NATIONAL AERONAUTICS AND SPACE ADMINISTRATION

Technical Memorandum 33-469

The Mariner VI and VII Flight Paths and Their Determination from Tracking Data

H. J. Gordon

D. W. Curkendall
D. A. O'Handley
N. A. Mottinger
P. M. Muller
C. C. Chao
B. D. Mulhall
V. J. Ondrasik
S. K. Wong
S. J. Reinbold
J. W. Zielenback
J. K. Campbell
R. T. Mitchell
J. E. Ball
W. G. Breckenridge
T. C. Duxbury
R. E. Koch

JET PROPULSION LABORATORY
CALIFORNIA INSTITUTE OF TECHNOLOGY
PASADENA, CALIFORNIA

December 1, 1970

NATIONAL AERONAUTICS AND SPACE ADMINISTRATION

Technical Memorandum 33-469

The Mariner VI and VII Flight Paths and Their Determination from Tracking Data

H. J. Gordon

D. W. Curkendall
D. A. O'Handley
N. A. Mottinger
P. M. Muller
C. C. Chao
B. D. Mulhall
V. J. Ondrasik
S. K. Wong
S. J. Reinbold
J. W. Zielenback
J. K. Campbell
R. T. Mitchell
J. E. Ball
W. G. Breckenridge
T. C. Duxbury
R. E. Koch

JET PROPULSION LABORATORY
CALIFORNIA INSTITUTE OF TECHNOLOGY
PASADENA, CALIFORNIA

December 1, 1970

Prepared Under Contract No. NAS 7-100
National Aeronautics and Space Administration

TABLE OF CONTENTS

CONTENTS (cont'd)

FIGURES

FIGURES (cont'd)

FIGURES (cont'd)

FIGURES (cont'd)

FIGURES (cont'd)

FIGURES (cont'd)

FIGURES (cont'd)

TABLES

TABLES (cont'd)

TABLES (cont' d)

SECTION I
INTRODUCTION

H. J. Gordon

This report describes the current best estimate (CBE) of the Mariner VI and VII flight paths, and the way in which they were determined. The flight paths are separated into three phases:

1) Launch to maneuver or pre-maneuver phase.

   This phase was characterized by the spacecraft velocity profile showing high sensitivity to its position relative to the earth. Under these conditions, the orbit could be very well determined after four or five days of continuous tracking.

   Results of pre-maneuver tracking showed how the trajectory would have appeared if no maneuver had been performed. Based upon these results, maneuvers were performed to attain the desired terminal conditions.

2) Cruise or post-maneuver phase.

   This phase was characterized by the spacecraft velocity profile showing very low sensitivity to its position in space. Under these conditions, the orbit determination process took several weeks to converge to as good an estimate as had been attained at the time the maneuver was performed. Due to the requirements to track other spacecraft, it was not possible to schedule continuous tracking coverage during this period, which additionally delayed the time at which good orbit estimates became available.

Initial results were used to determine whether or not a second maneuver would be necessary. In both cases, the maneuvers placed the spacecraft on sufficiently accurate trajectories so that all mission requirements were satisfied.

After accumulating a significant amount of tracking data, the results were used to plan detailed encounter sequences, which would be modified based on the tracking data accumulated during the encounter phase.

3) Encounter phase.

This phase was characterized by an increasing sensitivity of the spacecraft velocity profile to its position relative to Mars. Due to the high approach speeds, only the last few hours of pre-encounter data could be used to significantly increase the accuracy of the orbital estimates. In order to utilize as much tracking data as possible, final pre-encounter orbits were computed using tracking data taken up to approximately four hours before encounter. These final orbits were then used as the basis for positioning the scan platform to point the scientific instruments. Post-encounter tracking data, being very sensitive to the exact geometry near Mars closest approach, was then processed to very accurately determine the actual orbits.

These three basic mission phases covered different time intervals for the two spacecraft, and were interrupted by perturbing events which occurred on the spacecraft. Table 1-1 lists the events which affected the Mariner VI and VII flight paths.

There were two reasons for doing the Mariner VI maneuver as early as possible:

1) The trajectory geometry was such that the required pitch turns would have pointed the low gain antenna in a direction such that very poor telecommunications would have resulted if the maneuver were performed at L + 5 days, or later.

2) In case anything went wrong, analysis could have isolated a design flaw in time to take corrective action on the other spacecraft.

Table 1-1. Chronology of Events

Event	Time		Comment
	Mariner VI	Mariner VII	
1. Launch	25 Feb 1969 $01^h29^m02^s.013$	27 March 1969 $22^h22^m01^s.198$	Very accurate injection for both spacecraft.
2. Maneuver	1 March 1969 $00^h54^m44^s$ (L + 95 hr)	8 April 1969 $20^h22^m09^s$ (L + 286 hr)	Motor ignition time, at spacecraft. Both maneuvers were quite small and execution was sufficiently accurate to meet all mission requirements.
3. Scan unlatch	6 March 1969 $19^h11^m38^s$ (M + 138 hr)	8 May 1969 $19^h18^m26^s$ (M + 719 hr)	Accomplished by venting compressed nitrogen, which resulted in small velocity changes, of approximately 10 mm/sec.
4. Attempted Magellenic Cloud acquisition (MA VI)	30 April to 3 May 1969	N.A.	Non-standard sequence, attempted due to anomalous behavior of MA VI Canopus cone angle switching logic. Slight thrust unbalance between roll control jets (~0.7%) caused small velocity change, of approximately 2 mm/sec.
5. Pre-encounter anomaly (MA VII)	N.A.	Started on 30 July 1969 $22^h10^m58^s$	Apparent rupture of battery case and venting of solute caused loss of signal, electrical transients and damage to several telemetry channels, and a significant velocity change over a period of days. (Total velocity change was approximately 150 mm/sec).
6. Encounter	31 July 1969 $05^h19^m07^s$	5 August 1969 $05^h00^m50^s$	Time of closest approach.

Similarly, the scan platform unlatch was accomplished as soon as a reasonably good orbit determination was available, in order to allow time for any corrective action which might be necessary prior to the Mariner VII launch. When the unlatch occurred, the spacecraft went into a roll search. It was determined that though the spacecraft had been constructed under standard "clean room" conditions, dust particles were present on its surface. The nitrogen gas venting* dislodged some of these particles which subsequently reflected sunlight into the Canopus Star Tracker (CST) field of view and appeared to be brighter than Canopus so that they were tracked until they had moved away from the spacecraft. Canopus was automatically re-acquired approximately 26 min later. The short tracking data span between maneuver and scan unlatch did not allow a high precision orbit estimate to be made.

After the successful Mariner VII launch, telemetry showed that the Central Computer and Sequencer (CC&S) was in a non-standard mode. Subsequent analysis showed that there had not been any equipment failure, and a hypothesis based on spacecraft behavior during the launch environment explained the CC&S state. Right after launch, however, the CC&S behavior was not understood, and a decision was made to not transmit any ground commands until the CC&S state was clarified. This resulted in:

1) No ranging for the first five days of flight. (The spacecraft ranging transponder must be turned on by ground command – ranging was turned on for Mariner VI at L + 90 min.)

2) Automatic star acquisition logic resulted in acquisition of the star Vega as a roll reference. On April 1, a roll-search command was sent and Canopus was acquired. This rotated the high-gain antenna approximately 180 deg around the roll axis, and caused the non-radial components of solar pressure to act in opposite directions before and after Canopus acquisition.

The Mariner VII maneuver was executed on April 8. The required pitch turn, using Canopus as a roll reference would have tilted the solar panels 60 deg from the Sun direction, causing a battery share condition to occur. This

*The platform latch was a spring loaded device which was held latched by gas pressure. A leak in the pressurization system would automatically unlatch the scan platform so that it could perform its functions.

would not have been catastrophic, but it was undesirable. A roll search command was sent to acquire the star Sirius for roll reference a few hours before the maneuver was performed. The required pitch turn was then only 36 deg. After the maneuver was executed, Canopus was re-acquired.

The Mariner VII scan platform unlatch would have occurred automatically at the end of April, but operations personnel became heavily involved in trying to resolve a Mariner VI CST problem, so that it was postponed until May 8. The Canopus cone angle (Sun-spacecraft-star angle) changes as a function of time, since the spacecraft is oriented towards the Sun and Canopus is at a celestial latitude of 75 deg S. Therefore, the CST field of view must be adjusted in the cone angle direction periodically so that Canopus will not slip out of the field of view. On April 20, the CC&S automatically commanded such an adjustment, but the CST cone angle changed back to its prior position instead of stepping to its next position. This caused a loss of roll reference and an automatic roll search initiation. Several ground commands were sent to advance the CST cone angle, but it merely toggled back and forth. The only acquirable objects that would remain in the CST field of view through the encounter period were the Magellenic Clouds. Several attempts were made to acquire the brightest spot in the Greater Magellenic Cloud, but the extended source proved to be a very poor roll reference, and resulted in excessive attitude control gas utilization. On May 3, ground commands were again sent to advance the CST cone angle, and it did step to the proper position.

On May 8, the Mariner VII scan platform was unlatched by ground command. The spacecraft was first put into a gyro roll control mode so that the CST would not lose Canopus. During the nitrogen gas venting, telemetry indicated very high intensity error signals in the CST, but roll position was not disturbed. The spacecraft was returned to the normal cruise mode after the unlatch was completed.

On July 30, approximately 5 hr before the Mariner VI encounter, the radio signal from Mariner VII was suddenly lost. Mission operations personnel were deeply involved with the Mariner VI encounter sequence of events, so that only a small team could be spared to attempt to analyze Mariner VII. After the successful flyby was accomplished, operations personnel turned their

attention to the stricken spacecraft and sent a series of commands "in the blind" to switch the spacecraft transmitter from the high-gain antenna to the omni antenna. The spacecraft signal reappeared, 7 hr after being lost, indicating that the roll reference had been lost and the high-gain antenna had turned away from the Earth. The evidence which came pouring in indicated that a major spacecraft anomaly had occurred:

1) The doppler tone indicated a decrease in radial velocity of 1.89 cm/sec.

2) Only 70 telemetry channels were operating properly, 24 had been disabled.

3) There was evidence of many electrical transients having taken place.

After tracking for 71 min the signal was lost again, requiring 60 min to regain two-way lock, at which time additional electrical transients had occurred and the doppler tone indicated an additional decrease of 0.78 cm/sec in the radial velocity, which continued to decrease at an apparently exponentially decaying rate until well after the Mariner VII encounter. This behavior has been attributed to the battery case being ruptured, allowing solute to vent into the interior of the spacecraft and thence into space (Ref. 1). Great difficulty was experienced in processing tracking data influenced by an unknown (at that time) non-gravitational force which could not be properly modeled. An accurate orbit estimate was obtained in time to properly position the scan platform, and this flyby, too, was accomplished successfully.

Post-encounter analysis of all the tracking data accumulated to a time well past the time of closest approach has produced the CBE of the Mariner VI and VII orbits during their various mission phases. These CBEs are plotted in Figure 1-1 (see Figure 3-6 for aiming plane definition), and are included in other figures throughout this document for comparison with orbital estimates which were made at various times during the period of mission operations.

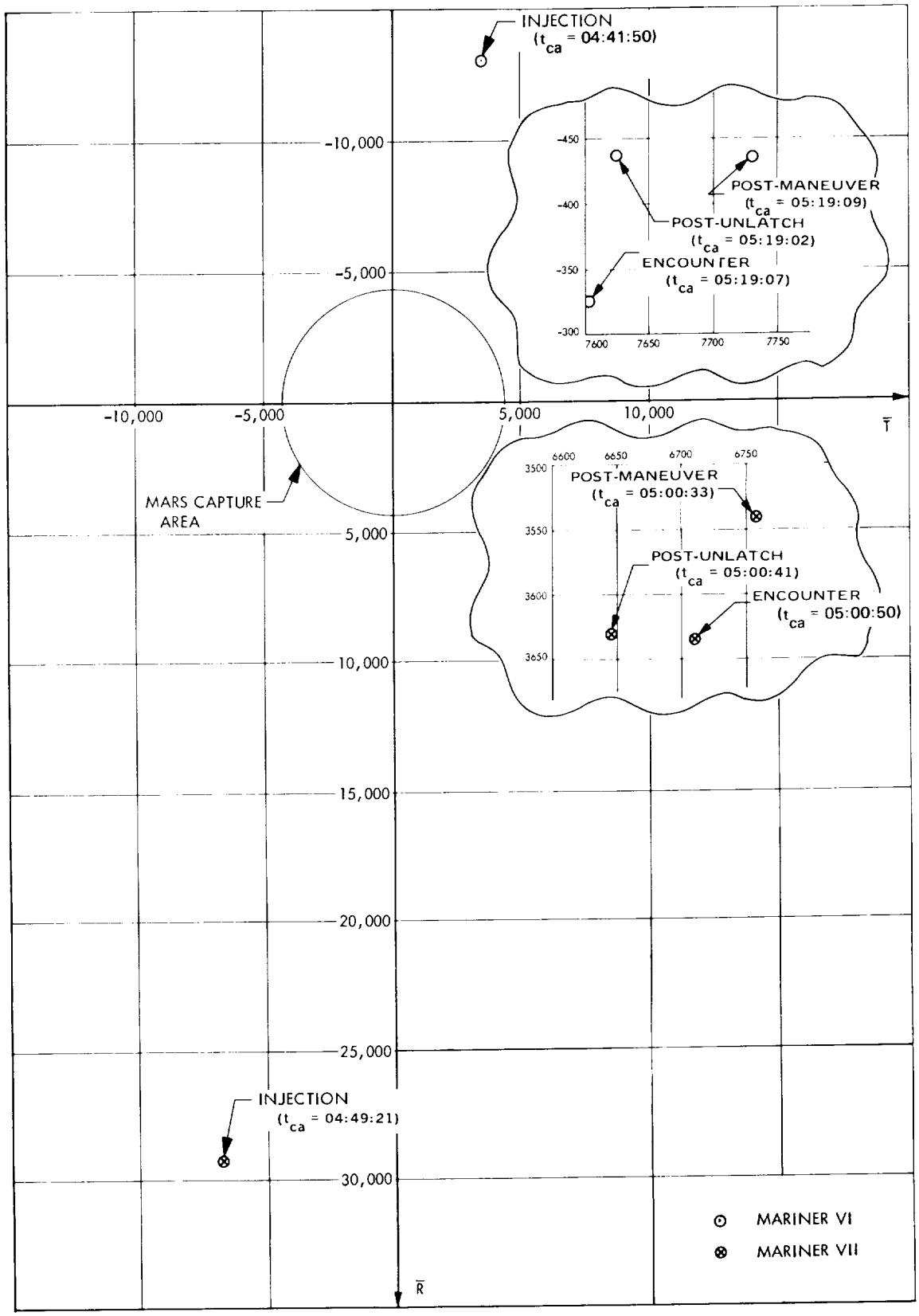

Figure 1-1. Current Best Estimates of Orbits for Various Mission Phases

SECTION II
ORBIT DETERMINATION FROM DSIF TRACKING DATA

A. PRECISION NAVIGATION PROJECT

1. Introduction — *D. W. Curkendall*

Early in the pre-flight planning stages of the Mariner Mars 1969 (MM' 69) mission it became apparent that in order to meet the science requirements, the pre-encounter trajectory had to be predicted to a much tighter tolerance than had been required or even demonstrated on earlier flights (see Mariner II-V Flight Path Reports for a detailed account of performance achieved). Specifically, the estimated B plane co-ordinates had to be accurate to within 250 km* in the direction perpendicular to the B vector.

Accordingly, in September of 1967, the Precision Navigation Project (PNP) was instituted with the unified goal of "delivering the software, procedures and estimates of DSS station locations" necessary to achieve this performance. The primary implied task of the project was to bring to completion the Double Precision Orbit Determination Program (DPODP) development. By merit of its improved physical models and extended precision it was determined that the DPODP could exhibit superior in-flight performance as compared to the Single Precision Orbit Determination Program (SPODP) and enhance the probability of meeting the MM'69 performance goals (see Ref. 2). In addition, the program was required for the more accurate determination of DSS station locations using tracking data from previous flights. The SPODP could also be

*Much later this number was relaxed to 300 km as performance data on the scientific instruments became more definite.

a beneficiary of improved station locations, since in general, this program can make advantageous use of location estimates of greater accuracy than can be produced with the program itself.

A version of the DPODP suitable for performing the station location work was delivered in December of 1968; the certified flight version was delivered May 1, 1969, culminating a development period of over five years.

As the mission period approached, the activities of the PNP broadened to coordinate the efforts in several areas needed to put together a comprehensive attack on the pre-encounter estimation problem. These included:

1) Improved timing and polar motion estimates and predictions.

2) Improved planetary ephemerides, particularly the Mars ephemeris, both for station location determination and in-flight activities.

3) An attempt to provide for the first time ionospheric calibrations for the tracking data both for past missions and the Mariner Mars 1969 mission itself.

4) A concerted effort was organized to define and formalize the estimation procedures to be employed for encounter.

These and other activities are discussed in the following subsections.

2. Flight Preparation

a. Ephemeris Development – *D. A. O'Handley*

- Introduction

Requirements for precision navigation of the spacecraft during the Mariner Mars 1969 mission resulted in a concentrated effort directed toward improving the ephemeris of Mars. The Development Ephemeris 40 (DE 40) represented the first dynamically consistent planetary ephemeris produced at the laboratory (see Ref. 3). This ephemeris resulted from a 56 parameter least squares fit to available radar and meridian circle observations over the period of 1950-1967. At the time of its release internally at JPL, it was known that the outer planets were improved over the currently available ephemerides, but also that there was a need to fit over a much longer arc to obtain

definitive ephemerides. Further, the longer arc of optical observations was needed to better determine the orientation of the ecliptic and the mean longitude of the earth-moon barycenter.

As a result of the needs of the Mariner Mars 1969 mission and the general improvement of planetary ephemerides a new 60-year numerical integration of the planets of the solar system was made. These ephemerides resulted from differential corrections obtained from a weighted least-squares fit to a data set spanning the period 1910-1968. The optical data set included over 34,000 meridian circle observations in right ascension and declination obtained with the Six-Inch Transit Circle and Nine-Inch Transit Circle of the U. S. Naval Observatory. These data were taken for the sun and all the planets except Pluto. The planetary radar data set includes over 700 time-delay measurements from the radio antennas at the Arecibo Ionospheric Observatory, the Jet Propulsion Laboratory, and Lincoln Laboratory of MIT. The radio tracking data set includes 214 time-delay points of 0.1 μsec* accuracy taken from Mariner V during its encounter with Venus in 1967 (see Ref. 4). This ephemeris (DE69) was delivered February 1, 1969 and was used for the initial determination of station locations with the DPODP and all pre-encounter flight operations.

- Mars Planetary Ranging Data

Development Ephemeris 69 was based upon Mars radar range data from Arecibo Ionospheric Observatory and MIT Haystack and optical data from the U. S. Naval Observatory. In order to check the accuracy of this ephemeris it was desirable to take some current radar time delay measurements based upon predictions using DE69. These residuals would be a measure of the accuracy of the ephemeris used.

On May 7, 1969, JPL made its first bistatic time delay measurement of Mars. The experiment consisted of using two antennas at the Goldstone Tracking Station of JPL. The Venus antenna was used to transmit a signal to the planet and the Mars antenna was used as the receiver. The Venus site comprises a 26-meter antenna with a 450-kW transmitter. The Mars antenna is 64-meters in diameter.

---

*Since time delay measurements are proportional to round-trip range the equivalence between a time delay measurement error and the metric range error is approximately 1 μsec = 150 m.

From May 7 to July 16, 1969, 239 accurate bistatic range measurements were made. The measurements made on the 18 nights are of better than 5 μsec accuracy. On each night of observation, an average of 15 round-trip measurements were made. The sub-earth point on Mars rotated with respect to surface features on Mars during an observation session, giving a longitude spread of approximately 180 deg. On a given evening's observation, the latitude remained almost constant with respect to the area on the surface of Mars. Because of the rotation of Mars and the motion of the earth, every 40 days the same longitude passes through the sub-earth point. The latitudes varied over this 2-month period from 3 deg N to 12 deg N.

The measured time delay is influenced by 1) the relative orbital positions of Mars and the earth, and 2) the variations in elevation on Mars at the sub-earth point.

- Comparison of Ranging Data With Theory

The initial comparison of these JPL-Mars range observations showed a negative bias of approximately 100 μsec (Figure 2-1) and an apparent "runoff" indicated by the smaller negative residuals after July 10 (JD2440412). The span of 80 μsec for residuals on a single date is the effect of topography covering approximately 12 km in altitude at the various latitudes.

- Ephemeris Improvement

It was highly desirable to use this 1969 Mars data to produce an improved ephemeris for use during the Mariner encounters. At the same time, Development Ephemeris (DE) 69 had been used for all the station location data processing, producing station estimates tied to this ephemeris. Time did not permit reprocessing all of the data with a completely updated ephemeris. Thus, the decision was made to use the Mars planetary data to update the Mars ephemeris only, leaving all other ephemerides fixed at their DE69 value.

The optical data and some radar range data had been used previously in DE69. The Arecibo data prior to 31 January 1965 were removed for this analysis because the quality of these data is poor compared to modern measurements. A summary of the Mars data used in the ephemeris development is given in Table 2-1.

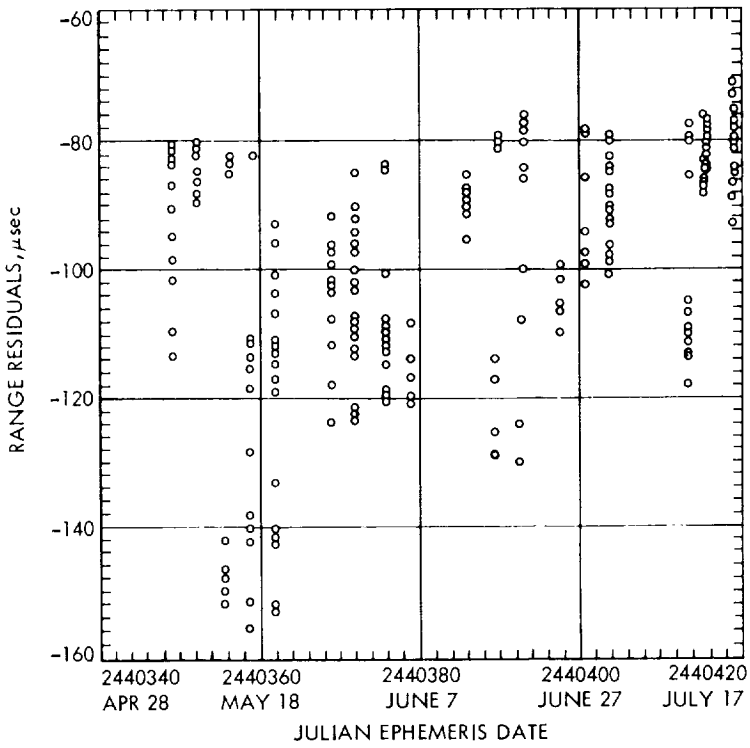

Figure 2-1. JPL 1969 Mars Range Residuals, DE69

Since the topography is imbedded in the range measurement, it was found that, by introducing a 10-σ weight for each point, the corrections to the ephemeris of Mars were within expected limits. The purpose was to minimize the effects of topography at that time. The ephemeris of Mars must be corrected first and realistic corrections for the topography can then be deduced.

- DE71 Solution

First, a simultaneous solution was made for 63 parameters: the elements of eight planets (Pluto excluded at this time), the right ascension and declination limb biases of Mercury and Venus, the radii of Mercury, Venus, and Mars, the six elements of Mariner V, the mass of Venus, and the astronomical unit.

Examination of the corrections for the ephemeris of the earth-moon barycenter for this global solution revealed that they were small with respect to the accuracy of optical data. This gave confidence that the errors introduced

Table 2-1. Mars Observations

Instrument	Period	Number of Observations	
		Right Ascension	Declination
6 in. Transit	242 4793.8-243 9658.5 (1926-1967)	549	528
9 in. Transit	242 0105.8-243 1164.5 (1913-1944)	122	120
	Total	671	648
(Range)			
Arecibo Ionospheric Observatory (AIO)	243 8803.8-243 8915.5 (1964-1965)	29	
Haystack (MIT)	243 8587.7-243 9643.5 (1967)	10 (compressed)	
Goldstone	244 0348.9-244 0418.8 (1969)	239	

by producing the Mars only ephemeris update were indeed small and the procedure was tractable. The stability of the corrections to the orbital elements of Mars with or without corrections to the earth is shown in Table 2-2. The 7 parameter solution was therefore used to create DE71.

The optical residuals are shown (Figures 2-2a and 2-2b) both in right ascension and declination. The total set of radar residuals shows (1) the relative accuracy of the modern measurements (Figure 2-3) compared to the first range measurements in 1964, and (2) the 80-μsec scatter due to topography in the 1969 measurements. If the 1969 residuals after solution are examined in detail, effects of improving the orbital elements and radius are seen (1) centering the residuals about zero, and (2) the alteration of the character of the residuals with time. The negative bias was removed primarily through the correction to the radius of Mars. The nominal radius of Mars from DE69 was 3375.6 km and the radius appropriate for DE71 is 3393.0 km. This new radar-determined radius agrees with the results of Dan L. Cain at JPL using Mariner IV spacecraft data.

Table 2-2. Corrections to DE69

63 Parameters/Rank 55			7 Parameters	
Earth-moon barycenter		Mars	Mars	
Set III* parameter	Corr.	Corr.	Corr.	
$\Delta l_o + \Delta r$	-".0007	+".0141	+".0148	±0.0017
Δp	+.0016	-.0626	-.0671	0.0107
Δq	+.0117	+.0097	+.0042	0.0134
$e\Delta r$	+.0004	+.0062	+0.0063	0.0014
$\Delta a/a$	$-.2 \times 10^{-6}$	-.0002	-0.0002	0.6×10^{-4}
Δe	-.0001	+.0168	+0.0170	0.0010
Radius		+16.9 km	+17.4 km	±1.4
AU		-1.1 km		

The total number observations is 1597. Standard deviation of data before solution is 2.78 - after solution is 0.67.

*Set III Parameters (defined in Ref. 5) are the standard coordinates used for ephemeris corrections and are quoted here for comparison purposes.

Recent work by A. J. Kliore and others, using occultation and trajectory information from Mariner VI, gives an equatorial radius of 3394 ±4.5 km and a flattening factor which reduces the polar radius by about 18 km (f = .0057 ±.002, which is close to the dynamic flattening factor).

- Comparison of DE69 and DE71

Since the pre-encounter activities were carried out using DE69 and the encounter activities used DE71 a comparison is given in Table 2-3.

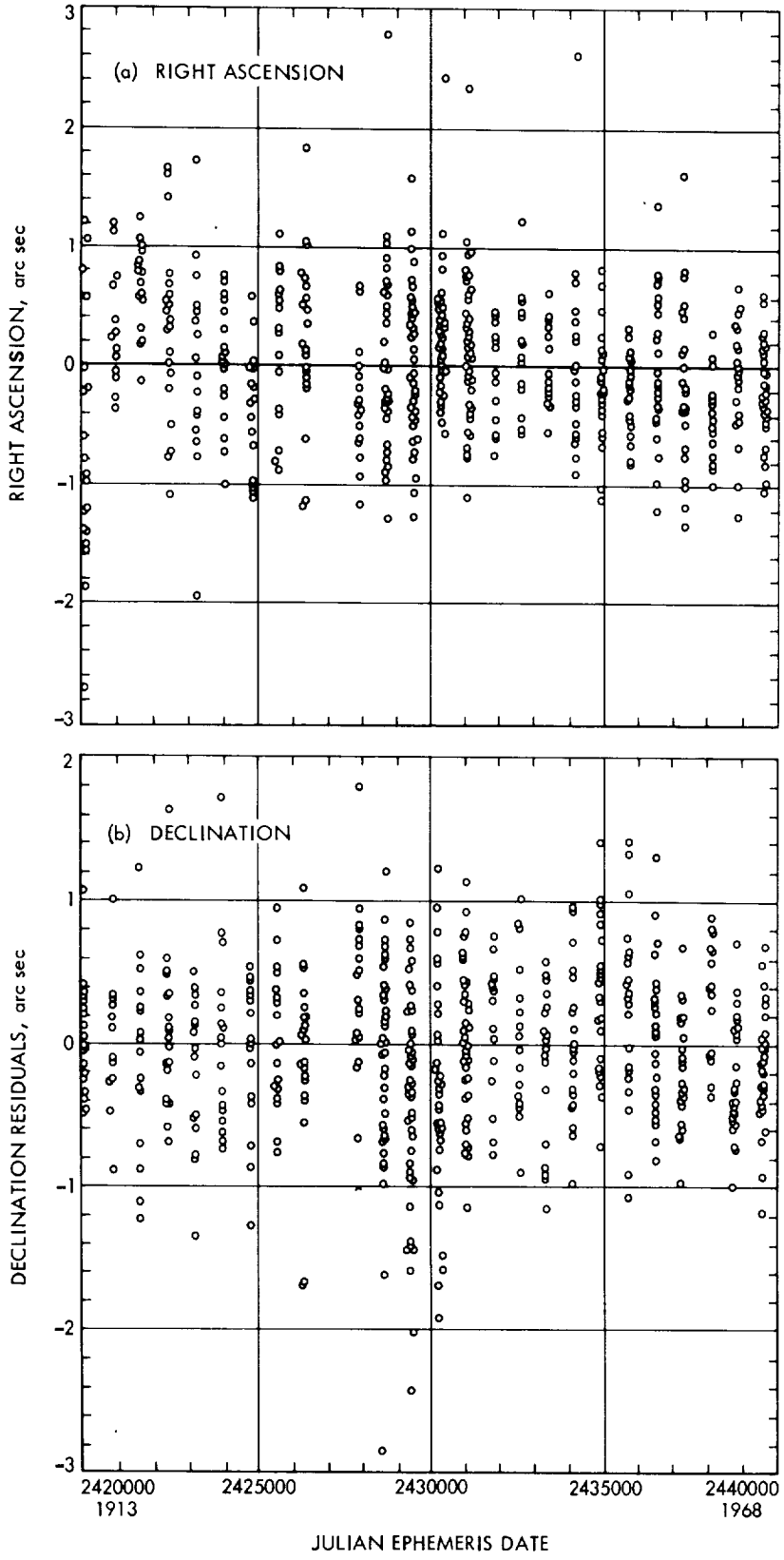

Figure 2-2. Optical Residuals, DE69 (1913-1969)

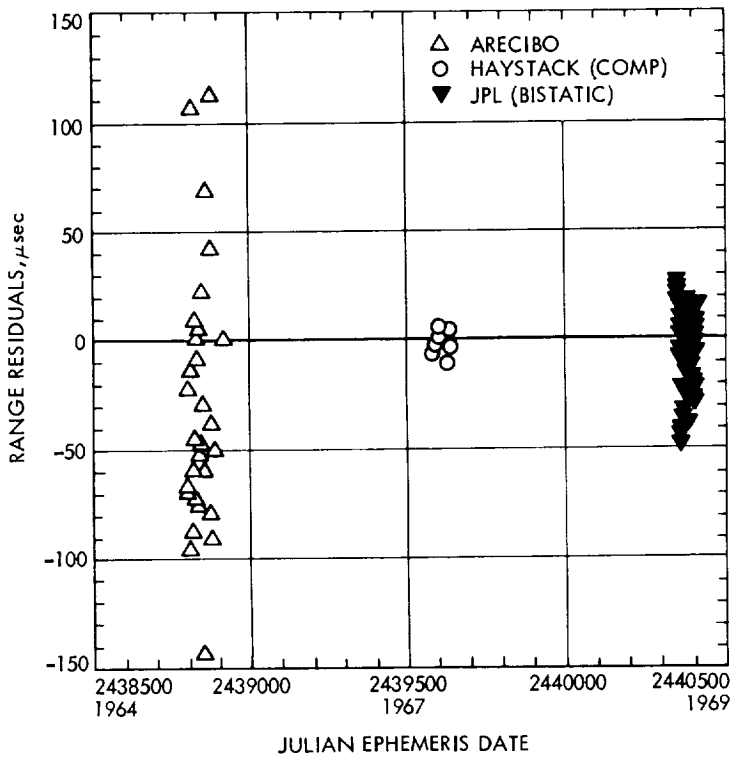

Figure 2-3. Radar Residuals, After Solution (1964-1969)

- Topography

It was indicated early that there were height variations imbedded in the range data. Having corrected the elements for Mars, the residuals of the range data compared to DE71 are plotted versus longitude (Figure 2-4). A negative residual represents an early return of a "high" area and conversely a positive residual represents a late return of a "low" area.

The highest area is Tharsis (105 deg) and the lowest is Amazonis (180 deg). Aeria (300 deg), which is 180 deg away from Tharsis, is a secondary high region and is approximately 4 km lower.

The residuals of Syrtis Major, a prominent dark feature, showed sharp variations of 7 km beginning at Aeria (295 deg) to Moeris Lacus (275 deg). The shallower slope from the northern tip of Mare Cimmerium westward is seen.

Another observation is that the variations in surface heights with longitude are real. Initially, comparisons of the later observations at high

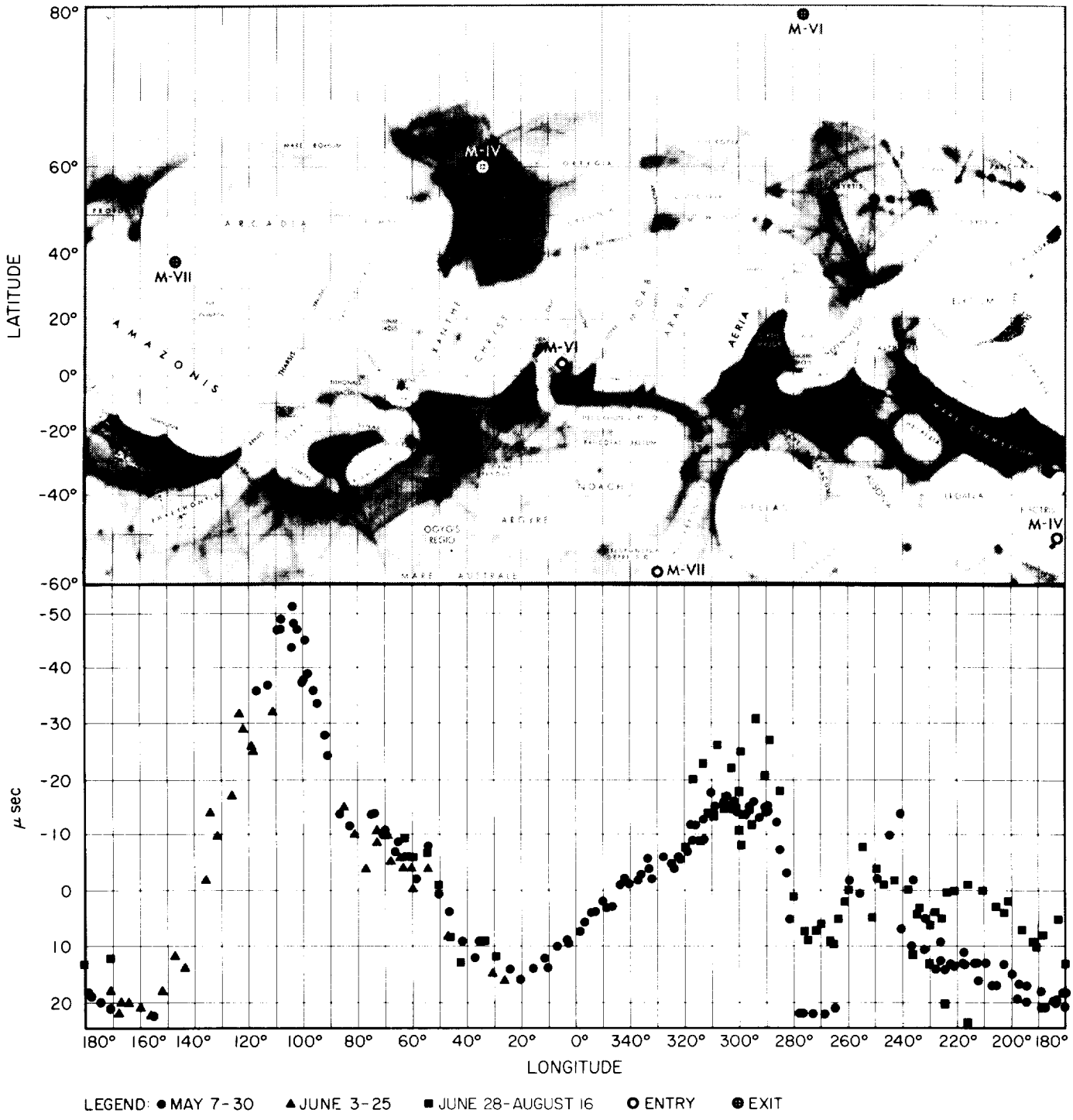

Figure 2-4. JPL - Mars Topography - 1969

Table 2-3. Mars (DE71 − DE69)

Date	ΔX (km)	ΔY (km)	ΔZ (km)	δR (km)	cos β dℓ (rad x 10^{-7})	δβ (rad x 10^{-7})
(July 30) 2449432.5	-19.1	-20.6	+15.5	~-7.7	-0.8507	+2.5879
(Aug. 7) 2440440.5	-18.5	-18.7	-47.7	~-9.3	-0.8020	+2.4077

where β and ℓ are the celestial latitude and longitude.

latitudes gave more negative residuals and this "run-off" was thought to be an ephemeris error. Subsequent analysis has shown that the region Aeria at 7.8 deg latitude is about 2 km lower than the same longitude at 12 deg latitude. Similarly, the Moeris Lacus region shows a variation between latitude 7.8 deg and 12 deg of about 2 km, and this tends to be maintained throughout the westward slope from the northern tip of Mare Cimmerium and what would appear a higher elevation at Trivium Chorontis.

- Conclusion

This new ephemeris of Mars performed satisfactorily during the encounter missions. The error in the ephemeris predictions was less than 5 km in the radial distance from earth to Mars as determined from the Mariner VI flyby. The flight version of DE71 which was used by the Mariner Mars 1969 mission is gravitationally inconsistent since the planetary ephemerides are those of DE69 except that DE71 Mars has been placed on the type 50 tape. This means corrections to the earth and Mars ephemerides from this mission should be carefully interpreted.

The topography that has been discussed seems to be well established by repeated measurements over the same longitudes and nearby latitudes. In the near future, the range measurements, along with the corrections for topography, will be published. Combining these JPL measurements with other Mars range data, it is hoped some contour plotting might be accomplished which would show relief between the latitudes of 3-22 deg N.

- Acknowledgments

The radar ranging of Mars was carried out by Richard M. Goldstein, George A. Morris, and George S. Downs. It is also a pleasure to acknowledge the assistances provided by Joyce Steinberg and Steve Ritchie in the ephemeris development and Don Johnson's work implementing the topography corrections into the radar predictions. William Melbourne and Douglas Holdridge were active in all portions of this research.

b. Station Locations — *N. A. Mottinger*

- Introduction

Often, the most reliable means of determining a spacecraft orbit before its encounter with the target planet is to use a restricted data arc (on the order of one week's tracking). This reduces the dependence of the estimation process on an accurate long term description of the physical mode. Specifically, the possible build-up of effects due to unpredictable non-gravitational forces arising from the spacecraft itself is guarded against by this strategy. However, the estimate thus obtained becomes highly dependent on an accurate *a priori* estimate of the locations of the DSS tracking stations.

In Ref. 2 Hamilton, Grimes and Trask analyzed the sensitivity of the orbit estimates of the Mariner Mars 1969 trajectories to station location errors and found them to be approximately

$$\frac{\Delta b_\delta}{\Delta r_s} = 39 \text{ km/m}$$

$$\frac{\Delta b_\alpha}{\Delta \lambda} = 16 \text{ km/m}$$

where

r_s = station distance from the Earth's spin axis

λ = station longitude

b_δ = projection on the B-plane of the error due to r_s, km

b_α = projection of error due to $\Delta\lambda$, km

On this basis, the goal was set to determine the station locations to an accuracy of 3 m standard deviation in both the r_s and λ components. The primary resource for determining locations at these accuracy levels was the tracking data from past spaceflight missions. To be an attractive data set for determining station locations, one of the following situations must be present:

1) The spacecraft trajectory must be established accurately irrespective of tracking station location accuracy. This occurs for a data span which includes a lunar or planetary encounter where the probe behavior is strongly influenced by the target's gravitational field, making the orbit parameters easy to discern. The data, which is always dependent on the station locations, can then be used to estimate these parameters as well.

2) The data is not affected strongly by the position of the spacecraft. This is a special circumstance and arises when the probe goes through zero geocentric declination. The dependence of the data on declination vanishes at this point (Ref. 6), but the dependence on r_s remains, making this a uniquely attractive situation to estimate the r_s component. Unfortunately, there is no analogous geometric separation between absolute station longitude and orbit parameters.

- Data Set

All pertinent missions for which Earth based radio tracking was available were considered as possible data sources for station location determination. These fell generally into two categories, lunar and planetary. None of the lunar missions offered zero declination cases independent of encounter (impact), whereas Mariner V offered two. One occurred during cruise and the other after encounter. Altogether, 21 different data periods were considered. In the final analysis, many had to be omitted due to the appearance of unexplained anomalies and/or lack of charged particle calibrations. In the case of the lunar missions disagreement with the planetary absolute longitude solutions exceeded allowable limits for combination. (This is probably due to inconsistencies between the lunar and planetary ephemerides.) The band of missions

used for determining station locations by the 1969 flight project was restricted to previous Mariner missions (Mars in 1965, Venus in 1967) and Pioneer VII, a total of five independent data blocks. Detailed discussion of this can be obtained in Refs. 7 and 8.

- Launch Station Locations

The set of station locations provided for the launch phase of Mariner 1969, Location Set (LS) 17, were obtained by processing radio tracking data with the DPODP. For the purposes of comparison, the previous reductions performed with the Single Precision Program were duplicated as best as possible as far as data content was concerned. The comparison between the sets of station locations produced with each program were detailed in Ref. 8. The average agreement between the two sets of solutions was 1 m in r_s, and 1.6 m in longitude. The largest disagreement noted was 3.3 m in r_s and 4.2 m in longitude. Such agreement was considered almost remarkable in view of the large physical model difference between the two data reduction programs and the manner in which these could have propagated into station location solutions.

- Encounter Station Locations

The determination of the encounter station locations incorporated many other variables in an effort to obtain still better locations. A limiting factor for the accuracy of the locations derived from the postflight analysis is the calibration for charged particle effects. The work necessary to prepare these in a form suitable for use in the DPODP is detailed in Ref. 7. The corrections which could be produced in the time available for the Mariner Mars 1969 encounter phase further reduced the number of missions which could be analyzed (Mariner IV and V only) and in some cases reduced the length of the data arcs. The application of the ionosphere corrections caused changes as large as 3.8 m in r_s and 3.2 m in longitude. The differences between the best set of station locations without the ionosphere, LS 24, and the set with corrections, LS 25, is shown in Table 2-4. It should be noted that the northern hemisphere stations underwent the greatest shift in r_s. This occurred because the height of the ionosphere activity occurred in the northern hemisphere at the times radio tracking data was available. Figures 2-5 and 2-6 show how the solutions available at the Goldstone complex compare before correction (top of each figure) and after the corrections were applied (bottom of each figure).

Table 2-4. Changes Due to Addition of Ionospheric Data (LS 25-LS 24)

DSS	Δr_s (m)	$\Delta\lambda$ (m)	Δ Relative λ (m) DSS 12 minus DSS
11	3.8	-0.94	
12	3.8	-0.94	
14	3.8	-0.96	
41	0.26	-3.24	2.3
42	-0.28	-0.32	-0.62
51	-0.61	-0.84	-0.1
61	3.47	-1.04	0.1
62	3.45	-1.08	0.14

Ionosphere corrected station locations, LS 25, will be used in this report to judge the accuracy of other locations used to support the mission, primarily the launch locations, LS 17. The differences between the two sets are shown in Table 2-5. For r_s these closely parallel those shown in Table 2-4, except for stations 51 and 61. The primary cause for the differences at these two stations has not been determined, but may be involved with the amount of data in the fits and the techniques used to produce LS 17 and LS 25. The longitude differences are between 7 and 9 m. This is due to changes made in the definition of UT1 disseminated by the USNO and to a smaller degree the ionosphere correction. After January 1, 1968 UT1 was changed by the USNO thereby introducing a discontinuity between the timing system used to process the previous data and the system for reducing the 1969 data. To counteract this, the longitude estimates were increased by 3×10^{-5} deg. However, during the later stages of the mission, timing data with the discontinuity removed was available and was used to reprocess the old data. Polar motion values also changed when the timing data were reissued. The changes in individual reductions agreed to within 0.3 m of the shift in UT1. So although the longitude values show large disagreements, they are explainable and do not represent errors in either set of station locations, but do show the sensitivity of the DSS longitude solutions to UT1.

The LS 24 values were used by the DPODP to support the majority of the encounter phase reductions. The ionosphere corrected station locations

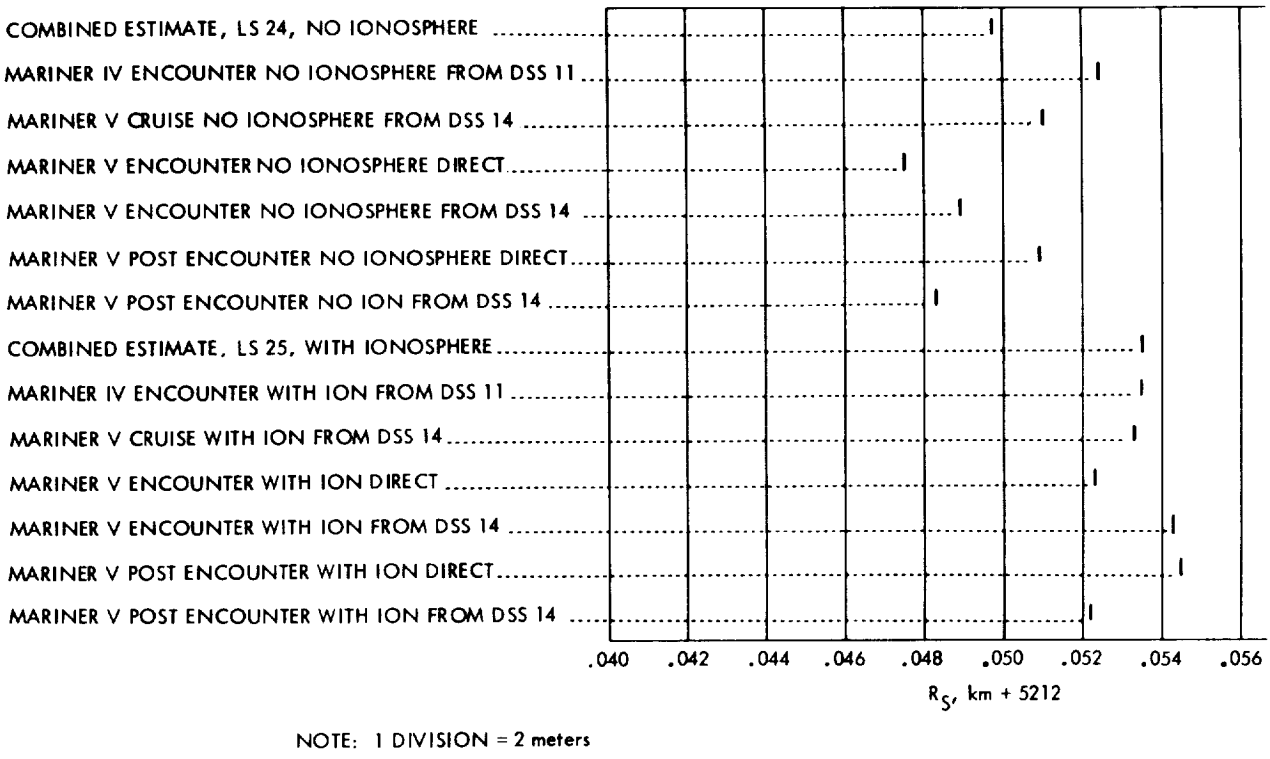

Figure 2-5. Distance Off Spin Axis, Earth Fixed System (1903.0 Pole) DSS 12

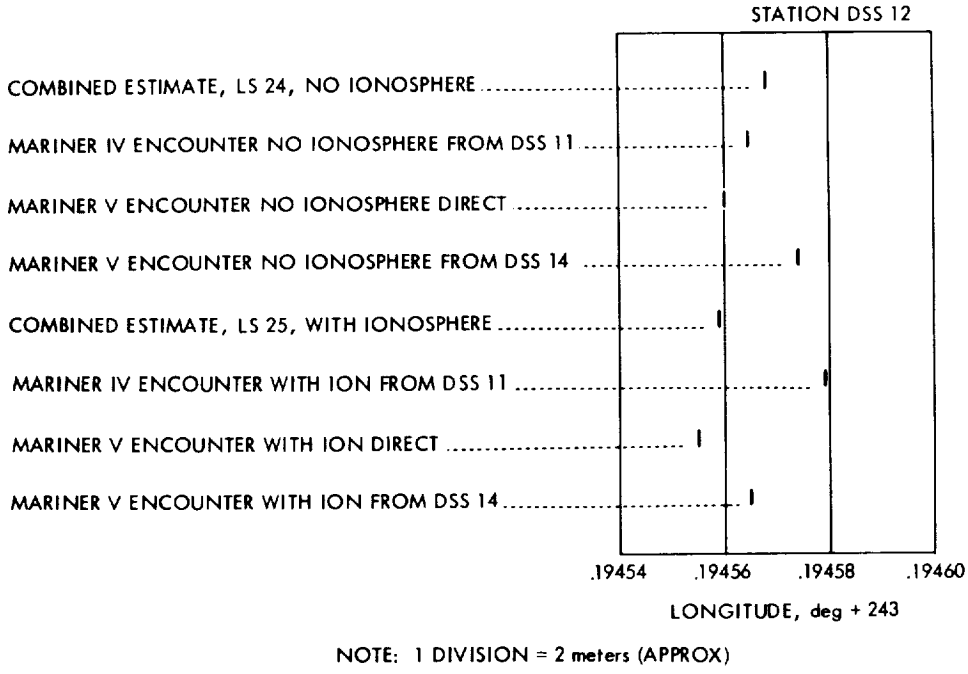

Figure 2-6. Geocentric Longitude, Earth Fixed System (1903.0 Pole) DSS 12

Table 2-5. Station Location Differences (LS 17-LS 25)*

DSS	Δr_s (m)	$\Delta\lambda$ (10^{-5} deg) ≈meters	ΔZ (m)
11	-3.7	7.3	-4
12	-3.7	7.1	-4
14	-3.9	7.7	-4
41	-0.3	9.3	5
42	0.1	7.9	18
51	-3.5	8.8	-16
61	-0.1	7.3	-56
62	-2.2	8.0	42

*LS 17 – Solution from Double Precision Orbit Determination Program used during launch; does not include ionospheric effects and without compensation for changes in UT1 made 1 January 1968.

LS 25 – Best estimate from DPODP, includes ionospheric correction and timing data with discontinuity removed.

were used only in conjunction with tracking data which could be corrected with the limited amount of charged particle data available during the time the mission was in progress. The method for doing this is described in Ref. 7 in the section on Station Locations. Although the charged particles had the most pronounced effects on station locations, a change was made in the refraction model for the neutral atmosphere which also affected them. The changes in the model are reported by Ondrasik in Section V of Ref. 7. Briefly they involved restricting the modeling of the troposphere to elevations above 15 deg. This new model was incorporated into the DPODP and due to the time available, only the Mariner V cruise zero declination case was refit to determine the effects on stations. Spin axis changes were of primary importance and no change was expected in the longitude solutions. The r_s changes derived from this reduction are listed in Table 2-6. These were applied to LS 24 to create LS 27 which was then used with the new troposphere model in the DPODP. Similarly changes were made to LS 25 to produce LS 26 which was used when ionosphere calibrations were applied to the tracking data.

Table 2-6. r_s Correction for New Troposphere Model

DSS	Value added to old solutions, m
11	0.5
12	0.5
14	0.6
41	0.8
42	0.8
51	0.8
61	0.7
62	0.7

Generally of minor concern in the reduction of doppler radio tracking is the accuracy associated with the distance of the station from the equator plane. The sensitivity of the doppler data in this component, Z, is nearly negligible. The Z values used came from several sources. Values for the stations at Goldstone, Woomera, and South Africa were based upon the Smithsonian Astrophysical Observatory values developed for their Standard Earth 1966. The remaining stations had Z values which trace back to geodetic surveys. Due to this low sensitivity, estimates of this component have not been available from previous doppler tracking, and have been of little consequence. However, when range data was included from several stations significant changes did exist between the orbit determined with both data types versus the doppler only solutions.

Although there were other factors affecting these solutions, the suspected error was the Z component of the tracking stations. Values were obtained for the DSN stations from K. K. Lambeck (private communication) who has reduced earth satellite data at the Smithsonian Astrophysical Observatory. Using these values produced a significant reduction in the conflict previously noted when range data was added to the doppler. The differences in this coordinate are shown for each station in Table 2-5.

- Location Uncertainty

The best estimate of contributing errors due to the ephemeris, UT1, troposphere, ionosphere and miscellaneous other items were RMSed in Ref. 9 to obtain estimates of the crust fixed uncertainty for Mariner IV and V. These were about 3.0 to 3.5 m, respectively. When the two estimates were combined to produce LS 25, the uncertainty was 2.3 m. Recall that this is also approximately the separation of the solutions from these two missions shown in Figure 2-6. Estimates of the spin axis uncertainty have not as yet been as rigorously determined. Based upon the distribution of the r_s solutions before and after the ionosphere corrections were applied, the estimated error would be approximately 4 m for the northern and 1 to 2 m for the southern hemisphere. The spin axis 1-σ uncertainty for LS 25 would be in the 1 to 2 m range for all stations.

The summarizing of errors here applies only to the post flight analysis performed to produce a particular Location Set. The error in the location of the station from the viewpoint of reducing the data in real time is an extension of this analysis in that pertinent quantities such as polar motion, UT1, charged particles and the ephemeris as discussed in other sections of this report all contribute to the success with which the true trajectory of the probe can be determined.

c. Timing and Polar Motion Errors — *P. M. Muller and C. C. Chao*

- Timing Errors

Three types of time are used when computing an orbit: Ephemeris Time (ET, used to look up positions of the celestial bodies), Universal Time (UT1, used to determine the location of a tracking station in space), and Station Time (t_s, the time tag that is associated with the actual tracking data) — (see Ref. 10). The behavior of these times with respect to a uniform time is schematically illustrated in Figure 2-7, where the abscissa is a uniform time defined for purposes of this discussion as A.1 (Atomic Time), and the ordinate represents units in one of the above three time systems.

The lack of precise knowledge of the relationships among the three times illustrated in Figure 2-7 can result in a degradation in the apparent quality of the tracking data, incorrect solutions for the tracking station locations,

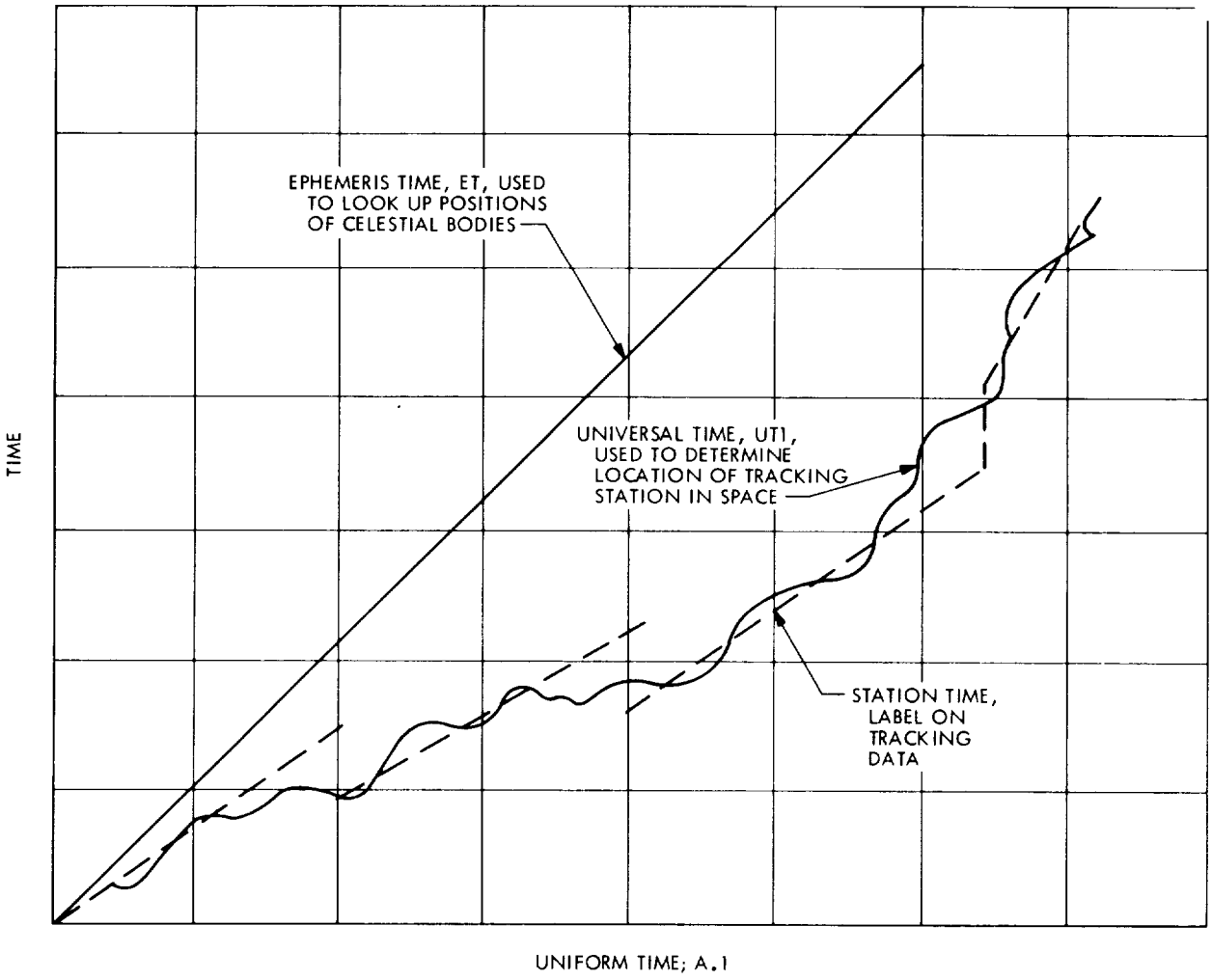

Figure 2-7. Relationship of Time Systems in the Orbit Determination Process.

and an erroneous prediction of the spacecraft coordinates near planetary encounter.

- Polar Motion Errors

The Earth's principal axis is not coincident with the spin axis; it moves with respect to the latter, causing the so-called polar motion. The precision with which we are seeking to evaluate DSN station locations requires consideration of this polar motion and its effects.

Polar motion, which is different from the Earth's precession and nutation (see Ref. 11), is observed indirectly through determinations of the variations in latitude of various observatories. The magnitude of this variation ranges from 5 to 20 m. Such an appreciable motion will obviously cause variations in DSN station location with the same order of magnitude of the polar motion. A maximum variation of 23.5 m was found at Goldstone during the period 1960 to 1966 (see Ref. 12). On this basis, polar motion has been modeled in the DPODP and special provisions were made during the Mariner Mars 1969 mission to represent and predict the polar motion as accurately as possible.

- Procedures for Implementing Corrections to the Data

Timing

Selection of Data Source. Currently, the quantity A.1-UT1 is determined by many agencies and observatories. The quality of A.1-UT1 data varies from observatory to observatory depending on their instrument and the local weather conditions throughout the year. Among them only two agencies were considered for our use because of their relative excellence in the observed data. They are the U. S. Naval Observatory (USNO), and the Bureau International de l'Heure (BIH). The USNO which has been in close contact with JPL in supplying data for earlier missions, has two stations, one at Washington, D.C., and one at Richmond, Florida. Both stations use PZT (Photographic Zenith Tube) to do the time measurement. An appreciable difference between the smoothed value of A.1-UT1 of the two stations has been found, and the USNO adopted A.1-UT1 as the linear combination of the two results by weighting Richmond two and Washington one, i.e., USNO A.1-UT1 = 2/3 Richmond (A.1-UT1) + 1/3 Washington (A.1-UT1). The relative weight of the two stations has no theoretical justification. It was adopted because previous experience has

shown Richmond to have more observations and better results than Washington. Thus, the USNO adopted A.1-UT1 may tend to have a bias toward one station's result when the other station has no observation due to bad weather. Therefore, when we use the USNO data, we use the result from one station (Richmond) all the time.

The BIH adopted A.1-UT1 results from combined UT observations of over 40 stations around the world including Washington and Richmond. A very sophisticated computing program (see Ref. 13) is employed by the BIH to solve for A.1-UT1. As claimed by BIH, their results are superior to that of USNO. The claimed uncertainty of A.1-UT1 from these sources is shown in Table 2-7. The estimated (not by JPL) uncertainties in Table 2-7 clearly suggests that we should use BIH adopted A.1-UT1. However, after a practical test with the previous mission results, Richmond A.1-UT1 (smoothed by JPL) turned out to be more consistent with the mission data than the BIH adopted value. This implied that a long term difference between the two data sources might exist.

Table 2-7. Claimed Short Term A.1-UT1 Uncertainties

Time when A.1-UT1 was determined	USNO		BIH	
	One-sigma msec	Worst case msec	One-sigma msec	Worst case msec
One night	6	30	Not applicable	Not applicable
1 year later final smoothed data	5	25 between Washington and Richmond	2	?

Finally, we decided that it is wise to stay with a single station which produces consistent results. Thus the nightly observed A.1-UT1 from Richmond was the source of timing data for the 1969 Mars mission.

Procedures of Processing the Data. A monthly daily observed raw data of A.1-UT1 of Richmond together with that of Washington were received

from USNO on keypunched cards around the 15th of each month. The JPL Timing Polynomial Computer Program (TPOLY) computes quadratic polynomials (first derivative continuous at the monthly breakpoints) for the received A.1-UT1 by employing the least-squares fitting techniques (see Ref. 14). In the meantime, TPOLY also generates the required prediction of A.1-UT1 for the mission. The output of TPOLY which is the fitted value of Richmond A.1-UT1 and the predicted values become the JPL adopted A.1-UT1. They are delivered to SPODP and DPODP for orbit determination via punched cards containing polynomials.

During the encounter period of Mariner VI and VII (E-30 to E+6 days), a special arrangement was made to receive the up-to-date data from USNO daily by teletype and/or telephone. This was to eliminate unnecessary error accumulated in the predicted A.1-UT1 to obtain better navigational accuracy during encounter.

Polar Motion

Selection of Data Source. The polar motion is measured independently by two organizations. They are the International Polar Motion Service (IPMS) (see Ref. 15) and the Bureau International de l'Heure (BIH) (see Ref. 13). IPMS utilizes measurements taken from five observatories which are at the same latitude and share the same star catalogue. BIH determines the polar motion by averaging the results from over 25 stations with distinct latitudes and catalogues. According to the data from 1956 to present, they differed by 3 m in worst case and 1.5 m in average.

Recently, as a research effort, the IPMS also computed the polar motion using the results from 26 stations (including the five original stations) from 1962 to 1968. Figure 2-8 shows the variations of the polar coordinates (X, Y) from BIH results, IPMS results and the research results of IPMS 26 stations. It clearly indicates that the BIH results are in better consistency with the IPMS 26 station results than the IPMS (5) results. It is probable, as pointed out by Yumi of IPMS (see Ref. 15) that the polar coordinates from only a few stations (five) are apt to be affected strongly by a local error of a certain station. This implies that the results from BIH, which uses more than 25 stations to compute the polar path, are superior to those of the five IPMS stations.

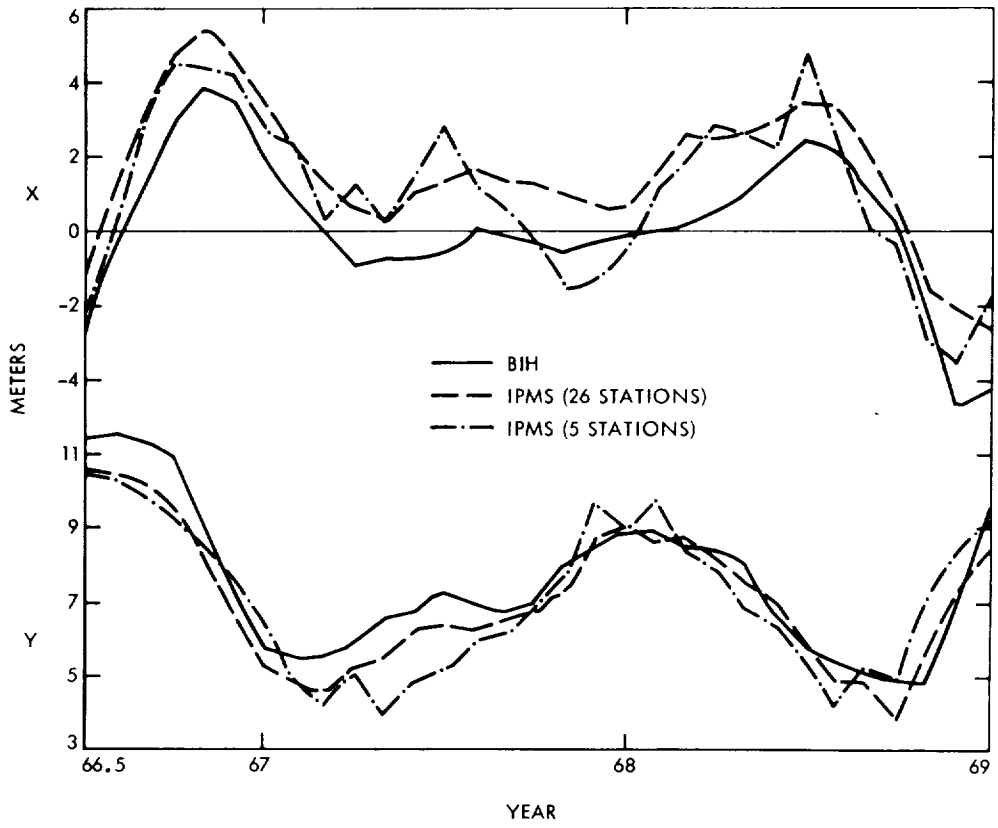

Figure 2-8. Comparison of Polar Motion Coordinates Between BIH and IPMS (5 Stations and 26 Stations)

Therefore, we chose the published results from BIH as JPL adopted polar motion data. Washington and Richmond UT1 is determined from UT0 via the BIH pole for consistency.

Procedure of Processing Data. Together with raw data of A.1-UT1, the BIH polar motion data were received from USNO on the same keypunched cards every month. TPOLY computes linear polynomials for the BIH polar data (X and Y). Although the BIH publishes final, as well as predicted polar motion data, we only use the final data and do our own prediction with the circular arc prediction model (see Ref. 14) in TPOLY. This is done because the BIH data always has a discontinuity between their final and predicted data.

Since the BIH requires one month to prepare their final polar motion, the prediction of polar motion for supplying up-to-date data becomes as important as that of A.1-UT1. An empirical method – the circular arc extrapolation was employed to do the prediction. The JPL predicted polar motion data

are expected to be good to 0.5 m with one month prediction, provided that the pole moves along its regular circular (relatively well-behaved) path. However, within one month prediction, the maximum deviation from final data should not exceed 1 m.

During the encounter period, a special computer run was made at BIH in order to supply us the final (last data on July 7) polar motion data on the 29th of July (E-2 of Mariner VI). This reduced the prediction length at encounter from two months to 25 days.

d. Ionosphere — *B. D. Mulhall*

- Charged Particle Effect on Radio Signals

The charged particles in the ionosphere and the interplanetary space plasma along the ray path of the radio signal transmitted to and received from a spacecraft have various effects upon the signal. Among these effects are absorption, refraction, scintillation, polarization rotation, phase path length decrease, and group path delay. For orbit determination, the two effects of concern are phase path decrease and group path delay.

As the number of charged particles along the ray path changes the phase path changes shifting the S-band carrier frequency. This frequency shift cannot be distinguished from the doppler effect unless the change in the number of charged particles is determined. Similarly, the charged particles delay the energy of the S-band signal increasing the round trip time (the group path length) and thereby corrupt ranging data since these measurements are based on the time required for the energy to propagate from the tracking station to the spacecraft and return.

As discussed in Ref. 7, random errors in the doppler observable can be reduced by taking data over many passes. Systematic errors cannot be reduced by averaging. Systematic errors which vary with a diurnal period are the most corruptive. The earth's ionosphere is caused by ultraviolet light from the sun ionizing the upper atmosphere. Consequently, the density of charged particles in the ionosphere increases and decreases with a diurnal period and corrupts inflight orbit determination solutions. Similarly, when post flight tracking data is used to estimate tracking station locations the ionosphere causes an error in the estimate of station location.

The tracking data from the Mariner IV and V missions have been calibrated for ionospheric effect. The Mariner IV spacecraft flew by the planet Mars in July 1965. The year 1965 was a period of very low solar activity, and consequently, concentrations of charged particles in the Earth's ionosphere were low. The ionospheric calibration from Mariner IV caused a change of about 1 m in the estimate of station location both in distance from the Earth's spin axis (spin radius) and longitude.

Mariner V flew during 1967, a period of much higher solar activity. The ionospheric calibration for this mission resulted in changes of about 6 m in the spin radius and longitude. The day by day ionospheric activity stated in terms of effective station location displacement is shown in Figure 2-9. From this graph it is apparent that errors greater than 10 m occurred on single days.

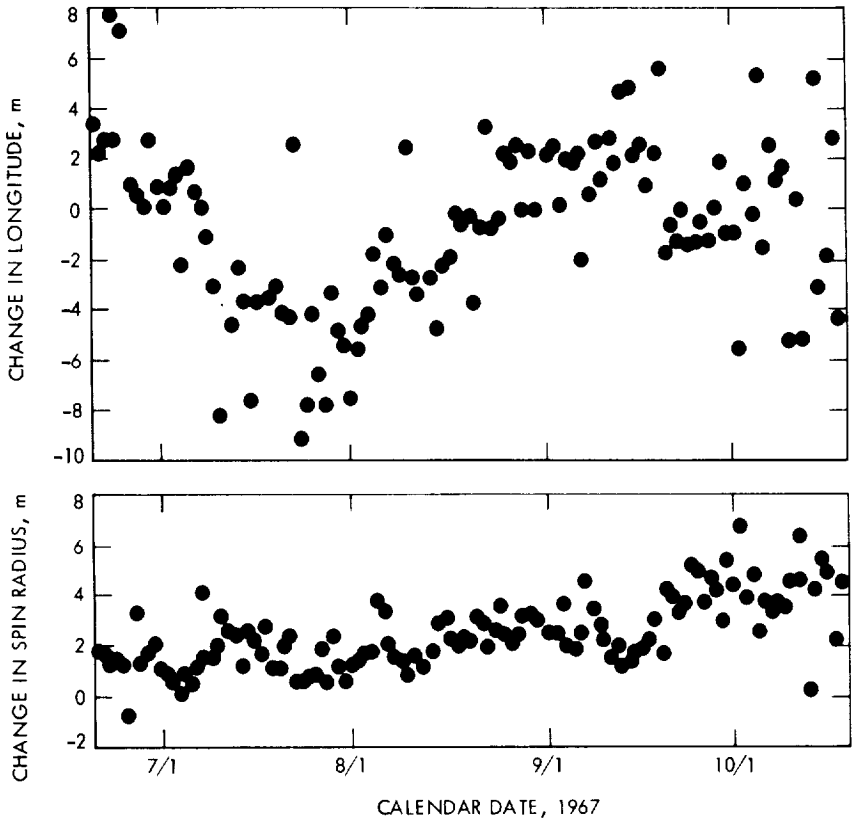

Figure 2-9. Effective Ionosphere Activity Referred to Location Perturbations for Mariner V

It was anticipated that solar activity in 1969 would be as great as in 1967, therefore, the Mariner Mars 1969 navigational accuracy goal of 3 m in spin radius and 3 m in longitude dictated that ionospheric calibration be performed. The 6 to 10 m errors in spin radius and longitude caused by the ionosphere in 1967 could have resulted in orbit estimating errors as high as 250 km at the Mariner Mars 1969 encounter.

Methods for Measuring Charged Particles

There are many techniques for measuring charged particles in the Earth's ionosphere and interplanetary space. Two techniques which were used as part of the ionospheric calibration effort were: Faraday rotation and vertical soundings (ionosonde). These techniques are discussed in the following paragraphs.

Faraday Rotation

The plane of polarization of a radio signal passing through a charged particle medium in the presence of a magnetic field is rotated by the Faraday effect (see Ref. 7). If the radio wave is linearly polarized and the initial polarization is constant with respect to some known frame of reference, then the polarization of the received signal can be used to measure the combined effect of the number of charged particles and the strength of the magnetic field encountered along the ray path. By modeling the tangential component of the Earth's magnetic field along the ray path, the number of charge particles can be computed.

Ionosonde

Before the advent of artificial satellites the only method of measuring the ionosphere was vertical sounding called ionosonde. A radio signal is transmitted vertically, reflected by the ionosphere, and received by the transmitting station. This process is repeated while increasing the transmitted frequency until the signal pierces the ionosphere. The density of electrons required to reflect a particular frequency is determined and by measuring the time of flight for each reflected frequency the altitude dependence of the electron density can be determined. This method measures densities for the lower or bottom side of the ionosphere, that is, up to the layer of maximum density called the F_2 layer. The topside electron content above the F_2 layer, must be estimated by employing a model in this region.

Comparisons of total electron content (E_c) computed from ionosonde data versus E_c measured by Faraday rotation indicate that total content can be estimated with usable accuracy from vertical soundings. As shown by comparing Faraday rotation measurements made by Stanford (mapped to the Point Arguello zenith) to Point Arguello ionosonde data (Figures 2-10 and 2-11) E_c

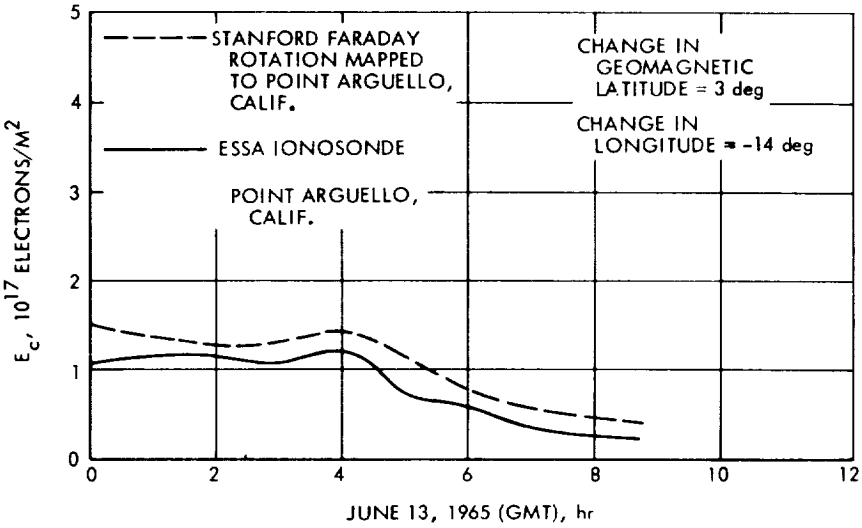

Figure 2-10. Comparison of Ionosphere Measurements, July 13, 1965

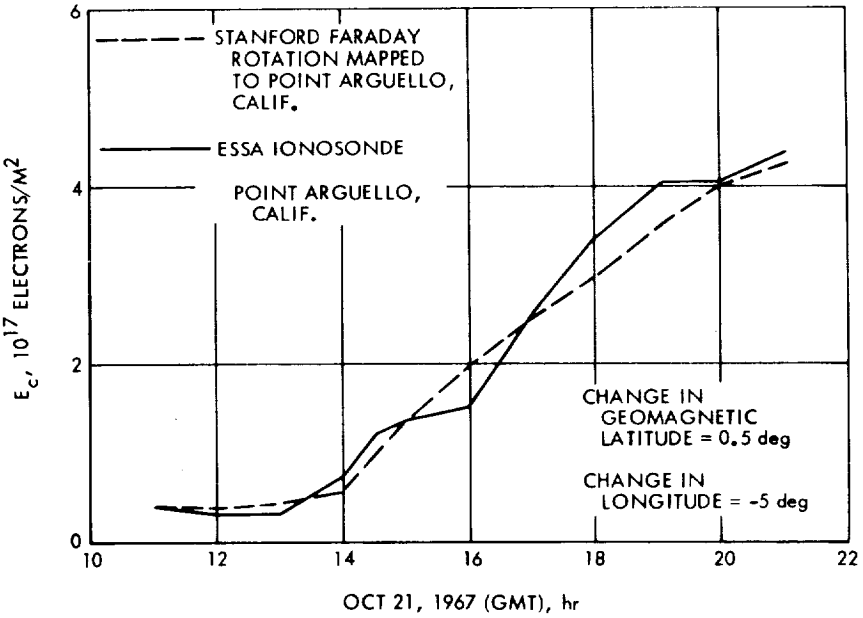

Figure 2-11. Comparison of Ionosphere Measurements, Oct. 2, 1967

computed by the Environmental Sciences Service Administration (ESSA) from ionosonde data is in better agreement with Faraday rotation measurements for quiet ionospheres, such as July 1965 (Figure 2-10) than for active ionospheres, such as October 1967 (Figure 2-11). Note also that the night time estimates are very accurate. The comparison seems poorest during the morning, probably because the sunlight initiates ionization more rapidly above the F_2 layer, the region the ionosonde does not measure.

Delays in obtaining E_c data from ionosonde measurements prevent the use of these data for inflight operations. Instead, E_c for overseas sites was estimated from measurements of the peak frequency reflected by the ionosphere ($F_{of\,2}$). The estimation procedure is described in Ref. 7.

Mapping of Measurements

Ideally, calibration of the spacecraft signal should be computed from measurements made along the signal's ray path. Both the Faraday rotation and ionosonde measurements must be related to the ionosphere actually pierced by the Mariner spacecraft signal. A computer program called ION has been developed to calculate the differences between the ionospheric conditions at the point where a measurement was taken and the points where the spacecraft signal pierced the ionosphere during an entire pass. Adjustments are due to differences in the length of the ray path through the ionosphere, in the local hour angle of the sun, and in the geomagnetic latitude.

Application of the Calibration

As shown in Figure 2-12 three 7094 computer programs were specifically involved with providing ionospheric calibrations to the DPODP. These are:

1) PREION – a preprocessor which reads in ionospheric data in various formats, converts the data to a standard form, and fits the data solving for the parameters of the temporal model of the ionosphere.

2) ION – the program that calculated the actual calibrations to range and doppler.

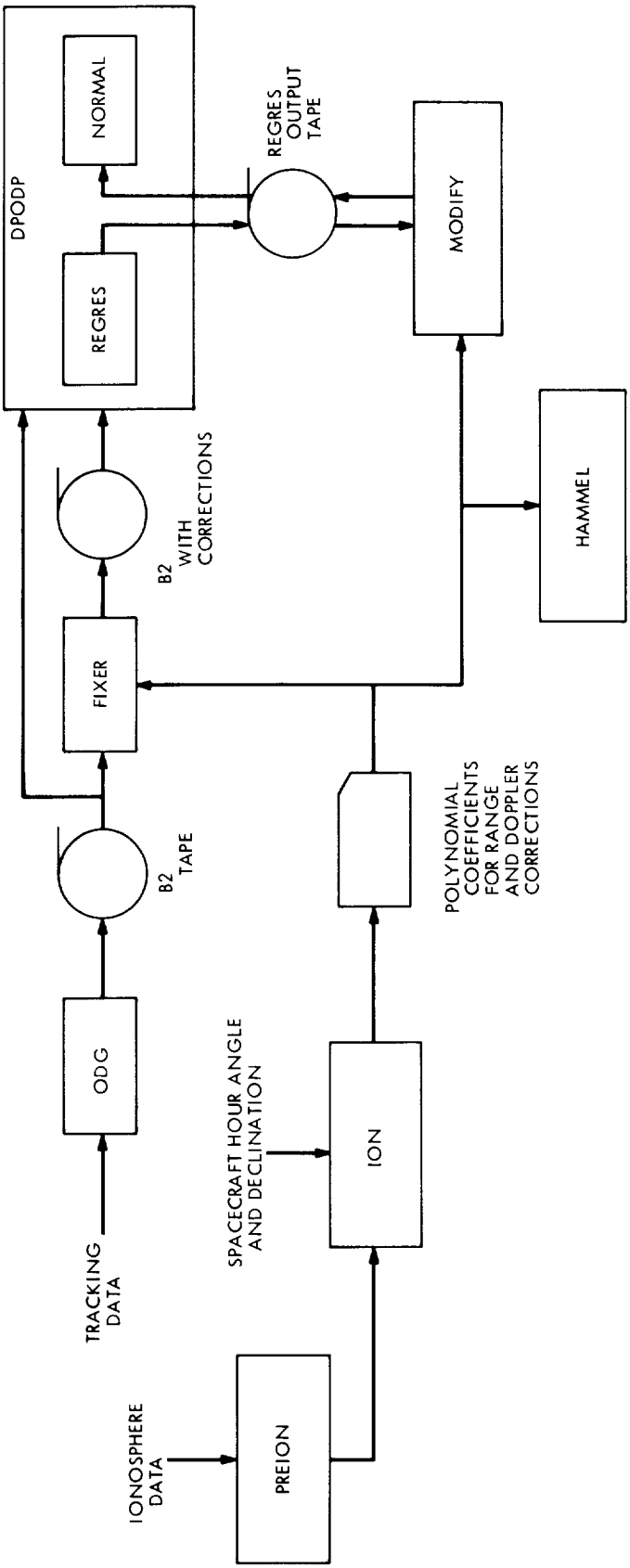

Figure 2-12. Ionospheric Calibration Data Processing

3) HAMMEL – a post-processor which predicts the effect of applying the calibration to assist in analysis of DPODP results and to detect erroneous calibrations.

PREION

Ionospheric measurements were received via teletype and punched on paper tape in the SFOF. These tapes in teletype, Baudot code were read into the PDP-7 computer which used the CONPAT program to write a magnetic tape record of the data. The magnetic tape was transferred to the 7094 computer where it was read in under control of the PREION program.

Data received from Goldstone was the unconditioned output of the receiver-polarimeter. This device measured Faraday rotations from 0 to 180 deg of the signal received from the ATS-1 satellite. This signal, transmitted at 137 MHz, underwent approximately two to five rotations of increase and decrease during the day. Consequently, algorithms had been developed within PREION to resolve the ambiguities in the data and reconstruct the daily variation. PREION was not capable of detecting every retrace and some hand corrections were required to remove the remaining ambiguities.

ION

ION read in the conditioned ionospheric data and information necessary to identify the pass of tracking data to be calibrated. This information consisted of the DSN station, the date of the pass, the rise and set times for the spacecraft, the topocentric hour angle and declination for the spacecraft, the nominal frequency of the S-band signal received from the spacecraft, the time interval for which corrections were to be calculated, and the type of calibration to be produced, doppler or doppler and range.

HAMMEL

HAMMEL is described in detail in Ref. 7. The program fits the doppler polynomial produced by ION with a constant, a sine wave, and a cosine wave. The amplitude of the sine wave determined the apparent change in station spin radius, r_s, while the cosine determined the change in longitude, λ. If the values of r_s and λ were reasonable, the correction could be assumed to be valid.

3. Range Data Validation

a. Non-Gravitational Forces — *V. J. Ondrasik*

During the early portion of the Mariner VI cruise it was noticed that the DPODP, state only, solutions were differing in the geocentric range by approximately 165 km depending upon whether doppler only or doppler plus range data was used. It was proposed that this range discrepancy was a manifestation of an incorrect modeling of the solar pressure forces. This indeed was the case. It was an early oversight not to realize that the high-gain, parabolic antenna which was mounted 41.6 deg off the roll axis, causing a non-negligible component of the solar pressure to be directed in the plane orthogonal to the probe-sun line would have to be modeled. When this additional force was included in the solutions, the apparent discrepancy between the range and doppler data vanished. We present a description and analysis of that situation here as a validation of the Mariner Mars 1969 ranging data in a circumstance which makes that data first appear to be incorrect and as a documentation of the extent that estimation errors can arise from small unmodeled forces. Tables 2-8 and 2-9 contain a summary of state only and state plus solar pressure DPODP solutions using range and range plus doppler data for twelve day and two day data arcs shortly after the midcourse maneuver.

A more thorough understanding of this problem may be obtained by using a simplified analytical model to find the cause of the differences in the solutions of Table 2-8. This model is based on a first order temporal expansion of the topocentric range rate and is given in Eq. (1) (see Ref. 16).

$$\dot{\rho}(t) = a + b \sin \omega t + c \cos \omega t + d\omega t + e\omega t \sin \omega t + f\omega t \cos \omega t \qquad (1)$$

where

$$a = \dot{r}_o$$

$$b = \omega r_s \cos \delta$$

$$c = \omega r_s \cos \delta \Delta\alpha$$

$$d = [a_g + r(\dot{\alpha}^2 \cos^2 \delta + \dot{\delta}^2)]/\omega = \ddot{r}_o$$

$$e = -r_s \sin \delta \dot{\delta}$$

Table 2-8. Results of Various DPODP Solutions With Data Between March 7 and March 19 With Epoch at March 1, 1967 and With *A priori* $\sigma_G = 1$

Data	Doppler only	Doppler plus range	Doppler only	Doppler plus range
Solve for parameters	State	State	State plus solar pressure	State plus solar pressure
$\Delta(G_r)$			-0.1347×10^{-2}	0.9602×10^{-2}
$\sigma(G_r)$			0.2073	1.1233
$\Delta(G_x)$			0.1988×10^{-1}	0.5835×10^{-2}
$\sigma(G_x)$			0.435	0.431
$\Delta(G_y)$			0.4870×10^{-1}	0.7149×10^{-1}
$\sigma(G_y)$			0.5563	0.5447
$\bar{B} \cdot \bar{R}$ (km)	-3.721×10^{2}	-4.765×10^{2}	-3.944×10^{2}	-2.847×10^{2}
$\sigma(\bar{B} \cdot \bar{R})$(km)	7.805×10	6.857×10	2.8904×10^{3}	2.866×10^{3}
$\bar{B} \cdot \bar{T}$ (km)	7.854×10^{3}	6.902×10^{3}	7.698×10^{3}	7.773×10^{3}
$\sigma(\bar{B} \cdot \bar{T})$	3.923×10^{2}	8.783×10	1.617×10^{3}	7.695×10^{2}
r(March 7)$^{(km)}$	2,996,667.48		2,996,500.67	2,996,501.38
x(March 7)$^{(0)}$	93.650528		93.650454	93.650378
r(March 17)$^{(km)}$	5,797,165.77		5,796,999.04	5,796,999.99
x(March 17)$^{(0)}$	102.985151		102.98552	102.98551

Table 2-9. Results of Two DPODP Solutions Using Data Between March 17 and March 19 With Epoch at March 1, 1969 and With *A priori* $\sigma_G = 1$

Data	Doppler only	Doppler plus range
Solve for parameters	State plus solar pressure	State plus solar pressure
$\Delta(G_r)$	-0.1752×10^{-1}	-0.1483×10^{-1}
$\sigma(G_r)$	0.9407	0.9371
$\Delta(G_x)$	0.4231×10^{-1}	0.3842×10^{-1}
$\sigma(G_x)$	0.6905	0.6720
$\Delta(G_y)$	0.4189	0.3871
$\sigma(G_y)$	0.3811	0.3561
r(March 17)	5,796,975.65	5,797,000.00
x(March 17)		102.98550

$f = r_s \dot{\alpha} \cos \delta$

r = geocentric range

α = right ascension

δ = declination

ω = earth angular rate

a_g = gravitational acceleration

r_s = distance of the tracking station off the Earth's spin axis

A Simplified Method of Predicting the Difference in the Geocentric Range

As shown in Ref. 16 for a near Earth spacecraft the range is determined primarily from the gravitational portion of term d, in Eq. (1). Improper

modeling of the solar pressure force produces a fictitious component to the gravitational acceleration given by Eq. (2) (see Ref. 17).

$$\Delta\ddot{r}(S.P.) = \frac{c_1 A_P}{m r_{SP}^2}\left[\Delta G_r(\underline{u}_{SP} \cdot \underline{u}_{EP}) + \Delta G_x(\underline{x}^* \cdot \underline{u}_{EP}) + \Delta G_y(\underline{y}^* \cdot \underline{u}_{EP})\right] \tag{2}$$

where

A_P = projected spacecraft area

r_{SP} = sun-probe distance

$\underline{u}_{EP}$ = unit vector in earth probe direction

$\underline{u}_{SP}$ = unit vector in Sun probe direction

$\underline{x}^*$ and $\underline{y}^*$ = unit vectors which are bisected by the probe-Canopus direction and together with $\underline{u}_{SP}$ form a right-hand orthogonal coordinate system

m = spacecraft mass

c_1 = multiplying constant

Figure 2-13 shows this unmodeled acceleration for values of ΔG_r, ΔG_x, and ΔG_y determined using both doppler and doppler plus range data. Although the two sets of the ΔGs are widely different they produce almost identical accelerations in the Earth-probe direction and may be represented to a first approximation by

$$\Delta\ddot{r} = -0.518 \times 10^{-11}\ \text{km/sec}^2 + 0.50 \times 10^{-18}\ \text{km/sec}^3 t \tag{3}$$

where

t = time in seconds past March 7, 1969

The DPODP will try to absorb this unmodeled solar pressure acceleration in the solar gravitational acceleration primarily by means of a range error Δr. The crucial partial derivative in this development will be the partial

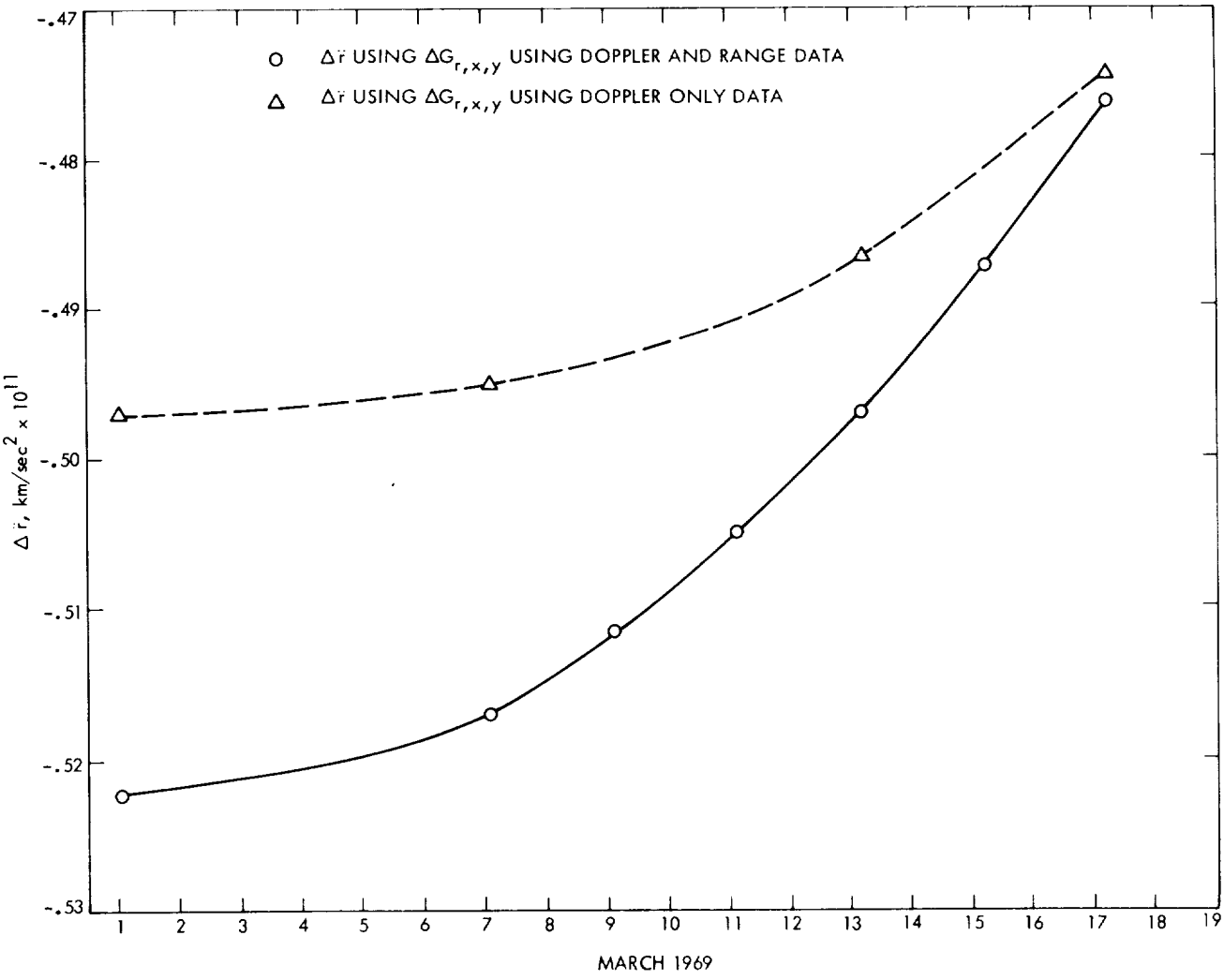

Figure 2-13. Solar Pressure Acceleration Produced by Using $\Delta G_{r,x,y}$, Determined from DPODP Solutions Using Doppler Only and Doppler and Range Data

of the gravitational acceleration w. r. t. the Earth probe range. This quantity may be easily determined in the following manner:

From the figure below, (the pertinent vectors and angles for development of $\partial a_y / \partial r$.)

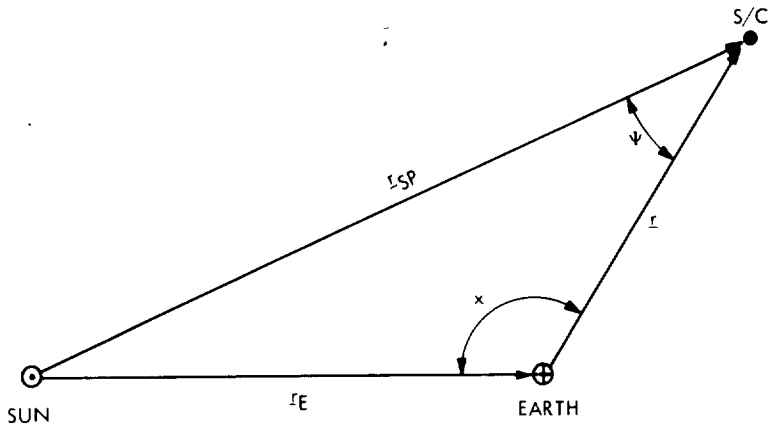

$$a_g = \frac{\underline{r} \cdot \ddot{\underline{r}}}{r} = GM\left[-\frac{\underline{r} \cdot \underline{r}_{SP}}{r r_{SP}^3} + \frac{\underline{r} \cdot \underline{r}_E}{r r_E^3}\right]$$

since

$$\frac{\partial}{\partial r}\frac{\underline{r}}{r} = 0$$

$$\frac{\partial a_g}{\partial r} = -GM\frac{\partial}{\partial r}\left[\frac{\underline{r} \cdot (\underline{r} + \underline{r}_E)}{r r_{SP}^3}\right]$$

$$= -GM\frac{\partial}{\partial r}\left[\frac{(r - r_E \cos x)}{\sqrt[3]{r^2 + r_E^2 - 2rr_E \cos x}}\right]$$

$$= \frac{GM}{r_{SP}^3}\left[3\frac{(r - r_E \cos x)^2}{r^2 + r_E^2 - 2rr_E \cos x} - 1\right]$$

$$= \frac{GM}{r_{SP}^3}\left[2 - 3\frac{r_E^2 \sin^2 x}{r_P^2}\right]$$

$$= \frac{GM}{r_{SP}^3}\left[2 - 3 \sin^2 \psi\right] \tag{5}$$

An approximate value of the range and range rate errors, Δr_o, and $\Delta \dot{r}_o$, caused by the unmodeled solar pressure accelerations may be obtained by ignoring periodic terms in Eq. (1). Thus, the geocentric range rate may be written as

$$\dot{r}(t) = \dot{r}_o + \ddot{r}_o t + \frac{1}{2}\dddot{r}_o t^2$$

An error in the acceleration of amount $\epsilon\ddot{r}$ will produce an error in the geocentric rate, $\epsilon\dot{r}$, of amount

$$\epsilon\dot{r}(t) = \epsilon\ddot{r}(t)t$$

where it is assumed that $\epsilon\dot{r}(0) = 0$. The ODP will try to account for the spurious acceleration by changing r_o and $\dot{r}_o$ to minimize $[\dot{r}(t) - \epsilon\dot{r}(t)]^2$ in a least squares sense. Thus since

$$\frac{\partial \dot{r}}{\partial \dot{r}_o} = 1$$

and

$$\frac{\partial \dot{r}}{\partial r_o} = \frac{\partial \ddot{r}}{\partial r_o} t + \frac{1}{2} \frac{\partial \dddot{r}}{\partial r_o} t^2$$

the usual least squares formulation gives

$$\begin{bmatrix} \Delta r_o \\ \Delta \dot{r}_o \end{bmatrix} = \begin{bmatrix} \int_{T_1}^{T_2} \left(\frac{\partial \ddot{r}}{\partial r_o} t + \frac{1}{2} \frac{\partial \dddot{r}}{\partial r_o} t^2 \right)^2 dt & \int_{T_1}^{T_2} \left(\frac{\partial \ddot{r}}{\partial r_o} t + \frac{1}{2} \frac{\partial \dddot{r}}{\partial r_o} t^2 \right) dt \\ \int_{T_1}^{T_2} \left(\frac{\partial \ddot{r}}{\partial r_o} t + \frac{1}{2} \frac{\partial \dddot{r}}{\partial r_o} t^2 \right) dt & \int_{T_1}^{T_2} dt \end{bmatrix}^{-1} \begin{bmatrix} \int_{T_1}^{T_2} \epsilon \dot{r}(t) \left(\frac{\partial \ddot{r}}{\partial r_o} t + \frac{1}{2} \frac{\partial \dddot{r}}{\partial r_o} t^2 \right) dt \\ \int_{T_1}^{T_2} \epsilon \dot{r}(t) \, dt \end{bmatrix} \tag{6}$$

where it has been assumed that the data is continuous between times T_1 and T_2 and is uniformly weighted. An examination of Figures 2-13 and 2-14 yield the numerical values of the quantities in the above equations, and they are

$$\epsilon \dot{r}(t) = -\left[0.518 \times 10^{-11} - 0.25 \times 10^{-18} t(\text{sec}) \right] \frac{\text{km}}{\text{sec}^2} t(\text{sec})$$

$$\frac{\partial \ddot{r}}{\partial r_o} = 0.395 \times 10^{-13} \frac{1}{\text{sec}^2}$$

$$\frac{\partial \dddot{r}}{\partial r_o} = 0.75 \times 10^{-20} \frac{1}{\text{sec}^3}$$

where it has been assumed that

$$\frac{d}{dt} \left(\frac{\partial \ddot{r}}{\partial r_o} \right) = \frac{\partial \dddot{r}}{\partial r_o}$$

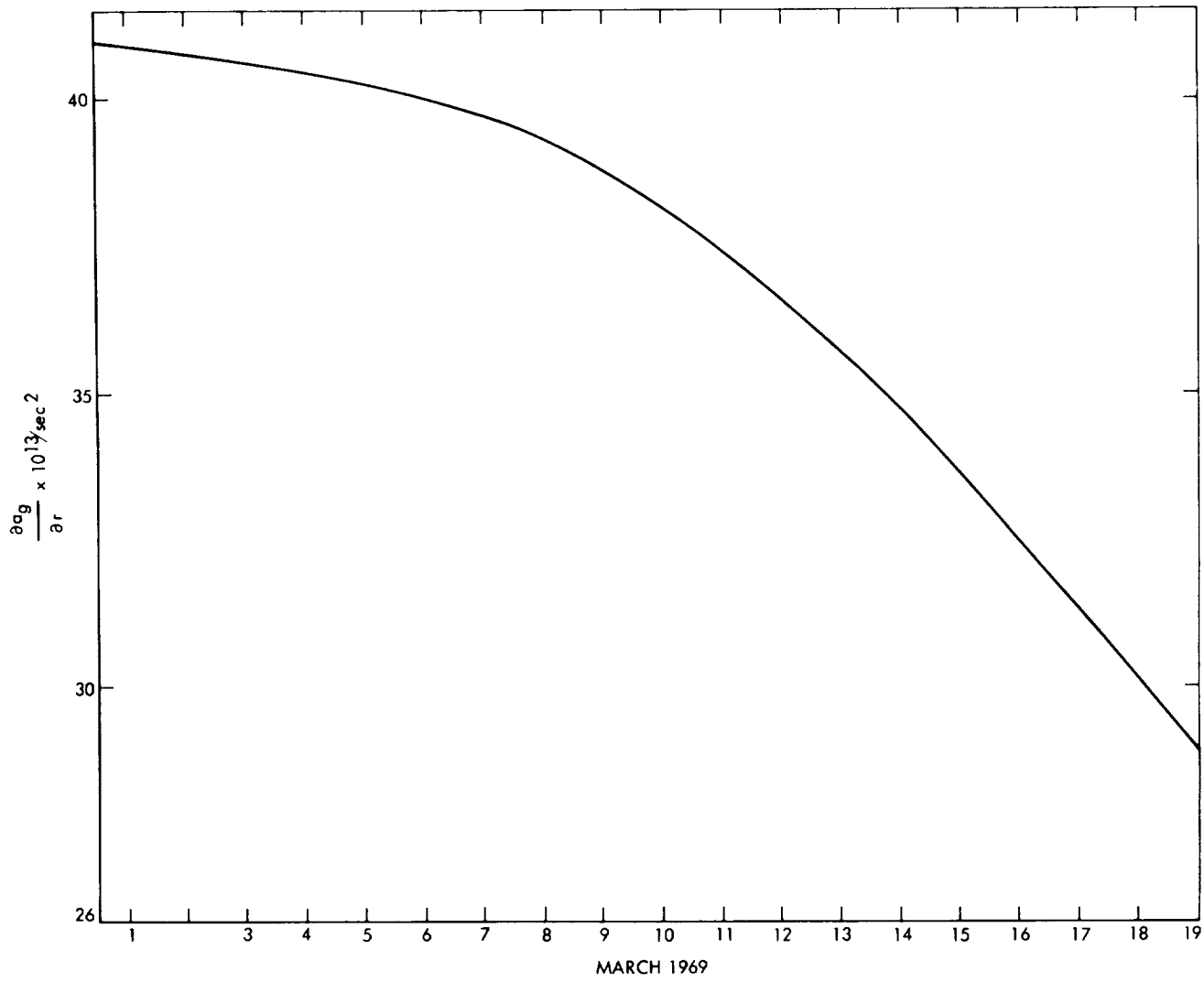

Figure 2-14. Partial of the Gravitational Acceleration w. r. t. Range.

Thus, Eq. (6) may be evaluated to give

$$\begin{bmatrix} \Delta r_o \\ \\ \Delta \dot{r}_o \end{bmatrix} = \begin{bmatrix} -141 \text{ km} \\ \\ 0.0 \times 10^{-5} \text{ km/sec} \end{bmatrix} \tag{7}$$

This result should be compared to the difference in the range values from the DPODP state only doppler solution and the state plus solar pressure doppler plus range solutions of -165 km and 1.1×10^{-6} km/sec. The discrepancy between the DPODP range change of 165 km and that given by Eq. (7) is probably due to the fact that part of the effect of the unmodeled solar pressure acceleration may be absorbed into other parameters than the range. For example, the change in the cross velocities between the two solutions mentioned immediately above may account for approximately 5 percent of this unmodeled acceleration. The discrepancy between the DPODP range rate change of 1.1×10^{-6} km/sec and 0.0×10^{-5} km/sec of Eq. (7) is insignificant because both are so small.

Reason Why Doppler Only Solutions Give Good Range Results

Deleting all the periodic terms in Eq. (1) allows the geocentric range rate of the spacecraft to be written as

$$\dot{r}(t) = \dot{r}_o + \ddot{r}_o t$$

For the spacecraft well into heliocentric space, this may be represented very well by

$$\dot{r}(t) = \dot{r}_o + a_g t \tag{8}$$

Clearly the $\dot{r}_o$ is determined early in the data arc while the range, which is obtained from a_g, will be obtained when the second term becomes comparable to the first. Hence a perturbation in the range, ϵ_r, will be approximately related to a perturbation in the range rate, $\epsilon_{\dot{r}}$, by the following equation

$$\epsilon_{\dot{r}}(t) = \frac{\partial a_g}{\partial r} \epsilon_r t \qquad \frac{\partial a_g}{\partial r} \approx 0.4 \times 10^{-13} \text{ sec}^2 \tag{9}$$

To keep the error in the doppler due to the range error below a typical residual value of 0.2×10^{-2} Hz requires ϵ_r to be less than 20 km for a data arc of 2 days and less than 3 km for a data arc of 12 days. Tables 2-8 and 2-9 show that the difference in the range between the state plus solar pressure solutions using either doppler only or doppler plus range are 24 km and 1 km for data arcs of 2 and 12 days respectively. These results agree fairly well with the numbers predicted by Eq. (9).

b. Effect of Station Location Distance From Equator on Radio Tracking — *N. A. Mottinger*

As discussed in Subsection II.A.2.B., the sensitivity of doppler tracking from deep space probes to the Z component of station locations is nearly negligible. However, when range data, ρ, is one of the data types included in the reduction and the probe declination becomes fairly large in absolute value, the computed range is sensitive to incorrect Z values. A simple equation relating the two is $\Delta\rho = \Delta Z \sin \delta$, where δ = geocentric declination of the spacecraft. The consequences of an error in the Z value had not been considered in the reduction of either the Mariner VI or VII range data. Problems had been encountered when fitting the doppler and range data from Mariner VI but appeared to have been resolved by including the accelerations produced by solar radiation striking the high gain antenna. Using the models available for this acceleration produced agreement between the doppler only and doppler and range solutions on the order of 1 km, as discussed in Section II.A.3.a. It was assumed that this had eliminated most of the significant problems outside of charged particle affects when the two data types were used. However, including the transverse solar acceleration for Mariner VII did not eliminate the conflict. In this case, range data was available from four stations whereas for Mariner VI it had only been available from one. When range data from only one station was used to complement the doppler, a stable solution could be obtained, but when range data from more than one station was used, conflicts arose.

Changes as large as 1400 km occurred in the B-plane when the range and doppler data were forced into the reduction. Examples of the incompatibility of the two data types is shown in Figure 2-15a where typical doppler and

range residuals are shown when data from the 8th of April to the 5th of May were fit. As is shown even the range data has not been successfully fit. Ranging from DSS 14 was weighted by 6 m and that from other stations by approximately 18 m. In light of the known range error induced from charged particle effects, up to 15 m, the choice of weights was thought to be a possible explanation. The reduction was repeated but omitting the DSS 14 range data. Typical residual plots are shown in Figure 2-15b. Although the fit has been improved, signatures on the doppler residuals still indicate that the problem is far from solved. It should be noted that the value for $\bar{B} \cdot \bar{R}$ obtained in this second case is more in line with solutions obtained fitting only the doppler data.

The suggestion was made that erroneous Z values for station locations might be causing these problems. K. Lambeck at the Smithsonian Astrophysical Observatory (SAO) was contacted for solutions obtained from the computation of the SAO Standard Earth 1969. He supplied estimates with associated uncertainties of 15 m and which differed from the values currently being used by as much as 56 m. A table of the differences shown in Section II.A. 2. a. is repeated here in Table 2-10. Also included is the range change computed from the equation given earlier. Due to the greater magnitude of declination for Mariner VI, -40 deg vs -30 deg for Mariner VII, the range corrections were larger. Another candidate for the range error is the charged particles in the Earth's ionosphere and generally in the interplanetary medium (space plasma). The former could account for as much as 15 m, as mentioned above, and the latter has been noted to account for as much as 25 m. Range residuals observed before the fit show variations on the order of 30 m which are easily attributed to charged particles, but they could also be caused by the new Z values.

An attempt to explain the erratic behavior of the doppler data under the influence of the range may be made in terms of the information on range rate implied by the range data. The doppler data may be thought of as a measurement of the change in range over a specified interval. Similar information is implied when more than one range point is taken. If the situation is such that range is being taken from more than one station, erroneous information on range rate is implied from the range data if the observables are not computed correctly. As an example, if range from DSS 41 and DSS 62 on April 9, 1969 is

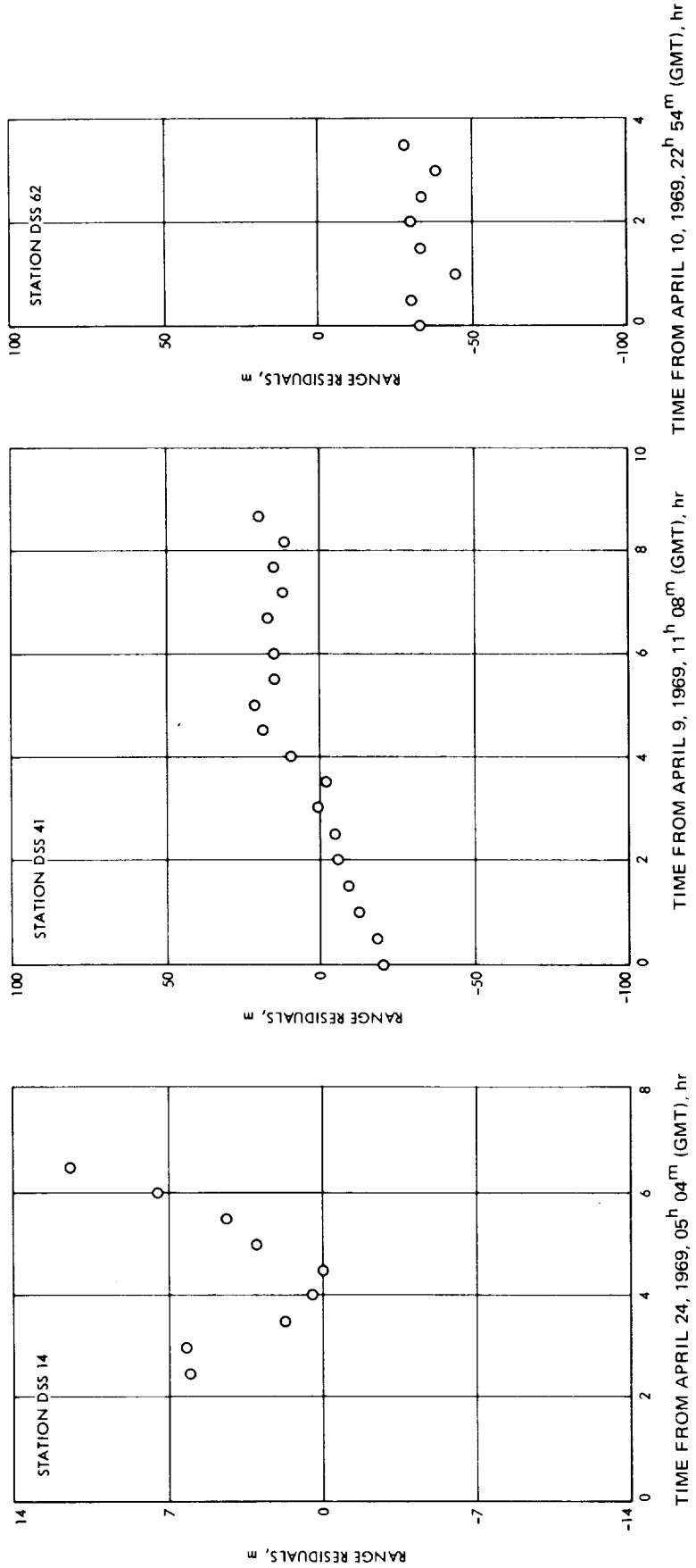

Figure 2-15a. Range Residuals After the Fit Including Range Data From DSSs 14, 41 and 62

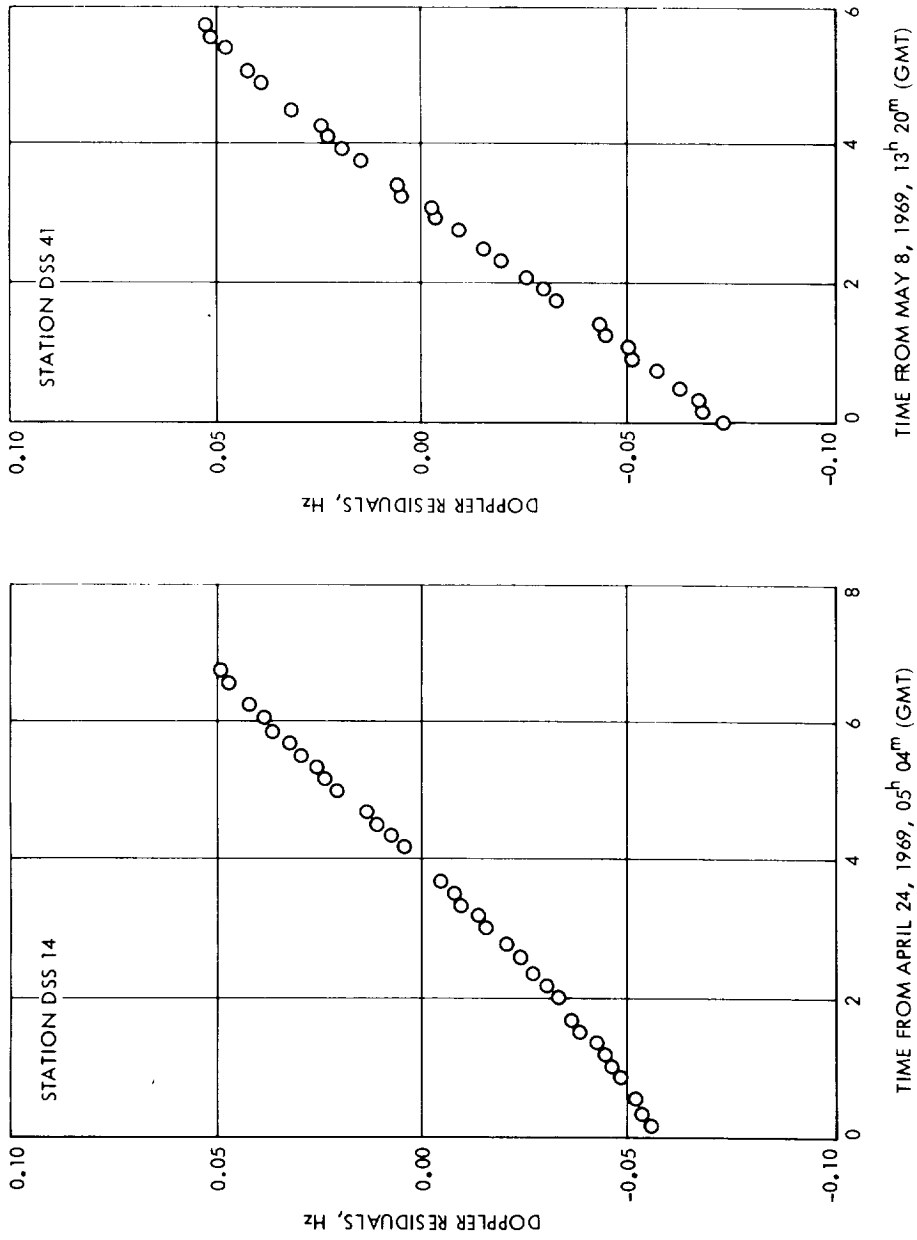

Figure 2-15a. Range Residuals After the Fit Including Range Data From DSSs 14, 41 and 62 (cont'd)

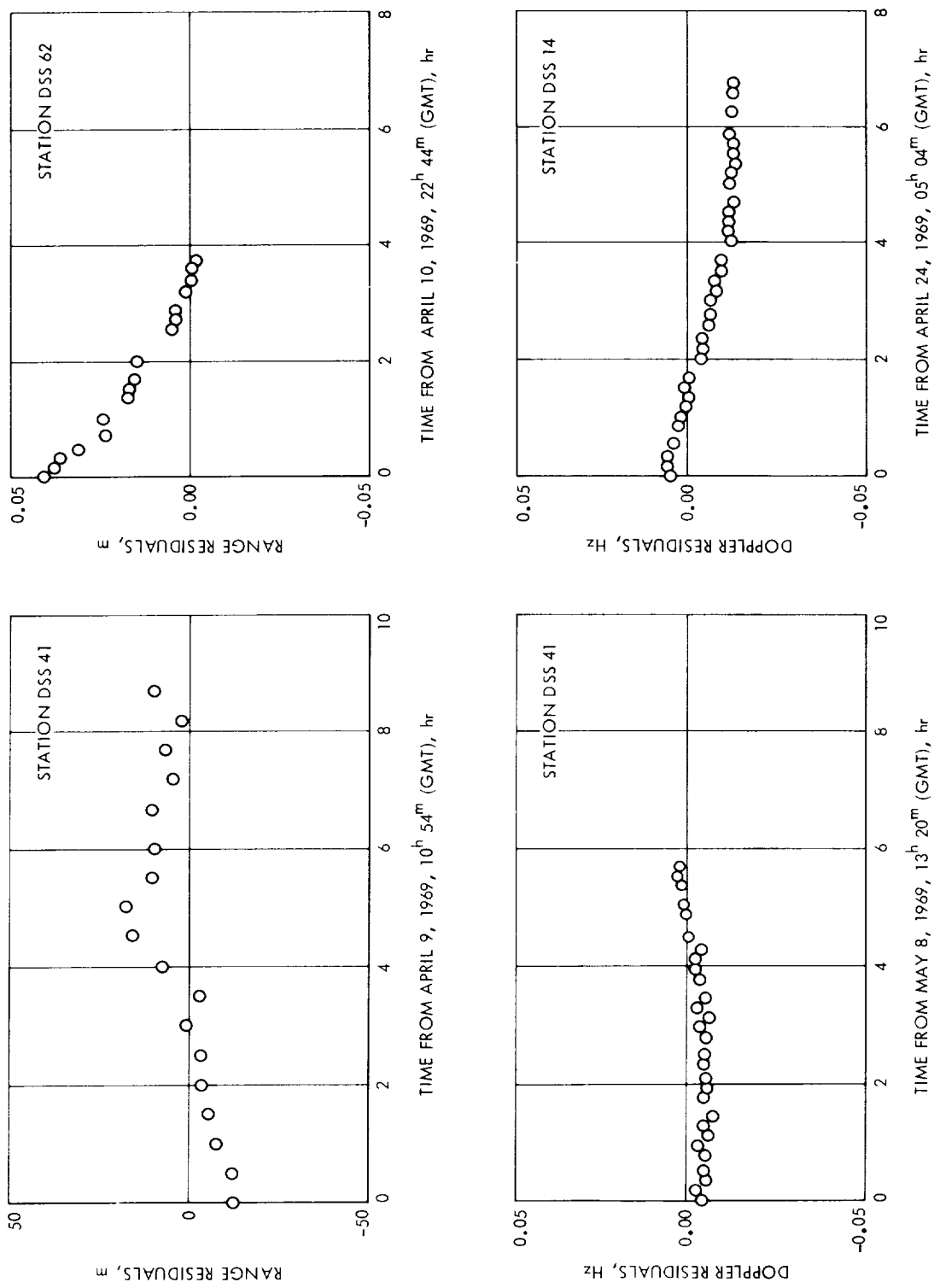

Figure 2-15b. Doppler Residuals After the Fit Including Range Data from DSSs 41 and 62

Table 2-10. Effects of Z* on Range Measurements

DSS	ΔZ, m	Δρ = ΔZ sin δ, m	
		Mariner VI	Mariner VII
11, 12, 14	-4	2.5	2
41	-5	3	3
42	-18	12	9
61	56	-36	-28
62	-42	27	21

*Distance of tracking station from Earth equatorial plane

used the error in computed range is approximately 18 m (obtained from Table 2-10 for Mariner VII). Range points were observed to be taken 2 hr apart during the interval in question. Dividing 8 m by 2 hr to give meters per sec which is then converted to hertz gives a value of 0.035 Hz. This is nearly the size of the residual noted for the two way doppler pass beginning on the 9th. Adding the DSS 14 range data, as noted earlier, totally disrupted the fit. Although the range error is approximately the same as for the DSSs 41 and 62, the increased weight used on the data would cause greater conflict between the doppler and the range change implied by the range itself.

B. FLIGHT OPERATIONS

1. Introduction — *S. K. Wong*

Mariner VI and VII were launched from Cape Kennedy on 25 February 1969 and 27 March 1969, respectively. Both spacecrafts fulfilled the mission objectives even though some nonstandard events were encountered by the two spacecrafts.

Mariner in-flight flight path analysis was the responsibility of the Mariner Flight Path Analysis and Command (FPAC) Team which was staffed by

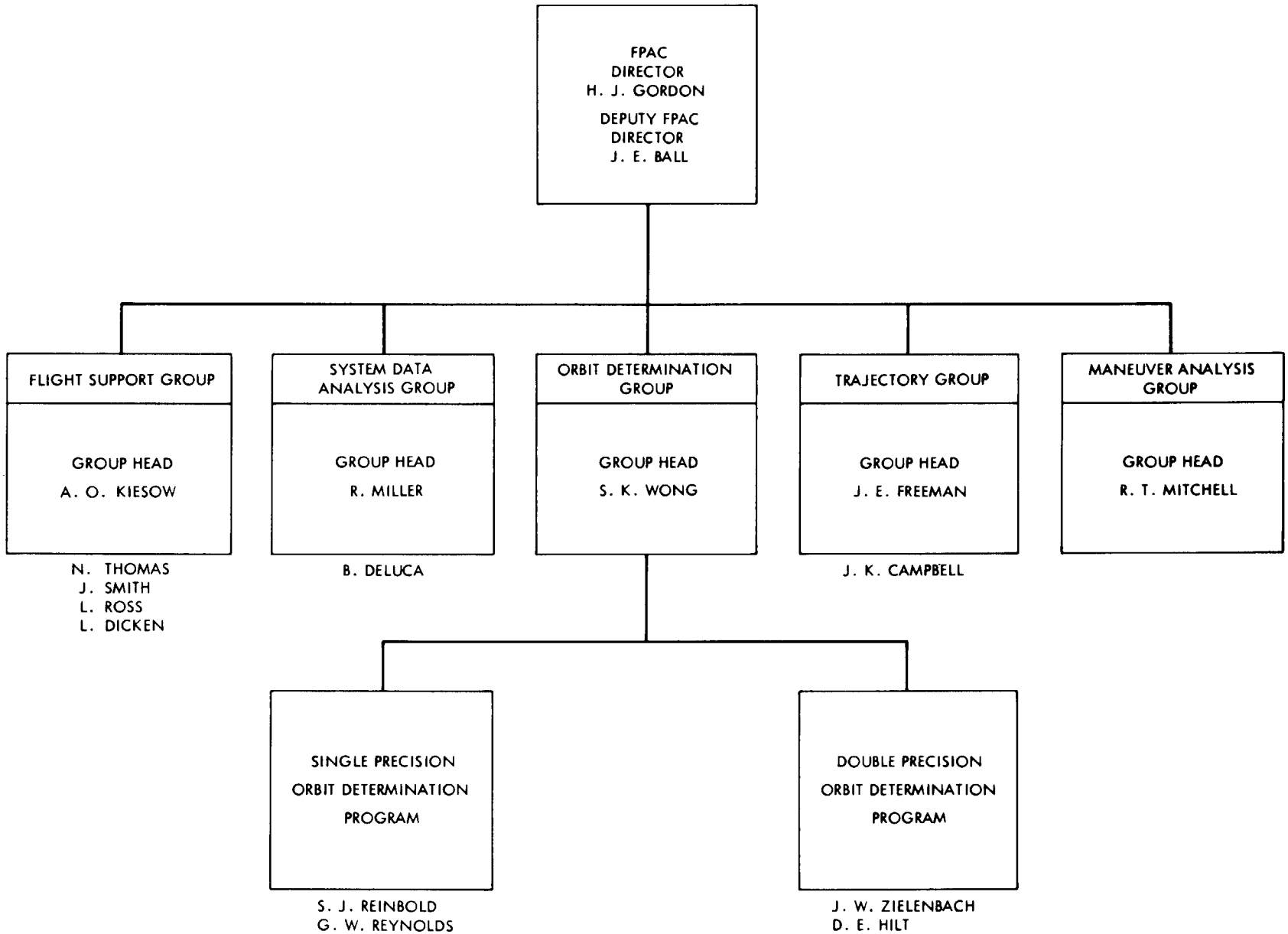

Figure 2-16. FPAC Organization

Jet Propulsion Laboratory personnel. The FPAC organization and participants for the mission are shown in Figure 2-16. The FPAC Team consisted of the following functional groups: System Data Analysis (SDA); Orbit Determination (OD); Maneuver Analysis (MA); Trajectory (TRAJ); and Flight Support (FS). The FPAC activities for Mariner VI and VII are described in Section II. B. 5 and Section II. B. 6, respectively.

The purpose of the preceding Section of this document is to give insight into the overall performance of orbit determination functions. For the sake of convenience, the mission has been separated into three distinct phases: pre-midcourse, cruise and encounter. The pre-midcourse maneuver phases of Mariner VI and VII are examined in Subsections II. B. 5. a and II. B. 6. a, respectively, which describe the orbit analysis during the interval from launch to midcourse maneuver. These results define how the entire trajectory would have appeared had there been no midcourse maneuver, such information being necessary to the planning of the maneuver.

The Mariner VI and VII cruise phase least squares orbit solutions are given in Subsections II. B. 5. b and II. B. 6. b, respectively. These Subsections discuss the cruise orbit solutions numerically integrated to Mars encounter.

The Mariner VI and VII encounter phase aiming point estimates are described in Subsections II. B. 5. c and II. B. 6. c. These results are numerically based on Radio Tracking Data obtained five days prior to Mars encounter and up to 3 hr before Mars encounter.

2. Locations of DSIF Tracking Stations and Physical Constants — *S. K. Wong, S. J. Reinbold*

The primary tracking support was provided by DSS 12 (Goldstone-Echo, California), DSS 14 (Goldstone-Mars, California), DSS 41 (Woomera, Australia), DSS 51 (Johannesburg, South Africa), DSS 62 (Cebreros, Spain). Tracking data was also provided by DSS 11 (Goldstone Pioneer, California), DSS 42 (Canberra, Australia) and MSFN 75 (Ascension Island).

There were four updates on the locations of the tracking stations used in the SPODP (Ref. 18) because of the correction for polar motion, which is time dependent.* The four updates were implemented on the following dates:

*The DPODP takes polar motion into account, the SPODP needs an average position for the data it is processing.

1st update: 17 May 1969

2nd update: 26 June 1969

3rd update: 23 July 1969

4th update: 23 July 1969

The 3rd and 4th updates were implemented on the same date. The 3rd update was for orbit computation using a short data arc (E - 5^d to closest approach). The 4th update was for orbit computation using a long data arc (platform unlatch to closest approach). The locations of the tracking stations used for orbit computation at the launch of Mariner VI and VII and at the four updates are given in Tables 2-11, 12, 13, 14 and 15. The set of station locations used for Mariner VI and VII launch were computed for polar motion between the two launch dates. The sets of station locations for updates 1, 2, 3 and 4 have polar motion corrected to 9 May 1969, 15 June 1969, 29 July 1969 and 25 June 1969, respectively. The set of physical constants used for inflight orbit computations is given in Table 2-16.

Table 2-11. Station Locations for Mariner VI and VII Launch

	Radius (km)	Latitude (Deg)	Longitude (Deg)	r_s (km)	Z (km)
DSS 11	6372.0061	35.208118	243.150710	5206.3319	3673.7679
DSS 12	6371.9904	35.118741	243.194640	5212.0435	3665.6329
DSS 14	6371.9891	35.244429	243.110600	5203.9887	3677.0569
DSS 41	6372.5534	-31.211440	136.887680	5450.1952	-3302.2430
DSS 42	6371.7003	-35.219559	143.981480	5205.3483	-3674.6311
DSS 51	6375.5290	-25.739504	27.685511	5742.9351	-2768.7663
DSS 61	6369.9899	40.238507	355.751200	4862.6086	4114.8279
DSS 62	6369.9924	40.263484	355.632400	4860.8163	4116.9489
DSS 72	6378.2386	-7.899908	345.673636	6317.7071	-876.6439

Table 2-12. Station Location for 1st Update

	Radius (km)	Latitude (Deg)	Longitude (Deg)	r_s (km)
DSS 11	6372.0061	35.208104	243.15068	5206.3319
DSS 12	6371.9904	35.118727	243.19461	5212.0435
DSS 14	6371.9891	35.244415	243.11057	5203.9887
DSS 41	6372.5534	-31.211472	136.88767	5450.1952
DSS 42	6371.7003	-35.219595	148.98147	5205.3483
DSS 51	6375.5290	-25.739471	27.68550	5742.9351
DSS 61	6369.9899	40.238546	355.75120	4862.6086
DSS 62	6369.9924	40.263524	355.63240	4860.8183
DSS 72	6378.2386	-7.899869	345.67363	6317.6439

Table 2-13. Station Location for 2nd Update

	Radius (km)	Latitude (Deg)	Longitude (Deg)	r_s (km)	Z (km)
DSS 11	6372.0065	35.208090	243.150580	5206.3339	3673.7656
DSS 12	6371.9907	35.118713	243.194510	5212.0456	3665.6305
DSS 14	6371.9895	35.244401	243.110470	5203.9908	3677.0545
DSS 41	6372.5535	-31.211468	136.887570	5450.1936	-3302.2457
DSS 42	6371.7002	-35.219594	148.981350	5205.3459	-3674.6342
DSS 51	6375.5316	-25.739451	27.685394	5742.9399	-2768.7621
DSS 61	6369.9869	40.238574	355.751090	4862.6016	4114.8316
DSS 62	6369.9922	40.263529	355.632290	4860.8128	4116.9525

Table 2-14. Station Location for 3rd Update

	Radius (km)	Latitude (Deg)	Longitude (Deg)	r_s (km)	Z (km)
DSS 11	6372.0084	35.208100	243.150590	5206.3348	3673.7676
DSS 12	6371.9927	35.118724	243.194520	5212.0464	3665.6327
DSS 14	6371.9915	35.244410	243.110470	5203.9918	3677.0565
DSS 41	6372.5561	-31.211504	136.887560	5450.1938	-3302.2505
DSS 42	6371.7103	-35.219730	148.981330	5205.3455	-3674.6524
DSS 51	6375.5247	-25.739303	27.685400	5742.9409	-2768.7443
DSS 61	6370.0235	40.238966	366.751080	4862.6013	4114.8885
DSS 62	6369.9643	40.263259	355.632270	4860.8110	4116.9116

Table 2-15. Station Locations for 4th Update

	Radius (km)	Latitude (Deg)	Longitude (Deg)	r_s (km)	Z (km)
DSS 11	6372.0084	35.208117	243.150590	5206.3338	3673.7691
DSS 12	6371.9927	35.118740	243.194520	5212.0454	3665.6341
DSS 14	6371.9915	35.244427	243.110470	5203.9908	3677.0580
DSS 41	6372.5561	-31.211508	136.887570	5450.1936	-3302.2509
DSS 42	6371.7103	-25.219730	148.981340	5205.3455	-2674.6525
DSS 51	6375.5247	-25.739316	27.685396	5742.9402	-2768.7456
DSS 61	6370.0235	40.239859	355.751090	4862.6018	4114.8879
DSS 62	6369.9643	40.263252	355.632280	4860.8115	4116.9110

Table 2-16. Nominal Physical Constants Used for MM'69 Mission

Constant	Value	SPODP Symbolic Designation	Space Symbolic Designation
Gravitational Coefficients km^3/sec^2			
Sun	$0.132712499 \times 10^{12}$		GMS
Earth	398601.2	KE	GME
Moon	4902.78	KM	GMM
Mercury	22181.598		GMR
Venus	324860.10		GMV
Mars	42828.444		GMA
Saturn	37926525.7		GMC
Jupiter	126707718.8		GMJ
Uranus	5787723.46		GMU
Neptune	6890576.3		GMN
Pluto	73240.893		GMP
Mars/Sun Mass Ratio	0.3227368×10^{-6}	MM	
Earth's Radius to Convert Lunar Ephemeris to km, km	6378.1492	RE	REM
Radius of Earth, km	6378.160		RE
Radius of Mars, km	3393.4	RSTOP	RA
Coefficient of Second Harmonic in Earth's Oblateness	0.00162405	J	J
Coefficient of Third Harmonic in Earth's Oblateness	-0.64×10^{-5}	H	H
Coefficient of Fourth Harmonic in Earth's Oblateness	0.69125×10^{-5}	D	D
Coefficient of Second Harmonic in Mars Oblateness	0.00197		J(2.0)
Astronomical Unit, km	149597893.0	AU	AU

Table 2-16. Nominal Physical Constants Used for MM'69 Mission (cont'd)

Constant	Value	SPODP Symbolic Designation	Space Symbolic Designation
Velocity of Light, km/sec	299792.5	C	
Area of MM'69 Spacecraft, meter^2	8.99079	ARMARS	ARA
Mass of MM'69 Spacecraft, kg	384.07915	MSMARS	MAS
Gamma B of MM'69 Spacecraft	0.34423	GBMARS	GB
Solar Radiation Pressure Constant km^3kg/sec^2m^2	1.0088×10^8	RADOPT	SC
Ephemeris Time – Universal Time, sec	39.5	DUT	DUT
Index of Refraction			
DSS 11, Pioneer	240	INDEX(2)	
DSS 12, Echo	240	INDEX(12)	
DSS 13, Venus	240	INDEX(15)	
DSS 14, Mars	240	INDEX(14)	
DSS 41, Woomera	340	INDEX(4)	
DSS 42, Canberra	310	INDEX(3)	
DSS 51, Johannesburg	240	INDEX(5)	
DSS 61, Madrid	300	INDEX(13)	
DSS 62, Madrid	300	INDEX(11)	
DSS 72, Ascension Is.	340	INDEX(1)	

3. Tracking Data — *S. K. Wong, S. J. Reinbold*

a. Data Types

The data types used in the computation of the orbit of the spacecraft are as follows:

1) Hour angle and declination (HA, DEC)
This data type is the pointing angle of the tracking antenna expressed in degrees; it is only used in the very early orbits.

2) S-band, phase coherent counted doppler (CC3) this is a measure of topocentric radial velocity of the spacecraft, and it is the prime orbit data type. Units: 1 m/s≈15.3 Hz (Figure 2-17).

3) Mark IA range unit (RU) this data type is defined as follows:

$$\rho_{DSIF} = \left[\frac{15(\Delta t + \epsilon)}{221}\ 96fq\right] \bmod 785762208$$

where
- ρ = measured round-trip interval, in RU
- t = round trip light time in UTC sec
- fq = transmitter reference frequency $\simeq 22MH_z$
- ϵ = time delay in seconds from station equipment, space transponder and intervening space plasma-ionospheric medium
- 785762208 RU = code length of system

The Mark 1A ranging system is limited to an effective one-way range of approx. 10,000,000 km.

4) The planetary ranging system at DSS 14 (Goldstone-Mars) measures the round trip delay directly in nanoseconds. The code length of the equipment is $\frac{1.00947}{1.0002}$ s, hence

$$\rho_{planetary} = 10^9(\Delta t + \epsilon) \bmod \frac{1.00947 \times 10^9}{1.0002}$$

Δt and ϵ is defined the same as for the Mark 1A range unit equation.

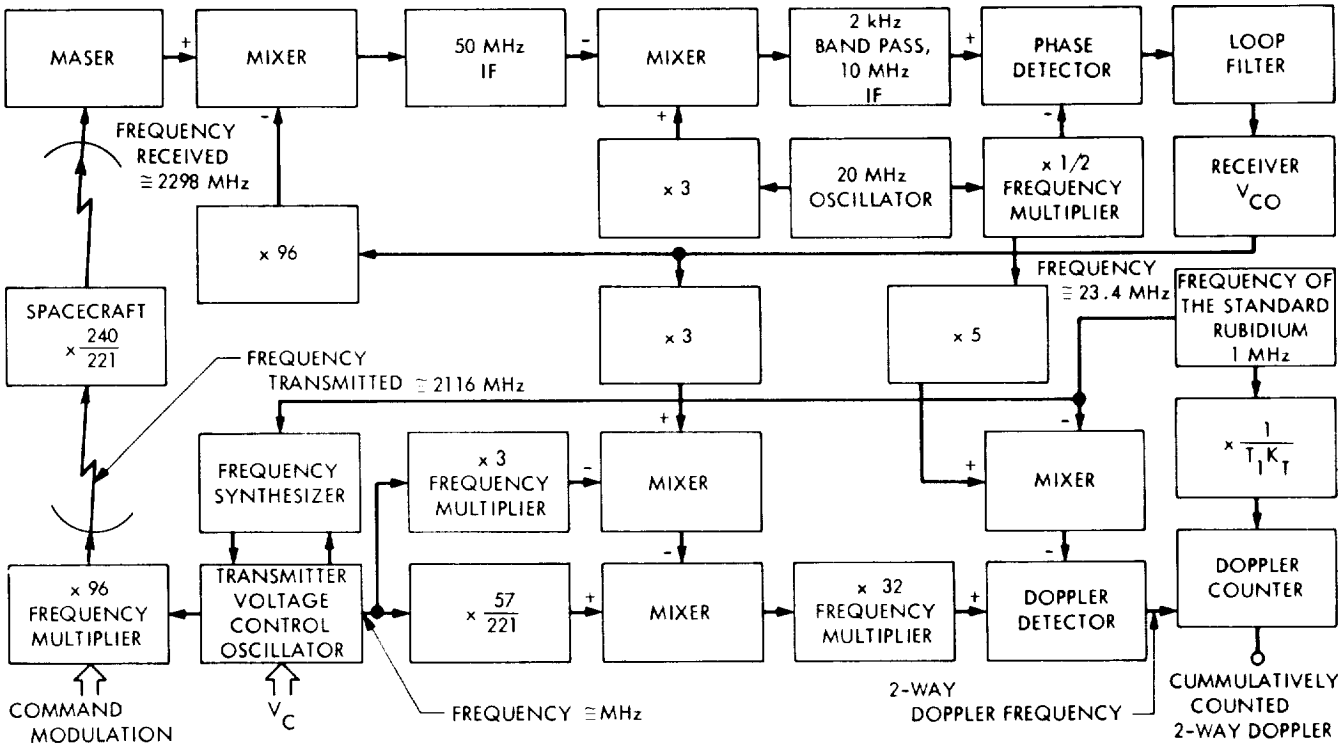

Figure 2-17. S-Band Two-Way Configuration

b. Compressed Data

Compressed data is averaged over some time interval greater than the actual count time (600 sec intervals were used for compression). This smoothing process is reflected in improved statistics for individual points.

For this mission, all tracking stations utilized a digital resolver for incrementing the sample time to the exact time of zero phase delay (±10) ns between transmitter and receiver. This has the advantage of eliminating counter truncation error.

4. Pre-Flight Encounter OD Strategy Plans — *J. W. Zielenbach*

The encounter orbit determination activities for the two Mariner '69 spacecraft were directed toward delivering an encounter time accurate to ±5 sec, at the time that the science system was turned on, and a position in the B plane with a circular uncertainty of 300 km by 3 hr before closest approach. By considering the effects of the various possible errors in the model being used, a plan of action was established for each of the two requirements. The plans were elaborated to allow information from the first spacecraft to influence the orbit determination of the second. The plans will be described first, followed by an indication of how they were implemented in practice.

- Strategy for Determining Encounter Time

Because the experimenters wanted their first TV picture to include the limb of Mars, and because the camera was to take exposures every 42.24 sec, it was necessary to determine the time of closest approach (and from that the time of limb passage) to within ±5 sec. Moreover, since the camera shuttering sequence, once started, could not be adjusted, and since this sequence included the far-encounter series of pictures, the time of encounter had to be delivered before the first TV pictures were taken, or 61 hr, prior to Mariner VI encounter, 78 hr prior to Mariner VII encounter.

The spacecraft's velocity relative to Mars was sufficiently high that the probe would be too far from the planet to produce the gravitational accelerations necessary to give a strong determination of the probe-planet range with doppler data alone at the time science power was energized. (This range, along with the spacecraft velocity would determine the time until encounter.) The range had to be obtained from the geocentric probe range, and the geocentric ephemeris of Mars. With the projected encounter speed of 7 km/sec, and the allowable uncertainty in time of 5 sec, the combined error of these range determinations could not exceed 35 km. Section II.A.2.a describes the ephemeris used for this portion of the mission, and indicates that the probable error in geocentric Mars range during the encounter period was less than 5 km. This put the burden on the flight OD engineer of determining the geocentric spacecraft range to better than 30 km.

The geocentric spacecraft range during cruise is determined primarily through observation of the heliocentric acceleration inferred from the doppler data of the probe and a knowledge of the heliocentric ephemeris of the earth. Doppler data can provide extremely accurate measurements of acceleration, but the deduction of range from such acceleration is quite susceptible to error in the presence of unknown or inadequately modeled non-gravitational forces. Since one never knows whether he is being affected by an unknown force, it is desirable, for safety's sake, to have an independent measurement of the earth-probe distance. It is for this reason, among others, that there was such insistence on spacecraft ranging during cruise and encounter.

Though ranging was provided by the DSN, determination of the spacecraft orbit using it was not an open and shut case. Experiences earlier in the mission had demonstrated quite strikingly both how powerful and how unforgiving this data type could be when the physical problem was mismodeled. (This is discussed in Section II. A. 3.) Because the errors in the Doppler data were small enough to limit the accumulated range error (integrated Doppler) over a pass to 1.5 m, the combination of range calibration and program modeling errors could not vary by more than this amount from day to day if one hoped to use all the range data in conjunction with the doppler data. A conservative approach seemed sensible because of the myriad of possible modeling errors that might amount to more than 1.5 m per pass. Moreover, when continuous Doppler would link the spacecraft's position from one time to another, it was obvious that a single range determination would be sufficient. Consequently, for the flight time determination, it was decided to use one point, or at most one pass, of ranging data as close to science turn on as possible, combined with as much Doppler as desired.

- Strategy for Determining B-Plane Parameters

An important variable in any interplanetary orbit determination strategy is the length of the data arc used in the final computation before encounter. For MM'69, even at E - 4 hr, the gravitational attraction of the planet was not strong enough to firmly establish with radio tracking a direct, planet-centered orbit; an earth-relative orbit had to be established and

then referred to Mars via the planetary ephemeris. Thus in determining the length of the data arc, the question resolves to deciding what arc gives the most accurate and reliable earth-relative orbit.

For comparison purposes, two extreme strategies were analyzed: 1) a short arc not exceeding 10 days of data and 2) a very long arc including all the cruise data. The case for the short arc says that this guards against the long term build-up of modeling errors. The case for the long data arc is that, not only does it produce better estimates because of a longer time to average data errors and a more solid geometry on which to have the estimate, but that often its susceptibility to certain model errors is less than the short arc. Although neither extreme can be totally relied upon, the preponderance of past evidence with the SPODP favored the short arc, primarily because of its difficulties in fitting very long arcs of data from Mariner IV and V.

However, with the improved modeling and increased computational precision of the DPODP, and the significant improvements in the knowledge of physical constants and station locations, it seemed appropriate to reconsider the long arc approach.

- Unmodeled Forces

Since charges of susceptibility to acceleration modeling errors were levied against each method, and used as the telling argument for each prosecution, an attempt was made to perform an analysis, using real data. The analysis of the solar pressure phenomenon early during the flight of Mariner 6 (Section II. A. 3. a.) exemplifies how these more subtle errors affect short arcs. The long arc problems were studied using the notoriously "dirty" Mariner IV spacecraft which had well-documented, long-term, unmodeled low-thrust forces due to its attitude control system. The results were rather surprising. The long arc solutions, though they fit the data poorly, gave consistently better predictions than the short arc solutions up to E - 1 day, without the instability that accompanied the short arcs.

The explanation proffered, but by no means proved here, is that a mean orbit was determined which best fit the existing data over the whole span within the confines of the existing model. In general, the unmodeled accelerations have little actual affect on the trajectory, but do their damage in the

filter where they can influence the state parameters being included in the solution. Over a long arc, this is more difficult and acceleration signatures which can be absorbed with a small amount of data may be forced out of the solutions.

In general, experience coping with unmodeled forces shows that when they are present, their effects on the orbit estimate are immediately apparent. (See Subsection II. A. 3. a, also II. B. 6. b. 3 and II. B. 6. b. 4). The effects when using long arcs are imperfectly understood, but the Mariner IV studies suggested that the B-plane predictions based on long arcs were more reliable than those based on short arcs.

Thus, since it was clear that no single strategy could be shown appropriate for the range of possible situations, the determination was made to prosecute both (and an intermediate length arc as well) and scrutinize the results of each for temporal stability of solutions, residual behavior, compatibility of doppler only and doppler plus range solutions, and single/multiple station consistency checks.

There were a variety of other known error sources which could have significant effect on the orbit determination. These errors and the techniques devised to reduce them are described in Section II. A. 2. How the OD strategy was designed around these will now be discussed.

- Ephemeris Errors

The plan finally adopted was designed to minimize susceptibility to ephemeris errors during the OD for the first spacecraft, and to capitalize on what was learned about the ephemeris for use with the second spacecraft.

Post-flight experience with Mariner V indicated how fatal an ephemeris error in geocentric range could be when ranging data was combined with Doppler and the target ephemeris was assumed known. The Mars-spacecraft acceleration provides the information to determine the range to the planet with doppler alone. This information comes after the flight-time determination at E - 2 to 3 days, but well before the final orbit estimate is made at E - 4 hr. The addition of ranging, then, is a separate means by which to deduce the probe-target range. This deduction must be made through the planetary ephemeris, and, if this is in error, the two independent range determinations will be in

conflict, a conflict that is resolved in part by moving the planet-centered latitude estimate of the probe. For MM'69, the possibility of such a movement was highly undesirable.

To avoid this difficulty, it was decided to include no ranging data that could be connected to encounter by continuous Doppler when solving for B-plane parameters for the first spacecraft. Having delivered the final estimate, all available ranging data would be used to evaluate the Mars ephemeris geocentric range error.

Because of the small uncertainty required in the direction normal to B in the B plane, the mission was extremely susceptible to ephemeris latitude errors. Unfortunately there was nothing that could be done from an OD standpoint to minimize this exposure for the first spacecraft. If the estimate for Mariner VI proved to be in error due to a combination of ephemeris and station location errors, the post-encounter data from Mariner VI could be used to attempt a rectification before the Mariner VII encounter. Planning for success, it was also recognized that if the first spacecraft proved the Mars ephemeris was accurate to under 5 km in the Earth Mars direction, then ranging data could be freely used during the Mariner VII encounter.

- Timing and Polar Motion Corrections

In view of the critical dependence of orbit determination results on the instantaneous value of UT1, every attempt was made to incorporate the timing information supplied from TPOLY as described in Section II.A.2.c. Because of the nature of the smoothing process the addition of one additional day's timing data often noticeably changed the smoothed UT1 for the previous two weeks from the values that were determined on the preceding day. From an operational point of view this meant that with every timing polynomial update, all previous short arc data had to be reprocessed, and at least the last two weeks of long arc data. Polar motion data was updated monthly with the last update ten days before the Mariner VI encounter and presented no particular operational problem to incorporate.

- Ionosphere

A large amount of research and analysis on charged particle effects was conducted prior to and during the flight. The results showed that

ionospheric effects could change the effective distance from the spin axis (r_s) for the prime tracking stations by as much as 5 m. Since it was felt that this would map into some 200 km in the $\overline{B} \cdot \overline{R}$ component, every effort was made using post flight data from other missions, to determine a set of "ionosphere-free" station locations, which could be used in flight with tracking data calibrated to remove the ionospheric effects.

Although there had been little previous experience with such phenomena on deep space missions, and the calibration procedures were still in the research and development phase, there was more to gain than to lose. It was decided to conduct a parallel series of runs (long and short arcs) using the ionosphere-free station locations and the calibrated tracking data. Because of the extreme unfamiliarity with,and uncertainty in this new procedure, the PNP plan was not to commit beforehand to an unalterable course of action in the event the two series of runs gave widely different results.

- Station Locations

Other than for consistency checks on long-arc solutions, it was decided not to attempt to solve for station locations during flight. The reason is that, except for very long arcs, these locations cannot be distinguished from the parameters of the orbit, geocentric right ascension and declination. More formally, the data partials with respect to probe state and earth station locations are, practically speaking, linearly dependent. From all past missions, more than enough data exists to determine the locations to an accuracy limited only by imperfections in the physical model used – the 1969 data arc, processed under the limitations imposed by the real-time operation could not help.

The above gives lack of motivation— there is yet a more compelling reason to even contraindicate a station solution. When estimating any two linearly dependent parameters, the data is simply apportioned between the two parameters in inverse proportion to the *a priori* knowledge assumed on each. Thus, a signal in the data indicating an error in either the probe state or the station location is blindly apportioned in this manner without any true discrimination as to its origin.

- Parameter Sets

On the basis of the foregoing discussion, it was decided to compare the following sets of OD solutions to arrive at a prediction of B-plane parameters:

a) The short arc, involving data from E - 5 days to E - 4 hr. Both Doppler only and Doppler and range solutions would be made, solving for the cartesian state and the gravitational constant (GM) of Mars.

b) The long arc, involving data from the last major dynamic spacecraft activity (midcourse or the Magellanic cloud mapping)* to E - 4 hr. Both Doppler only and Doppler and range solutions would be made solving for the cartesian state, 3 components of solar pressure and the gravitational constants for the moon and for Mars.

There was the tacit understanding that if ranging were used in either arc and caused the solution to disagree markedly from the Doppler only results, in the absence of any extenuating circumstances, the solutions with ranging were to be discarded in favor of the Doppler-only ones because of the ephemeris geocentric range error phenomenon.

5. Mariner VI Inflight Orbit Determination Analysis

a. Premidcourse Orbit Estimates — *S. K. Wong, S. J. Reinbold*

- Introduction

The Mariner VI spacecraft was injected into its Earth-Mars trajectory on February 25, 1969 at $01^h41^m11^s.6$ GMT. The nominal closest approach point was 6339.59 km from the center of Mars, to be reached on 30 July 1969; however, at injection, this was deliberately biased out to 20,859 km from the center of Mars to avoid any chance of impacting the planet. Hence, a midcourse maneuver was planned at the outset to achieve the nominal aiming point. This spacecraft had the capability to perform two maneuvers.

*The Mariner VII pre-encounter anomaly which occurred at E - 127 hr degraded all long- and medium-arc solutions (see Subsection II.B.6.c).

- Estimation of Spacecraft Premaneuver Orbit

The "ETR check orbit" was computed at JPL using only 7 data points from Antigua. These seven data points were obtained between the Centaur main engine cut-off and the Centaur-spacecraft separation. Therefore this orbit was biased* from the actual spacecraft orbit computed later during the flight. This orbit indicated a B-miss of 103,670 km.

The first estimate of the spacecraft orbit was completed at L + 2h 25 min and was based on approx 1 hour of DSS-51 angular and two-way doppler data. When this solution was mapped forward to target, the B-plane estimates indicated that the solution was very close to the nominal premaneuver aiming point ($\overline{B} \cdot \overline{R}$ = -13,300 km, $\overline{B} \cdot \overline{T}$ = 17,100 km, t_{ca} = $05^{h}\,01^{m}\,32^{s}$) and that the correction required to achieve the nominal post-maneuver aim point was well within the midcourse correction capability. This was verified by the second (ICEV) and third (PREL) orbit computations completed at L + 5 hr and L + 11 hr respectively.

During the second orbit computation period a comparison was made between solutions with and without angular (HA, DEC) data. One orbit was computed using DSS 51 angular and doppler data in the least squares fit. The other orbit was computed using only DSS 51 two-way doppler data in the fit. The comparison showed a magnitude difference in the B vector of 10,830 km. Since it is known that angular data are biased, the sole purpose of using angular data is to obtain early solutions until enough doppler data is obtained to converge independently to a reasonable solution.

During the data consistency (DACO) computation period from L + 14 hr to L + 27 hr, seven orbital solutions were obtained using various combinations of DSS 41, 51, 12 and MSFN 75 (Ascension) data. The solutions obtained from these computations indicated that the DSS 41, 51 and 12 data were consistent. However, the MSFN 75 data appeared to be biased and this bias is probably due to the inaccuracy of the surveyed station location. Since only one hour of tracking data was obtained from MSFN 75, it was decided not to use this data in any later orbit computations.

---

*A spring separation device changes the spacecraft velocity by approximately 0.6 m/sec when it is separated from the Centaur.

During the DACO computation period, orbit solutions were also computed using doppler data only, ranging data only, and doppler and ranging data. These three solutions are in fairly good agreement with the amount of the data in the solutions. The comparison between the three solutions is given below:

	Doppler Only	Ranging Only	Doppler and Ranging
B	13361.13	13540.22	13377.03
$\bar{B} \cdot \bar{R}$	-12983.65	-13044.16	-12985.47
$\bar{B} \cdot \bar{T}$	3153.51	3631.4355	3212.83
t_{ca} (7/31/69)	$04^h\,41^m\,27^s.83$	$04^h\,40^m\,20^s.09$	$04^h\,41^m\,20^s.74$

The nominal maneuver (NOMA) orbit computation time block started at approximately L + 40 hr. The NOMA 2XK orbit solution was used for midcourse maneuver computation. The following amount of data was used in the computation:

	Doppler	Ranging
DSS 41	23.5 hr	23.5 hr
DSS 51	27.0 hr	15.5 hr
DSS 12	3.0 hr	3.0 hr

The orbit estimated only the state vector and when this solution was mapped to target, it indicated the following results:

$$B = 13407.02 \text{ km}$$

$$\bar{B} \cdot \bar{R} = -12909.08 \text{ km}$$

$$\bar{B} \cdot \bar{T} = 3619.95 \text{ km}$$

$$t_{ca} = 04^h\,40^m\,14^s.379$$

Examining the observed minus computed (o - c) residual plots of the NOMA 2XK solution, the data fit appeared to be reasonably good.

However, it indicated that some small perturbation probably was not accounted for. Estimating for station locations, solar pressure in the Sun-Probe direction, Earth ephemeris elements, and changing the values of the index of refraction for the tracking stations did not improve the data fit. An orbit solution estimating the gravitational constant of the earth (KE) along with state vector did improve the data fit but it changed KE by the unrealistic amount of 7 km^3/sec^2. It was suspected that the perturbation was due to an acceleration caused by the solar pressure in the tangential direction or a small gas leak. Since the SPODP was unable* to estimate the solar pressure in the tangential direction nor the gas leaks and the DPODP has not yet been certified, it was decided to use the NOMA 2XK solution for maneuver computation.

During this time a similar orbit solution to NOMA 2XI was computed by the Double Precision Orbit Determination Program (DPODP). The solution estimated the state vector by using the doppler data only. The ranging data was not used because the program that converted the SPODP data tape to a DPODP data tape handled the ranging data incorrectly. The comparison of these solutions is given below:

Target Parameters	SPODP	DPODP	ΔSPODP-DPODP
B	13439 km	13425 km	14 km
$\bar{B} \cdot \bar{R}$	-12936 km	-12929 km	-7 km
$\bar{B} \cdot \bar{T}$	3641 km	3617 km	24 km
t_{ca}	$04^h40^m05^s.7$	$04^h40^m14^s.2$	-8.5 sec

The last premidcourse (LAPM) orbit computation time block was between midcourse minus 10 hours (M - 10 hr) to M - 1 hr. The orbits computed during this time block indicated solutions very close to the NOMA 2XK solution which was used for maneuver computation. Therefore, the midcourse maneuver was performed on the NOMA 2XK solution.

The numerical results of the premaneuver orbit computations are presented in Table 2-17. Figures 2-18 and 2-19 show the B-plane estimates

*The flight version of the software system had been "frozen" with several known "bugs" in the SPODP. These were corrected after the Mariner VII maneuver was performed.

Table 2-17. Mariner VI Pre-midcourse Orbit Computations

Orbit ID	B, km	$\bar{B} \cdot \bar{R}$, km	$\bar{B} \cdot \bar{T}$, km	t_{ca}*	Time of Last Data Point, GMT	Stations Used in Orbit	Data Types Used	Estimated Parameters
ETR[1]	103669.74	43657.477	94014.989	$15^h43^m01^s.509$	$2/25\text{-}01^h42^m06^s$	Antigua	Range, AZ, EL	State Vector
PROR-X[1]	24777.882	-14636.396	19992.982	$04^h11^m56^s.727$	$2/25\text{-}03^h50^m02^s$	DSS 51	CC3, Angles	State Vector
ICEV-Y[2]	13948.287	-13575.227	-3204.3617	$04^h52^m40^s.721$	$2/25\text{-}03^h32^m00^s$	DSS 51	CC3	State Vector
ICEV-X[1]	13816.627	-12999.501	4681.0404	$04^h38^m32^s.189$	$2/25\text{-}05^h59^m00^s$	DSS 51	RU, CC3	State Vector
PREL-X[2]	13584.248	-13122.211	3512.7392	$04^h40^m32^s.790$	$2/25\text{-}08^h10^m32^s$	DSS 51	CC3	State Vector
PREL-XB[1]	12751.511	-12698.872	1157.4472	$04^h45^m46^s.506$	$2/25\text{-}08^h52^m32^s$	ACN DSS 51	RU, CC3	State Vector
PREL-XC[2]	14386.036	-12522.663	7091.0269	$04^h34^m05^s.708$	$2/25\text{-}09^h17^m32^s$	ACN DSS 51	CC3	State Vector
PREL-XE[2]	13639.018	-12981.023	4185.1942	$04^h39^m20^s.199$	$2/25\text{-}09^h17^m32^s$	Station 5	RU, CC3	State Vector
DACO-YA[2]	12995.738	-12879.224	1736.3124	$04^h44^m36^s.425$	$2/25\text{-}15^h06^m32^s$	ACN DSS 51, 12	CC3	State Vector
DACO-YB[2]	13224.917	-12916.457	2839.6431	$04^h42^m19^s.224$	$2/25\text{-}21^h00^m32^s$	ACN DSS 12, 41, 51	CC3	State Vector
DACO-YC[2]	13239.561	-12915.764	2410.1594	$04^h42^m10^s.773$	$2/25\text{-}22^h03^m32^s$	ACN DSS 41, 51	CC3	State Vector
DACO-YD[2]	13360.799	-12976.379	3181.9094	$04^h41^m26^s.213$	$2/25\text{-}23^h28^m32^s$	DSS 41, 12, 51	CC3	State Vector
DACO-YE[2]	13540.218	-13044.163	3531.4355	$04^h40^m20^s.088$	$2/26\text{-}00^h24^m02^s$	DSS 41, 12, 51	RU	State Vector
DACO-YF[2]	13377.026	-12985.474	3212.8273	$04^h41^m20^s.742$	$2/26\text{-}03^h05^m02^s$	DSS 41, 51, 12	RU, CC3	State Vector
NOMA-XA[2]	13411.275	-12980.636	3371.2605	$04^h41^m05^s.511$	$2/26\text{-}17^h11^m32^s$	DSS 51, 12, 41	CC3	State Vector
NOMA-XD[3]	13434.670	-13024.689	3293.6037	$04^h41^m08^s.229$	$2/27\text{-}00^h07^m32^s$	DSS 41, 51, 12	CC3	State Vector
NOMA-XE[2]	13413.430	-12988.397	3349.8718	$04^h41^m06^s.928$	$2/27\text{-}00^h07^m32^s$	DSS 41, 51, 12	CC3	State Vector
NOMA-XF[2]	13336.354	-12899.804	3384.2877	$04^h41^m03^s.594$	$2/27\text{-}00^h07^m32^s$	DSS 41, 51, 12	CC3	State Vector

*The date of closest approach is July 31, 1969 for all solutions.

Table 2-17. Mariner VI Pre-midcourse Orbit Computations (cont'd)

Orbit ID	B, km	$\bar{B} \cdot \bar{R}$, km	$\bar{B} \cdot \bar{T}$, km	t_{ca}	Time of Last Data Point. GMT	Stations Used in Orbit	Data Types Used	Estimated Parameters
NOMA-XH*2	13486.224	-12806.334	4228.0090	$04^h38^m27^s.560$	$2/27\text{-}01^h31^m32^s$	DSS 41, 51, 12	RU, CC3	State Vector
NOMA-XI*2	13478.042	-12839.830	4098.3379	$04^h38^m53^s.035$	$2/27\text{-}02^h57^m32^s$	DSS 41, 51, 12	CC3	State Vector
NOMA-XJ*3	13472.616	-12977.150	3620.0775	$04^h39^m57^s.906$	$2/27\text{-}02^h57^m32^s$	DSS 41, 51, 12	CC3	State Vector
NOMA-XK*3	13488.059	-12871.664	4030.8833	$04^h39^m30^s.227$	$2/27\text{-}02^h57^m32^s$	DSS 41, 51, 12	RU, CC3	State Vector
NOMA-2XA*2	1341.097	-12896.523	3686.5803	$04^h40^m06^s.322$	$2/27\text{-}16^h22^m32^s$	DSS 41, 51, 12	CC3	State Vector
NOMA-2XB*3	13432.471	-12918.651	3679.6365	$04^h40^m04^s.921$	$2/27\text{-}16^h22^m32^s$	DSS 41, 51, 12	CC3	State Vector
NOMA-2XG*2	13427.490	-12903.507	3714.4307	$04^h40^m01^s.803$	$2/27\text{-}21^h44^m32^s$	DSS 41, 51, 12	CC3	State Vector
NOMA-2XH*2	13437.303	-12907.753	3735.1078	$04^h39^m58^s.599$	$2/27\text{-}21^h44^m32^s$	DSS 41, 51	CC3	State Vector
NOMA-2XI*3	13439.148	-12936.403	3641.4497	$04^h40^m05^s.702$	$2/27\text{-}21^h44^m32^s$	DSS 41, 51, 12	CC3	State Vector
NOMA-2XJ*3	13415.121	-12909.190	3649.4222	$04^h40^m10^s.654$	$2/27\text{-}22^h18^m32^s$	DSS 41, 51, 12	CC3	State Vector
NOMA-2XK*2	13407.024	-12909.075	3619.9528	$04^h40^m14^s.379$	$2/27\text{-}23^h45^m32^s$	DSS 41, 51, 12	RU, CC3	State Vector
NOMA-2XL*3	1343.518	-12930.540	3648.8711	$04^h40^m09^s.659$	$2/28\text{-}02^h25^m32^s$	DSS 41, 51, 12	CC3	State Vector-Station Location
LAPM-XC*3	13430.326	-12934.428	3615.8279	$04^h40^m13^s.618$	$2/28\text{-}20^h37^m32^s$	DSS 41, 51, 12	CC3	State Vector-Station Location
LAPM-XD*2	13402.332	-12912.415	3590.5486	$04^h40^m18^s.363$	$2/28\text{-}22^h00^m32^s$	DSS 41, 51, 12	RU, CC3	State Vector
LAPM-XE*3	13427.237	-12933.272	3608.4884	$04^h40^m15^s.082$	$2/28\text{-}22^h00^m32^s$	DSS 41, 51, 12	CC3	State Vector
LAPM-XF*3	13428.050	-12929.883	3623.6262	$04^h40^m12^s.042$	$2/28\text{-}23^h38^m32^s$	DSS 41, 51, 12	CC3	State Vector

*The first 18 orbits, through NOMA-XF used: spacecraft mass, MASS = 384.1932 Kg reflectivity coefficient, GB = 0.23998. Those values were in error, and were corrected to: MASS = 385.69458 Kg GB = 0.34423

[1]Epoch taken to be $2/25/69\ 01^h40^m40^s.645$

[2]Epoch taken to be $2/25/69\ 02^h33^m00^s.000$

[3]Epoch taken to be $2/25/69\ 10^h39^m00^s.000$

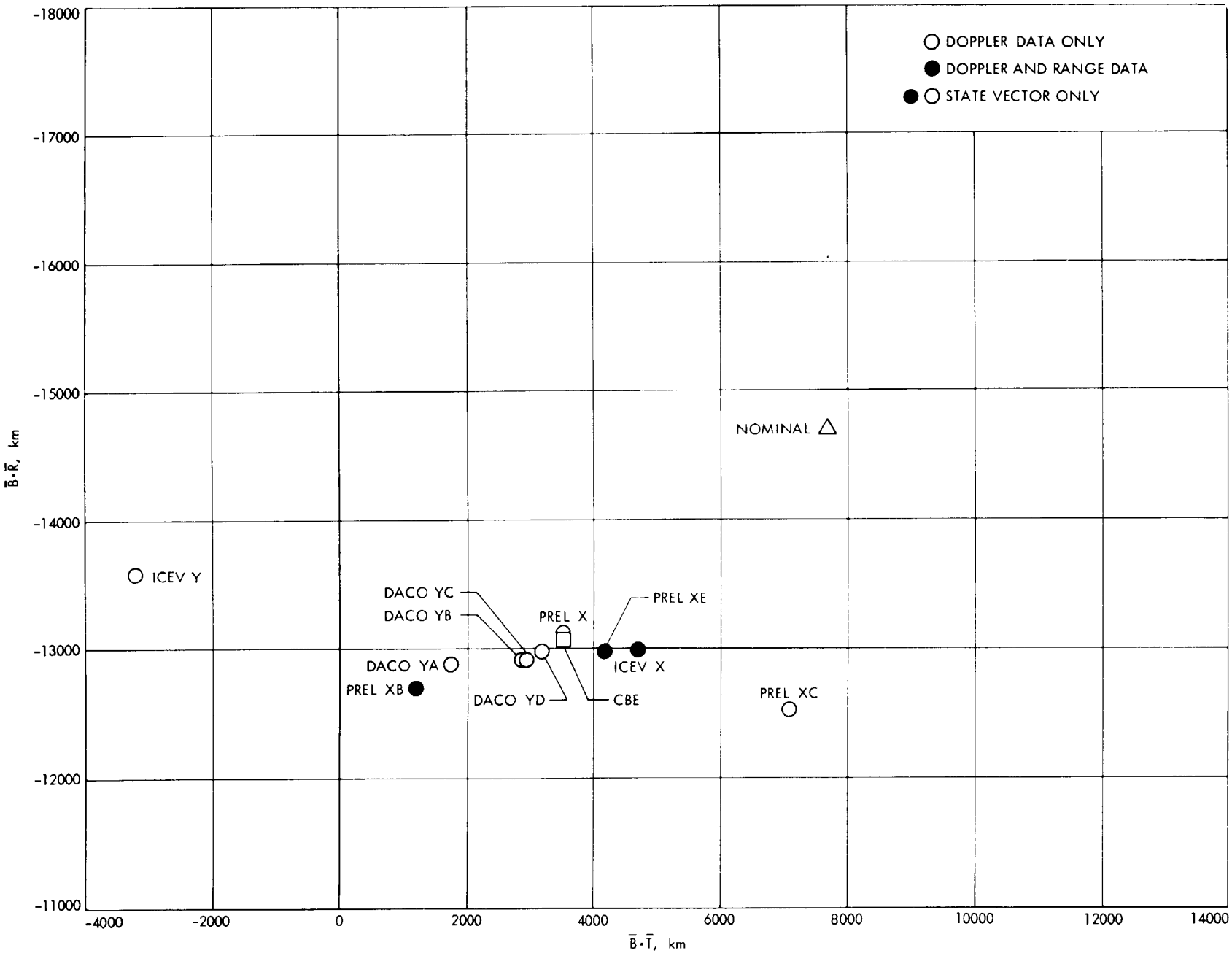

Figure 2-18. Mariner VI Pre-Midcourse Orbit Estimates

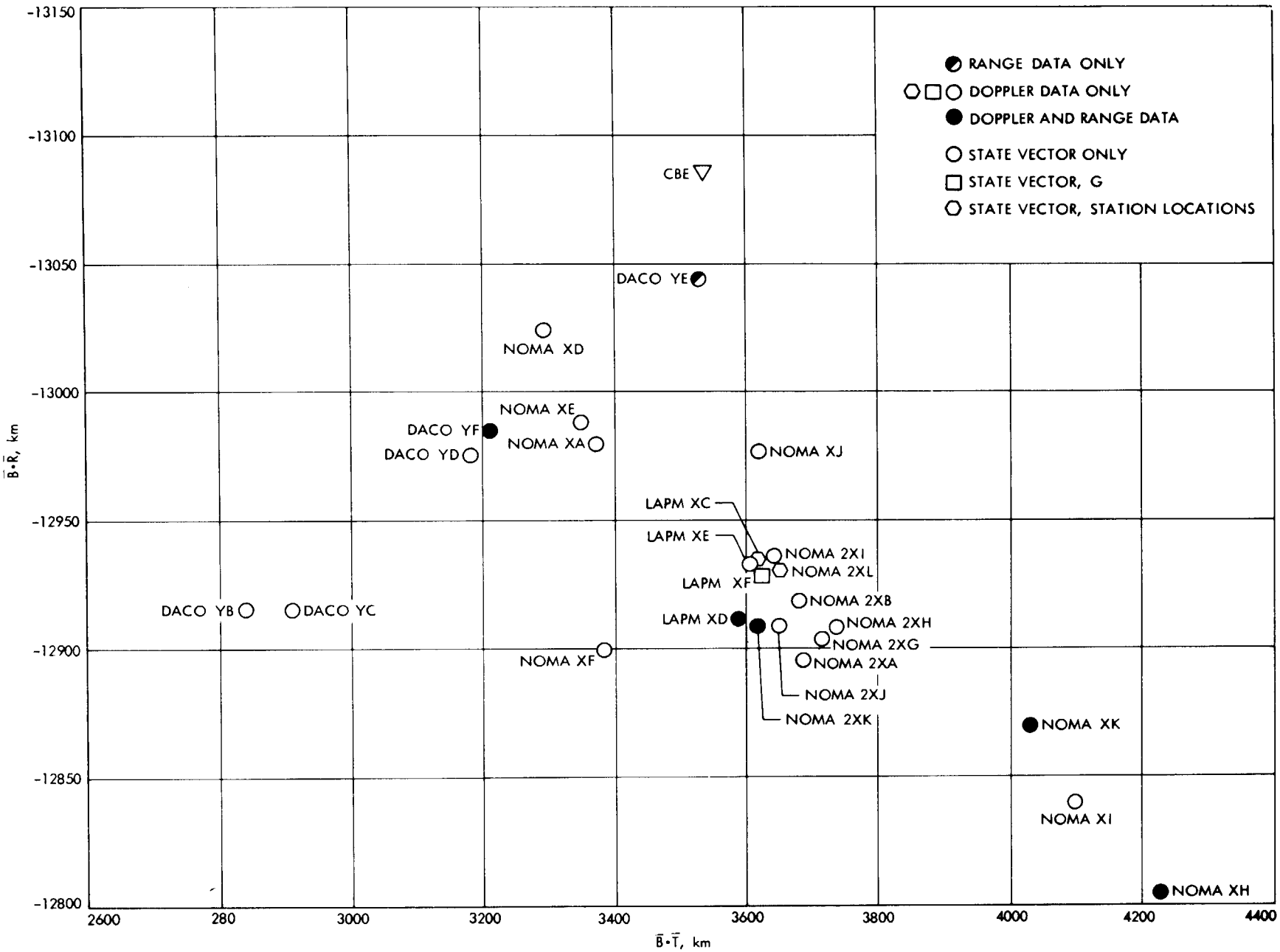

Figure 2-19. Mariner VI Pre-Midcourse Orbit Estimates

of the orbits computed during pre-midcourse, Figures 2-20 and 2-21 show the time of closest approach of the pre-midcourse orbits.

b. Post-midcourse Orbit Estimates — *S. K. Wong, S. J. Reinbold*

- Introduction

The command to initiate the Mariner VI spacecraft maneuver was transmitted by DSS 41 at 23^h19^m GMT on February 28 and Canopus was reacquired at 01^h11^m GMT on March 1. The maneuver was performed approximately four days after launch.*

Less than 6 days after the maneuver, the scan platform was unlatched by ground command DC 45 transmitted at 19^h11^m GMT, March 6 from DSS 41. This scan platform unlatch was performed by venting compressed nitrogen which perturbed the orbit of the spacecraft. Continuous tracking coverage was provided from midcourse maneuver (M) to M + 10 days. Thereafter, the tracking coverage was intermittent and averaged about 45 hr/wk. At encounter minus 9 days continuous tracking coverage was again provided until encounter plus 6 days.

- Estimation of Spacecraft Pre-unlatch Orbit

The first post-midcourse orbit computed at approximately M + 6 hr indicated that the orbit was quite different than the expected orbit. After detailed analysis, it was discovered that the DSS 41 doppler data had a timing error. With these data rejected, another orbit was computed using approximately 20 hr of tracking data (doppler and range). This orbit estimated only the state vector and when this solution was mapped to target, it appeared to be quite close to the expected orbit.

Orbit Post 1	Maneuver Aiming Point (M.A.P.)	ΔPost 1 - M.A.P.
$\bar{B} \cdot \bar{R} = -460$ km	$\bar{B} \cdot \bar{R} = -643$ km	$\Delta\bar{B} \cdot \bar{R} = 183$ km
$\bar{B} \cdot \bar{T} = 7779$ km	$\bar{B} \cdot \bar{T} = 7452$ km	$\Delta\bar{B} \cdot \bar{T} = 327$ km
$t_{ca} = 05^h17^m28^s$	$t_{ca} = 05^h17^m50^s$	$\Delta t_{ca} = -22^s$

*The maneuver and the scan unlatch were done as early as possible in order to have time to correct any deficiencies before Mariner VII was launched (see Section I).

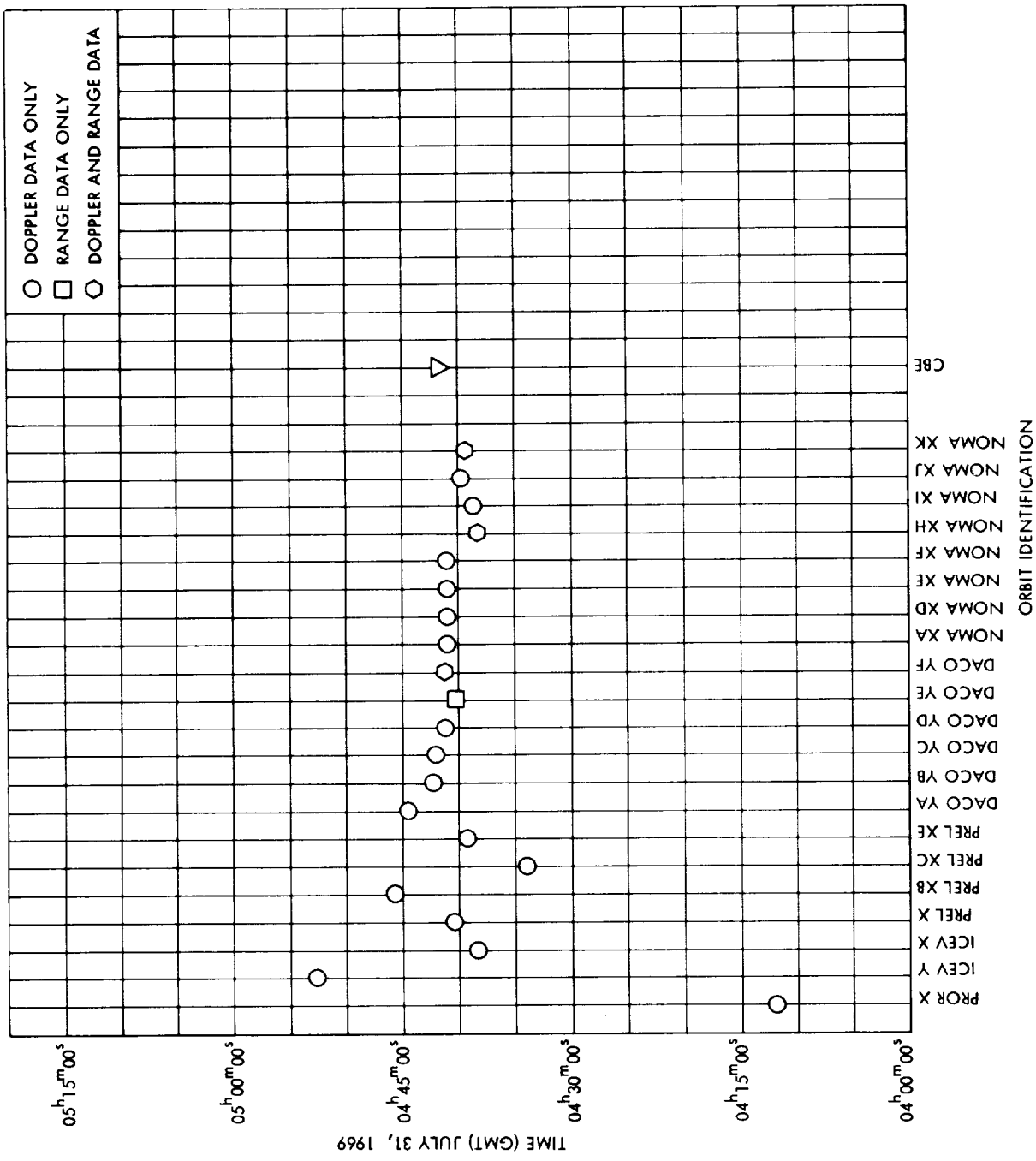

Figure 2-20. Mariner VI Pre-Midcourse Time of Closest Approach

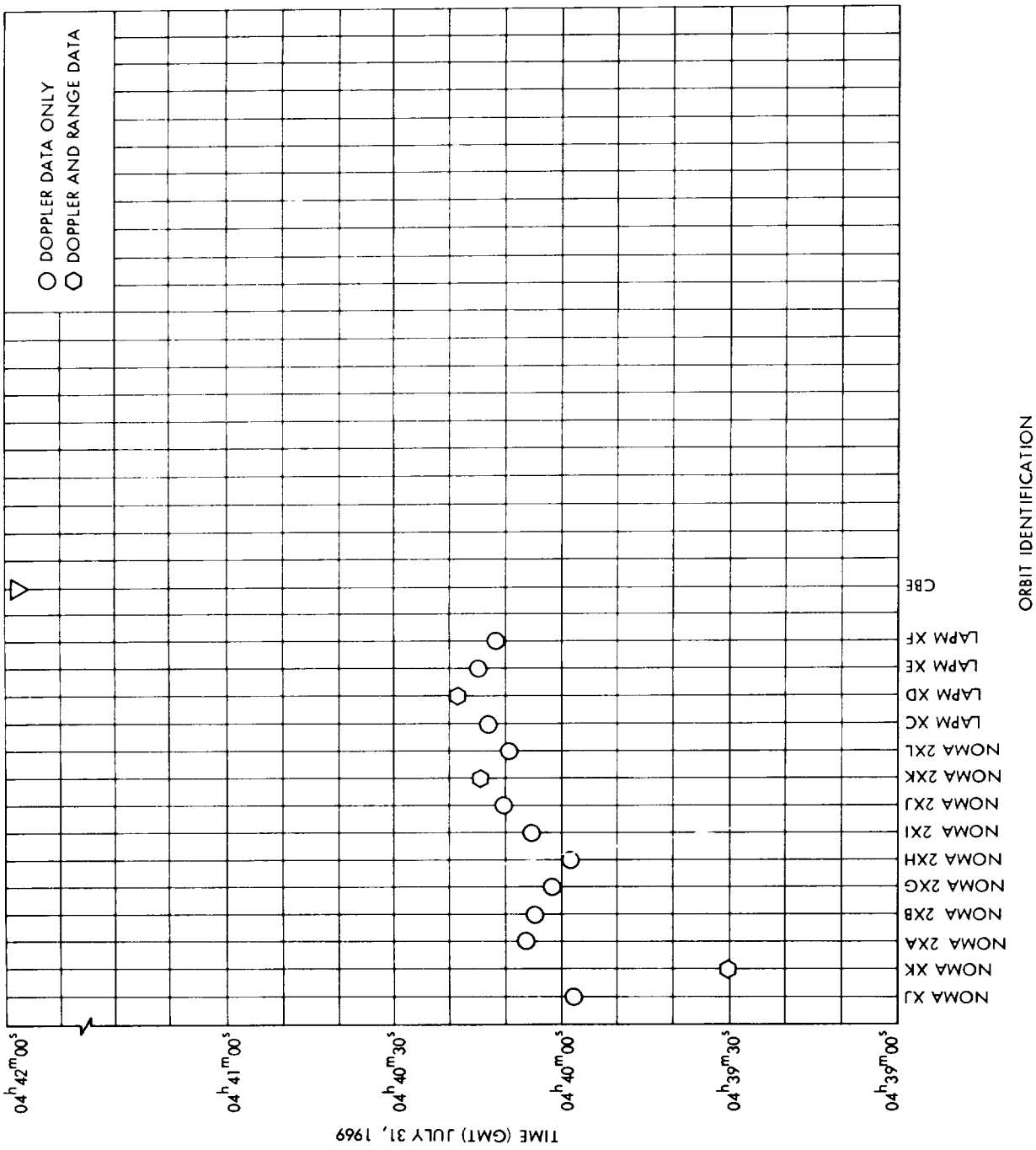

Figure 2-21. Mariner VI Pre-Midcourse Time of Closest Approach

With about 1 day of data, the orbit solutions computed using doppler and range data agreed with the orbit solutions computed using doppler data only. However, with additional data the two types of solutions began to diverge and at the time of the platform unlatch the two solutions were:

Doppler Only	Doppler and Range
$B = 7649$ km	$B = 7410$
$\bar{B} \cdot \bar{R} = -384$ km	$\bar{B} \cdot \bar{R} = -412$
$\bar{B} \cdot \bar{T} = 7639$ km	$\bar{B} \cdot \bar{T} = 7398$
$t_{ca} = 05^h18^m03^s.493$	$t_{ca} = 05^h18^m16^s.123$

These solutions estimated only the state vector. Even though these two solutions indicated possible inconsistency between doppler and range data, the data fit of both solutions was good. This was what led us to believe that with additional data the two solutions might converge. The best inflight estimate of the pre-unlatched orbit was:

$$B = 7797 \text{ km}$$

$$\bar{B} \cdot \bar{R} = -410 \text{ km}$$

$$\bar{B} \cdot \bar{T} = 7786 \text{ km}$$

$$t_{ca} = 05^h18^m44^s.244$$

This solution used only doppler data and estimated the state vector, the three components of solar pressure and station locations.

- Estimation of Spacecraft Post-Unlatch Orbit

The characteristics of redetermination of the orbit during this phase was that it took much longer for the orbit to stabilize. This was due to the placement of the epoch (i.e., no near-Earth data) and the lack of continuous tracking data. With about 5 days of intermittent tracking data the orbits differed by at least 1200 km when one orbit was computed with *a priori* statistics and another was computed without *a priori* statistics. The two solutions are given as follows:

With *a priori*	Without *a priori*
$B = 7108$	$B = 8348$
$\bar{B} \cdot \bar{R} = -423$	$\bar{B} \cdot \bar{R} = -348$
$\bar{B} \cdot \bar{T} = 7095$	$\bar{B} \cdot \bar{T} = 8340$
$t_{ca} = 05^h18^m35.^s646$	$t_{ca} = 05^h16^m27.^s106$

These solutions were computed using doppler data only and estimating only the state vector.

With about 18 days of intermittent tracking data the orbit solutions were slowly moving toward each other. The solutions are as follows:

With *a priori*	Without *a priori*
$\bar{B} \cdot \bar{R} = -392$ km	$\bar{B} \cdot \bar{R} = -344$ km
$\bar{B} \cdot \bar{T} = 7590$ km	$\bar{B} \cdot \bar{T} = 8022$ km
$t_{ca} = 05^h17^m45.^s228$	$t_{ca} = 05^h17^m05.^s492$

With about 43 days of intermittent tracking data the orbit solutions with and without *a priori* statistics were approximately the same.

Without *a priori*

$\bar{B} \cdot \bar{R} = -377$ km

$\bar{B} \cdot \bar{T} = 7598$ km

$t_{ca} = 05^h17^m46.^s390$

On April 30, the attitude control jets were fired attempting to acquire the Greater Magellanic Cloud by the Canopus tracker. The reason for performing this procedure was that the Canopus tracker must be stepped in cone-angle to keep Canopus in view. The spacecraft had apparently lost this capability and had stepped the cone-angle to an improper position. Due to the difficulties in staying locked to the Greater Magellanic Cloud another attempt

was made to step the tracker field-of-view to acquire Canopus and it was successful.

During this procedure the doppler residuals showed a total doppler change of 0.03 Hz and once again the spacecraft orbit was slightly perturbed.

The orbit of the spacecraft was redetermined using only the tracking data obtained after the Magellanic Cloud activity. With approximately 2 months of intermittent tracking data, the following orbit solutions were obtained:

Solution A	Solution B	Solution C
$B = 7550$ km	$B = 7616$ km	$B = 7628$ km
$\bar{B} \cdot \bar{R} = -511$ km	$\bar{B} \cdot \bar{R} = -418$ km	$\bar{B} \cdot \bar{R} = -367$ km
$\bar{B} \cdot \bar{T} = 7533$ km	$\bar{B} \cdot \bar{T} = 7604$ km	$\bar{B} \cdot \bar{T} = 7619$ km
$t_{ca} = 05^h19^m13.^s114$	$t_{ca} = 05^h19^m08.^s376$	$t_{ca} = 05^h19^m05.^s539$

Solution A was computed using only doppler data and estimated only the state vector. Solution B was computed using only doppler data and estimated the state vector, the 3 components of solar pressure and station locations. Solution C was computed using doppler and planetary ranging data and estimated the same parameters as Solution B.

The following solutions were computed with data up to E - 5 days.

Orbit	3 Post 49	3 Post 89	3 Post 91	3 Post 47
Data Used	Doppler	Doppler	Doppler and Range	Doppler and Range
Parameters Estimated	State Vector, 3 Components of Solar Pressure	State Vector, 3 Components of Solar Pressure, Station Locations	State Vector, 3 Components of Solar Pressure	State Vector, 3 Components of Solar Pressure, Station Locations
B, km $\bar{B} \cdot \bar{R}$, km $\bar{B} \cdot \bar{T}$, km t_{ca}	7586 -302 7580 $05^h18^m53.^s889$	7599 -359 7591 $05^h18^m54.^s147$	7575 -320 7568 $05^h19^m03.^s754$	7587 -402 7577 $05^h19^m02.^s441$

The four solutions agreed quite well. However, much more confidence was placed on the time of closest approach computed using doppler and range data.

The numerical results of the pre-unlatch, post-unlatch, and post-Magellanic orbit computations are presented in Table 2-18. Figures 2-22, 2-23, and 2-24 show the B-plane estimates of the orbits computed during pre-unlatch, post-unlatch and post-Magellanic Cloud phases. Figures 2-25, 2-26 and 2-27 show the time of closest approach of the pre-unlatch, post-unlatch and post-Magellanic orbits.

c. Encounter Orbit Estimates

- Introduction

The basic encounter strategy was that orbit solutions would be computed for a long data arc and a short data arc. The long data arc had a data span from the Magellanic Cloud activity to the latest data point. The short data arc had a data span from E - 5^d to the latest data point. The parameter set to be estimated for the short data arc included the state vector and the mass ratio of Mars to Sun; the long-data-arc parameter set included the state vector, mass ratio of Mars to Sun and the solar pressure coefficients.

- Estimation of the Spacecraft Pre-Encounter Orbit — *S. K. Wong, S. J. Reinbold*

At encounter minus 61 hr, the best available time of closest approach was needed for the spacecraft platform update. The reason for the importance of this update was that the camera shuttering sequence would not be adjusted after it was started. At this time, the DPODP encounter operations team recommended the following value for the time of closest approach:

$$\text{July 31, 1969 } 05^h19^m05^s.412$$

The DPODP long-data-arc orbit solutions at E - 5^d are given as follows:

Table 2-18. Mariner VI Pre-Unlatch, Post-Unlatch, and Post-Magellanic Orbit Computations

Orbit ID	B, km	$\bar{B} \cdot \bar{R}$, km	$\bar{B} \cdot \bar{T}$, km	t_{ca}	Time of Last Data Point, GMT	Stations Used in Orbit	Data Types Used	Estimated Parameters
Post 1	7793.0214	-460.19057	7779.4223	$05^h17^m27^s.575$	$3/01\text{-}21^h54^m02^s$	DSS 41, 51, 12	RU, CC3	State Vector
Post 2	7801.5570	-452.76303	7788.4078	$05^h17^m28^s.080$	$3/01\text{-}21^h43^m32^s$	DSS 41, 51, 12	CC3	State Vector
Post 3	7831.6724	-448.18057	7818.8376	$05^h17^m25^s.818$	$3/02\text{-}01^h14^m32^s$	DSS 41, 51, 12	RU, CC3	State Vector
Post 4	7519.9435	-314.07063	7513.2819	$05^h18^m23^s.792$	$3/02\text{-}14^h56^m32^s$	DSS 41, 51, 12	RU, CC3	State Vector
Post 5	7498.8235	-367.30898	7589.9407	$05^h18^m06^s.153$	$3/02\text{-}19^h44^m32^s$	DSS 41, 51, 12	CC3	State Vector
Post 6	7520.8736	-341.91268	7513.0975	$05^h18^m19^s.516$	$3/03\text{-}15^h26^m32^s$	DSS 41, 51, 12	CC3	State Vector
Post 7	7421.5097	-338.52906	7413.7848	$05^h18^m29^s.219$	$3/03\text{-}15^h26^m32^s$	DSS 41, 51, 12	RU, CC3	State Vector
Post 8	7433.1472	-346.04453	7425.0875	$05^h18^m26^s.429$	$3/03\text{-}22^h10^m32^s$	DSS 41, 51, 12	CC3	State Vector
Post 9	7852.3048	-371.35706	7843.5185	$04^h17^m45^s.335$	$3/04\text{-}00^h54^m32^s$	DSS 41, 51, 12	CC3	State Vector and G
Post 10	7876.3022	-370.36533	7867.5896	$05^h17^m42^s.795$	$3/04\text{-}00^h54^m32^s$	DSS 41, 51, 12	CC3	State Vector
Post 11	7816.4545	-358.72908	7808.2183	$05^h17^m51^s.893$	$3/04\text{-}18^h56^m32^s$	DSS 41, 51, 12	CC3	State Vector
Post 12	7431.2828	-392.38301	7420.9160	$05^h18^m18^s.262$	$3/04\text{-}19^h51^m32^s$	DSS 41, 51, 12	RU, CC3	State Vector
Post 13	7807.0068	-360.90796	7798.6602	$05^h17^m52^s.380$	$3/04\text{-}21^h15^m32^s$	DSS 41, 51, 12	CC3	State Vector
Post 14	7542.1301	-381.79101	7532.4603	$05^h18^m19^s.830$	$3/04\text{-}21^h15^m32^s$	DSS 41, 51, 12	CC3	State Vector
Post 15	7721.3483	-351.07192	7713.3629	$05^h18^m03^s.304$	$3/04\text{-}18^h30^m32^s$	DSS 41, 51, 12	CC3	State Vector
Post 16	7383.5481	-388.59577	7373.3149	$05^h18^m24^s.069$	$3/05\text{-}19^h40^m32^s$	DSS 41, 51, 12	RU, CC3	State Vector
Post 17	7409.1778	-383.41172	7399.2503	$05^h18^m22^s.650$	$3/04\text{-}22^h26^m32^s$	DSS 41, 51, 12	RU, CC3	State Vector
Post 18	7392.6953	-388.20316	7382.4956	$05^h18^m23^s.214$	$3/05\text{-}22^h24^m32^s$	DSS 41, 51, 12	RU, CC3	State Vector
Post 19	7648.6165	-384.31128	7638.9550	$05^h18^m03^s.493$	$3/04\text{-}18^h32^m32^s$	DSS 41, 51, 13	CC3	State Vector
Post 20	7397.2372	-417.82706	7385.4274	$05^h18^m17^s.192$	$3/06\text{-}18^h39^m32^s$	DSS 41, 51, 12	RU, CC3	State Vector
Post 21	7409.6218	-411.67594	7398.1763	$05^h18^m17^s.123$	$3/06\text{-}18^h54^m02^s$	DSS 41, 51, 12	RU, CC3	State Vector
2 Post 4	7651.1004	-357.15901	7642.7595	$05^h17^m44^s.949$	$3/10\text{-}09^h29^m32^s$	DSS 41, 51	CC3	State Vector
2 Post 11	7718.8713	-393.71728	7708.8235	$05^h17^m30^s.490$	$3/11\text{-}15^h28^m32^s$	DSS 41, 51, 12	CC3	State Vector

Table 2-18. Mariner VI Pre-Unlatch, Post-Unlatch, and Post-Magellanic Orbit Computations (cont'd)

Orbit ID	B, km	$\bar{B} \cdot \bar{R}$, km	$\bar{B} \cdot \bar{T}$, km	t_{ca}	Time of Last Data Point, GMT	Stations Used in Orbit	Data Types Used	Estimated Parameters
2 Post 13	7150.8454	-476.80965	7134.9311	$05^h18^m39^s.625$	$3/12-17^h45^m32^s$	DSS 41, 51, 12	CC3	State Vector and G
2 Post 14	7203.0341	-472.11011	7187.5452	$05^h18^m17^s.842$	$3/12-17^h45^m32^s$	DSS 41, 51, 12	CC3	State Vector, Station Location
2 Post 15	7251.9190	-473.42394	7236.4490	$05^h18^m13^s.023$	$3/12-17^h45^m32^s$	DSS 41, 51, 12	CC3	State Vector
2 Post 18	8025.9455	-352.70477	7998.1720	$05^h17^m04^s.945$	$3/13-19^h38^m32^s$	DSS 41, 51, 12	CC3	State Vector
2 Post 19	7255.1697	-413.63569	7243.3686	$05^h18^m19^s.010$	$3/16-08^h58^m32^s$	DSS 41, 51, 12	CC3	State Vector
2 Post 21	7159.5740	-451.59686	7145.3171	$05^h18^m34^s.135$	$3/17-19^h35^m02^s$	DSS 41, 51, 12	CC3	State Vector G and Station Location
2 Post 23	7020.7920	-451.77824	7006.2411	$05^h18^m37^s.722$	$3/19-16^h54^m02^s$	DSS 41, 51, 12, 14	PRU, CC3	State Vector
2 Post 24	7409.7139	-411.02479	7398.3049	$05^h18^m01^s.708$	$3/19-08^h41^m02^s$	DSS 41, 51, 12, 14	CC3	State Vector
2 Post 28	7535.1354	-413.10636	7523.7996	$05^h17^m58^s.681$	$3/20-18^h30^m02^s$	DSS 41, 51, 12, 14	CC3	State Vector and G
2 Post 29	7545.1992	-397.43958	7534.7242	$05^h17^m50^s.533$	$3/20-18^h30^m02^s$	DSS 41, 51, 12, 14	CC3	State Vector
2 Post 32	7600.23	-391.81	7590.13	$05^h17^m45^s.228$	$3/24-17^h56^m02^s$	DSS 42, 41, 51, 12, 14	CC3	State Vector
2 Post 38	8099.24	-340.94	8092.06	$05^h16^m57^s.464$	$3/25-07^h54^m02^s$	DSS 42, 41, 51, 12, 14	CC3	State Vector
2 Post 40	7957.13	-354.67	7949.22	$05^h17^m10^s.601$	$3/29-14^h14^m02^s$	DSS 42, 41, 51, 12, 14	CC3	State Vector
2 Post 41	7754.1692	-360.57140	7745.7813	$05^h17^m31^s.125$	$4/03-12^h36^m02^s$	DSS 42, 41, 51, 12, 14	CC3	State Vector
2 Post 42	7688.0597	-370.29846	7679.1366	$05^h17^m37^s.123$	$4/07-10^h54^m02^s$	DSS 42, 41, 51, 12, 14	CC3	State Vector
2 Post 43	7681.3892	-369.87816	7672.4785	$05^h17^m37^s.862$	$4/09-13^h12^m02^s$	DSS 14, 12, 51, 41	CC3	State Vector

Table 2-18. Mariner VI Pre-Unlatch, Post-Unlatch, and Post-Magellanic Orbit Computations (cont'd)

Orbit ID	B, km	$\bar{B} \cdot \bar{R}$, km	$\bar{B} \cdot \bar{T}$, km	t_{ca}	Time of Last Data Point, GMT	Stations Used in Orbit	Data Types Used	Estimated Parameters
2 Post 44	7626.0869	-377.70226	7616.7277	$05^h17^m44^s.069$	$4/18\text{-}21^h31^m02^s$	DSS 42, 41, 51, 62, 12, 14	CC3	State Vector
2 Post 48	7415.5997	-540.24786	7395.8932	$05^h17^m58^s.148$	$4/18\text{-}21^h31^m02^s$	DSS 42, 41, 51, 62, 12, 14	CC3, PRU	State Vector
2 Post 50	7605.9919	-378.02251	7596.5918	$05^h17^m46^s.462$	$4/23\text{-}17^h35^m02^s$	DSS 42, 41, 51, 62, 12, 14	CC3	State Vector
2 Post 55	7583.8298	-368.51970	7574.8705	$05^h17^m50^s.382$	$4/30\text{-}14^h02^m02^s$	DSS 42, 41, 51, 62	CC3	State Vector
3 Post 2	7517.1291	-477.36714	7501.9564	$05^h19^m01^s.457$	$6/02\text{-}02^h16^m12^s$	DSS 41, 51, 62, 12	CC3	State Vector
3 Post 3	7552.1426	-428.35860	7539.9844	$05^h19^m04^s.285$	$6/02\text{-}02^h16^m12^s$	DSS 41, 51, 62	CC3	State Vector, Solar Pressure, Station Location
3 Post 5	7535.5111	-459.40841	7521.4936	$05^h19^m07^s.358$	$6/16\text{-}22^h01^m02^s$	DSS 41, 51, 62, 12	CC3	State Vector
3 Post 6	7585.9066	-378.59128	7576.4530	$05^h19^m07^s.910$	$6/16\text{-}22^h01^m02^s$	DSS 41, 51, 62, 12	CC3	State Vector, Solar Pressure, Station Location
3 Post 7	7543.2270	-476.64540	7528.1526	$05^h19^m11^s.255$	$6/23\text{-}00^h49^m02^s$	DSS 41, 51, 62, 12	CC3	State Vector
3 Post 8	7606.2994	-377.447761	7597.0754	$05^h19^m09^s.831$	$6/25\text{-}01^h35^m02^s$	DSS 41, 51, 62, 12	CC3	State Vector, Solar Pressure, Station Location
3 Post 9	7544.4506	-472.42847	7529.6442	$05^h19^m12^s.699$	$6/30\text{-}07^h33^m02^s$	DSS 42, 41, 51, 62, 12	CC3	State Vector
3 Post 10	7617.2135	-380.69839	7607.6940	$05^h19^m09^s.592$	$6/30\text{-}07^h53^m02^s$	DSS 42, 41, 51, 62, 12	CC3	State Vector, Solar Pressure, Station Location
3 Post 16	7617.8870	-400.86622	7607.3323	$05^h19^m08^s.174$	$7/07\text{-}14^h12^m02^s$	DSS 42, 14, 12, 62, 51, 41, 72	CC3	State Vector
3 Post 17	7628.0903	-367.87485	7619.2142	$05^h19^m05^s.517$	$7/07\text{-}14^h12^m02^s$	DSS 42, 41, 42, 72, 51, 12, 14	CC3	State Vector, Solar Pressure, Station Location

Table 2-18. Mariner VI Pre-Unlatch, Post-Unlatch, and Post-Magellanic Orbit Computations (cont'd)

Orbit ID	B, km	$\overline{B} \cdot \overline{R}$, km	$\overline{B} \cdot \overline{T}$, km	t_{ca}	Time of Last Data Point, GMT	Stations Used in Orbit	Data Types Used	Estimated Parameters
3 Post 19	7624.1379	-369.0434	7615.2008	$05^h19^m07^s.907$	$7/14\text{-}07^h49^m02^s$	DSS 41, 72, 51, 62, 12, 14	CC3	State Vector, Solar Pressure, Station Location
3 Post 22	7609.5196	-254.50233	7605.2623	$05^h19^m06^s.992$	$7/14\text{-}07^h49^m02^s$	DSS 41, 51, 62, 12, 14	CC3, PRU	State Vector
3 Post 30	7471.3125	-491.26776	7455.1431	$05^h19^m30^s.799$	$7/21\text{-}04^h50^m02^s$	DSS 11, 41, 51, 62, 12, 14	CC3	State Vector
3 Post 31	7603.5634	-370.44968	7594.5336	$05^h19^m02^s.151$	$7/21\text{-}04^h50^m02^s$	DSS 41, 72, 51, 62, 12, 14	CC3	State Vector, Solar Pressure, Station Location
3 Post 32	7600.2911	-383.62063	7590.6032	$05^h19^m03^s.640$	$7/21\text{-}04^h50^m02^s$	DSS 41, 72, 51, 62, 12, 14	CC3, PRU	State Vector, Solar Pressure, Station Location
3 Post 37	7583.7563	-318.64433	7577.0590	$05^h19^m00^s.631$	$7/23\text{-}16^h00^m02^s$	DSS 41, 72, 51, 62, 12, 14	CC3	State Vector, KM, Solar Pressure
3 Post 38	7579.3768	-321.75321	7572.5441	$05^h19^m04^s.035$	$7/23\text{-}16^h00^m02^s$	DSS 41, 72, 51, 62, 12, 14	CC3, PRU	State Vector, KM, Solar Pressure
3 Post 39	7593.1372	-381.63736	7583.5402	$05^h19^m01^s.713$	$7/23\text{-}16^h00^m02^s$	DSS 41, 72, 51, 62, 12, 14	CC3	State Vector, KM, Solar Pressure, Station Location
3 Post 46	7474.4644	-346.66963	7466.4204	$05^h18^m56^s.876$	$7/23\text{-}06^h31^m32^s$	DSS 14	PRU	State Vector
3 Post 47	7587.2651	-401.9796	7576.6089	$05^h19^m02^s.441$	$7/26\text{-}06^h21^m02^s$	DSS 41, 72, 51, 62, 12, 14	CC3, PRU	State Vector, KM, Solar Pressure, Station Location
3 Post 48	7592.8269	-385.52853	7583.0326	$05^h18^m59^s.990$	$7/26\text{-}06^h21^m02^s$	DSS 41, 72, 51, 62, 12, 14	CC3	State Vector, KM, Solar Pressure, Station Location
3 Post 49	7586.4945	-302.46619	7580.4625	$05^h18^m53^s.889$	$7/26\text{-}06^h21^m02^s$	DSS 41, 51, 62, 12, 14	CC3	State Vector, KM, Solar Pressure
3 Post 89	7599.913	-358.82755	7591.4371	$05^h18^m54^s.147$	$7/26\text{-}02^h30^m02^s$	DSS 41, 72, 51, 62, 12, 14	CC3	State Vector, MM, Solar Pressure, Station Location
3 Post 91	7574.7801	-320.2213	7568.0079	$05^h19^m03^s.754$	$7/26\text{-}02^h30^m02^s$	DSS 41, 72, 51, 62, 12, 14	CC3, PRU	State Vector, MM, Solar Pressure

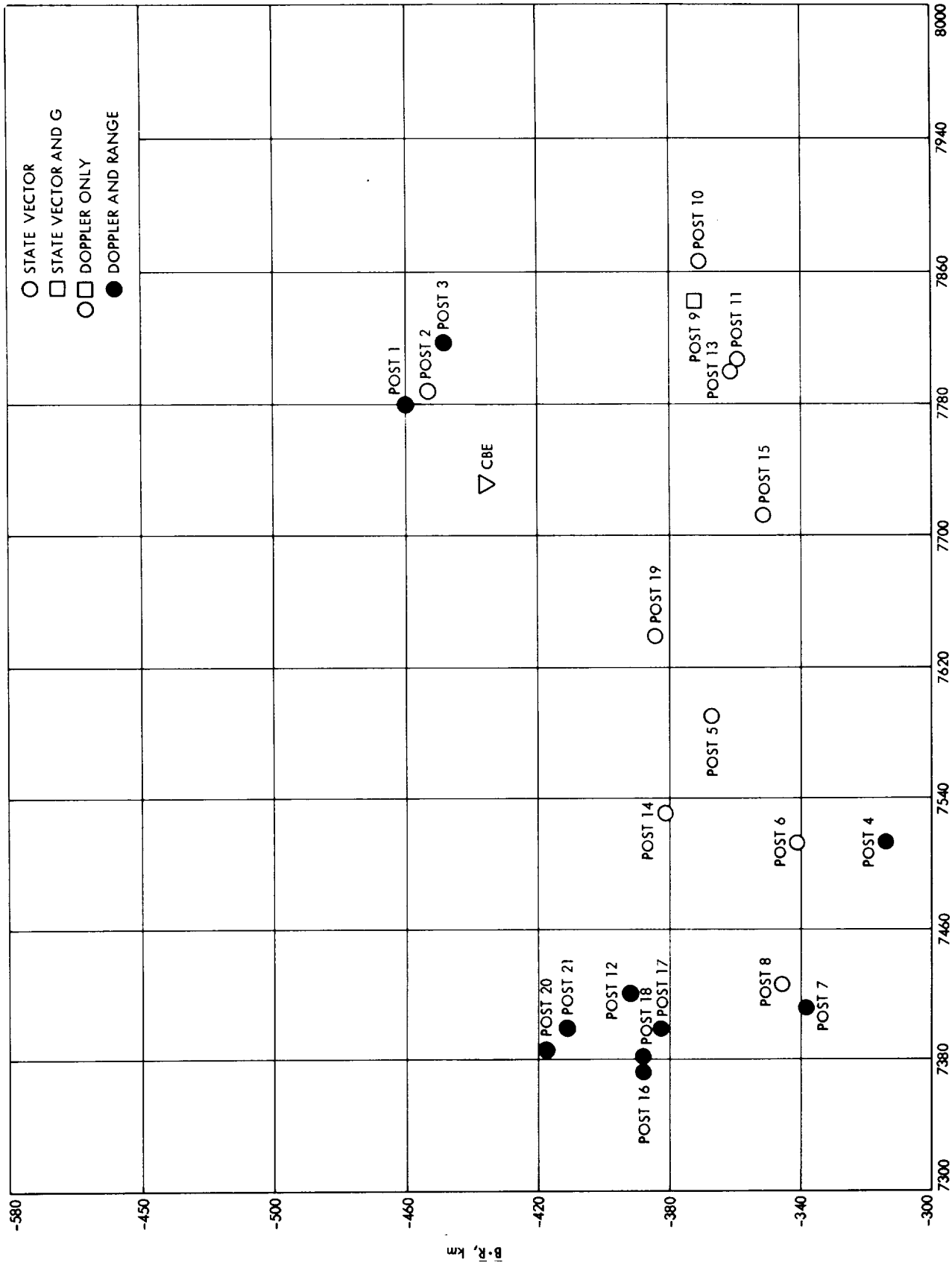

Figure 2-22. Mariner VI Post-Midcourse Orbit Estimates

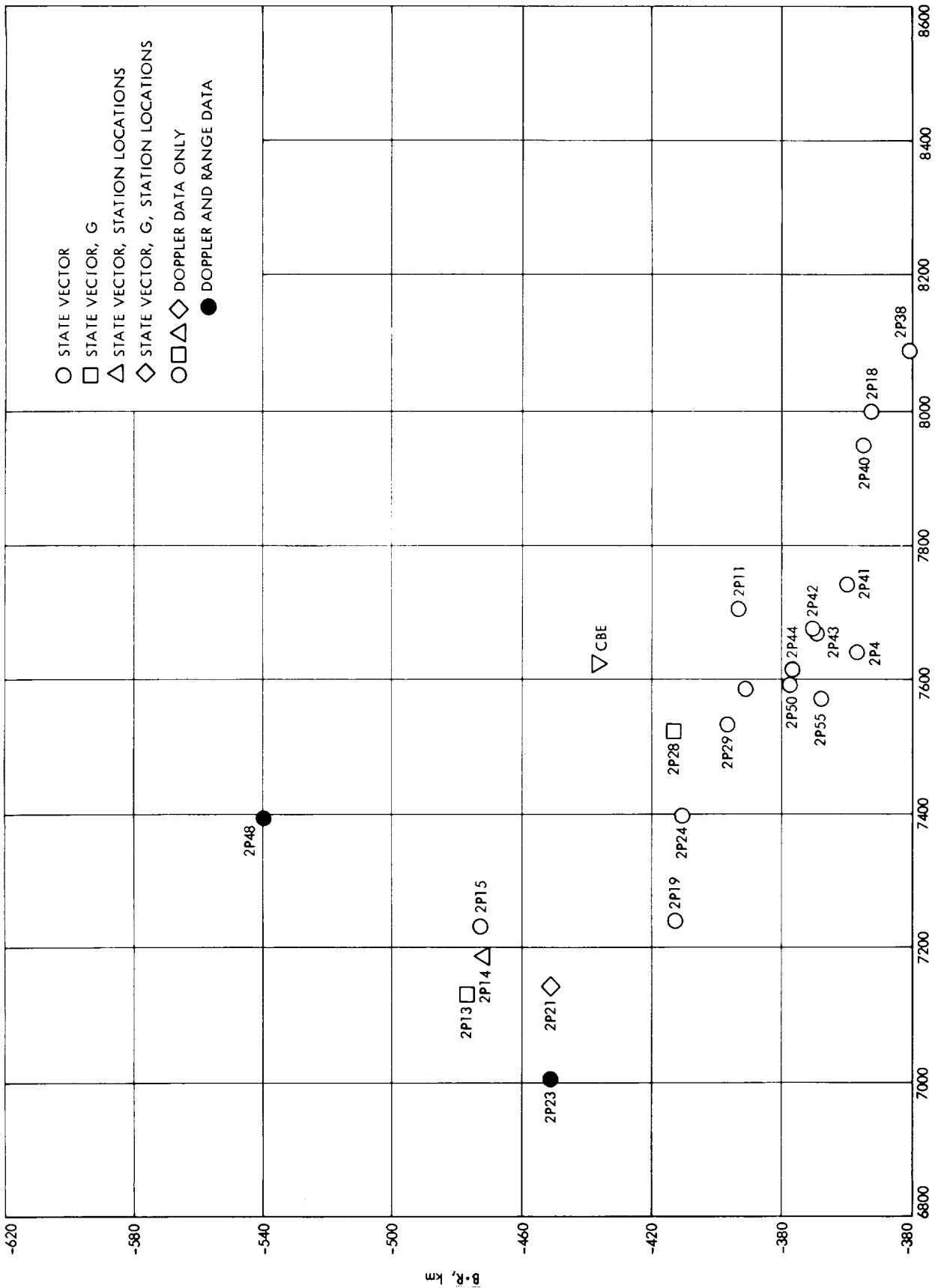

Figure 2-23. Mariner VI Post-Unlatch Orbit Estimates

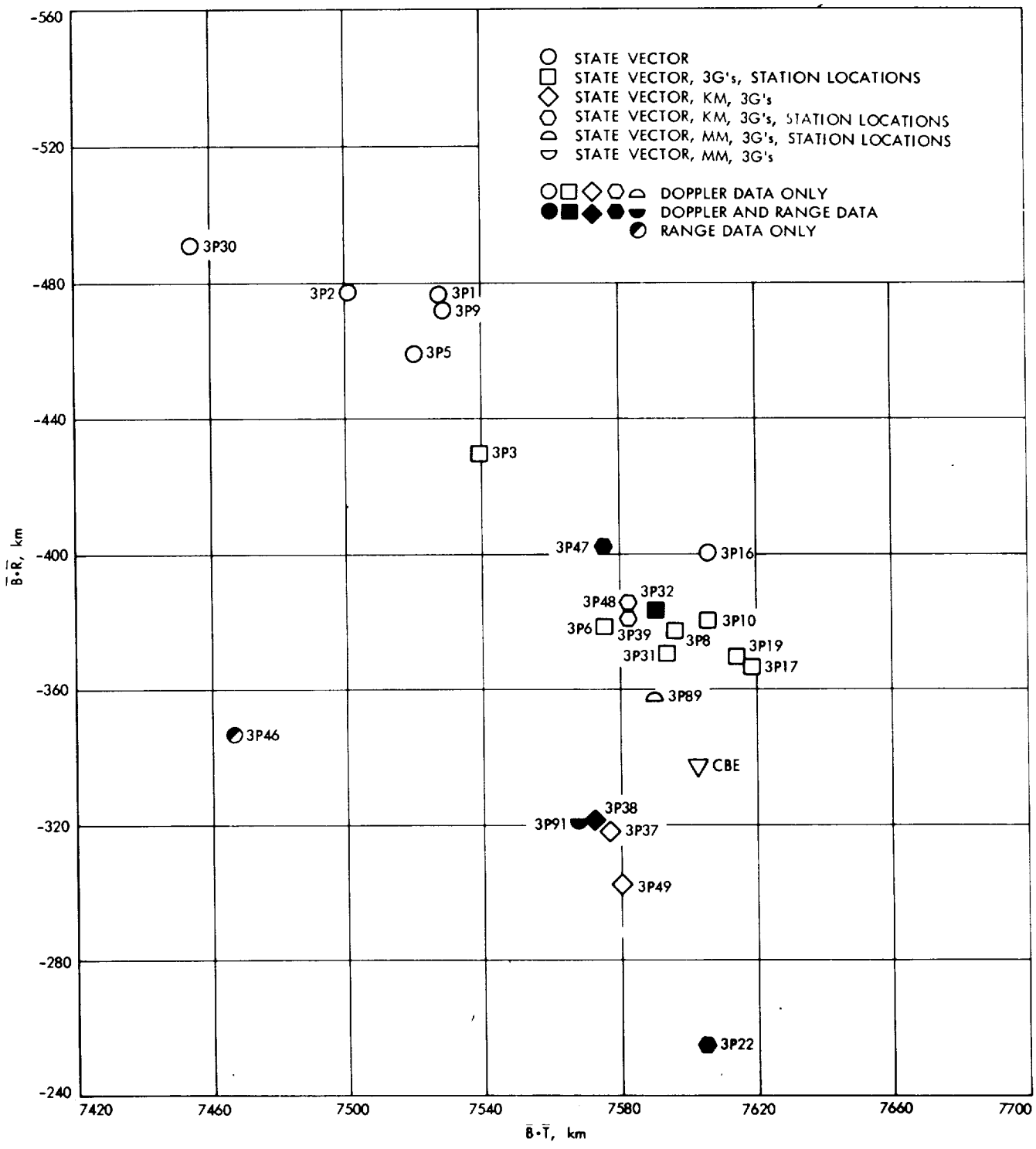

Figure 2-24. Mariner VI Post-Magellanic Cloud Orbit Estimates

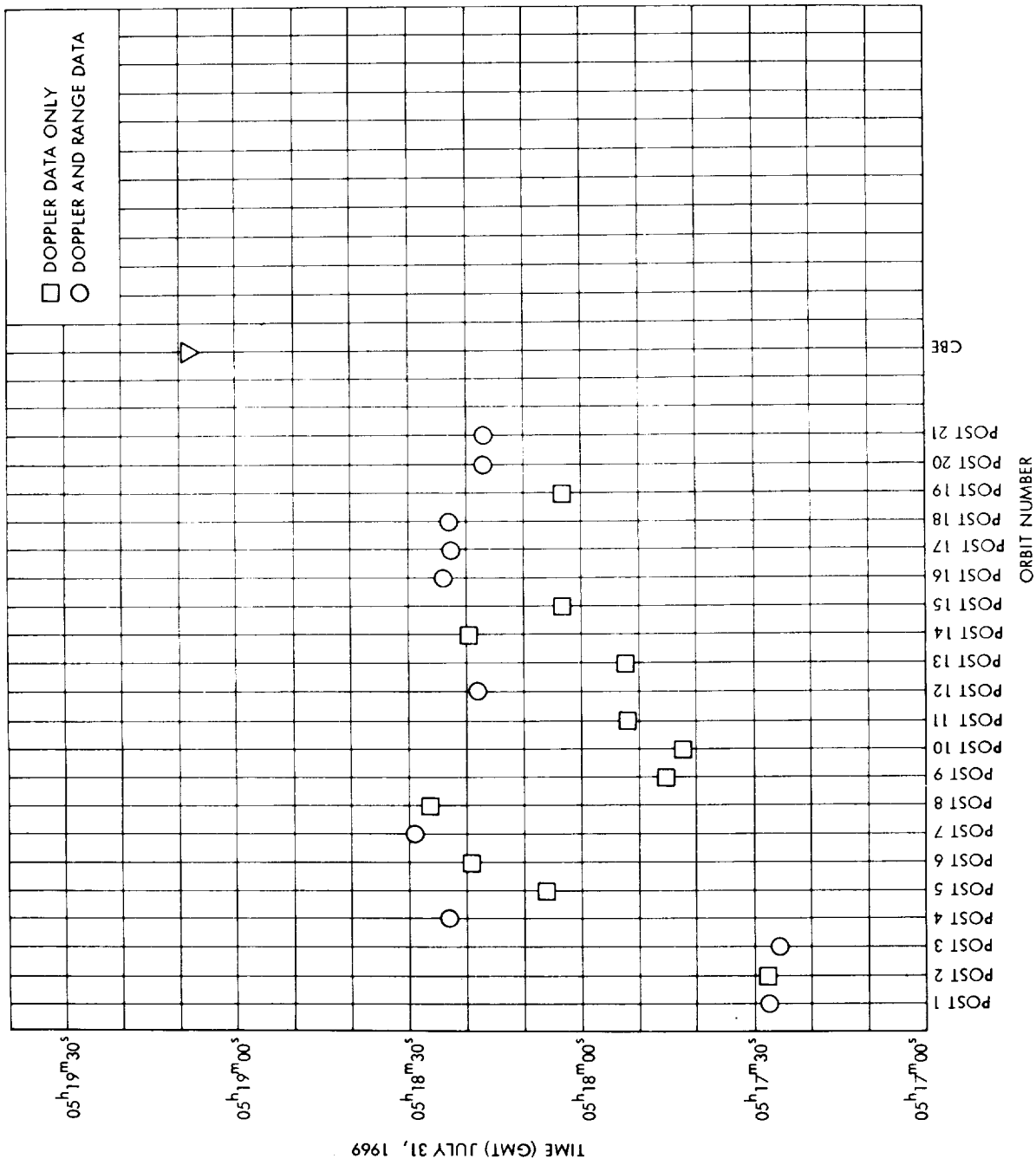

Figure 2-25. Mariner VI Post-Midcourse Time of Closest Approach

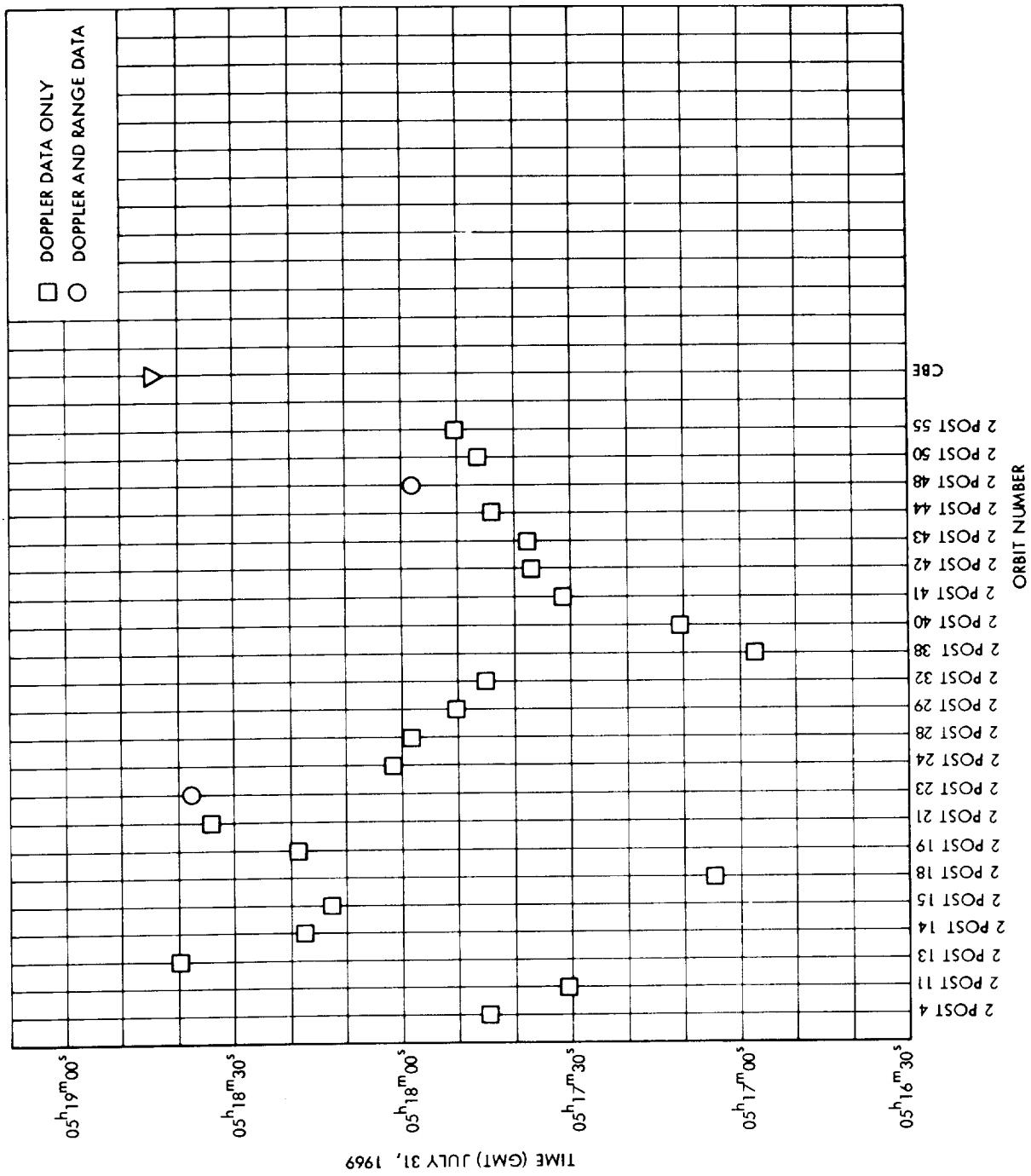

Figure 2-26. Mariner VI Post-Unlatch Time of Closest Approach

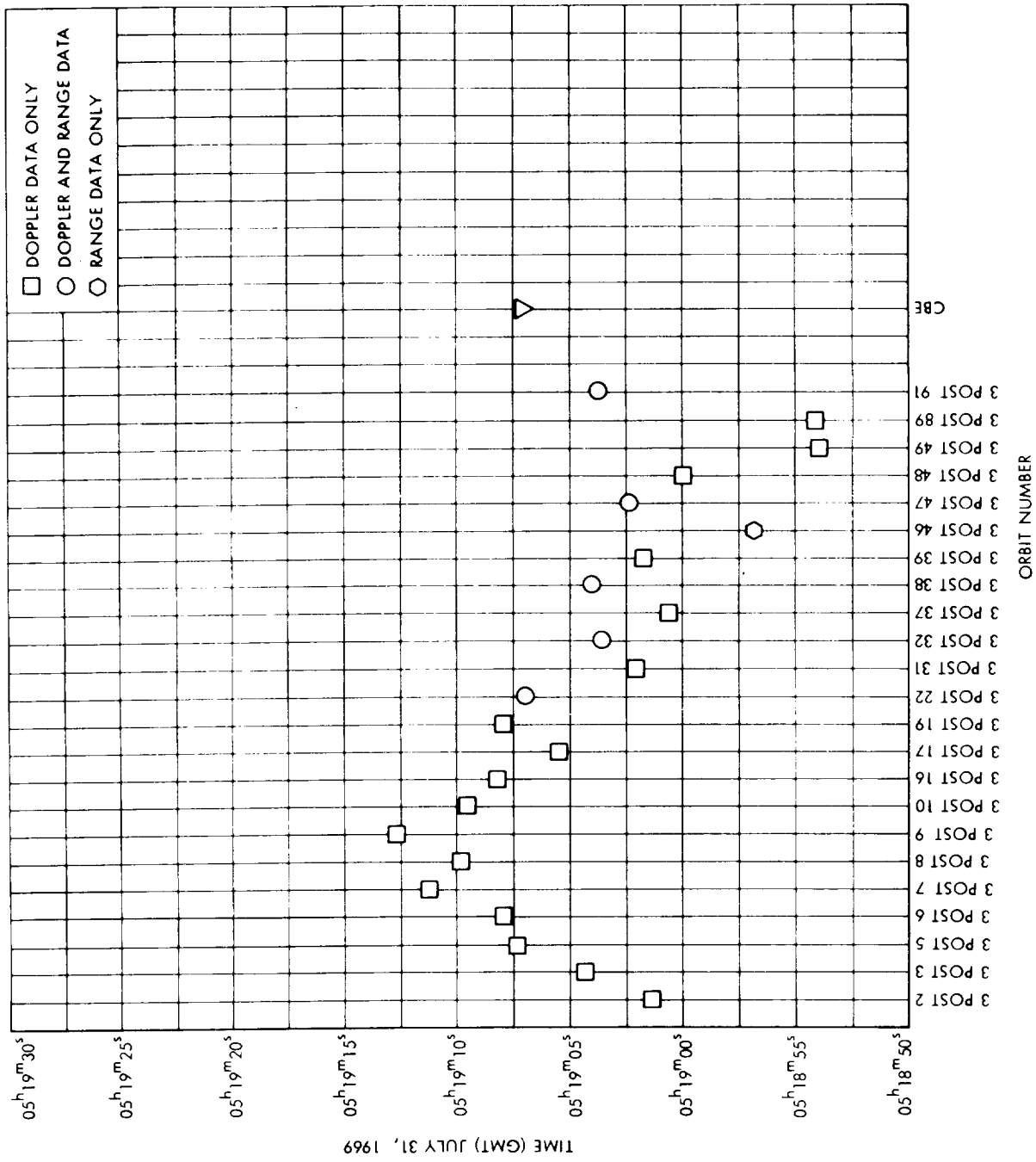

Figure 2-27. Mariner VI Post-Magellanic Cloud Time of Closest Approach

Orbit	CM1	CM3	CM2	CM4
Data Used	Doppler	Doppler	Doppler and Range	Doppler and Range
Parameters Estimated	State Vector Solar Pressure Coefficients	State Vector Solar Pressure Coefficients Station Locations	State Vector Solar Pressure Coefficients	State Vector Solar Pressure Coefficients Station Locations
B, km $\bar{B} \cdot \bar{R}$, km $\bar{B} \cdot \bar{T}$, km t_{ca}	7565 -331 7557 $05^h19^m11.^s263$	7572 -383 7562 $05^h19^m11.^s592$	7594 -290 7589 $05^h19^m06.^s893$	7591 -329 7584 $05^h19^m05.^s698$

The SPODP long-data-arc orbit solutions are given below:

Orbit	3 Post 49	3 Post 89	3 Post 91	3 Post 47
Data Used	Doppler	Doppler	Doppler and Range	Doppler and Range
Parameters Estimated	State Vector, 3 Components of Solar Pressure	State Vector, 3 Components of Solar Pressure, Station Locations	State Vector, 3 Components of Solar Pressure	State Vector, 3 Components of Solar Pressure, Station Locations
B, km $\bar{B} \cdot \bar{R}$, km $\bar{B} \cdot \bar{T}$, km t_{ca}	7586 -302 7580 $05^h18^m53.^s889$	7599 -359 7591 $05^h18^m54.^s147$	7575 -320 7568 $05^h19^m03.^s754$	7587 -402 7577 $05^h19^m02.^s441$

With the recommendation of the time of closest approach and the E - 5^d orbit solutions of SPODP and DPODP, the following orbit solution was recommended by the Orbit Determination Group to the MM'69 Project at E - 61 hours:

$$\bar{B} \cdot \bar{R} = -339 \text{ km}$$

$$\bar{B} \cdot \bar{T} = 7560 \text{ km}$$

$$t_{ca} = 05^h19^m05^s$$

A problem that occurred during early encounter operations was the change of phase from heliocentric phase to target center (aerocentric) phase. During this change of phase the data appeared to be noisy and biased. Orbits were computed ignoring the data obtained during change of phase. However, the confidence on the long-data-arc orbit solutions were somewhat lessened. Therefore, after this time, efforts by the SPODP were concentrated on the short-data-arc which has a data span with an epoch located after the change of phase.

At approximately 1 day before encounter, the following short-data-arc orbit solutions were computed:

Orbit	3 Post 106	3 Post 109	3 Post 105	3 Post 107
Data Used	Doppler	Doppler	Doppler and Range	Doppler and Range
Parameters Estimated	State Vector	State Vector Station Locations	State Vector	State Vector Station Locations
B, km $\bar{B} \cdot \bar{R}$, km $B \cdot T$, km t_{ca}	7482 -373 7473 $05^h19^m13^s.381$	7497 -404 7487 $05^h19^m12^s.131$	7598 -429 7586 $05^h19^m01^s.688$	7613 -398 7602 $05^h19^m03^s.396$

The short-data-arc orbit solutions computed using doppler and range data agreed quite well with long-data-arc solutions. However, the orbit solutions computed with doppler data only were about 100 km in $\bar{B} \cdot \bar{T}$ from the long-data-arc solutions and these solutions were still moving toward the long-data-arc solutions.

At approximately E - 3^h, the SPODP and DPODP short-data-arc orbit solutions were:

Orbit	SPODP	SPODP	DPODP	DPODP
Data Used	Doppler	Doppler	Doppler	Doppler and Range
Parameters Estimated	State Vector Mass Ratio of Mars to Sun	State Vector Mass Ratio of Mars to Sun Station Locations	State Vector Gravitational Constant of Mars	State Vector Gravitational Constant of Mars
$\bar{B} \cdot \bar{R}$, km $\bar{B} \cdot \bar{T}$, km t_{ca}	-364 7463 $05^h19^m09^s.476$	-371 7585 $05^h19^m07^s.272$	-385 7475 $05^h19^m08^s.81$	-298 7579 $05^h19^m06^s.30$

The DPODP orbit solution computed using ionospheric correlations to the tracking data was:

$$\bar{B} \cdot \bar{R} = -387 \text{ km}, \ \bar{B} \cdot \bar{T} = 7615 \text{ km}, \ t_{ca} = 05^h19^m06^s.2$$

From the above inputs (the short data arc and long data arc orbit solutions) the Orbit Determination Group recommended the following orbit to the MM'69 project for the final spacecraft platform update:

$$\bar{B} \cdot \bar{R} = -380 \text{ km}, \ \bar{B} \cdot \bar{T} = 7580 \text{ km}, \ t_{ca} = 05^h19^m06^s$$

The one sigma dispersion ellipse associated with this orbit was 100 km by 40 km with the semi-major axis approximately parallel to the R-axis in the B-plane.

The recommended solution was used as input to the Pegasis Program and when the platform clock angle was rounded off to an achievable value the orbit that was actually used for the final platform update was as follows:

$$\bar{B} \cdot \bar{R} = -350 \text{ km}, \ \bar{B} \cdot \bar{T} = 7560 \text{ km}, \ t_{ca} = 05^h19^m05^s$$

The numerical results of the encounter orbit computations are presented in Table 2-19. Figure 2-28 shows the B-plane estimates of the orbits computed during encounter. Figure 2-29 shows the time of closest approach of the encounter orbits.

Table 2-19. Mariner VI Post-Magellanic Orbit Computations

Orbit ID	B, km	$\overline{B} \cdot \overline{R}$, km	$\overline{B} \cdot \overline{T}$, km	t_{ca}*	Time of Last Data Point, GMT	Stations Used in Orbit	Data Types Used	Estimated Parameters
3 Post 53	7574.2687	-466.98688	7559.8590	$05^h18^m59^s.660$	$7/27\text{-}15^h03^m02^s$	DSS 41, 51, 62, 12, 14	CC3, PRU	State Vector, KM, Solar Pressure, Station Location
3 Post 54	7583.3042	-309.40463	7576.9895	$05^h18^m50^s.040$	$7/27\text{-}15^h03^m02^s$	DSS 41, 51, 62, 12, 14	CC3	State Vector, KM, Solar Pressure
3 Post 55	7584.7068	-366.35194	7575.8535	$05^h18^m54^s.566$	$7/27\text{-}15^h03^m02^s$	DSS 41, 51, 62, 12, 14	CC3	State Vector, KM, Solar Pressure, Station Location
3 Post 64	7580.1992	-434.60336	7567.7298	$05^h19^m01^s.082$	$7/27\text{-}15^h03^m02^s$	DSS 41, 51, 62, 12, 14	CC3, PRU	State Vector, KM, Solar Pressure, Station Location
3 Post 66	7591.4688	-378.99110	7582.0028	$05^h19^m00^s.736$	$7/27\text{-}15^h03^m02^s$	DSS 41, 51, 62, 12, 14	CC3	State Vector, KM, Solar Pressure, Station Location
3 Post 67	7588.6468	-315.74644	7582.0750	$05^h18^m52^s.905$	$7/27\text{-}15^h03^m02^s$	DSS 41, 51, 62, 12, 14	CC3	State Vector, KM, Solar Pressure
3 Post 69	7575.3787	-405.03638	7564.5425	$05^h19^m01^s.409$	$7/27\text{-}15^h03^m02^s$	DSS 51, 62, 12, 14	CC3, PRU	State Vector
3 Post 85	7550.4154	-346.01244	7542.4828	$05^h19^m00^s.398$	$7/28\text{-}20^h59^m02^s$	DSS 41, 51, 62, 12, 14	CC3, PRU	State Vector, KM, Solar Pressure
3 Post 86	7582.9349	-351.65693	7574.7762	$05^h19^m01^s.000$	$7/28\text{-}20^h59^m02^s$	DSS 41, 51, 62, 12, 14	CC3, PRU	State Vector
3 Post 87	7565.8782	-446.76131	7552.6758	$05^h18^m59^s.654$	$7/28\text{-}20^h59^m02^s$	DSS 41, 51, 62, 12, 14	CC3, PRU	State Vector, KM, Solar Pressure, Station Location
3 Post 88	7406.6729	-402.70448	7395.7167	$05^h19^m58^s.255$	$7/28\text{-}20^h59^m02^s$	DSS 41, 51, 62, 12, 14	CC3	State Vector
3 Post 90	7590.3538	-309.14269	7584.0557	$05^h18^m53^s.049$	$7/28\text{-}02^h30^m02^s$	DSS 41, 62, 12, 14	CC3	State Vector, MM, Solar Pressure
3 Post 92	7578.0047	-407.11572	7567.0610	$05^h19^m01^s.227$	$7/29\text{-}17^h50^m02^s$	DSS 41, 51, 62, 12, 14	CC3, PRU	State Vector
3 Post 93	7432.5854	-353.84335	7424.1573	$05^h19^m25^s.164$	$7/29\text{-}17^h50^m02^s$	DSS 41, 51, 62, 12, 14	CC3	State Vector

*The date of closest approach is July 31, 1969 for all solutions.

Table 2-19. Mariner VI Post-Magellanic Orbit Computations (cont'd)

Orbit ID	B, km	$\overline{B}\cdot\overline{R}$, km	$\overline{B}\cdot\overline{T}$, km	t_{ca}	Time of Last Data Point, GMT	Stations Used in Orbit	Data Types Used	Estimated Parameters
3 Post 94	7586.4957	-414.20109	7575.180	$05^h19^m01^s.547$	$7/29\text{-}17^h50^m02^s$	DSS 41, 51, 62, 12, 14	CC3, PRU	State Vector, Station Location
3 Post 95	7460.5489	-386.05775	7450.5533	$05^h19^m22^s.785$	$7/29\text{-}17^h50^m02^s$	DSS 14, 41, 51, 62, 12	CC3	State Vector, Station Location
3 Post 96	7564.0199	-345.93851	7556.1047	$05^h18^m41^s.033$	$7/29\text{-}17^h50^m02^s$	DSS 41, 51, 62, 12, 14	CC3	State Vector, MM, Solar Pressure, Station Location
3 Post 97	7570.8595	-331.182087	7563.584	$05^h18^m32^s.722$	$7/29\text{-}17^h50^m02^s$	DSS 41, 51, 62, 12, 14	CC3	State Vector, MM, Solar Pressure
3 Post 105	7597.7125	-428.56446	7585.6156	$05^h19^m01^s.688$	$7/30\text{-}01^h06^m02^s$	DSS 41, 51, 62, 12, 14	CC3, PRU	State Vector
3 Post 106	7482.9207	-373.06805	7472.9207	$05^h19^m13^s.381$	$7/30\text{-}01^h06^m02^s$	DSS 41, 51, 52, 12, 14	CC3	State Vector
3 Post 107	7612.6347	-398.4893	7602.1976	$05^h19^m03^s.396$	$7/30\text{-}01^h06^m02^s$	DSS 41, 51, 62, 12, 14	CC3	State Vector, Station Location
3 Post 108	7616.9150	-413.17172	7605.7005	$05^h19^m03^s.253$	$7/30\text{-}01^h06^m02^s$	DSS 41, 51, 62, 12, 14	CC3, PRU	State Vector, MM, Station Location
3 Post 109	7497.4719	-403.87088	7486.5860	$05^h19^m12^s.131$	$7/30\text{-}01^h06^m02^s$	DSS 41, 51, 62, 12, 14	CC3	State Vector, Station Location
3 Post 110	7551.0103	-347.61898	7543.0043	$05^h19^m01^s.417$	$7/30\text{-}01^h06^m02^s$	DSS 41, 51, 62, 12, 14	CC3, PRU	State Vector, KM, Solar Pressure
Enc 1	7656.9162	-337.28006	7649.4839	$05^h19^m07^s.664$	$7/30\text{-}15^h17^m02^s$	DSS 41, 51, 62, 12, 14	CC3, PRU	State Vector, MM
Enc 2	7494.8485	-371.36799	7485.6421	$05^h19^m10^s.551$	$7/30\text{-}15^h17^m02^s$	DSS 41, 51, 62, 12, 14	CC3	State Vector, MM, Station Location
Enc 3	7616.1762	-289.02332	7610.6901	$05^h19^m06^s.452$	$7/30\text{-}15^h17^m02^s$	DSS 41, 51, 62, 12, 14	CC3, PRU	State Vector, MM, Station Location
Enc 4	7465.4401	-372.70959	7456.1304	$05^h19^m11^s.298$	$7/30\text{-}15^h17^m02^s$	DSS 41, 51, 62, 12, 14	CC3	State Vector, MM
Enc 14	7603.2390	-261.92297	7598.7259	$05^h19^m06^s.400$	$7/30\text{-}18^h09^m02^s$	DSS 41, 51, 62, 12, 14	CC3, PRU	State Vector, MM, Station Location

Table 2-19. Mariner VI Post-Magellanic Orbit Computations (cont'd)

Orbit ID	B, km	$\overline{B}\cdot\overline{R}$, km	$\overline{B}\cdot\overline{T}$, km	t_{ca}	Time of Last Data Point, GMT	Stations Used in Orbit	Data Types Used	Estimated Parameters
Enc 15	7530.5783	-374.79631	7521.2456	$05^h19^m09^s.126$	$7/30\text{-}18^h09^m02^s$	DSS 41, 51, 62, 12, 14	CC3	State Vector, MM, Station Location
Enc 17	7627.6784	-315.56244	7621.1479	$05^h19^m06^s.552$	$7/30\text{-}21^h55^m02^s$	DSS 41, 51, 62, 12, 14	CC3, PRU	State Vector, MM
Enc 18	7594.4701	-248.91543	7590.8901	$05^h19^m06^s.200$	$7/30\text{-}21^h55^m02^s$	DSS 41, 51, 62, 12, 14	CC3, PRU	State Vector, MM, Station Location
Enc 19	7467.7610	-380.160	7458.0782	$05^h19^m09^s.609$	$7/30\text{-}21^h55^m02^s$	DSS 41, 51, 62, 12, 14	CC3	State Vector, MM
Enc 20	7559.3544	-323.65788	7552.4221	$05^h19^m07^s.683$	$7/30\text{-}21^h55^m02^s$	DSS 51, 41, 62, 12, 14	CC3	State Vector, MM, Solar Pressure, Station Location
Enc 21	7539.5023	-389.53211	7529.4328	$05^h19^m08^s.689$	$7/30\text{-}21^h55^m02^s$	DSS 41, 51, 62, 12, 14	CC3	State Vector, MM, Station Location
Enc 26	7471.989	-363.78475	7463.1278	$05^h19^m09^s.476$	$7/31\text{-}01^h05^m02^s$	DSS 41, 51, 62, 12, 14	CC3	State Vector, MM
Enc 28	7569.1796	-373.1961	7559.9737	$05^h19^m07^s.359$	$7/31\text{-}01^h05^m02^s$	DSS 41, 62, 12, 14	CC3	State Vector, MM, Station Location
Enc 29	7565.739	-346.90921	7557.7813	$05^h19^m07^s.673$	$7/30\text{-}22^h56^m32^s$	DSS 41, 51, 62, 12, 14	CC3	State Vector, MM
Enc 30	7584.8663	-339.77107	7577.2522	$05^h19^m07^s.094$	$7/30\text{-}23^h44^m02^s$	DSS 51, 62, 12, 14	CC3	State Vector, MM, Station Location
Enc 31	7594.0646	-371.27483	7584.9833	$05^h19^m07^s.272$	$7/31\text{-}01^h52^m32^s$	DSS 41, 51, 62, 12, 14	CC3	State Vector, MM, Station Location

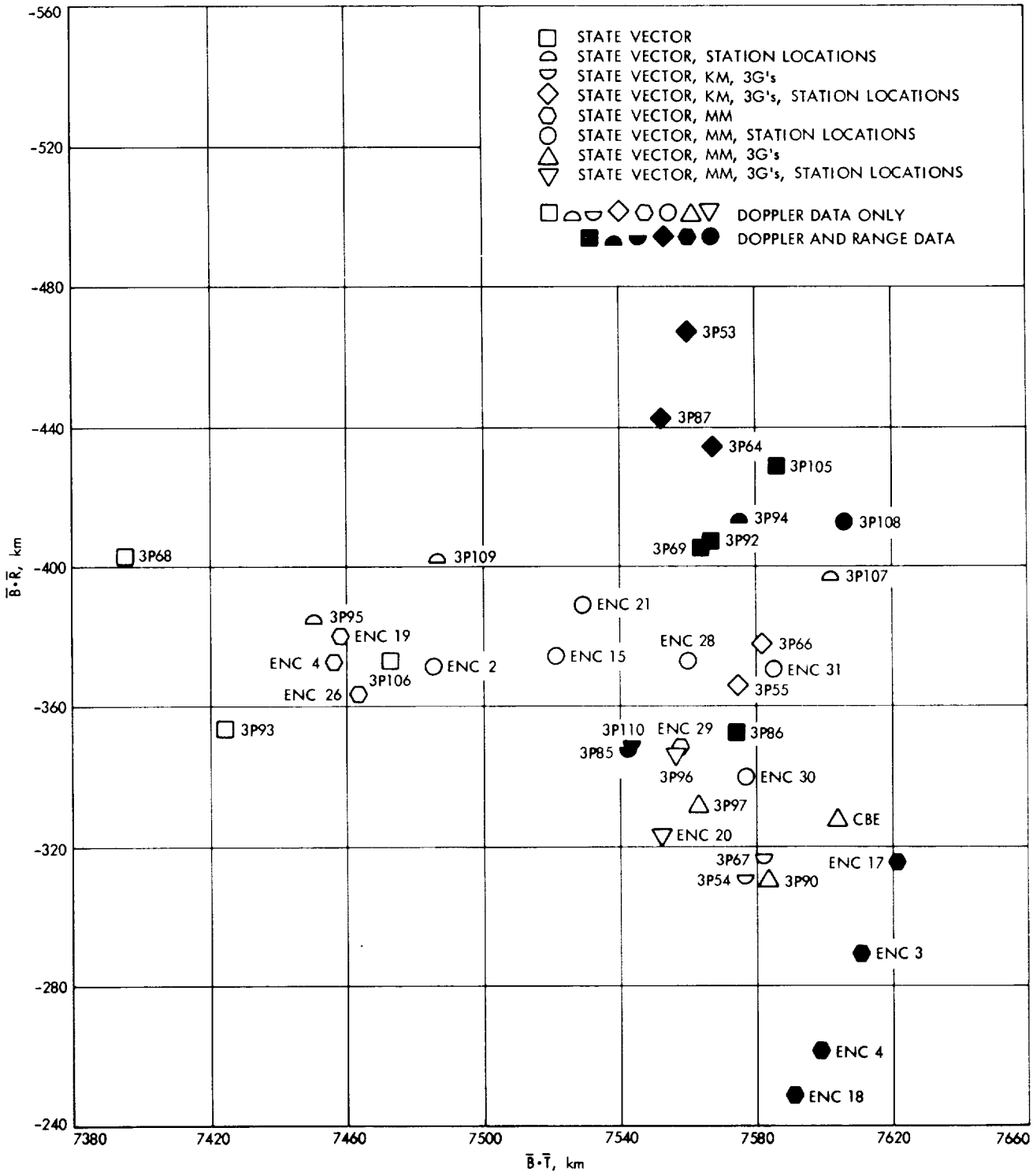

Figure 2-28. Mariner VI Encounter Orbits

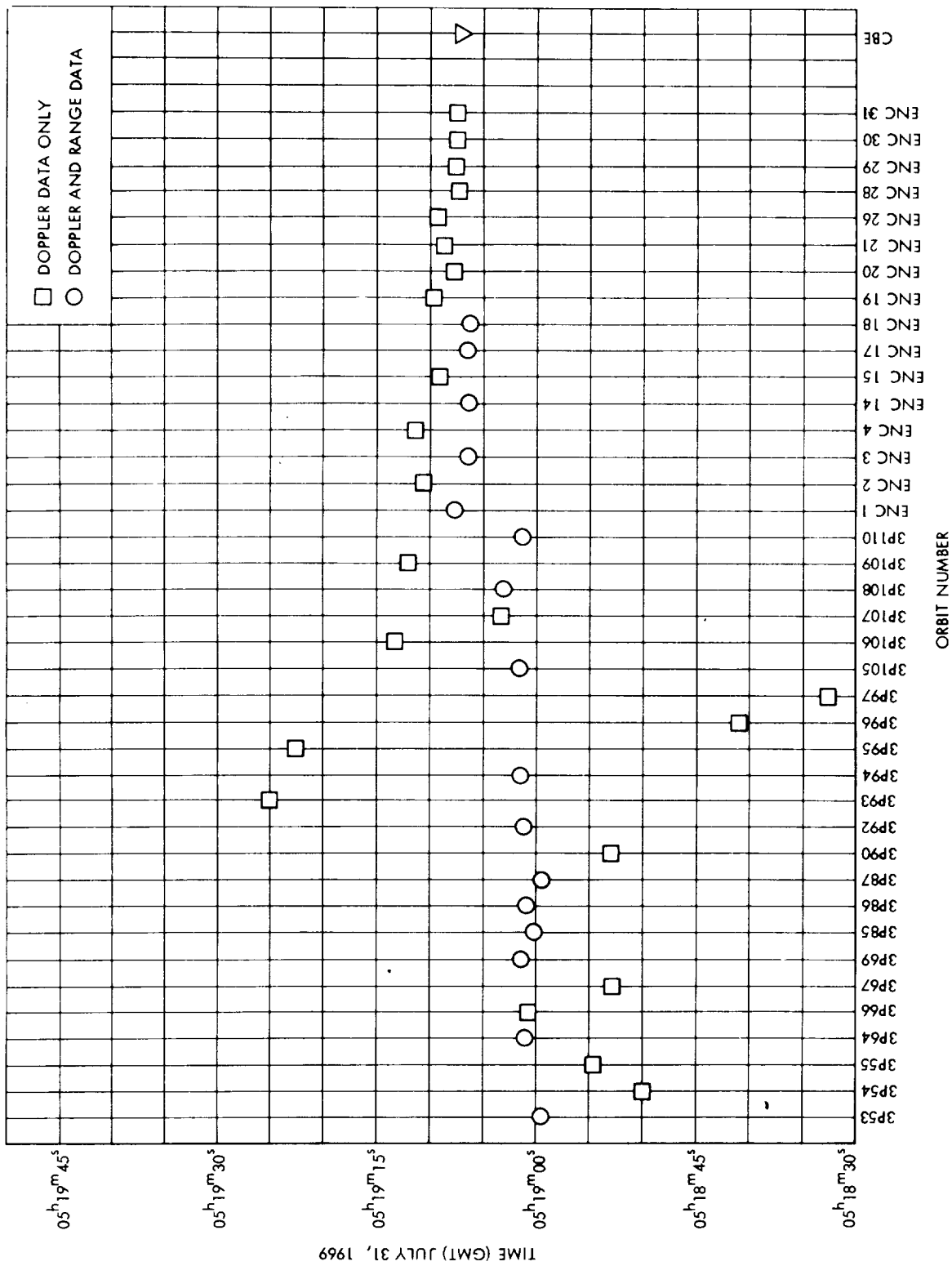

Figure 2-29. Mariner VI Encounter Orbits Time of Closest Approach

- Analysis — *J. W. Zielenbach*

1) Time of Closest Approach (t_{ca})

The plan recommended an orbit based on doppler and range data. For safety's sake, if there were any suspicious behavior when all the ranging were included the prediction would be based on an orbit with one point, or at most one pass of ranging, taken as close to E - 61 hr as possible.

The t_{ca} portion of Figure 2-30 shows that for at least 3 weeks before encounter, the DPODP long arc predictions based on Doppler and ranging vary less than 2 sec from the final post flight value. If one excludes the multi-pass range solutions after July 25, there is less than 0.5 sec variation from the final value in the predicted time of closest approach. The long arc predictions based on Doppler alone, obtained only for comparison, were consistently from 5 to 11 sec too late.

The short arc portion of the graph shows the 15 sec discordance between the Doppler-only and Doppler-and-range predictions at E - 64 hr. The solutions converge thereafter, but not sufficiently to be of use for controlling the shuttering sequence at E - 61 hr. It is interesting to note that even with ranging, the solution at E - 64 hr was 6 sec off.

The behavior after July 25 will be explained below.

Based on the data plotted before July 25, and the single ranging pass solution, the DPODP group recommended a closest approach time of $05^h19^m05^s.4$ at E - 61 hr.

2) B-plane Parameters

The plans called for a comparison of long and short arc runs using Doppler by itself and Doppler with ranging. Figure 30 displays the DPODP solutions considered for the inflight prediction of B-plane positions.

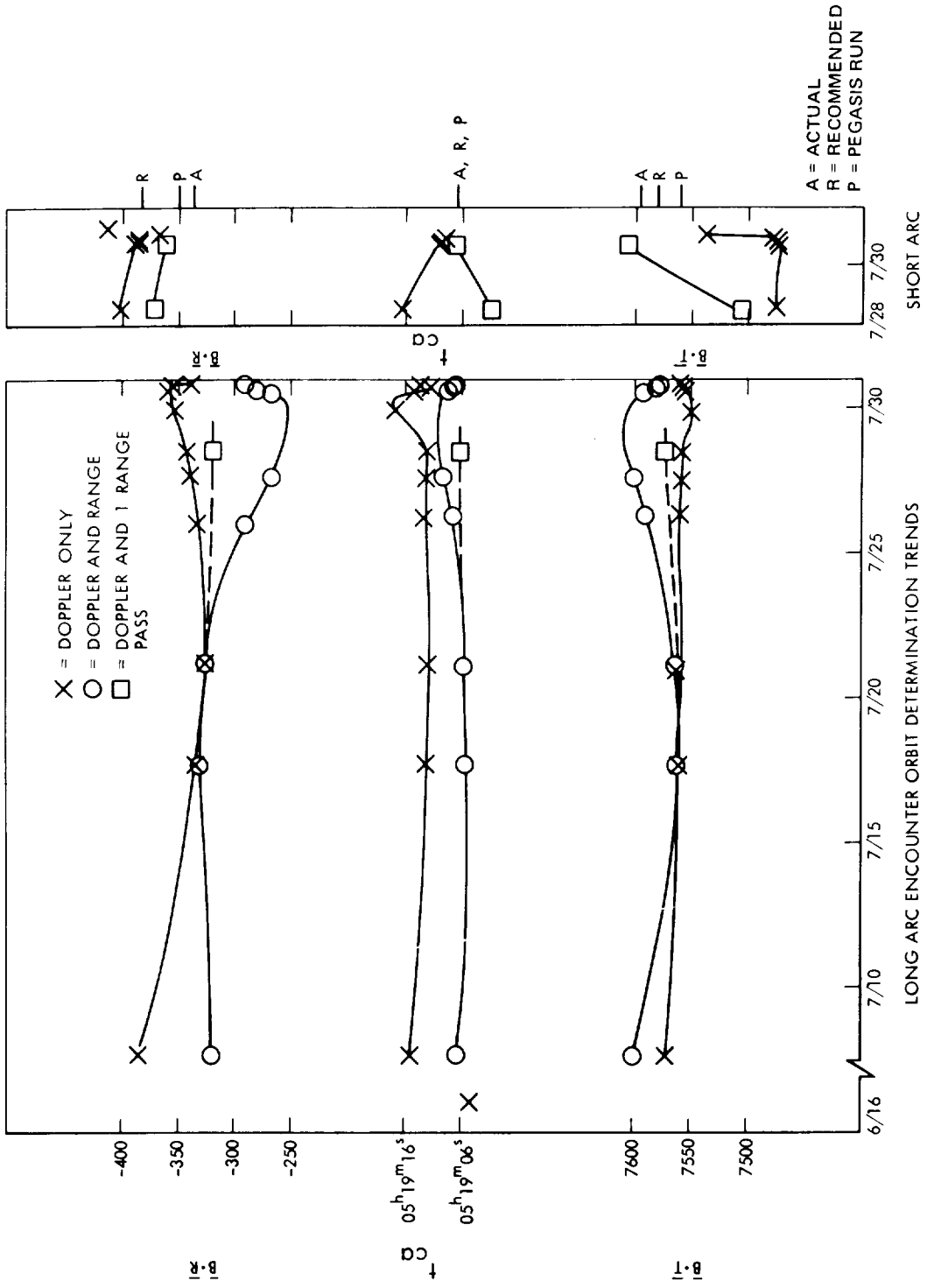

Figure 2-30. Mariner VI Encounter Orbit Determination Trends

Long Arc Results

The long arc solutions using Doppler-only vs Doppler and range differ by no more than 100 km in $\overline{B} \cdot \overline{R}$ and 50 km in $\overline{B} \cdot \overline{T}$ for at least 6 weeks before encounter. All solutions were within 70 km of the final value in $\overline{B} \cdot \overline{R}$ and 40 km in $\overline{B} \cdot \overline{T}$ throughout the same period. The last long arc Doppler only solution (at E - 7 hr), was in error by only 5 km in $\overline{B} \cdot \overline{R}$ and 35 km in $\overline{B} \cdot \overline{T}$. The final solution with ranging (at E - 7 hr) erred by 45 km in $\overline{B} \cdot \overline{R}$ and 20 km in $\overline{B} \cdot \overline{T}$.

The largest difference between the long arc solutions using the two data sets occurred during the last 5 days before encounter. The solutions with ranging took the larger excursions from the true values. This was due to an inaccurate computation of the trajectory which resulted from an inappropriate choice of parameters input to the automatic stepsize control for the numerical integrator. The truncation error rose from less than 1 m to over 50 m between July 17 and July 27. Because the effective weight of each ranging pass was comparable to that of a single point with a standard deviation of 2 m, and there was ranging before and after this error appeared, an inconsistency developed between the numerical model and the physical universe. The error finally affected the Doppler-only solutions about E - 2 days. By this time the accumulated range error had increased to more than 100 m.

During this period a solution was made using a single ranging pass, marked as a square □ . This was the conservative approach recommended for incorporating ranging and achieved the full benefit of the ranging without any desirable side effects.

Short Arc Results

The DPODP short arc solutions were all within 80 km of the final value in $\overline{B} \cdot \overline{R}$ and 150 km in $\overline{B} \cdot \overline{T}$. The final solution

without ranging erred by 80 km in $\overline{B} \cdot \overline{R}$ and 60 km in $\overline{B} \cdot \overline{T}$. The final doppler and ranging prediction (E - 7 hr) was in error by 25 km in $\overline{B} \cdot \overline{R}$ and 10 km in $\overline{B} \cdot \overline{T}$. It is interesting to note that the short arc doppler only $\overline{B} \cdot \overline{T}$ solution changed more than 70 km in the period between E - 7 hr and E - 4 hr. (The final doppler solution plotted solved for station locations.)

On the basis of the long and short-arc-solutions discussed here, a preliminary prediction of $\overline{B} \cdot \overline{R} = -340$ km and $\overline{B} \cdot \overline{T} = 7600$ km was prepared.

Recommended Values

The plans allowed freedom in use of results on ionospheric calibrations. All the evidence available up to E - 4 hr indicated that the probable effect of neglecting the ionosphere was an estimate 60 km too high (positive) in $\overline{B} \cdot \overline{R}$. Engineering judgment was applied to this figure after reexamination of the trends in Figure 2-30 and the final recommendation became:

$\overline{B} \cdot \overline{R} = -380$ km

$\overline{B} \cdot \overline{T} = 7580$ km

$t_{ca} = 05^h 19^m 06^s$

d. Mariner VI Postflight Orbit Determination Analysis — *S. K. Wong, S. J. Reinbold*

- Introduction

The purpose of this subsection is to present the best estimate of the Mariner VI Flight Path and other significant results obtained from analysis of the DSS tracking data. The analysis verified that premidcourse and encounter inflight orbit solutions were within the Mariner Project orbit determination accuracy requirements. For the postflight orbital computations and analysis, only two-way doppler and planetary range data were used. The Double Precision Orbit Determination Program was the principle analysis tool used for this postflight orbit determination study.

The tracking data was divided into four logical blocks:

1) Premidcourse maneuver data was taken between transfer orbit injection and attitude maneuver prior to midcourse thrust.

2) Pre-unlatch data was taken between the midcourse maneuver and the unlatching of the scan platform.

3) Post-unlatch data was taken between the unlatching of the platform and the attempted Magellanic Cloud acquisition.

4) Encounter data was taken from encounter minus 5 days to encounter plus 5 days.

All the known bad data points were removed by the Orbit Data Generator Program (ODG) before the start of the postflight analysis. The postflight solution differs from the inflight DPODP solutions in the following manner:

1) The tracking data in the early portion of the Mariner '69 mission was processed through the Single Precision ODG; whereas in postflight these data were processed through the Double Precision ODG.

2) In postflight a nominal value for G_B* of 0.31925 was input in the pre-midcourse and pre-unlatch phases of orbit computations. A value of 0.310 was input as a nominal value for G_B in the post-unlatch and encounter phases of orbit solutions. The nominal value used for inflight solutions was 0.34423. This is significant because the premidcourse and pre-unlatch phase data have very little information on the value of G_B. Therefore the actual G_B value that was used in orbit computation was very close to the nominal input value. The G_B values of 0.31925 and 0.310 were obtained from the inflight results from the data which have information on G_B.

3) In postflight the orbit analysis can be more detailed than the analysis performed inflight.

---

*G_B is the solar reflectivity coefficient along the Sun to spacecraft direction.

In the postflight studies a number of solutions from each phase were examined. Solutions estimated different sets of parameters and used different combinations of *a priori* for the estimated parameters. The solution that showed the best data fit was declared the current best estimate of the orbit for that phase and this solution is presented in the following sections for each phase of the mission.

- Premidcourse Maneuver Orbit Estimate

The inflight midcourse orbit (NOMA 2XK) which was used for midcourse maneuver computation estimated only the state vector. Examining the observed minus computed (O - C) residual plots of the NOMA 2XK solution, the data fit indicated that some small perturbation probably was not accounted for. It was suspected that the perturbation was due to an acceleration caused by the solar pressure on the high gain antenna. The current best estimate of the premidcourse orbit was computed postflight using only two-way doppler data. This solution estimated the state vector, the three components of solar pressure, the gravitational constant of the Earth, and station location parameters. This solution showed a significant improvement in data fit and when it was mapped to target, it indicated the following results:

$$B = 13558.5 \text{ km}$$

$$\bar{B} \cdot \bar{R} = -13088.7 \text{ km}$$

$$\bar{B} \cdot \bar{T} = 3538.4 \text{ km}$$

$$t_{ca} = \text{July } 31\ 04^{h}41^{m}50.^{s}327$$

The current best estimate of the premidcourse orbit solution is given in Table 2-20. The B-plane estimates of the two solutions and the difference between the solutions are given in Table 2-21.

- Pre-Unlatch Orbit Estimates

The inflight results indicated inconsistent B-plane estimates between orbit solutions computed using doppler data only and the solutions computed using doppler and range data. The range data included Mark 1A ranging and planetary ranging data. The difference in $\bar{B} \cdot \bar{T}$ between the two solutions was approximately 200 km. The current best estimate of the pre-unlatch orbit was

Table 2-20. Mariner VI Pre-midcourse Parameter Solution

Parameters	*A priori* Value	*A priori* Statistics, 1σ	CBE	CBE Statistics, 1σ
X(km)	-61251.33398	10000.0	-61251.76268	0.649883
Y(km)	-96329.52441	10000.0	-96329.69280	0.735315
Z(km)	-106262.1455	10000.0	-106262.5245	0.720146
DX(km/sec)	-1.186937898	1.0	-1.186940970	0.654348×10^{-5}
DY(km/sec)	-2.758124083	1.0	-2.758119643	0.547100×10^{-5}
DZ(km/sec)	-2.690982878	1.0	-2.690982230	0.508885×10^{-5}
GR	1.31925	0.03	1.319887900	0.029988
GX	0	0.05	-0.048173428	0.034347
GY	0	0.05	-0.035089870	0.042086
GM Earth (km^3/sec^2)	398601.20	1.0	398601.4350	0.98315
DSS 41				
R_s(km)	5450.19860	0.008	5450.201991	0.006383
λ(deg)	136.887507	0.00010	136.887532	0.0000661
DSS 51				
R_s(km)	5742.9417	0.008	5742.93953	0.006544
λ(deg)	27.685432	0.00010	27.6854219	0.0000670
DSS 12				
R_s(km)	5212.0535	0.008	5212.052368	0.007759
λ (deg)	243.194559	0.00010	243.194543	0.0000721

Table 2-21. Mariner VI Pre-midcourse B-plane Estimates

	B km	$\bar{B} \cdot \bar{R}$ km	$\bar{B} \cdot \bar{T}$ km	t_{ca} (July 31, 1969, GMT)
Inflight Solution (Solution used for Maneuver computation)	13407.0	-12909.1	3619.95	$04^h40^m14^s.379$
Current Best Solution (Postflight)	13558.5	-13088.7	3538.4	$04^h41^m50^s.327$
Δ Inflight - CBE	-151.5	179.6	81.55	-95.948 sec

computed using doppler and planetary range data. This solution estimated the state vector, the three components of solar pressure, and station location parameters. When it was mapped to target, it indicated the following results:

$B = 7745.2$ km

$\bar{B} \cdot \bar{R} = -436.34$ km

$\bar{B} \cdot \bar{T} = 7732.90$ km

$t_{ca} =$ July 31 $05^h19^m08^s.683$

The postflight doppler only solution agreed extremely well with the current best solution. The *a priori* input values and 1σ statistics are given in Table 2-22 along with the current best estimate of pre-unlatch orbit solution.

- Evaluation of Midcourse Maneuver Based on DSIF Tracking Data

The evaluation of the midcourse maneuver based on DSIF tracking data was done by taking the current best estimate of the premidcourse orbit and mapping the state vector of this orbit to an epoch just after the midcourse maneuver. This mapped forward state vector was subtracted from the state vector of the current best estimate of the pre-unlatch orbit at the same epoch. The results of this comparison are given in the following table:

	ΔDX m/sec	ΔDY m/sec	ΔDZ m/sec	ΔV m/sec
OD Estimate*	-0.57138	+2.3647	-1.9969	3.1474
Commanded Maneuver**	-0.54048	+2.3053	-1.9507	3.0679
Maneuver Error***	+0.03090	-0.0594	+0.0462	-0.0813

*OD Estimate = Current best pre-unlatch estimate minus current best premaneuver estimate mapped to the pre-unlatch epoch.

**Commanded Maneuver = Midcourse velocity increment computed by the Manuever Group based on NOMA 2XK orbit.

***Maneuver Error = Commanded maneuver minus OD estimates.

Table 2-22. Mariner VI Pre-Unlatch Parameter Solution

Parameters	*A priori* Value	*A priori* Statistics, 1σ	CBE	CBE Statistics, 1σ
X (km)	-376348.8164	1,000.0	-376359.5533	2.2768
Y (km)	-856430.8672	1,000.0	-856459.3172	1.5900
Z (km)	-840356.9531	1,000.0	-840384.1263	1.6519
DX (km/sec)	-0.9733621627	0.001	-0.973360595	0.10383×10^{-4}
DY (km/sec)	-2.3654279113	0.001	-2.365423033	0.697065×10^{-5}
DZ (km/sec)	-2.283865690	0.001	-2.283870054	0.623579×10^{-5}
GR	1.319250	0.03	1.31886173	0.02984
GX	0	0.05	-0.03734427	0.031603
GY	0	0.05	-0.02867134	0.040392
DSS 41				
R_s (km)	5450.19860	0.010	5450.20424	0.007093
λ (deg)	136.887507	0.00010	136.887537	0.0000624
DSS 51				
R_s (km)	5742.94170	0.010	5742.93961	0.007373
λ (deg)	27.685432	0.00010	27.68542321	0.0000624
DSS 12				
R_s (km)	5212.0535	0.010	5212.0499	0.008753
λ (deg)	243.194559	0.00010	243.194538	0.0000644
DSS 14				
R_s (km)	5203.99890	0.010	5203.9989	0.009999
λ (deg)	243.110513	0.00010	243.110513	0.0000999

The effect of these errors when mapped to the target may be seen in the following table:

	$\Delta\bar{B} \cdot \bar{R}$, km	$\Delta\bar{B} \cdot \bar{T}$, km	Δt_{ca}, sec
Overall Error*	207	281	79
OD Error**	-180	-82	96
Maneuver Error***	387	363	-17

*Overall Errors = Current best estimate of pre-unlatch orbit minus maneuver aiming point.

**OD Errors = Current best premaneuver estimate minus orbit used for maneuver computation.

***Manuever Errors = Overall errors minus OD errors.

The evaluation of midcourse maneuver was performed assuming that the current best estimate of the spacecraft orbit is exact.

- Post-Unlatch Orbit Estimates

The inflight results indicated that this phase required a much longer time for the orbit to converge. An explanation for this is the placement of the epoch and the lack of continuous tracking data near epoch. Another cause for the orbit convergence problem at this time is that the SPODP did not have the capability to estimate the solar reflectivity coefficients which were not along the Sun-spacecraft direction until some time later inflight. To demonstrate the orbit convergence problem the inflight post-unlatch orbits with five days, 18 days, and 43 days of intermittent tracking data are given below:

Inflight Post-Unlatch Solution

Days of Intermittent Tracking Data	$\bar{B} \cdot \bar{R}$ km	$\bar{B} \cdot \bar{T}$ km	t_{ca} (July 31, 1969, GMT)
5 days	-348	8340	$05^h16^m27^s.106$
18 days	-344	8022	$05^h17^m05^s.492$
43 days	-377	7598	$05^h17^m46^s.390$

The above solution estimated only the state vector and were computed using doppler data only.

To show the effect of the solar reflectivity coefficients on orbit computation, post-unlatch orbits were computed with 5 days, 10 days, 15 days and 20 days of intermittent tracking data in postflight. The solutions estimated the state vector, solar reflectivity coefficients, gravitational constant of the Moon, and station location parameters, The solutions are given below:

Postflight Post-Unlatch Solution

Days of Intermittent Tracking Data	B km	$\overline{B} \cdot \overline{R}$ km	$\overline{B} \cdot \overline{T}$ km	t_{ca} (July 31, 1969, GMT)
5 days	7648.23	-379.44	7638.81	$05^h18^m05^s.145$
10 days	7646.18	-372.42	7637.11	$05^h18^m25^s.933$
15 days	7560.66	-434.66	7548.16	$05^h19^m06^s.140$
20 days	7576.89	-434.56	7564.42	$05^h19^m04^s.472$

The orbit solutions with 5 days and 10 days of intermittent tracking data are computed using doppler data only because no planetary ranging data was obtained prior to this time in the post-unlatch phase. The other two solutions are computed using doppler and planetary ranging data.

Comparing the inflight and postflight solutions, the effect of the solar reflectivity coefficients is obvious.

The current best estimate of the post-unlatch orbit was computed using doppler and planetary ranging data. This solution estimated the state vector, solar reflectivity coefficients, gravitational constant of the Moon, and station location parameters. The solution indicated the following B-plane estimates.

$B = 7638.27$ km

$\bar{B} \cdot \bar{R} = -437.48$ km

$\bar{B} \cdot \bar{T} = 7625.73$ km

$t_{ca} =$ July 31 $05^h 19^m 02^s.316$

The *a priori* input values and 1σ statistics are given in Table 2-23 along with the current best estimate of the post-unlatch orbit solution.

- An Evaluation of the Mariner VI Platform Unlatch

The current best estimate of the pre-unlatch and post-unlatch orbits were used to evaluate the change in velocity due to the unlatch. The state vector from the current best pre-unlatch orbit was mapped to the post-unlatch epoch and compared with the best estimate of the state vector obtained from the post-unlatch orbit at the same epoch. The velocity change is given below:

$\Delta DX = +0.0076$ m/sec

$\Delta DY = -0.0071$ m/sec

$\Delta DZ = +0.0010$ m/sec

$\Delta V = 0.01045$ m/sec

It should be pointed out that the uncertainties associated with the velocity component of the spacecraft are nearly as large as the differences presented above.

The amount that the orbit was perturbed due to the platform unlatch can be obtained by differencing the B-plane estimates of the current best pre-unlatch and post-unlatch orbits.

$\Delta B = -106.93$ km

$\Delta\bar{B} \cdot \bar{R} = -1.14$ km

$\Delta\bar{B} \cdot \bar{T} = -107.17$ km

$\Delta t_{ca} = -6.352$ sec

Δ = the current best post-unlatch orbit minus current best pre-unlatch orbit.

Table 2-23. Mariner VI Post-Unlatch Parameter Solutions

Parameters	*A priori* Value	*A priori* Statistics	CBE	CBE Statistics, 1σ
X (km)	-853027.2422	1000.0	-853030.1628	4.6395
Y (km)	-2024180.4844	1000.0	-2024177.7788	3.1833
Z (km)	-1966943.6406	1000.0	-1966944.6301	3.2970
DX (km/sec)	-0.9346082285	0.001	-0.934613735298	0.4972×10^{-5}
DY (km/sec)	-2.30250093341	0.001	-2.30249721581	0.4365×10^{-5}
DZ (km/sec)	-2.2211188376	0.001	-2.2211201540	0.4586×10^{-5}
GR	1.3100	0.03	1.313549	0.012879
GX	0.0	0.05	-0.03151718	0.018787
GY	0.0	0.05	-0.02559797	0.022983
GM/MARS (km^3/sec^2)	4902.8200	1.0	4902.79381	0.03779
DSS 41				
R_s (km)	5450.19860	0.008	5450.20269	0.005120
λ (deg)	136.887507	0.00010	136.88747266	0.00004585
DSS 51				
R_s (km)	5742.94170	0.008	5742.93792	0.005521
λ (deg)	27.685432	0.00010	27.6853598	0.00004704
DSS 62				
R_s (km)	4860.81760	0.008	4860.81723	0.007874
λ (deg)	355.63220	0.00010	355.6321799	0.00007047
DSS 12				
R_s (km)	5212.05350	0.008	5212.05464	0.006992
λ (deg)	243.194559	0.00010	243.1945249	0.00005441
DSS 14				
R_s (km)	5203.99890	0.008	5203.99890	0.007906
λ (deg)	243.110513	0.00010	243,1104901	0.00007813

- Encounter Orbit Estimates

At approximately 3 hr before encounter the Orbit Determination Group recommended the following orbit to the MM'69 project for the final scan platform update:

$\bar{B} \cdot \bar{R} = -380$ km

$\bar{B} \cdot \bar{T} = 7580$ km

$t_{ca} = 05^h19^m06^s$ on July 31, 1969

The one-sigma dispersion ellipse associated with this orbit was 100 km by 40 km with the semi-major axis approximately parallel to the R-axis in the B-plane. The recommended solution was used as input to the Pegasis Program and when the platform clock angle was rounded off to an achievable value, the orbit that was actually used for the final platform update was as follows:

$\bar{B} \cdot \bar{R} = -350$ km

$\bar{B} \cdot \bar{T} = 7560$ km

$t_{ca} = 05^h19^m05^s$ on July 31, 1969

In post-flight the encounter orbit solutions were computed using data spans of E - 5 days to E - 45 min and E - 5 days to E + 5 days. A current best estimate of encounter orbit is given for each of the above data spans. For the data span from E - 5 days to E - 45 min, the current best estimate of the pre-encounter orbit was computed using doppler and planetary range data. This solution estimated the state vector, the gravitational constant of Mars, and station location parameters. This solution indicated the following B-plane parameters:

$B = 7603.81$ km

$\bar{B} \cdot \bar{R} = -335.63$ km

$\bar{B} \cdot \bar{T} = 7596.40$ km

$t_{ca} = 05^h19^m06^s.430$ on July 31, 1969

The reason for taking data up to E - 45 min is that the IRS gas venting started at that time. The a priori input values and 1σ statistics are given in Table 2-24 along with the current best estimate of the pre-encounter orbit solution.

For the data span from E - 5 days to E + 5 days, the current best estimate of the encounter orbit was computed using doppler and planetary range data. This solution estimated the state vector, the gravitational constant of Mars, and station location parameters. When it was mapped to target it indicated the following results:

$$B = 7610.25 \text{ km}$$

$$\bar{B} \cdot \bar{R} = -327.01 \text{ km}$$

$$\bar{B} \cdot \bar{T} = 7603.23 \text{ km}$$

$$t_{ca} = 05^h 19^m 07^s.102 \text{ on July 31}$$

The data residuals (observed minus computed) indicate that all orbit solutions computed using pre- and postencounter data do not have good data fits. This is because the IRS gas venting caused some non-gravitational perturbation. These data will be examined again at a later date. However, this solution will still be our current best estimate of the encounter orbit. The three-sigma dispersion ellipse associated with this orbit was 15 km by 10 km with the semi-major axis approximately parallel to the R-axis in the B-plane.

To evaluate the accuracy of the encounter orbit that was recommended to the MM'69 Project at E - 3 hr, the B-plane estimate of the recommended orbit was subtracted from the current best estimate of the encounter orbit. The differences are presented below:

$$\Delta\bar{B} \cdot \bar{R} = 53 \text{ km}$$

$$\Delta\bar{B} \cdot \bar{T} = 23 \text{ km}$$

$$\Delta t_{ca} = 1.1 \text{ sec}$$

This indicates that our recommended orbit was in error by 53 km in $\bar{B} \cdot \bar{R}$, 23 km in $\bar{B} \cdot \bar{T}$ and 1.1 sec in the time of closest approach.

The orbit used for the final platform update was in error by 23 km in $\bar{B} \cdot \bar{R}$, 43 km in $\bar{B} \cdot \bar{T}$ and 2.1 sec in the time of closest approach.

Table 2-24. Mariner VI Encounter Parameter Solutions

Parameters	*A priori* Value	*A priori* Statistics	CBE	CBE Statistics, 1σ
X (km)	-40567115.000	1,000.0	-40567052.1089	32.5735
Y (km)	-70320687.000	1,000.0	-70320620.7348	59.9250
Z (km)	-36815322.000	1,000.0	-36815523.2881	150.1590
DX (km/sec)	-0.74423141777	0.001	-0.7443833898	0.7314×10^{-4}
DY (km/sec)	-15.1647220135	0.001	-15.1616194820	0.1343×10^{-3}
DZ (km/sec)	-6.2199977636	0.001	-6.2195392604	0.3369×10^{-3}
GM/MARS (km^3/sec^2)	42828.44390	2.0	42828.42294	1.2328
DSS 41				
R_s (km)	5450.19860	0.008	5450.200797	0.003753
λ (deg)	136.8875070	0.00010	136.887493666	0.00004467
DSS 51				
R_s (km)	5742.94170	0.008	5742.941223	0.005963
λ (deg)	27.6854320	0.00010	27.685410883	0.00006271
DSS 62				
R_s (km)	4860.81760	0.008	4860.816231	0.005503
λ (deg)	355.632200	0.00010	355.63218806	0.00005141
DSS 12				
R_s (km)	5212.05350	0.008	5212.051686	0.005293
λ (deg)	243.1945590	0.00010	243.19453860	0.00005037
DSS 14				
R_s (km)	5203.99890	0.008	5203.996480	0.005872
λ (deg)	243.1105130	0.00010	243,11049882	0.00005275

- Mariner VI Inflight and Postflight* Solutions for Physical Constants and Station Locations

Solar Radiation Pressure

The high gain antenna is located on the front of the spacecraft facing the Sun. The orientation of the antenna boresight is at a clock angle of 268.9 deg and a cone angle of 41.1 deg. It has a circular parabolic reflector with a diameter of 40 in. (see Figure 2-31). Due to the orientation of this parabolic reflector, there were added solar pressure effects in directions other than the direction along the Sun-spacecraft line.

During pre-midcourse and the early portion of cruise phase, the perturbative spacecraft acceleration resulting from solar radiation pressure was modeled by (In SPODP)

$$\Delta\ddot{R} = \frac{KA}{M_R{}^2}(1 + G_B)$$

where

R is the probe-Sun distance, in km.

$K = 1.0088 \times 10^8$, a solar radiation constant.

A is the spacecraft effective area normal to R, nominally $8.99079\ m^2$.

M is the spacecraft mass, nominally 384.07915 kg.

G_B is the reflectivity coefficient of the spacecraft along the Sun-spacecraft line, nominally 0.34423.

Approximately two months after midcourse maneuver the solar radiation pressure model was expanded to

$$\Delta\ddot{R} = \frac{KA}{M_R{}^2}\left[(1 + G_B)\bar{R} + (G_T)\bar{T} + (G_N)\bar{N}\right]$$

*The inflight solutions in this subsection are computed using SPODP and the postflight solutions are computed using DPODP.

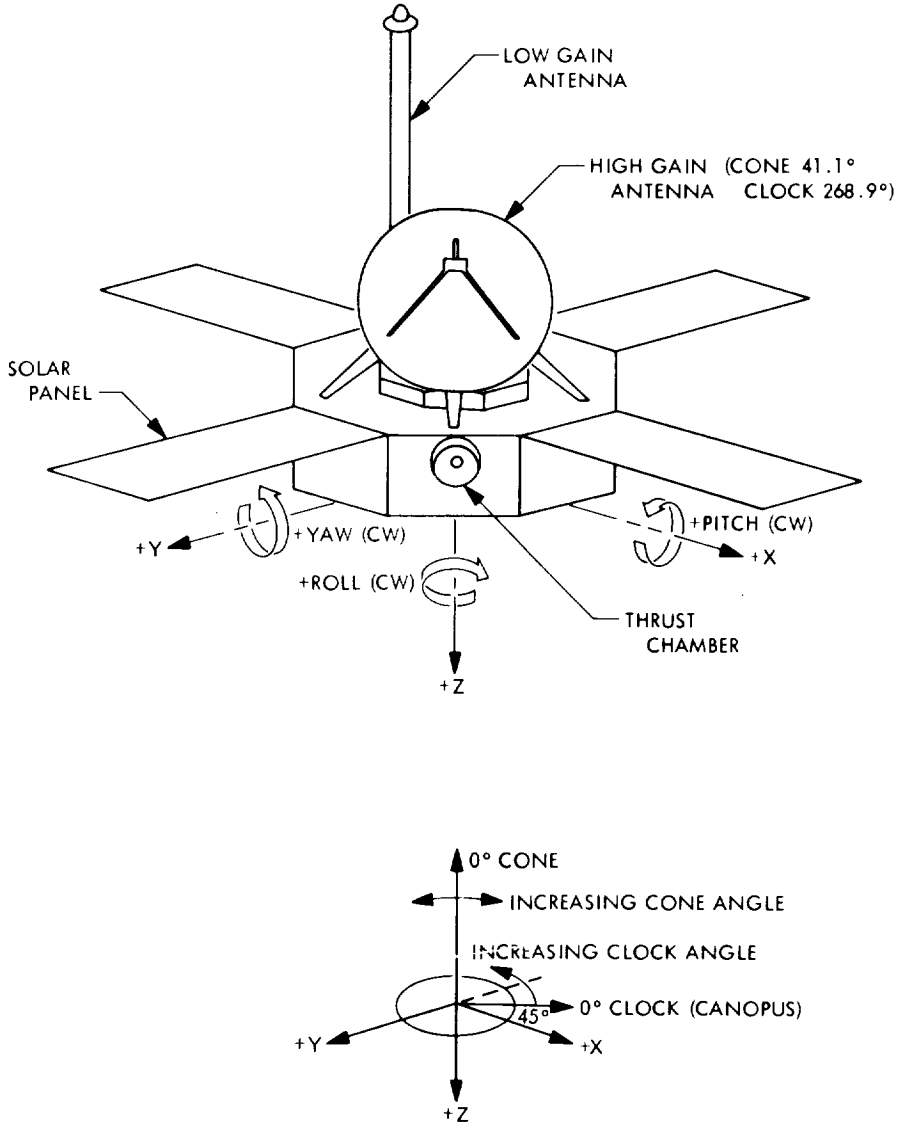

Figure 2-31. Mariner Mars '69 Spacecraft Configuration

where

G_T and G_N are solar reflectivity coefficients in directions defined by unit vectors $\overline{T}$ and $\overline{N}$.

$\overline{R}$ is a unit vector directed out from Sun to spacecraft.

$\overline{T}$ is a unit vector corresponding to the spacecraft + X direction (pitch axis).

$\overline{N}$ is a unit vector corresponding to the spacecraft + Y direction (yaw axis).

The least squares estimates were made of the solar reflectivity coefficients in the pre-midcourse phase, the post-midcourse to unlatch phase, the unlatch to Magellanic Cloud acquisition phase and the Magellanic Cloud acquisition to encounter phase. For each phase, the solar reflectivity coefficients were estimated using a data span from the beginning of that phase to sometime later within the same phase. The time history of these solutions are shown in Figures 2-32, 2-33 and 2-34. These figures show the estimated reflectivity coefficient vs the time of last data point of the solutions. All three solutions indicate a trend toward lower pressure with increasing time. The observed change in G_B is on the order of 0.025 between the pre-midcourse solution and late cruise solution. The observed change was over a period of 5 months. The physical interpretation of this decrease in solar pressure could be that an actual degradation of the total reflectance of the spacecraft and a decrease in specularity of the solar panels took place during cruise. The temperature monitoring of solar panels showed an increase of approximately 2% which indicates that the reflectance of the solar panel had decreased. The decrease in reflectance and in specularity of the solar panel can easily account for the 2% change observed in the radial solar pressure.

Assuming that the high gain antenna is the only source contributing solar radiation force in a direction other than the Sun-spacecraft direction, then $G_M = A_M/A$, where A_M is the effective area normal to $\overline{M}$, A is the spacecraft effective area normal to $\overline{R}$ and G_M is the reflectivity coefficient in direction defined by the unit vector $\overline{M}$ (defined in the following diagram).

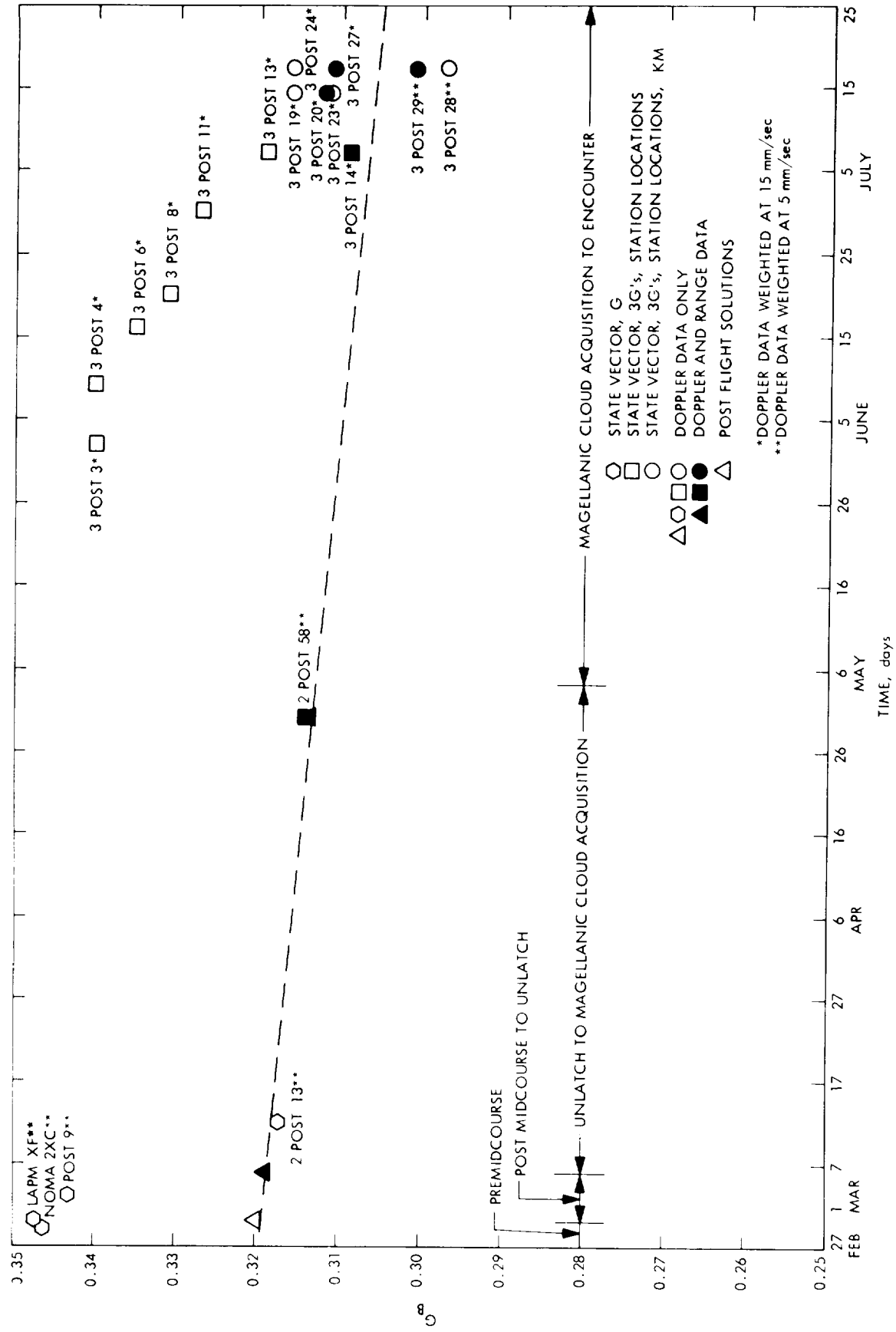

Figure 2-32. Mariner VI Solution for Solar Pressure Coefficient G_B

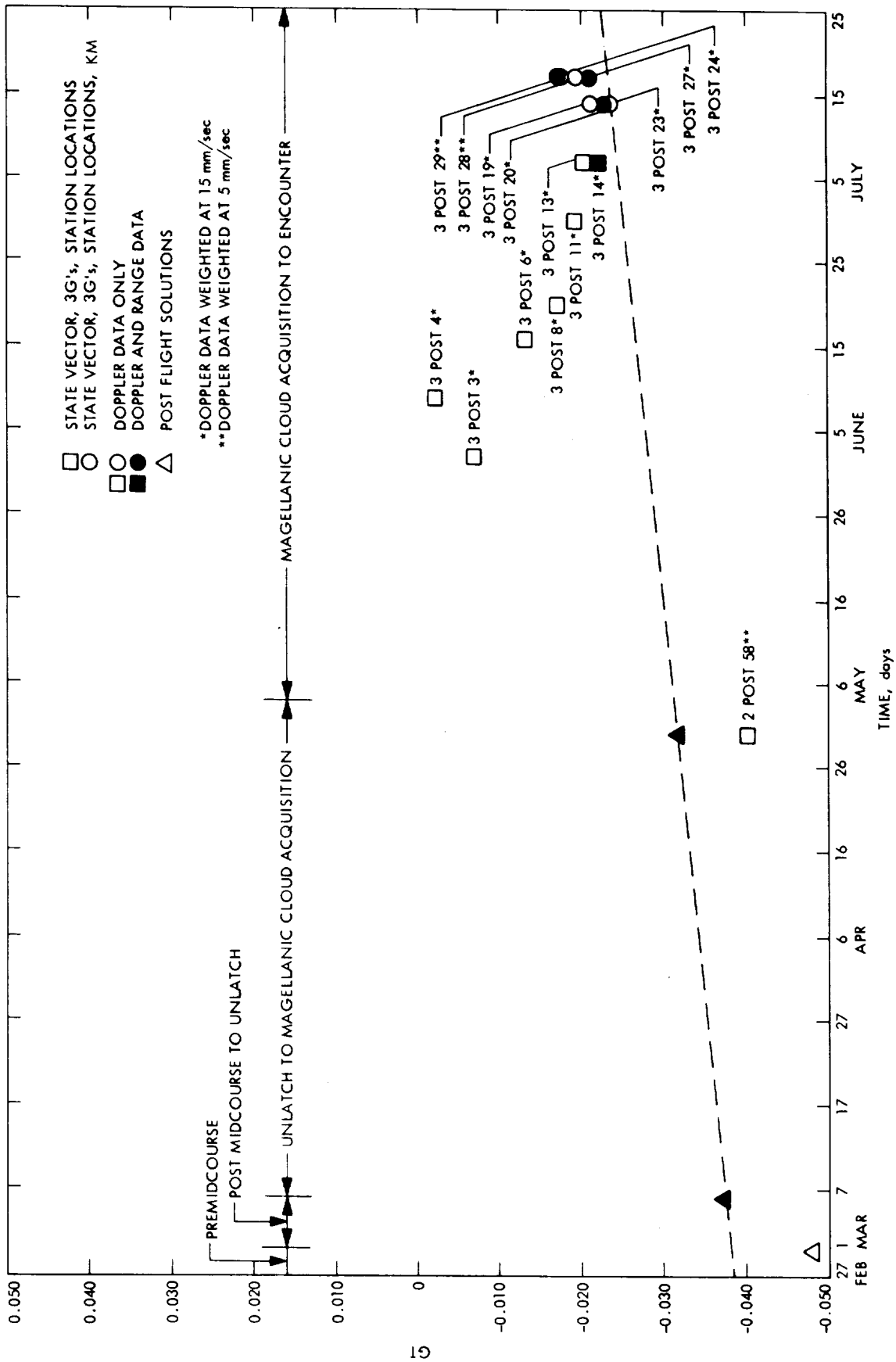

Figure 2-33. Mariner VI Solution for Solar Pressure Coefficient G_T

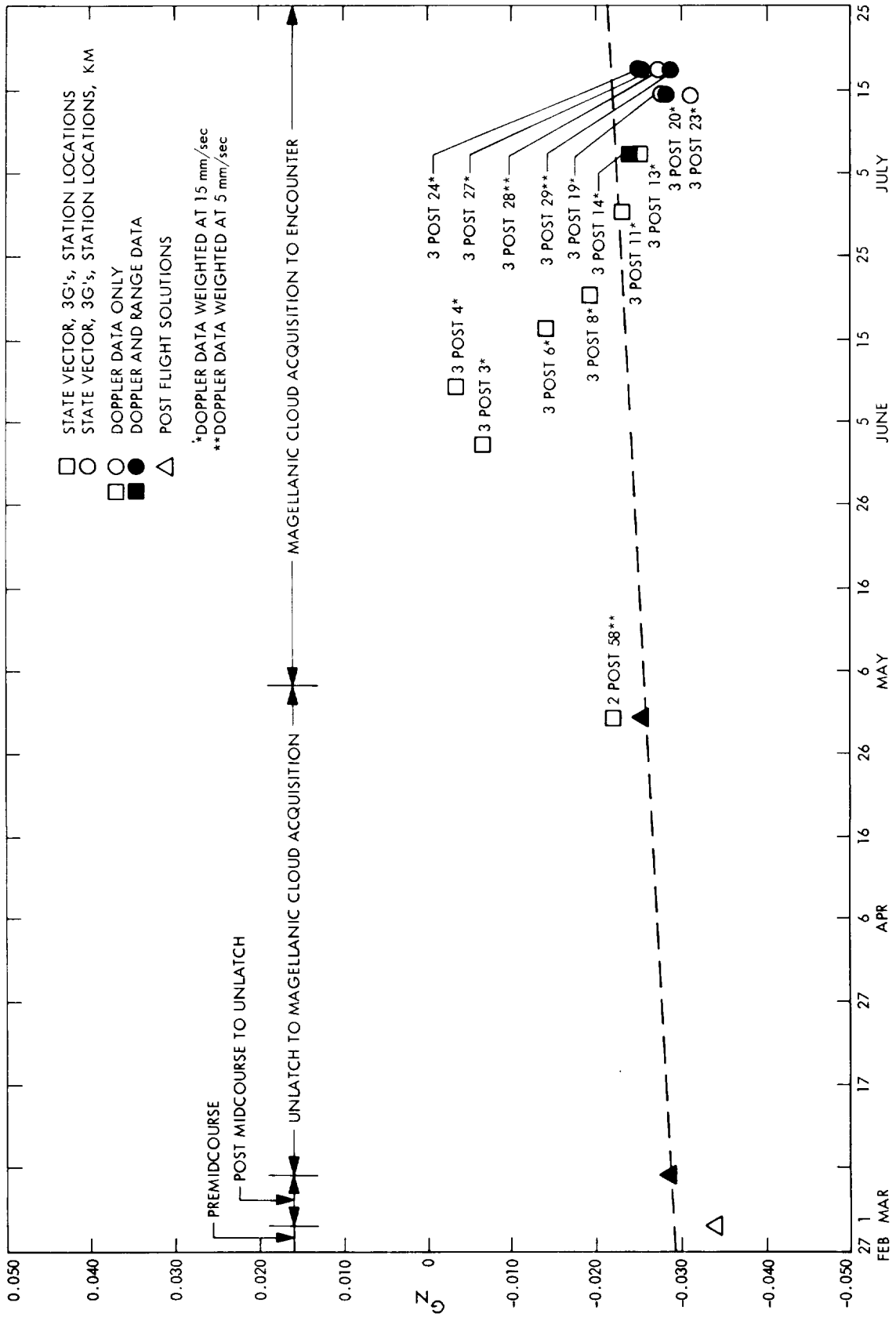

Figure 2-34. Mariner VI Solution for Solar Pressure Coefficient G_N

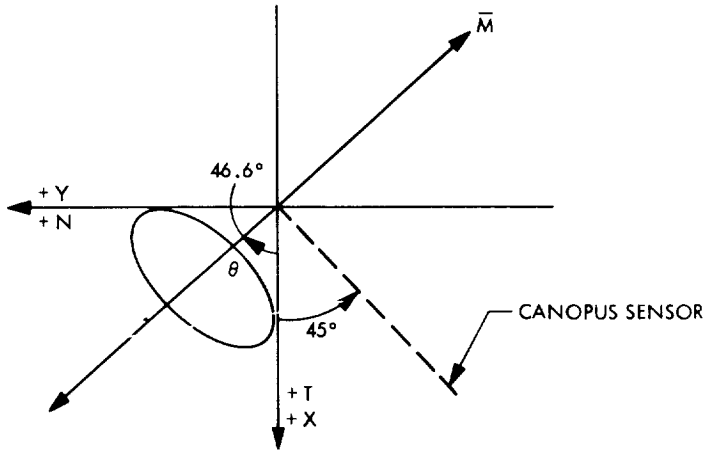

With A_M equal to 1160.2 in.^{2*} and A equal to 16908 in.^{2}, G_M is computed to be 0.0686. Therefore G_T and G_N can be calculated by the following equations:

$$G_T = -G_M \cos 46.6 = -0.0686 \times 0.687 = -0.0471$$

$$G_N = -G_M \sin 46.6 = -0.0686 \times 0.727 = -0.0499$$

The least squares estimates of the magnitude of G_N and G_T computed inflight were smaller than those values computed above. The reason may be that some solar radiation force from other surfaces partially offset the solar pressure contributed by the high gain antenna.

Figures 2-32, 2-33, and 2-34 indicate a fast down trend of solar pressure between solutions with data ending at June 2nd and solutions with data

*These numbers were obtained from an IOM by J. W. Stuart, Jr. dated 15 January 1969.

ending at July 17th. This is not due to a change in solar pressure, but indicates that the data at that time have very little information on the solar pressure to be able to change the nominal input values which were zeros for G_N and G_T and 0.344 for G_B. As more data were used in the orbit solution, the solar reflectivity coefficient gradually moved toward the actual value. The estimation of the solar pressure is complicated by the fact that much of the tracking data taken during cruise were in 2-3 hr blocks and limited amounts of tracking data were taken.

In summary, the G_B estimates obtained inflight were from 0.317 near midcourse to 0.297 near encounter. The G_N estimates obtained were from -0.022 at 1 May to -0.030 near-encounter. The G_T estimates computed were from -0.040 at 1 May to -0.023 near encounter.

The least squares estimate of $G_X(G_T)$* and $G_Y(G_N)$ were computed in post-flight for the premidcourse, pre-unlatch and post-unlatch phases and the following results were obtained:

	Premidcourse	Pre-Unlatch	Post-Unlatch
$G_R(G_B)$	0.31989	0.31886	0.31355
$G_X(G_T)$	-0.04817	-0..03734	-0.03152
$G_Y(G_N)$	-0.03509	-0.02867	-0.02560

The post-flight results agree quite well with the in-flight results; the observed change in G_B in post-flight was slightly less than the change observed in-flight. Figures 2-32, 2-33 and 2-34 show the time history of the post-flight solutions along with the in-flight solutions.

- The Mass of Mars

  The post-flight Mariner VI solution is

$$GM_{MARS} = 42828.42 \pm 1.2 \text{ km}^3/\text{sec}^2$$

*The postflight solutions are computed using DPODP. The symbols for solar reflectivity coefficients in DPODP are G_R, G_X, G_Y and these are equivalent to G_B, G_T and G_N in SPODP.

This solution, which corresponds to a sun-Mars mass ratio of 3,098,702 ±80, along with the Mariner VI inflight solution, Mariner IV solution, and previous astronomical determination are given in Table 2-25. This solution is based on an AU value of 149,597,893 km.

- The Gravitational Constant of the Moon.

The lunar gravitational constant estimate for Mariner VI is given in Table 2-38 along with the solutions from Mariner VII and previous missions. The table indicates that the $GM_{\mathbb{C}}$ solutions from the lunar missions are lower than the solutions from the interplanetary missions. This is due to the fact that in lunar missions, the $GM_{\mathbb{C}}$ estimate was obtained by measuring the effect of the lunar gravity field on the probe acceleration and in the interplanetary missions, the $GM_{\mathbb{C}}$ estimate was obtained by measuring the barycentric motion of the tracking stations over the long cruise interval; therefore, in reality, the results are a determination of the earth-moon mass ratio, assuming a known value of earth-moon distance. The $GM_{\mathbb{C}}$ estimate for Mariner II was 4902.8442 km^3/sec^2 based on the earth gravitational constant, $GM_{\oplus}$ = 398601.27 km^3/sec^2, yielding an earth/moon mass ratio μ^{-1} = 81.3000 ±0.0011. Based on the same earth gravitational constant as in Mariner II, Mariner IV obtained μ^{-1} = 81.30147 ±0.0016 from $GM_{\mathbb{C}}$ = 4902.756 ±0.1 km^3/sec^2. The Mariner V realtime cruise solutions for $GM_{\mathbb{C}}$ range from 4902.68 km^3/sec^2 to 4902.86 km^3/sec^2. The representative value of the Mariner V real time $GM_{\mathbb{C}}$ was 4902.77 km^3/sec^2. All Mariner V solutions assumed a $GM_{\oplus}$ value of 398601.33 km^3/sec^2, the corresponding real time estimate of μ^{-1} is 81.30125 ±0.00166. The Mariner V post flight processing yields $GM_{\mathbb{C}}$ = 4902.81 ±0.5 km^3/sec^2 and μ^{-1} = 81.30059 ±0.00083. The real time $GM_{\mathbb{C}}$ estimate for Mariner VI is 4902.8205 ±0.023 km^3/sec^2. Based on the $GM_{\oplus}$ value of 398601.20, the corresponding real time estimate of μ^{-1} is 81.30039 ±0.0001. This value agrees extremely well with the Mariner II and the Mariner V post-flight processing solution.

The post-flight Mariner VI solution is:

$$GM_{\mathbb{C}} = 4902.794 \pm 0.04 \text{ km}^3/\text{sec}$$

Table 2-25. Estimates of the sun-Mars Mass Ratio

Source	Sun-Mars Mass Ratio
De Sitter, 1938 weighted mean (Ref. 19)	3,085,000 ±6700
Van Den Bosch, 1927 Martian Satellites (Ref. 20)	3,088,000 ±6700
MIT 1967 RADAR AND OPTICAL OBSERVATION OF PLANETS (Ref. 21)	3,111,000 ±9000
JPL 1965 Mariner IV (Ref. 22)	3,098,708 ±9
JPL 1969 Mariner VI (In-flight)	3,098,697 ±80
JPL 1969 Mariner VI (Post-flight)	3,098,702 ±80

Since the value $GM_{\oplus} = 398,601.20$ was used for the $GM_{\leftmoon}$ solution, the earth-moon mass ratio may be computed as:

$$\mu^{-1} = 81.30083 \pm 0.00067$$

- The Gravitational Constant of earth

The In-flight Mariner VI solution was

$$GM_{\oplus} = 398,601.67 \pm 0.97 \text{ km}^3/\text{sec}^2$$

The post-flight Mariner VI solution is

$$GM_{\oplus} = 398,601.435 \pm 0.983 \text{ km}^3/\text{sec}^2$$

These values are consistent with the $GM_{\oplus}$ estimates obtained inflight and in previous missions as given in Table 2-38.

Station Locations*

The least square estimates of station locations based on pre-midcourse maneuver phase, cruise phase, and encounter phase tracking data are presented in Figures 2-35 through 2-46 in a natural coordinate system (r_s, λ, z) where r_s is the distance off the spin axis (in the station meridian), λ is the longitude and z is along the earth spin axis. The *a priori* standard deviations for spin axis distance r_s and longitude λ are given in Table 2-26. The estimates were reduced to the mean pole of 1903 and plotted by N. Mottinger of JPL. In general, the numerical results indicate that the r_s and λ solutions are consistent to ±3m with the exception of the station location change that occurred at orbit 3P10. This will be explained later. Some small variations of r_s and λ can be expected due to the following conditions: (1) a change in the estimated parameters list, (2) a change in the time polynomials which were

*Station locations had been determined as accurately as possible by reprocessing data from previous missions (see section II. A. 2. b.). These solutions were made so that consistency could be checked, and so that any unmodeled effects could be absorbed, if present, as equivalent station location errors.

Table 2-26. Information Relating to the Computation of Station Locations

Orbits	Data Span	Estimated[b] Parameters	Station Location *A priori*	T Poly	ELMIN[c]	Data Wt of 2 Way Doppler
LAXC	2/25 10:00-2/28 20:37	Set 1	$\tilde{\sigma}\, r_s$ = 8m $\tilde{\sigma}_\lambda$ = 10m	#1	10°	5 mm/s
2P14	3/06 20:00-3/12 17:45	Set 1		#1	10°	5 mm/s
3P3	5/04 00:00-6/02 02:16	Set 2		#1	10°	15 mm/s
3P4	5/04 00:00-6/09 03:40	Set 2		#2	10°	15 mm/s
3P6	5/04 00:00-6/16 22:01	Set 2		#1	10°	15 mm/s
3P10	5/04 00:00-6/30 07:53	Set 1		#3	10°	15 mm/s
3P13	5/04 00:00-7/07 14:12	Set 2		#3	15°	15 mm/s
3P14[a]	5/04 00:00-7/07 14:12	Set 2		#3	15°	15 mm/s
3P19	5/04 00:00-7/14 07:49	Set 3		#3	15°	15 mm/s
3P20[a]	5/04 00:00-7/14 07:49	Set 3		#3	15°	15 mm/s
3P28	5/04 00:00-7/17 16:19	Set 3		#3	15°	5 mm/s
3P29[a]	5/04 00:00-7/17 16:19	Set 2		#3	15°	5 mm/s
3P33	7/01 05:00-7/21 04:50	Set 1		#3	15°	5 mm/s
3P34[a]	7/01 05:00-7/21 04:50	Set 1		#3	15°	5 mm/s
3P44[a]	7/17 09:00-7/23 16:00	Set 1		#4	15°	5 mm/s
3P52	7/01 05:00-7/26 06:21	Set 1		#5	15°	5 mm/s
3P94[a]	7/26 02:00-7/29 17:50	Set 1		#6	15°	5 mm/s
3P95	7/26 02:00-7/29 17:50	Set 1		#6	15°	5 mm/s
3102	7/26 02:00-7/29 21:44	Set 1		#7	15°	5 mm/s
3104[a]	7/26 02:00-7/29 21:44	Set 1		#7	15°	5 mm/s
3107[a]	7/26 02:00-7/30 01:06	Set 1		#7	15°	5 mm/s
3108[a]	7/26 02:00-7/30 01:06	Set 4		#7	15°	5 mm/s
Enc 2	7/26 02:00-7/30 15:17	Set 4		#7	15°	5 mm/s
Enc 3[a]	7/26 02:00-7/30 15:17	Set 4	$\tilde{\sigma}\, r_s$ = 8m $\tilde{\sigma}_\lambda$ = 10m	#7	15°	5 mm/s
E 15	7/26 02:00-7/30 18:09	Set 4	$\tilde{\sigma}\, r_s$ = 20 $\tilde{\sigma}_\lambda$ = 25m	#7	15°	5 mm/s
E 16[a]	7/26 02:00-7/30 18:09	Set 4		#7	15°	5 mm/s
E 28	7/26 02:00-7/31 01:05	Set 4		#7	15°	5 mm/s
E 32	7/26 02:00-7/30 23:44	Set 4	$\tilde{\sigma}\, r_s$ = 20 $\tilde{\sigma}_\lambda$ = 25 m	#7	15°	5 mm/s

[a]Orbit Solution computed using planetary ranging along with 2-way doppler data.

[b]Set 1 - State vector and station locations.

Set 2 - State vector, station locations and solar reflectivity coefficients.

Set 3 - State vector, station locations, solar reflectivity coefficients and gravitational constant of moon.

Set 4 - State vector, station locations, mass ratio of Mars to Sun.

[c]The minimum elevation angle which the data were taken and still used in orbit solution.

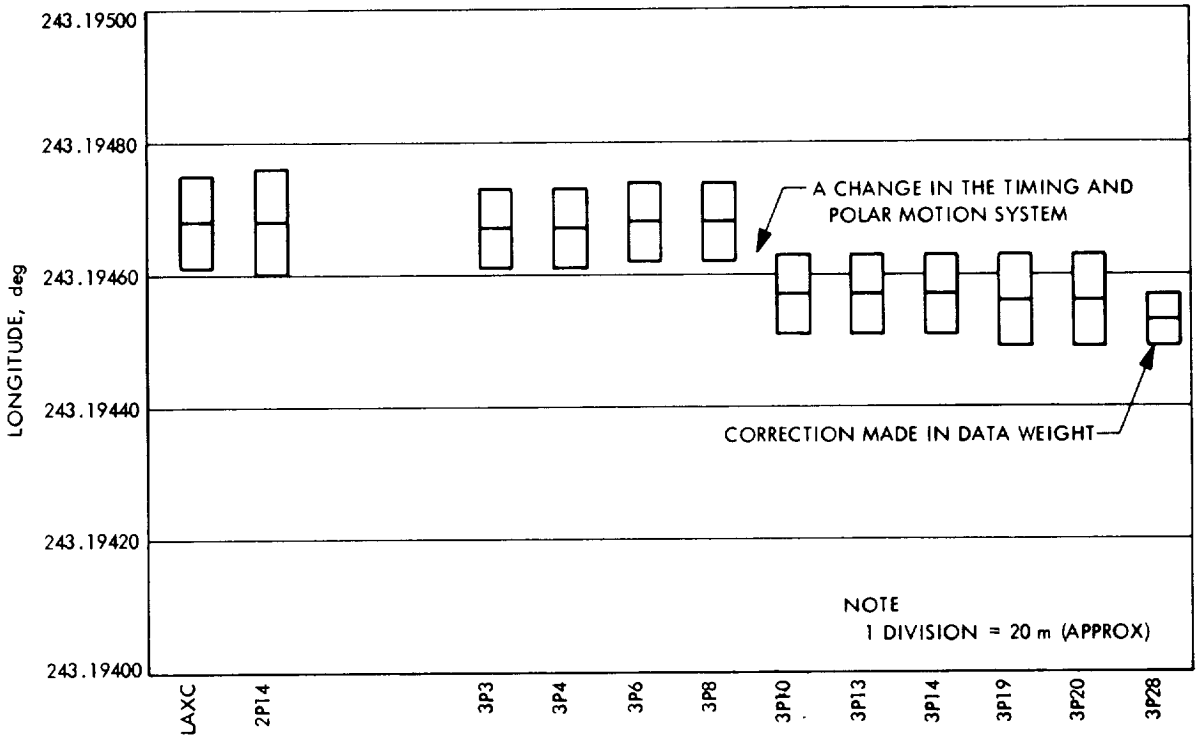

(a)

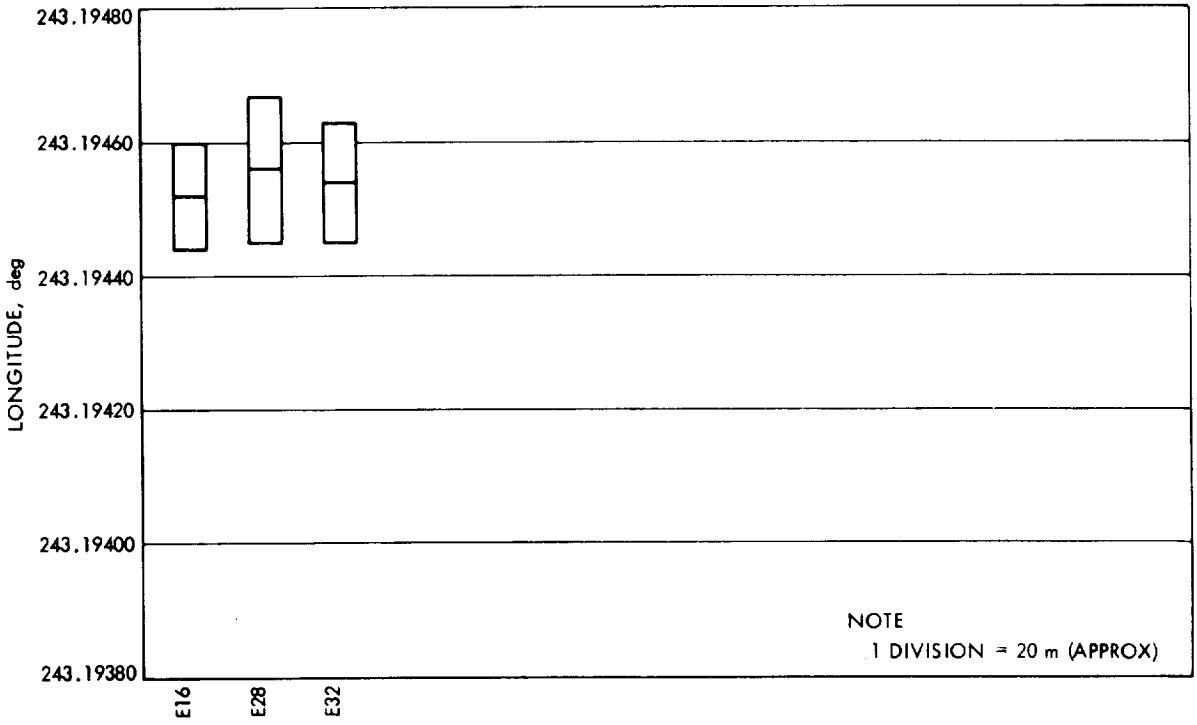

(b)

Figure 2-35. Geocentric Longitude, DSS 12

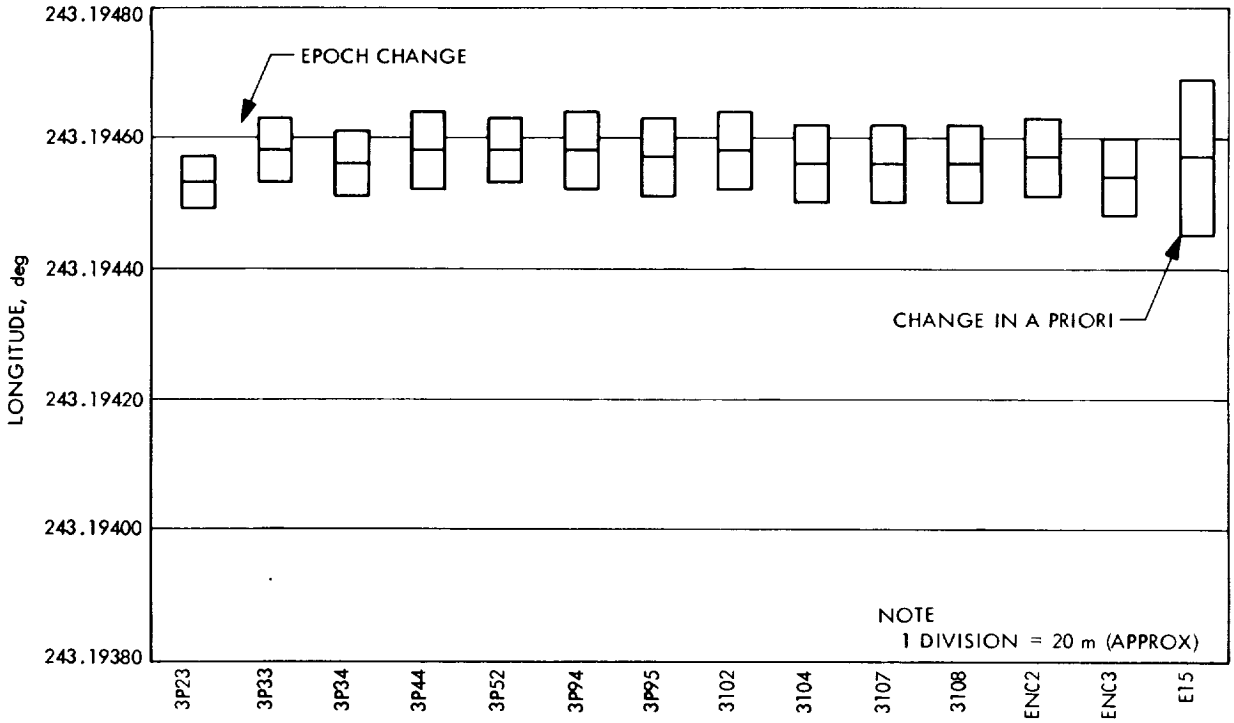

(c)

Figure 2-35. Geocentric Longitude, DSS 12 (cont'd)

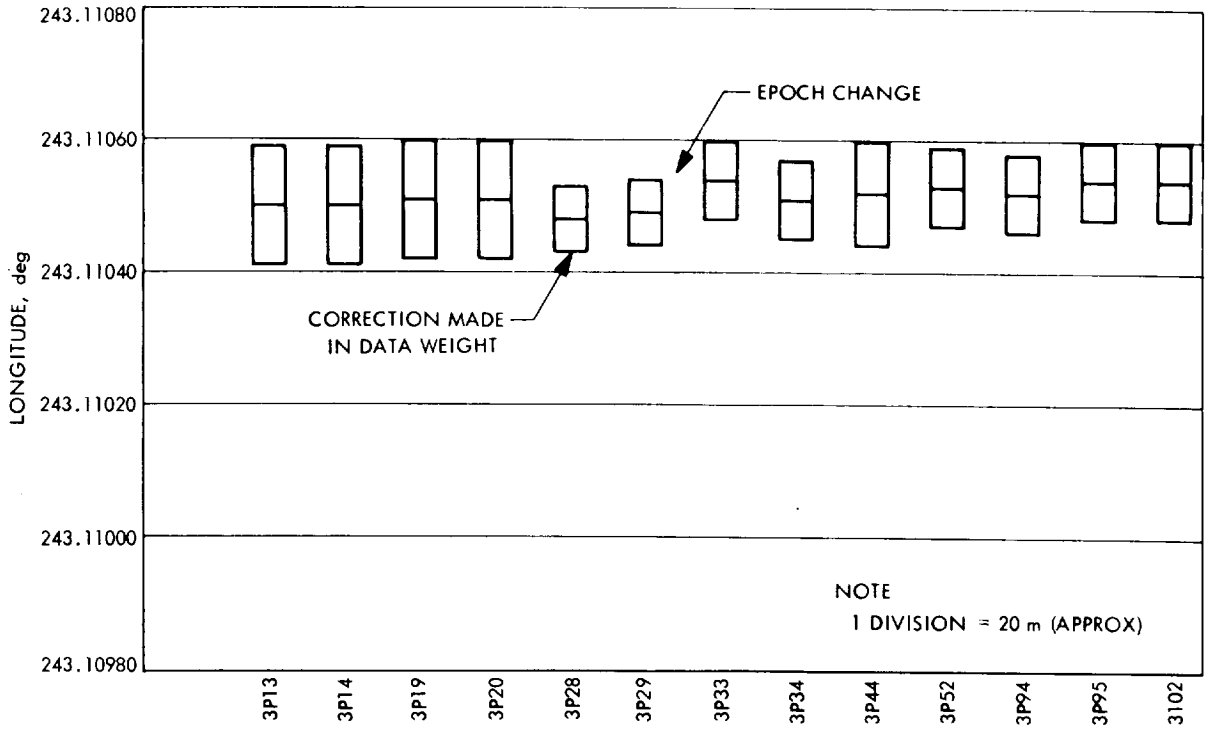

(a)

Figure 2-36. Geocentric Longitude, DSS 14

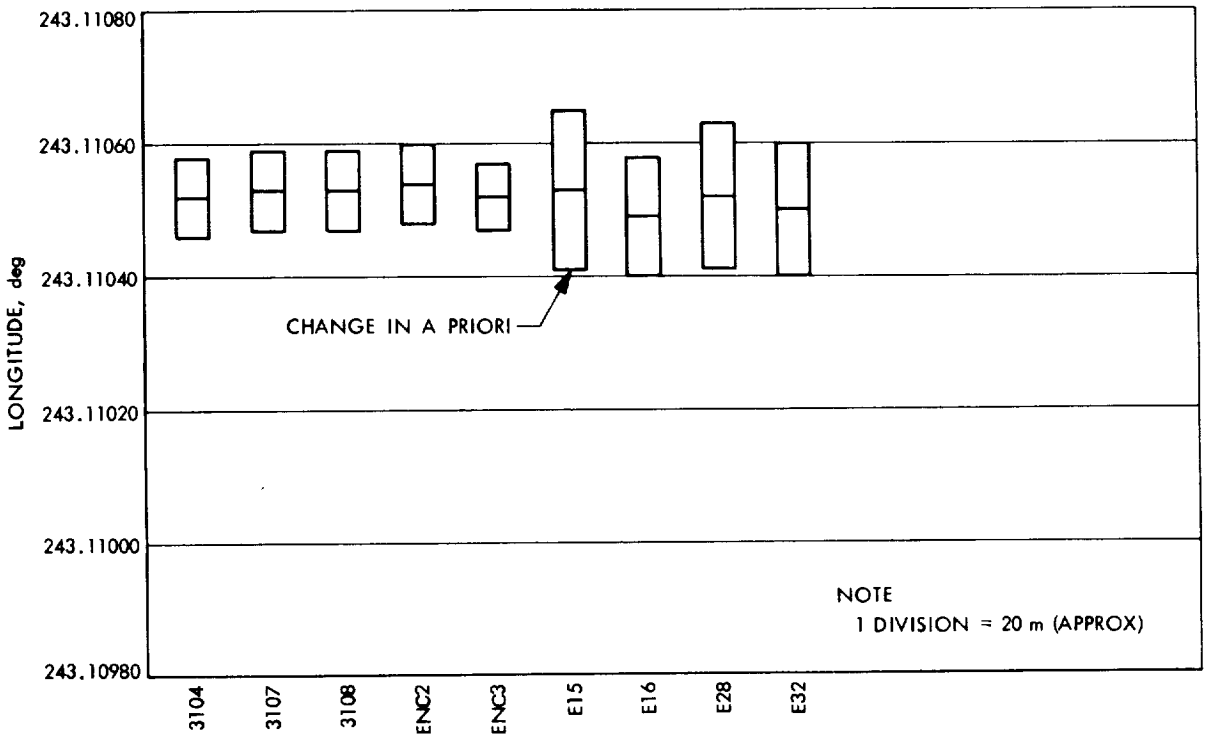

(b)

Figure 2-36. Geocentric Longitude, DSS 14 (cont't)

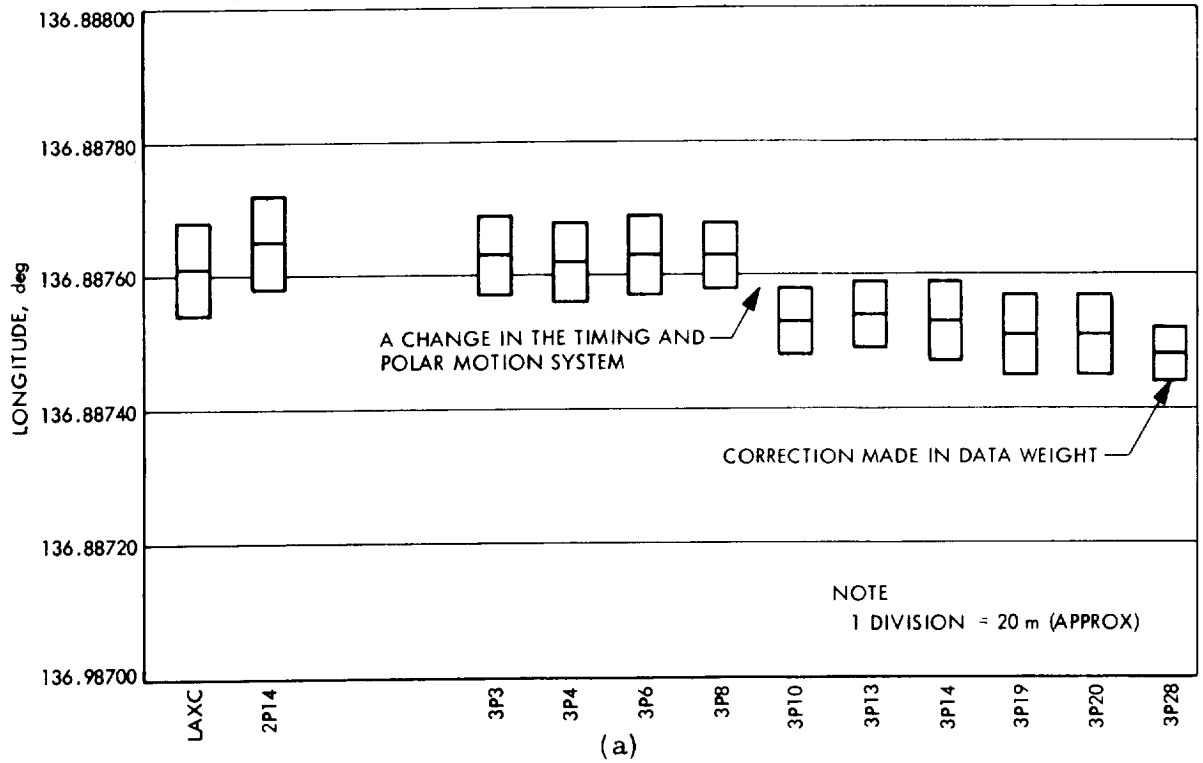

(a)

Figure 2-37. Geocentric Longitude, DSS 41

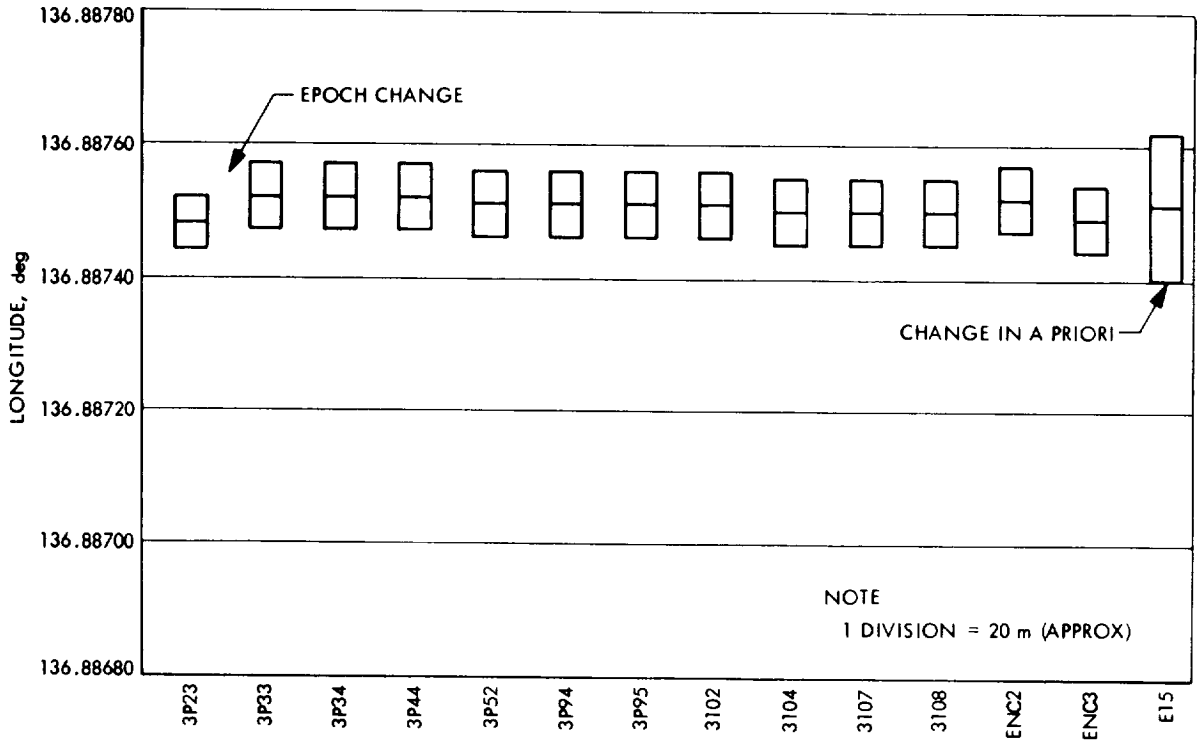

(b)

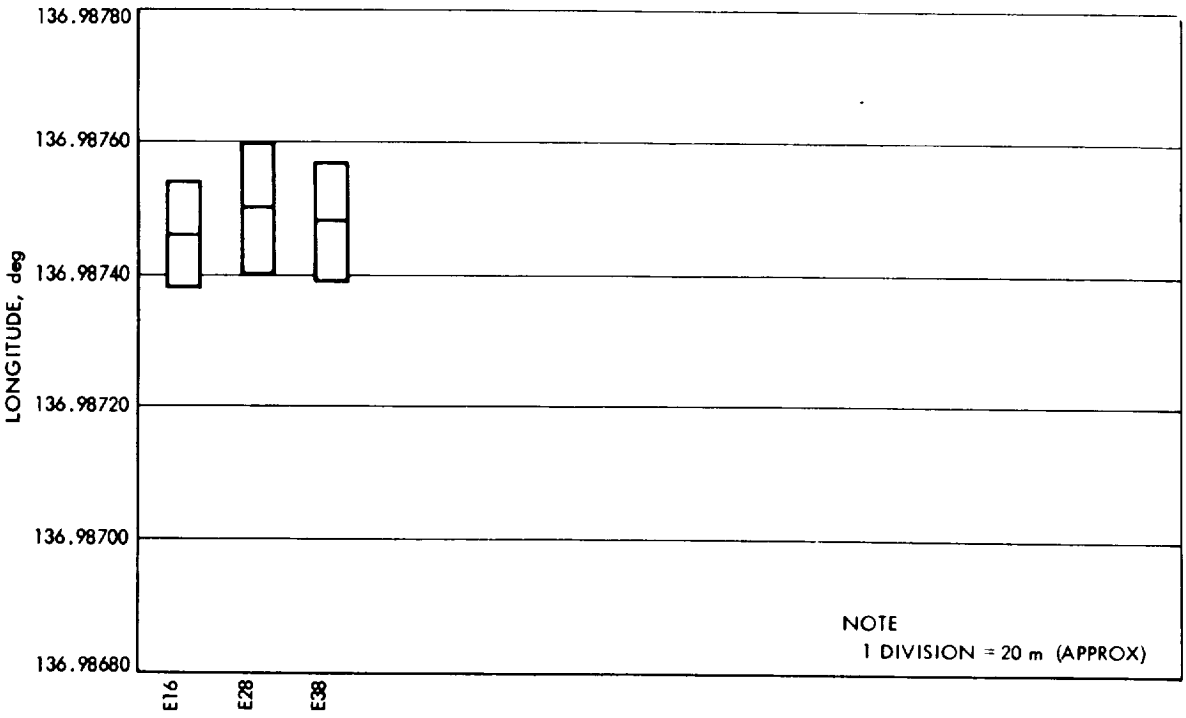

(c)

Figure 2-37. Geocentric Longitude, DSS 41 (cont'd)

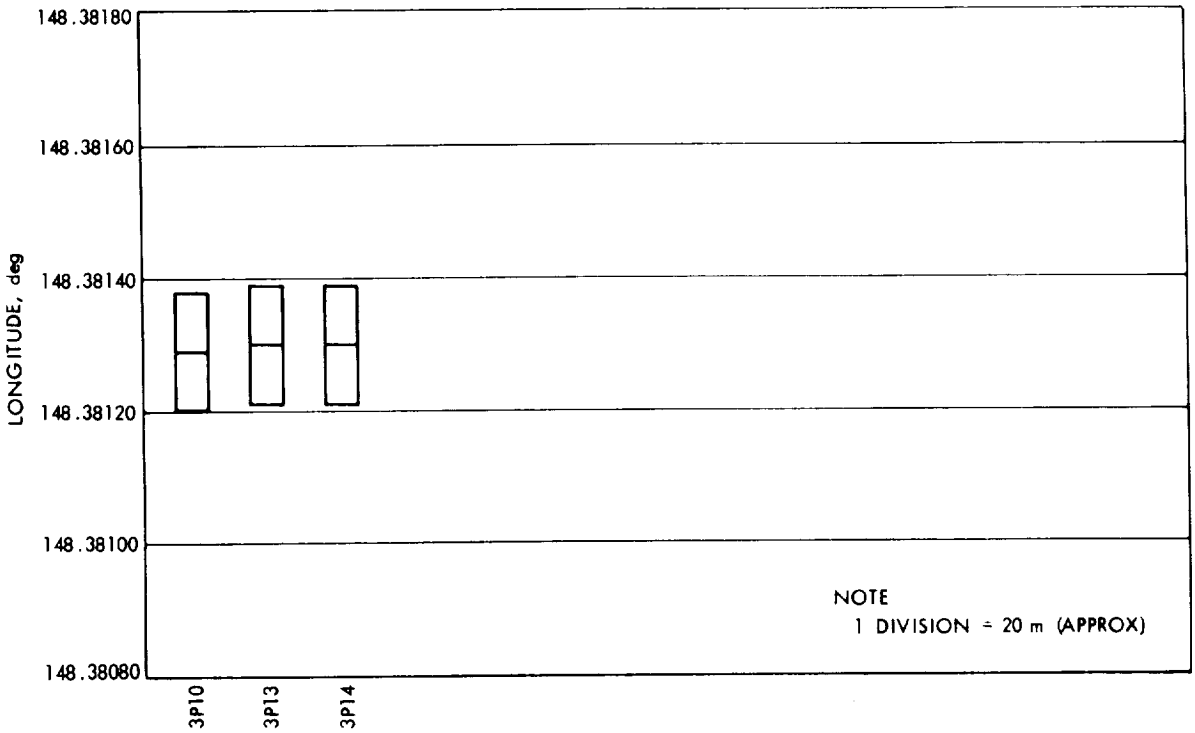

Figure 2-38. Geocentric Longitude, DSS 42

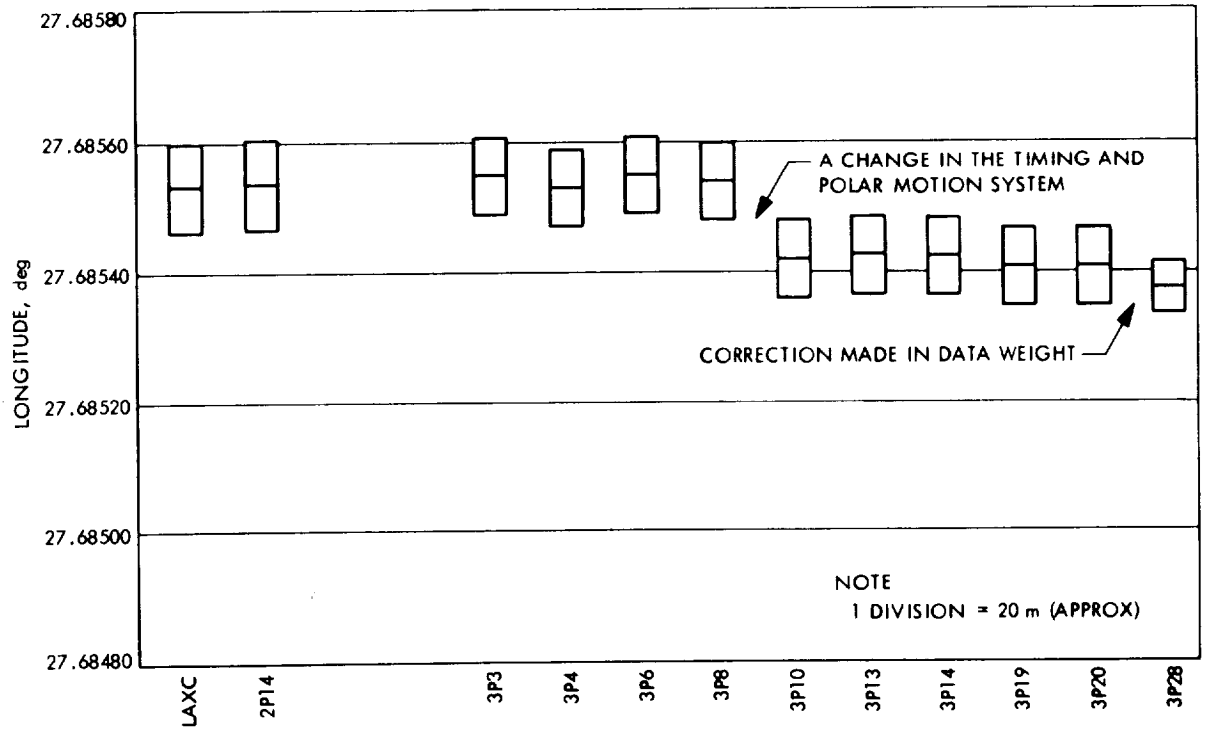

(a)

Figure 2-39. Geocentric Longitude, DSS 51

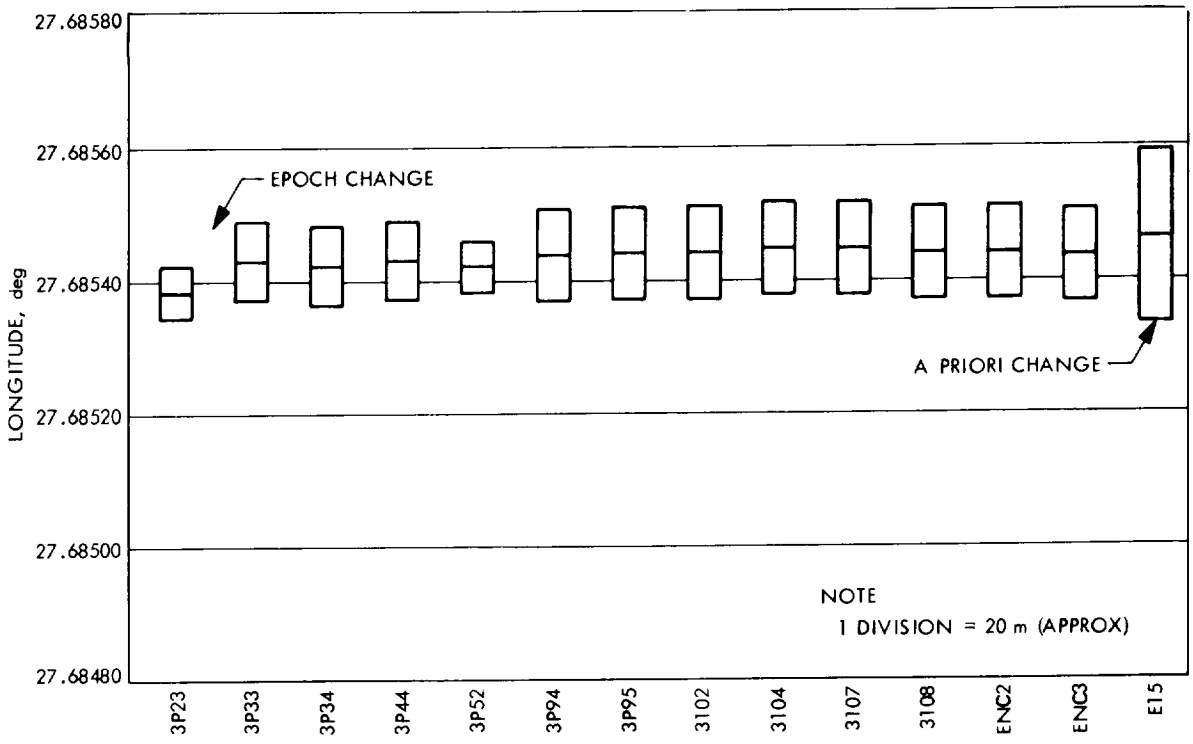

(b)

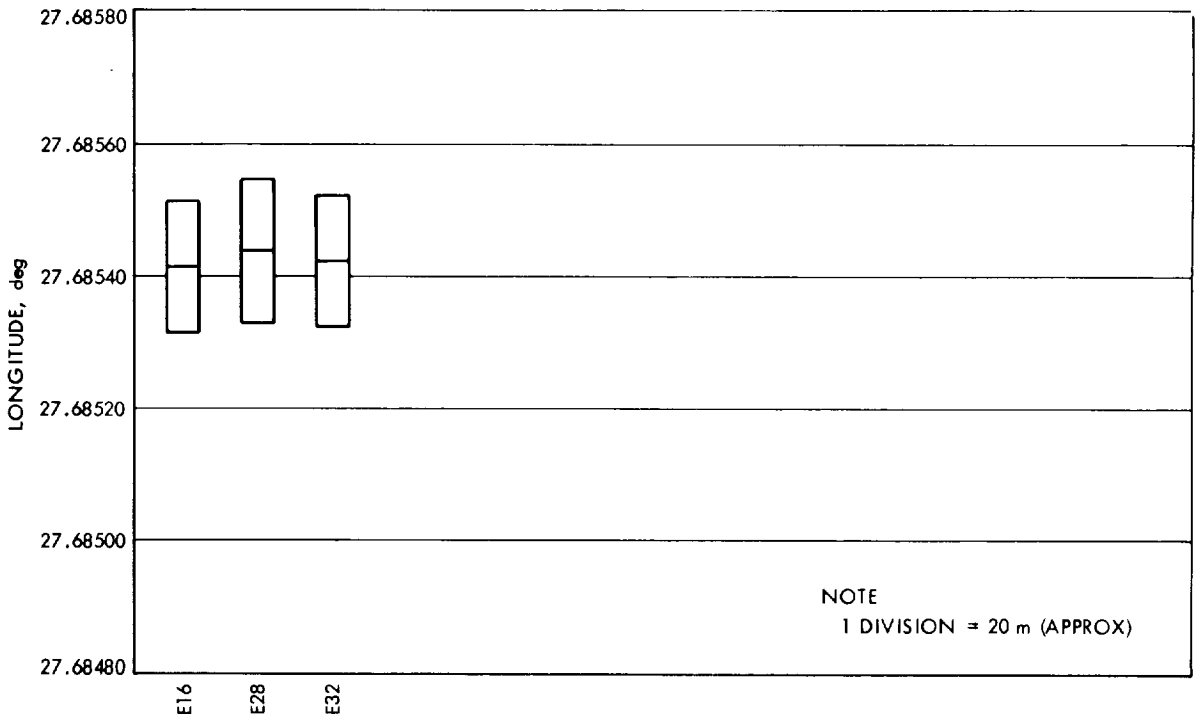

(c)

Figure 2-39. Geocentric Longitude, DSS 51 (cont'd)

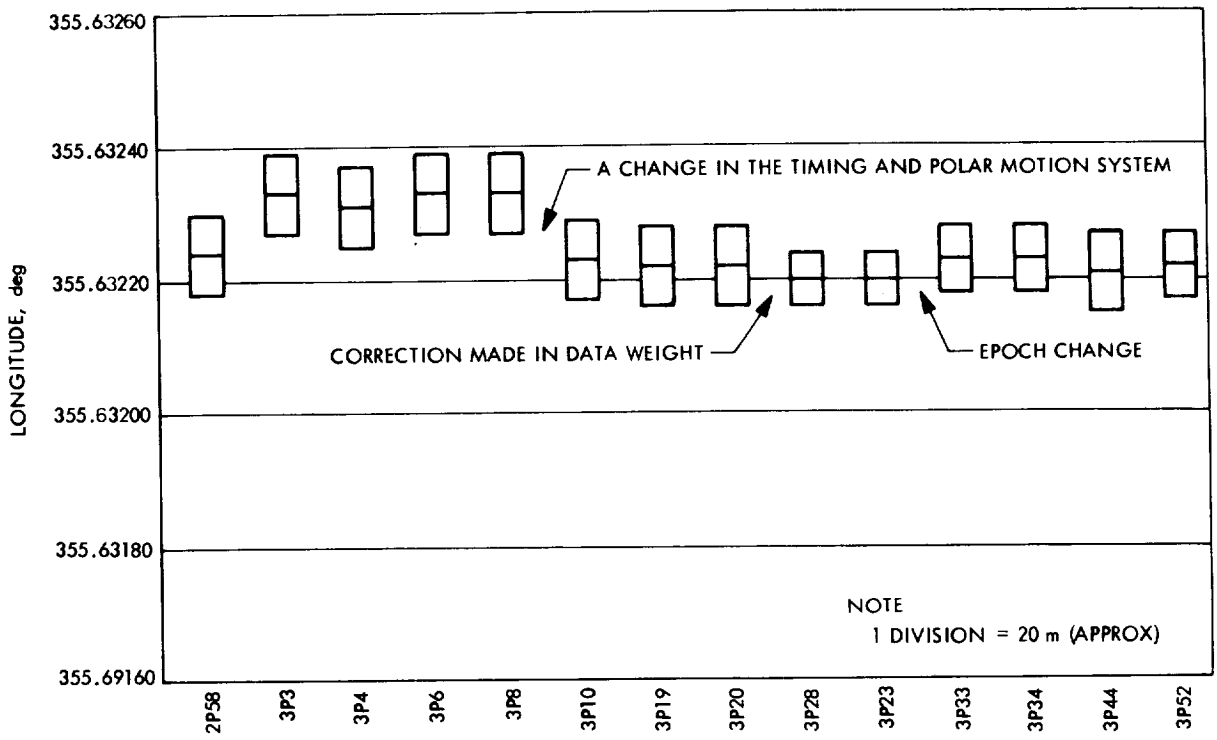

(a)

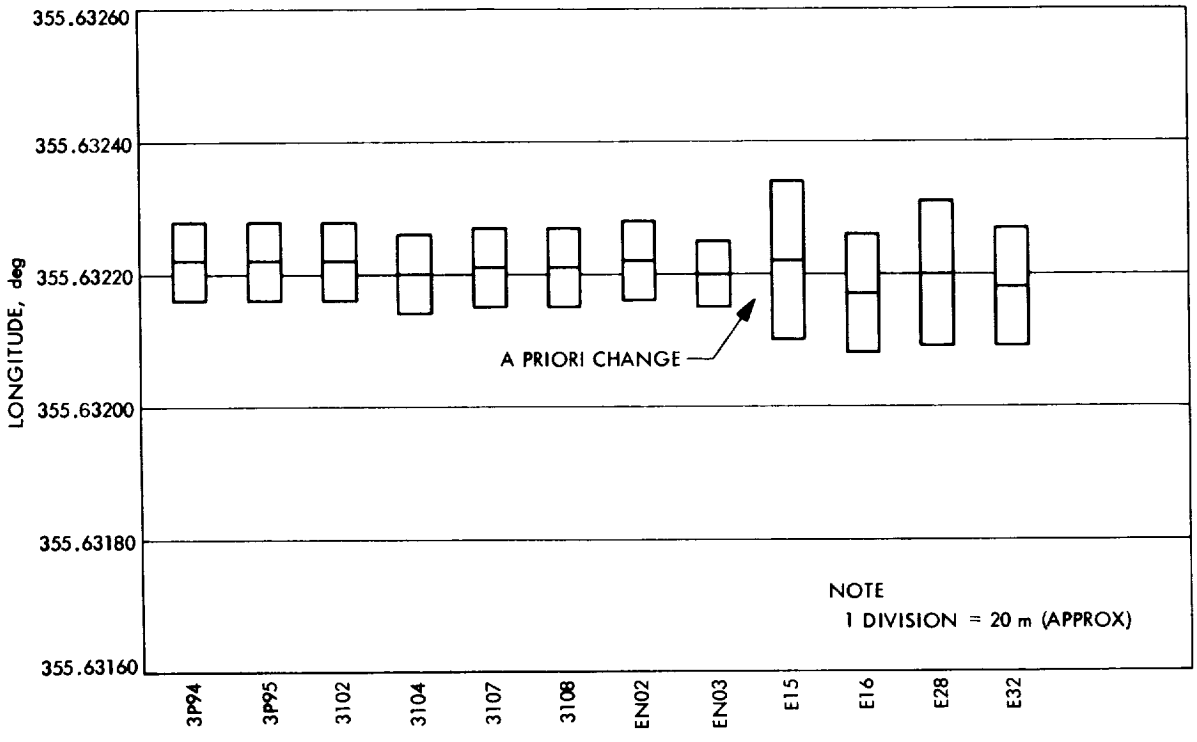

(b)

Figure 2-40. Geocentric Longitude, DSS 62

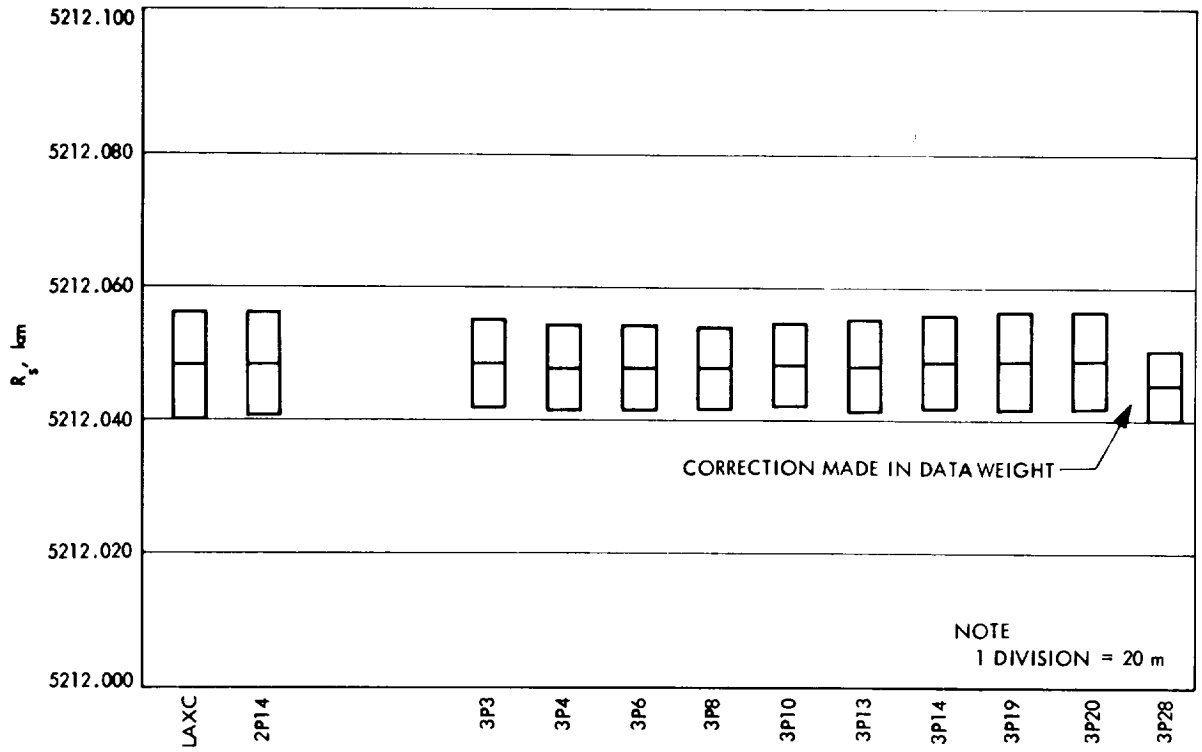

(a)

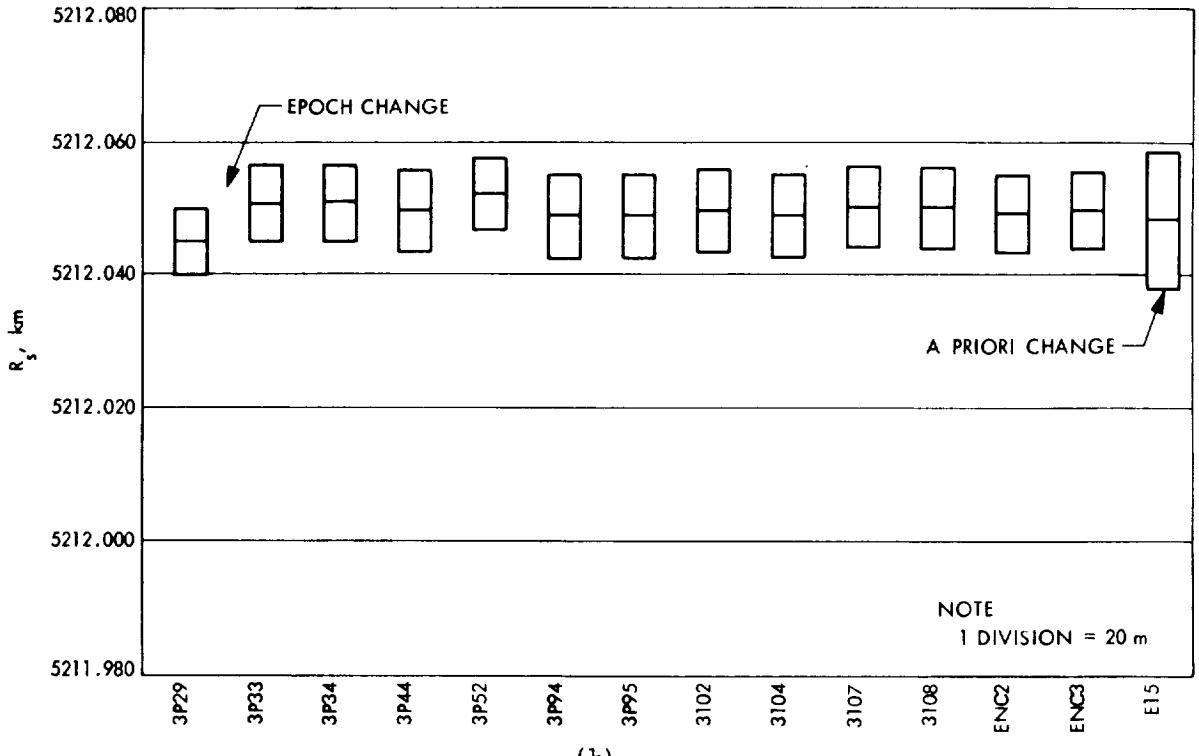

(b)

Figure 2-41. Distance Off Spin Axis, DSS 12

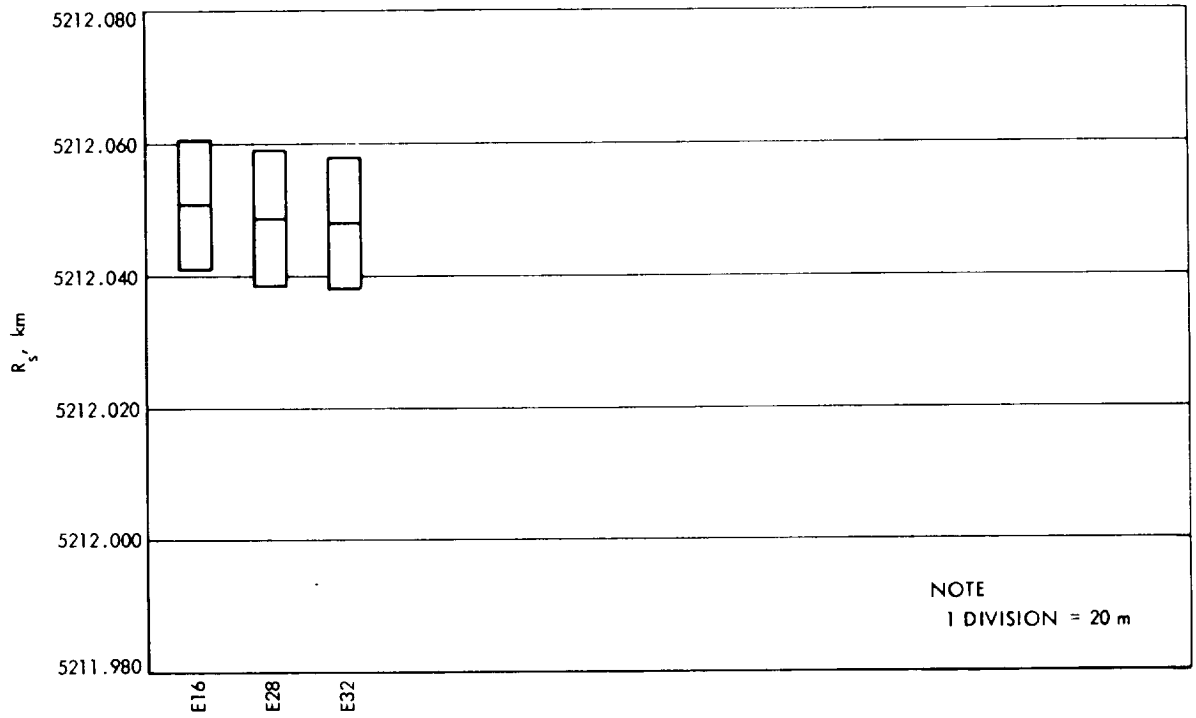

(c)

Figure 2-41. Distance Off Spin Axis, DSS 12 (cont'd)

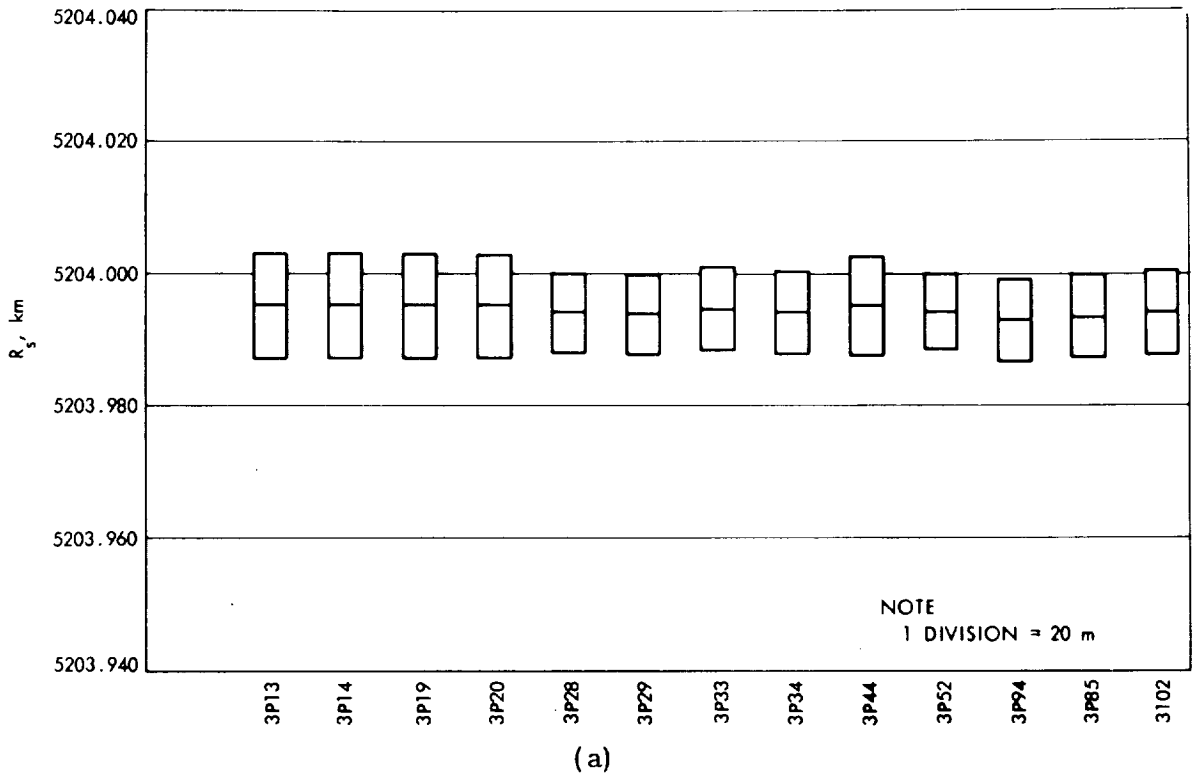

(a)

Figure 2-42. Distance Off Spin Axis, DSS 14

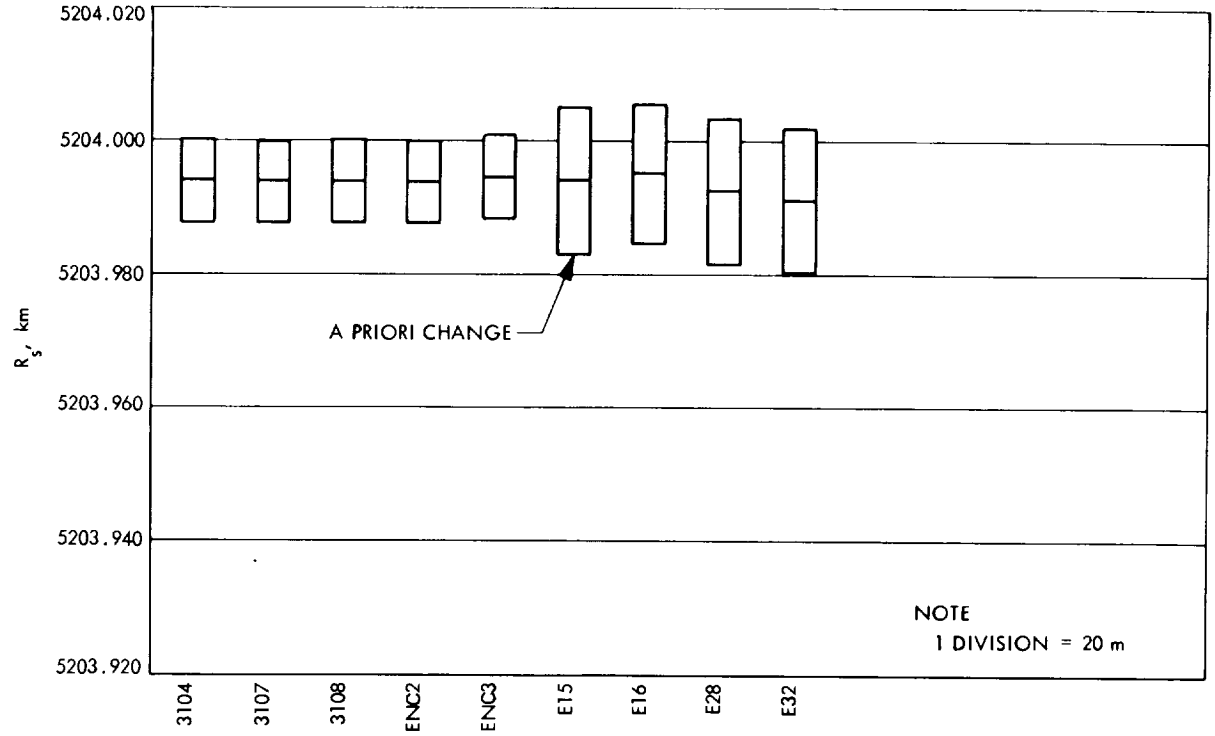

(b)

Figure 2-42. Distance Off Spin Axis, DSS 14 (cont'd)

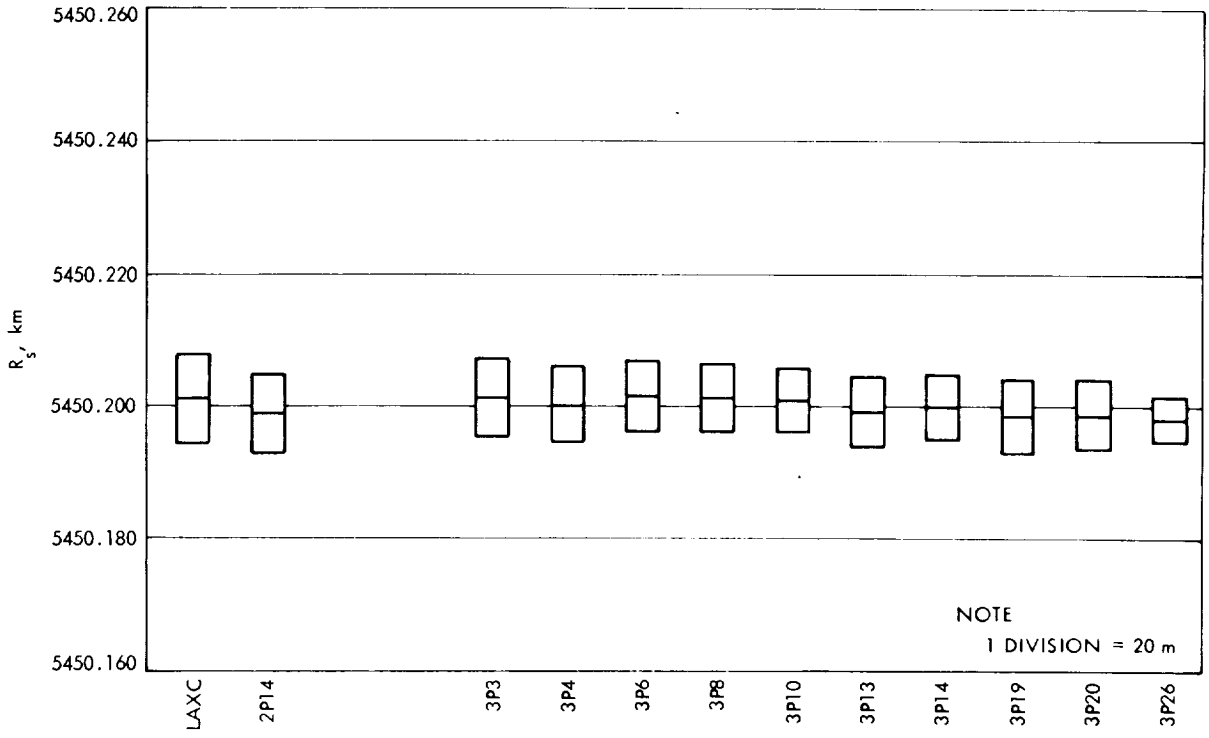

(a)

Figure 2-43. Distance Off Spin Axis, DSS 41

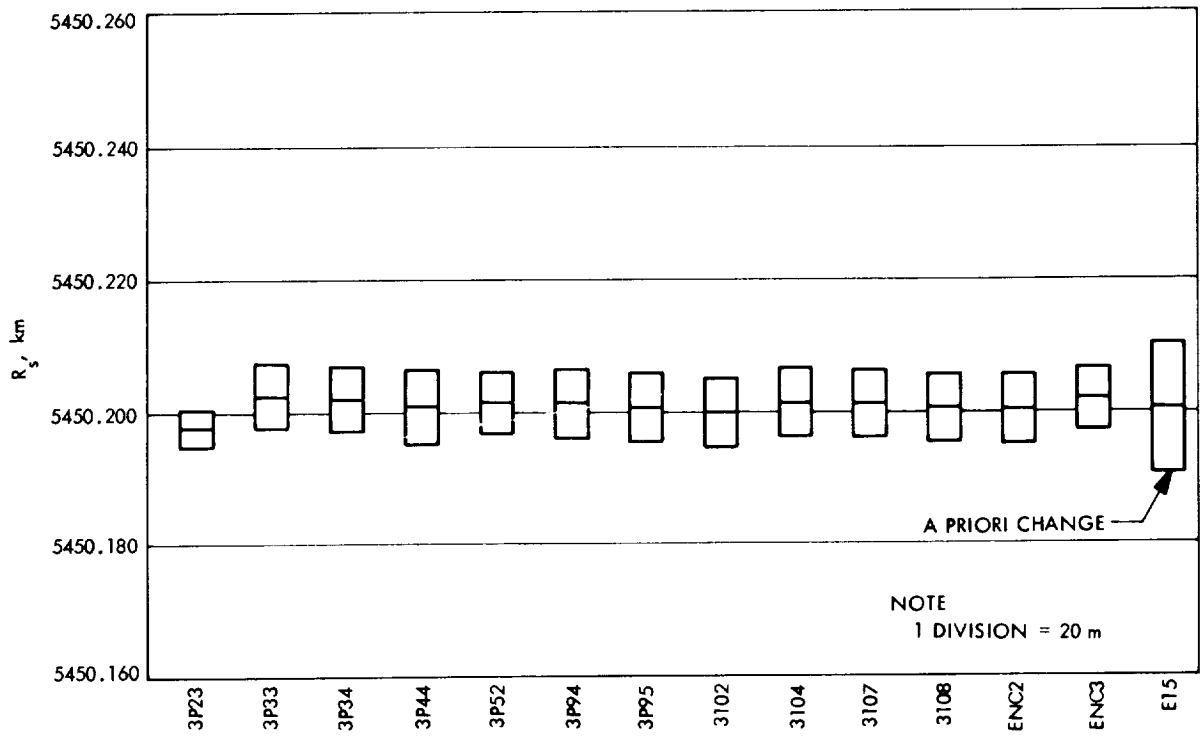

(b)

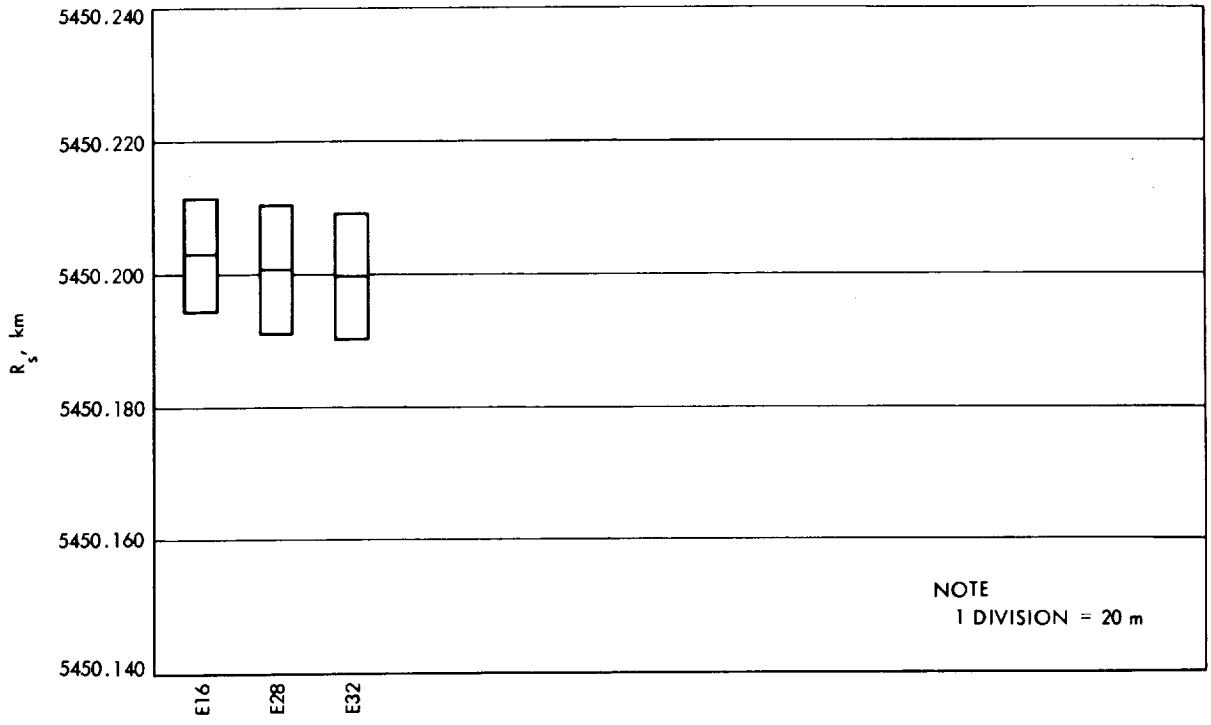

(c)

Figure 2-43. Distance Off Spin Axis, DSS 41 (cont'd)

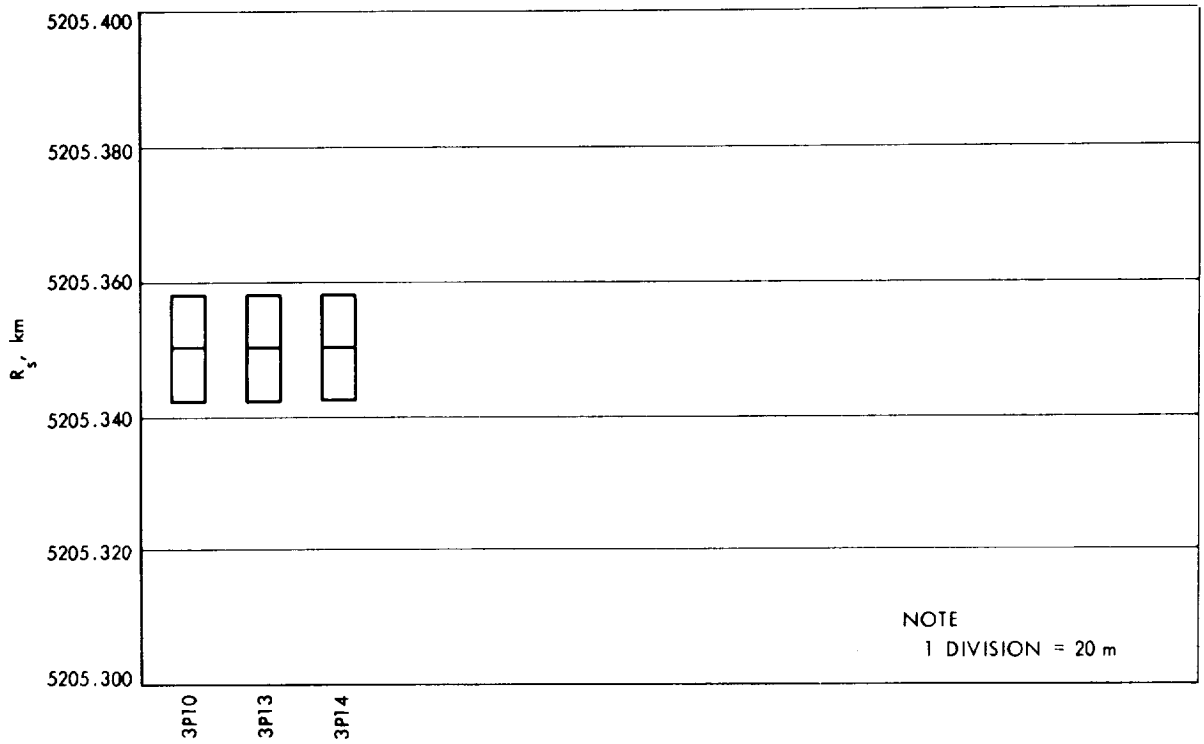

Figure 2-44. Distance Off Spin Axis, DSS 42

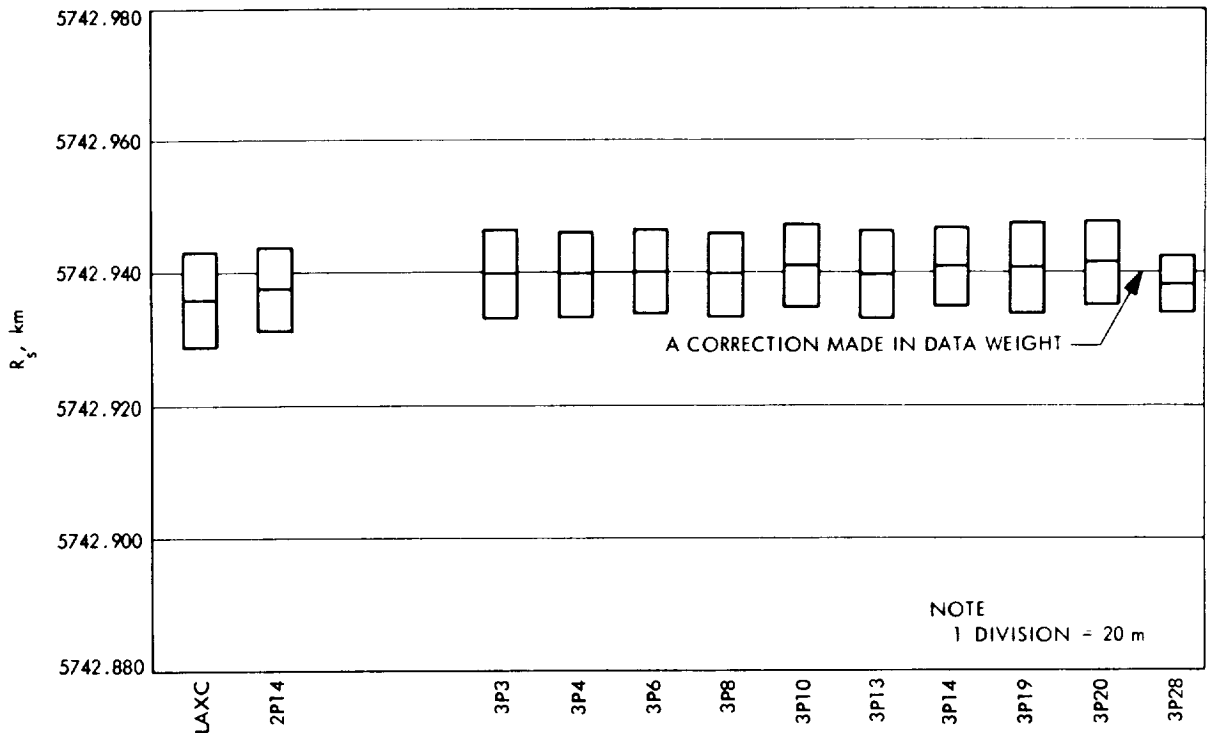

(a)

Figure 2-45. Distance Off Spin Axis, DSS 51

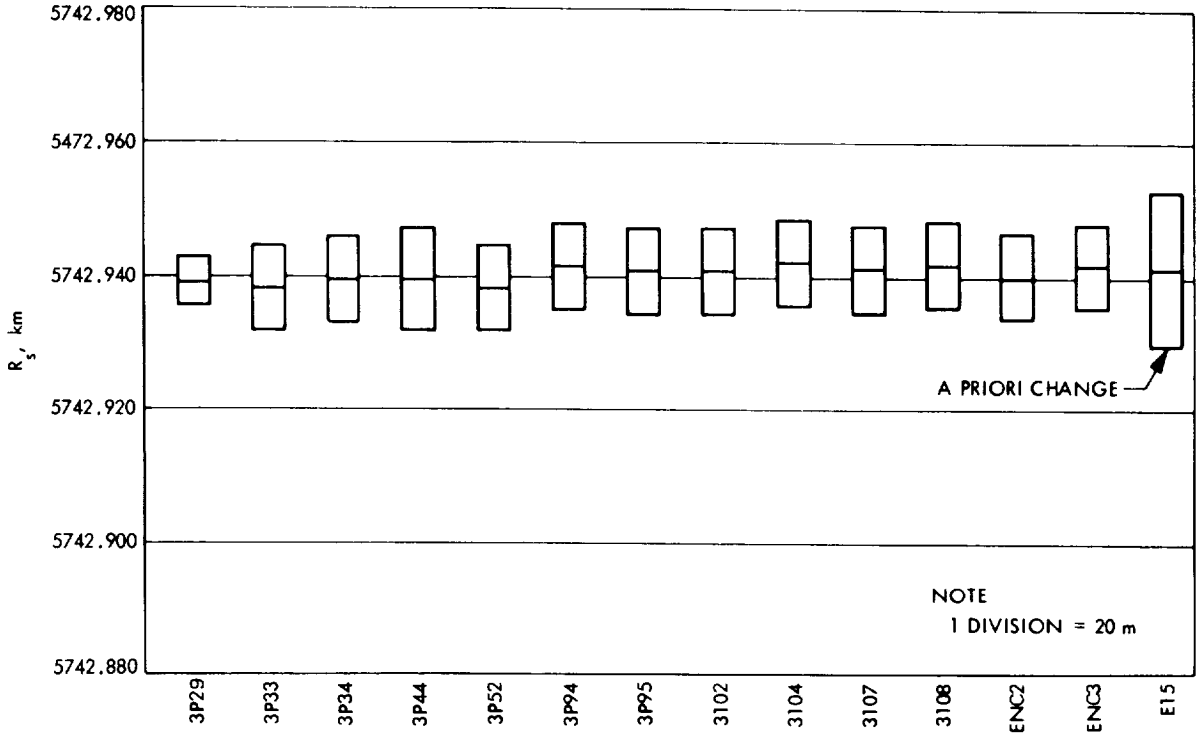

(b)

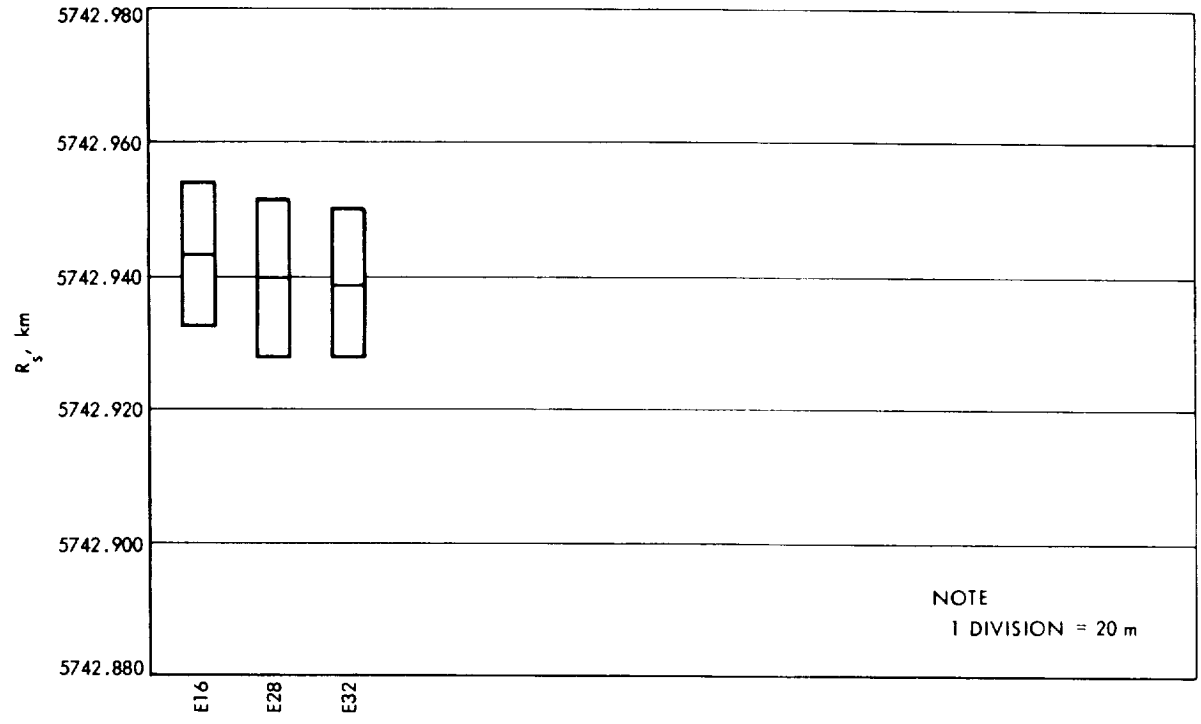

(c)

Figure 2-45. Distance Off Spin Axis, DSS 51 (cont'd)

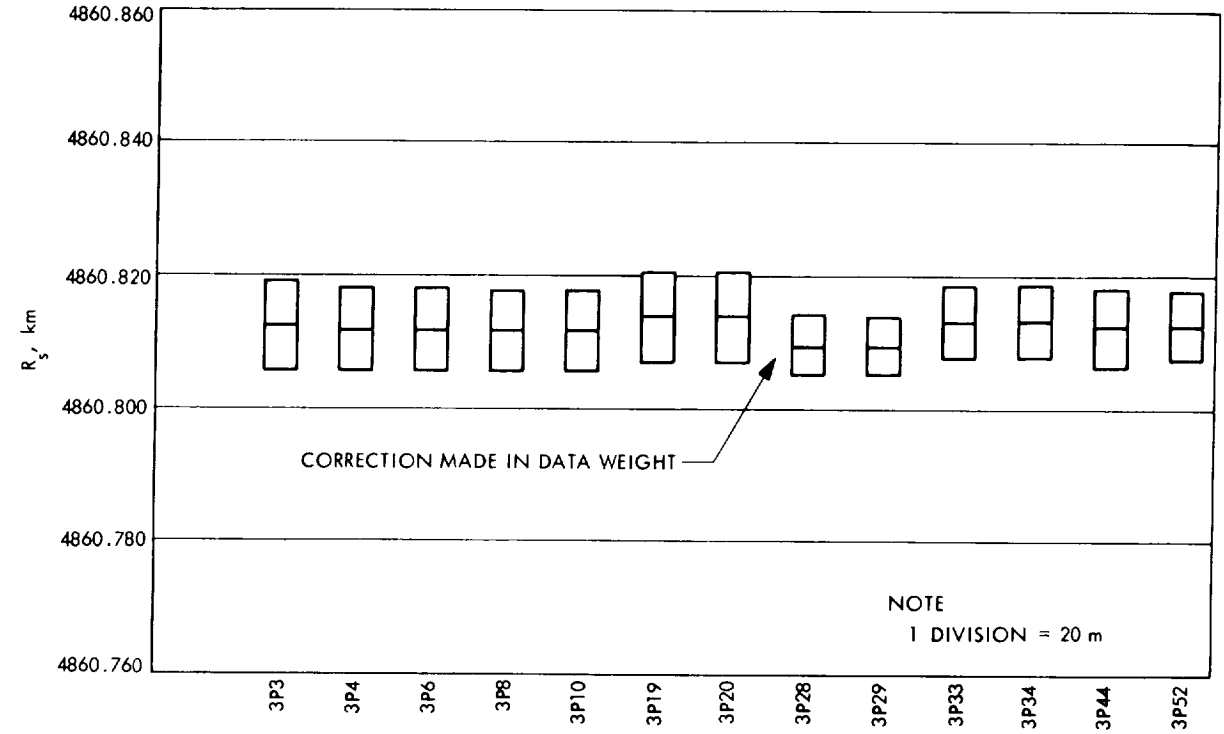

(a)

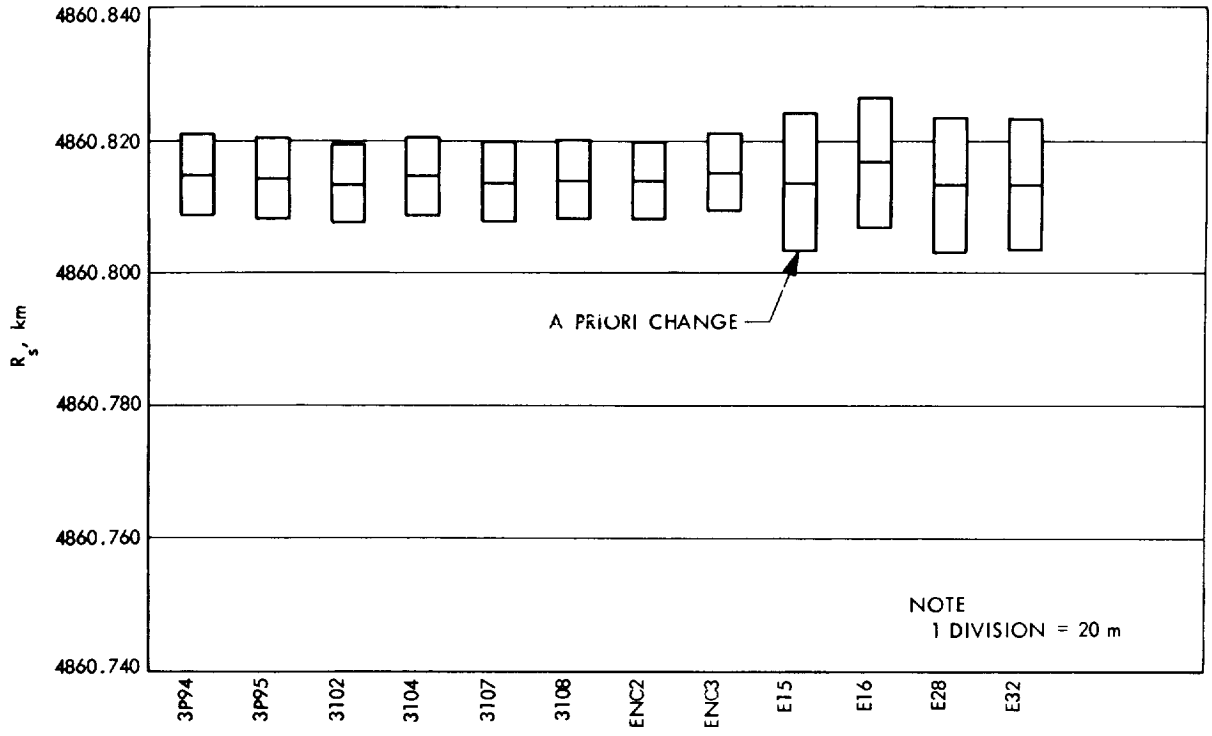

(b)

Figure 2-46. Distance Off Spin Axis, DSS 62

produced by the TPOLY program to initialize the orbit determination program for time handling, (3) a change in the *a priori* of the estimated parameters, (4) a change in the minimum elevation of tracking data, and (5) a change in the data weight. All the above conditions occurred inflight. Information regarding the above changes corresponding to the orbits are given in table 2-26. The change of data weight in orbit 3P3 was unintentional. It came about when the new updated Mariner '69 software system was implemented on approximately 13 May 1969. The updated Mariner '69 software system included some modification in the ODG which caused the data weight of the compressed data (600 sec count time) to be the same data weight as the 60 sec data, when the compressed data should have been weighted 10 times more than the 60 sec data. This data weight change was discovered and corrected on orbits 3P28 and subsequent ones. The nominal minimum elevation angle at which the data were taken and still used in the orbit solution was 15 deg, however, significant amounts of data obtained during premidcourse, pre-unlatch and early portions of the cruise phase are below 15 deg and, therefore, 10 deg was used at these times.

A new set of station locations and timing polynomials were implemented into the flight version of the SPODP just prior to orbit 3P10. The changes in observed station locations at this point are due to the changes which have been made in the timing and the polar motion system used by JPL*. The changes were made in the computation of Universal Time and the determination of pole positions. The following station longitude changes were observed when the timing polynomials were updated:

Station	$\Delta\lambda$
DSS 41	12 meters
DSS 51	11 meters
DSS 62	12 meters
DSS 12	12 meters

No noticeable changes were observed in the station distance from the spin axis.

*It is well known that a timing error is equivalent to a station longitude error: a 1 sec clock error corresponds to a station longitude error of approximately 416 m.

The post-flight Mariner VI station location solutions for premidcourse, pre-unlatch, post-unlatch and encounter phases are given in Table 41 in II B 6.d along with Mariner VII and previous interplanetary missions. The station location solutions are given in r_s, the distance from the Earth spin axis and λ, the longitude.* Of the four sets of station locations (one for each phase), the set computed using encounter tracking data is probably best because the tracking data was almost continuous, and the station tracking passes were longer than those taken during the cruise phase. In addition, the encounter tracking data has more information on station locations than the tracking data from other phases. There are some expected differences between the Mariner VI solutions and the solutions from other missions because of a difference in the ephemeris used in the computation. Mariner VI solutions used Development Ephemeris 71 and solutions of other missions used Development Ephemeris 69.

*Doppler data is quite sensitive to r_S and λ, but insensitive to z, the distance along the spin axis (corresponding to latitude). Section II. A. 3. b points out that range data is sensitive to z and can be used to estimate this third component of station locations.

6. Mariner VII Inflight Orbit Determination Analysis

a. Pre-midcourse Orbit Estimates — *S. K. Wong, S. J. Reinbold*

- Introduction

The Mariner VII spacecraft was injected into its Earth-Mars trajectory on March 27, 1969 at $22^h33^m43^s.500$ GMT. The nominal closest approach point was 7200 km from the center of Mars, to be reached on August 5, 1969; however, at injection, this was deliberately biased out to 21,131 km from the center of Mars to avoid any chance of impacting the planet. Hence, a midcourse maneuver was planned at the outset to achieve the nominal aiming point. This spacecraft had the capability to perform two maneuvers.

- Estimation of Spacecraft Pre-maneuver Orbit

The ETR check orbit was computed at JPL using only 14 data points from Antigua. These fourteen data points were obtained between the Centaur main engine cut-off and the Centaur-spacecraft separation. Therefore this orbit was biased from the actual spacecraft orbit computed later during the flight. This orbit indicated a B-miss of 42,047 km.

The first estimate of the spacecraft orbit was completed at L + 2h and was based on approximately 1 hour of DSS 51 angular and two-way doppler data. When this solution was mapped forward to target, the B-plane estimates indicated that the solution was close to the nominal pre-maneuver aiming point ($\bar{B} \cdot \bar{R}$ = 20994 km, $\bar{B} \cdot \bar{T}$ = 2402 km, $t_{ca} = 04^h31^m31^s.76$) and that the correction required to achieve the nominal post-maneuver aim point was within the midcourse correction capability. This was verified by the second (ICEV) and third (PREL) orbit computations completed at L + 5 h and L + 11h respectively

During the second orbit computation period, the angular data was dropped from the solutions. Since it is known that angular data are biased, the sole purpose of using angular data is to hold the orbit until enough doppler data is obtained to converge independently to a reasonable solution.

During the data consistency (DACO) computation period from L + 14h to L + 27h, orbital solutions were obtained using various combinations of DSSs 41, 51, 12 and MSFN 75 data. The solutions obtained from these computations indicated that the DSSs 41, 51 and 12 data were consistent. However, the

MSFN 75 data appeared to be biased just as it was for Mariner VI. It is believed that this bias is probably due to the inaccuracy of the surveyed station location. The MSFN data was not used in any later orbit computations.

The nominal maneuver (NOMA) orbit computation time block started at approximately L + 40h. The NOMA XF orbit was computed at approximately L + 3.5 days and the following amount of data was used:

DSS	Doppler Data
41	26 hours
62	14 hours
12	8.5 hours

No ranging data was obtained prior to this time. The orbit estimated only the state vector and when this solution was mapped to target, it indicated the following results:

$$B = 30095 \text{ km}$$

$$\bar{B} \cdot \bar{R} = 29355 \text{ km}$$

$$\bar{B} \cdot \bar{T} = -6632 \text{ km}$$

$$t_{ca} = 04^h48^m45^s.623$$

The Canopus tracker had been locked on the star Vega since 00^h24^m GMT on March 28, but at 16^h45^m GMT on April 1, DSS-41 transmitted a DC 21 command which caused the spacecraft to unlock and roll until Canopus was acquired. This spacecraft roll created some difficulties in the orbit computations. The difficulties arise from the fact that non-radial components of solar pressure force on the high gain antenna had changed direction due to the spacecraft roll. This change in direction of the solar pressure force caused some inconsistency between the data when the Canopus tracker was locked to the star Vega and the data when the Canopus tracker was locked on Canopus. Because of the inconsistency between the two data blocks, a decision had to be made as to which data block to use to compute the orbit for maneuver calculation or to ignore the inconsistency between the two data blocks and use all the data. The orbit solutions for each of the data blocks and the combination of the two data blocks are given below:

Vega Data Block (Orbit-NOMA 2XE)	Canopus Data Block (Orbit-LAPM XH)	Combined Data Blocks (Orbit-LAPM XG)
$B = 30085$ km	$B = 30093$ km	$B = 30082$ km
$\bar{B} \cdot \bar{R} = 29348$ km	$\bar{B} \cdot \bar{R} = 29297$ km	$\bar{B} \cdot \bar{R} = 29309$ km
$\bar{B} \cdot \bar{T} = -6622$ km	$\bar{B} \cdot \bar{T} = -6874$ km	$\bar{B} \cdot \bar{T} = -6777$ km
$t_{ca} = 04^h48^m45^s$	$t_{ca} = 04^h49^m23^s$	$t_{ca} = 04^h48^m22^s$

The orbit solutions given above estimated only the state vector and used only doppler data. The SPODP did not have the capability to estimate all three components of solar pressure. This capability was added after the maneuver of the Mariner VII spacecraft.

The DPODP orbit solutions for the two data blocks estimated only the state vector and were computed using only the doppler data. When the solutions were mapped to target, they indicated the following results:

Vega Data Block (state only)	Canopus Data Block (state only)
$B = 30083$ km	$B = 30100$ km
$\bar{B} \cdot \bar{R} = 29327$ km	$\bar{B} \cdot \bar{R} = 29291$ km
$\bar{B} \cdot \bar{T} = -6701$ km	$\bar{B} \cdot \bar{T} = -6931$ km
$t_{ca} = 04^h48^m01^s$	$t_{ca} = 04^h49^m09^s$

These results agree quite closely with the SPODP orbit solutions.

When the DPODP orbit solutions for the two data blocks estimated the 3 components of the solar pressure along with the state vector the following results were obtained:

Vega Data Block (State + 3G's)	Canopus Data Block (State + 3G's)
$B = 30085$ km	$B = 30056$ km
$\bar{B} \cdot \bar{R} = 29322$ km	$\bar{B} \cdot \bar{R} = 29260$ km
$\bar{B} \cdot \bar{T} = -6723$ km	$\bar{B} \cdot \bar{T} = -6869$ km
$t_{ca} = 04^h48^m10^s$	$t_{ca} = 04^h49^m14^s$

The DPODP orbit solutions indicated the difference between the two data blocks were as follows:

Estimate State Only		Estimate State + 3G's	
ΔB	= 17 km	ΔB	= 29 km
$\Delta \bar{B} \cdot \bar{R}$	= 36 km	$\Delta \bar{B} \cdot \bar{R}$	= 62 km
$\Delta \bar{B} \cdot \bar{T}$	= 230 km	$\Delta \bar{B} \cdot \bar{T}$	= 137 km
Δt_{ca}	= 38 sec	Δt_{ca}	= 64 sec

The Canopus data block solution had the latest data on the spacecraft, but having an epoch at approximately 5 days from injection and having only approximately 6 days of data, there were some doubts as to whether this was enough to compute a stable, accurate orbit. When the last orbit was computed before the maneuver using the Canopus block of data the solution was still moving very slightly toward the less negative value in $\bar{B} \cdot \bar{T}$.

The LAPM XG orbit solution was used for midcourse maneuver computation. The solution was computed using doppler data from both data blocks and estimated only the state vector. This solution is between the solutions for the two data blocks.

The ranging data was not included in the final solution because an apparent inconsistency between range and doppler had been observed. DPODP orbit solutions on the Canopus data block were computed using doppler data only, ranging data only, and doppler and ranging data. The comparison between the three solutions is given below:

	Doppler Only	Range Only	Doppler and Range
B	30100 km	30688 km	30800 km
$\bar{B} \cdot \bar{R}$	29291 km	29815 km	29922 km
$\bar{B} \cdot \bar{T}$	-6932 km	-7268 km	-7302 km
t_{ca}	$04^h49^m09^s$	$04^h48^m39^s$	$04^h48^m47^s$

These solutions estimated only the state vector.

The numerical results of the premaneuver orbit computations are presented in Table 2-27. The SMAA and SMIA of orbit LAPM XG quoted inflight for midcourse calculation are 400 km by 400 km. Figure 2-47 shows the B-plane estimates of the orbits computed. Figures 2-48 and 2-49 show the time of closest approach of the premidcourse orbits.

Table 2-27. Mariner VII Premidcourse Orbit Computations

Orbit ID	B, km	$\bar{B}\cdot\bar{R}$, km	$\bar{B}\cdot\bar{T}$, km	t_{ca}	Time of Last Data Point, GMT	Stations Used in Orbit	Data Types Used	Estimated Parameters
ETR	42046.92	21938.25	-35869.99	$07^h39^m43^s.09$	$3/27\text{-}22^h35^m24^s$	Antigua	R, AZ, EL	State Vector
PROR YA	28079.11	27601.8	-5155.28	$05^h23^m46^s.41$	$3/28\text{-}00^h02^m02^s$	DSS 51	HA, DEC, CC3	State Vector
PROR XA	27254.76	26740.687	-5268.56	$05^h20^m47^s.39$	$3/28\text{-}00^h43^m32^s$	DSS 51, 62	CC3, C3	State Vector
ICEV XA	22239.54	21978.57	-3397.00	$04^h57^m48^s.28$	$3/28\text{-}03^h18^m02^s$	DSS 51	CC3	State Vector
PREL XA	29914.58	29191.05	-6539.45	$04^h48^m42^s.88$	$3/28\text{-}16^h33^m32^s$	DSS 41, 51, 12	CC3	State Vector
DACO XA	29839.32	29121.08	-6507.54	$04^h48^m35^s.55$	$3/28\text{-}18^h03^m32^s$	DSS 41, 51	CC3	State Vector
DACO XB	29634.21	28957.30	-6297.73	$04^h48^m34^s.81$	$3/28\text{-}11^h11^m32^s$	DSS 51, 12	CC3	State Vector
DACO XC	29927.47	29209.59	-6515.59	$04^h48^m45^s.84$	$3/28\text{-}18^h03^m32^s$	DSS 41, 12	CC3	State Vector
NOMA XA	30051.32	29309.22	-6637.11	$04^h48^m44^s.81$	$3/29\text{-}17^h49^m32^s$	DSS 41, 51, 62, 12	CC3	State Vector
NOMA XC	30134.81	29395.97	-6632.03	$04^h48^m55^s.18$	$3/29\text{-}19^h46^m32^s$	DSS 41, 51, 62	CC3	State Vector
NOMA XD	30141.56	29403.11	-6631.05	$04^h48^m55^s.61$	$3/29\text{-}19^h46^m32^s$	DSS 41, 62, 12	CC3	State Vector
NOMA XE	30136.03	29401.19	-6614.41	$04^h48^m50^s.43$	$3/29\text{-}19^h46^m32^s$	DSS 41, 62, 12	CC3	State Vector and G
NOMA XF	30094.82	29355.08	-6631.55	$04^h48^m45^s.62$	$3/31\text{-}17^h33^m32^s$	DSS 41, 62, 13	CC3	State Vector
NOMA XH	30087.18	29349.31	-6622.44	$04^h48^m45^s.59$	$4/01\text{-}17^h59^m02^s$	DSS 41, 62, 12, 14	CC3	State Vector
NOMA 2XA	30074.31	29331.94	-6640.88	$04^h48^m40^s.57$	$4/02\text{-}17^h18^m02^s$	DSS 41, 62, 12, 14	CC3	State Vector
NOMA 2XC	30052.56	29303.49	-6667.99	$04^h48^m33^s.38$	$4/03\text{-}18^h00^m02^s$	DSS 41, 62, 12, 14	CC3	State Vector
NOMA 2XE	30085.27	29347.56	-6621.52	$04^h48^m45^s.49$	$4/01\text{-}16^h24^m32^s$	DSS 41, 62, 12, 14	CC3	State Vector
LAPM XC	30146.31	29327.55	-6978.16	$04^h48^m52^s.55$	$4/04\text{-}18^h02^m02^s$	DSS 41, 62, 12, 14	CC3	State Vector
LAPM XD	24343.02	21965.52	-10492.78	$04^h23^m23^s.21$	$4/04\text{-}18^h02^m02^s$	DSS 41, 62, 12, 14	RU, CC3	State Vector
LAPM XE	30132.42	29331.74	-6900.10	$04^h49^m28^s.22$	$4/06\text{-}19^h00^m02^s$	DSS 41, 62, 12, 14	CC3	State Vector, G and Station Location
LAPM XF	30057.32	29332.10	-6562.83	$04^h48^m15^s.22$	$4/01\text{-}16^h24^m32^s$	DSS 41, 62, 12, 14	CC3	State Vector, G and Station Location
LAPM XG	30082.44	29309.03	-6777.44	$04^h48^m22^s.01$	$4/06\text{-}10^h03^m02^s$	DSS 41, 62, 12, 14	CC3	State Vector
LAPM XH	30092.89	29297.17	-6814.41	$04^h49^m22^s.63$	$4/07\text{-}19^h01^m02^s$	DSS 41, 62, 12, 14	CC3	State Vector
LAPM 2XC	30047.91	29251.12	-6873.80	$04^h49^m24^s.73$	$4/08\text{-}10^h37^m02^s$	DSS 41, 62, 12, 14	CC3	State Vector

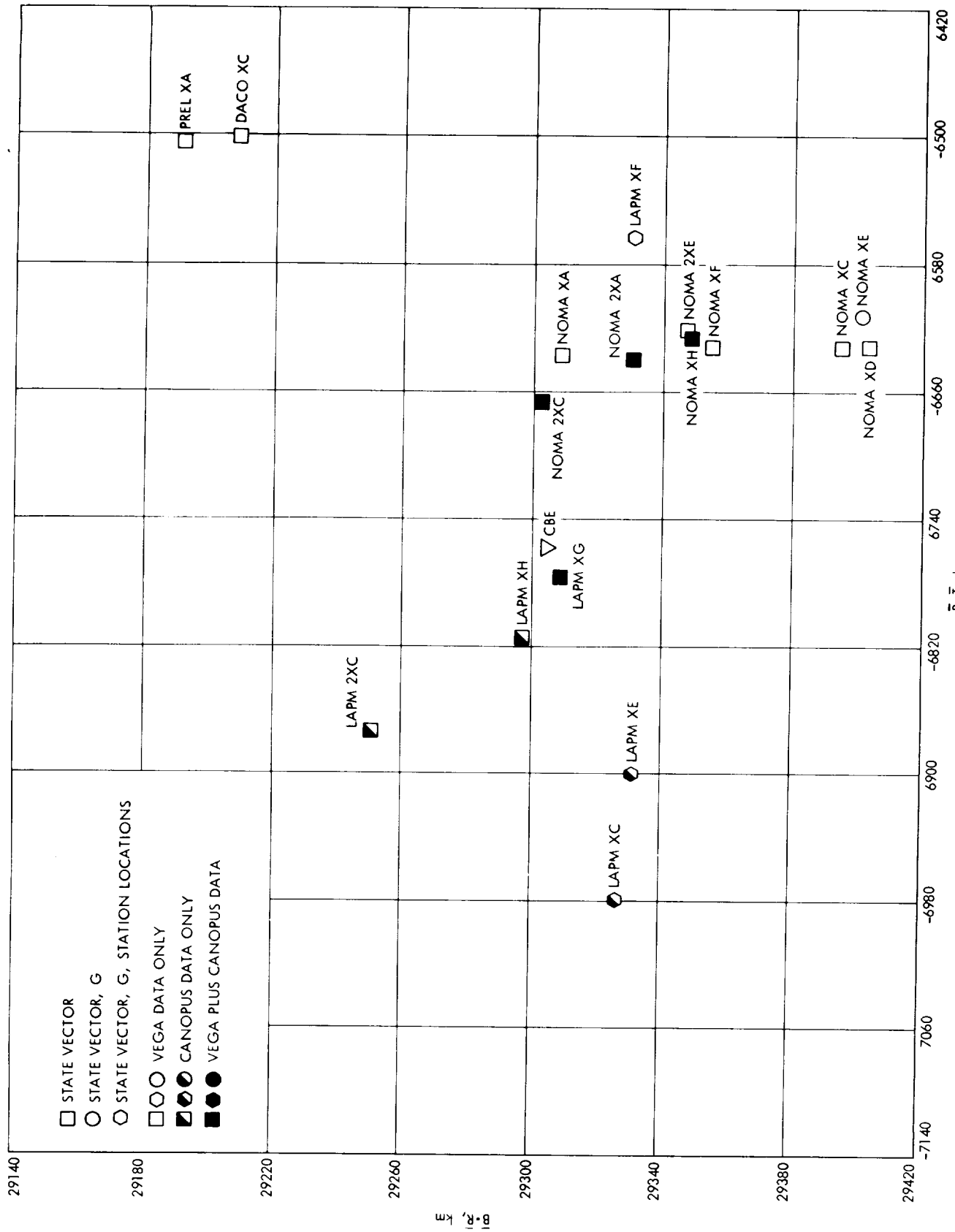

Figure 2-47. Mariner VII Pre-midcourse Inflight Orbits

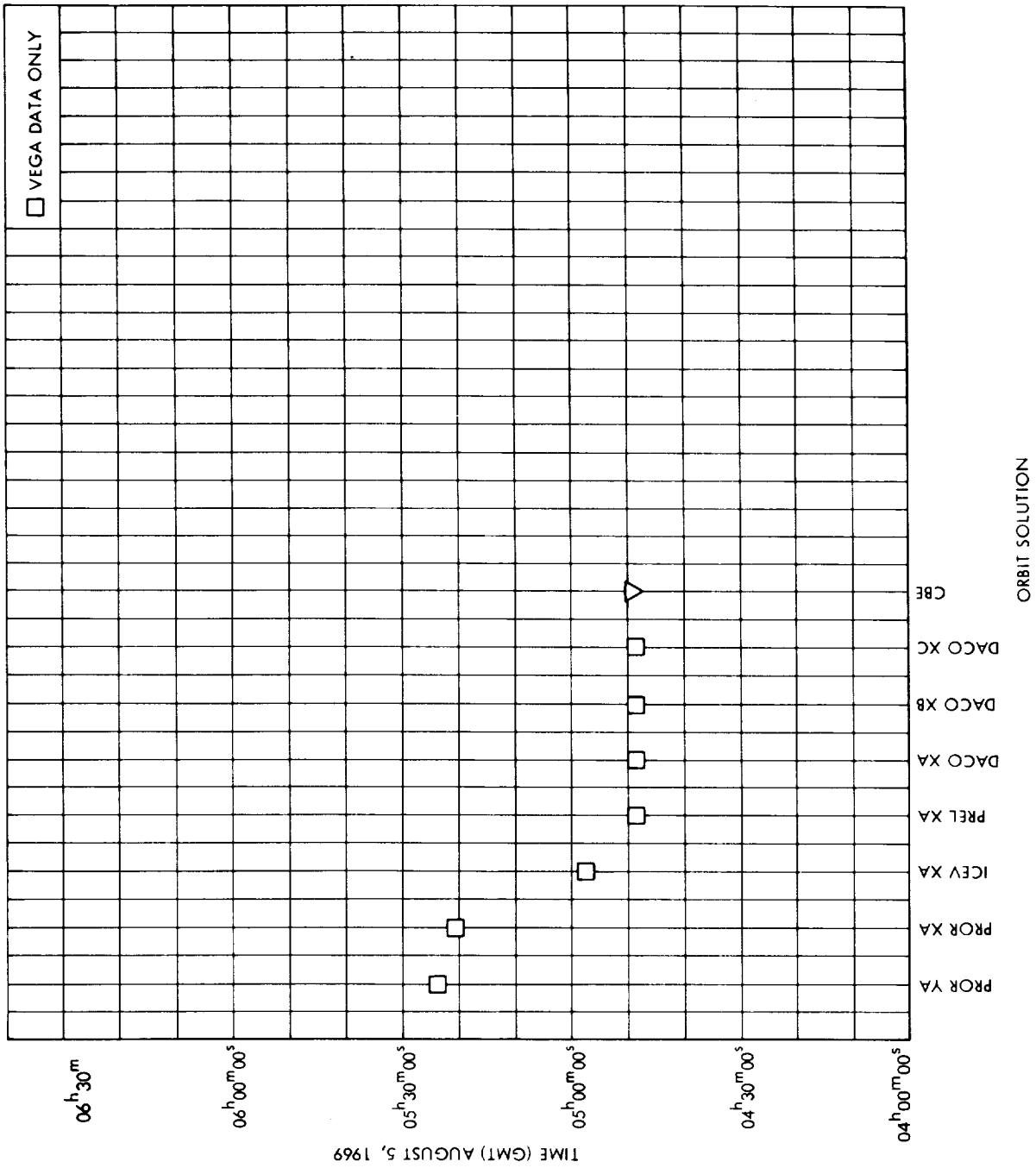

Figure 2-48. Mariner VII Pre-Midcourse Time of Closest Approach

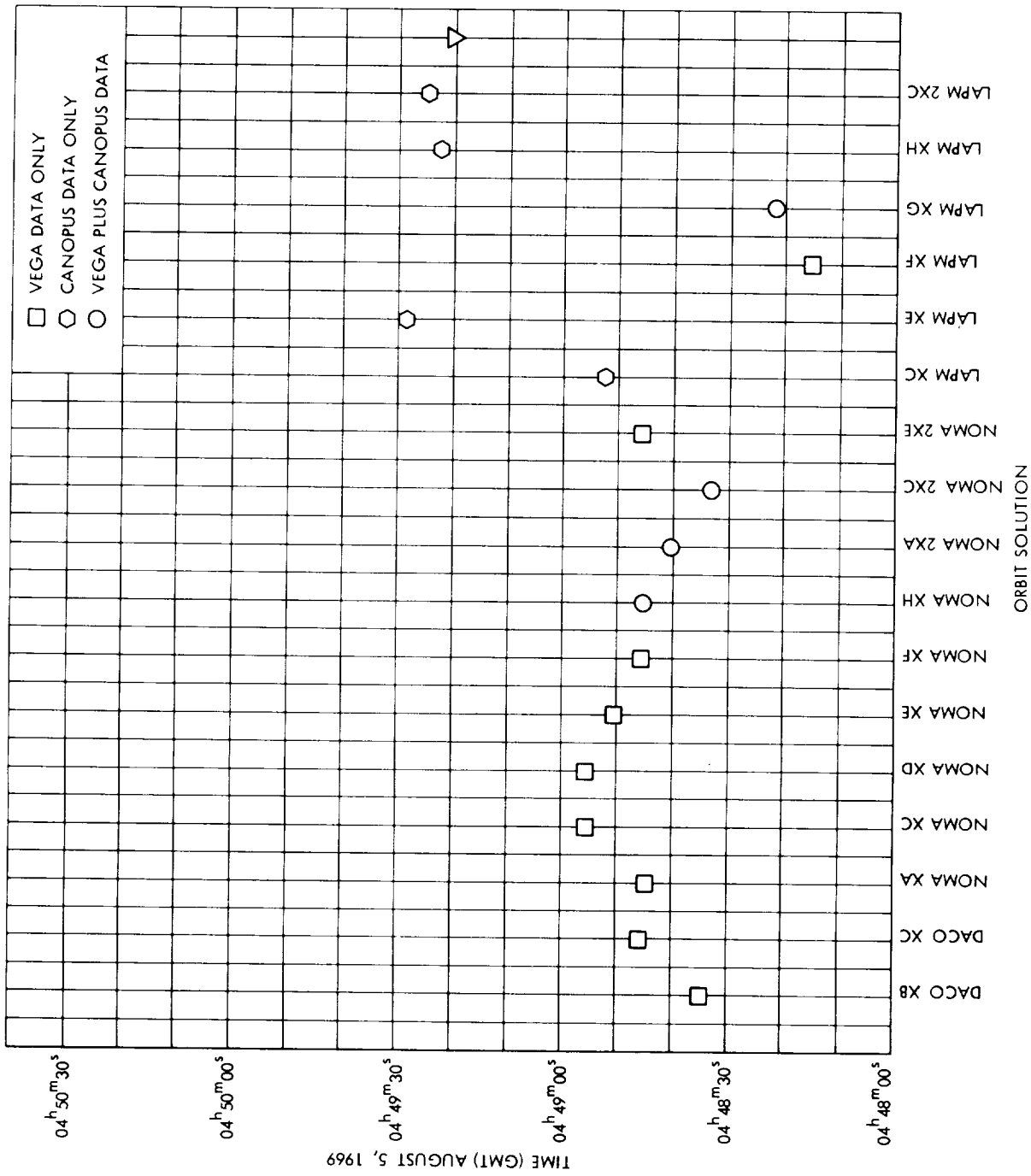

Figure 2-49. Mariner VII Pre-midcourse Time of Closest Approach

b. Post Midcourse Orbit Estimates — *S. K. Wong, S. J. Reinbold*

- Introduction

The command to initiate the Mariner VII spacecraft maneuver was transmitted by DSS 41 at $18^h51^m14^s$ GMT on April 8 and Canopus was reacquired at 21^h16^m GMT. The maneuver was performed approximately 12 days after launch.

Unlatching of the platform was preprogrammed in the central computer and sequencer of Mariner VII to occur about five weeks after launch. It was delayed because the operations team was very busy with Mariner VI due to its Canopus tracker problem and attempts to acquire the Greater Magellanic Cloud. The scan platform was unlatched by the ground command transmitted at 19^h18^m GMT, May 8 from DSS 41. This scan platform operation slightly perturbed the orbit of the spacecraft.

- Estimation of Spacecraft Pre-Unlatched Orbit

With about 2 days of tracking data, orbit solutions were computed using doppler and range data. These orbits estimated only the state vector and when these solutions were mapped to target, they showed the following results:

Orbit Post 4 (Doppler Only)	Orbit Post 5 (Doppler and Range (RU))	Maneuver Aiming Point
$\overline{B} \cdot \overline{R}$ = 2959 km	$\overline{B} \cdot \overline{R}$ = 3540 km	$\overline{B} \cdot \overline{R}$ = 3440 km
$\overline{B} \cdot \overline{T}$ = 6684 km	$\overline{B} \cdot \overline{T}$ = 6409 km	$\overline{B} \cdot \overline{T}$ = 6528 km
$t_{ca} = 05^h00^m59^s.333$	$t_{ca} = 04^h58^m55^s.716$	$t_{ca} = 05^h01^m09^s$

The differences between these results and the maneuver aim point are presented below:

Δ = Post 4 - M. A. P.	Δ = Post 5 - M. A. P.
$\Delta\overline{B} \cdot \overline{R}$ = -481 km	$\Delta\overline{B} \cdot \overline{R}$ = 10 km
$\Delta\overline{B} \cdot \overline{T}$ = 156 km	$\Delta\overline{B} \cdot \overline{T}$ = -119 km
Δt_{ca} = -9.667 sec	Δt_{ca} = -134 sec

Once again, an apparent inconsistency was observed between doppler and range data. With approximately 7 days of tracking data and the solutions estimating only the state vector, the following orbits were obtained:

Doppler Only	Doppler and Range (RU)	Doppler and Range (RU) and Range (PRU)
B = 7368 km	B = 7362 km	B = 7345 km
$\overline{B} \cdot \overline{R}$ = 3427 km	$\overline{B} \cdot \overline{R}$ = 4136 km	$\overline{B} \cdot \overline{R}$ = 3566 km
$\overline{B} \cdot \overline{T}$ = 6522 km	$\overline{B} \cdot \overline{T}$ = 6094 km	$\overline{B} \cdot \overline{T}$ = 6421 km
$t_{ca} = 04^h59^m54^s.409$	$t_{ca} = 04^h59^m24^s.316$	$t_{ca} = 04^h59^m14^s.300$

The range (RU) is the data from the Mark IA ranging system for near Earth tracking. The Range (PRU) is the data from the planetary ranging system for tracking at greater distances. The doppler and range (PRU) solution was not computed during inflight. This apparent inconsistency between the two data types was also observed in the DPODP orbit solutions. The comparison is given below:

Doppler Only (DPODP)	Doppler and Range (RU) and Range (PRU) (DPODP)
B = 7380 km	B = 7324 km
$\overline{B} \cdot \overline{R}$ = 3434 km	$\overline{B} \cdot \overline{R}$ = 3941 km
$\overline{B} \cdot \overline{T}$ = 6532 km	$\overline{B} \cdot \overline{T}$ = 6173 km
$t_{ca} = 04^h59^m50^s.981$	$t_{ca} = 04^h59^m14^s.717$

The solutions estimated only the state vector and used approximately 8 days of data.

When the scan platform was unlatched at 19^h18^m GMT, May 8, the inflight pre-unlatch orbit solution indicated the following results:

Post 30

$B = 7553$ km

$\overline{B} \cdot \overline{R} = 3536$ km

$\overline{B} \cdot \overline{T} = 6674$ km

$t_{ca} = 05^h 00^m 21^s.538$

This solution was computed estimating the state vector, solar pressure coefficient along the Sun-spacecraft direction, and station locations. The current best estimate of the pre-unlatched orbit is given below:

$B = 7549$ km

$\overline{B} \cdot \overline{R} = 3537$ km

$\overline{B} \cdot \overline{T} = 6669$ km

$t_{ca} = 05^h 00^m 11^s.324$

This solution estimated the state vector, gravitational constants of the moon, and the solar pressure coefficients and used the doppler and range (PRU) data.

- Estimation of Spacecraft Post-Unlatch Orbit

Similar to the estimation of the Mariner VI post unlatch orbit, the redetermination of the orbit during this phase took much longer for the orbit to stabilize than the previous phases which was due to the placement of the epoch and the lack of continuous tracking data. With about 5 days of intermittent tracking data the post-unlatch orbit solution was:

$B = 7412$ km

$\overline{B} \cdot \overline{R} = 3724$ km

$\overline{B} \cdot \overline{T} = 6409$ km

$t_{ca} = 04^h 59^m 29^s.766$

This orbit solution estimated only the state vector and used doppler data only. There were no ranging data taken until June 27.

With about 2-1/2 months of intermittent tracking data the following orbit solutions were obtained:

Orbit	2 Post 39	2 Post 40	2 Post 41
Data Used	Doppler and Range	Doppler and Range	Doppler
Parameters Estimated	State Vector, Solar Pressure Coefficients, Gravitational Constant of Moon	State Vector, Solar Pressure Coefficients, Gravitational Constant of Moon, Station Locations	State Vector, Solar Pressure Coefficients, Gravitational Constant of Moon, Station Locations
B, km	7544	7554	7526
$\overline{B} \cdot \overline{R}$, km	3545	3544	3498
$\overline{B} \cdot \overline{T}$, km	6659	6671	6664
t_{ca}, 8/5/69	$05^h00^m38^s.075$	$05^h00^m38^s.745$	$05^h00^m42^s.278$

At approximately encounter minus 5 days the following orbit solutions were available:

2 Post 39	2 Post 44
Doppler and Range (PRU)	Doppler Only
$B = 7544$ km	$B = 7502$ km
$\overline{B} \cdot \overline{R} = 3545$ km	$\overline{B} \cdot \overline{R} = 3513$ km
$\overline{B} \cdot \overline{T} = 6659$ km	$\overline{B} \cdot \overline{T} = 6629$ km
$t_{ca} = 05^h00^m38^s.075$	$t_{ca} = 05^h00^m39^s.942$

The 2 Post 39 orbit solution estimated the state vector, gravitational constant of the Moon, and the solar pressure coefficients. The 2 Post 44 orbit solution estimated the same parameters plus the station location parameters. These two orbit solutions agreed quite well.

The current best estimate of the post-unlatch orbit is given below: $B = 7522$ km, $\overline{B} \cdot \overline{R} = 3531$ km, $\overline{B} \cdot \overline{T} = 6642$ km, $t_{ca} = 05^h00^m36^s.626$. This solution was computed using doppler and range (PRU) data and estimated the state vector, solar pressure coefficients and the gravitational constant of the Moon.

The numerical results of the post-midcourse and post-unlatch orbit computations are presented in Table 2-28. Figures 2-50 and 2-51 show the B-plane estimates of the post-midcourse and post-unlatch inflight orbits. Figures 2-52 and 2-53 show the time of closest approach of the post-midcourse and post-unlatch inflight orbits.

Table 2-28. Mariner VII Pre-Unlatch and Post-Unlatch Orbit Computation

Orbit ID	B, km	$\bar{B}\cdot\bar{R}$, km	$\bar{B}\cdot\bar{T}$, km	t_{ca}	Time of Last Data Point, GMT	Stations Used in Orbit	Data Types Used	Estimated Parameters
Post 1	7586.4872	3392.5023	6785.6991	$05^h00^m42^s.476$	$4/09\text{-}00^h30^m32^s$	DSS 41, 62	CC3	State Vector
Post 4	7309.2714	2958.5062	6683.7628	$05^h00^m59^s.333$	$4/10\text{-}16^h45^m32^s$	DSS 41, 62, 12	CC3	State Vector
Post 5	7278.5541	3449.6747	6409.1412	$04^h58^m55^s.716$	$4/10\text{-}16^h45^m32^s$	DSS 41, 62, 12	RU, CC3	State Vector
Post 7	7270.9879	3360.9996	6447.5535	$04^h58^m50^s.859$	$4/11\text{-}16^h49^m32^s$	DSS 41, 62, 12	RU, CC3	State Vector
Post 8	7345.9110	3411.5881	6505.6492	$04^h59^m48^s.385$	$4/11\text{-}18^h16^m32^s$	DSS 41, 62, 12	CC3	State Vector
Post 11	7359.4929	3415.7120	6518.8225	$04^h59^m55^s.759$	$4/14\text{-}19^h52^m02^s$	DSS 41, 62, 12	CC3	State Vector
Post 13	7362.4530	4136.4199	6093.6275	$04^h59^m24^s.316$	$4/15\text{-}20^h36^m02^s$	DSS 41, 62, 14	RU, CC3	State Vector
Post 14	7367.6791	3426.3727	6522.3727	$04^h59^m54^s.409$	$4/15\text{-}20^h36^m02^s$	DSS 41, 62, 12, 14	CC3	State Vector
Post 15	7344.9639	3565.9663	6421.2441	$04^h59^m14^s.300$	$4/15\text{-}20^h36^m02^s$	DSS 41, 62, 12, 14	PRU, RU, CC3	State Vector
Post 17	7027.2827	3502.7279	6092.0930	$04^h58^m06^s.300$	$4/15\text{-}20^h36^m02^s$	DSS 41, 62, 12, 14	RU, PRU	State Vector
Post 21	7384.4751	3404.3237	6552.9419	$04^h59^m38^s.997$	$4/23\text{-}00^h33^m02^s$	DSS 41, 62, 12, 14	CC3	State Vector, G, Station Location
Post 22	7337.5640	3445.0600	6478.5341	$04^h59^m09^s.190$	$4/23\text{-}00^h33^m02^s$	DSS 41, 62, 12, 14	PRU, CC3, RU	State Vector
Post 25	7412.1574	3429.2021	6571.1986	$04^h59^m57^s.734$	$4/29\text{-}11^h26^m02^s$	DSS 42, 41, 62, 12, 14	CC3	State Vector
Post 26	7415.7140	3440.0118	6569.5618	$04^h59^m57^s.210$	$5/05\text{-}01^h06^m12^s$	DSS 42, 41, 62, 12, 13	CC3	State Vector
Post 27	7560.4195	3525.3227	6688.1902	$05^h00^m17^s.826$	$5/05\text{-}01^h06^m12^s$	DSS 41, 62, 12, 14	CC3	State Vector, Solar Pressure, Station Location
Post 30	7553.1920	3536.2973	6674.2270	$05^h00^m21^s.538$	$5/08\text{-}13^h53^m02^s$	DSS 62, 12, 41, 14	CC3	State Vector, Solar Pressure, Station Location
Post 31	7461.9857	3480.8462	6600.374	$05^h00^m11^s.553$	$5/08\text{-}18^h53^m02^s$	DSS 41, 62, 12	CC3	State Vector

Table 2-28. Mariner VII Pre-Unlatch and Post-Unlatch Orbit Computation (cont'd)

Orbit ID	B, km	$\bar{B}\cdot\bar{R}$, km	$\bar{B}\cdot\bar{T}$, km	t_{ca}	Time of Last Data Point, GMT	Stations Used in Orbit	Data Types Used	Estimated Parameters
2 Post 2	7412.3244	3724.4544	6408.6654	$04^h59^m29^s.766$	$5/12\text{-}23^h09^m02^s$	DSS 41, 51, 62, 12	CC3	State Vector
2 Post 3	7494.5804	3515.0269	6619.1630	$05^h00^m32^s.155$	$5/26\text{-}23^h47^m02^s$	DSS 41, 51, 62, 12	CC3	State Vector
2 Post 4	7538.6452	3600.3692	6623.3303	$05^h00^m35^s.020$	$5/31\text{-}23^h47^m02^s$	DSS 41, 51, 62, 12	CC3	State Vector
2 Post 5	7556.9090	3552.6944	6669.7250	$05^h00^m42^s.611$	$6/02\text{-}00^h26^m02^s$	DSS 41, 51, 62, 12, 14	CC3	State Vector, Solar Pressure, Station Location
2 Post 8	7542.2323	3574.8431	6641.2169	$05^h00^m38^s.514$	$6/05\text{-}00^h26^m02^s$	DSS 41, 51, 62, 12, 14	CC3	State Vector
2 Post 13	7535.0961	3489.7965	6678.2470	$05^h00^m44^s.466$	$6/16\text{-}12^h22^m02^s$	DSS 41, 51, 62, 12	CC3	State Vector
2 Post 14	7553.4587	3522.860	6681.631	$05^h00^m44^s.658$	$6/16\text{-}12^h22^m02^s$	DSS 41, 51, 62, 12	CC3	State Vector, Solar Pressure, Station Location
2 Post 16	7542.6396	3536.126	6662.3736	$05^h00^m43^s.749$	$6/23\text{-}01^h19^m02^s$	DSS 11, 41, 51, 62, 12, 14	CC3	State Vector
2 Post 17	7549.9826	3553.5243	6661.434	$05^h00^m43^s.530$	$6/23\text{-}01^h19^m02^s$	DSS 41, 51, 62, 12, 14	CC3	State Vector, Solar Pressure, Station Location
2 Post 20	7539.0735	3498.3012	6678.2865	$05^h00^m45^s.672$	$6/30\text{-}11^h51^m02^s$	DSS 41, 12, 14, 51, 62	CC3	State Vector, Solar Pressure, Station Location
2 Post 21	7590.0065	3592.0584	6686.2032	$05^h00^m39^s.336$	$6/30\text{-}11^h51^m02^s$	DSS 62, 14, 51, 41, 12	CC3, PRU	State Vector, Solar Pressure, Station Location
2 Post 24	7515.2819	3459.6721	6671.5909	$05^h00^m47^s.856$	$7/07\text{-}10^h49^m01^s$	DSS 62, 14, 51, 41, 12	CC3	State Vector
2 Post 25	7513.8685	3414.9761	6692.9930	$05^h00^m47^s.628$	$7/07\text{-}10^h49^m02^s$	DSS 41, 14, 11, 12, 51	CC3	State Vector, Solar Pressure, Station Location

Table 2-28. Mariner VII Pre-Unlatch and Post-Unlatch Orbit Computation (cont'd)

Orbit ID	B, km	$\bar{B}\cdot\bar{R}$, km	$\bar{B}\cdot\bar{T}$, km	t_{ca}	Time of Last Data Point, GMT	Stations Used in Orbit	Data Types Used	Estimated Parameters
2 Post 27	7545.9401	3505.9699	6682.0196	$05^h00^m46^s.297$	$7/14\text{-}21^h50^m02^s$	DSS 41, 51, 62, 12, 14	CC3	State Vector, Solar Pressure, Station Location
2 Post 28	7580.6531	3537.6862	6704.5561	$05^h00^m40^s.331$	$7/14\text{-}21^h50^m02^s$	DSS 41, 51, 62, 12, 14	CC3, PRU	State Vector, Solar Pressure, Station Location
2 Post 32	7586.855	3736.4204	6602.9938	$05^h00^m47^s.604$	$7/14\text{-}21^h50^m02^s$	DSS 41, 51, 62, 12, 14	CC3	State Vector
2 Post 33	7652.719	3902.4348	6582.9405	$05^h00^m41^s.642$	$7/14\text{-}21^h50^m02^s$	DSS 41, 51, 62, 12, 14	CC3, PRU	State Vector
2 Post 34	7556.4342	3542.9296	6674.3799	$05^h00^m43^s.212$	$7/21\text{-}07^h12^m02^s$	DSS 41, 51, 62, 12, 14	CC3	State Vector, Solar Pressure, Station Location
2 Post 35	7575.3661	3566.1848	6683.4494	$05^h00^m40^s.089$	$7/21\text{-}07^h12^m02^s$	DSS 41, 51, 62, 12, 14	CC3, PRU	State Vector, Solar Pressure, Station Location
2 Post 39	7544.2336	3545.2972	6659.3035	$05^h00^m38^s.075$	$7/22\text{-}20^h55^m02^s$	DSS 51, 41, 62, 12, 14	CC3, PRU	State Vector, KM, Solar Pressure
2 Post 40	7553.7557	3544.1185	6670.7155	$05^h00^m38^s.745$	$7/22\text{-}20^h55^m02^s$	DSS 41, 51, 62, 12, 14	CC3, PRU	State Vector, KM, Solar Pressure, Station Location
2 Post 41	7526.2818	3498.2350	6663.8778	$05^h00^m42^s.278$	$7/22\text{-}20^h55^m02^s$	DSS 41, 51, 62, 12, 14	CC3	State Vector, KM, Solar Pressure, Station Location
2 Post 44	7502.3278	3512.8554	6629.0849	$05^h00^m39^s.942$	$7/26\text{-}07^h15^m02^s$	DSS 41, 72, 51, 62, 14, 12	CC3	State Vector, KM, Solar Pressure, Station Location

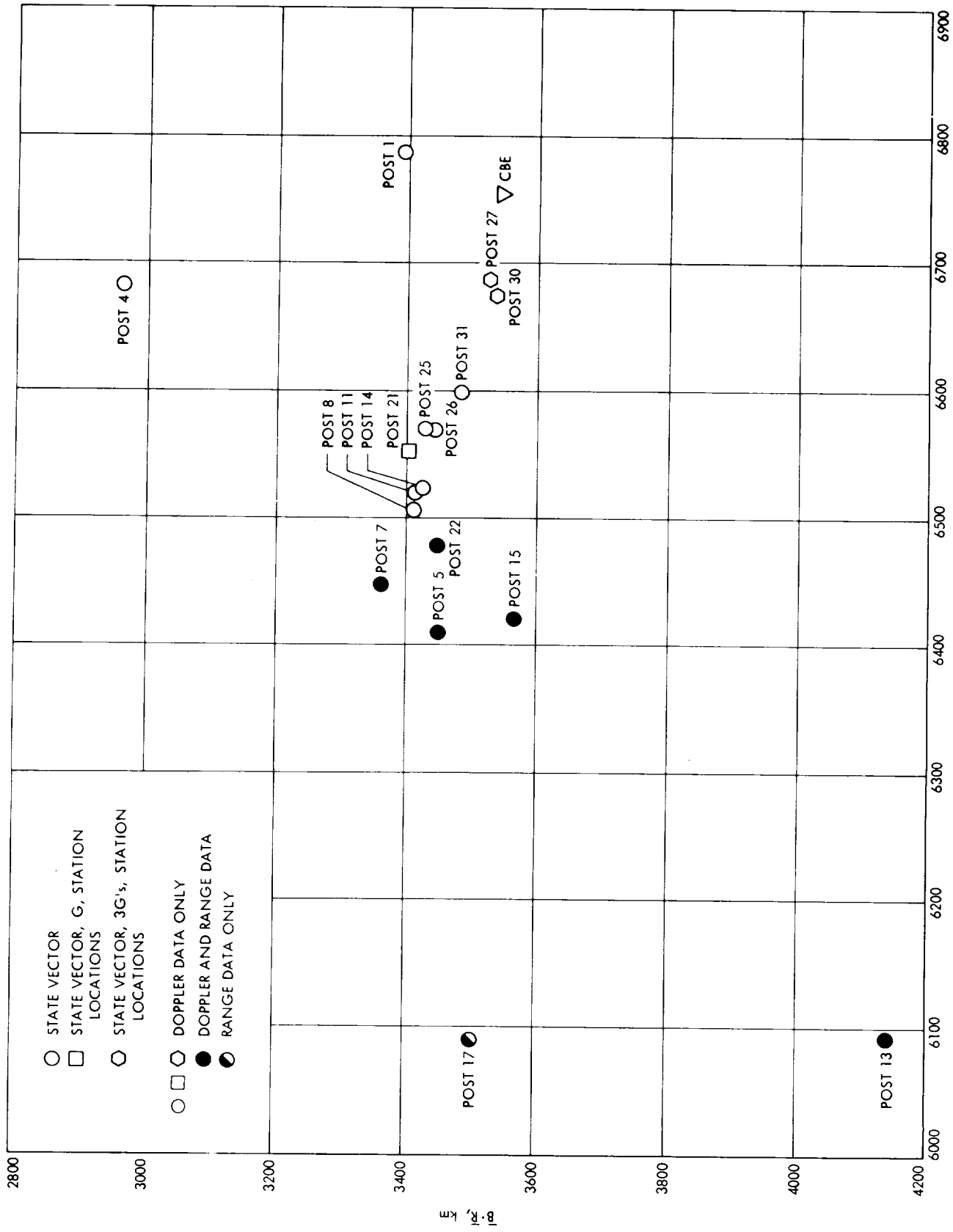

Figure 2-50. Mariner VII Post-Midcourse Orbit Estimates

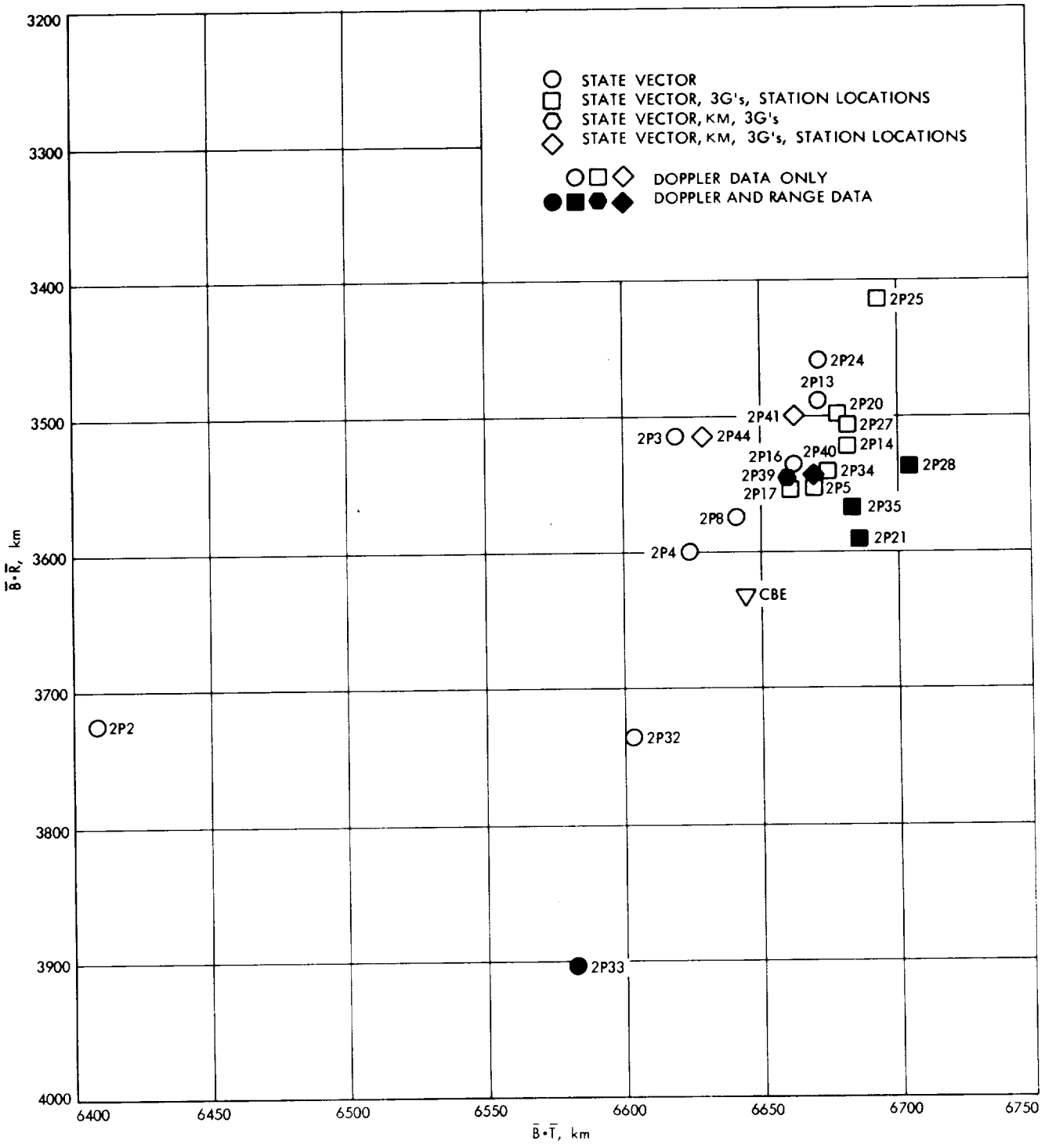

Figure 2-51. Mariner VII Post-Unlatch Orbit Estimates

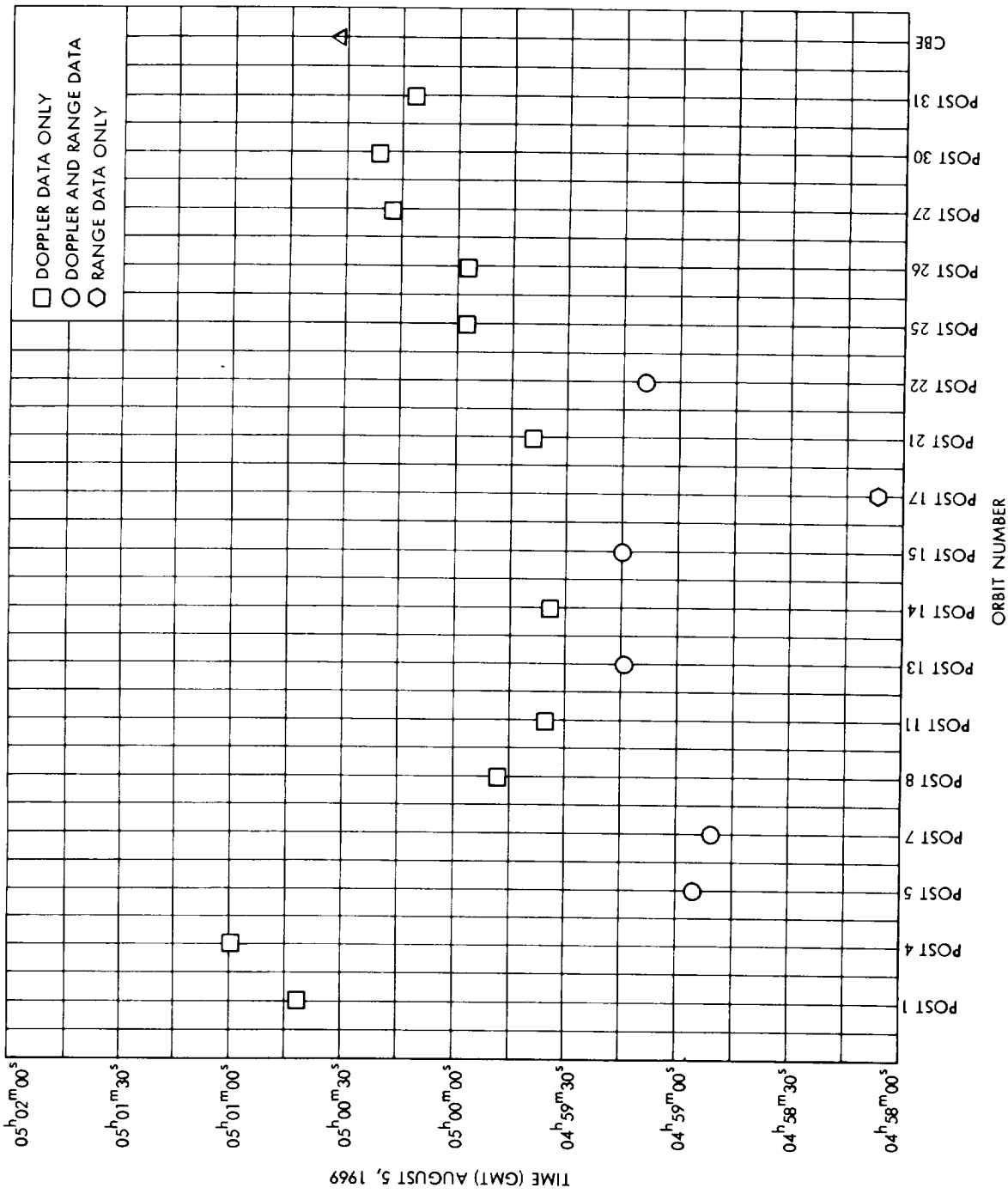

Figure 2-52. Mariner VII Post-Midcourse Time of Closest Approach

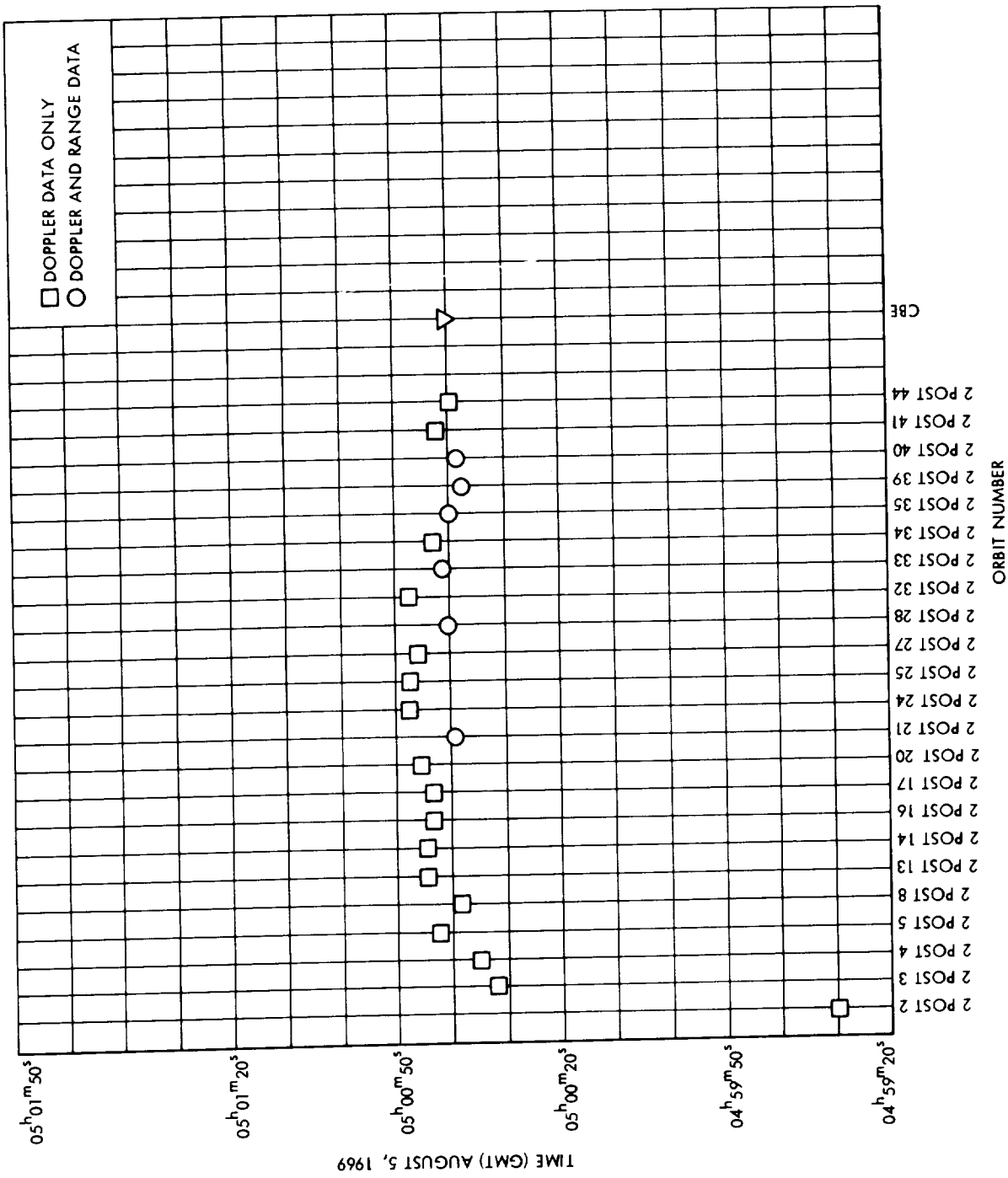

Figure 2-53. Mariner VII Post-Unlatch Time of Closest Approach

c. Encounter Orbit Estimates

- Introduction — *H. J. Gordon*

At 127 hours before its scheduled encounter with Mars, the radio signal from Mariner VII was lost abruptly. When the signal was reacquired after 7 hours and 12 minutes (following ground commands to switch to the low gain antenna), the doppler tone showed that the radial velocity had decreased by 1.89 cm/sec. There were indications that several electrical transients had occurred, and 24 telemetry channels (out of a total of 94) were found to be disabled. The doppler tone remained constant for 71 minutes, at which time two-way lock and telemetry data were lost again for 60 minutes. When two-way lock was reacquired, the radial velocity had decreased by an additional 0.78 cm/sec, and continued to decrease at an apparently exponentially decaying rate. Telemetry showed that several additional electrical transients had occurred.

There were several hypotheses to explain these events, all having the common feature of gas venting for the extended period of time during which non-gravitational acceleration continued. Operationally, it was imperative to accurately redetermine the orbit so that all science instruments could be optimally pointed during the encounter.

Post-encounter analysis ultimately led to the conclusion that at least one battery cell had spontaneously failed during a charging sequence which began on July 26. (The charge current profile had been quite non-standard. Tests conducted on August 12 and 13 showed that the battery was in an open circuit condition.) Between July 26 and July 30, the cell pressure had increased, breaking through the cell walls in one monoblock (there were six monoblocks, with three cells in each) and finally rupturing the battery case and venting into the interior of the spacecraft. Internal pressure built up and allowed corona arcing to occur in the Canopus Star Tracker 700 volt power supply. This caused the electrical transients, and also caused an apparent loss of Canopus, initiating a roll search. Dust particles dislodged from the spacecraft were acquired so that the spacecraft did not continue to roll, but did roll enough to sweep the high gain antenna away from the Earth. Gas escaped through asymmetrically located openings in the thermal blanket, producing the translational

forces. Meanwhile, the crack in the battery case was cooled by the evaporating solute and was restricted and frozen over, until the battery approached thermal equilibrium and the crack opened again. (Restriction of a venting aperture is common, special precautions being required to avoid this phenomenon when designing such apertures.) The battery temperature was 7°F cooler after the second loss of signal (LOS) than it had been immediately before. A similar temperature drop is assumed to have occurred after the first LOS, but was not seen due to the long interval between the time that the crack was sealed and the time that the signal was reacquired. The battery construction was such that about 10% of the solute is "free," 90% being entrapped in capillary tubes in the cell walls. Therefore the initial evaporation rate would have been much higher than the subsequent rates, and tests indicate that it would take about two weeks for such a cell to "dry out" in a hard vacuum.

- Estimation of The Spacecraft Pre-Encounter Orbit — *S. K. Wong, S. J. Reinbold*

The first orbit after the trajectory perturbation was computed with approximately 1 day of Doppler data. The epoch of this orbit was at 22^h00^m GMT, July 31. The solution indicated a change of 600-700 km in $\overline{B} \cdot \overline{R}$ and a change of 260-270 km in $\overline{B} \cdot \overline{T}$. However, with only one day of data, the uncertainties of this solution were larger than the indicated differences. From previous studies, results indicated that short data arc solutions would not be tied down until the near-target data (taken during the final 3-4 hours before encounter) was used in the orbit solution.

As more orbit solutions were computed with more data added, the solutions indicated that the spacecraft still had a small acceleration. Knowing that there was a small acceleration acting on the spacecraft, the strategies were:

1) To model the small acceleration in the orbit computation.

2) To keep the data arc used in computing the orbit solution as short as possible to minimize the model error.

In the SPODP, this small acceleration may be modeled by the solar pressure model, or the attitude control jet model. Both of these models were tried and the two solutions were quite similar. The solutions computed with Doppler and range data up to E - 9h are given below:

Solar Pressure Model	Attitude Control Model
$B = 7713$ km	$B = 7687$ km
$\bar{B} \cdot \bar{R} = 3927$ km	$\bar{B} \cdot \bar{R} = 3986$ km
$\bar{B} \cdot \bar{T} = 6638$ km	$\bar{B} \cdot \bar{T} = 6626$ km
$t_{ca} = 05^h00^m49^s.680$	$t_{ca} = 05^h00^m48^s.368$

At approximately E - 3h, orbit solutions were computed using doppler and range data with a data span from E - 53h to E - 4h. The solutions are presented below:

Solution E23	Solution E26	Solution E27
$B = 7692$ km	$B = 7578$ km	$B = 7535$ km
$\bar{B} \cdot \bar{R} = 3769$ km	$\bar{B} \cdot \bar{R} = 3829$ km	$\bar{B} \cdot \bar{R} = 3811$ km
$\bar{B} \cdot \bar{T} = 6705$ km	$\bar{B} \cdot \bar{T} = 6540$ km	$\bar{B} \cdot \bar{T} = 6500$ km
$t_{ca} = 05^h00^m49^s.774$	$t_{ca} = 05^h00^m52^s.788$	$t_{ca} = 05^h00^m53^s.520$

Solution E23 estimated the state vector, mass ratio of Mars to Sun, Attitude Control Jets, and station locations using Doppler and range data in the solution. Solution E26 estimated the same parameters as E23, but it used only doppler in the orbit solution. Solution E27 used only doppler data and estimated only the state vector.

The orbit solutions obtained prior to E - 6h were concentrated in the region of 3850 - 3920 km in $\bar{B} \cdot \bar{R}$. As more near-target data were added up to E - 3h, there were 3 orbit solutions that moved past 3800 km up to about 3769 km.

At approximately E - 3h, two DPODP estimates of the spacecraft orbit were obtained. The estimates are given below:

Solution A	Solution B
$\overline{B} \cdot \overline{R} = 3450$	$\overline{B} \cdot \overline{R} = 3780$
$\overline{B} \cdot \overline{T} = 6800$	$\overline{B} \cdot \overline{T} = 6640$
$t_{ca} = 05^h00^m47^s.7$	$t_{ca} = 05^h00^m49^s.7$

Solution B was computed using the short data arc and estimated the state vector, solar pressure coefficients, and the mass of Mars. Solution A used a longer data arc than Solution B and attempted to model a motor burn through the "happening."

It was decided to use the short data arc. Considering Solution B and the SPODP solutions, the following orbit solution was recommended to the MM'69 project for the final spacecraft platform update:

$\overline{B} \cdot \overline{R} = 3800$ km

$\overline{B} \cdot \overline{T} = 6670$ km

$t_{ca} = 05^h00^m50^s$

The one-sigma dispersion ellipse associated with this solution was 300 km circular.

It was decided to choose an orbit, which if in error, would minimize the effect of the OD errors on science results. Therefore, the FPAC director recommended at the E - 3hr meeting a $\overline{B} \cdot \overline{R} = 3700$ km and "rounded" the platform clock angle to the larger achievable value. The actual orbit that was used for the final spacecraft platform update was:

$\overline{B} \cdot \overline{R} = 3650$ km

$\overline{B} \cdot \overline{T} = 6725$ km

$t_{ca} = 05^h00^m47^s$

Table 2-29 presents the encounter orbit determination results. Figures 2-54 and 2-55 show the B-plane estimates for doppler only and doppler plus ranging solutions. Figure 2-56 shows the time of closest approach for the encounter orbits.

Table 2-29. Mariner VII Encounter Orbit Computations

Orbit ID	B, km	$\overline{B}\cdot\overline{R}$, km	$\overline{B}\cdot\overline{T}$, km	t_{ca}	Time of Last Data Point, GMT	Stations Used in Orbit	Data Types Used	Estimated Parameters
3 Post 1	7326.4719	3620.5259	6369.3784	$05^h01^m32.^s229$	$8/01\text{-}00^h15^m02^s$	DSS 11	CC3	State Vector
3 Post 2	8124.5777	4191.0274	6960.1759	$05^h00^m05.^s735$	$8/01\text{-}20^h23^m32^s$	DSS 11, 41, 51	CC3	State Vector
3 Post 5	7870.9892	4084.6202	6728.1684	$05^h00^m58.^s731$	$8/02\text{-}03^h49^m32^s$	DSS 11, 41, 51, 62, 14	CC3, PRU	State Vector
3 Post 6	7678.0366	3913.6062	6605.7499	$05^h01^m31.^s245$	$8/02\text{-}03^h49^m32^s$	DSS 11, 41, 51, 62, 14	CC3	State Vector
3 Post 9	7772.4686	3847.7373	6753.2349	$05^h00^m54.^s495$	$8/02\text{-}03^h49^m32^s$	DSS 11, 41, 51, 62, 14	CC3, PRU	State Vector, Station Location
3 Post 10	7774.2539	3816.4406	6773.0203	$05^h00^m48.^s350$	$8/02\text{-}15^h34^m32^s$	DSS 11, 41, 51, 62, 14	CC3	State Vector, Station Location
3 Post 11	7742.3102	3851.1216	6716.5038	$05^h00^m52.^s412$	$8/02\text{-}15^h34^m32^s$	DSS 11, 41, 51, 62, 14	CC3, PRU	State Vector
3 Post 12	7749.6709	3809.7215	6748.5863	$05^h00^m53.^s305$	$8/02\text{-}12^h34^m32^s$	DSS 11, 41, 51, 62, 14	CC3, PRU	State Vector, Station Location
3 Post 16	7861.1400	3826.4310	6867.0186	$05^h00^m27.^s276$	$8/03\text{-}20^h32^m32^s$	DSS 11, 41, 51, 62, 14	CC3	State Vector, Station Location
3 Post 17	7767.0004	3888.9461	6723.2725	$05^h00^m53.^s617$	$8/02\text{-}20^h32^m32^s$	DSS 41, 51, 62, 14	CC3, PRU	State Vector, Station Location
3 Post 20	7688.2803	3883.0558	6635.6260	$05^h01^m17.^s622$	$8/02\text{-}20^h32^m32^s$	DSS 41, 51, 62, 14	CC3	State Vector
3 Post 21	7763.2170	3936.3765	6691.2241	$05^h00^m52.^s937$	$8/02\text{-}20^h32^m32^s$	DSS 41, 51, 62, 14	CC3, PRU	State Vector
3 Post 25	7742.0462	3986.6265	6689.9608	$05^h00^m51.^s930$	$8/03\text{-}15^h37^m32^s$	DSS 41, 51, 62, 14	CC3, PRU	State Vector
3 Post 27	7726.3851	3981.8348	6674.6271	$05^h00^m50.^s943$	$8/03\text{-}15^h17^m02^s$	DSS 41, 51, 62, 14	CC3, PRU	State Vector
3 Post 28	7662.7104	3829.3290	6637.2911	$05^h00^m47.^s258$	$8/03\text{-}15^h17^m02^s$	DSS 62, 14, 41, 51	CC3, PRU	State Vector, Station Location
3 Post 30	7885.4538	3930.3092	6836.1574	$04^h59^m43.^s946$	$8/03\text{-}21^h02^m32^s$	DSS 41, 52, 14	CC3	State Vector, Station Location

Table 2-29. Mariner VII Encounter Orbit Computations (cont'd)

Orbit ID	B, km	$\bar{B}\cdot\bar{R}$, km	$\bar{B}\cdot\bar{T}$, km	t_{ca}	Time of Last Data Point, GMT	Stations Used in Orbit	Data Types Used	Estimates Parameters
3 Post 34	7662.7104	3829.3290	6637.2711	$05^h00^m47^s.258$	$8/03\text{-}15^h17^m02^s$	DSS 41, 51, 62, 14	CC3, PRU	State Vector, Station Location
Enc 6	7810.9285	3935.8620	6746:8207	$05^h00^m41^s.033$	$8/04\text{-}15^h19^m02^s$	DSS 41, 62, 14	CC3	State Vector, Solar Pressure, Station Location
Enc 7	7686.7592	3896.2547	6626.1197	$05^h00^m48^s.368$	$8/04\text{-}15^h19^m02^s$	DSS 41, 62, 14	CC3, PRU	State Vector, Gas Jets, Station Location
Enc 10	7716.8320	3839.0414	6694.1208	$05^h00^m50^s.872$	$8/04\text{-}20^h19^m02^s$	DSS 41, 62, 14	CC3, PRU	State Vector, Gas Jets
Enc 11	7712.7685	3926.9575	6638.2078	$05^h00^m49^s.680$	$8/03\text{-}16^h07^m02^s$	DSS 41, 62, 14	CC3, PRU	State Vector, Solar Pressure, Station Location
Enc 12	7722.9194	3887.3479	6673.2308	$05^h00^m50^s.666$	$8/04\text{-}20^h19^m02^s$	DSS 41, 62, 14	CC3, PRU	State Vector, Solar Pressure, Station Location
Enc 14	7722.8371	3901.9613	6664.6012	$05^h00^m50^s.729$	$8/04\text{-}20^h19^m02^s$	DSS 41, 52, 14	CC3, PRU	State Vector, Gas Jets, Station Location
Enc 15	7650.3105	3906.3579	6577.8124	$05^h00^m51^s.538$	$8/04\text{-}22^h53^m02^s$	DSS 41, 62, 14	CC3	State Vector, MM, Solar Pressure, Station Location
Enc 16	7707.6027	3857.9457	6672.580	$05^h00^m50^s.106$	$8/04\text{-}22^h53^m02^s$	DSS 41, 62, 14	CC3, PRU	State Vector, Gas Jets, Station Location
Enc 17	7724.6774	3936.4614	6646.4209	$05^h00^m50^s.359$	$8/04\text{-}22^h53^m02^s$	DSS 41, 62, 14	CC3, PRU	State Vector, MM, Solar Pressure, Station Location
Enc 20	7688.1067	3792.2613	6687.7301	$05^h00^m49^s.590$	$8/04\text{-}22^h53^m02^s$	DSS 41, 62, 14	CC3, PRU	State Vector, MM, Gas Jets, Station Location
Enc 21	7686.7158	3766.4942	6700.6806	$05^h00^m49^s.552$	$8/04\text{-}22^h53^m02^s$	DSS 41, 62, 14	CC3, PRU	State Vector, MM, Gas Jets, Station Location

Table 2-29. Mariner VII Encounter Orbit Computations (cont'd)

Orbit ID	B, km	$\overline{B} \cdot \overline{R}$, km	$\overline{B} \cdot \overline{T}$, km	t_{ca}	Time of Last Data Point, GMT	Stations Used in Orbit	Data Types Used	Estimated Parameters
Enc 23	7692.1020	3768.9396	6705.4848	$05^h00^m49^s.774$	$8/05\text{-}01^h12^m02^s$	DSS 41, 62, 14	CC3, PRU	State Vector, MM, Gas Jets, Station Location
Enc 26	7578.1699	3829.0213	6539.6675	$05^h00^m52^s.788$	$8/05\text{-}01^h12^m52^s$	DSS 41, 62, 14	CC3	State Vector, MM, Gas Jets, Station Location
Enc 27	7535.1539	3811.3938	6500.1401	$05^h00^m53^s.520$	$8/05\text{-}01^h12^m02^s$	DSS 41, 62, 14	CC3	State Vector
Enc 32*	7638.5430	3763.5883	6647.0099	$05^h00^m49^s.691$	$8/05\text{-}04^h14^m57^s$	DSS 41, 62, 14	CC3	State Vector, MM, Gas Jets, Station Location
Post Enc 29*	7631.764	3630.9142	6712.6954	$05^h00^m49^s.984$	$8/08\text{-}18^h47^m02^s$	DSS 11, 42, 41, 51, 62, 12, 14	CC3	State Vector, MM, Solar Pressure

*Computed after the final platform update. Post Enc 29 is the current best estimate of the Mariner VII orbit.

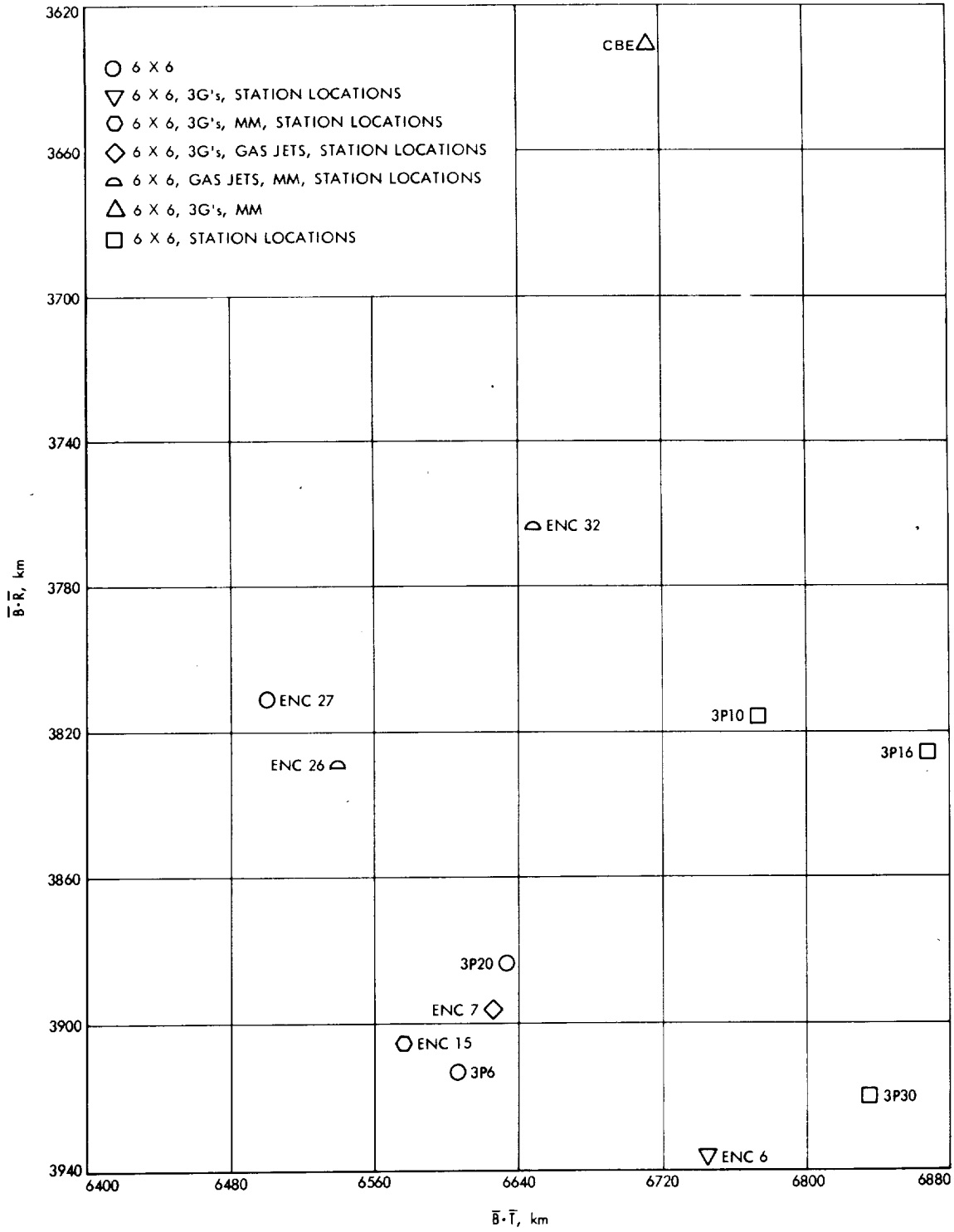

Figure 2-54. Mariner VII Encounter Orbit Solutions Doppler Data Only

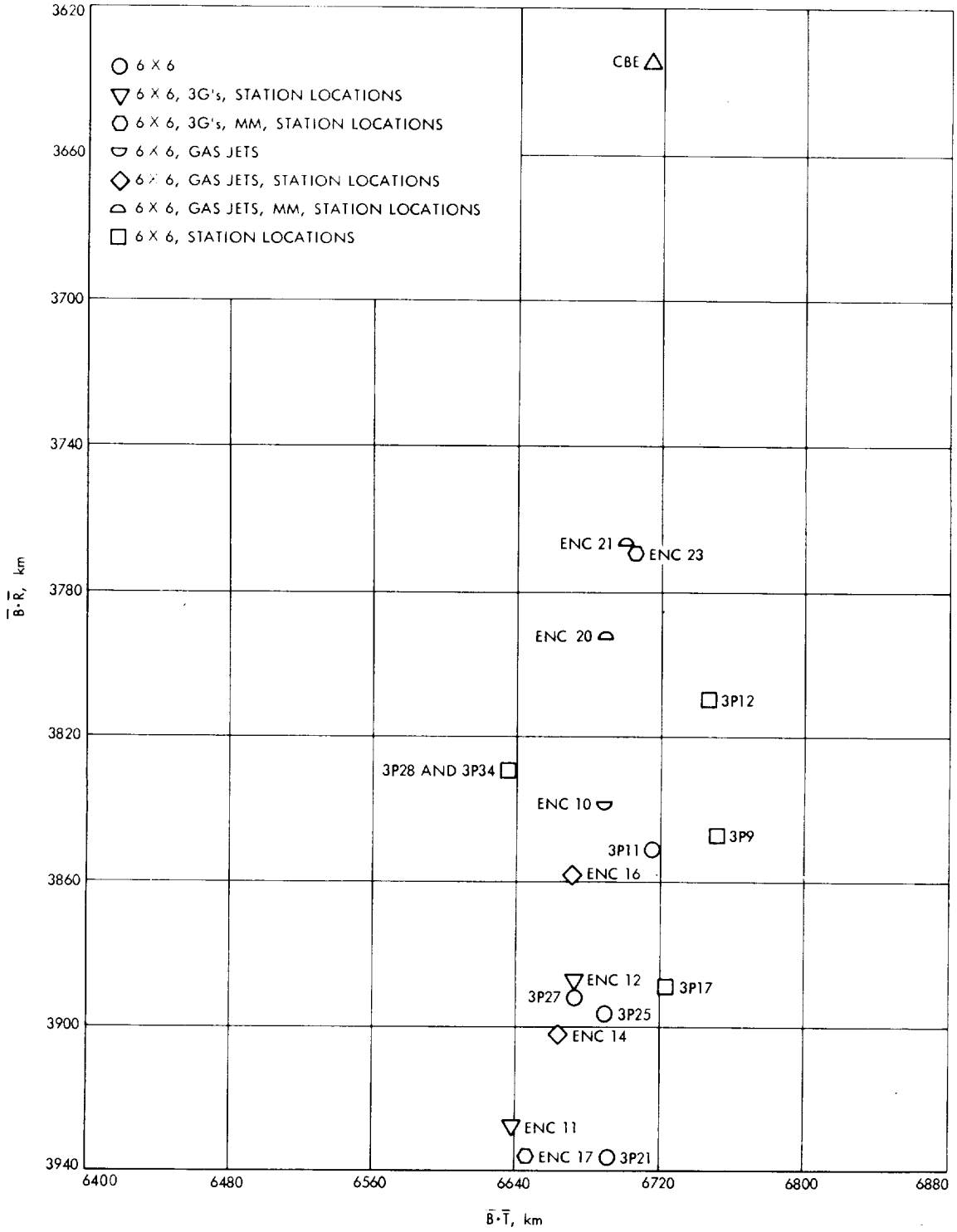

Figure 2-55. Mariner VII Encounter Orbit Solutions Doppler and Range Data

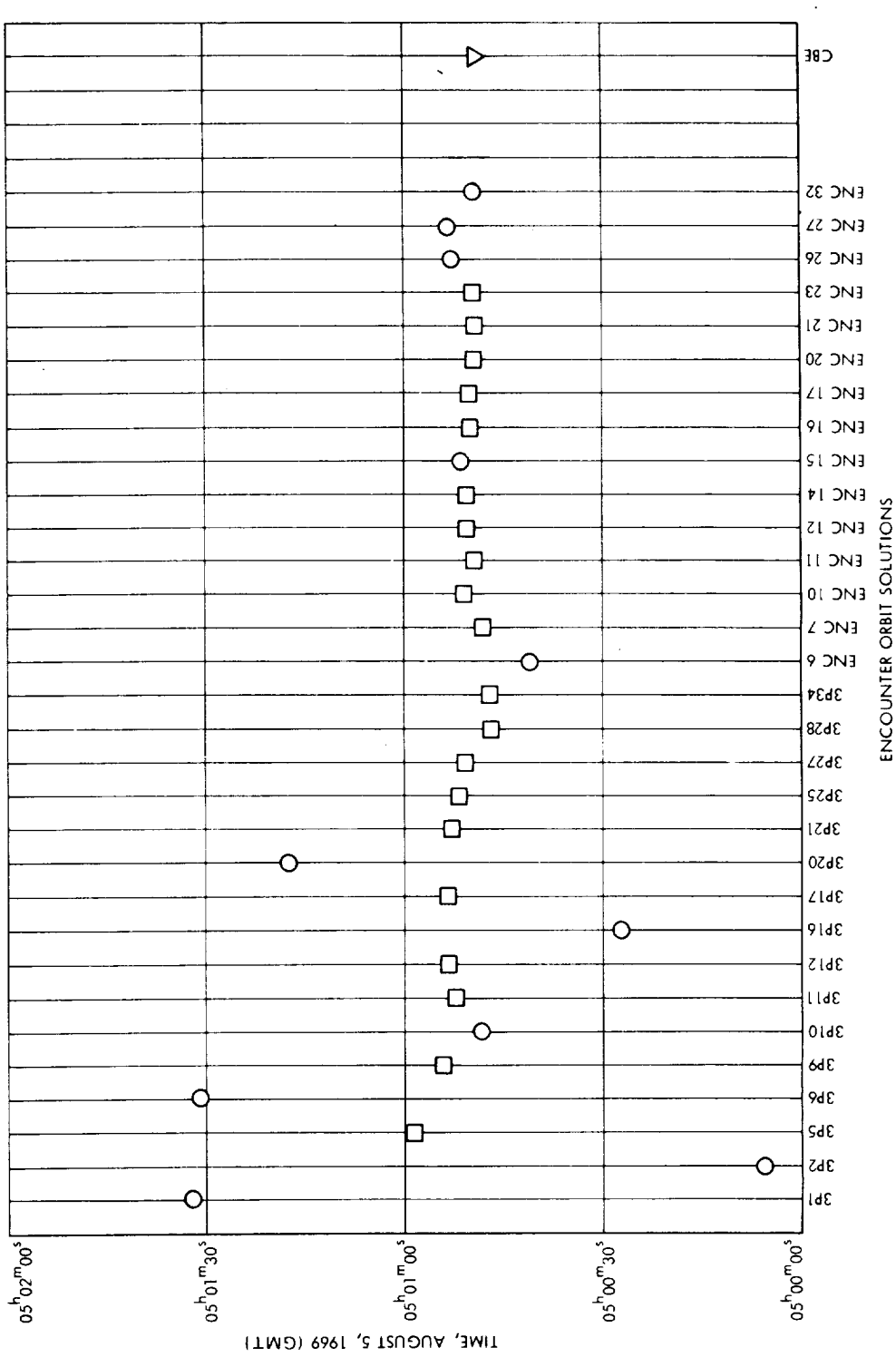

Figure 2-56. Mariner VII Time of Closest Approach

- Analysis — *J. W. Zielenbach*

Recommendations for Mariner VII based on Mariner VI Results

The plans called for a conservative approach to Mariner VI, avoiding as much as possible those techniques which were susceptible to the errors discussed earlier. (See Subsection II. B. 4.) In order to capitalize on the Mariner VI information, it was necessary to examine all those solutions which were made in the hope that they would point out modeling deficiencies.

The fact that ranging could be used near encounter without solving for the ephemeris meant that the geocentric ephemeris range error was within acceptable bounds and could be used without any special precautions.

It soon became apparent that the long arc solutions somehow had modified the effect of the ionosphere so there was little need to try to calibrate this effect for Mariner VII.

It was impossible to separate the effects of the other error sources mentioned in time to be used for Mariner VII. From the Mariner VI performance it could only be concluded that their combination was within acceptable bounds and that no special approach need be taken for Mariner VII.

Mariner VII (Refer to Figure 2-57)

Seven hours before Mariner VI encounter, something happened to Mariner VII causing what was later referred to as the "Happening" (see Figure 2-58). It became apparent that the spacecraft had received a line of sight velocity increment of about 6 cm/sec and was undergoing a slowly decreasing acceleration. This "Happening" and the subsequent acceleration began a new chapter of the OD history and drastically changed the approach to B-plane parameter predictions from that originally planned.

Many of the telemetry channels were disabled during the "Happening" including those that read out the scan platform position in the Near-encounter position. Indications of electrical transients which had stepped the reference position potentiometers made it essential to construct and carry out a calibration sequence at the start of the Far-encounter sequence. Therefore science

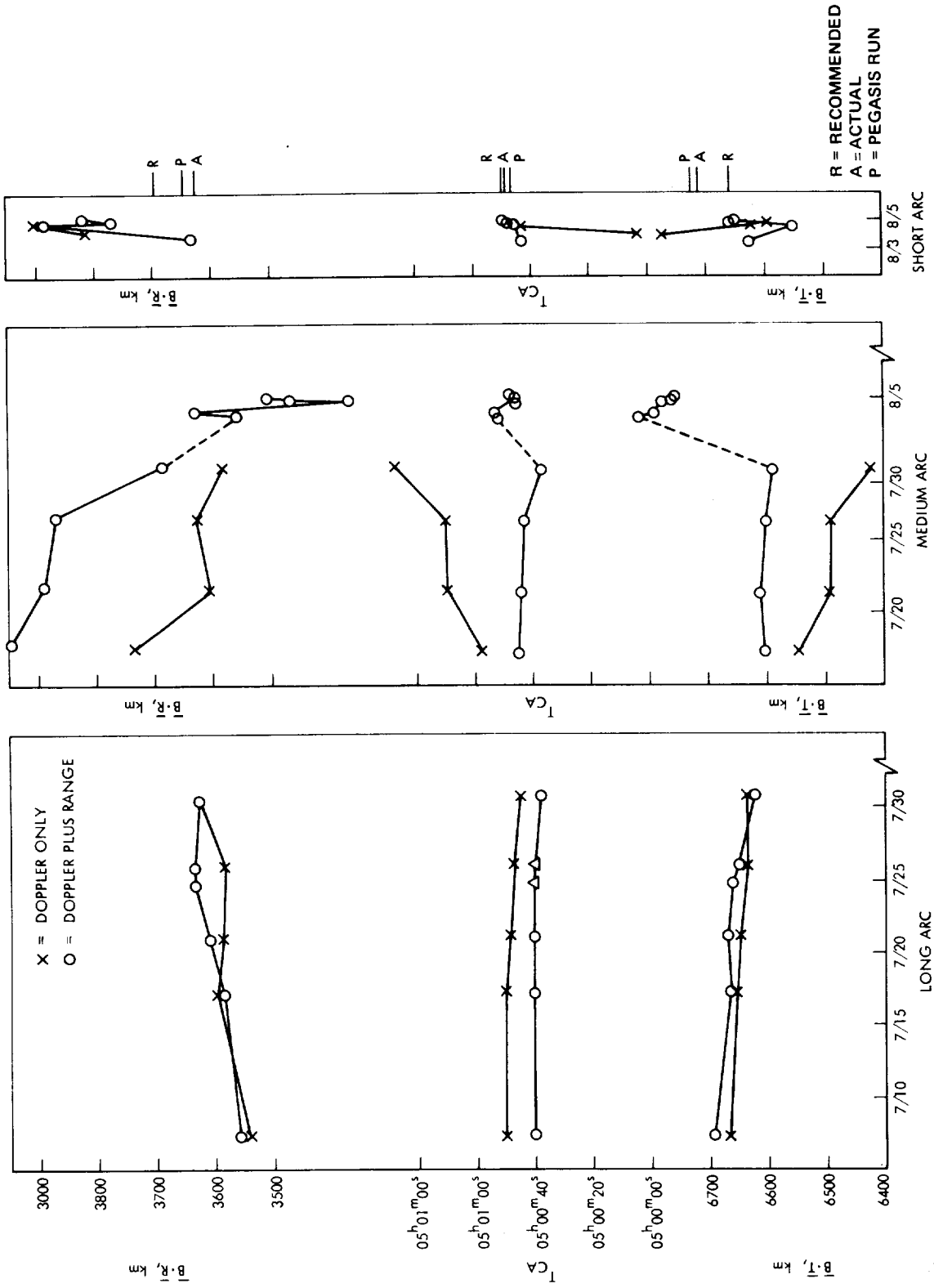

Figure 2-57. Mariner VII Encounter OD Trends

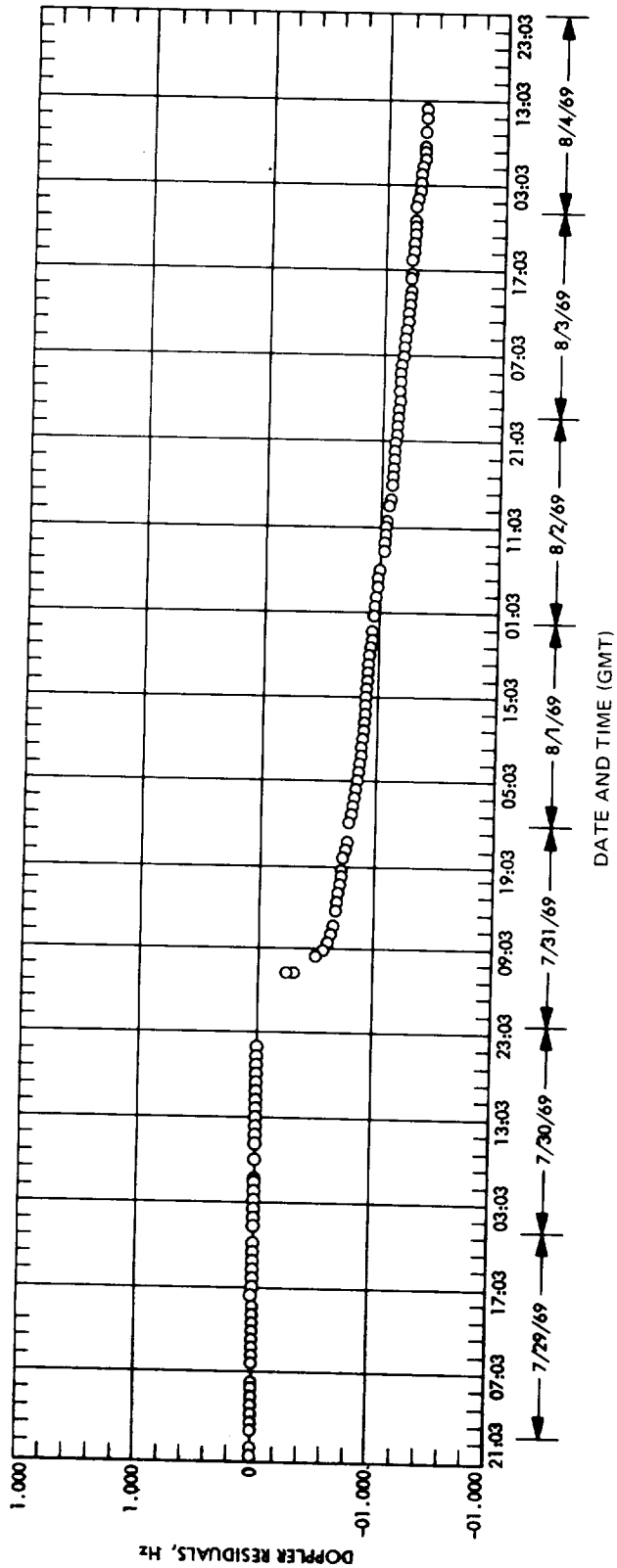

Figure 2-58. Doppler Residuals Before and After the Mariner VII Pre-Encounter Anomaly

power was turned on at approximately E - 78 hrs with no attempt to correlate turn on time and the desired limb picture being taken at the right time during the TV shuttering sequence.

Until the time of the "Happening" the long arc prediction based on Doppler vs those with Doppler and ranging were in remarkable agreement in $\overline{B} \cdot \overline{R}$ and $\overline{B} \cdot \overline{T}$, showing no evidence of the truncation errors which affected Mariner VI. (The trajectory step size problem had been discovered and rectified just before the Mariner VI encounter.) The difference between their time of encounter predictions was slowly decreasing from 10 to 5 seconds. The best DPODP pre-happening long arc prediction was:

$$\overline{B} \cdot \overline{R} = 3625 \text{ km}$$

$$\overline{B} \cdot \overline{T} = 6625 \text{ km}$$

$$t_{ca} = 05^h 00^m 40^s$$

Three conceptually different sets of short-arc solutions were obtained, two of which were based on initial conditions provided by the OD engineer. The first set involved the SPODP initial conditions in Table 2-30 and is unique in that it included data before $00^h 00^m$ August 2. These predictions were the first obtained and were wildly different (1000 km in $\overline{B} \cdot \overline{R}$) from the pre-happening long-arc results. These solutions were discarded as incredible and rationalized as due to the shortness of the arc combined with the larger non-gravitational acceleration at that time.

The second set of solutions used the same initial conditions but used only data after $00^h 00^m$ August 2. These solutions are displayed in Figure 2-57. Both Doppler-only and Doppler and range data sets were used, although the solutions with ranging were of primary importance because it was felt that they restricted the amount of non-gravitational acceleration that could be absorbed by the spacecraft state. The behavior as even more data was added was quite erratic but eventually was restricted to solutions within about 65 km of 3840 for $\overline{B} \cdot \overline{R}$, 50 km of 6600 for $\overline{B} \cdot \overline{T}$, and 3 seconds of $05^h 00^m 48^s$ for t_{ca}.

Each of this second set of solutions solved for the Cartesian state and the GM for Mars, using a spherical *a priori* uncertainty of 1000 km on position and 1 m/sec on velocity, with 5 km^3/sec^2 on GM. The initial conditions provided by the OD engineer had been derived by a multi-iterative fit to earlier Doppler data and differed from the state on the unperturbed long arc trajectory mapped to the same epoch by the amounts in Table 2-30.

This second series of solutions were called into question eventually because it was felt that insufficient use was being made of the *a priori* knowledge about the orbit, at a time when every available bit of information was needed to help tie it down. A discussion of the physics of any mechanism that would cause the observed velocity increment over the 7 hr period when the spacecraft was incommunicado precluded the possibility of changes to the y and z initial coordinates of the magnitude seen in Table 2-30. On the basis of the long arc solution with ranging, the position of the probe at the time of the "Happening" was known to at least a few tens of kilometers. The second set of solutions did not take advantage of this information; rather they started with positions hundreds of kilometers different and assumed they had uncertainties of 1000 km.

A third series of solutions were conducted that do not appear in Figure 2-57. These started with conditions (b) of Table 2-30 and involved varying *a priori* uncertainties on position, while the velocities were assumed known to 1.0 m/sec. The predictions based on the various solutions are listed below:

$\sigma_{x,y,z}$ (km)	$\bar{B} \cdot \bar{R}$ (km)	$\bar{B} \cdot \bar{T}$ (km)	t_{ca} (Aug 5, 1969)
25	3384	6791	$05^h00^m47^s.8$
100	3540	6889	$05^h01^m57^s.9$
300	3569	6877	$05^h01^m57^s.8$
1000	3906	6564	$05^h00^m47^s.0$

Table 2-30. First Estimate of "Happening" Effects

	Conditions Provided by OD Engineer (Multi-Iterative Fit to Early Data) (a)	Conditions Obtained from Unperturbed Long Arc Mapped to Same Epoch (b)	Difference (a) - (b)
x, km	282637.6	282544.5	93.1
y, km	2448779.2	2448477.6	301.6
z, km	903517.7	903281.8	225.9
$\dot{x}$, km/sec	-0.7753319	-0.7746952	-0.0006367
$\dot{y}$, km/sec	-6.5938139	-6.5942226	+0.0004087
$\dot{z}$, km/sec	-2.4442887	-2.4442644	-0.0000243

Conditions are Mars-centered, Earth mean equatorial 1950.0 coordinates.
Epoch is 31 July $22^h00^m00^s$.

Because of the noticeable change in $\overline{B} \cdot \overline{R}$ when the 100 km position uncertainty was admitted, it was felt that in fact much needed information was being thrown away in the second series of solutions and that probably the $\overline{B} \cdot \overline{R}$ value was closer to 3450 than to 3850.

As an extension of the philosophy of using *a priori* information, a solution using data before and after the "Happening" was suggested. The only checked out capability in the program for estimating trajectory discontinuities was the impulsive burn model. From an examination of Figure 2-59 and the realization that 6 degrees of freedom might be necessary because of the accelerations involved, it was decided to estimate 2 impulsive maneuvers, at 0^h and 12^h on July 31. Soon it began to look like the burns would cancel each other and so the first one was discarded. The central set of plots in Figure 2-57 represents this medium arc solution series, using data from July 1 to the time of the plotted points, solving for the Cartesian state, 3 components of solar pressure, mass of Mars, and the second impulsive burn (after the "Happening").

The initial position and velocity (at July 1) were assumed known to only 1000 km and 1 m/sec, on the assumption that one month's data would determine them sufficiently well. The impulsive burn was assigned a spherical 0.5 m/sec uncertainty. The solutions eventually began to cluster within 70 km of 3440 for $\overline{B} \cdot \overline{R}$, within 20 km of 6780 for $\overline{B} \cdot \overline{T}$ and within 1 sec of $05^h00^m48^s$ for t_{ca}.

A correspondence was sought between the estimated components of the burn and the velocity adjustments in the short-arc-solutions. The fact that the second series of short-arc-solutions experienced velocity increments opposite in direction to the burn components, was and still is quite perplexing. It was felt at the time that the short-arc-velocity adjustments were in effect trying to affect the erroneous initial positions as well as account for the actual velocity increment, and this only served to further discredit that approach.

Final Recommendations

Because the philosophy of the second series of short arc solutions was questionable, and because of the apparent agreement between the medium arc solutions with burn and the 25 km *a priori* run of the third short arc series, a solution of

$$\overline{B} \cdot \overline{R} = 3450$$

$$\overline{B} \cdot \overline{T} = 6800$$

$$t_{ca} = 05^h 00^m 48^s$$

was recommended.

Still, the two basic approaches yielded answers nearly 400 km apart, in a direction and of a magnitude such that if the scientific instruments had been aligned exactly in accordance with the dictates of either solution and the other were correct, serious degradation in the scientific return from the mission would have resulted. This, then, was a crucial recommendation.

To express this uncertainty in a manner that could be assimilated by the project as rapidly as possible, it was decided to make an "alternate" (for lack of a better word) recommendation of

$$\overline{B} \cdot \overline{R} = 3780$$

$$\overline{B} \cdot \overline{T} = 6640$$

$$t_{ca} = 05^h 00^m 50^s$$

to express the possibility that the southerly clustering of answers was the right area. This, however, was supplied with a strong rejoinder that it was not the preferred solution. The actual values that were used for the final platform update, as discussed in the preceding section, were almost exactly mid-way between these two recommendations, and proved to be quite accurate (see Section II. B. 6. d).

d. Mariner VII Postflight Orbit Determination Analysis – *S. K. Wong, S. J. Reinbold*

- Introduction

The purpose of this section is to present the best estimate of the Mariner VII flight path and other significant results obtained from analysis of the DSS tracking data. The analysis verified that premidcourse, postmidcourse and encounter inflight orbit solutions were within the Mariner Project orbit determination accuracy requirements. For the postflight orbital computations and analysis, as for Mariner VI, only two-way Doppler and planetary range data were used. The Double Precision Orbit Determination Program of the Jet Propulsion Laboratory was the principle analysis tool used for the Mariner VII postflight orbit determination study.

The tracking data was divided into four logical blocks:

1) Premidcourse maneuver data was taken between transfer orbit injection and attitude maneuver prior to midcourse thrust.

2) Pre-unlatch data was taken between midcourse maneuver and the unlatching of the scan platform.

3) Post unlatch data was taken between the unlatching of the platform and the spacecraft "happening" that occurred on July 30, 1969.

4) Encounter data was taken from encounter minus 2 days to encounter plus 2 days.

See Subsection II. B. 5. d. for a description of differences in data reduction for post-flight analysis. The solution that showed the best data fit is declared the current best estimate (CBE) of the orbit for that phase and this solution is presented in the following sections for each phase of the mission.

- Premidcourse Maneuver Orbit Estimate

The Mariner VII premidcourse data were essentially divided into two blocks. One data block had the Canopus tracker locked on the star Vega, and the other data block had the Canopus tracker on Canopus.

The data span for this block is from 00^h24^m GMT on March 28 to 16^h45^m GMT on April 1. At approximately 16^h45^m GMT on April 1 the spacecraft was unlocked from the star Vega and rolled to acquire Canopus. It stayed locked to Canopus until near midcourse maneuver. The inflight DPODP orbit solutions for the two data blocks that estimated the 3 components of the solar pressure along with the state vector are as follows:

Vega Data Block	Canopus Data Block
$B = 30085$ km	$B = 30056$ km
$\bar{B} \cdot \bar{R} = 29322$ km	$\bar{B} \cdot \bar{R} = 29260$ km
$\bar{B} \cdot \bar{T} = -6732$ km	$\bar{B} \cdot \bar{T} = -6869$ km
$t_{ca} = 04^h48^m10^s$ GMT (Aug. 5, 1969)	$t_{ca} = 04^h49^m14^s$ GMT (Aug. 5, 1969)

These solutions were computed using Doppler data only.

The LAPM XG orbit solution was used for midcourse maneuver computation. This solution was computed using Doppler data from the two data blocks and estimated only the state vector. This solution was:

Orbit LAPM XG
$B = 30082$ km
$\bar{B} \cdot \bar{R} = 29309$ km
$\bar{B} \cdot \bar{T} = -6777$ km
$t_{ca} = 04^h48^m22^s$ GMT (Aug. 5, 1969)

Examination of the residual plots of the LAPM XG solution indicated a poor data fit. This was caused by the inconsistency between the two data blocks.

The current best estimate of the premidcourse orbit was computed postflight using only the Canopus data block. The solution estimates the state vector, and three components of solar pressure, the gravitational constant of Earth and the station location parameters. This solution was computed using Doppler and planetary range data, and it indicated the following results:

$$B = 30074.2 \text{ km}$$
$$\overline{B} \cdot \overline{R} = 29305.0 \text{ km}$$
$$\overline{B} \cdot \overline{T} = -6758.31 \text{ km}$$
$$t_{ca} = 04^h49^m20.^s844 \text{ GMT (Aug. 5, 1969)}$$

The *a priori* input values and the one-sigma statistics along with the current best estimate of premidcourse orbit solution are given in Table 2-31.
The B-plane estimates of the inflight solution used for maneuver computation and the current best estimate of the premidcourse solution are given below along with the difference between the two solutions.

	B, km	$\overline{B} \cdot \overline{R}$, km	$\overline{B} \cdot \overline{T}$, km	t_{ca} (Aug. 5, 1969, GMT)
Solution Used for Maneuver Computation (Inflight)	30082	29309	-6777	$04^h48^m22^s$
Current Best Estimate (Postflight)	30074	29305	-6758	$04^h49^m21^s$
ΔInflight - CBE	8	4	-19	-59 sec

- Pre-Unlatch Orbit Estimates

The inflight DPODP orbit solutions indicated an apparent inconsistency between doppler and range (RU) data. The comparison is given below:

Doppler Only	Doppler and Range (RU) and Range (PRU)
$B = 7380$ km	$B = 7324$ km
$\overline{B} \cdot \overline{R} = 3434$ km	$\overline{B} \cdot \overline{R} = 3941$ km
$\overline{B} \cdot \overline{T} = 6532$ km	$\overline{B} \cdot \overline{T} = 6173$ km
$t_{ca} = 04^h59^m50.^s981$ GMT (Aug. 5, 1959)	$t_{ca} = 04^h59^m14.^s717$ (Aug. 5, 1969)

The above solutions estimated only the state vector and used approximately 8 days of data.

Table 2-31. Mariner VII Premidcourse Parameter Solution

Parameters	*A priori* Value	*A priori* Statistics 1σ	Current Best Solution	CBE Solution Statistics 1σ
X (km)	-1097136.5781	10.0	-1097141.1697	2.6516
Y (km)	-1075657.1563	10.0	-1075658.5171	2.4560
Z (km)	-902391.2422	10.0	-902393.0974	3.5118
DX (km/sec)	-2.5389167666	1×10^{-4}	-2.538923065	0.8345×10^{-5}
DY (km/sec)	-2.5392206609	1×10^{-4}	-2.5392156881	0.8400×10^{-5}
DZ (km/sec)	-2.1074835658	1×10^{-4}	-2.1074806221	0.10965×10^{-4}
G_B	0.31925	0.03	0.30272	0.02350
G_T	0.0	0.05	-0.02974	0.04016
G_N	0.0	0.05	-0.02411	0.04386
GME (km^3/sec^2)	398601.2000	1.0	398601.2307	0.9976
DSS 41				
R_s (km)	5450.19860	0.008	5450.20085	0.00592
λ (deg)	136.887507	0.00010	136.887512	0.5532×10^{-4}
DSS 62				
R_s (km)	4860.81760	0.008	4860.81546	0.00667
λ (deg)	355.632200	0.00010	355.632219	0.5790×10^{-4}
DSS 12				
R_s (km)	5212.05350	0.008	5212.05336	0.00745
λ (deg)	243.194559	0.00010	243.194551	0.6359×10^{-4}
DSS 14				
R_s (km)	5203.99890	0.008	5203.99961	0.00719
λ (deg)	243.110513	0.00010	243.110509	0.6863×10^{-4}

The current best estimate of the pre-unlatch orbit is computed using Doppler and planetary range data. This solution estimated the state vector, the three components of solar pressure, the gravitational constant of the Moon, and station location parameters. When it was mapped to target, it indicated the following results:

$$B = 7628.38 \text{ km}$$
$$\bar{B} \cdot \bar{R} = 3540.95 \text{ km}$$
$$\bar{B} \cdot \bar{T} = 6756.77 \text{ km}$$
$$t_{ca} = 05^h 00^m 33.^s 357 \text{ GMT (Aug. 5, 1969)}$$

The postflight Doppler only solution agreed extremely well with the current best solution. The *a priori* input value and 1σ statistics are given in Table 2-32 along with the current best estimate of pre-unlatch orbit solution.

- Evaluation of the Midcourse Maneuver Based on DSIF Tracking Data

The evaluation of the midcourse maneuver based on DSIF tracking data was done by taking the current best estimate of the premidcourse orbit and mapping the state vector of this orbit to an epoch after the midcourse maneuver. This mapped forward state vector was then subtracted from the state vector of the current best estimate of the pre-unlatch orbit at the same epoch. The results of this comparison are given in the following table:

	ΔDX m/sec	ΔDY m/sec	ΔDZ m/sec	ΔV m/sec
OD Estimate*	-1.7088	-0.59290	3.8840	4.2845
Commanded Maneuver**	-1.6947	-0.56477	3.9026	4.2920
Maneuver Error***	0.0141	0.02813	0.0186	0.0366

*OD Estimate = Current best pre-unlatch estimate minus current best pre-maneuver estimate mapped to the pre-unlatch epoch.
**Commanded Maneuver = Midcourse velocity increment computed by the Maneuver Group based on LAPM XG orbit.
***Maneuver Error = Commanded maneuver minus OD estimates.

Table 2-32. Mariner VII Pre-unlatch Parameter Solution

Parameters	*A priori* Value	*A priori* Statistics 1σ	Current Best Solution	CBE Solution Statistics 1σ
X (km)	-2693596.2187	1000.0	-2693600.2094	6.6091
Y (km)	-2640756.0000	1000.0	-2640749.4359	7.9351
Z (km)	-2197889.1875	1000.0	-2197892.4652	8.9171
DX (km/sec)	-2.6322803497	0.001	-2.6322881158	0.7934×10^{-5}
DY (km/sec)	-2.5072045624	0.001	-2.5071950648	0.8914×10^{-5}
DZ (km/sec)	-2.0627239943	0.001	-2.0627243412	0.10953×10^{-5}
G_B	0.31925	0.03	0.30972	0.01435
G_T	0.0	0.05	-0.02688	0.03899
G_N	0.0	0.05	-0.02868	0.03661
GMM (km^3/sec^2)	4902.82000	1.0	4902.84581	0.07808
DSS 41				
R_s (km)	5450.19860	0.008	5450.20068	0.0053
λ (deg)	136.887507	0.00010	136.887522	0.000055
DSS 62				
R_s (km)	4860.81760	0.008	4860.81572	0.0066
λ (deg)	355.632200	0.00010	355.632219	0.000057
DSS 12				
R_s (km)	5212.05350	0.008	5212.05337	0.0063
λ (deg)	243.194559	0.00010	243.194549	0.000058
DSS 14				
R_s (km)	5203.99890	0.008	5203.99823	0.0063
λ (deg)	243.110513	0.00010	243.110496	0.000061

The effect of these errors when mapped to the target may be seen in the following table:

	$\Delta\bar{B} \cdot \bar{R}$, km	$\Delta\bar{B} \cdot \bar{T}$, km	Δt_{ca}, sec
Overall Error*	101	229	-36
OD Error**	-4	19	59
Maneuver Error***	105	210	-95

*Overall Errors = Current best estimate of pre-unlatch orbit minus maneuver aiming point.
**OD Errors = Current best premaneuver estimate minus orbit used for maneuver computation.
***Maneuver Errors = Overall errors minus OD errors.

The evaluation of midcourse maneuver is performed assuming that the current best estimate of the spacecraft orbit is exact.

- Post-Unlatch Orbit Estimates

A postflight orbit solution based on estimating the state vector, solar reflectivity coefficients, gravitational constant of the Moon, and station location parameters was obtained. This orbit solution was computed using Doppler and planetary range data. Examination of the residuals indicated inconsistency in some of the planetary range data. To isolate the bad ranging data, orbit solutions were computed using different combinations of passes of range data. The analysis indicated that the ranging data passes on July 8 and 9 were biased by 1300 nanoseconds (approximately 195 meters). With these two passes of planetary range data excluded from the computation, the current best estimate of the post-unlatch orbit is:

$$B = 7571.99 \text{ km}$$
$$\bar{B} \cdot \bar{R} = 3630.82 \text{ km}$$
$$\bar{B} \cdot \bar{T} = 6644.71 \text{ km}$$
$$t_{ca} = \text{Aug. 5, 1969 } 05^h00^m40.^s665 \text{ GMT}$$

The *a priori* input values and 1σ statistics are given in Table 2-33 along with the current best estimate of post-unlatch orbit solution.

Table 2-33. Mariner VII Post-Unlatch Parameter Solution

Parameters	*A priori* Value	*A priori* Statistics 1σ	Current Best Solution	CBE 1σ Statistics
X (km)	-11182300.1250	10000.0	-11182303.8569	24.6104
Y (km)	-9794473.2500	10000.0	-9794475.6043	25.5460
Z (km)	-7608393.1875	10000.0	-7608379.7722	31.8334
DX (km/sec)	-4.1169092655	1.0	-4.1169059203	0.3551×10^{-5}
DY (km/sec)	-3.3549144268	1.0	-3.3549049491	0.1112×10^{-4}
DZ (km/sec)	-2.2417705655	1.0	-2.2417852938	0.1669×10^{-4}
G_B	0.31000	0.030	0.29561	0.01374
G_T	0.0	0.050	-0.01582	0.03754
G_N	0.0	0.050	+0.00532	0.03118
GMM (km^3/sec^2)	4902.820000	1.0	4902.828471	0.02987
DSS 11				
R_s (km)	5206.34190	0.008	5206.33918	0.00599
λ (deg)	243.150627	0.00010	243.150652	0.46×10^{-4}
DSS 42				
R_s (km)	5205.35040	0.008	5205.35160	0.00484
λ (deg)	148.981301	0.00010	148.981298	0.46×10^{-4}
DSS 41				
R_s (km)	5450.19860	0.008	5450.20220	0.00390
λ (deg)	136.887507	0.00010	136.887500	0.33×10^{-4}
DSS 51				
R_s (km)	5742.94170	0.008	5742.94152	0.00429
λ (deg)	27.685432	0.00010	27.685410	0.33×10^{-4}
DSS 62				
R_s (km)	4860.81760	0.008	4860.81328	0.00452
λ (deg)	355.632200	0.00010	355.632203	0.35×10^{-4}
DSS 12				
R_s (km)	5212.0535	0.008	5212.05323	0.00556
λ (deg)	243.194559	0.00010	243.194529	0.40×10^{-4}
DSS 14				
R_s (km)	5203.99890	0.008	5203.99794	0.00596
λ (deg)	243.110513	0.00010	243.110516	0.46×10^{-4}

- An Evaluation of the Mariner VII Platform Unlatch

The current best estimate of the pre-unlatch and post unlatch orbits were used to evaluate the change in velocity due to the unlatch. The state vector from the current best pre-unlatch orbit was mapped to the post-unlatch epoch and compared with the best estimate of the state vector obtained from the post-unlatch orbit at the same epoch. The velocity change is given below:

$$\Delta DX = 0.0016 \text{ m/sec}$$
$$\Delta DY = 0.0101 \text{ m/sec}$$
$$\Delta DZ = 0.0036 \text{ m/sec}$$
$$\Delta V = 0.0108 \text{ m/sec}$$

Δ = the state vector of current best estimate of post-unlatch orbit minus the mapped forward state vector of the current best estimate of pre-unlatch orbit.

It should be pointed out that the uncertainties associated with the velocity component of the spacecraft are nearly as large as the differences presented above.

The amount that the orbit was perturbed due to the platform unlatch can be obtained by differencing the B-plane estimates of the current best pre-unlatch and post-unlatch orbits.

$$\Delta B = -56.39 \text{ km}$$
$$\Delta\overline{B} \cdot \overline{R} = 89.87 \text{ km}$$
$$\Delta\overline{B} \cdot \overline{T} = -112.06 \text{ km}$$
$$\Delta t_{ca} = 7.308 \text{ sec}$$

Δ = the current best post-unlatch orbit minus current best pre-unlatch orbit.

- An Evaluation of the Mariner VII "Happening"

At $22^h\ 11^m$ GMT on the 30th of July, something happened to the Mariner VII spacecraft that caused DSS 51 (Johannesburg, South Africa) to lose the radio signal. When DSS 11 (Goldstone-Pioneer, California) reacquired the spacecraft at $05^h 22^m$ GMT on the 31st of July the Doppler residuals indicated a Doppler shift of 0.287 Hz or approximately 18.7 mm/s. The Doppler residuals

can be seen in Figure 2-59. The DSS-11 doppler residuals between 05^h22^m and 06^h33^m GMT indicated that some spacecraft acceleration had occurred. Figure 2-59 shows that DSS-11 lost lock on the spacecraft again at 06^h33^m GMT on the 31st of July. When the spacecraft was reacquired again at 07^h23^m GMT on the 31st of July by DSS-41 (Woomera, Australia) the Doppler residuals indicated that additional spacecraft acceleration had occurred, and was continuing. This section makes a preliminary evaluation of the velocity change caused by the "happening" and describes the spacecraft acceleration which occurred afterward. The postflight analysis of the "happening" was performed using the Single Precision Orbit Determination Program as the principle tool.

An estimate of the spacecraft acceleration along the Earth-Probe direction may be obtained by passing the orbit computed using the pre-"happening" data through the post-"happening" data. From the Doppler residuals of the post-"happening" data the acceleration can be calculated for different times. This acceleration at some selected times are given in Table 2-34. The estimates are quite sensitive to the orbit which passed through the post-"happening" data and any errors in the data (ionospheric, timing, etc.) will directly affect the acceleration estimates.

The perturbative spacecraft acceleration resulting from the "happening" was modeled by a solar pressure force (see Section II. B. 5. d. for a description of the SPODP solar pressure model). By inputs to the orbit determination program $\bar{U}_{sp}$, $\bar{T}$, and $\bar{N}$ correspond to the +Z, +Y and +X axis of the spacecraft coordinate system respectively. The solar pressure equation models the acceleration inversely proportional to R^2. However, the change in R is relatively small compared to its magnitude. If R^2 is assumed as a constant the solar pressure model becomes a constant acceleration model. In applying a constant acceleration model to a non-constant acceleration trajectory, the model will not be effective over a long data span. Therefore orbit computations were made using data spans of one to 6 hours. The computed results are given in Table 2-35. The results indicate that the spacecraft accelerations obtained by the solar pressure model compared quite well with the accelerations computed from the Doppler residuals (Table 2-34). The spacecraft acceleration as a function of time is given in Figures 2-60 through 2-63.

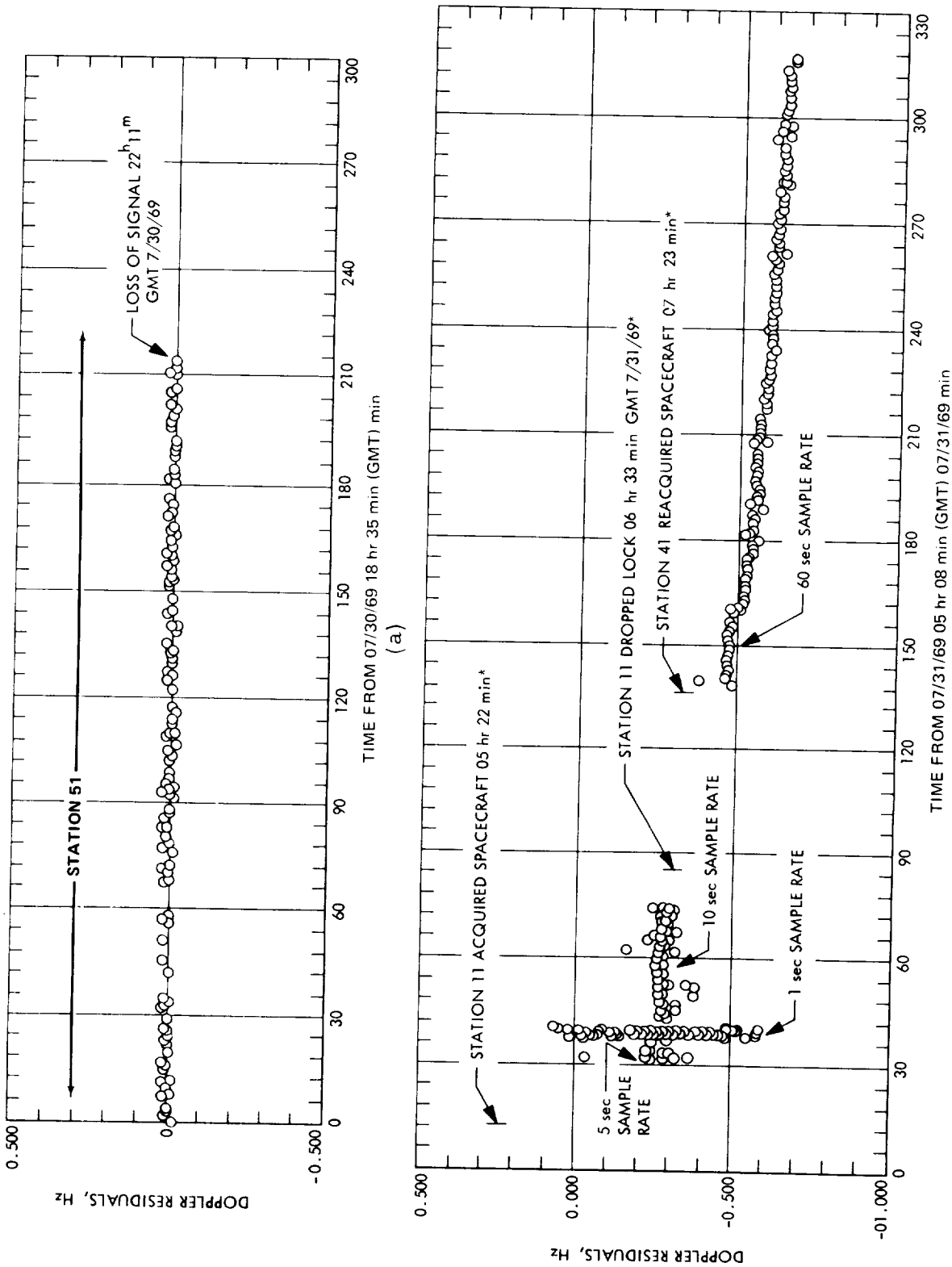

Figure 2-59. Doppler Residuals (Observed-Computed) of the "Happening"

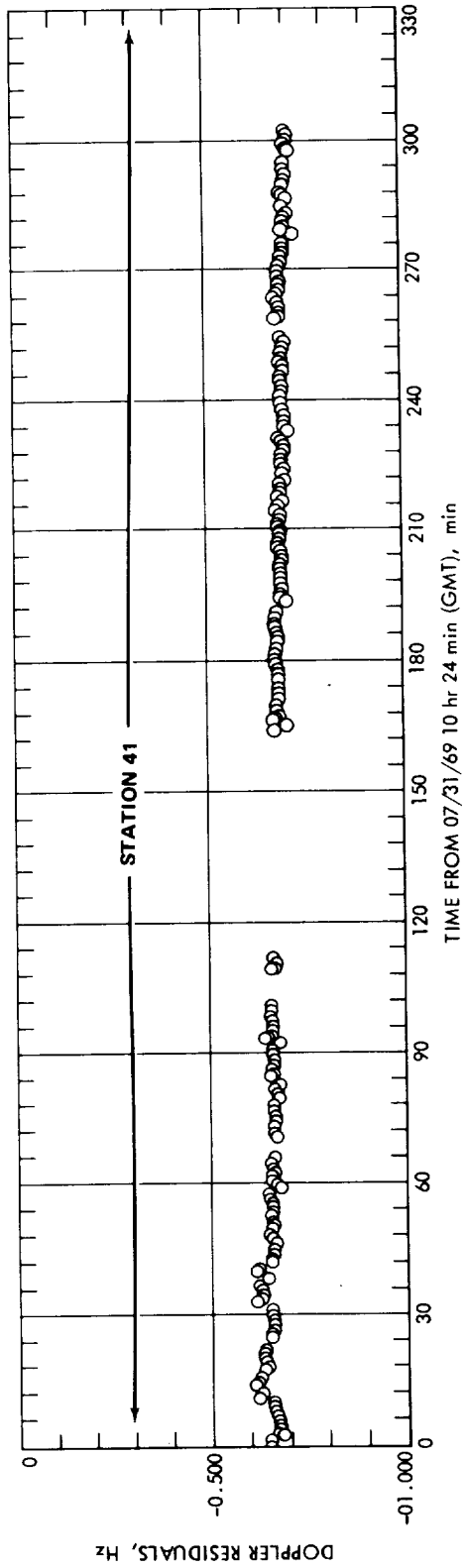

(c)

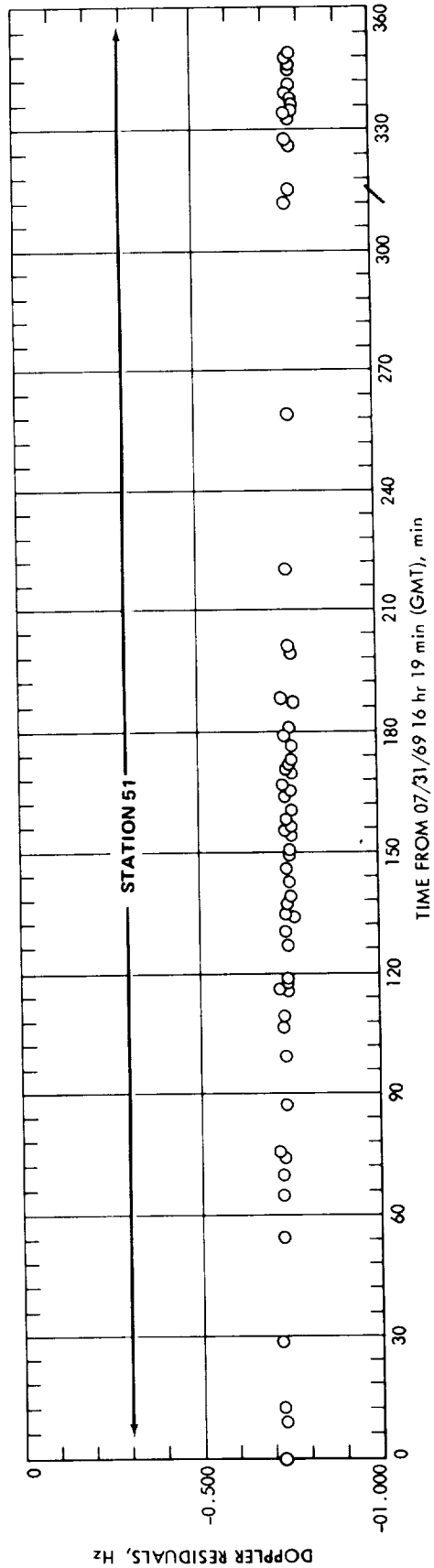

(d)

Figure 2-59. Doppler Residuals (Observed-Computed) of the "Happening" (Cont'd)

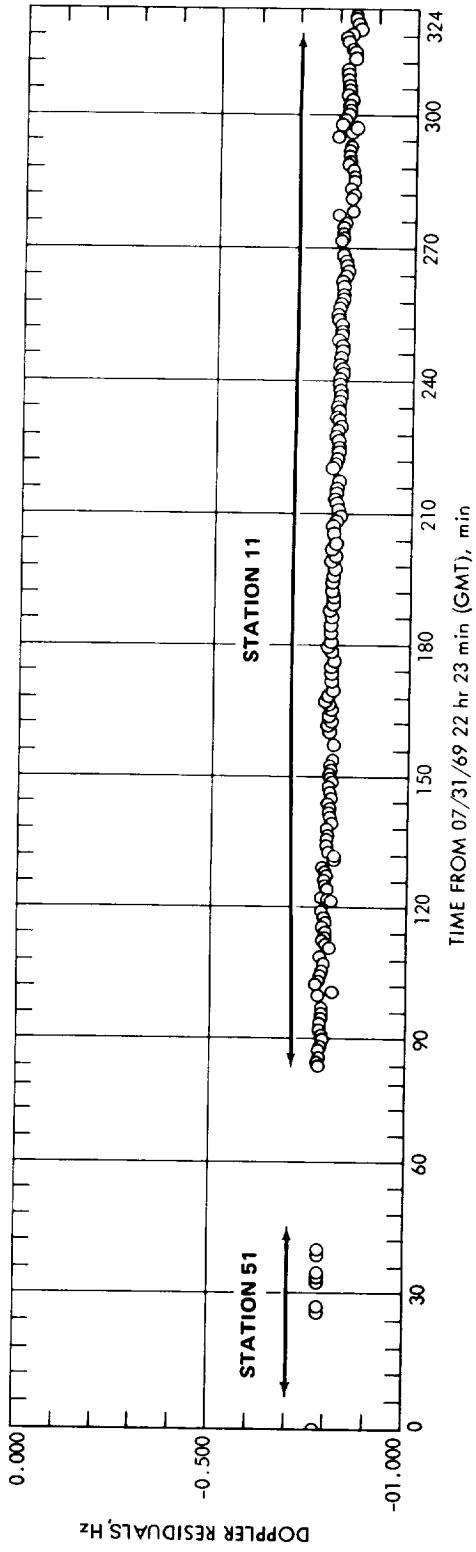

(e)

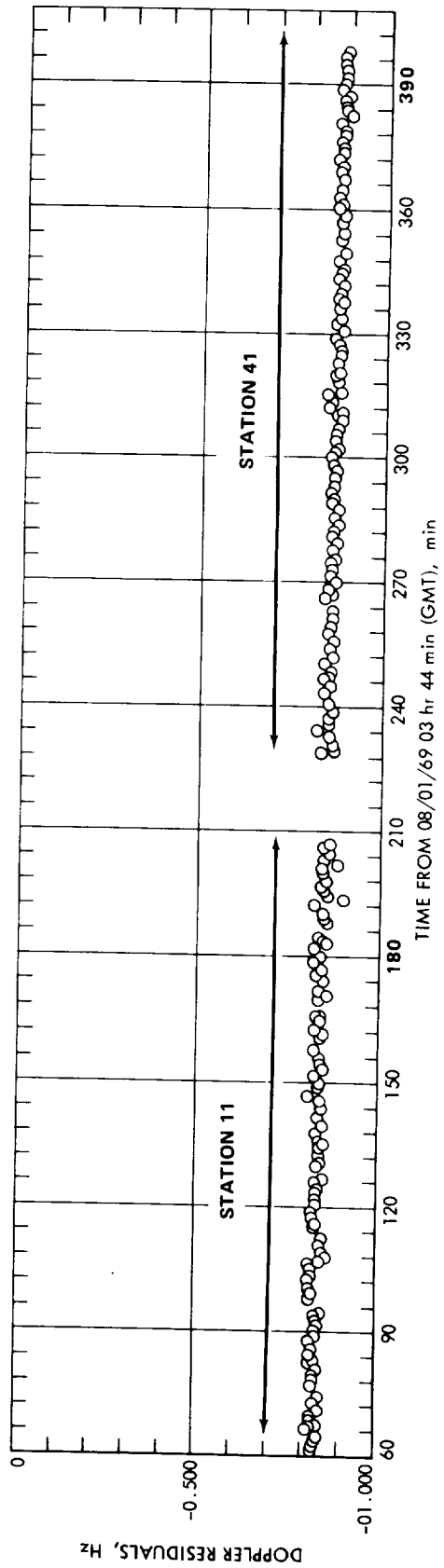

(f)

Figure 2-59. Doppler Residuals (Observed-Computed) of the "Happening" (Cont'd)

Table 2-34. Spacecraft Acceleration in Earth-Probe Direction

	Doppler Residuals, Hz	Δ Range Rate in time interval Δt, km/sec	Δt, sec	Spacecraft Acceleration in Earth-Probe Direction, km/sec^2
7/31 $05^h40^m00^s$	-0.2871	0.3835×10^{-6}	2520	-1.5218×10^{-10}
06 01 00				
06 22 00	-0.2930			
$07^h30^m00^s$	-0.4792	5.044×10^{-6}	3000	-16.813×10^{-10}
07 55 00				
08 20 00	-0.5568			
$08^h10^m00^s$	-0.5484	3.120×10^{-6}	3600	-8.667×10^{-10}
08 40 00				
09 10 00	-0.5964			
$09^h10^m00^s$	-0.5964	2.379×10^{-6}	3600	-6.608×10^{-10}
09 40 00				
10 10 00	-0.6330			
$10^h10^m00^s$	-0.6330	1.638×10^{-6}	3600	-4.550×10^{-10}
10 40 00				
11 10 00	-0.6582			
$11^h10^m00^s$	-0.6582	0.9685×10^{-6}	3300	-2.935×10^{-10}
11 37 30				
12 05 00	-0.6731			
$12^h05^m00^s$	-0.6731	1.872×10^{-6}	7500	-2.496×10^{-10}
13 07 30				
14 10 00	-0.7019			
$14^h10^m00^s$	-0.7019	1.8915×10^{-6}	12000	-1.576×10^{-10}
15 50 00				
17 30 00	-0.7310			
$17^h30^m00^s$	-0.7310	3.991×10^{-6}	21640	-1.844×10^{-10}
20 50 00				
8/1 00 10 00	-0.7924			
$00^h10^m00^s$	-0.7924	6.318×10^{-6}	43200	-1.463×10^{-10}
06 10 00				
12 10 00	-0.8896			

Table 2-35. Spacecraft Accelerations

Day	Time	Az* km/sec^2	Ax** km/sec^2	Ay*** km/sec^2
7/31	05^h56^m	-1.848×10^{-10}	1.122×10^{-10}	1.275×10^{-10}
	07^h50^m	-15.766×10^{-10}	8.778×10^{-10}	9.970×10^{-10}
	08^h40^m	-7.607×10^{-10}	4.031×10^{-10}	4.577×10^{-10}
	09^h40^m	-4.640×10^{-10}	2.524×10^{-10}	2.865×10^{-10}
	11^h40^m	-2.085×10^{-10}	1.163×10^{-10}	1.320×10^{-10}
	13^h10^m	-1.679×10^{-10}	0.895×10^{-10}	1.105×10^{-10}
	15^h40^m	-1.269×10^{-10}	0.865×10^{-10}	0.978×10^{-10}
	20^h40^m	-1.142×10^{-10}	0.684×10^{-10}	0.818×10^{-10}
8/1	06^h10^m	-1.149×10^{-10}	0.583×10^{-10}	0.677×10^{-10}

*Acceleration along the spacecraft Z axis.
**Acceleration along the spacecraft X axis.
***Acceleration along the spacecraft Y axis.

To determine the effects of unmodeled accelerations, a simulation was performed with known accelerations that could be treated as unknown. The results of this simulation is described in Subsection II. B. 6. e.

- Encounter Orbit Estimates

Knowing that there was a small acceleration acting on the spacecraft, the inflight strategies were:

1) To model the small acceleration in the orbit computation.

2) To keep the data arc used in computing the orbit solution as short as possible to minimize the model error.

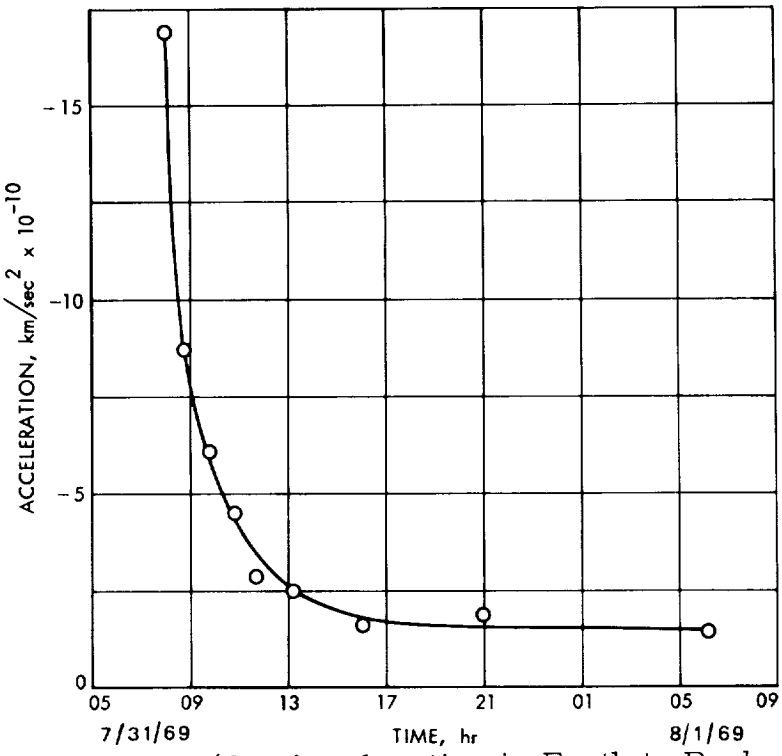

Figure 2-60. Acceleration in Earth to Probe Direction vs Time

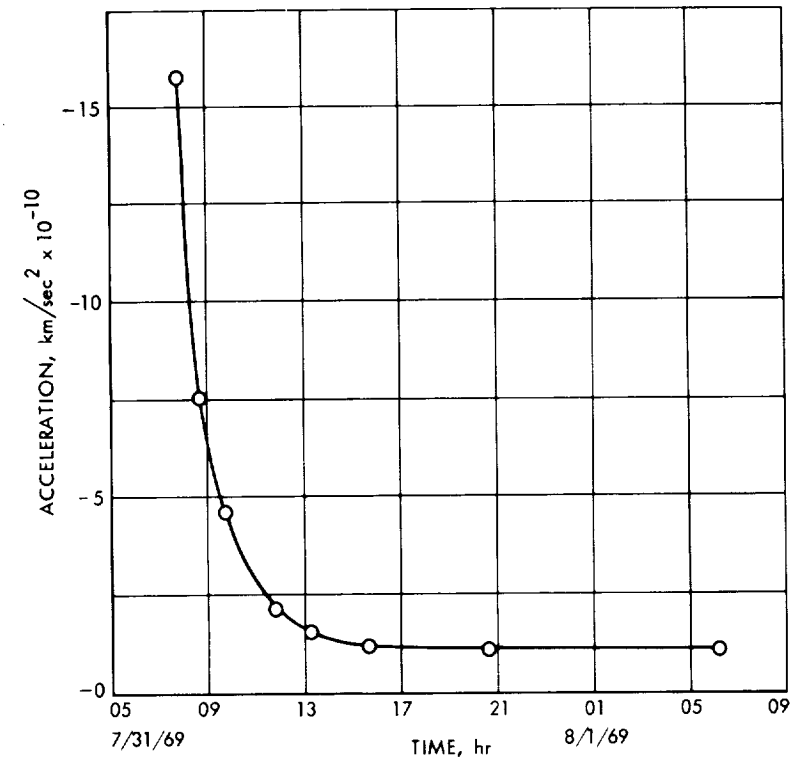

Figure 2-61. Acceleration in Sun to Probe Direction vs Time

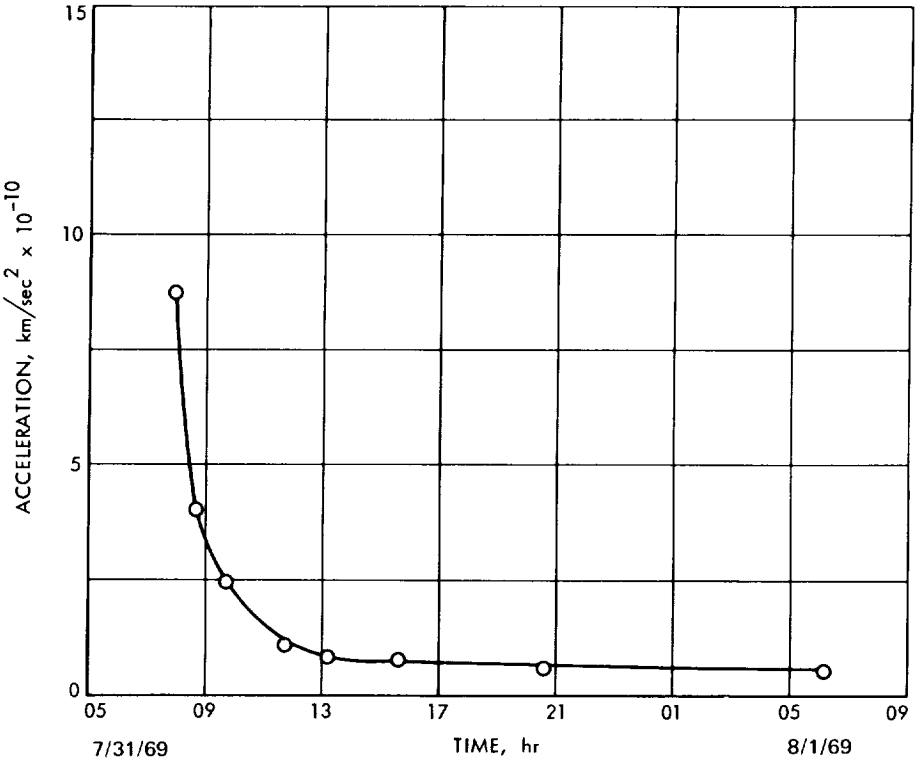

Figure 2-62. Acceleration Along the Spacecraft's Positive X-Axis vs Time

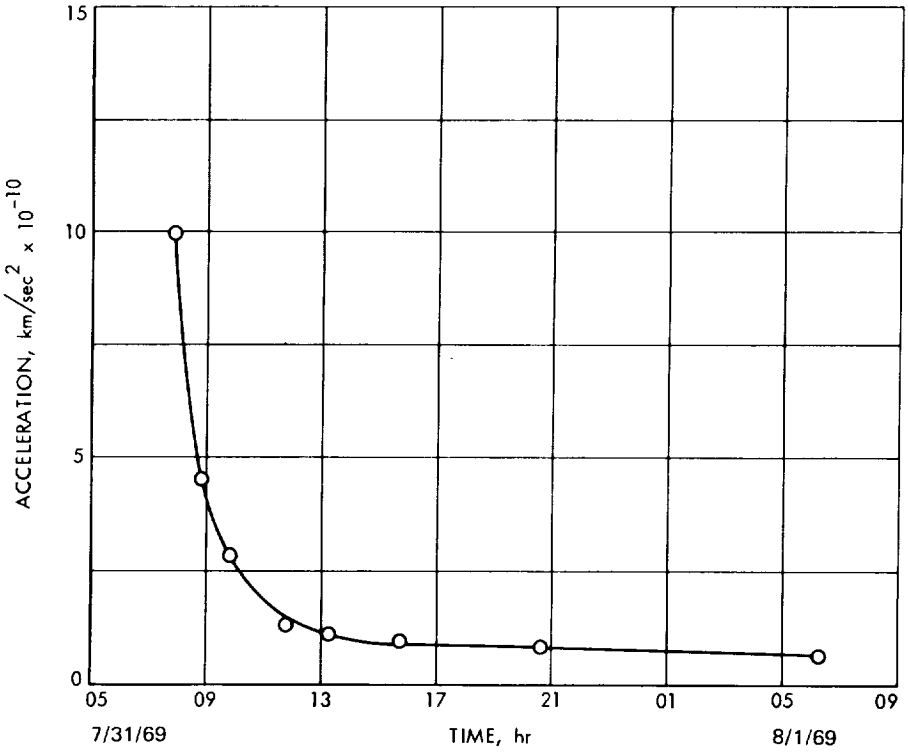

Figure 2-63. Acceleration Along the Spacecraft's Positive Y-Axis vs Time

At approximately 3 hours before encounter the Orbit Determination Group recommended an orbit solution to the MM'69 Project for the final spacecraft platform update. When the PEGASIS program was run, and achievable platform pointing angles were selected, the orbit corresponded to:

$$\overline{B} \cdot \overline{R} = 3650 \text{ km}$$
$$\overline{B} \cdot \overline{T} = 6725 \text{ km}$$
$$t_{ca} = 05^h 00^m 47^s \text{ GMT (Aug. 5, 1969)}$$

The one-sigma dispersion ellipse associated with this orbit was 300 km circular.

In post-flight, the encounter orbit solutions were computed using data spans of E - 2 days 5 hours to E - 45 minutes and E - 2 days 5 hours to E + 2 days 5 hours. A current best estimate of encounter orbit is given for each of the above data spans. For the data span from E - 2 days 5 hours to E - 45 minutes, the current best estimate of the pre-encounter orbit was computed using Doppler and planetary range data. This solution estimated the state vector, the gravitational constant of Mars, and the attitude control jets, and indicated the following B-plane parameters:

$$B = 7634.97 \text{ km}$$
$$\overline{B} \cdot \overline{R} = 3640.54 \text{ km}$$
$$\overline{B} \cdot \overline{T} = 6711.13 \text{ km}$$
$$t_{ca} = 05^h 00^m 49^s.064 \text{ GMT (Aug. 5, 1969)}$$

The data span was started at E - 2 days 5 hours in order to keep the data arc as short as possible to minimize the model error. The data span stopped at E - 45 min because the IRS gas venting started at that time. The *a priori* input values and 1σ statistics are given in Table 2-36 along with the current best estimate of pre-encounter parameters.

For the data span from E - 2 days 5 hr to E + 2 days 5 hr, the current best estimate of the encounter orbit was computed using Doppler and planetary range data. This solution estimated the state vector, the gravitational constants of Mars, astronomical unit, and station location parameters. When it was mapped to target it indicated the following results:

$$B = 7632.09 \text{ km}$$
$$\bar{B} \cdot \bar{R} = 3634.56 \text{ km}$$
$$\bar{B} \cdot \bar{T} = 6711.09 \text{ km}$$
$$t_{ca} = 05^h00^m49^s.284 \text{ GMT (Aug. 5, 1969)}$$

Table 2-36. Mariner VII Encounter Parameter Solution (E - 2d 5h to E - 45m)

Parameters	*A priori* Value	*A priori* Statistics	Current Best Solution	CBE 1σ Statistics
X (km)	-40092267.5000	1000.0	-40091727.3023	61.4339
Y (km)	-78177128.0000	1000.0	-78177480.5104	60.5968
Z (km)	-40250032.0000	1000.0	-40249859.8790	144.6974
DX (km/sec)	1.2293577939	0.001	1.2266569018	0.375236×10^{-3}
DY (km/sec)	-16.0433413982	0.001	-16.0413951021	0.280968×10^{-3}
DZ (km/sec)	-6.9812358618	0.001	-6.9821924135	0.709406×10^{-3}
Az (km/sec^2)	0.0	1×10^{-10}	-0.8353×10^{-11}	0.7861×10^{-10}
Ax (km/sec^2)	0.0	1×10^{-10}	-0.9843×10^{-11}	0.9387×10^{-10}
Ay (km/sec^2)	0.0	1×10^{-10}	-0.12538×10^{-11}	0.9224×10^{-10}
GM (Mars) (km^3/sec^2)	42828.4439	2.0	42829.7150	1.5904

The three-sigma dispersion ellipse associated with this orbit is 15 km by 10 km with the semi-major axis approximately perpendicular to the B-vector in the B-plane. The *a priori* input values and 1σ statistics are given in Table 2-37.

To evaluate the accuracy of the encounter orbit that was recommended to the MM'69 Project at E - 3h, the B-plane estimate of the recommended orbit was subtracted from the current best estimate of the encounter orbit. The differences are presented below:

Table 2-37. Mariner VII Encounter Parameter Solution
(E - 5d 2h to E + 2d 5h)

Parameters	*A priori* Value	*A priori* Statistics	Current Best Solution	CBE 1σ Statistics
X (km)	-40092267.5000	10000.0	-40091823.7262	79.3557
Y (km)	-78177128.0000	10000.0	-78177642.2530	45.3306
Z (km)	-40250032.0000	10000.0	-40249449.7087	163.9992
DX (km/sec)	1.229357739	1.0	1.2269649017	0.41487×10^{-3}
DY (km/sec)	-16.0433413982	1.0	-16.0404533231	0.24688×10^{-3}
DZ (km/sec)	-6.9812358618	1.0	-6.9843405339	0.88385×10^{-3}
Az (km/sec^2)	0.0	1×10^{-9}	0.14412×10^{-8}	0.3342×10^{-9}
Ax (km/sec^2)	0.0	1×10^{-9}	-0.7818×10^{-8}	0.8621×10^{-9}
Ay (km/sec^2)	0.0	1×10^{-9}	-0.1683×10^{-8}	0.5885×10^{-9}
AU (km)	149597893.00	100	149597897.41	0.40
GM (Mars) (km^3/sec^2)	42828.4439	1.0	42829.2724	0.8197
DSS 41				
R_s (km)	5450.19860	0.008	5450.20157	0.0033
λ (deg)	136.887507	0.0001	136.887500	0.37×10^{-4}
DSS 62				
R_s (km)	4860.81760	0.008	4860.81191	0.0053
λ (deg)	355.632200	0.0001	355.632165	0.43×10^{-4}
DSS 12				
R_s (km)	5212.05350	0.008	5212.05309	0.0078
λ (deg)	243.194559	0.0001	243.194565	0.66×10^{-4}
DSS 14				
R_s (km)	5203.99890	0.008	5203.99467	0.0047
λ (deg)	243.110513	0.0001	243.110459	0.41×10^{-4}

$$\Delta\bar{B} \cdot \bar{R} = -165.44 \text{ km}$$

$$\Delta\bar{B} \cdot \bar{T} = 41 \text{ km}$$

$$\Delta t_{ca} = -0.716 \text{ sec}$$

The orbit used for the final platform update was in error by -15.44 km in $\bar{B} \cdot \bar{R}$, -13.91 km in $\bar{B} \cdot \bar{T}$ and 2.284 sec in the time of closest approach.

- Mariner VII Solutions for Solar Pressure and Physical Constants

Solar Radiation Pressure

Since the Mariner VI and VII spacecraft were identical, the solar radiation effect on the spacecraft due to the high gain antenna discussed in Subsection II. B. 5. d for Mariner VI also applies to Mariner VII. During premidcourse and early portions of the cruise phase, the perturbative spacecraft acceleration resulting from solar radiation pressure was modeled by (In SPODP):

$$\Delta\ddot{R} = \frac{KA}{MR^2}(1 + G_B)$$

On approximately May 1, the model was expanded to

$$\Delta\ddot{R} = \frac{KA}{MR^2}\left[1 + G_B\bar{R} + G_T\bar{T} + G_N\bar{N}\right]$$

The definitions of the terms are given in Section II. B. 5. d.

The least squares estimates were computed for the solar reflectivity coefficients in the pre-midcourse phase, pre-unlatch phase, and post-unlatch phase. For each phase the solar reflectivity coefficients were estimated using data span from the beginning of that phase to some later time within the same phase. The time history of these solutions are shown in Figures 2-64, 2-65 and 2-66. These figures show the estimated reflectivity coefficient vs the time of the last data point of the solutions. The G_B solutions showed a similar down trend in solar pressure with increasing time for the Mariner VI solutions. The

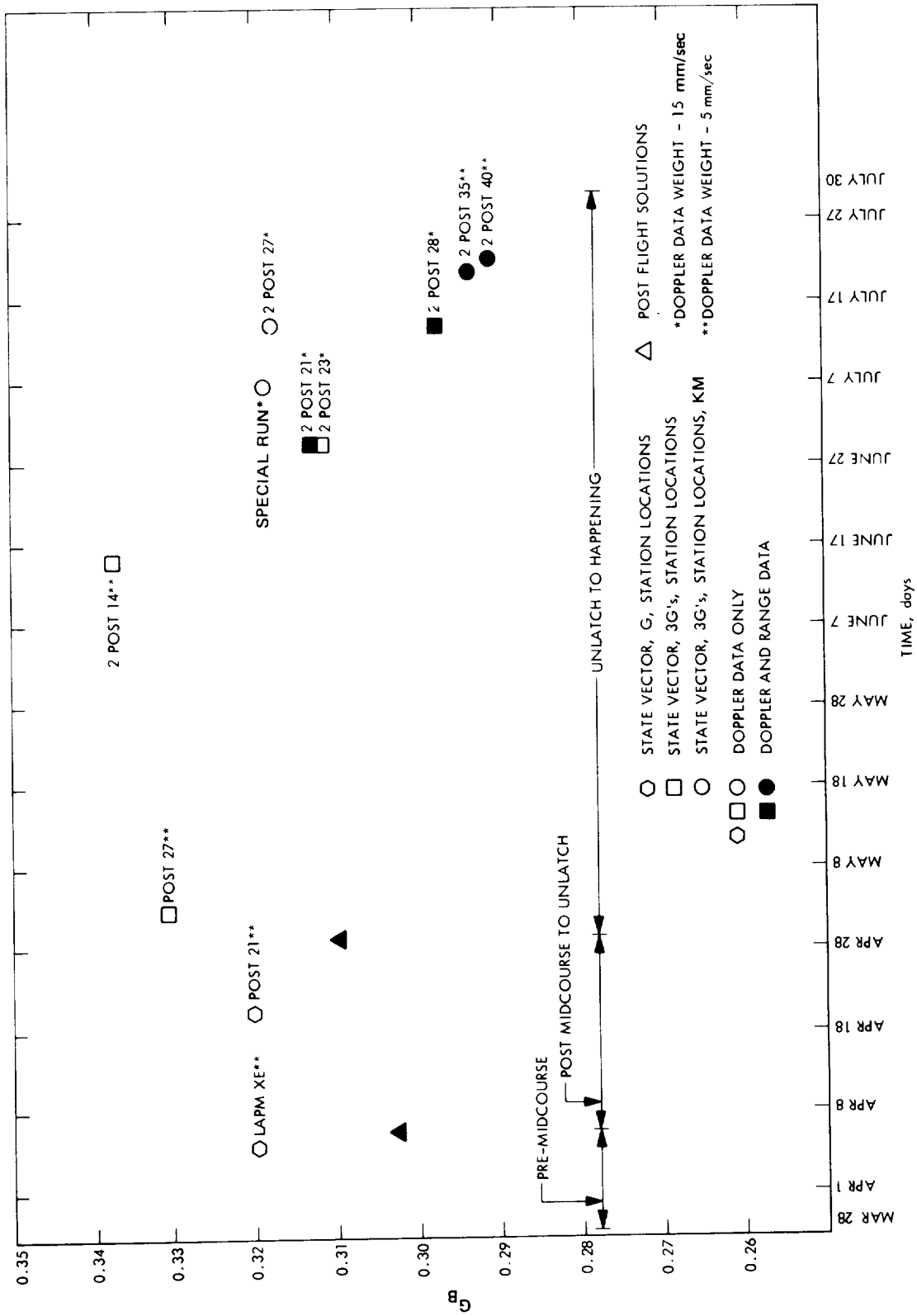

Figure 2-64. Mariner VII Solution for Solar Pressure Coefficient C_B

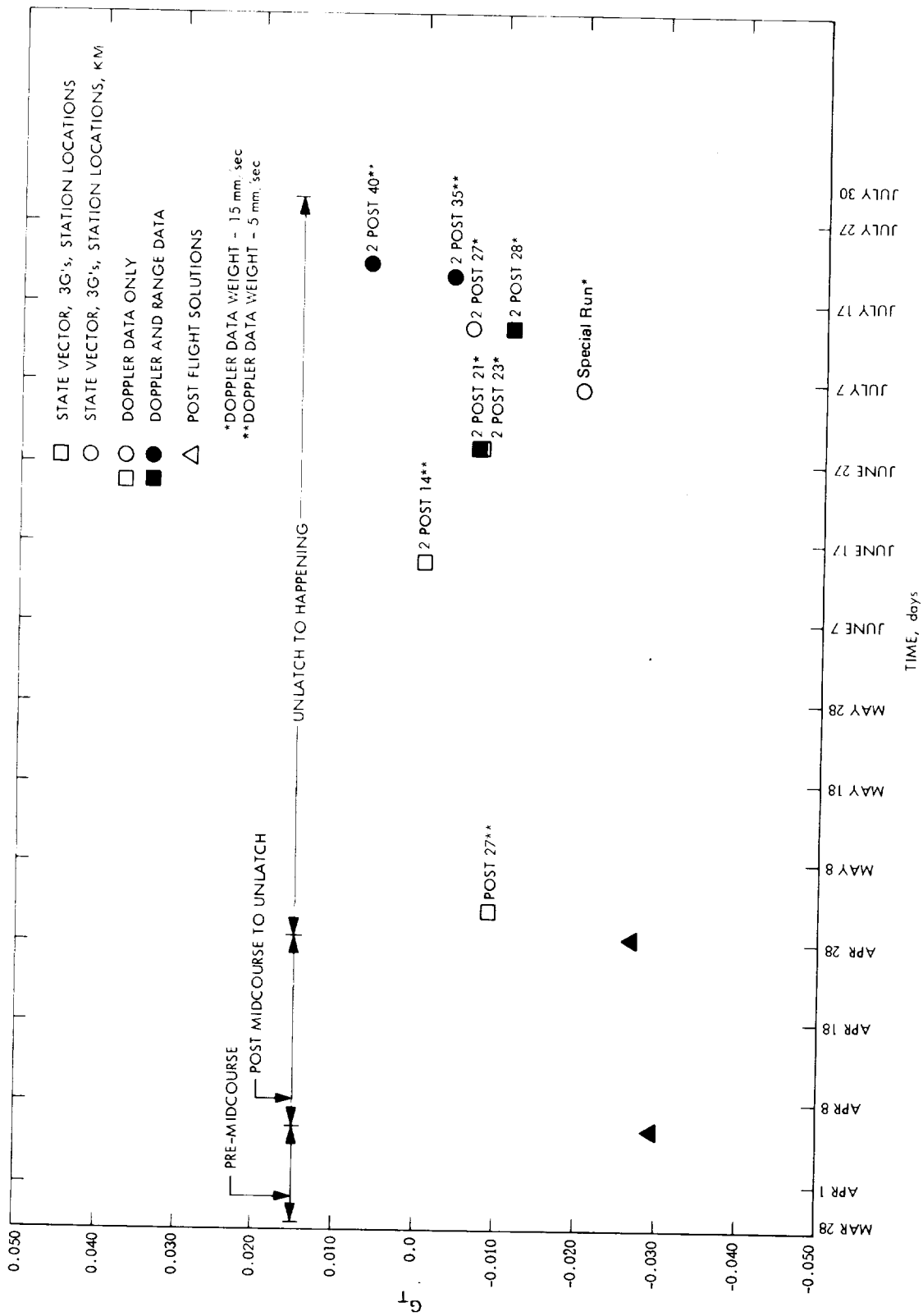

Figure 2-65. Mariner VII Solution for Solar Pressure Coefficient G_T

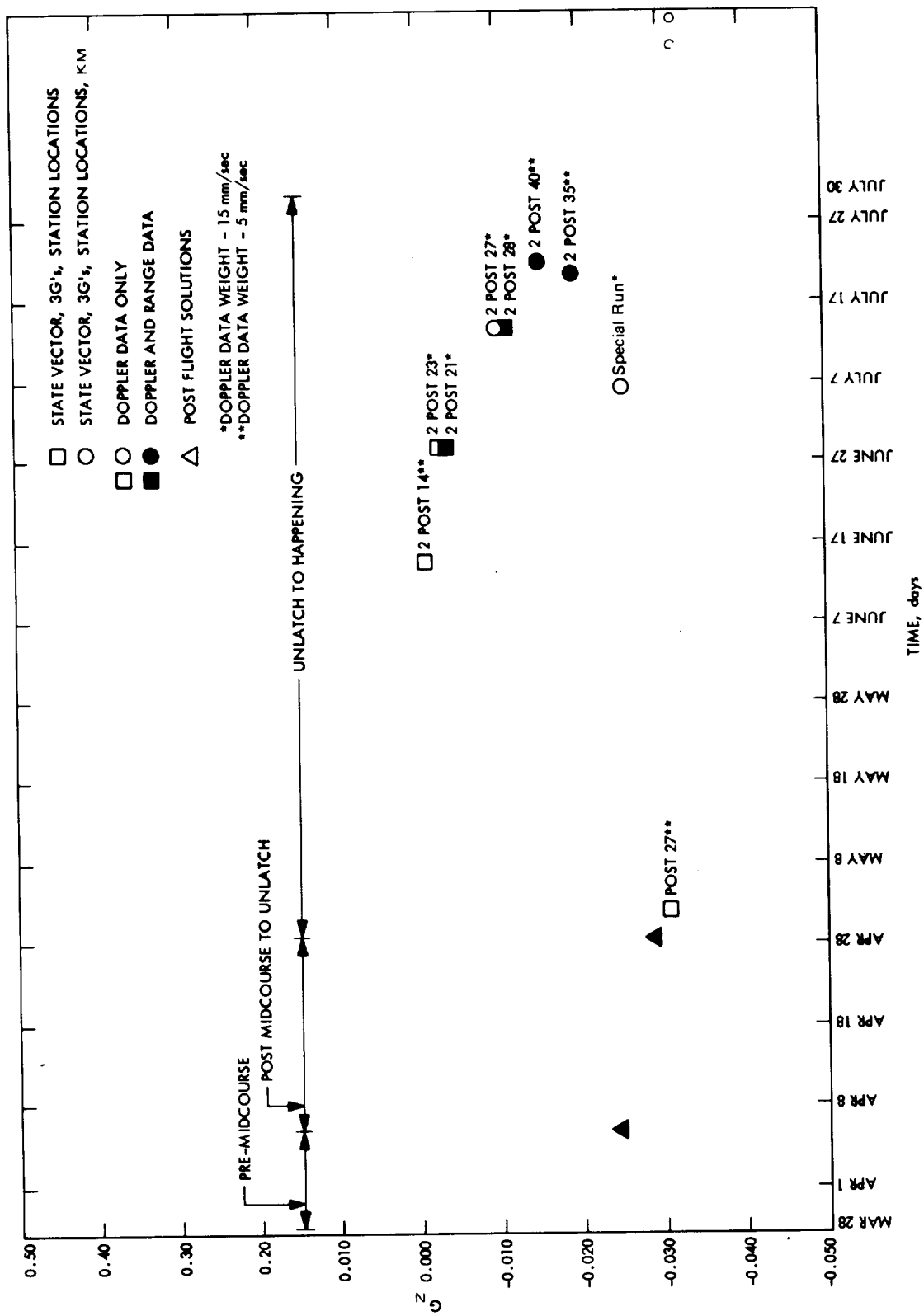

Figure 2-66. Mariner VII Solution for Solar Pressure Coefficient G_N

observed change in G_B between the pre-midcourse solution and the late cruise solution was on the order of 0.026 as compared to 0.025 for Mariner VI. This observed change was over a period of 4 months. This change is probably caused by the degradation of the total reflectance of the spacecraft and a decrease in specularity of the solar panels which took place during cruise.

The expected G_N and G_T values, using effective areas, were calculated as -0.0499 and -0.0471 respectively.

The least squares solution closest to the calculated values above was:

$$G_N = -0.0109 \qquad G_T = -0.0112$$

The difference between the calculated G_N and G_T values and the least squares estimates can be explained by:

1) The least squares G_N and G_T solutions for Mariner VII indicated that the data had very little information on G_N and G_T.

2) The calculated G_N and G_T were obtained assuming that the high gain antenna was the only source contributing solar radiation force in a direction other than the sun-spacecraft direction, and it is possible that some solar radiation force from other surfaces partially offset the solar pressure contributed by the high gain antenna.

The G_B estimates with data span ending between June 16 and July 22 showed a fast down trend of solar pressure. This is not caused by a change in solar pressure, but is due to the fact that the initial data had very little information on solar pressure and was unable to change the nominal input values which were zero for G_N and G_T and 0.338 for G_B in solutions prior to 2 POST 23. After 2 POST 23 the nominal value of 0.319 was input for G_B. As more data were used in the orbit solution, the estimated solar reflectivity coefficient gradually moved toward the actual value.

The least-squares estimate of G_B, G_T and G_N were computed in postflight for the premidcourse and pre-unlatch phases. The following results were obtained:

	Premidcourse	Pre-Unlatch
G_B	0.30272	0.30972
G_T	-0.02974	-0.02688
G_N	-0.02411	-0.02868

The postflight results agree quite well with the inflight results and the Mariner VI postflight results. Figures 2-64, 2-65, and 2-66 show the time history of the postflight solutions along with the inflight solutions.

Solution for Gravitational Constant of the Moon

The lunar gravitational constant estimates for Mariner VII are given in Table 2-38 along with solutions from previous missions. As mentioned in Section II. B. 5. d., the $GM_{\mathbb{C}}$ solutions from the lunar missions are lower than the solutions from the interplanetary missions. This is due to the fact that in lunar missions, the $GM_{\mathbb{C}}$ estimate was obtained by measuring the effect of the lunar gravity field on the probe acceleration and in the interplanetary missions, the $GM_{\mathbb{C}}$ estimate was obtained by measuring the barycentric motion of the tracking station over the long cruise interval; therefore, in reality, the results are a determination of the earth-moon mass ratio, assuming a known value of earth-moon distance. The real time $GM_{\mathbb{C}}$ estimate for Mariner VII is:

$$GM_{\mathbb{C}} = 4902.8703 \pm 0.033 \text{ km}^3/\text{sec}^2$$

Based on the value $GM_{\oplus} = 398601.20 \text{ km}^3/\text{sec}^2$, the earth-moon mass ratio is computed to be

$$\mu^{-1} = 81.29956 \pm 0.001$$

Table 2-38. $GM_{\oplus}$ and $GM_{\mathbb{C}}$ Solutions from Planetary and Lunar Flights

Source	$GM_{\oplus}$, km^3/sec^2	1σ Standard Deviation km^3/sec^2	$GM_{\mathbb{C}}$, km^3/sec^2	1σ Standard Deviation km^3/sec^2	Earth/Moon Mass Ratio μ^{-1}	1σ Standard Deviation
Lunar Missions:						
Lunar Orbiter II (Doppler Only)	398600.88	2.14	4902.6605	0.29	81.3030	0.0048
Lunar Orbiter II (Doppler and Range)	398600.37	0.68	4902.7562	0.13	81.3015	0.0022
Ranger VI	398600.69	1.13	4902.6576	0.185	81.3029	0.0030
Ranger VII	398601.34	1.55	4902.5371	0.167	80.3051	0.0029
Ranger VIII	398601.14	0.72	4902.6304	0.119	81.3035	0.0018
Ranger IX	398601.42	0.60	4902.7073	0.299	81.3023	0.0048
Combined Rangers (Ref. 23)	398601.22	0.37	4902.6309	0.074	81.3035	0.0012
Surveyor I	398601.27	0.78	4902.6492	0.237	81.3032	0.0040
Surveyor III	398601.11	0.84	4902.6420	0.246	81.3033	0.0040
Surveyor IV	398601.19	0.99	4902.6297	0.247	81.3036	0.0040
Surveyor V	398601.10	0.60	4902.6298	0.236	81.3036	0.0040
Surveyor VI	398601.11	0.54	4902.6425	0.235	81.3033	0.0039
Surveyor VII (Ref. 24)	398601.11	0.80	4902.6429	0.235	81.3033	0.0039

Table 2-38. $GM_{\oplus}$ and $GM_{\leftmoon}$ Solutions from Planetary and Lunar Flights (cont'd)

Source	$GM_{\oplus}$, km^3/sec^2	1σ Standard Deviation km^3/sec^2	$GM_{\leftmoon}$, km^3/sec^2	1σ Standard Deviation km^3/sec^2	Earth/Moon Mass Ratio μ^{-1}	1σ Standard Deviation
Interplanetary Missions:						
Mariner II			4902.8442	0.07	81.3001	0.0013
Mariner IV	398601.83	1.4	4902.756	0.10	81.3015	0.0016
Mariner V (Ref. 25)	398600.49	0.4	4902.81	0.5	81.3006	0.0008
Mariner VI (Inflight)	398601.67	0.97	4902.8205	0.08	81.3004	0.0013
Mariner VII (Inflight)	NA	NA	4902.8703	0.08	81.2996	0.0013
Mariner VI (Postflight)	398601.44	0.98	4902.794	0.05	81.3008	0.0007
Mariner VII (Postflight)	398601.23	0.99	4902.828	0.03	81.3002	0.0005

The postflight Mariner VII solution is

$$GM_{\leftmoon} = 4902.828 \pm 0.03 \text{ km}^3/\text{sec}^2$$

and the Earth-Moon mass ratio may be computed as

$$\mu^{-1} = 81.3002 \pm 0.0005$$

The Gravitational Constant of Earth

The post-flight Mariner VII solution is

$$GM_{\oplus} = 398601.231 \pm 0.997 \text{ km}^3/\text{sec}^2$$

This value is consistent with the $GM_{\oplus}$ estimates obtained in previous missions as given in Table 2-38. Comparison between the uncertainty of the estimate and the input *a priori* indicates that the data has very little information on the gravitational constant of Earth. (This is due to the lack of near-Earth ranging data and the change in solar pressure force when the roll reference was changed from Vega to Canopus at L + 5 days.)

Mariner VII Solutions for Station Locations*

The least squares estimates of station locations based on pre-midcourse maneuver phase, cruise phase tracking data are presented in Figures 2-67 through 2-76 in a natural coordinate system (r_s, λ, z) where r_s is the distance off the spin axis (in the station meridian), λ is the longitude and Z is along the Earth spin axis. The station location solutions for the encounter phase are excluded here because of the spacecraft anomaly which occurred on 30 July 1969 causing significant spacecraft acceleration which was not very well modeled for the inflight solutions. The *a priori* standard deviation for the

*Station locations have been determined as accurately as possible by reprocessing data from previous missions (see Section II. A. 2. b.). These solutions were made so that consistency could be checked, and so that any unmodeled effects, if present, could be absorbed as equivalent station location errors.

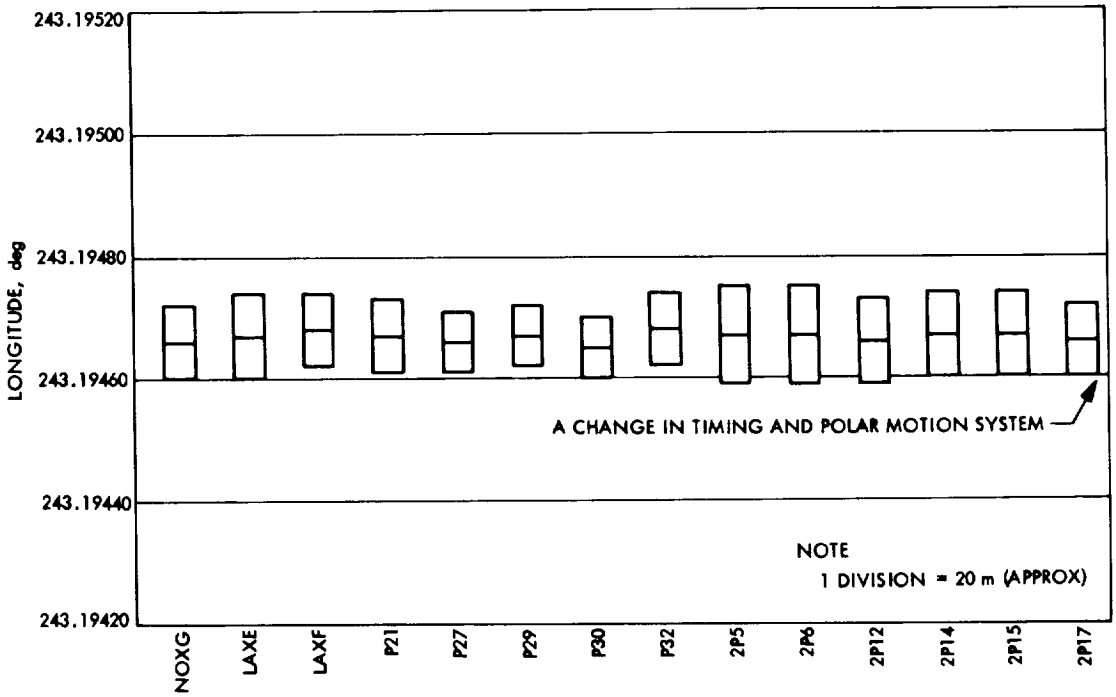

(a)

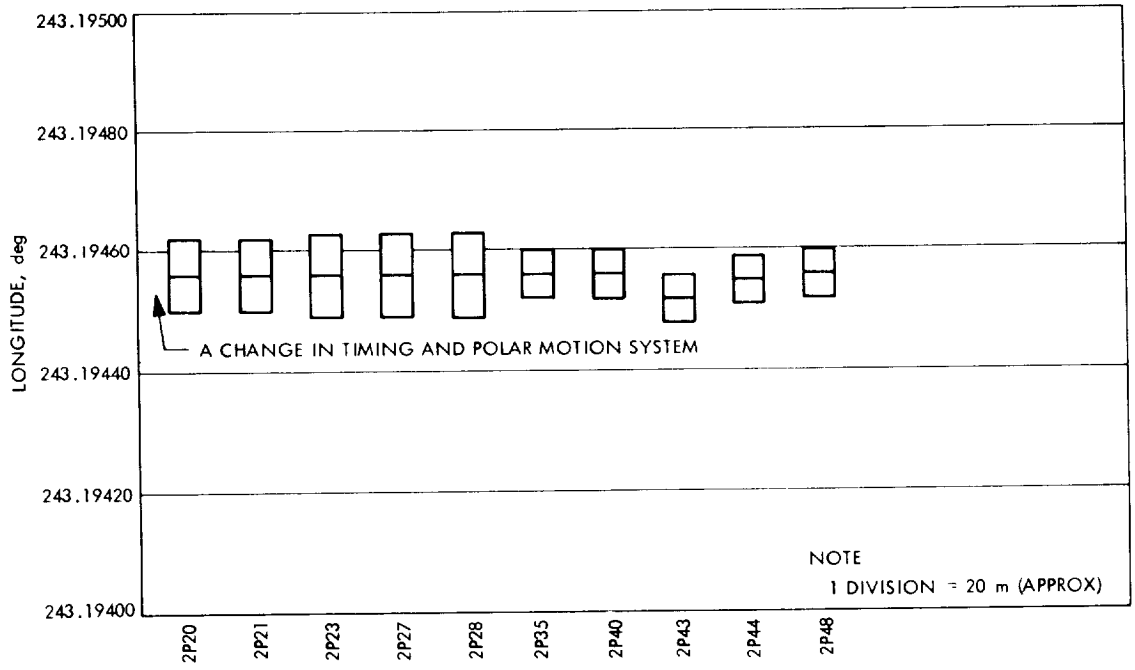

(b)

Figure 2-67. Geocentric Longitude, DSS 12

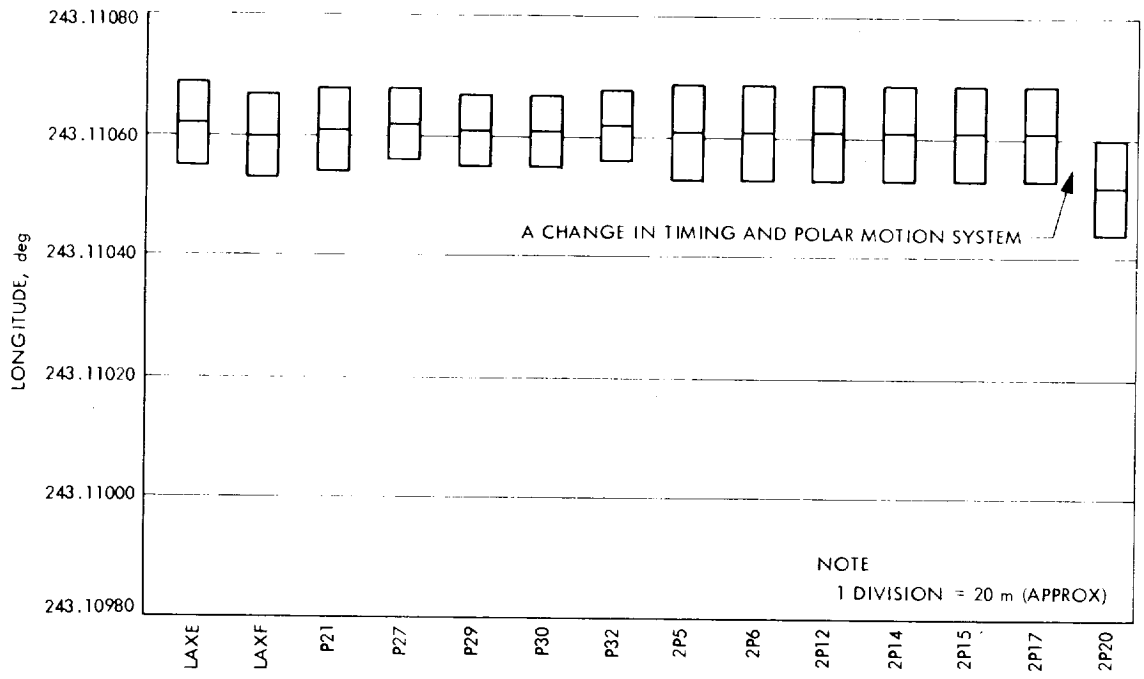

(a)

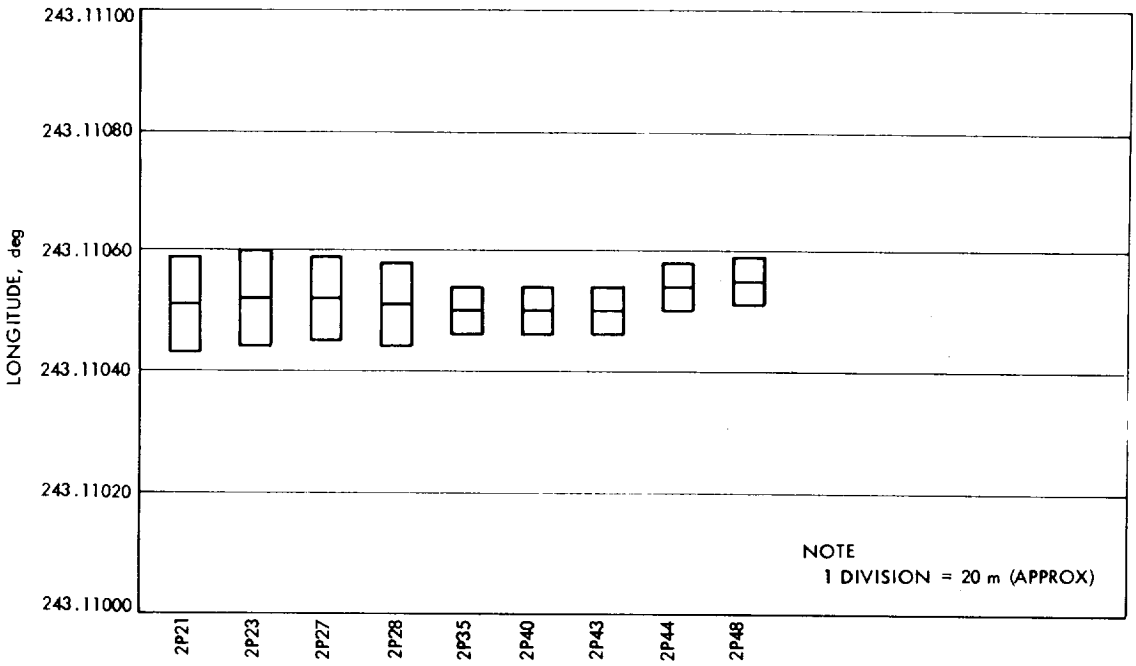

(b)

Figure 2-68. Geocentric Longitude, DSS 14

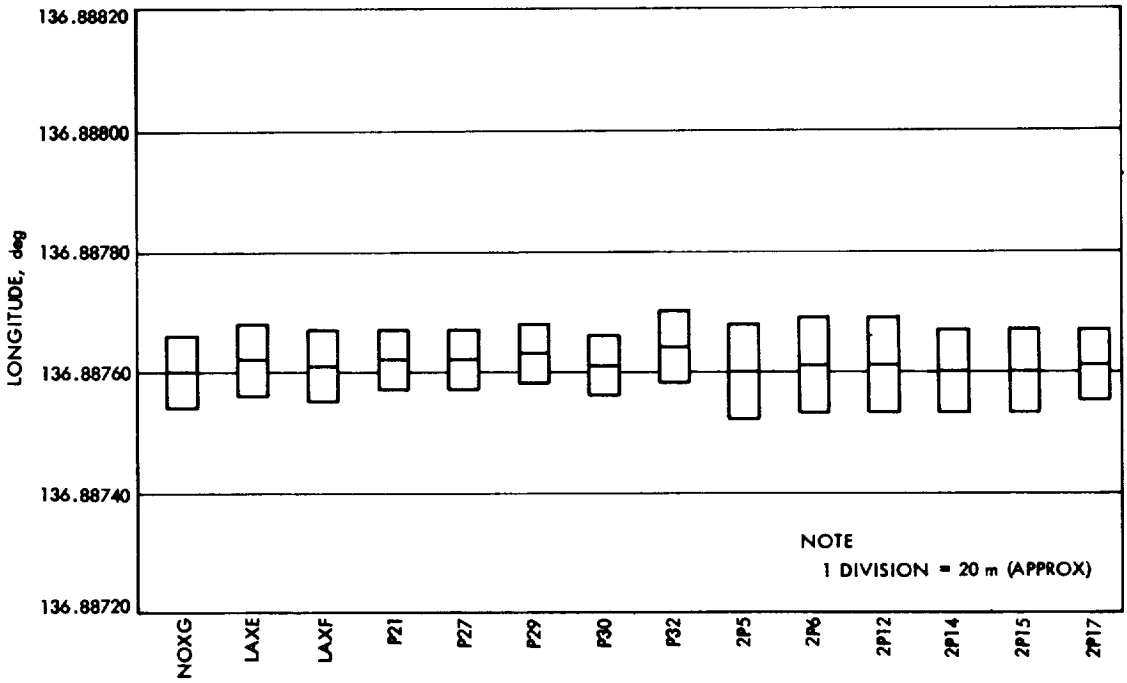

(a)

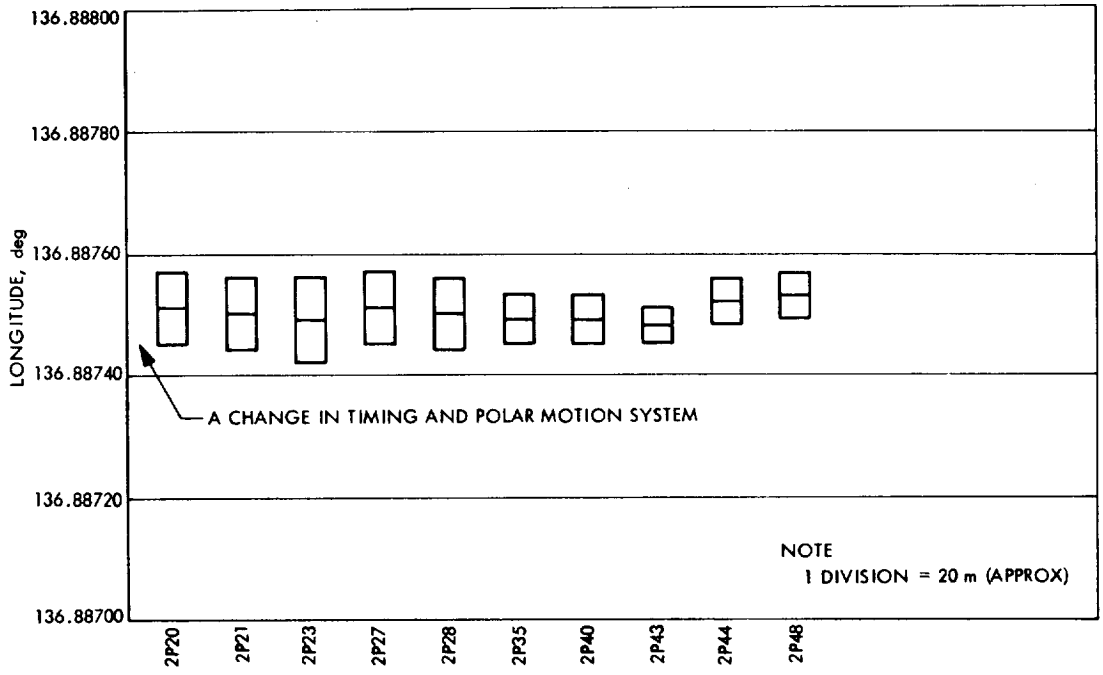

(b)

Figure 2-69. Geocentric Longitude, DSS 41

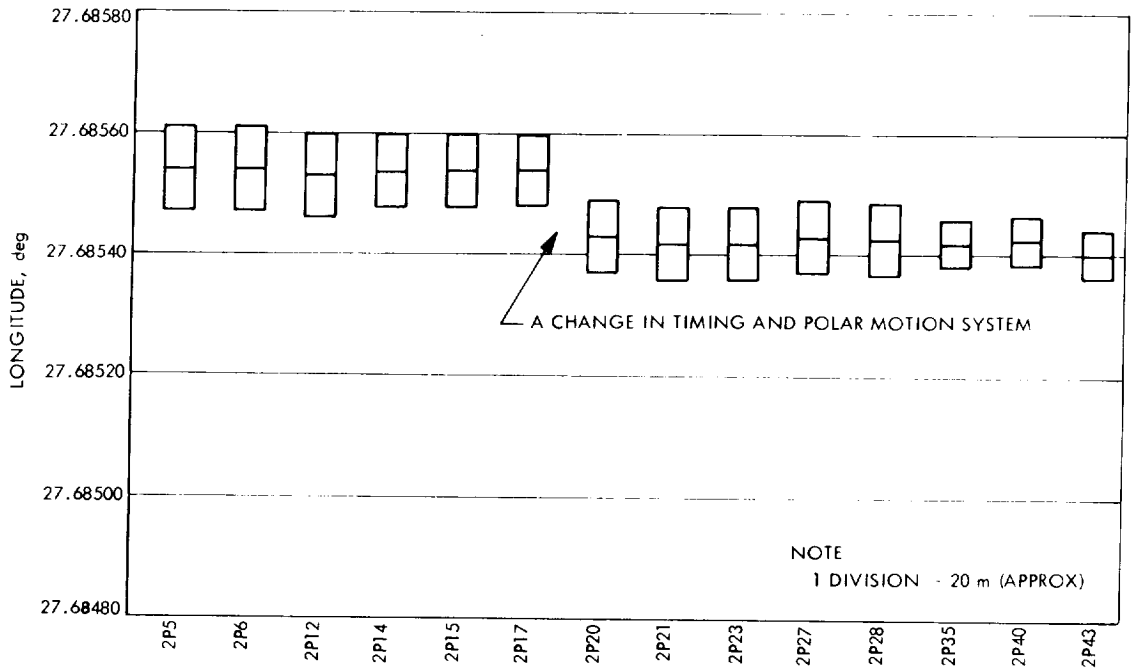

(a)

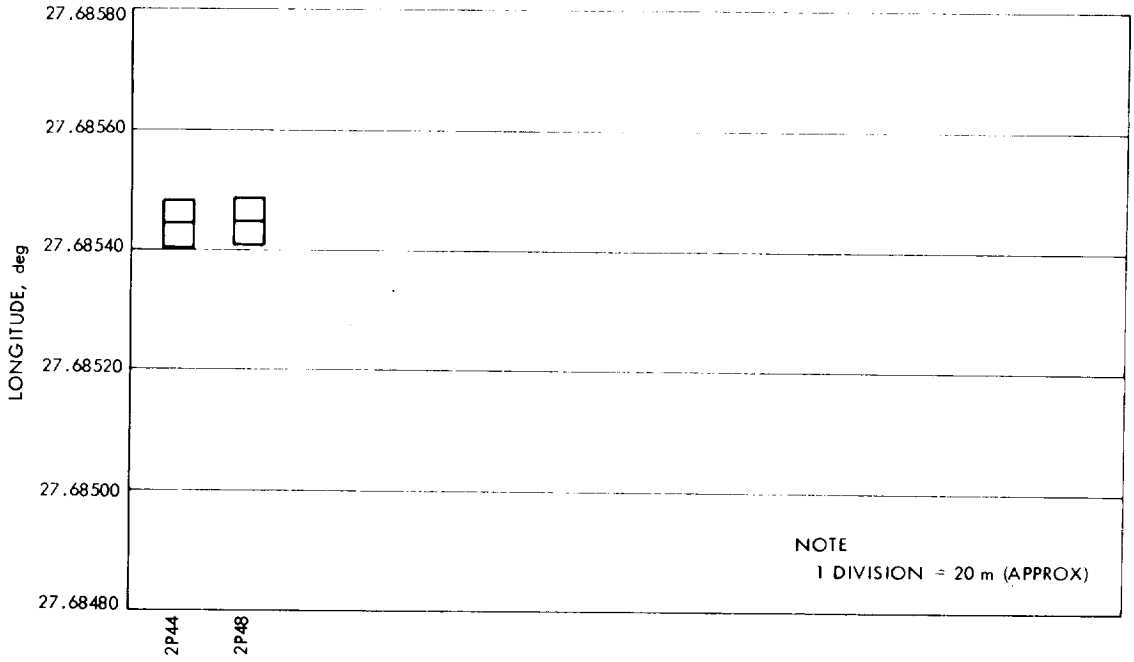

(b)

Figure 2-70. Geocentric Longitude, DSS 51

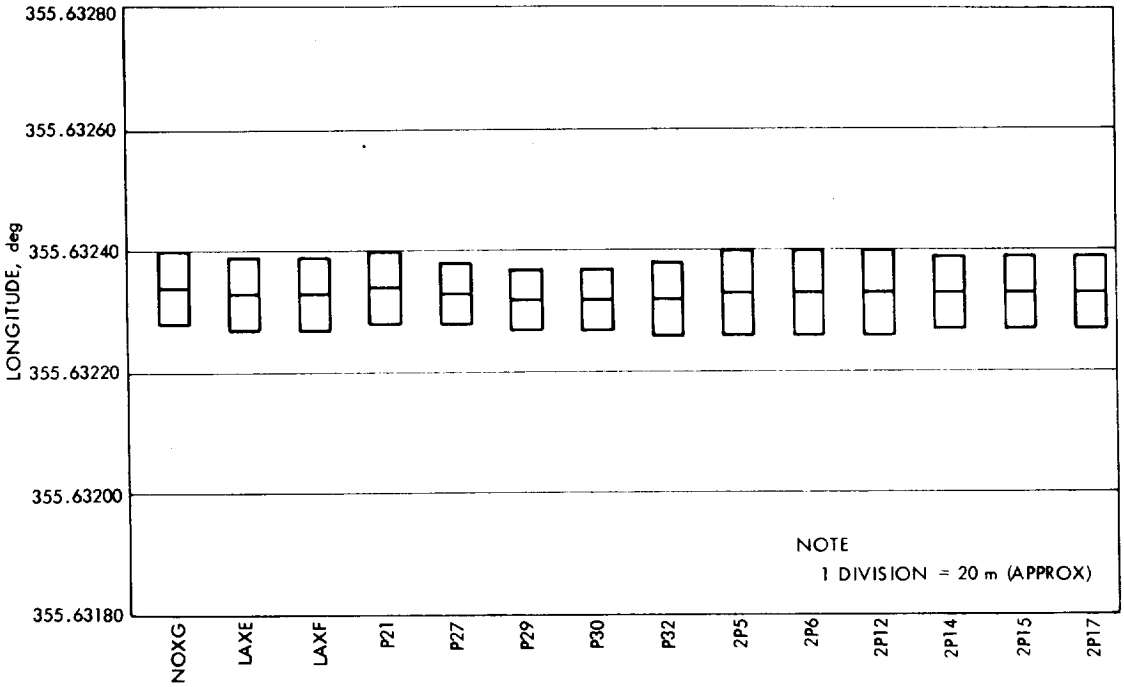

(a)

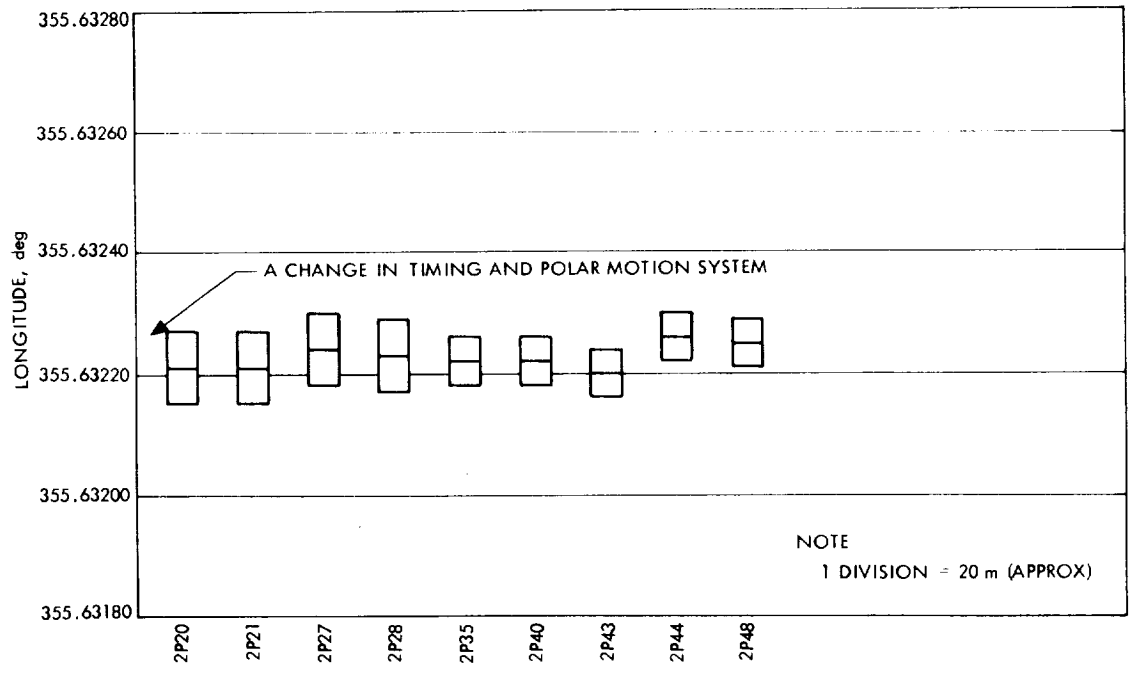

(b)

Figure 2-71. Geocentric Longitude, DSS 62

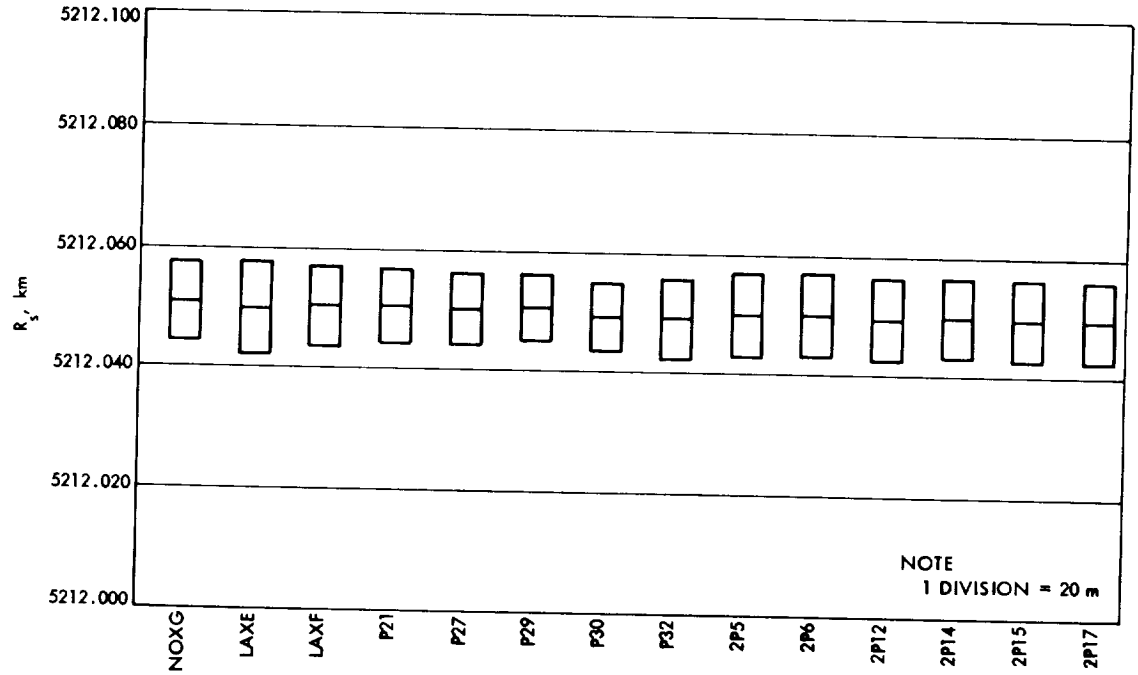

(a)

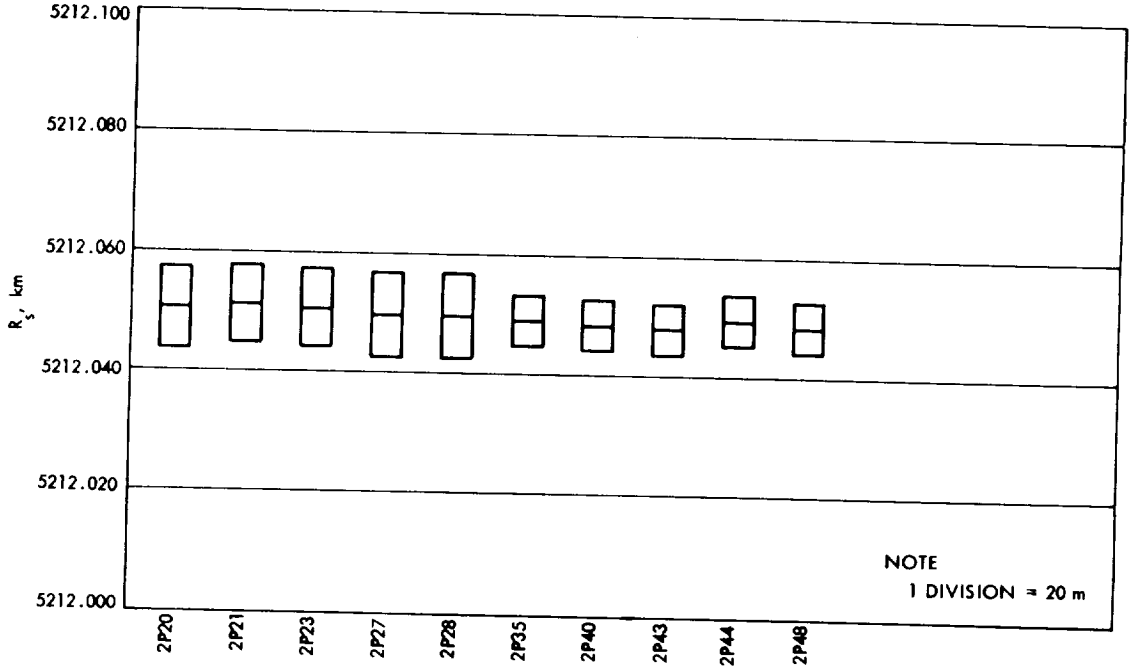

(b)

Figure 2-72. Distance Off Spin Axis, DSS 12

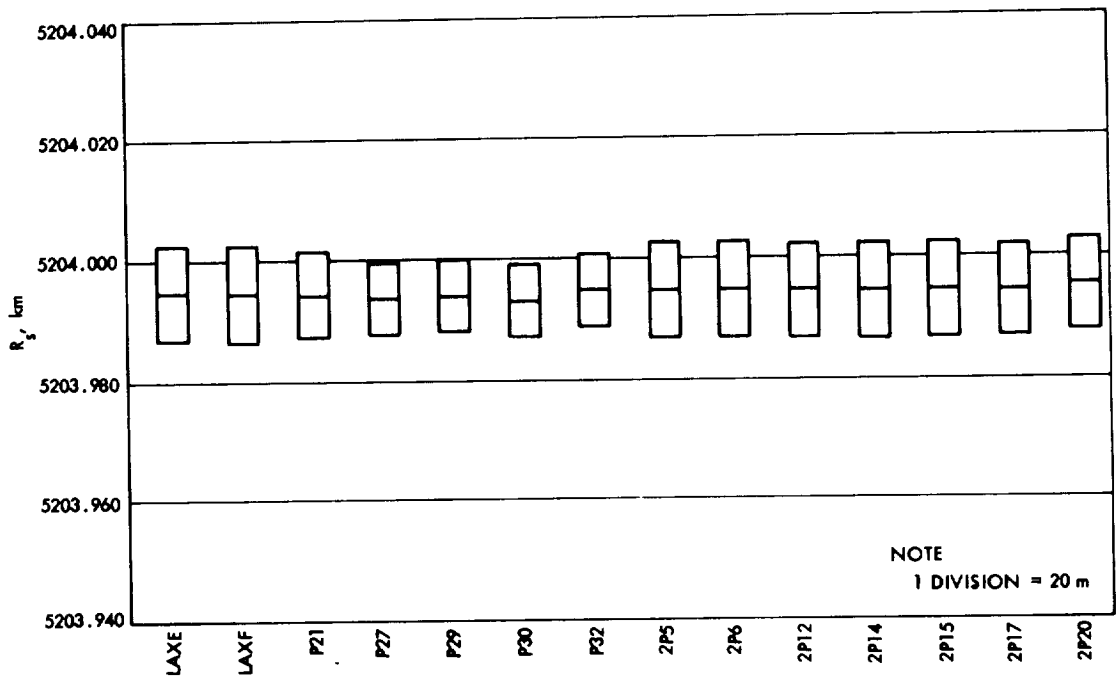

(a)

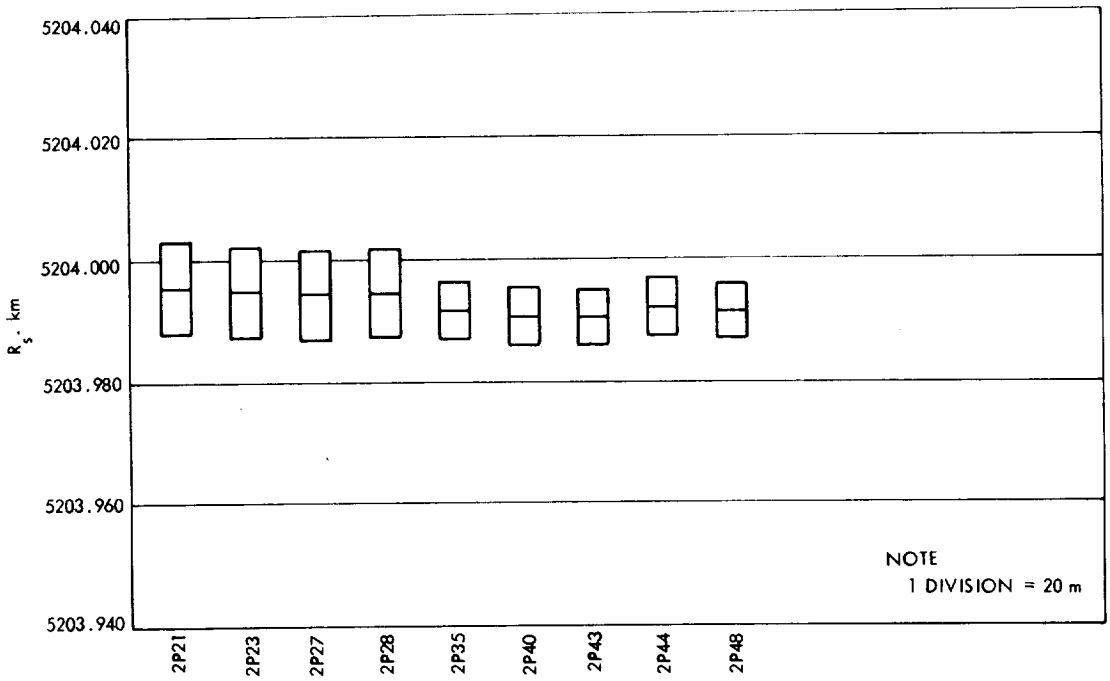

(b)

Figure 2-73. Distance Off Spin Axis, DSS 14

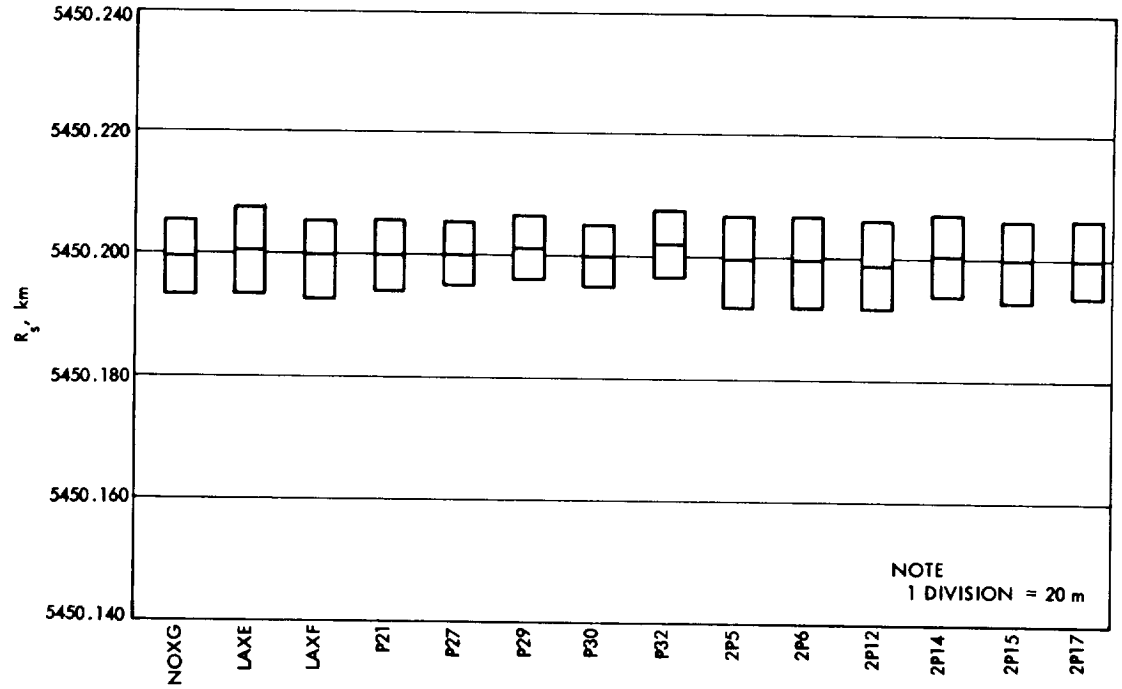

(a)

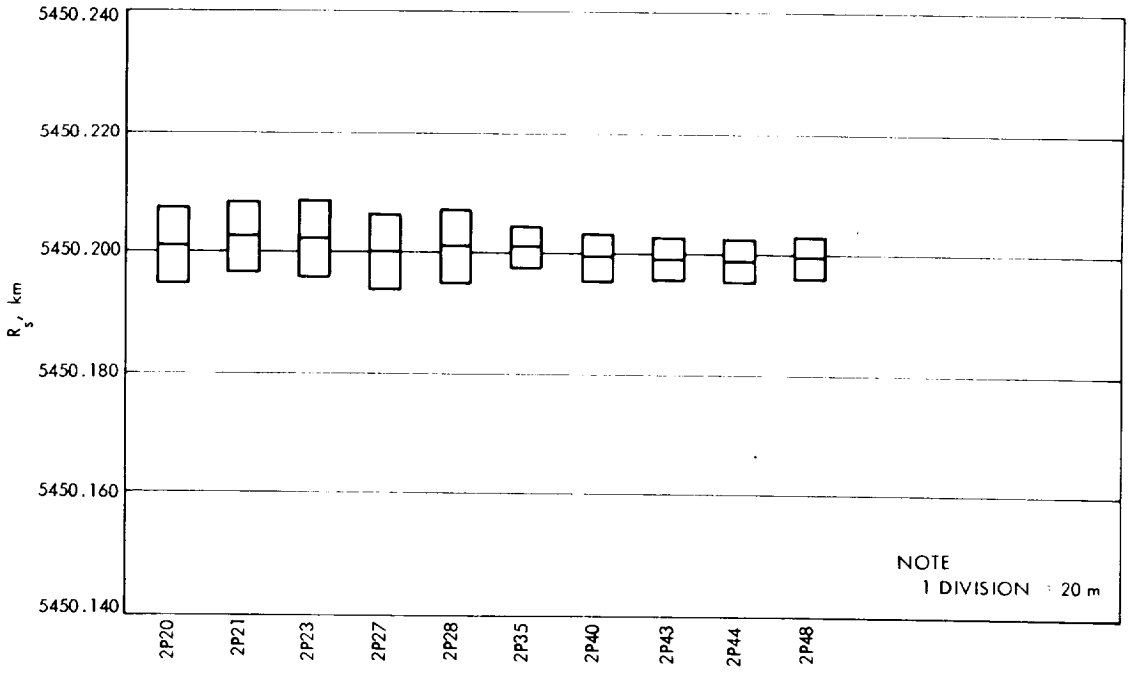

(b)

Figure 2-74. Distance Off Spin Axis, DSS 41

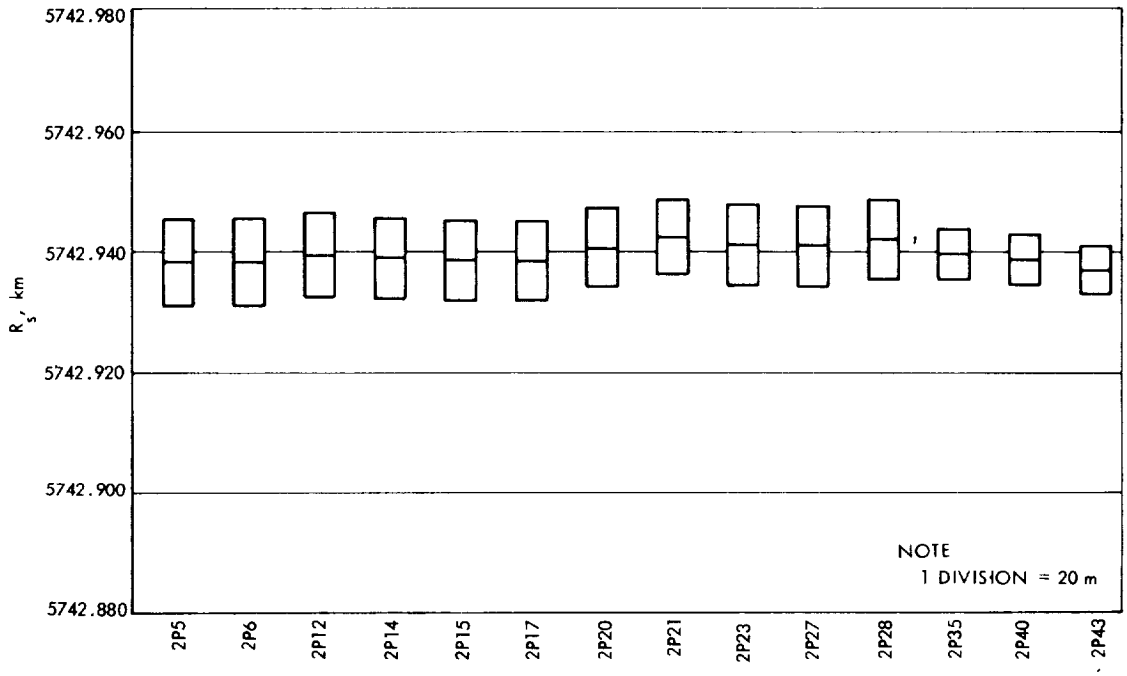

(a)

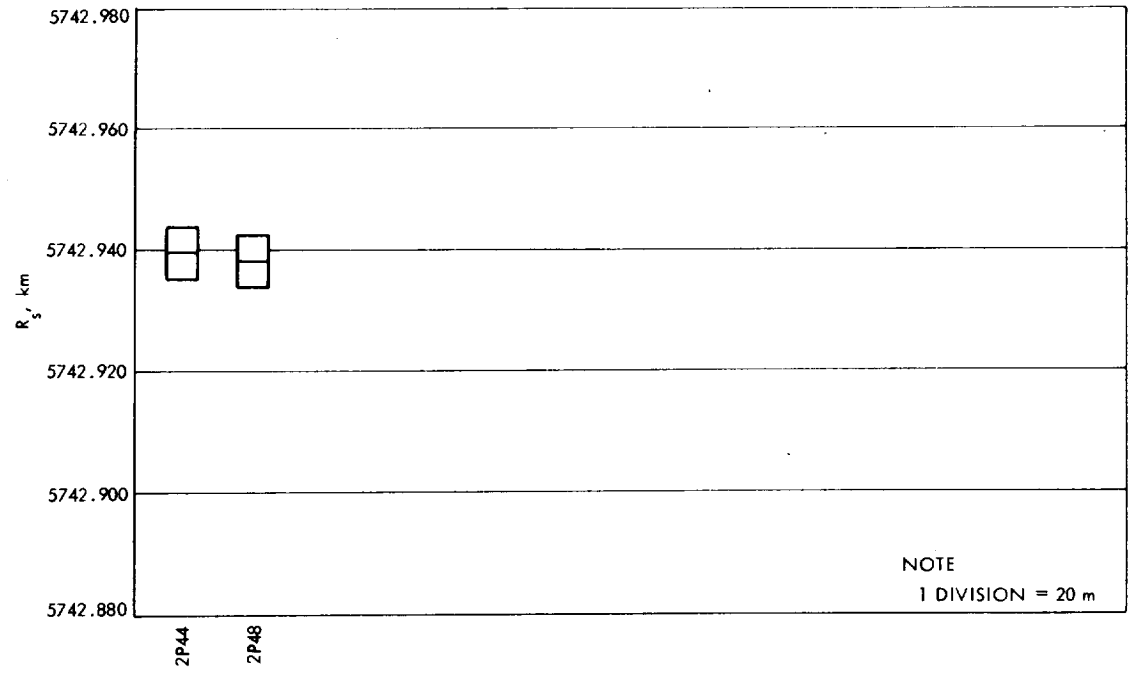

(b)

Figure 2-75. Distance Off Spin Axis, DSS 51

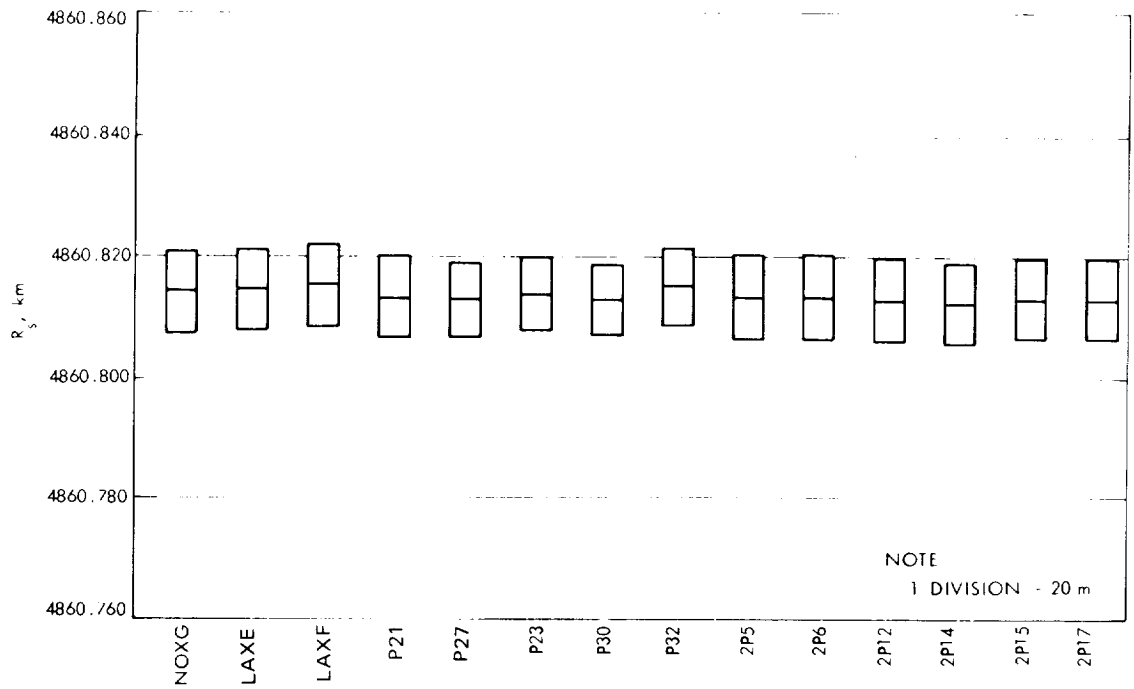

(a)

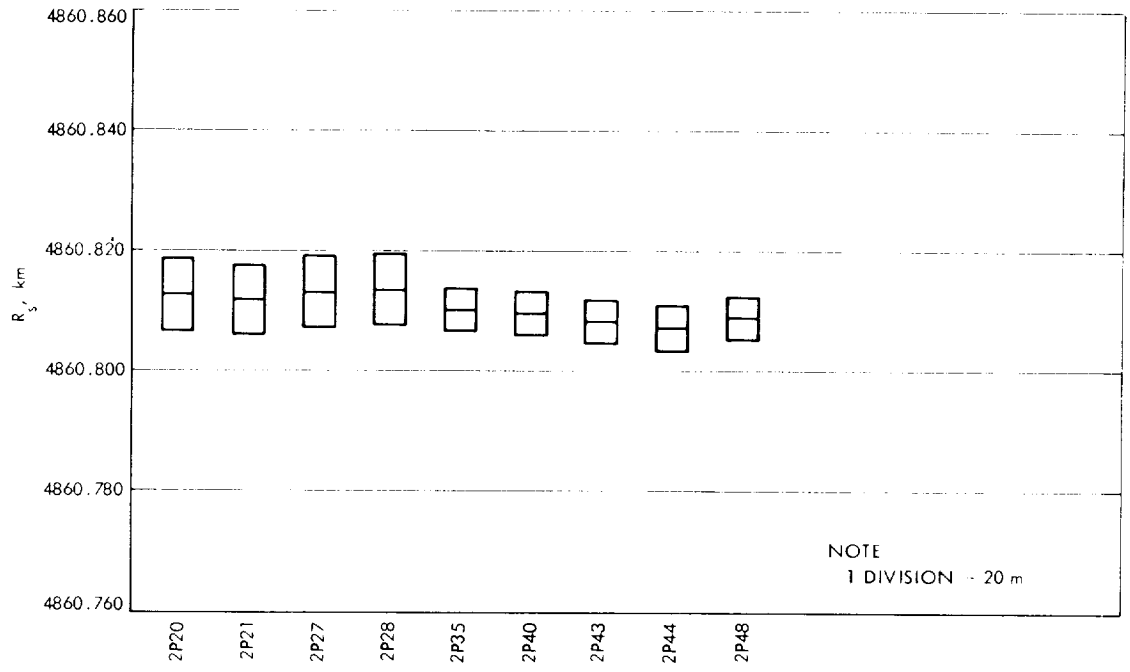

(b)

Figure 2-76. Distance Off Spin Axis, DSS 62

spin axis distance r_s and longitude λ are $\tilde{\sigma}_{r_s}$ = 8m $\tilde{\sigma}_{\lambda}$ = 10m. The station location estimates were reduced to the mean pole of 1903 and plotted by N. Mottinger of JPL. The Mariner VII numerical results for station locations indicate that the r_s and λ solutions are more consistent than the Mariner VI results. An explanation for this is that the maximum elevation angles for Mariner VII tracking data are higher than for the Mariner VI tracking data and that much of the Mariner VI pre-midcourse and early cruise phase data are below 15 degrees in elevation.

A new set of station locations and timing polynomials were implemented into the flight version of SPODP just prior to orbit 2P20. The changes observed in the station locations at this point are similar to the changes observed just prior to 3P10 in the Mariner VI solutions and the causes are the same. The jump in the station location solutions is due to the changes which were made in the timing and the polar motion system used by JPL. The changes were made in the computation of Universal Time and the determination of the pole positions. The observed changes in station longitude are given below: (The Mariner VI changes in station longitude, are also given here for comparison purposes.)

Station	$\Delta\lambda$ (Mariner VI)	$\Delta\lambda$ (Mariner VII)
DSS-12	12 meters	11 meters
DSS-14	NA	9 meters
DSS-41	12 meters	11 meters
DSS-51	11 meters	11 meters
DSS-62	12 meters	10 meters

The average value of the station location estimates for each station was computed for Mariner VI and Mariner VII and they are presented in Table 2-39. Two average values were computed for each station. One average value is for the station location estimates before the changes made in timing and polar motion system. The other average value is for the station location

Table 2-39. Station Location Solutions for Mariner VI and VII

	MARINER VI		MARINER VII	
	Pre-System Change*	Post-System Change	Pre-System Change*	Post-System Change
DSS 12				
r_s	5212.0481	5212.0490	5212.0499	5212.0496
λ	243.19468	243.19456	243.19467	243.19456
DSS 14				
r_s	NA	5203.9941	5203.9942	5203.9932
λ	NA	243.11052	243.11061	243.11052
DSS 41				
r_s	5450.2006	5450.2004	5450.2000	5450.2006
λ	136.88763	136.88751	136.88761	136.88750
DSS 42				
r_s	NA	5205.3501	NA	NA
λ	NA	148.98130	NA	NA
DSS 51				
r_s	5742.9386	5742.9395	5742.9386	5742.9403
λ	27.685537	27.685425	27.685537	27.685428
DSS 62				
r_s	4860.8119	4860.8133	4860.8136	4860.8107
λ	355.63233	355.63221	355.63233	355.63223

*System Change – The change made in the computation of Universal Time and the determination of the Earth pole position.

estimates after the change. The differences in the station locations between Mariner VI and VII are presented in Table 2-40 which shows that the station locations are consistent to ±1 m.

The Mariner VII postflight station location solutions for premidcourse, pre-unlatch and post-unlatch phase are given in Table 2-41 along with previous interplanetary missions. The station location solutions for the encounter phase are not given because of the inadequacy of the model for the spacecraft acceleration. The station location solutions are given in r_s, the distance from the Earth spin axis and λ, the longitude. The Mariner VII solutions agree very well with the Mariner VI solutions. There are some differences expected between the solutions for Mariners VI and VII and solutions for previous missions because of a difference in the ephemeris used in the computation. Mariners VI and VII solutions used Development Ephemeris '71 and solutions for previous missions used Development Ephemeris '69.

Table 2-40. The Difference in Station Location Between Mariner VI and VII

Δ Mariner VII — Mariner VI		
Pre System Change*		Post System Change
DSS 12		
r_s	2 meters	1 meter
λ	-1 meter	0
DSS 14		
r_s		-1 meter
λ		0
DSS 41		
r_s	-1 meter	0
λ	-2 meters	-1 meter
DSS 51		
r_s	0	0
λ	0	0
DSS 62		
r_s	2 meters	-2 meters
λ	0	2 meters

*System Change – The change made in the computation of Universal Time and the determination of the Earth pole position.

Table 2-41. Absolute Station Locations and Statistics

DSS	Data Source	Distance Off Spin Axis, km	1-σ Standard Deviation, m	Geocentric Longitude, deg	1-σ Standard Deviation 10^{-5} deg	Distance Along* Spin Axis, km
11		5206.3XXX		243.15XXXX		3673.7XXX
	Mariner IV Encounter	408	2.9	0633	5.6	590
	Pioneer VIIA	408	1.6	0454	17.0	590
	Pioneer VIIIA	382	1.9	0686	109.0	590
	Mariner VII Post-Unlatch	392	6.0	0653	4.7	630
12		5212.0XXX		243.19XXXX		3665.6XXX
	Mariner V Encounter	475	2.1	4560	3.6	240
	Mariner V Post-encounter	509	1.9	4588	9.8	240
	Pioneer VIIA	508	1.2	4382	16.5	240
	Pioneer VIIIB	484	3.6	4318	77.4	240
	Pioneer IX	469	5.8	4498	61.0	240
	Mariner VI Premidcourse	524	7.8	4543	7.2	280
	Mariner VI Pre-Unlatch	499	8.8	4538	6.4	280
	Mariner VI Post-Unlatch	546	7.0	4525	5.4	280
	Mariner VI Encounter	517	5.3	4539	5.0	280
	Mariner VII Premidcourse	534	7.5	4552	6.4	280
	Mariner VII Pre-Unlatch	534	6.3	4549	5.8	280
	Mariner VII Post-Unlatch	532	5.6	4529	4.0	280
14		5203.9XXX		243.11XXXX		3677.XXX
	Mariner V Cruise	964	2.4	0531	9.2	048
	Mariner V Encounter	942	1.7	0528	3.6	048
	Mariner V Post-encounter	936	3.0	0523	9.8	048
	Pioneer VIIB	957	2.5			
	Pioneer IX	992	5.7	0438	62.0	048
	Mariner VI Pre-Unlatch	989	10.0	0513	10.0	052
	Mariner VI Post-Unlatch	999	7.9	0490	7.8	052
	Mariner VI Encounter	965	5.9	0499	5.3	052
	Mariner VII Premidcourse	996	7.2	0509	6.9	052
	Mariner VII Pre-Unlatch	982	6.4	0497	6.1	052
	Mariner VII Post-Unlatch	979	6.0	0517	4.6	052
41		5450.XXXX		136.88XXXX		-3302.XXX
	Mariner V Encounter	1975	2.1	7531	3.0	238
	Mariner V Post-encounter	2000	2.4	7578	9.7	238
	Pioneer VIIA	2006	8.0	7365	17.6	238
	Mariner VI Premidcourse	2020	6.4	7532	6.6	243
	Mariner VI Pre-Unlatch	2042	7.1	7537	6.2	243
	Mariner VI Post-Unlatch	2027	5.1	7473	4.6	243
	Mariner VI Encounter	2008	3.8	7494	4.5	243
	Mariner VII Premidcourse	2009	5.9	7513	5.5	243
	Mariner VII Pre-Unlatch	2007	5.4	7523	5.5	243
	Mariner VII Post-Unlatch	2022	3.9	7501	3.4	243
42		5205.3XXX		148.98XXXX		-3674.XXX
	Mariner IV Encounter	494	2.9	1288	5.0	628
	Mariner V Cruise	503	1.4	1311	9.3	628
	Pioneer VIIA	519	1.6	1129	16.5	628
	Pioneer VIIIA	478	1.6	1378	108.0	628
	Pioneer VIIIB	475	2.1	1004	75.7	628
	Pioneer IX	424	7.8	1268	62.0	628
	Mariner VII Post-Unlatch	516	4.8	1299	4.7	646
51		5742.9XXX		27.68XXXX		-2768.XXX
	Mariner IV Encounter	408	2.6	5432	4.5	760
	Pioneer VIIIB	307	2.4	5192	75.7	760
	Pioneer IX	397	9.1	5396	62.0	760
	Mariner VI Premidcourse	395	6.5	5422	6.7	744
	Mariner VI Pre-Unlatch	396	7.4	5423	6.2	744
	Mariner VI Post-Unlatch	379	5.5	5360	4.7	744
	Mariner VI Encounter	412	6.0	5411	6.3	744
	Mariner VII Post-Unlatch	415	4.3	5410	3.4	744
62		4860.8XXX		355.63XXXX		4116.XXX
	Mariner V Cruise	149	2.1	2219	9.8	950
	Mariner V Encounter	151	2.0	2221	3.3	950
	Mariner V Postencounter	155	2.4	2234	10.0	950
	Pioneer IX	127	8.1	2075	69.0	950
	Mariner VI Post-Unlatch	172	7.9	2180	7.0	908
	Mariner VI Encounter	162	5.5	2188	5.1	908
	Mariner VII Premidcourse	155	6.7	2220	5.8	908
	Mariner VII Pre-Unlatch	157	6.7	2220	5.7	908
	Mariner VII Post-Unlatch	133	4.5	2203	3.5	908

*Distance along spin axis was input but not solved for.

e. Analysis of Simulated Data — *V. J. Ondrasik*

- Introduction

During the Mariner VII operations and the post-encounter analysis, many strategies were employed to determine the spacecraft's orbit under the influence of the unknown perturbation. To try and formulate a "best" strategy to deal with such perturbations, and to obtain some idea of how well the orbit may be determined, simulated data was produced so that the actual trajectory was a known quantity.

The first block of simulated data consisted of producing two-way doppler points and the associated partial derivatives every 10 minutes starting on July 31 at $22^h 00^m$ and continuing to August 10, for a nominal orbit with no perturbations. To avoid having to simulate and fit data for every perturbation which was to be studied, the following procedure was followed:

1) A simple trajectory run was made applying the desired perturbation and obtaining perturbed values of the geocentric range.

2) These perturbed geocentric range values were differenced with the unperturbed values.

3) These range differences were used to produce the corresponding doppler changes by means of the program ION (described in III.A.2.d.) with all features peculiar to the ionosphere deleted.

4) The resulting doppler corrections were then treated as residuals in the nominal unperturbed run.

This method produced the necessary quantities needed to study the effects of any desired perturbation in less than one-tenth of the time of simulating original data and performing a fit.

The effects of five perturbations were studied, namely, a constant acceleration of magnitude 0.26×10^{-8} km/sec^2 in the r and y directions and an exponential acceleration of magnitude 0.26×10^{-8} exp (-t/18 hr) km/sec^2 in the r, x, and y directions. (These directions correspond to the principal spacecraft axes, roll, pitch and yaw, respectively.)

The constant acceleration was chosen because the orbit determination program has the capability of solving for it, and the exponential was chosen because it best approximates the actual acceleration thought to have been experienced by Mariner VII. Table 2-42 shows the effects these accelerations have on the B-plane parameters, and Figures 2-77, 2-78, and 2-79 show the resulting changes in the range and range rate for the exponential perturbations.

The numbers of Table 2-42 are easily predicted from the following equation

$$\begin{bmatrix} \Delta B \\ \Delta(\overline{B}\cdot\overline{R}) \\ \Delta(\overline{B}\cdot\overline{T}) \end{bmatrix} = \begin{bmatrix} \overline{U}_B \\ \overline{R} \\ \overline{T} \end{bmatrix} \int_0^{T_{CA}} \int \Delta\ddot{\overline{r}}\, dt^2$$

where $\Delta\ddot{\overline{r}}$ is the perturbing acceleration

For example, the changes in B for the constant accelerations in the r, x, and y directions are

$$\Delta B(\ddot{r}, \ddot{x}, \ddot{y}) = -45, 39, 125 \text{ km}$$

which should be compared to the trajectory run results of -42.4, 40.5 and 127.8 respectively. In order to determine if these results could be applied in a linear fashion to perturbations of a different magnitude and direction, a trajectory run was performed with an acceleration of 0.26×10^{-8} km/sec^2 in all three directions simultaneously. The changes in the B-plane parameters, from the nominal, for this run agreed to within 1 km of the sum of the changes as produced by applying the accelerations separately.

- Pre-Encounter Solutions

Figures 2-80 and 2-81 show plots of the partial derivatives of doppler data with respect to the state parameters. It is obvious from these figures that the pre-encounter solutions, which can use data only up to E - 4 hours,

Table 2-42. Effects of Perturbing Accelerations*

Description	B, km	$\bar{B} \cdot \bar{R}$, km	$\bar{B} \cdot \bar{T}$, km	t_{ca} (8/5/69)	B (pert.) - B (nom), km	$\bar{B} \cdot \bar{R}$ (pert.) - $\bar{B} \cdot \bar{R}$ (nom), km	$\bar{B} \cdot \bar{T}$ (pert.) - $\bar{B} \cdot \bar{T}$ (nom), km	t_{ca} (pert.) - t_{ca} (nom), sec
nominal	7604.0	3360.5	6821.1	$05^h01^m28^s.1$				
r direction (constant)	7561.6	3373.9	6769.0	$05^h01^m09^s.3$	-42.4	13.4	-52.1	-18.8
x direction (constant)	7644.5	3260.0	6908.0	$05^h01^m22^s.3$	40.5	-100.5	86.9	-5.8
y direction (constant)	7731.7	3462.0	6913.4	$05^h01^m25^s.9$	127.8	101.5	92.3	-2.2
r direction (exponential)	7590.7	3363.9	6804.6	$05^h01^m22^s.1$	-13.3	3.4	-16.5	-6.0
x direction (exponential)	7616.6	3329.9	6850.1	$05^h01^m26^s.3$	12.6	-30.6	29.0	-1.8
y direction (exponential)	7644.6	3392.8	6850.5	$05^h01^m27^s.4$	40.6	32.3	29.4	-0.7

*The first three rows show the effect of a constant acceleration of magnitude 0.26302×10^{-8} km/sec^2 in the r, x and y directions, respectively.

The last three rows show the effect of an expontially decaying acceleration, of magnitude $0.26302 \times 10^{-8} \exp^{(-t/18\ hr)}$ km/sec^2, in the r, x and y direction, respectively, where t is the time from 22^h00^m, July 31.

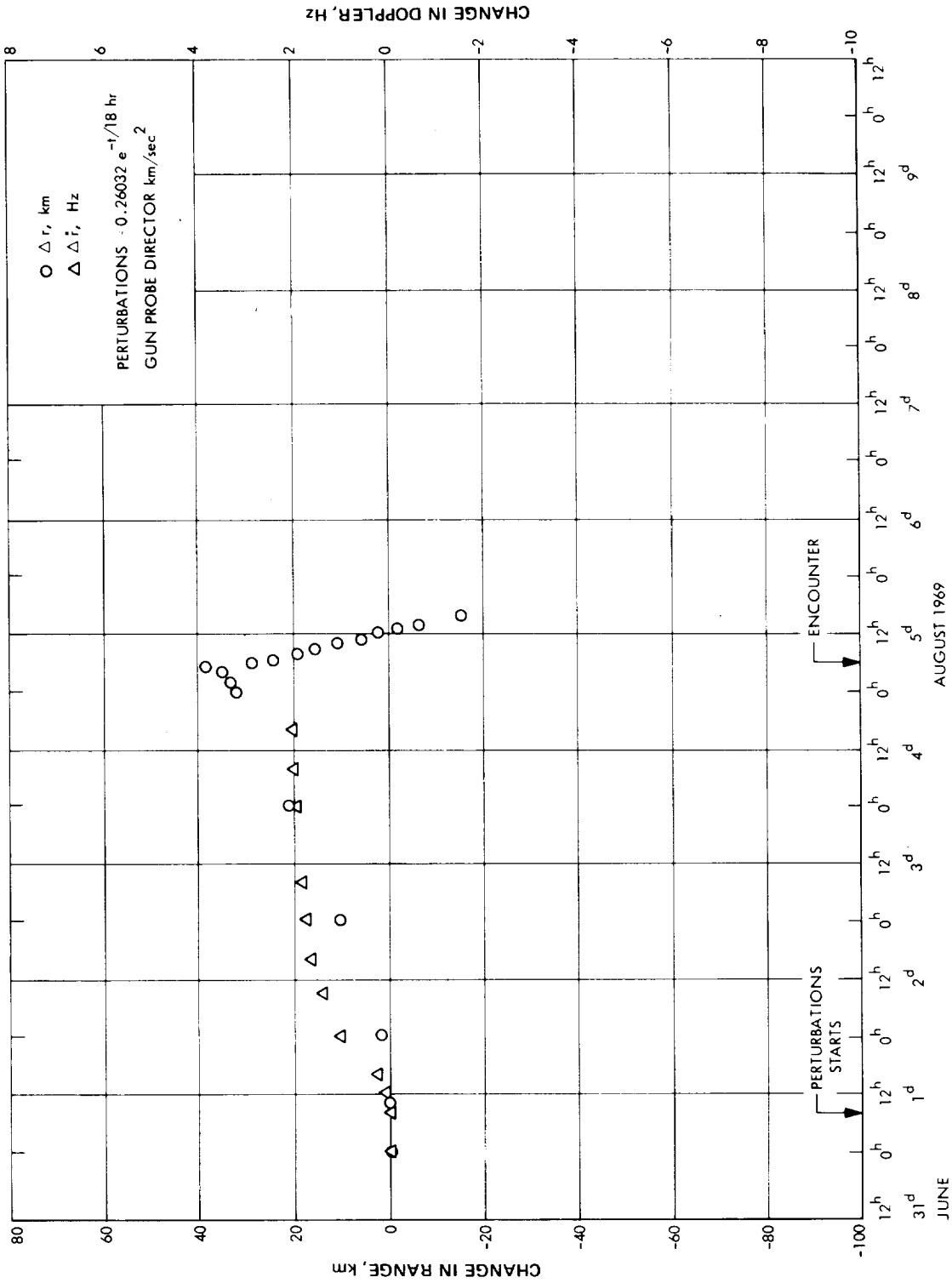

Figure 2-77. Doppler and Range Changes Produced by an Exponential Acceleration in R Direction

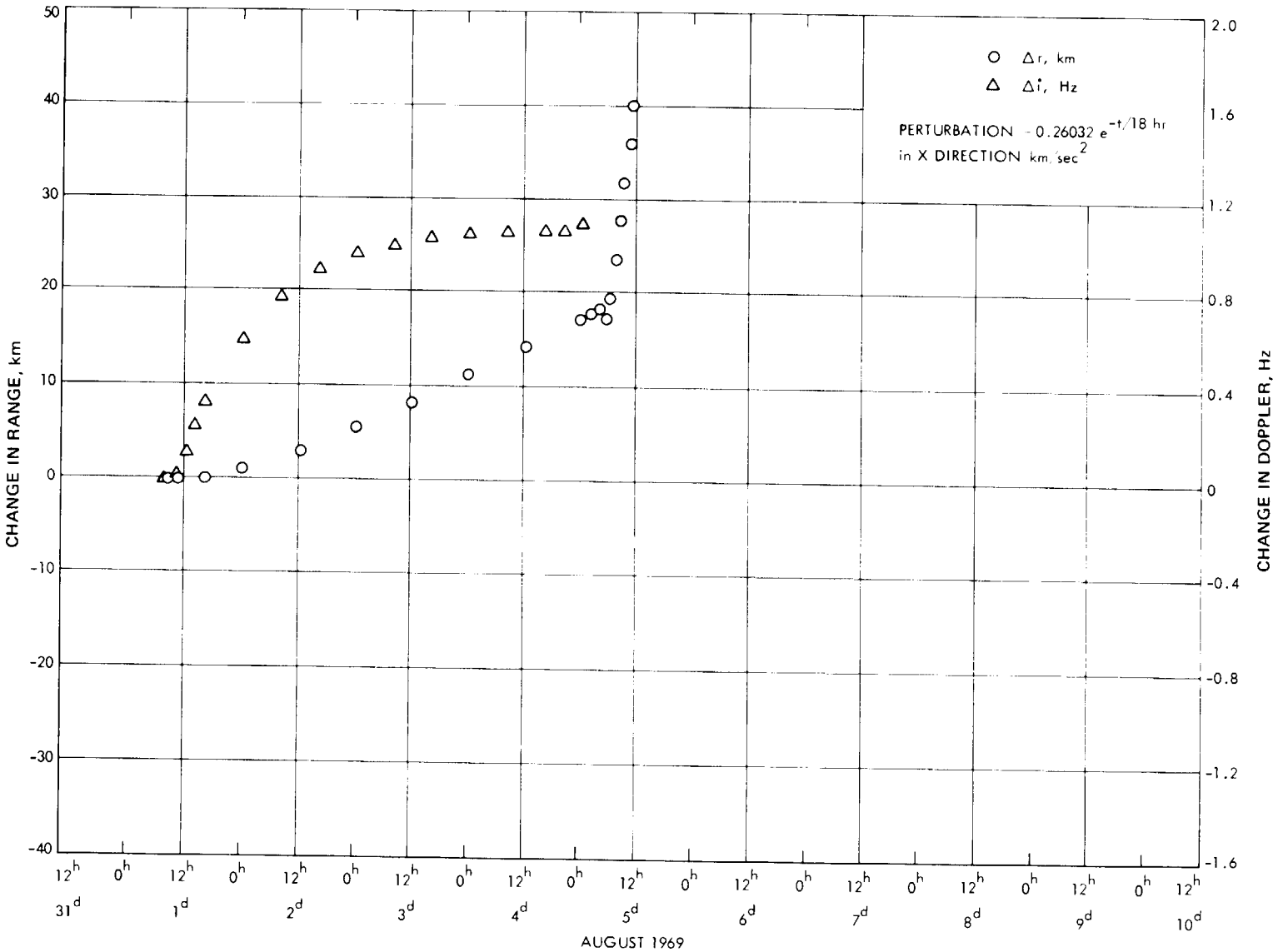

Figure 2-78. Doppler and Range Changes Produced by an Exponential Acceleration in X Direction

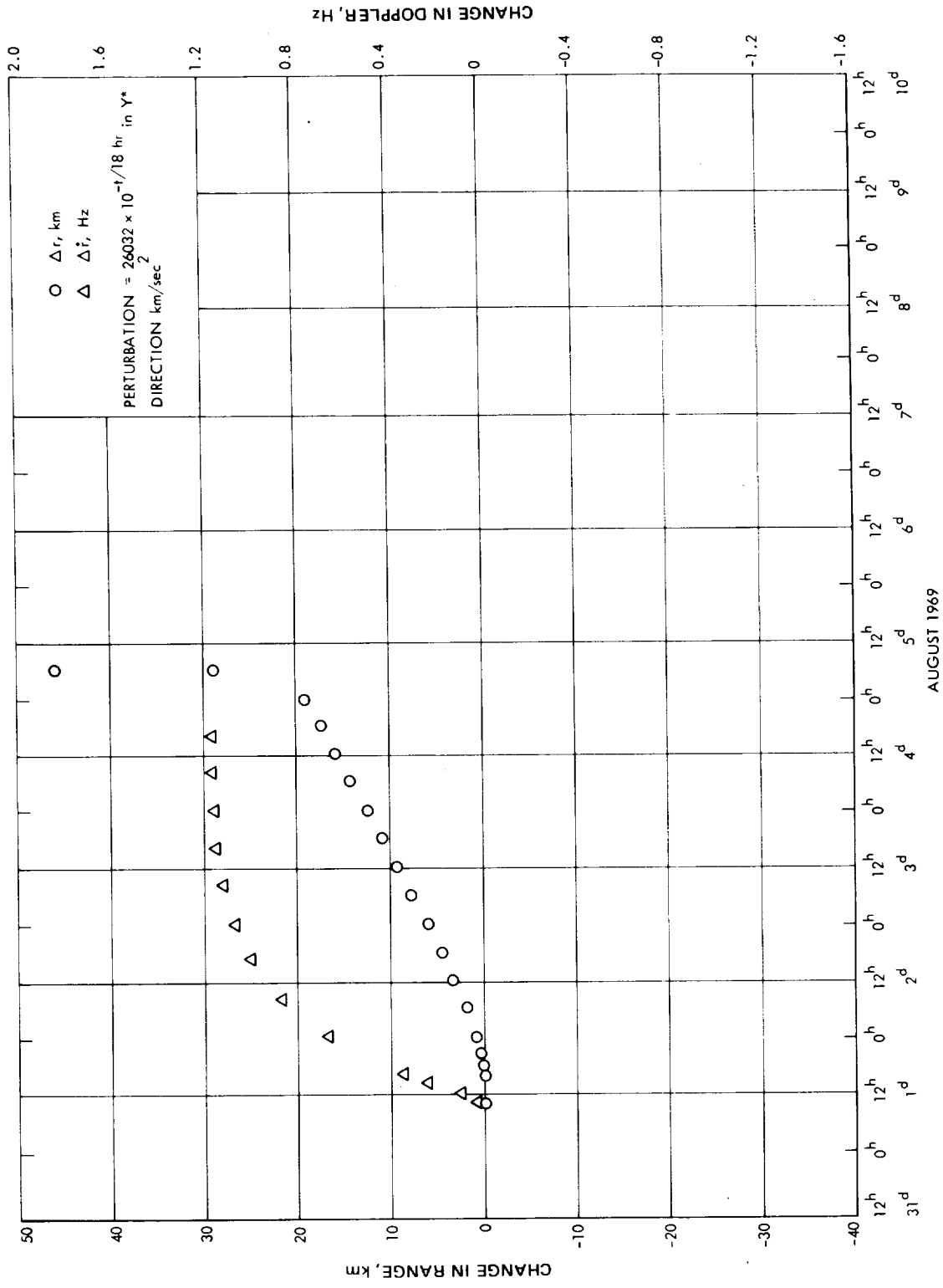

Figure 2-79. Doppler and Range Changes Produced by an Exponential Acceleration in Y Direction

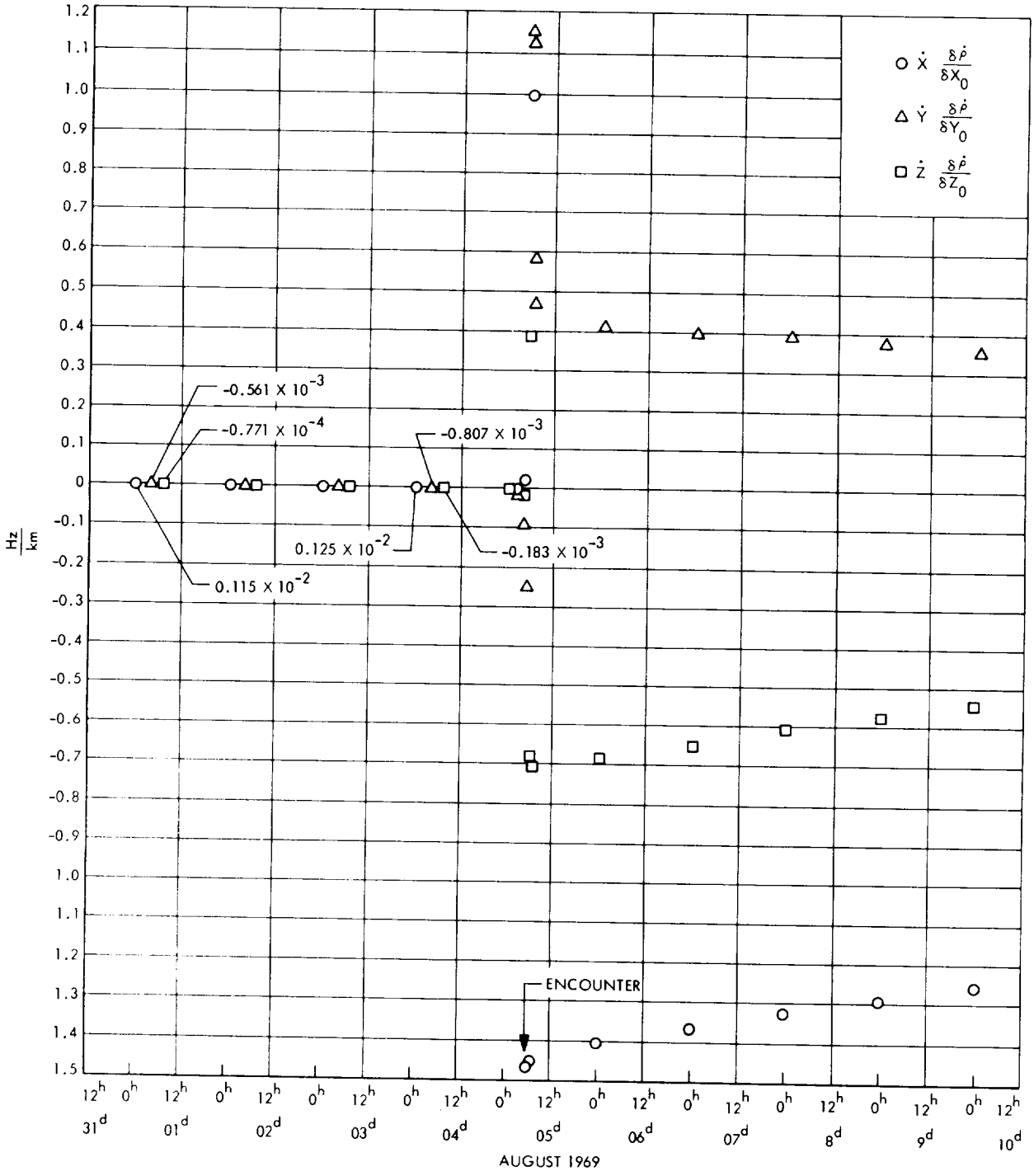

Figure 2-80. Doppler Partial w. r. t. Position

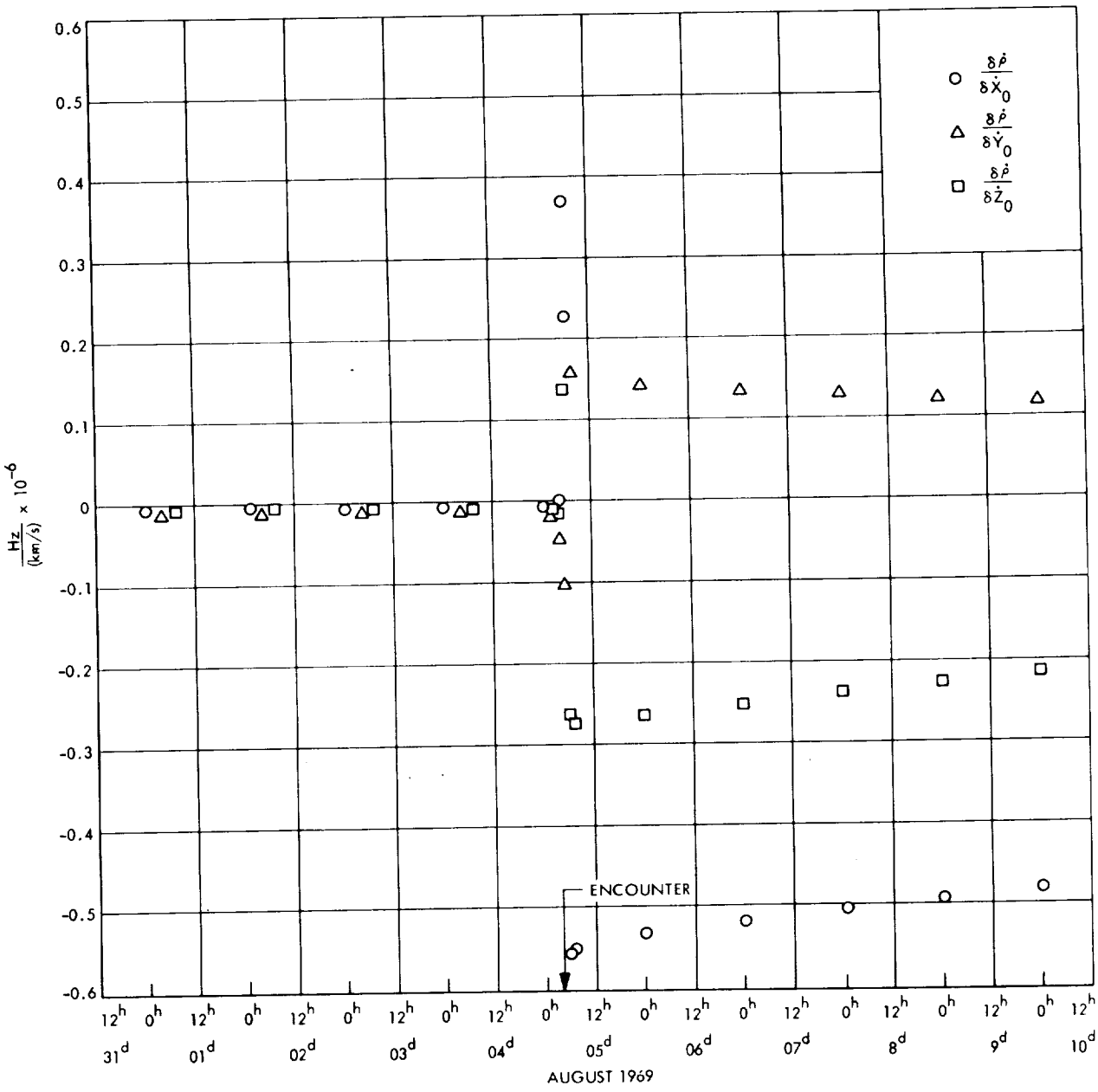

Figure 2-81. Doppler Partial w. r. t. Velocity

received very little help from the planet centered accelerations to resolve uncertainties arising from the unmodeled forces.

- Pre-Encounter Data

Tables 2-43 through 2-47 give the results of orbit determination solutions using various data arcs, *a priori*, and estimation parameters, for exponential and constant accelerations. All of these tables substantiate the well known fact that large unmodeled accelerations have disasterous effects upon the solution, and in this case may give errors in the encounter parameters of thousands of kms. An approximation to the change in orbital elements may be obtained by considering a first order temporal expansion of the range rate given by the following equation (Ref. 16).

$$\dot{\rho}(t) = \dot{r}_o + r_s \omega \cos\delta (\sin\omega t + \Delta\lambda \cos\omega t) + \left[a_g + r(\dot{\alpha}^2 \cos^2\delta + \dot{\delta}^2)\right] t$$

$$- r_s \omega t \dot{\delta} \sin\delta \sin\omega t - r_s \omega t \dot{\alpha} \cos\delta \cos\omega t \qquad (1)$$

where

ρ = topocentric range

r = geocentric range

δ = declination

$\Delta\lambda$ = an error in right ascension

r_s = distance of tracking station of the spin axis

a_g = gravitational acceleration

$r(\dot{\alpha}^2 \cos^2\delta + \dot{\delta}^2) = v_\perp^2/r$ = centrifugal acceleration

The orbit determination program will modify the elements r_o, $\dot{r}_o$, α_o, $\dot{\alpha}_o$, δ_o, and $\dot{\delta}_o$ to account for the unmodeled acceleration. For example, consider in a very simplified manner, the effects of a constant acceleration in the sun probe direction of magnitude 0.26×10^{-8} km/sec^2. The coefficients of the fourth term must rearrange themselves to account for this acceleration. Thus,

$$0.20 \times 10^{-8} \text{ km/sec}^2 = \left[\frac{\partial a_g}{\partial r} + (\dot{\alpha}^2 \cos^2 \delta + \dot{\delta}^2)\right]\Delta r + \frac{\partial a_g}{\partial \alpha}\Delta\dot{\alpha}$$

$$+ \frac{\partial a_g}{\partial \delta}\Delta\delta + 2rv_\perp \Delta v_\perp \qquad (2)$$

The gravitational partials are so small that it would require changes in the range of 0.2×10^6 km or changes in α or δ of approximately 1 deg to account for the unmodeled acceleration gravitationally. These possibilities must be eliminated as being unreasonably large. In addition the second or third choices are in conflict with the determination of α and δ from the second and third terms of Eq. (1). Thus, by assuming that the effects of the unmodeled accelerations will be absorbed in the perpendicular velocity, equation (2) yields

$$\Delta v_\perp = \frac{0.20 \times 10^{-8} \text{ km}^2/\text{sec}^2}{1.72 \times 10^{-7} \text{ km/sec}} = 0.0116 \text{ km/sec}$$

This agrees quite well with the DPODP result of 0.0123 km/sec. Unfortunately the correlation between the various coefficients of Eq. (1) prohibits such easy prediction of the changes in other quantities. However, an examination of the results given in Tables 2-43 through 2-47 have shown that the changes in both position and velocity are mostly perpendicular to the earth-probe direction.

Tables 2-43, 2-44, and 2-45 show that deleting increasing amounts of data where the exponential acceleration is large continually improves the state only solution. Finally, using only one day's worth of data shortly before encounter gives solutions whose B-plane parameters are usually within 30 km of the correct result with associated sigmas of approximately 60 km. However, the errors appear to be a function of the choice of *a priori* , even to the extent of changing sign, and for some particular parameters may be as large as 118 km. Comparing the one day data arc, state only solutions in Tables 2-43, 2-44, and 2-45 with perturbed minus nominal results of Table 2-42 show that errors in the solutions are almost always larger than actual differences in the perturbed and nominal trajectories. Thus the effect of the unmodeled acceleration degrades the state only solutions to such an extent that the use of these

Table 2-43. Pre-Encounter Solutions for $\Delta\ddot{r}_r = 0.26032 \times 10^{-8} e^{-t/18\ hr}\ km/sec^2$

(All data stops at E - 6 hr)

Start of Data Arc	Acceleration at Start of Data Arc, km/sec^2	A priori Standard Deviations	$\Delta x, y, z$, km	$\Delta\dot{x}, \dot{y}, \dot{z}$, km/sec	Δ(Attitude Control Parameters)*	B (DPODP) - B (traj), km	$\bar{B} \cdot \bar{R}$ (DPODP) - $\bar{B} \cdot \bar{R}$ (traj), km	$\bar{B} \cdot \bar{T}$ (DPODP) - $\bar{B} \cdot \bar{T}$ (traj), km	t_{ca} (DPODP) - t_{ca} (traj), sec
E - 3^d19^h	0.26×10^{-8}	10^4 km 1 km/sec	0.16×10^4 0.76×10^4 -0.13×10^5	-0.59×10^{-2} -0.28×10^{-1} 0.61×10^{-1}		2488.6	-10,111.6	682.7	93.5
E - 2^d19^h	0.065×10^{-8}	10^4 km 1 km/sec	0.38×10^3 0.22×10^4 -0.40×10^4	-0.11×10^{-2} -0.74×10^{-2} 0.15×10^{-1}		543.6	-1762.5	58.1	3.6
E - 2^d19^h	0.065×10^{-8}	100 km 10 m/sec $\sigma(a_r) = 10^{-6}$ $\sigma(b_r) = 10^{-12}$	0.28×10^3 -0.28×10^3 -0.23×10^3	-0.17×10^{-2} 0.80×10^{-3} 0.11×10^{-3}	$\Delta a_r = 0.11 \times 10^{-5}$ $\Delta b_r = -0.30 \times 10^{-4}$	388.8	181.7	343.9	-7.1
E - 1^d6^h	0.008×10^{-8}	100 km 10 m/sec	-0.86×10^2 -0.64×10^2 0.12×10^2	0.25×10^{-3} -0.35×10^{-3} 0.89×10^{-4}		-27.6	-67.6	2.5	-0.1
E - 1^d6^h	0.008×10^{-8}	1000 km 10 m/sec	-0.13×10^3 0.13×10^3 -0.14×10^3	0.21×10^{-3} -0.58×10^{-3} 0.61×10^{-3}		16.3	-114.9	73.8	-1.3
E - 1^d6^h	0.008×10^{-8}	100 km 1 m/sec $\sigma(a_r) = 10^{-9}$ $\sigma(b_r) = 10^{-14}$	-0.70 x 10 -0.51 x 10 -0.19 x 10	-0.32×10^{-4} -0.79×10^{-4} -0.36×10^{-4}	$\Delta a_r = 0.31 \times 10^{-9}$ $\Delta b_r = -0.95 \times 10^{-15}$	24.1	0.0	26.9	-0.9
E - 1^d6^h	0.008×10^{-8}	100 km 1 m/sec $\sigma(a_{r,x,y}) = 10^{-9}$ $\sigma(b_{r,x,y}) = 10^{-14}$	-0.58 x 10 -0.62 x 10 -0.23 x 10	-0.20×10^{-4} -0.82×10^{-4} -0.40×10^{-4}	$\Delta a_r = 0.19 \times 10^{-9}$ $\Delta a_x = 0.96 \times 10^{-10}$ $\Delta a_y = 0.11 \times 10^{-10}$ $\Delta b_r = 0.53 \times 10^{-15}$ $\Delta b_x = 0.43 \times 10^{-15}$ $\Delta b_y = -0.30 \times 10^{-15}$	25.3	2.0	27.2	-0.9

*Modelled as a constant plus linear acceleration, i.e., $\ddot{r}_i = a_i + b_i t$ where i = r, x or y and t is time from 22^h00^m on July 31.

Table 2-44. Pre-Encounter Solutions for $\Delta\ddot{r}_x = 0.26032 \times 10^{-8}\ e^{-t/18\ hr}\ km/sec^2$

(All data stops at E - 6 hr)									
Start of Data Arc	Acceleration at Start of Data Arc km/sec^2	*A priori* Standard Deviations	Δ x, y, z km	$\Delta\dot{x}, \dot{y}, \dot{z}$ km/sec	Δ (Attitude Control Parameters)*	B (DPODP) - B (traj) km	$\bar{B} \cdot \bar{R}$ (DPODP) - $-\bar{B} \cdot \bar{R}$ (traj) km	$\bar{B} \cdot \bar{T}$ (DPODP) - $-\bar{B} \cdot \bar{T}$ (traj) km	t_{ca} (DPODP) - t_{ca} (traj) sec
E - 3^d19^h	0.26×10^{-5}	10^4 km	0.11×10^4	-0.39×10^{-2}		298.9	-6575.2	427.7	47.1
		1 km/sec	0.49×10^4	-0.18×10^{-1}					
			-0.84×10^4	0.39×10^{-1}					
E - 1^d6^h	0.008×10^{-8}	100 km	-0.22×10^2	0.22×10^{-4}		-43.1	-66.1	-15.5	0.5
		10 m/sec	0.38×10^2	-0.13×10^{-3}					
			0.12×10^2	0.52×10^{-4}					
E - 1^d6^h	0.008×10^{-8}	1000 km	-0.35×10^2	0.48×10^{-5}		-32.1	-81.4	0.1	0.2
		10 m/sec	0.63×10^2	-0.21×10^{-3}					
			-0.40×10^2	0.23×10^{-3}					
E - 1^d6^h	0.008×10^{-8}	100 km	0.58 x 10	-0.55×10^{-4}	$\Delta a_y = 0.13 \times 10^{-9}$	-25.4	-37.5	-9.8	0.2
		1 m/sec	0.14×10^2	-0.52×10^{-4}	$\Delta b_y = -0.57 \times 10^{-15}$				
		$\sigma(a_r) = 10^{-9}$	0.84×10^1	0.91×10^{-6}					
		$\sigma(b_r) = 10^{-14}$							
E - 1^d6^h	0.008×10^{-8}	100 km	0.65 x 10	-0.69×10^{-4}	$\Delta a_r = 0.61 \times 10^{-10}$	-24.3	-35.9	-9.4	0.2
		1 m/sec	0.13×10^2	-0.41×10^{-4}	$\Delta a_x = 0.49 \times 10^{-10}$				
		$\sigma(a_{r,x,y}) = 10^{-9}$	0.79 x 10	-0.10×10^{-4}	$\Delta a_y = 0.53 \times 10^{-10}$				
		$\sigma(b_{r,x,y}) = 10^{-4}$			$\Delta b_r = -0.35 \times 10^{-15}$				
					$\Delta b_x = -0.64 \times 10^{-16}$				
					$\Delta b_y = 0.18 \times 10^{-16}$				

*Modelled as a constant plus linear acceleration, i.e., $\ddot{r}_i = a_i + b_i t$ where i = r, x or y and t is time from 22^h00^m July 31.

Table 2-45. Pre-Encounter Solutions for $\Delta\ddot{r}_y = 0.26032 \times 10^{-8}\ e^{-t/18\ hr}\ km/sec^2$

(All data stops at E - 6h)									
Start of Data Arc	Acceleration at Start of Data Arc km/sec^2	A priori Standard Deviations	$\Delta x, y, z$ km	$\Delta\dot{x}, \dot{y}, \dot{z}$ km/sec	Δ(Attitude Control Parameters)*	B (DPODP) - B (traj) km	$\overline{B} \cdot \overline{R}$ (DPODP) - $-\overline{B} \cdot \overline{R}$ (traj) km	$\overline{B} \cdot \overline{T}$ (DPODP) - $-\overline{B} \cdot \overline{T}$ (traj) km	t_{ca} (DPODP) - t_{ca} (traj) sec
E - 3^d19^h	0.26×10^{-8}	10^4 km	0.98×10^3	-0.35×10^{-2}		16.7	-5796.0	373.8	38.3
		1 km/sec	0.43×10^4	-0.16×10^{-1}					
			-0.75×10^4	-0.35×10^{-1}					
E - 2^d19^h	0.065×10^{-8}	100 km	0.56×10^3	-0.25×10^{-2}	$\Delta a_x = 0.17 \times 10^{-8}$	369.0	26.7	395.9	-4.3
		10 m/sec	-0.21×10^3	0.57×10^{-3}	$\Delta b_x = -0.29 \times 10^{-14}$				
		$\sigma(a_r) = 10^{-6}$	-0.61×10^3	0.15×10^{-2}					
		$\sigma(b_r) = 10^{-12}$							
E - 1^d6^h	0.008×10^{-8}	100 km	-0.18×10^2	0.24×10^{-4}		-20.1	-4.1	20.4	0.3
		10 m/sec	0.28×10^2	-0.13×10^{-3}					
			0.52×10	0.65×10^{-4}					
E - 1^d6^h	0.008×10^{-8}	1000 km	-0.28×10^2	-0.25×10^{-5}		-10.1	-20.9	-1.1	-0.1
		10 m/sec	0.66×10^2	-0.25×10^{-3}					
			-0.77×10^2	0.32×10^{-3}					
E - 1^d6^h	0.008×10^{-8}	100 km	0.10×10	0.48×10^{-6}	$\Delta a_x = 0.21 \times 10^{-9}$	-8.8	34.6	-26.9	0.0
		1 m/sec	0.98×10	-0.45×10^{-4}	$\Delta b_x = -0.77 \times 10^{-5}$				
		$\sigma(a_r) = 10^{-9}$	0.47×10^2	-0.46×10^{-4}					
		$\sigma(b_r) = 10^{-14}$							
E - 1^d6^h	0.008×10^{-8}	100 km	0.34×10	-0.13×10^{-4}	$\Delta a_r = 0.79 \times 10^{-10}$	-7.8	39.3	-27.8	-0.1
		1 m/sec	0.79×10	-0.39×10^{-4}	$\Delta a_x = 0.38 \times 10^{-10}$				
		$\sigma(a_{r,x,y}) = 10^{-9}$	0.46×10	-0.40×10^{-4}	$\Delta a_y = 0.53 \times 10^{-10}$				
		$\sigma(b_{r,x,y}) = 10^{-14}$			$\Delta b_r = -0.27 \times 10^{-15}$				
					$\Delta b_x = -0.24 \times 10^{-15}$				
					$\Delta b_y = -0.24 \times 10^{-15}$				

*Modelled as a constant plus linear acceleration, i.e., $\ddot{r}_i = a_i + b_i t$ where $i = r$, x or y and t is time from 22^h00^m July 31.

Table 2-46. Pre-Encounter Solutions for $\Delta\ddot{r}_r = 0.26032 \times 10^{-8}$ km/sec^2

(All data between E - 3 days 19 hr and E - 6 hr)								
A priori Standard Deviations	$\Delta x, y, z$, km	$\Delta\dot{x}, \dot{y}, \dot{z}$, km/sec	Δ(Attitude Control Parameters)*	Standard Deviation for Solution Attitude Controls	B (DPODP) - B (traj), km	$\bar{B} \cdot \bar{R}$ (DPODP) - $\bar{B} \cdot \bar{R}$ (traj), km	$\bar{B} \cdot \bar{T}$ (DPODP) - $\bar{B} \cdot \bar{T}$ (traj), km	t_{ca} (DPODP) - t_{ca} (traj), sec
10^6 km	-0.19×10^4	0.12×10^{-1}			1165.3	1515.4	-2439.5	15.2
1 km/sec	0.58×10^3	-0.66×10^{-3}						
	0.28×10^4	-0.15×10^{-1}						
25 km	-0.20×10	0.46×10^{-4}	$a_r = 0.26 \times 10^{-8}$	0.27×10^{-10}	-7.7	14.5	-14.9	-0.8
1 m/sec	0.22×10	-0.98×10^{-3}						
$\sigma(a_r) = 10^{-7}$	-0.44×10	-0.29×10^{-4}						
100 km								
10 m/sec								
$\sigma(a_{r,x,y}) = 10^{-6}$								
100 km	0.52×10^2	-0.32×10^{-3}	$a_r = 0.66 \times 10^{-7}$	0.71×10^{-8}	-8.3	11.9	-14.5	-1.9
10 m/sec	-0.30×10^2	0.47×10^{-3}	$a_x = 0.13 \times 10^{-7}$	0.22×10^{-7}				
$\sigma(a_{r,x,y}) = 10^{-6}$	-0.22×10^2	-0.57×10^{-3}	$a_y = -0.81 \times 10^{-8}$	0.95×10^{-8}				
$\sigma(b_{r,x,y}) = 10^{-10}$			$b_r = 0.30 \times 10^{-13}$	0.55×10^{-13}				
			$b_x = -0.92 \times 10^{-13}$	0.16×10^{-12}				
			$b_y = 0.36 \times 10^{-13}$	0.56×10^{-13}				

*Modelled as a constant plus linear acceleration, i.e., $\ddot{r}_i = a_i + b_i t$ where i = r, x or y and t is time from 22^h00^m July 31.

Table 2-47. Pre-Encounter Solutions for $\Delta\ddot{r}_y = 0.26032 \times 10^{-8}$ km/sec^2

(All data between E - 3 days 19 hr and E - 6 hr)								
A priori Standard Deviations	$\Delta x, y, z$, km	$\Delta\dot{x}, \dot{y}, \dot{z}$, km/sec	Δ(Attitude Control Parameters)*	Standard Deviation for Solution Attitude Controls	B (DPODP) - B (traj), km	$\bar{B} \cdot \bar{R}$ (DPODP) - $\bar{B} \cdot \bar{R}$ (traj), km	$\bar{B} \cdot \bar{T}$ (DPODP) - $\bar{B} \cdot \bar{T}$ (traj), km	t_{ca} (DPODP) - t_{ca} (traj), sec
10^6 km								
1 km/sec								
25 km	0.14×10^2	0.70×10^{-4}	$\Delta a_y = 0.257 \times 10^{-8}$	0.10×10^{-10}	-24.3	-24.3	-15.1	0.0
1 m/sec	0.21×10^2	-0.90×10^{-4}						
$\sigma(a_y) = 10^{-7}$	0.11×10^2	0.10×10^{-3}						
100 km	0.42×10^2	0.84×10^{-4}	$\Delta a_r = -0.17 \times 10^{-9}$	0.86×10^{-9}	-40.5	-35.9	-27.4	0.2
10 m/sec	0.12×10^2	-0.19×10^{-4}	$\Delta a_x = 0.81 \times 10^{-9}$	0.44×10^{-8}				
$\sigma(a_{r,x,y}) = 10^{-6}$	0.18×10^2	-0.42×10^{-4}	$\Delta a_y = 0.21 \times 10^{-8}$	0.25×10^{-8}				
100 km	0.37×10^2	0.35×10^{-4}	$\Delta a_r = 0.14 \times 10^{-8}$	0.57×10^{-8}	+2.3	50.3	-22.0	0.4
10 m/sec	0.67 x 10	-0.13×10^{-3}	$\Delta a_x = -0.59 \times 10^{-8}$	0.20×10^{-7}				
$\sigma(a_{r,x,y}) = 10^{-2}$	0.47 x 10	0.23×10^{-3}	$\Delta a_y = 0.56 \times 10^{-8}$	0.94×10^{-8}				
$\sigma(b_{r,x,y}) = 10^{-10}$			$\Delta b_r = -0.18 \times 10^{-13}$	0.54×10^{-13}				
			$\Delta b_x = 0.58 \times 10^{-13}$	0.15×10^{-13}				
			$\Delta b_y = -0.22 \times 10^{-13}$	0.54×10^{-13}				

*Modelled as a constant plus linear acceleration, i.e., $\ddot{r}_i = a_i + b_i t$ where i = r, x or y and t is time from $22^h 00^m$ July 31.

orbits would incur larger errors than the use of the nominal orbit, determined before the acceleration was initiated.

The orbit solutions for the exponentially perturbed spacecraft are considerably improved if some non-gravitational force is included in the estimate list along with the state parameters. For example, the errors in the 2d 13h data arc solutions, although still several hundred km, are improved by approximately a factor of five over the state only solutions. Figure 2-82 shows how the orbit determination program tries to fit the exponential acceleration with a constant plus linear acceleration over the 2d 13h and 1 day data arcs when the direction of the acceleration is assumed to be known. As shown by the last entry in Tables 2-43, 2-44, and 2-45 including attitude control accelerations in directions other than the perturbing acceleration in the estimate list produces hardly any change in the solution. Comparing these results with the perturbed minus nominal trajectory runs of Table 2-42 show the solution errors in B-plane parameters are smaller than the actual changes produced by the acceleration if these changes are large. Thus, if the perturbing acceleration can be fairly well modeled by attitude control forces it appears that this orbit determination solution is preferable to the nominal trajectory.

- Solving for Known Accelerations

By examining the before the fit residuals produced by an unknown perturbative acceleration the gross temporal characteristics of this acceleration may be determined. Thus, if the orbit determination program contains solve-for accelerations of this character it may be possible to determine the magnitude and direction of the perturbing accelerations. Tables 2-46 and 2-47, contain orbit determination solutions in r, and y directions. These tables show that by applying relatively tight *a priori* and solving only for the state and the constant acceleration, a, the magnitude of the acceleration can be solved for very nicely. Unfortunately, the solution contains errors in the B-plane parameters of up to 30 km. Loosening the *a priori* and including constant accelerations in all three directions somewhat degrades the solution for the accelerations but does not effect the B-plane parameters substantially. If in addition to the constant accelerations, linear accelerations are included in the list of solve for parameter the solution for the direction and magnitude of the force is severely degraded, but once again the B-plane parameters are not substantially changed.

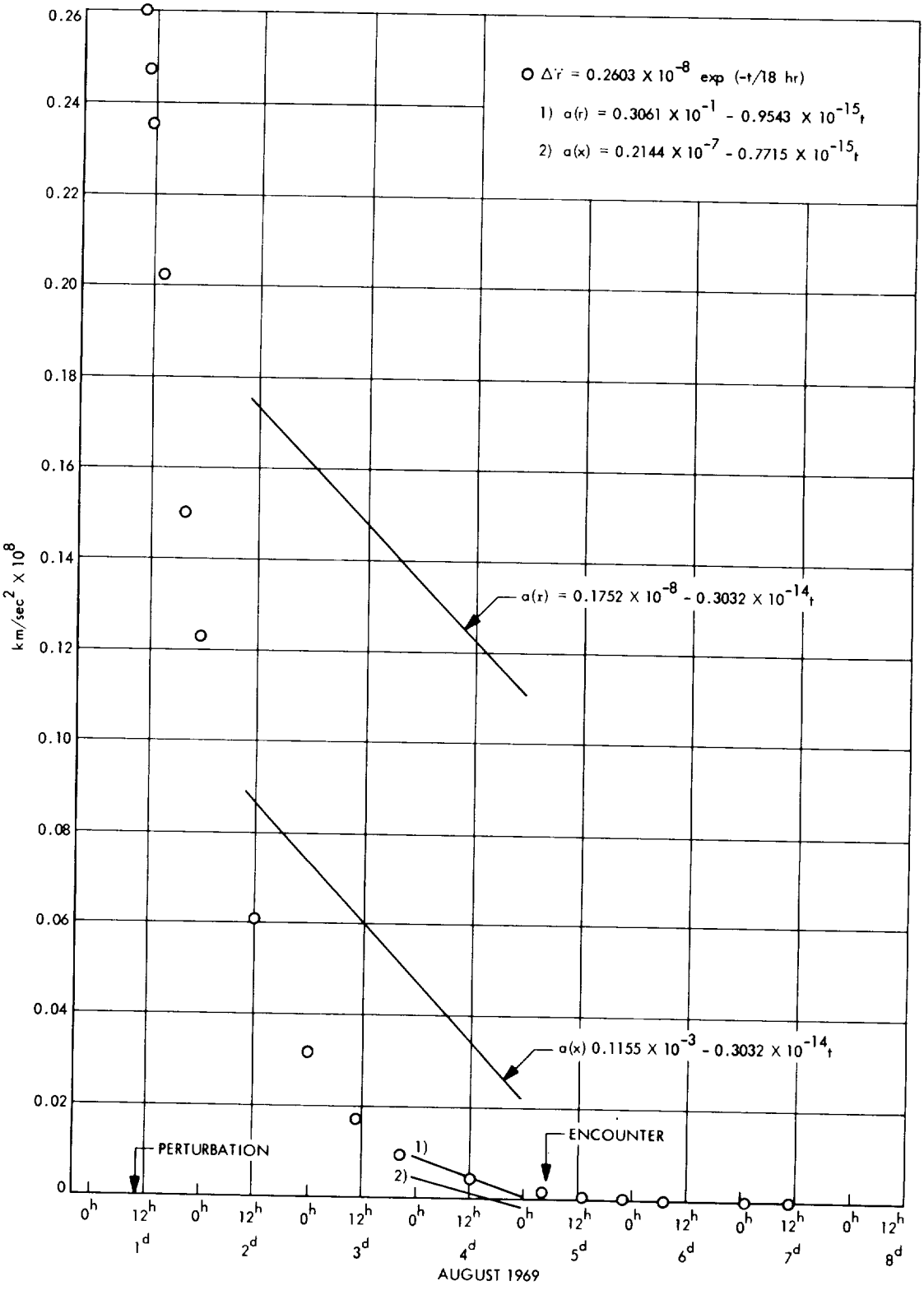

Figure 2-82. Const. + Linear Attitude Control Acceleration Fits to the Exponential Perturbation for Various Data Arcs

- Post Encounter Solutions

Once the spacecraft has passed the planet so that both post encounter and pre-encounter data are available the solution for the encounter parameters is greatly improved. Tables 2-48 and 2-49 show the results of using this post and pre-encounter data for orbits produced by exponential and constant accelerations respectively. These tables show that even deleting the data from E - 6h to E + 11h give B-plane errors which exceed 15 km only once for the exponential perturbations and 30 km only twice for the constant acceleration.

An order of magnitude prediction of the effect unmodeled accelerations have on the parameter B may be obtained in the following way. Consider the spacecraft to be in a hyperbolic orbit about the encounter planet as shown in Figure 2-83.

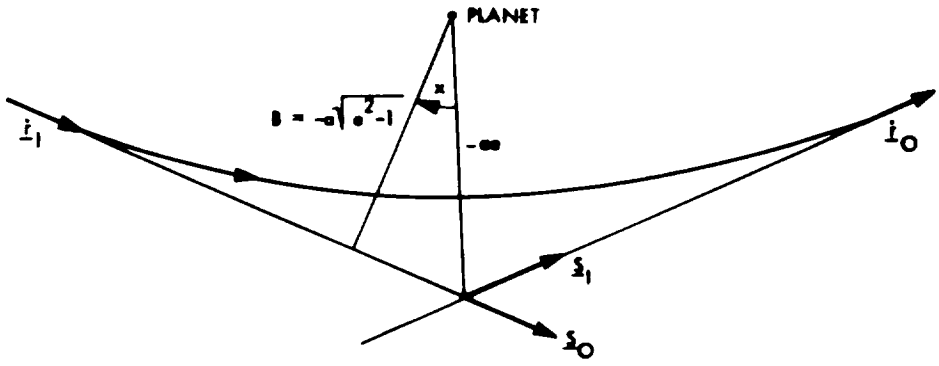

Figure 2-83. Planet Centered Hyperbolic Trajectory

The simplest situation to examine is when the perturbing acceleration is always directed toward the planet. For this case the angular momentum, per unit mass,

$$h = B\dot{s}$$

is conserved so that

$$\frac{\Delta B}{B} = -\frac{\Delta \dot{s}}{\dot{s}} \qquad (2a)$$

Table 2-48. Post-Encounter Solutions for Exponential Perturbations

Data Arc	Perturbation Direction	*A priori* Standard Deviation	$\Delta x, y, z$	$\Delta \dot{x}, \dot{y}, \dot{z}$	B (DPODP) - B (traj) km	$\bar{B} \cdot \bar{R}$ (DPODP) - $\bar{B} \cdot \bar{R}$ (traj) km	$\bar{B} \cdot \bar{T}$ (DPODP) - $\bar{B} \cdot \bar{T}$ (traj) km	t_{ca} (DPODP) - t_{ca} (traj) sec
Enc - $4^d 7^h$ E + $5^d 11^h$ No 14 or 42 on enc	r	10^4 km	-0.14×10^3	0.43×10^{-3}	-10.5	-0.1	+11.5	-1.1
		1 km/sec	-0.49×10^3	0.12×10^{-2}				
			0.11×10^4	-0.31×10^{-2}				
Enc - $4^d 7^h$ to E + $5^d 11^h$ No 14 or 42 on enc	x	10^4 km	-0.22×10^3	0.53×10^{-3}	4.3	10.5	-0.4	7.7
		1 km/sec	0.11×10^4	-0.30×10^{-2}				
			-0.19×10^4	0.52×10^{-2}				
Enc - $4^d 7^h$ to Enc + $5^d 11^h$ No 14 or 42 on enc no	y	10^4 km	-0.66×10^3	0.18×10^{-2}	-1.2	+25.2	-14.0	6.4
		1 km/sec	0.16×10^3	0.13×10^{-3}				
			0.88×10^3	-0.23×10^{-2}				

Table 2-49. Post-Encounter Solutions for Constant Perturbations

Data Arc	Perturbation Direction	*A priori* Standard Deviation	$\Delta x, y, z$	$\Delta \dot{x}, \dot{y}, \dot{z}$	B (DPODP) - B (traj) km	$\overline{B} \cdot \overline{R}$ (DPODP) - $-\overline{B} \cdot \overline{R}$ (traj) km	$\overline{B} \cdot \overline{T}$ (DPODP) - $-\overline{B} \cdot \overline{T}$ (traj) km	t_{ca} (DPODP) - t_{ca} (traj) sec
End - $4^d 7^h$ to $E + 5^d 11^h$ No 14 or 42 on enc	r	10^4 km	-0.48×10^4	0.13×10^{-1}	2.3			-68.7
		1 km/sec	-0.22×10^4	0.42×10^{-2}				
			0.80×10^4	-0.22×10^{-1}				
Enc - $4^d 7^h$ to $E + 5^d 11^h$ No 14 or 42 on enc	y	10^4 km	-0.46×10^4	0.12×10^{-1}	-19.3	67.8	-56.1	-85.0
		1 km/sec	-0.49×10^4	0.15×10^{-1}				
			0.15×10^5	-0.42×10^{-1}				

Tables 2-46 and 2-47 have shown that a state only solution for the orbit perturbed by a constant acceleration using pre-encounter data alone may give errors in the velocity up to 10^{-2} km/sec. Using this value for $\Delta\dot{s}$ in Eq. (2a) predicts an error of 10 km in B. This agrees quite well with the results in Table 2-49 which contains errors in B from 10 to 30 km.

If the perturbation is not in the spacecraft planet direction the situation is not so simple, but still tractable using some very reasonable assumptions. Once more consider the spacecraft to be in a hyperbolic orbit about the planet as shown in Figure 2-83.

From the figure

$$\cos x = \frac{\sqrt{e^2 - 1}}{e}$$

upon expanding and neglecting terms of the order $1/e^2$ and higher

$$x = \frac{1}{e} \tag{3}$$

The incoming and outgoing asymptote unit vectors, $\underline{S}_I$ and $\underline{S}_o$, are given by

$$\underline{S}_I = \frac{\dot{\underline{r}}_I}{\dot{s}}$$

and

$$\underline{S}_o = \frac{\dot{\underline{r}}_o}{\dot{s}}$$

and the dot product between them may be written as

$$\underline{S}_I \cdot \underline{S}_o = \cos^2 x = 1 - \frac{2}{e^2}$$

Thus an error in the eccentricity is related to errors in velocity quantities by the following equation

$$\Delta e = -\frac{e^2}{4}\left[\underline{S}_o \cdot \frac{\Delta \dot{\underline{r}}_I}{\dot{s}} - 2\underline{S}_I \cdot \underline{S}_o \frac{\Delta \dot{s}}{\dot{s}} + \underline{S}_I \cdot \frac{\Delta \dot{\underline{r}}_o}{\dot{s}}\right] \tag{4}$$

since

$$\Delta \underline{S} = \frac{\Delta \dot{\underline{r}}}{\dot{s}} - \underline{S}\frac{\Delta \dot{s}}{\dot{s}} \tag{5}$$

For a two-body orbit the incoming and outgoing speeds must be the same so that $\Delta \dot{s}$, $\Delta \dot{\underline{r}}_s$, and $\Delta \dot{\underline{r}}_o$ must satisfy the following equation.

$$\Delta \dot{s} = \underline{S}_I \cdot \Delta \dot{\underline{r}}_I = \underline{S}_o \cdot \Delta \dot{\underline{r}}_o$$

Thus writing Eq. (4) as

$$\Delta e = -\frac{e^2}{4}\left[(\underline{S}_o - \underline{S}_I + \underline{S}_I) \cdot \Delta \dot{\underline{r}}_I + (\underline{S}_I - \underline{S}_o + \underline{S}_o) \cdot \Delta \dot{\underline{r}}_o - 2\underline{S}_I \cdot \underline{S}_o \Delta \dot{s}\right]$$

and substituting in Eq. (5) gives

$$\Delta e = -\frac{e^3}{4}\left[(\underline{S}_o - \underline{S}_I) \cdot (\Delta \dot{\underline{r}}_I - \Delta \dot{\underline{r}}_o) + 2(1 - \underline{S}_I \cdot \underline{S}_o)\Delta \dot{s}\right] \tag{6}$$

From Eq. (3) it may be seen that

$$(1 - \underline{S}_I \cdot \underline{S}_o) = \frac{2}{e^2}$$

and

$$|(\underline{S}_o - \underline{S}_I)| = \frac{2}{e}$$

Therefore since for any reasonable perturbative accelerations

$$|\Delta\dot{\underline{r}}_I - \Delta\dot{\underline{r}}_o| \propto \frac{1}{e}\Delta\dot{s}$$

and for convenience it will be assumed the constant of proportionality equals 2.

$$\Delta e \sim -2e\frac{\Delta\dot{s}}{\dot{s}} \tag{7}$$

The eccentricity may also be written in terms of the energy and the impact parameter according to the well known equation given below

$$e = \sqrt{1 + (k\dot{s}^2 B)^2}$$

where k is a constant. Differentiating and then expanding this equation in powers of 1/e gives to the first order

$$\Delta e = 2e\frac{\Delta\dot{s}}{\dot{s}} + e\frac{\Delta b}{b}$$

Combining this equation with Eq. (7) gives

$$\frac{\Delta b}{b} \sim -4\frac{\Delta\dot{s}}{\dot{s}}$$

Once more using the value $\Delta\dot{s} = 10^{-2}$ km/sec obtained from Tables 2-46 and 2-47, the above equation predicts $\Delta b = 40$ km. This is in good agreement with the orbit determination program results in Table 2-49 of errors in B which range from 10 to 30 km.

- Summary and Conclusions

An examination of the various orbit determination solutions using the simulated data suggests the following conclusions:

1) All data perturbed by an acceleration which cannot be modeled should be deleted.

2) Even if the accelerations can be modeled closely, the solutions will contain very little information about the direction of the perturbations.

3) The combination of pre- and post-encounter data should allow the B-plane parameters to be determined to within 10 or 15 km for these types of perturbations.

7. Accuracy Evaluation

a. Ionosphere — *B. D. Mulhall*

As described in Subsection II. A. 2. d., ionospheric measurements were obtained from the Faraday rotation polarimeters at the Venus site and at the University of New England, Armidale, Australia and from ionosonde vertical sounding stations at Tortosa, Spain, Mount Stromlo, Australia, Woomera, Australia and Johannesburg, South Africa. These measurements were converted to total electron content, mapped to the Mariner ray path, and range and doppler corrections were computed and applied to Mariner VI and VII radio tracking data and resulted in the recommended changes shown in Table 2-50.

Table 2-50. Recommended Changes Due to Ionospheric Effect, Mariner Mars 1969 Mission

	$\Delta\overline{B} \cdot \overline{R}$, km	$\Delta\overline{B} \cdot \overline{T}$, km
Mariner VI	-53	48
Mariner VII	-40	20

$\overline{B} \cdot \overline{T}$ is the component of the B vector (a vector from the center of the planet to the aiming point) in the ecliptic plane and $\overline{B} \cdot \overline{R}$ is the component perpendicular to $\overline{B} \cdot \overline{T}$.

The recommended changes listed in Table 2-50 were determined by differencing the results of Double Precision Orbit Determination Program (DPODP) solutions using inflight data which had not been calibrated for the ionosphere with station locations based on post-flight solutions using uncalibrated data versus DPODP runs using ionospherically calibrated data and station locations based on post-flight calibrated data. These differences are not necessarily the actual ionospheric effect on the orbit determination since the error introduced by the ionosphere into the inflight data would be masked in part by the uncalibrated station location.

For example, Figure 2-9 of Section II. A. 2. d. shows that for Mariner V, the ionosphere caused an error which consistently increased the

apparent station spin radius, r_s. It is very likely that the ionosphere had a similar effect for Mariner 1969. Consequently, station locations based on uncalibrated Mariner V data would compensate in part for the ionospheric error in Mariner 1969 data.

The ionospheric effect was considerably lower than was anticipated. Although 1969 had been a year of high ionospheric concentration due to solar flare activity, during the period when the calibration was performed, July 1 to August 5, 1969, the ionosphere was relatively inactive. This low activity was particularly noticeable in the southern hemisphere where the total columnar electron ionospheric content was typically less than half of the content in the northern hemisphere. Due to the southerly declination of the Mariner spacecraft most of the radio tracking data were obtained from southern latitude stations. Consequently, the smaller effect of the southern ionosphere outweighed the effect in the northern ionosphere and reduced the magnitude of the calibration for the entire net.

A great part of the resources of the ionospheric calibration team were spent in devising schemes to automatically collect, process, and produce calibration data for the Mariner 1969 encounter. Hand processing of data consumed another large portion of the team's resources where automated approaches could not be used or there was not sufficient time to develop automated techniques. The problem arises from using the data of various agencies, institutions, and observations from all corners of the world. Though these organizations proved extremely cooperative and helpful, the requested data could not be transmitted in the standard format.

To make calibration procedures operational on a routine, as opposed to a research, basis the following steps should be taken.

1) Models to predict the effect that requires calibration should be developed and perfected to eliminate the need for making measurements especially for inflight calibration.

2) Instrumentation to measure the effects requiring calibration should be installed at each DSS and connected into the tracking data acquisition system so that collection and processing of calibration is as nearly automated as possible.

3) Measurement techniques which hold the most promise of inherent accuracy should be exploited as opposed to techniques which have inherent limitation in accuracy which will make them obsolete for future missions. For example, techniques which provide measurements along the entire probe-DSS ray path should be developed over techniques which do not.

b. Timing and Polar Motion — *C. C. Chao, P. M. Muller*

It was found, as expected, that the JPL adopted A.1-UT1 data are perturbed each time newly received data is input into the TPOLY program (Ref. 14, Subsection II.A.2.c.). This is due to the fact that the least squares fitting curve will alter its path in order to fit the new data points. An analysis was made on such perturbations from launch to encounter of Mariner VI and VII (Ref. 26). The greatest magnitude of the perturbation reached 14 milliseconds which is twice as great as the uncertainty allowed by mission requirements, and the perturbation penetrated backward (at a lesser amplitude) two to three weeks from the last data point.

Figure 2-84 looks back over the time period during the Mariner 1969 mission and charts what is now thought to be the error in A.1-UT1 calibrations at the time the calibrations were first made. That is, on a particular day, say June 13, a TPOLY run was made including observations up to that day, in this case June 13. Based on current knowledge, the ordinate plots the "errors" (4 ms) in the estimated June 13 A.1-UT1 on June 13. It is seen that this error can be quite large — the worst case was on July 17 and was 14 ms. This error is equivalent to nearly a 6 m station longitude error and should be compared to the goal of determining the station locations to an accuracy of 3 m.

By itself, however, Figure 2-84 presents a pessimistic picture in the sense that in any given TPOLY determination of A.1-UT1, the error will (in general) be highest on the last day (assuming of course a prediction of UT1 is not required). This error will decay rapidly for days before the final day since they will have the benefit of USNO data on each side of the date in question. Moreover, any orbit estimate will normally be formed using data at least two weeks in arrears of the last data point received and will be influenced by errors in UT1 equally for each day's worth of data. To emphasize this point, Figure 2-85 plots the estimated error in the worst case July 17 polynomial for the two weeks leading up to the 17th. Had a highly important OD run been made on the 17th using only two week's data, the effective station longitude error could well be approximated by the average of the errors shown, or 5.7 ms (2.3 m).

This represents the worst case, which did not occur during a critical portion of either mission. The actual errors for the encounter for both

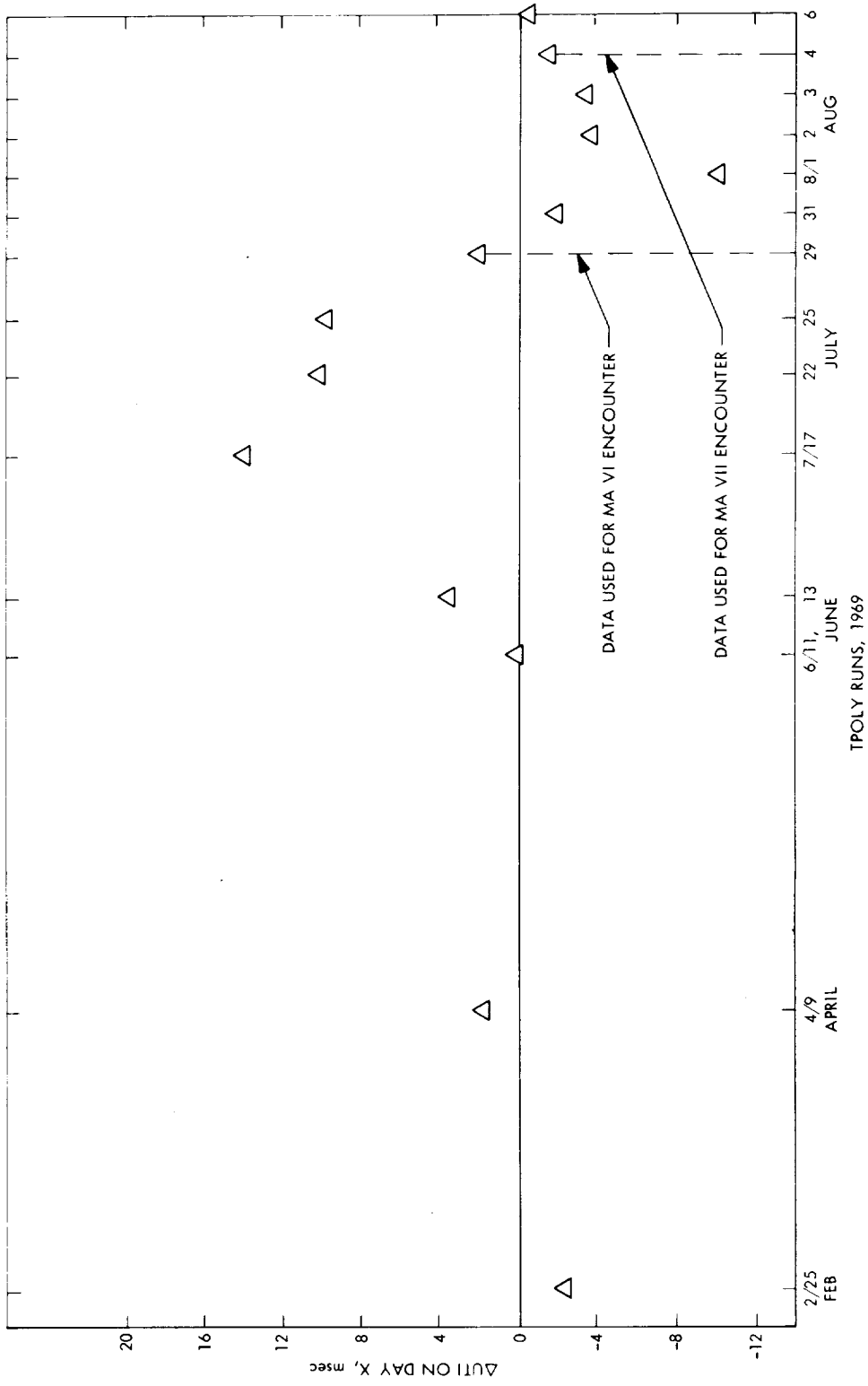

Figure 2-84. Variation of A.1-UT1 Perturbations on Day X With Respect to the TPOLY Results on September 4, 1969

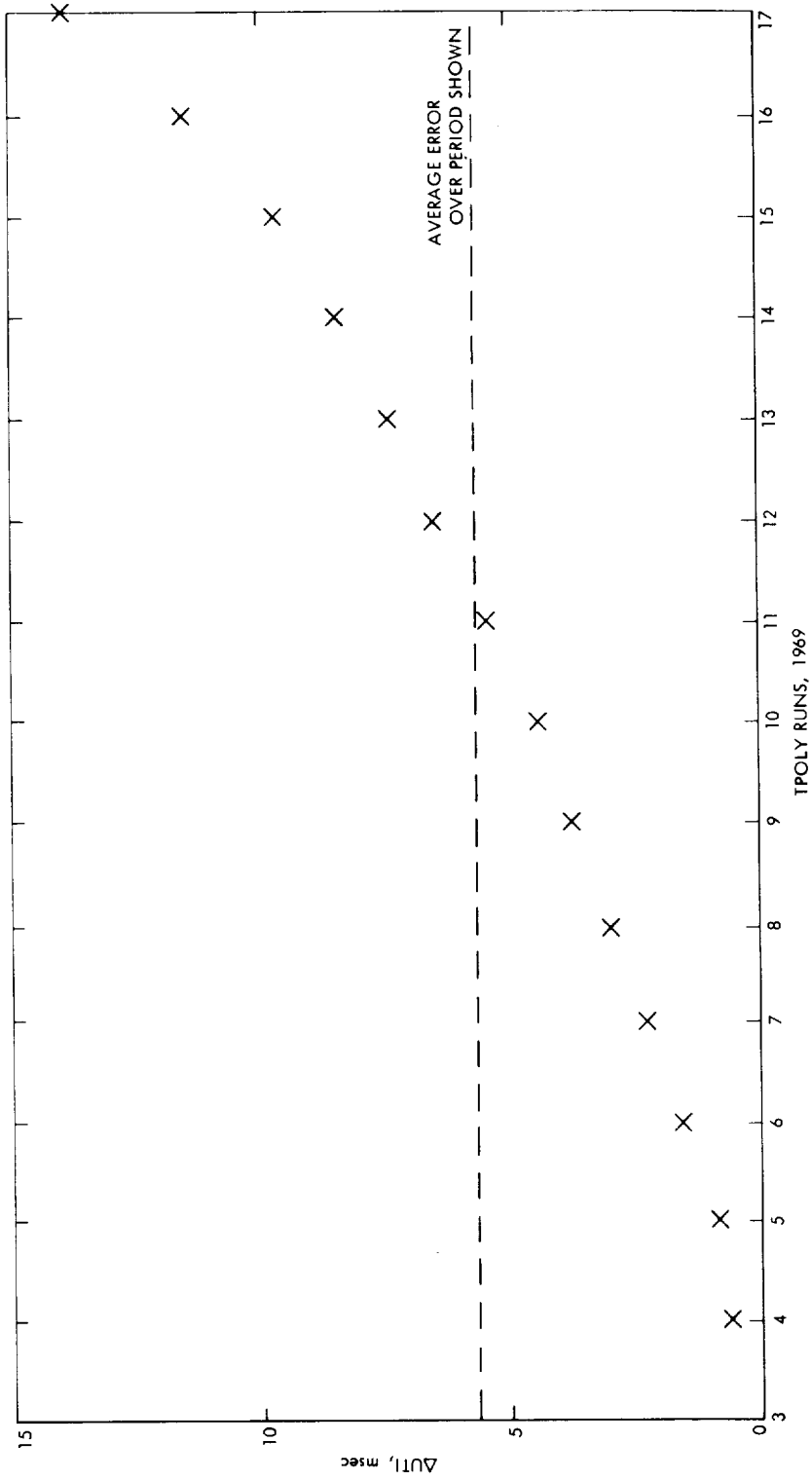

Figure 2-85. UT1 Errors from the TPOLY Run Made on July 17, 1969

spacecraft are noted on Figure 2-84, and then plotted for a week leading backwards from encounter on Figure 2-86. These show more typical behavior and yield average errors of 1 to 2 ms (0.5 to 1 m in equivalent station location error).

A similar plot was made for the deviation in polar motion data in Figure 2-87. For Mariner VI encounter, the 25 day predicted value of polar motion gave a 0.011 arc sec (1/3 m) difference in x and a 0.028 arc sec (0.9 m) difference in y. For Mariner VII encounter, the difference in x and y increased to 0.022 arc sec (3/4 m) and 0.032 arc sec (1.03 m) respectively due to the longer prediction arc.

The error of the one month prediction of the polar motion exceeded our expected value (1/2 m) because the linear rate at which the pole was moving during the crucial period was higher than normal.

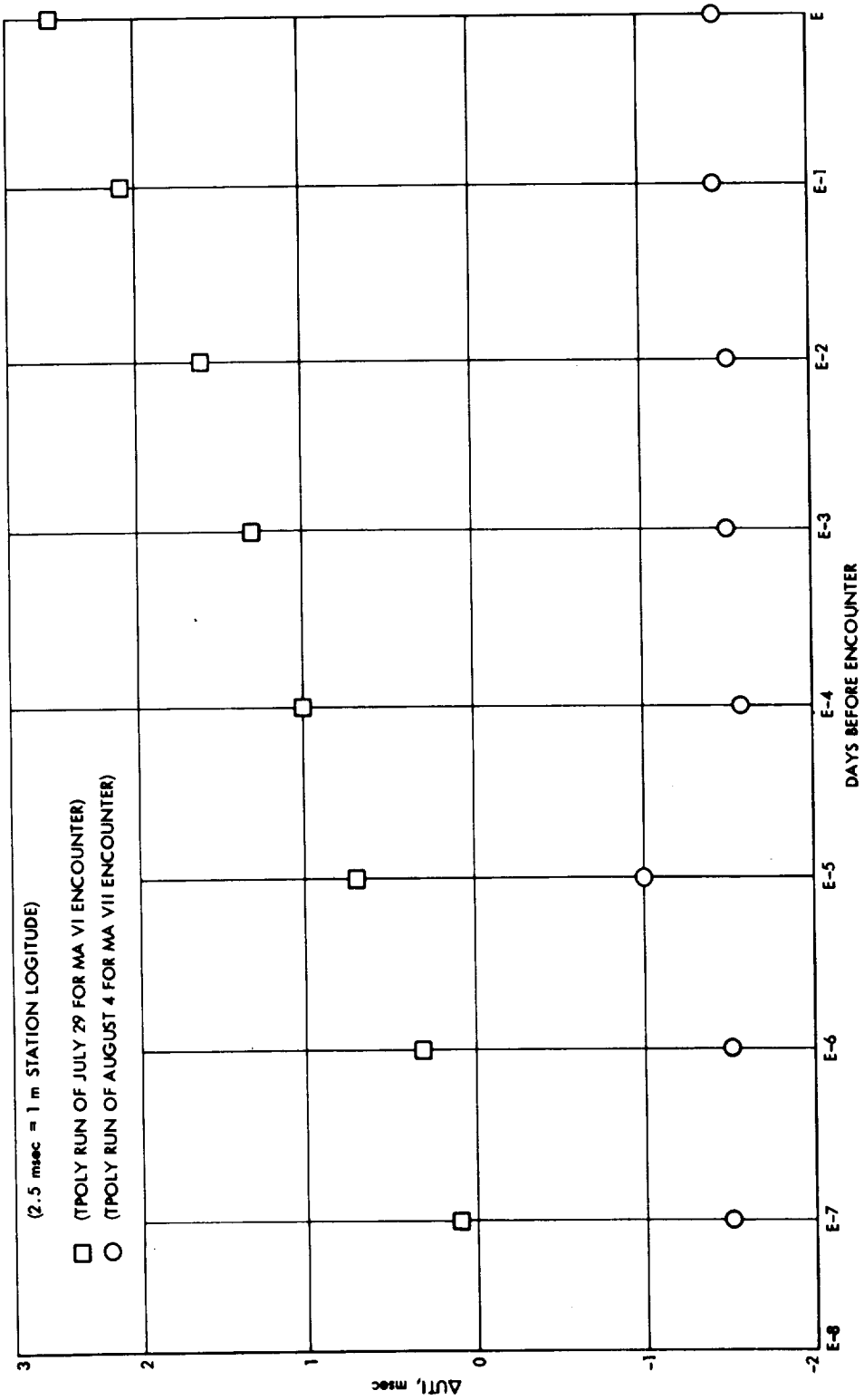

Figure 2-86. Deviations of A.1-UT1 from the Correct Reference (TPOLY Result of Feb 9, 1970) at the MM'69 Encounters

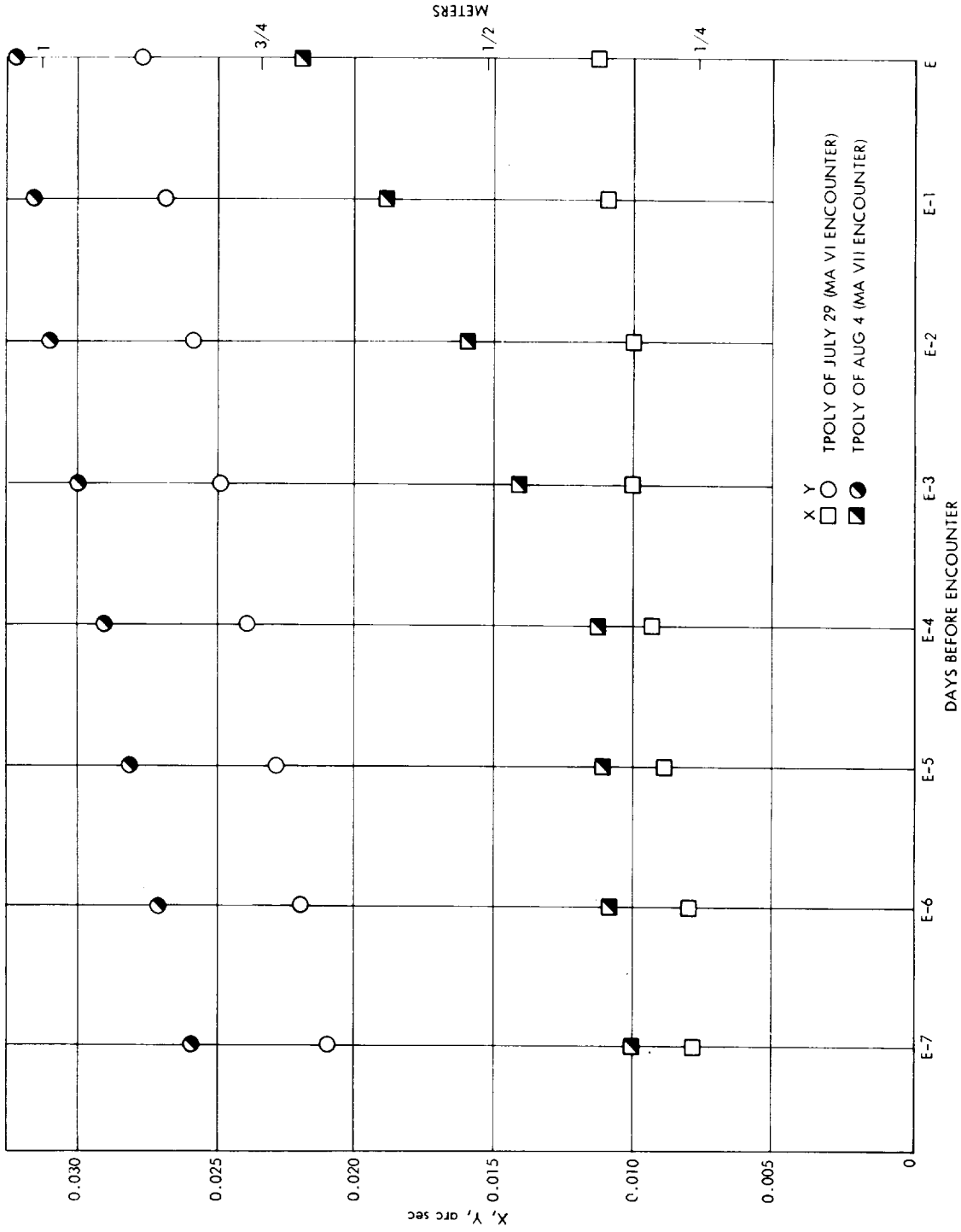

Figure 2-87. Deviations of Predicted Polar Motion (x and y) Data at MM'69 Encounters

SECTION III
MARINER VI AND VII TRAJECTORIES

J. K. Campbell

A. MARINER VI

1. Launch to Maneuver

Mariner VI was launched by Atlas/Centaur 20 on a direct ascent trajectory from Air Force Eastern Test Range (AFETR), complex 36B, on February 25, 1969, $01^h29^m02^s.013$ GMT. The launch window had opened 35 min earlier, at 00 hr 54 min. Figure 3-1 illustrates the Atlas/Centaur sequence of events. A programmed 13 sec roll brought the vehicle to an inertial azimuth 108 deg east of north. The pitch program was then initiated and completed at booster engine cutoff (BECO) which occurred at $01^h31^m33^s.2$. The Atlas booster was jettisoned 3 sec later at $01^h31^m36^s.2$.

At BECO +8 sec the initial yaw maneuver took place. The yaw maneuver actually consisted of two separate maneuvers. The first yaw was performed during the Atlas sustainer phase and had a "yaw index" of 9.25. The term "yaw index" is used to describe the magnitude of the yaw maneuver, and is a function of the trajectory inclination at Centaur main engine cutoff. If the desired inclination requires a planar azimuth heading greater than 115 deg, an initial yaw is made to a 115 deg parallel azimuth heading and then a final yaw maneuver is initiated shortly after Centaur main engine start (MES), to align the vehicle with the desired final heading. Yaw index equals the yaw rates multiplied by the yaw times, and is thus approximately equal to the total yaw angle turned during powered flight (see Figures 3-2 and 3-3). The final yaw maneuver had a yaw index of 9.

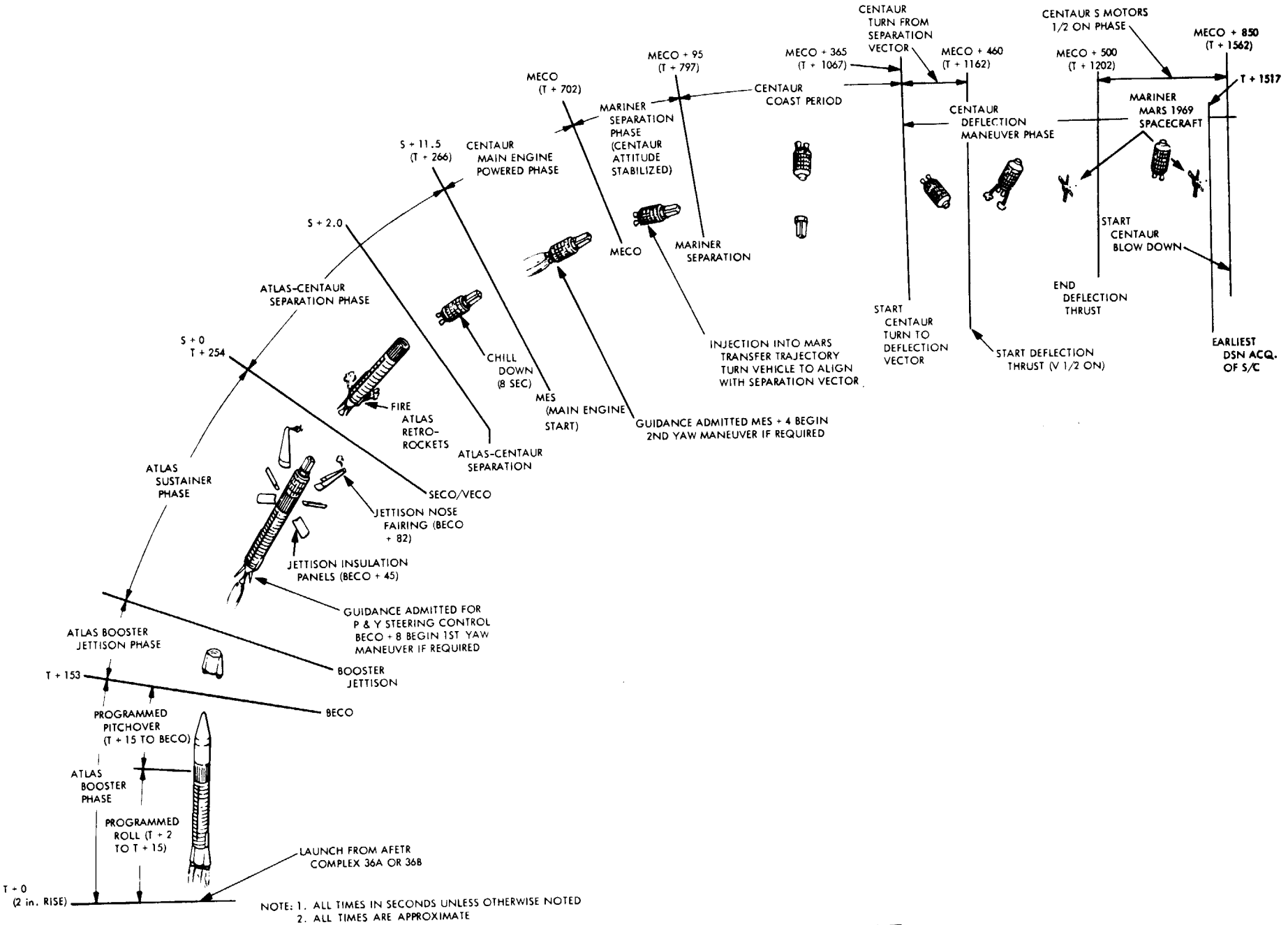

Figure 3-1. Typical Atlas/Centaur Sequence of Events

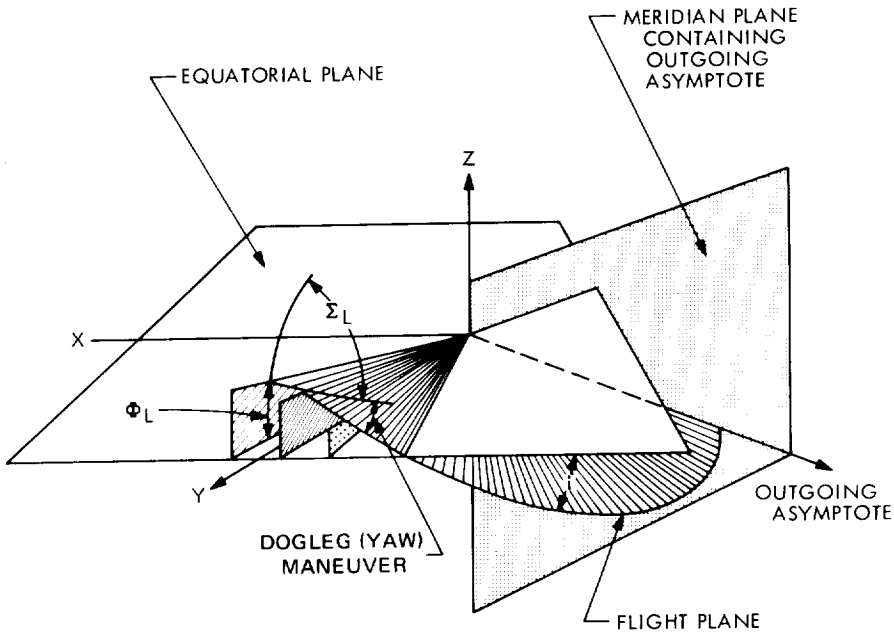

Figure 3-2. Dog-leg Maneuver to Increase Inclination

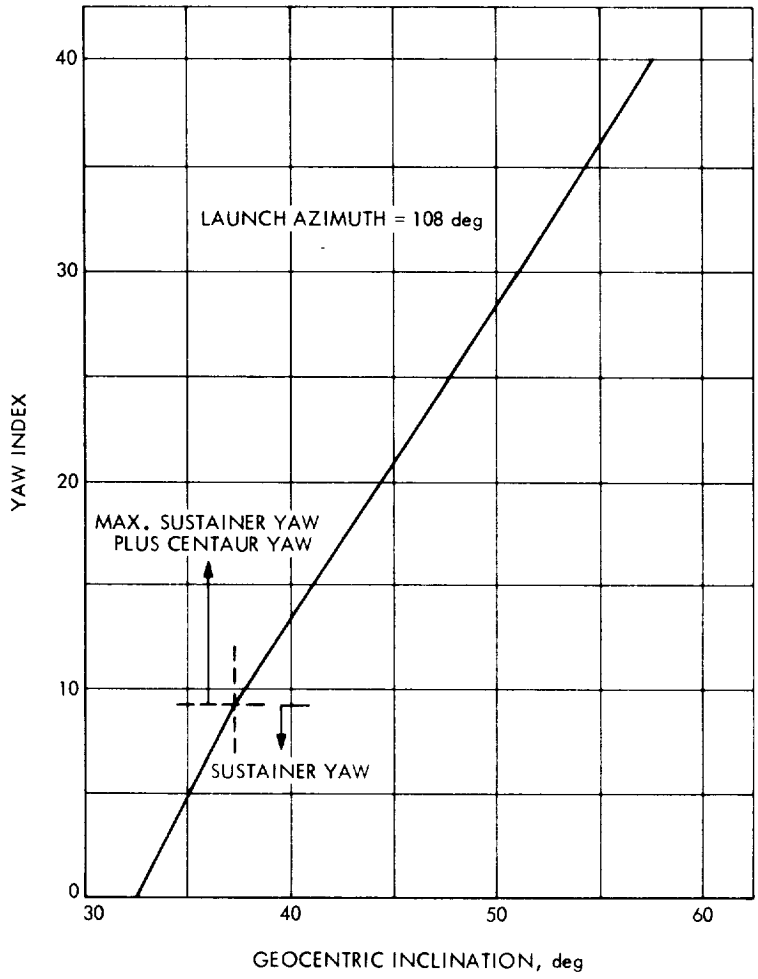

Figure 3-3. Yaw Index vs Geocentric Inclination

After rising above a significant portion of the atmosphere, the Centaur insulation panels and nose fairing, which protect the spacecraft during ascent, were jettisoned at $01^h32^m18^s.4$ and $01^h32^m54^s.6$ respectively. During the Atlas sustainer phase, the sustainer and vernier engines adjusted vehicle velocity and attitude until sustainer engine cutoff/vernier engine cutoff (SECO/VECO), which occurred at $01^h33^m37^s.3$. The sustainer stage was separated from the Centaur at $01^h33^m40^s.0$, and after an 8.9 sec coast, the main engine of the Centaur was ignited at $01^h33^m48^s.9$. The main engine cutoff (MECO) at $01^h41^m11^s.6$, when C_3 was computed to be 11.1906 km^2/sec^2. Immediately after Centaur MECO, the Centaur guidance system initiated a turning maneuver to bring the vehicle into alignment with the separation direction, which was primarily determined by telecommunication and planetary quarantine requirements. The pre-separation turning maneuver continued until approximately MECO +95 sec, and was completed at $01^h42^m47^s.3$. At the completion of this maneuver separation occurred, and the spacecraft was placed onto its Mars transfer trajectory by a spring deflection from the Centaur.

The Mars transfer trajectory was a Type I transfer, that is, the total heliocentric central transfer angle from earth at launch to Mars at encounter was less than 180 deg. Table 3-1 gives the elements and injection conditions of the transfer orbit, at separation. At the completion of separation the spacecraft initiated several events. First, the tip-off rates resulting from separation were nulled out. Next, the solar panels were deployed at $01^h46^m45^s$. The spacecraft left earth's shadow at $01^h55^m12^s$ and sun acquisition was initiated. After completing sun acquisition at $01^h58^m35^s$, the spacecraft then initiated Canopus acquisition at $05^h25^m01^s$, which was completed by $05^h42^m20^s$. The spacecraft was now attitude stabilized.

While the spacecraft was performing the above events, the Centaur was prepared for its deflection maneuver. Following a 270 sec coast after separation, the Centaur began to pitch to a new direction, nearly perpendicular to the spacecraft separation direction, at $01^h47^m17^s$. Two of the Centaur vernier engines were then ignited ($01^h48^m52^s$) and the Centaur began to thrust itself away from the spacecraft and thus away from the Mars transfer trajectory. Approximately 40 sec later the vernier engines were cut off and two settling

Table 3-1. Geocentric Orbital Elements at Injection

Element	Mariner VI	Mariner VII
Periapsis, km	6863.	6884.
Semi-major axis, km	-35820.	-23639.
Longitude of ascending node, deg*	318.27	325.85
Argument of periapsis deg*	135.99	119.32
Eccentricity	1.18	1.27
Inclination, deg*	43.33	31.01
Time of periapsis, GMT	2/25/69 $01^h40^m40^s.6$	3/27/69 $22^h30^m10^s.0$

*With respect to Earth Equatorial plane and vernal equinox.

motors thrusted for 350 sec. Following this thrust period, the Centaur began its propellant blowdown at $01^h55^m24^s$ to achieve the final deflection of the Centaur from the spacecraft. The blowdown lasted until all propellants, liquids and gases, were expelled. Figure 3-4 shows the ground track of Mariner VI for about 8 hr after launch.

- Mariner VI Injection Aiming Point

In order to satisfy various planetary quarantine constraints, it was necessary to aim the spacecraft at injection (post-separation) to a point farther from the planet than the actual desired aiming point. The particular biasing direction chosen was dictated primarily by the desire to keep the midcourse velocity increment small, as well as to minimize the trajectory dispersions which would result from a larger-than-expected error in velocity increment. This bias was then removed by the midcourse maneuver. The injection aiming point, as defined in Figures 3-5 and 3-6, achieved by Mariner VI was $\overline{B} \cdot \overline{T}$ = 3,620 km, $\overline{B} \cdot \overline{R}$ = 12,909 km. Closest approach would have occurred at

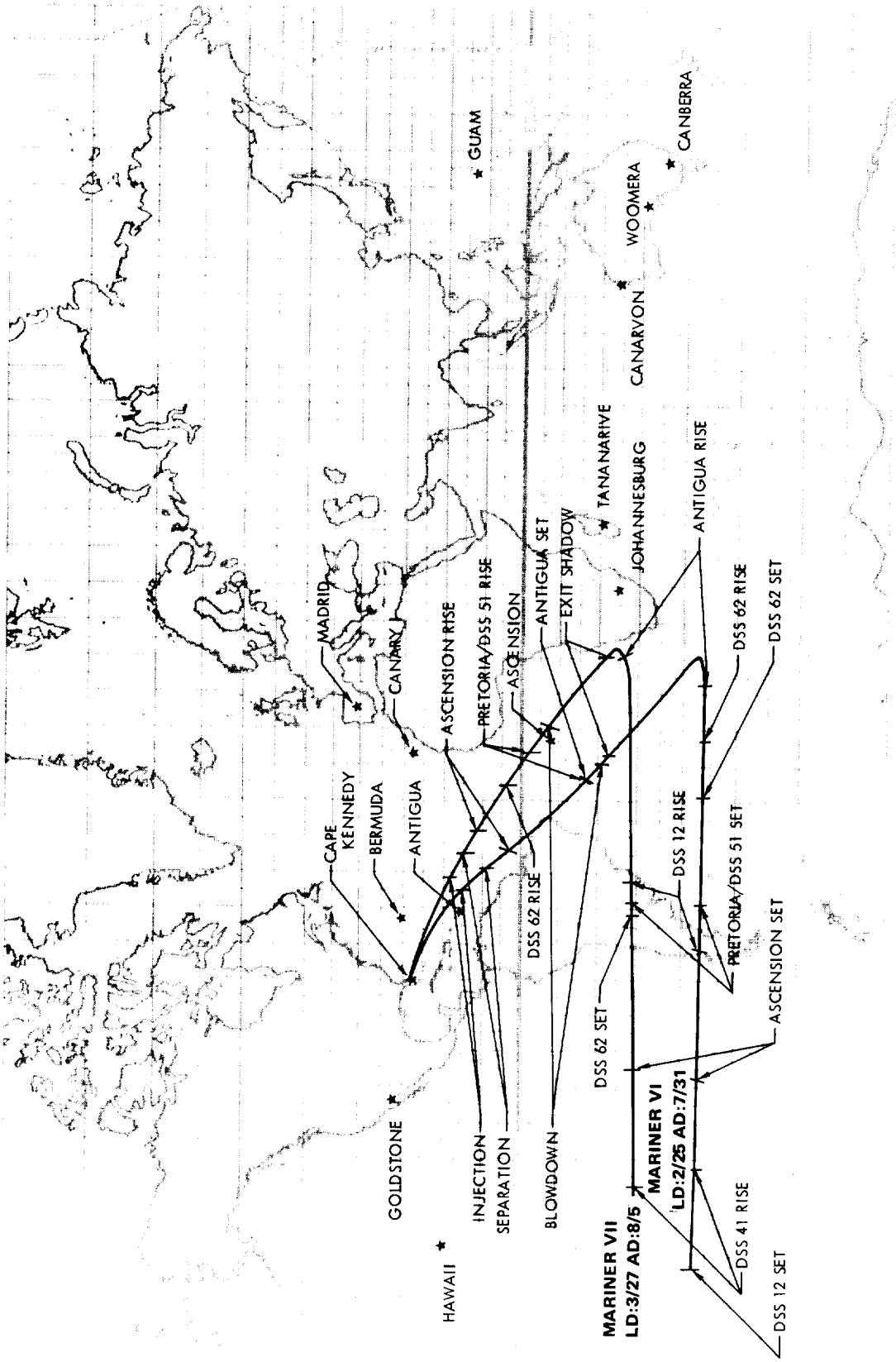

Figure 3-4. Ground Tracks of Mariner VI, VII

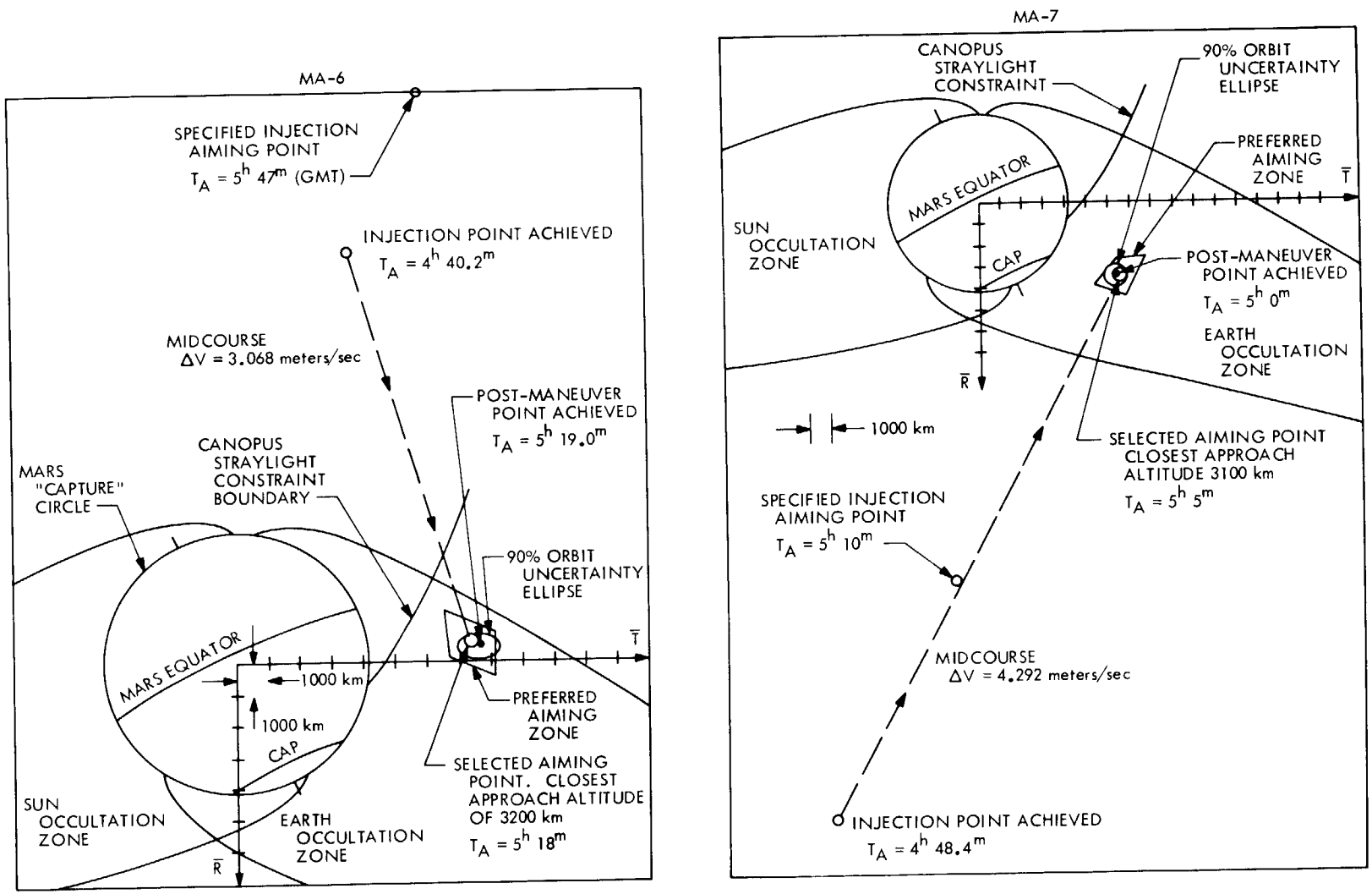

Figure 3-5. Mariner VI, VII Injection and Midcourse Aiming Points Shown in Aiming-Plane View

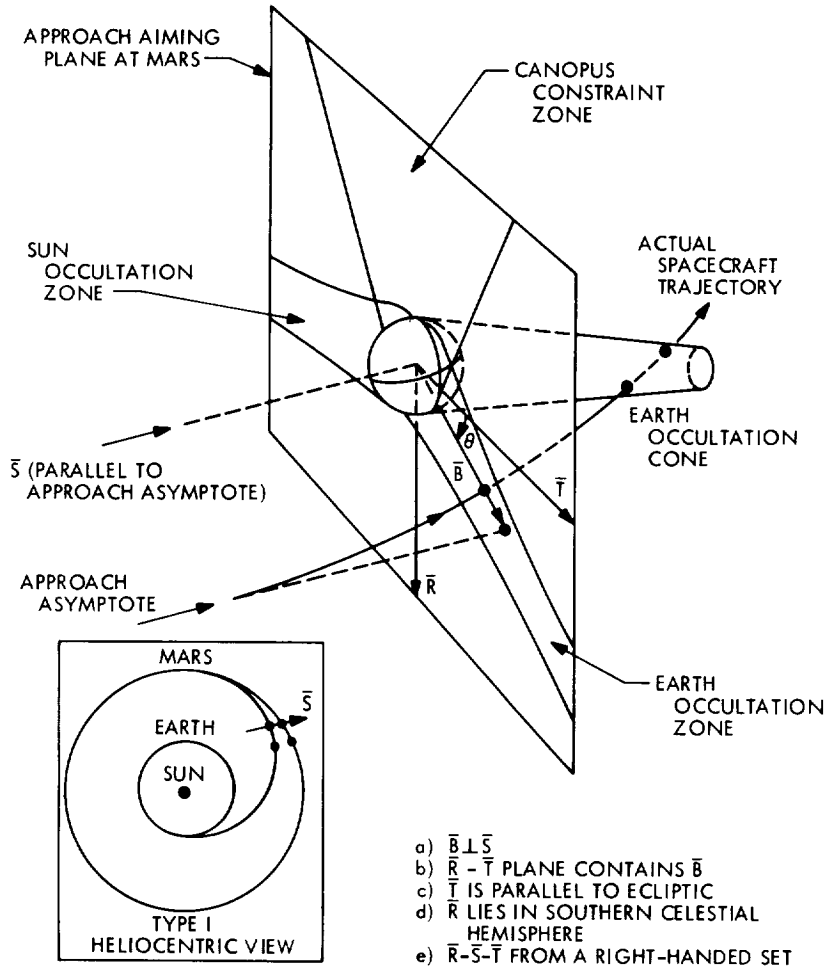

Figure 3-6. Diagram of Aiming Plane

$04^h40^m14^s$ GMT on 31 July 1969. Thus the Atlas/Centaur, the most accurate launch vehicle combination used to date, would have delivered Mariner VI to an aiming point only about 5600 km 'southwest' of the specified aiming point, as illustrated in Figure 3-5. The preferred aiming zone shown was selected by the scientific experimenters for a high-value science return. Because of the aim point biasing needed to satisfy quarantine constraints, and the Centaur injection errors (which were well within tolerance), a midcourse correction was required to adjust the velocity vector, to deliver the spacecraft to the preferred aiming point. Although each spacecraft could perform two maneuvers, only one maneuver was needed to meet the accuracy requirements. The midcourse motor was ignited at $00^h54^m44^s$ GMT on 1 March 1969 and the resulting change in the spacecraft trajectory is illustrated by a comparison of the aiming plane coordinates: $\overline{B} \cdot \overline{T}$ was now 7786 km, $\overline{B} \cdot \overline{R}$ was -410 km, and closest approach time was $05^h18^m44^s$ GMT on July 31, 1969. Table 3-2 contains the post-midcourse heliocentric orbital elements.

2. Cruise

After leaving the vicinity of the earth, the spacecraft proceeded on an approximately elliptical trajectory about the sun until it reached the vicinity of Mars. Figure 3-7 illustrates the heliocentric view of the Mariner VI trajectory. Figures 3-8 through 3-17 show various geometric trajectory parameters for Mariner VI, such as celestial latitude, longitude, earth-spacecraft range, heliocentric distance, and cone and clock angles of earth. The figures illustrate the geometric behavior of both spacecraft projected out to 1975.

Several days after the midcourse maneuver, the scan platform, on which the science instruments were mounted, was unlatched from its stowed position. The unlatching involved the releasing of compressed nitrogen and the resulting velocity vector change slightly altered the spacecraft trajectory. Table 3-3 shows the heliocentric orbital elements of the post-unlatch trajectory.

A small anomaly occurred during the heliocentric cruise, on about April 20, 1969. The cone angle of Canopus changes during cruise (see Figure 3-15), such that Canopus slips out of the field of view of the Canopus tracker

Table 3-2. Post-Midcourse Heliocentric Orbital Elements

Element	Mariner VI	Mariner VII
Periapsis, 10^6 km	148.11	145.18
Semi-major axis, 10^6 km	194.44	190.01
Longitude of ascending node, deg*	335.94	6.73
Argument of periapsis, deg*	179.91	148.81
Eccentricity	0.2383	0.2383
Inclination, deg*	1.99	1.60
Time of periapsis, GMT	2/24/69 $15^h25^m49^s$	2/27/69 $20^h36^m48^s$

*With respect to ecliptic plane and vernal equinox.

if the tracker's cone angle is not updated. During the update period around 22^h30^m GMT on April 20, 1969 the Canopus cone angle was anomalously switched to the incorrect position. The subsequent loss of Canopus and the many roll jet actuations while trying to acquire the brightest spot in the Larger Magellenic Cloud resulted in a 2 mm/sec change in radial velocity. The aiming point at Mars changed slightly, by 50 km in the B-plane and 12 sec in arrival time. The post-anomaly heliocentric orbital elements are given in Table 3-4.

3. Encounter

The spacecraft approached the vicinity of Mars (~2 x 10^6 km) with an areocentric speed of about 7 km/sec. The orbital path with respect to Mars could be approximated by a hyperbolic trajectory with an asymptotic speed of 7.2 km/sec. Mars gravitational attraction caused the hyperbolic asymptote

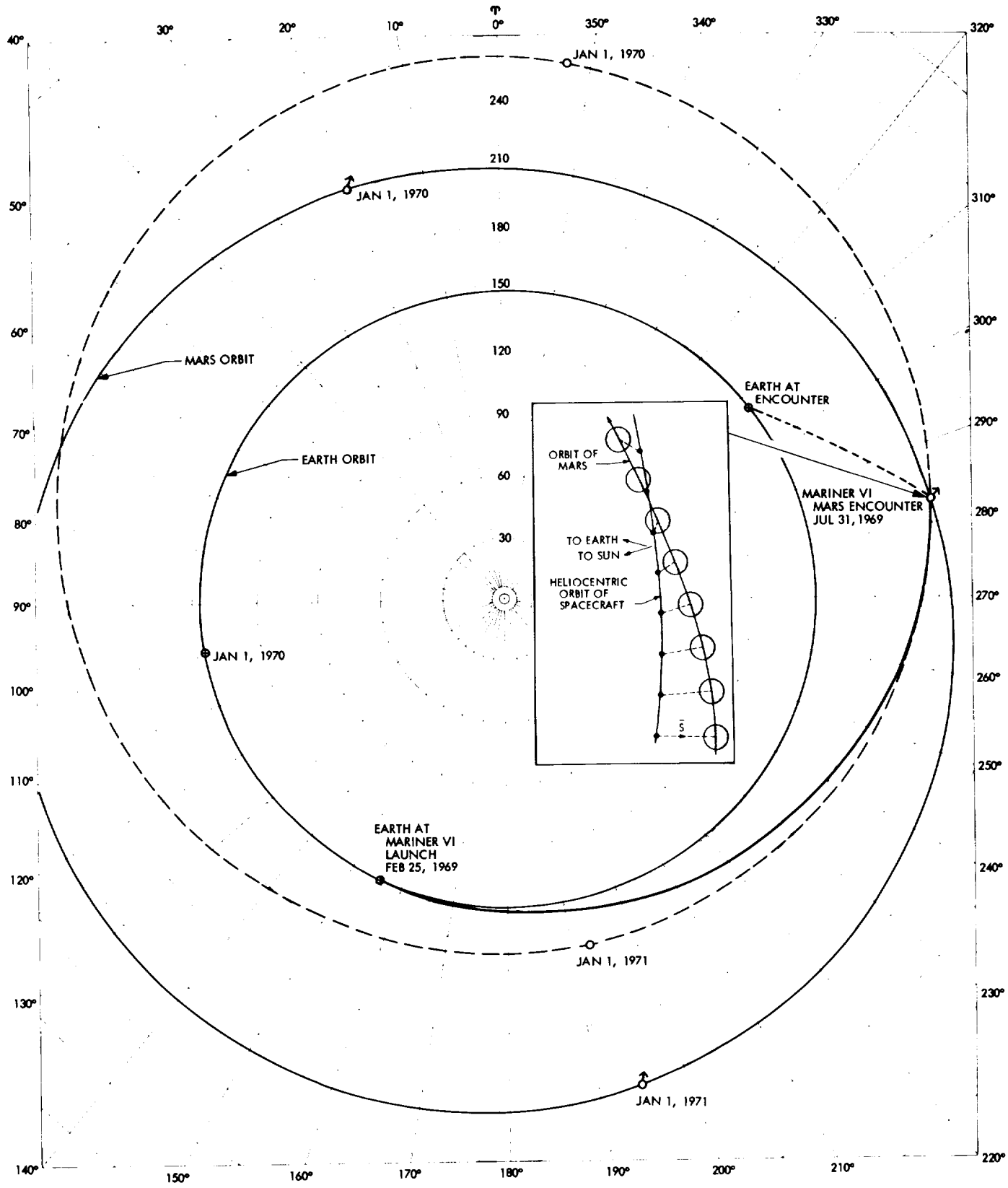

Figure 3-7. Heliocentric View of Mariner VI Trajectory

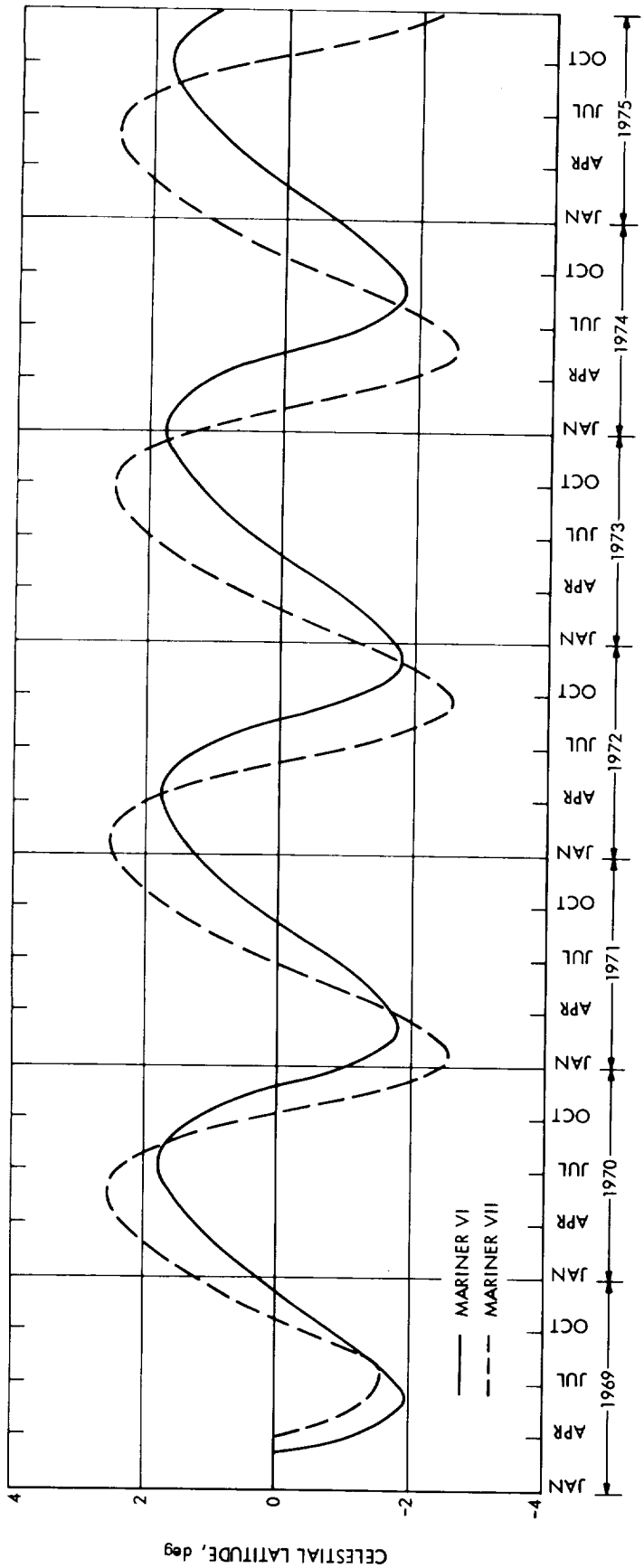

Figure 3-8. Celestial Latitude of Spacecraft vs Time, Mariner VI-VII

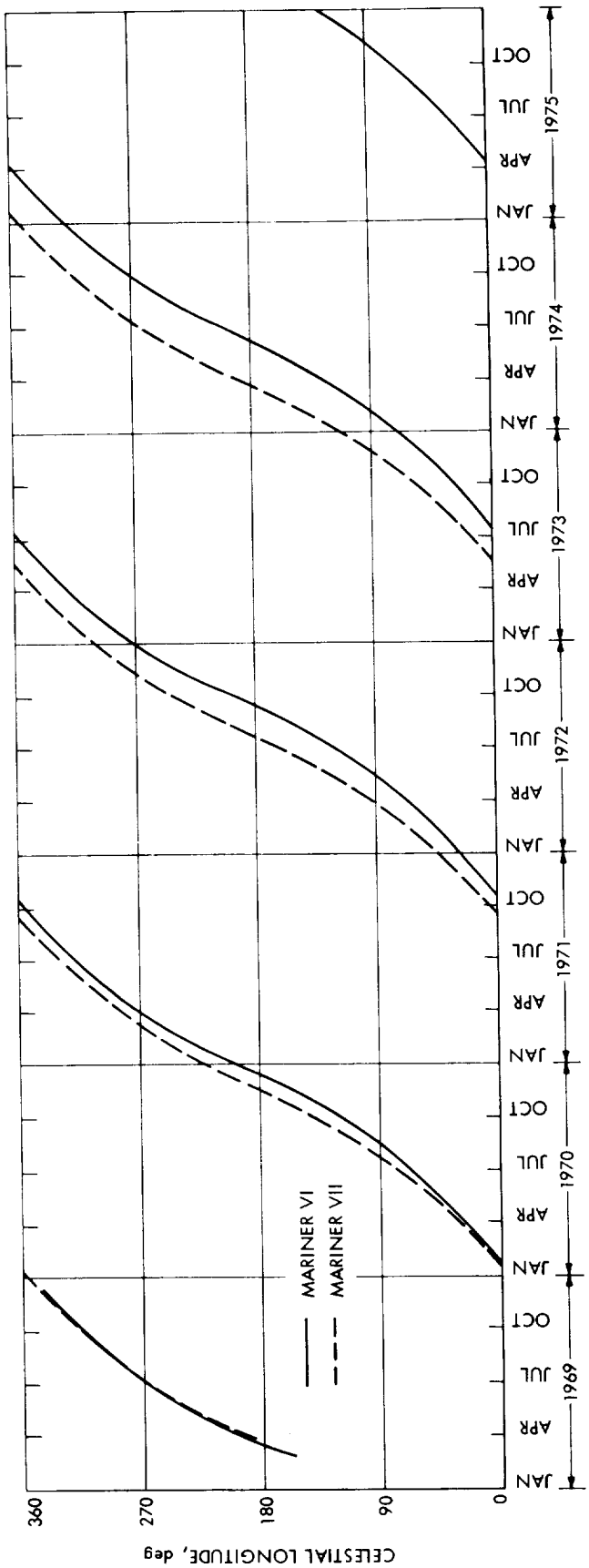

Figure 3-9. Celestial Longitude of Spacecraft vs Time, Mariner VI-VII

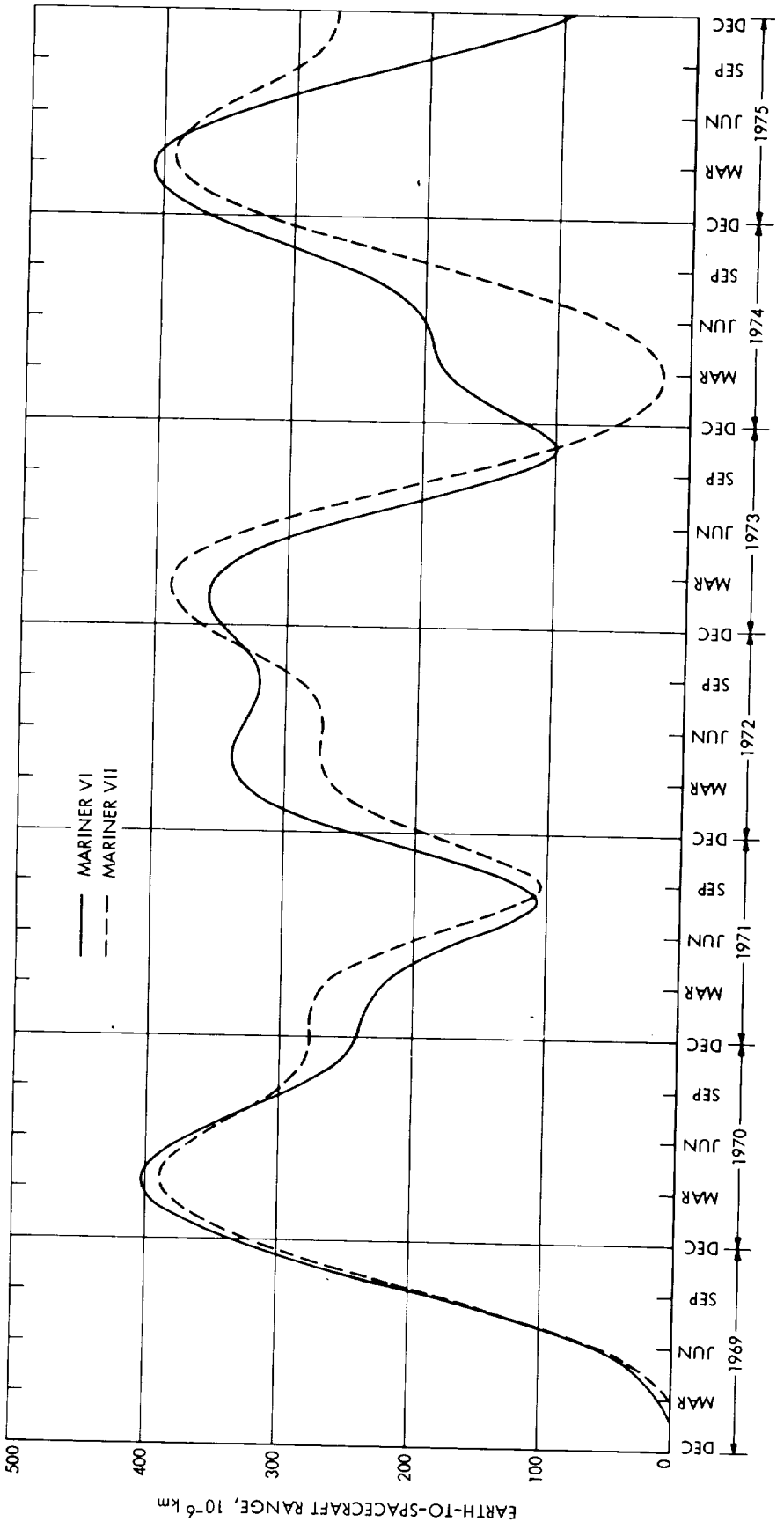

Figure 3-10. Earth-Spacecraft Range vs Time, Mariner VI-VII

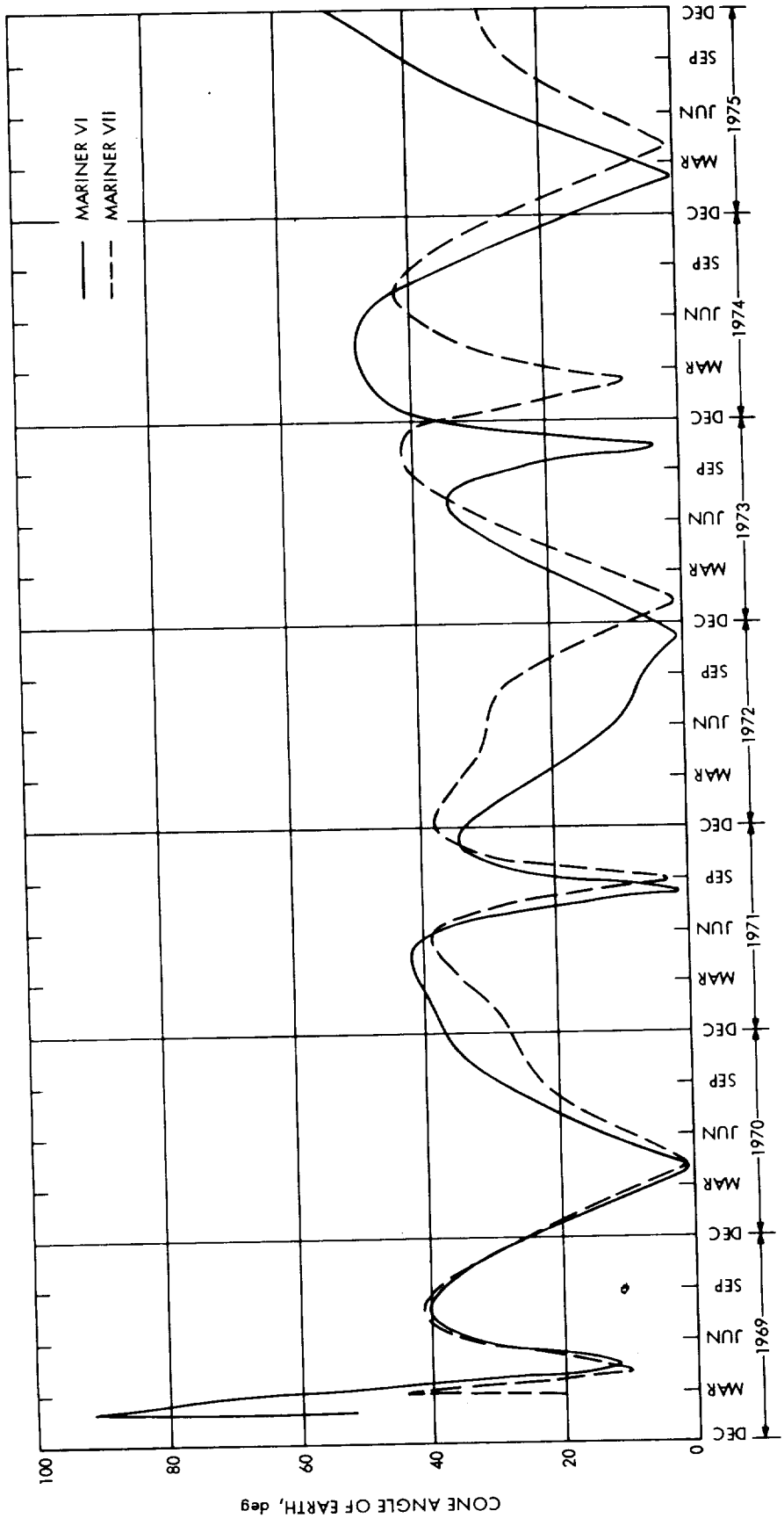

Figure 3-11. Cone Angle of Earth vs Time, Mariner VI-VII

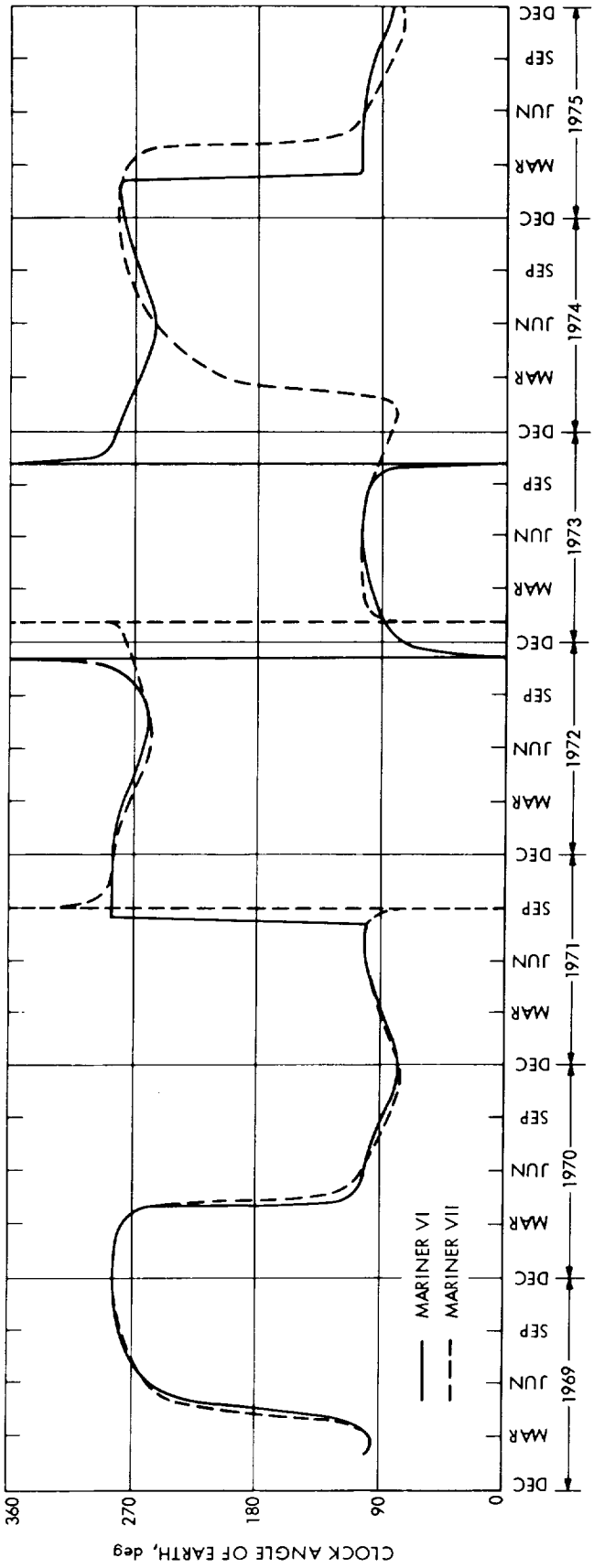

Figure 3-12. Clock Angle of Earth vs Time, Mariner VI-VII

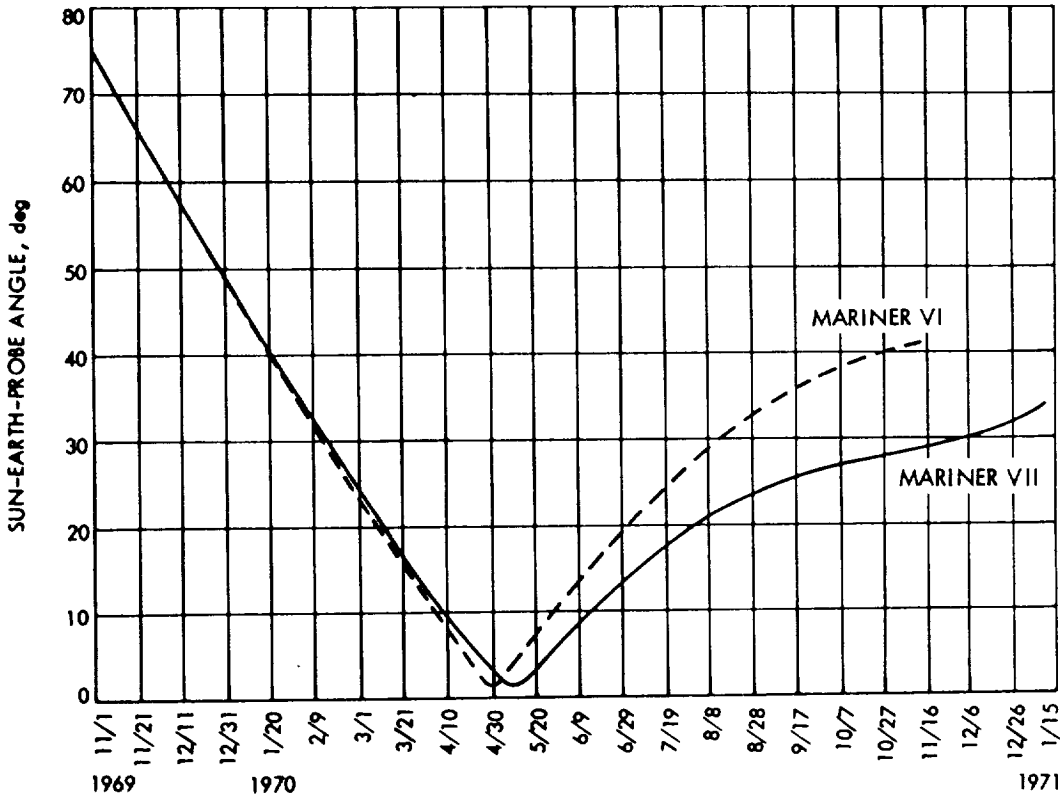

Figure 3-13. Sun-Earth-Spacecraft Angle vs Time, Mariner VI-VII

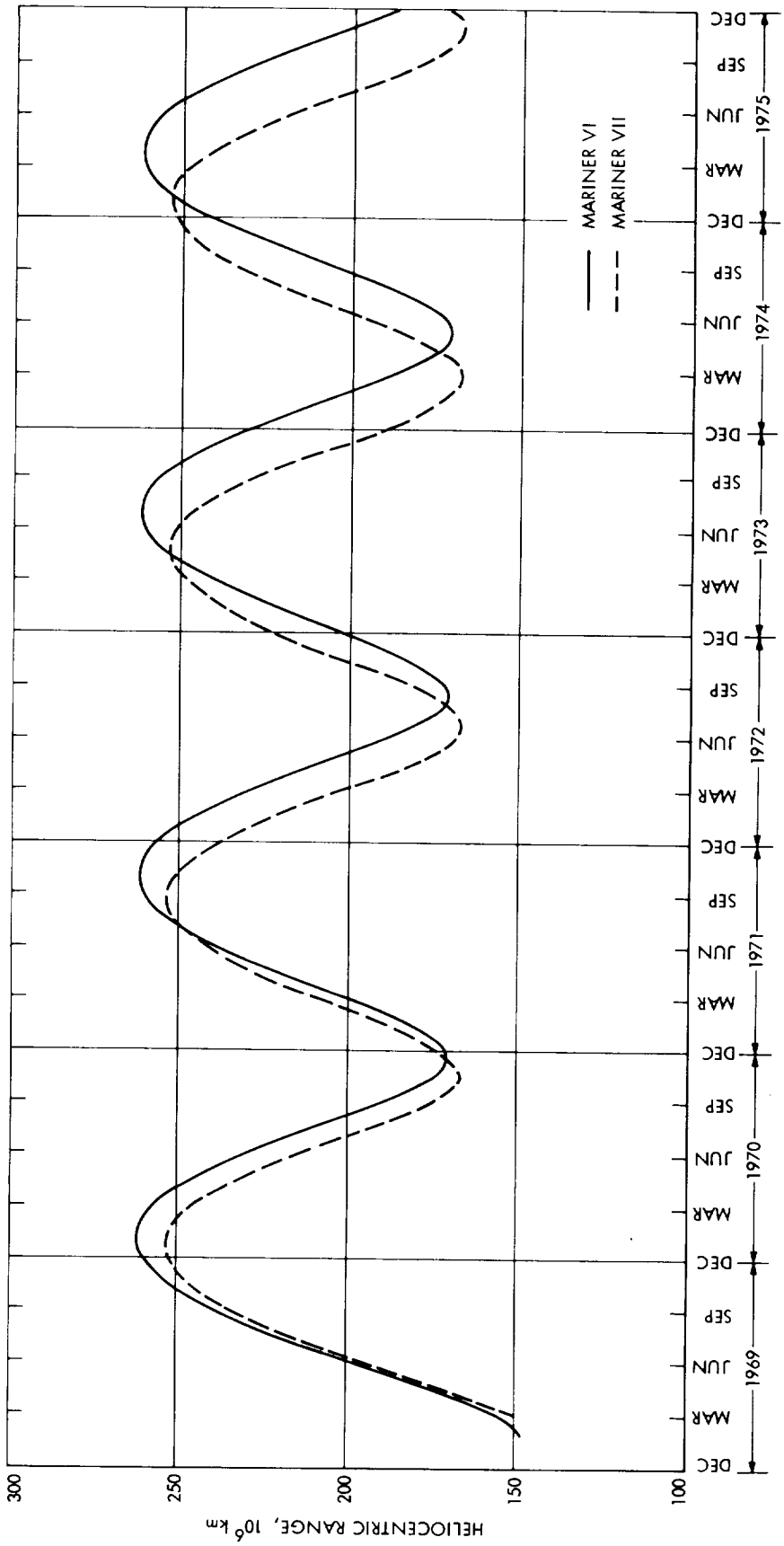

Figure 3-14. Heliocentric Range vs Time, Mariner VI-VII

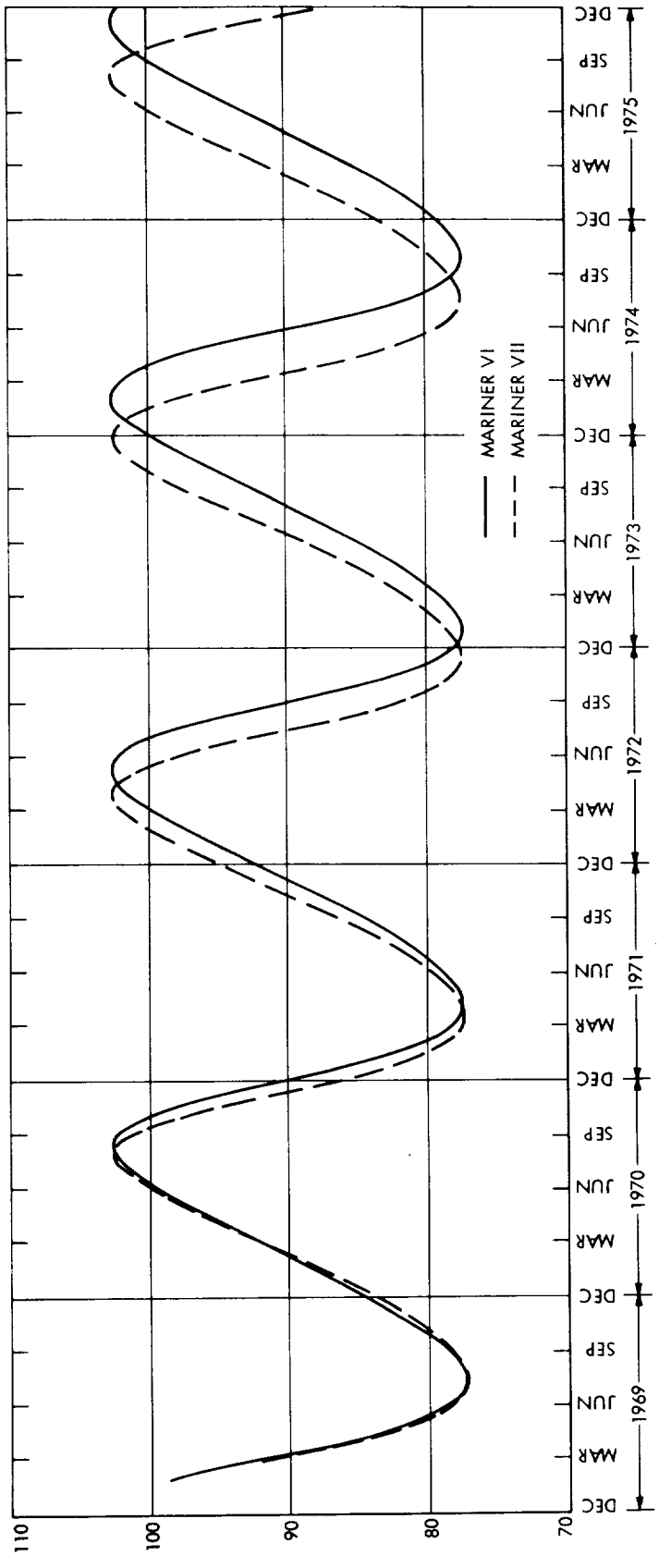

Figure 3-15. Cone Angle of Canopus vs Time, Mariner VI-VII

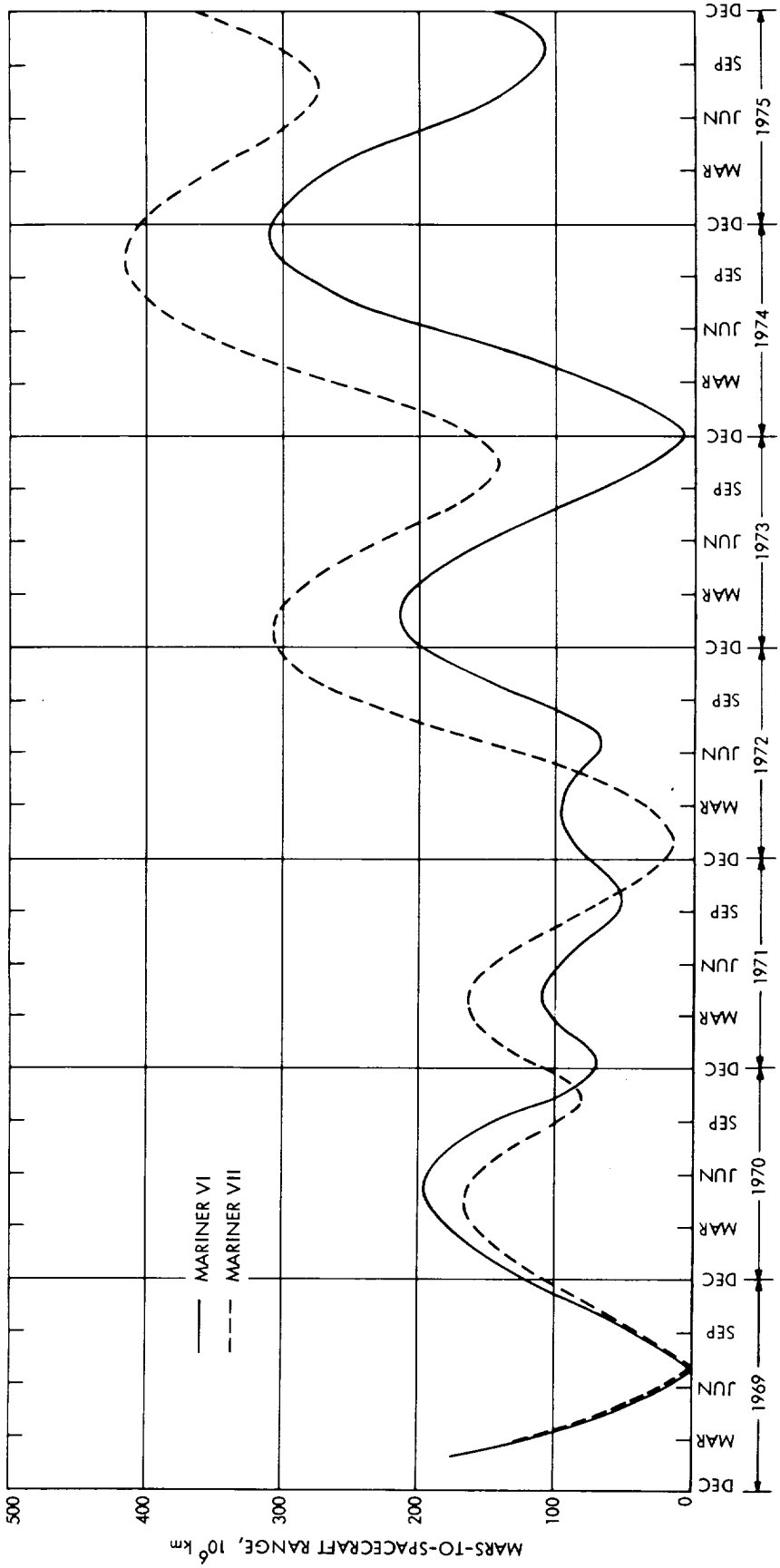

Figure 3-16. Areocentric Range vs Time, Mariner VI-VII

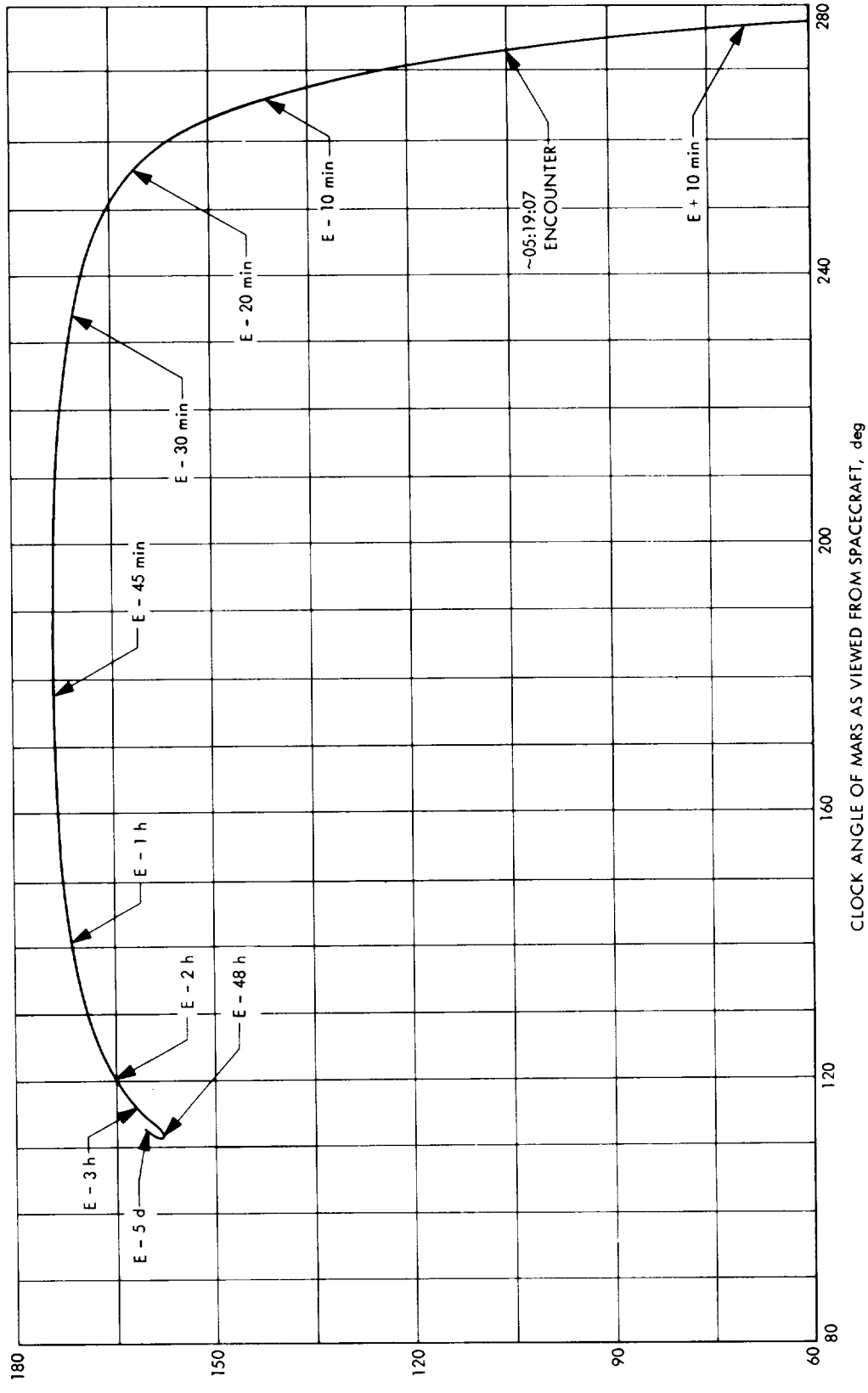

Figure 3-17. Cone Angle vs Clock Angle of Mars at Mariner VI Encounter

Table 3-3. Post-Unlatch* Heliocentric Orbital Elements

Element	Mariner VI	Mariner VII
Periapsis, 10^6 km	148.10	145.21
Semi-major axis, 10^6 km	193.40	189.88
Longitude of ascending node, deg**	335.82	6.66
Argument of periapsis, deg**	179.91	148.88
Eccentricity	0.2342	0.2353
Inclination, deg**	1.96	1.60
Time of periapsis, GMT	2/24/69 $12^h50^m17^s$	2/29/69 $20^h06^m42^s$

*Unlatch of scan platform
**With respect to ecliptic plane and vernal equinox.

direction to be altered by about 15 deg after Mars encounter. Tables 3-5, 3-6, and 3-7 contain the pre-encounter, encounter, and post-encounter areocentric orbital elements for the Mariner VI encounter trajectory. The flyby of Mars was geometrically accomplished by the spacecraft crossing the orbit of Mars in an outgoing heliocentric direction (see Fig. 3-7). The spacecraft passed the trailing edge of Mars, that is, Mars in its orbit had the larger tangential component of heliocentric velocity, and essentially passed the spacecraft. At about 04^h30^m GMT on July 31, Mars overtook the spacecraft, i.e., the celestial longitude defining the Sun-Mars line became larger than the celestial longitude defining the Mars-spacecraft line. Now before this time, Mars as viewed from the spacecraft appeared with its morning terminator to the left. The last far-encounter TV picture was shuttered at about 22^h21^m GMT on July 30, so that all of the far-encounter TV pictures show several degrees of the morning terminator to the left in the planet.

Table 3-4. Post-Magellanic Cloud Heliocentric Orbital Elements for Mariner VI (May 4, 1969 $00^h00^m00^s$)

Element	Mariner VI
Periapsis, 10^6 km	148.10
Semi-major axis, 10^6 km	192.86
Longitude of ascending node, deg*	335.60
Argument of periapsis, deg*	180.02
Eccentricity	0.2321
Inclination, deg*	1.94
Time of periapsis, GMT	2/24/69 $09^h44^m29^s$

*With respect to ecliptic plane and vernal equinox.

The near-encounter phase was initiated after the spacecraft crossed the Sun-Mars line. Now Mars appeared from the spacecraft with the evening terminator dividing the planet disk nearly in half. During the close-encounter phase, several key science instrument events had to be accurately placed within the encounter sequence of events. Hence, it was necessary to combine estimates of the encounter aim point with the desires of the principal investigators to maximize the data returned from the four scientific instruments. The trajectory estimate determined the scan platform angles needed to point a planet sensor which could initiate cooldown of the infrared spectrometer. In addition, the projection of the ultraviolet spectrometer slit had to be parallel to the local horizon 100 km above the surface of Mars. Further, the TV experimenters wanted the first recorded wide-angle TV picture to be shuttered at the limb-crossing of the center of the projected TV frame. It had been determined that a closest approach trajectory of about 3000 km altitude and passing

Table 3-5. Pre-Encounter* Areocentric Orbital Elements

Element	Mariner VI	Mariner VII
Periapsis, km	6169.9	6238.8
Semi-major axis, 10^6 km	-824.4	-857.3
Longitude of ascending node, deg**	163.10	259.05
Argument of periapsis, deg**	16.70	282.72
Eccentricity	8.48	8.28
Inclination, deg**	6.35	32.20
Time of periapsis, GMT	7/31/69 $05^h16^m21^s$	8/15/69 $04^h57^m58^s$

*Spacecraft approaching vicinity of Mars (approximately 2,000,000 km from Mars).
**With respect to ecliptic plane and vernal equinox.

approximately 20 deg below Mars' equator would best satisfy the desires of the principal investigators. Table 3-6 gives the areocentric orbital elements of the actual trajectory, which very closely matched the desired trajectory. After the TV line of sight crossed the bright-side limb of the planet, the scan platform was slewed to four new directions, again to allow maximum scientific return in viewing various regions on Mars. Platform slews were performed in 1 deg steps over a broad cone and clock angle range, and were initiated by the central computer and sequencer (CC&S) shortly after frame readout started for selected TV pictures. The picture numbers and the cone and clock steps were stored in the CC&S memory, and were altered several times during the pre-encounter flight, as the trajectory estimates became more accurate and the investigators pinpointed the desired viewing regions on the planet. The spacecraft attitude was inertially stabilized by gyros, and the scan platform motion was accomplished by electric motors such that extremely small resulting torques were felt by the spacecraft.

Table 3-6. Areocentric Orbital Elements at Encounter

Element	Mariner VI	Mariner VII
Periapsis, km	6842.	6812.
Semi-major axis, km	-825.8	-858.8
Longitude of ascending node, deg*	148.21	258.14
Argument of periapsis, deg*	30.89	282.98
Eccentricity	9.29	8.96
Inclination, deg*	6.92	28.15
Time of periapsis, GMT	7/31/69 $05^h19^m06^s.2$	8/05/69 $05^h00^m49^s.5$

*With respect to ecliptic plane and vernal equinox.

The factors which dictated each of the five platform positions will now be summarized briefly. Mariner VI returned 25 pictures of the lighted side of Mars during the close-encounter pass. The general locations of these pictures are illustrated in Figure 3-18. The odd-numbered frames are wide-angle (TV-A) pictures, and the even-numbered frames are narrow-angle (TV-B) pictures. Picture No. 1 was shuttered approximately 13^m59^s before encounter (closest approach), and picture No. 25 was shuttered approximately 2^m55^s after encounter. The pictures were spaced at 42.24 sec intervals. The initial platform cone angle was selected such that (at the initial clock angle used) the digital tape recorder (DTR) would start at the "appropriate" time and, also, the first picture would be a suitable wide-angle picture of the limb. By "appropriate" is meant that the DTR would still be running some 30 to 60 sec after the IRS viewing axis had crossed the dark limb (at the final platform cone and clock angle position). This was done to ensure recovery of the dark-side data on the DTR in the event that the real-time high-rate (16,200 bps) channel did not

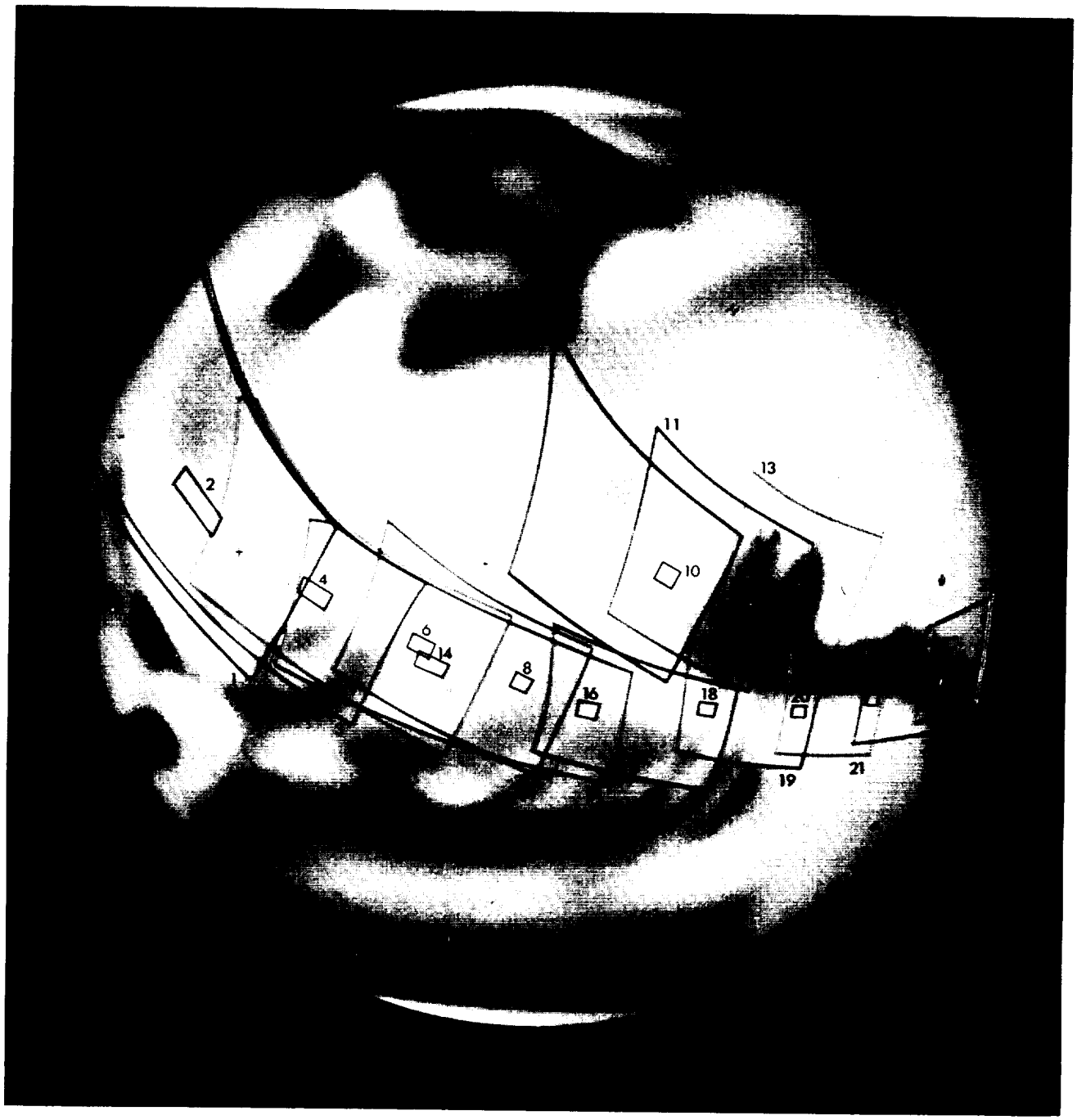

Figure 3-18. Mariner VI Near Encounter TV Coverage

Table 3-7. Post-Encounter* Areocentric Orbital Elements

Element	Mariner VI	Mariner VII
Periapsis, km	7228.7	7107.7
Semi-major axis, km	-824.20	-857.12
Longitude of ascending node, deg**	139.04	254.95
Argument of periapsis, deg**	40.29	286.11
Eccentricity	9.77	9.29
Inclination, deg**	7.94	24.43
Time of periapsis, GMT	7/31/69 $05^h21^m59^s.3$	8/05/69 $05^h03^m44^s.6$

*Spacecraft leaving vicinity of Mars (approximately 2,000,000 km from Mars).
**With respect to ecliptic plane and vernal equinox.

function properly. The initial platform clock angle for the first swath was selected such that (for the initial cone angle used) the UVS viewing slit would be aligned with the local horizontal at an altitude of 100 km above the bright limb. A sufficient number of pictures were taken along this first swath to ensure that the trailing UVS field-of-view (FOV) had scanned the lower atmosphere, had crossed the limb, and had even passed a small distance across the planet surface. Approximately 8 sec after frame No. 8 was shuttered the CC&S instructed the platform to slew to its second position. A negative slew in clock angle carried the instrument viewing axes to the north in order to view such interesting surface features as Margaritifer Sinus, Oxia Palus, Meridiani Sinus, and a small part of the western side of Sabaeus Sinus. The amount of clock angle slew was limited so that some overlap would be maintained with the last picture swath across the lighted side. The platform had to be slewed after picture

No. 13 in order to carry the UVS back off the limb to a sufficient altitude where it could make a second scan of the atmosphere. The third platform orientation was therefore determined by slewing to the final cone angle position (≈100 deg) and that clock angle position which would again align the UVS slit with the tangent plane at 100 km altitude above the bright limb. This slew-back also provided the UVS with its shortest slant-range view of the atmosphere above the limb. In order to again give the UVS ample time to scan the atmosphere, cross the limb, and pass onto the planet surface, the next platform slew was not made until 8 sec after picture No. 17 had been shuttered. After picture No. 17 had been shuttered, the platform clock angle was diminished by 2 deg, thus moving the instrument traces slightly to the north on Mars. This fourth platform position was chosen to accomplish three objectives:

1) Maintain some overlap with frames No. 11 and 13.

2) View the southern boundary and most of Sabaeus Sinus.

3) Obtain a good pass completely across Syrtis Major on the dark side with the IRR and IRS.

A final platform slew was performed on the dark side (after frame No. 32) in order to view Libya and extend dark-side viewing time for the non-TV instruments.

Closest approach occurred at $05^h19^m06^s.9$ GMT on July 31, at a Martian latitude of -23.0 deg and 19.9 deg east longitude. Shortly thereafter, the spacecraft crossed the evening terminator, and then occulted the earth at $05^h34^m33^s$ GMT when loss of radio signal occurred. Occultation occurred on the dark side of Mars at 3.7 deg latitude and 355.7 deg east longitude. The spacecraft areocentric position was -8.7 deg latitude, 64.5 deg east longitude. Occultation ended and the signal reappeared at 79.3 deg latitude, 87.1 deg east longitude. The spacecraft areocentric position at exit occultation was 0.6 deg latitude, 80.3 deg longitude. The spacecraft was reacquired at $05^h54^m28^s$ GMT. Figure 3-19 shows the areocentric Mariner VI trajectory and the relation of the spacecraft and science events. The events, some of which are labeled on Figure 3-19, are as follows:

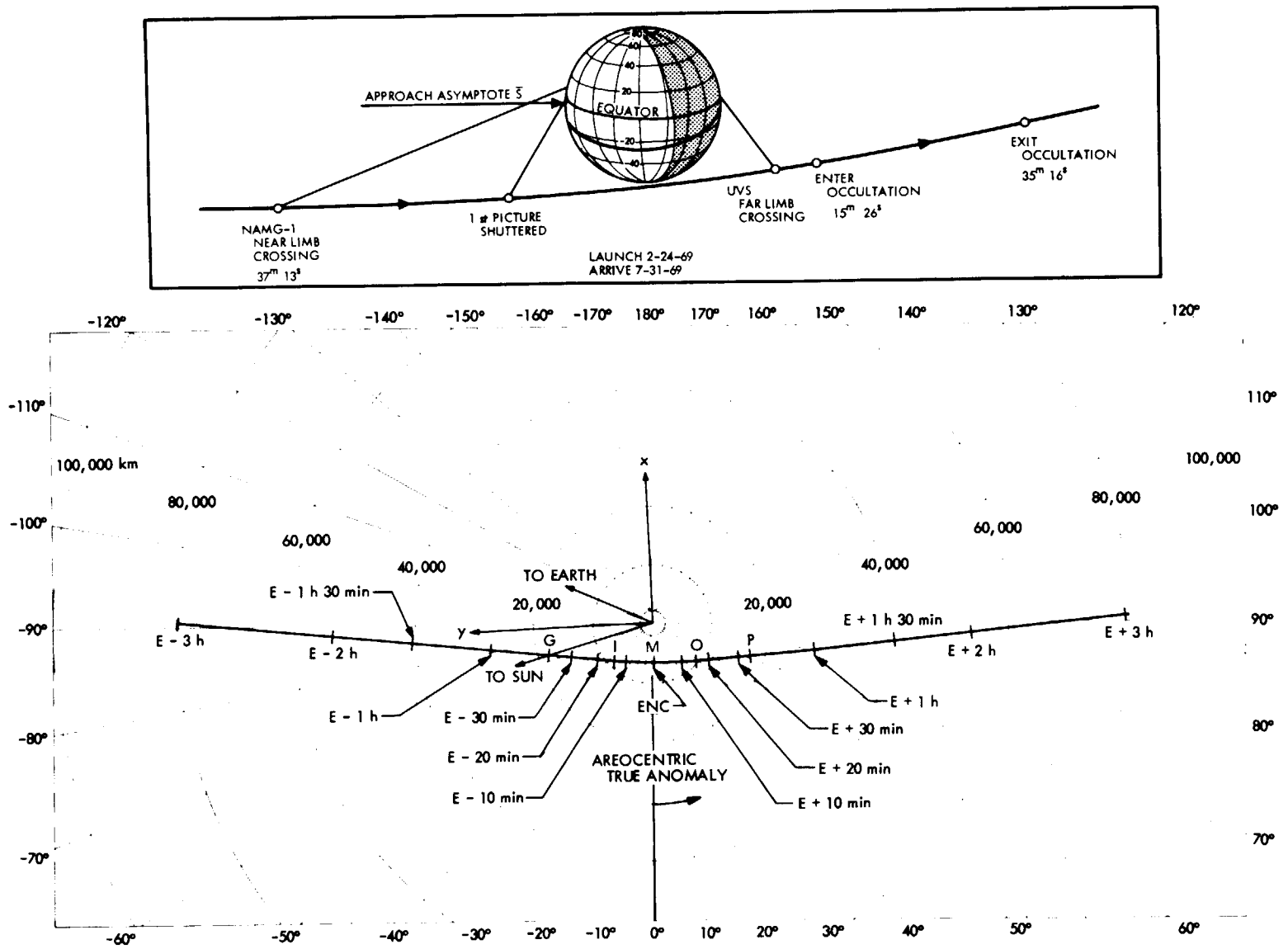

Figure 3-19. Ecliptic View of Near-Mars Mariner VI Trajectory

A Spacecraft 2,000,000 km from Mars, July 28, $00^h21^m51^s$

B Science instrument and scan encounter power turned on July 29, $01^h22^m21^s$

C Scan control switched to far-encounter references July 29, $01^h56^m31^s$

D Far-Encounter TV-B Picture No. 1 shuttered July 29, $05^h28^m48^s$

E Far-Encounter TV-B Picture No. 50 shuttered July 30, $22^h21^m42^s$

F Scan control switched to near-encounter references July 30, $22^h23^m28^s$

G Spacecraft crosses sun-Mars line July 31, $\sim 04^h38^m08^s$

H IRS cooldown squibs fired by Pyro - IRS motor started July 31, $04^h41^m54^s$

I Near-encounter TV-A Picture No. 1 shuttered July 31, $05^h05^m08^s$

J Initiation of 1st Platform Slew, approximately -14 deg in clock, performed after shuttering of 8th TV picture, $05^h10^m12^s$

K Initiation of 2nd Platform Slew, approximately +20 deg in clock, to 100.0 deg cone, performed after shuttering of 13th TV picture, $05^h13^m42^s$

L Initiation of 3rd Platform Slew, approximately 02 deg in clock, performed after shuttering of 15th TV picture, $05^h16^m32^s$

M Closest approach to Mars, $05^h19^m07^s$

N Initiation of 4th Platform Slew, approximately +6 deg in clock performed after shuttering of 32nd TV picture, $05^h27^m06^s$

O Spacecraft occults earth, $05^h34^m33^s$

P Spacecraft exits earth occultation, $05^h54^m23^s$

B. MARINER VII

1. Launch to Maneuver

Mariner VII was launched by Atlas/Centaur 19 on a direct ascent trajectory from AFETR, complex 36A, on March 27, 1969, $22^h22^m01^s$ GMT. The spacecraft was launched in sunlight, and entered the earth's shadow at $22^h38^m27^s$ GMT. The launch window had opened at $21^h35^m00^s$ about 47 min before the launch actually occurred. The launch azimuth was 102.79 deg, requiring no yaw maneuver. BECO occurred at $22^h24^m32^s$. The Atlas/Centaur sequence of events for Mariner VII was otherwise the same as for Mariner VI. The Centaur insulation panels and nose fairing were jettisoned at $22^h25^m16^s$, and $22^h25^m53^s$, respectively. The Atlas sustainer engine cutoff occurred at $22^h26^m16^s$, and the sustainer stage separated from the Centaur two seconds later. After a 10 sec coast, the Centaur main engine was started at $22^h26^m28^s$. Centaur MECO occurred at $22^h33^m53^s$, when C_3 was computed to be 16.8612 km^2/sec^2. Spacecraft separation occurred at $22^h35^m28^s$. The solar panels were deployed at $22^h38^m28^s$ and the Centaur deflection maneuver was initiated at $22^h40^m01^s$. The spacecraft exited the earth's shadow at $23^h12^m45^s$ and sun acquisition was completed at $23^h14^m33^s$. Figure 3-4 shows the ground track of Mariner VII for about 8 hr after launch.

- Mariner VII Injection Aiming Point

The injection aiming point achieved by Mariner VII had the following aiming plane coordinates at Mars: $\bar{B}\cdot\bar{T}$ = -6777 km, $\bar{B}\cdot\bar{R}$ = 29,309 km, t_{ca} = $04^h48^m22^s$ GMT, August 5, 1969 (see Figure 3-5 and 3-6). The Mariner VII injection aiming point was also biased, the bias being removed by the midcourse maneuver. The maneuver is ordinarily computed and executed with the star Canopus as the standard roll position reference. However, for Mariner VII the star Sirius was used as reference, in order to minimize the pitch turn magnitude so that the solar panels would not be tilted away from the sun significantly. On April 7, 1969 commands were sent to acquire Sirius and the motor burn was initiated at about 20^h22^m on April 8, 1969. Subsequent to the midcourse maneuver, Mariner VII headed for an aiming point about 190 km from the selected aiming point. Tables 3-1, 3-2, and 3-3 give the geocentric and heliocentric orbital elements at injection, post-midcourse, and post-scan platform unlatch for both spacecraft.

2. Cruise

After leaving the vicinity of the earth, the spacecraft proceeded on an approximately elliptical trajectory about the sun until it reached the vicinity of Mars. Figure 3-20 illustrates the heliocentric view of the Mariner VII trajectory. Figures 3-8 to 3-16 and Figure 3-21 show various geometric trajectory parameters for Mariner VII, such as celestial latitude, longitude, earth-spacecraft range, heliocentric distance, and cone and clock angles of earth. The figures illustrate the geometric behavior of both spacecraft projected out to 1975.

One month after the midcourse maneuver, the scan platform, on which the science instruments were mounted, was unlatched from its stowed position. The unlatching involved the releasing of compressed nitrogen and the resulting velocity vector change slightly altered the spacecraft trajectory. Table 3-3 shows the heliocentric orbital elements of the post-unlatch trajectory.

The Mariner VII spacecraft experienced a sequence of anomalies, initiated by a loss of radio signal at approximately 22^h11^m GMT on July 30, and concluded with the reacquisition of spacecraft roll reference at 11^h35^m on July 31. The series of anomalies had a large effect on the subsequent encounter mission operations. The result of the anomalies was to change the velocity of the spacecraft by -7.67 cm/sec in the earth-radial direction. (See Section II. B. 6. f. for a complete description of the Mariner 7 anomalies.) Table 3-5 gives the areocentric pre-encounter orbital elements for the Mariner VII orbit.

3. Encounter

The Mariner VII encounter trajectory closely matched the Mariner VI encounter trajectory, with the exception that the trajectory plane was inclined about 55 deg south with respect to the Mars equator. Table 3-5 gives the areocentric orbital elements for the actual Mariner VII encounter trajectory. The sequence of near-encounter events for the Mariner VII encounter was similar to the Mariner VI sequence. The factors which dictated each of the five Mariner VII platform positions will now be summarized briefly. Mariner VII returned 33 pictures of the lighted side of Mars during the near-encounter pass. The general locations of these pictures are shown in Figure 3-23. The odd-numbered frames are TV-A, and the even-numbered frames are TV-B. Picture No. 1 was shuttered approximately 20^m26^s before closest approach, and

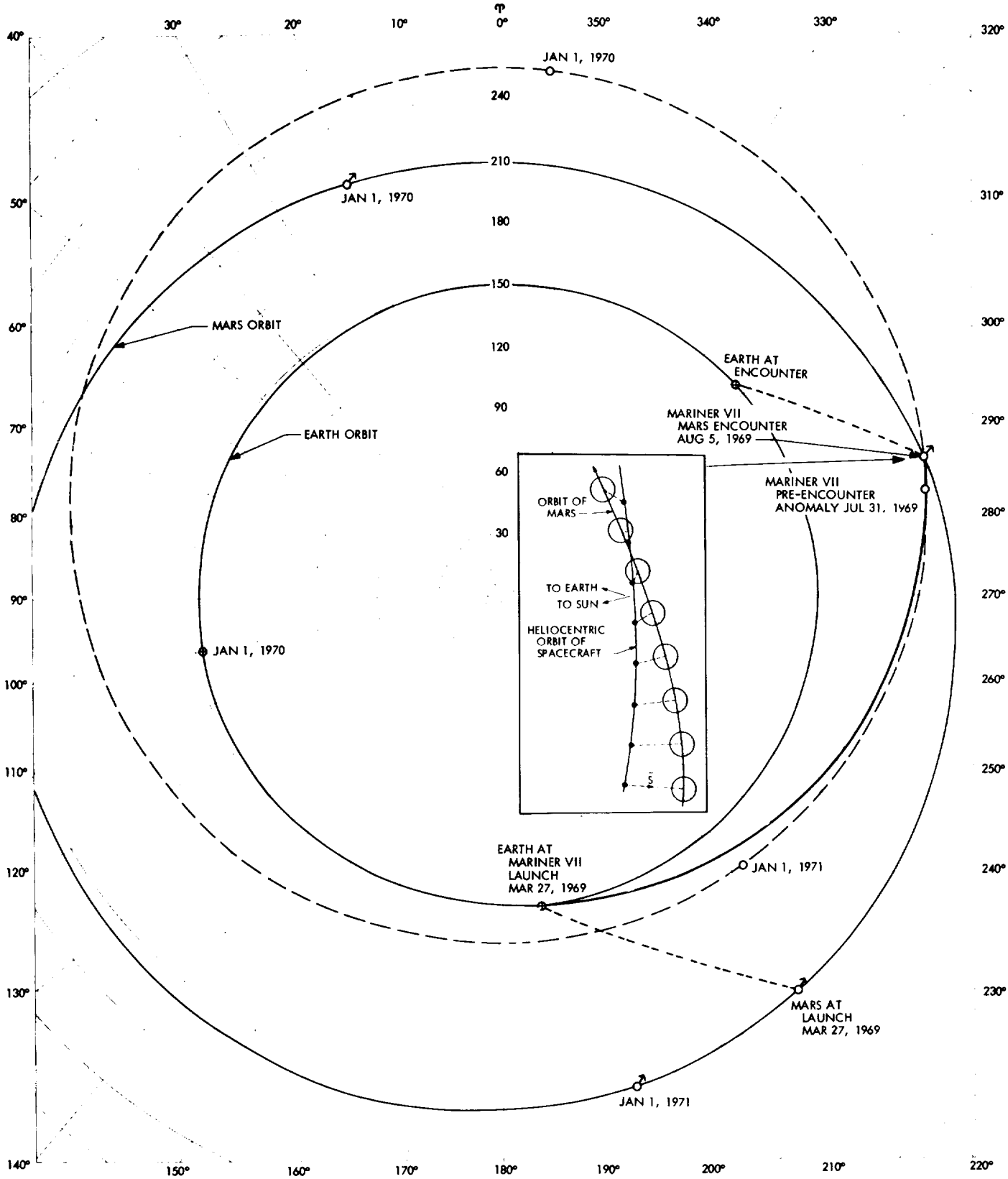

Figure 3-20. Heliocentric View of Mariner VII Trajectory

picture No. 33 was shuttered approximately $2^{m}6^{s}$ after closest approach. The pictures were spaced at 42.24 second intervals. Four different platform viewing orientations were used during the TV portion of the flyby pass.

Since the high-rate channel had worked successfully for Mariner VI FE and NE (and for Mariner VII FE), and because the FE pictures had further increased the interest in the southern polar cap, it was decided to take more NE pictures for Mariner VII, with more of them on the southern polar cap. The initial platform cone angle was therefore increased to about 135 deg in order to start the sequence properly and fill the analog tape recorder (ATR) with 33 pictures of the lighted side of Mars. The initial cone angle value was based upon knowledge of the time the TV would cross the terminator (with the platform slewed back to CA $\approx$ 100 deg, KA $\approx$ 234 deg), and assuming that initial value of platform clock angle which would properly align the UVS slit projection at 100 km altitude above the bright limb. The initial platform position also resulted in obtaining very desirable coverage of Meridiani Sinus under different viewing conditions than had been present during the second Mariner VI NE platform position. A sufficient number of pictures were taken along this first swath to ensure that the trailing UVS field-of-view had scanned the atmosphere, had crossed the limb, and had passed a short distance across the planet surface.

Approximately 8 sec after picture No. 9 had been shuttered, the CC&S instructed the scan platform to slew to its second position in order to view the southern polar cap. This required a very large positive clock slew of 33 deg, as well as a positive cone slew of 9 deg. The chosen cone and clock angles (CA $\approx$ 144 deg, KA $\approx$ 250 deg) gave all instruments the opportunity to view the regions north of the cap boundary, to make the transition across the thaw region and cap boundary with continuity to progress well onto the cap, and, finally, to obtain wide-angle pictures (see frames No. 17 and 19) of the terminator while on the polar cap. The platform had to be slewed after picture No. 20 in order to carry the UVS back off the limb to a sufficient altitude where it could begin a second scan through the atmosphere.

The third platform position was therefore determined by slewing to the final cone angle position ($\approx$100 deg) and that clock angle value ($\approx$234 deg) which would again align the UVS slit with the tangent plane at 100 km altitude above

the bright limb. This slew back also provided the UVS with its shortest slant-range view of the atmosphere above the limb. Motion along this third swath continued for a sufficient time to permit the UVS to complete its scan of the atmosphere and, in addition, to permit the TV and IRR to cross the western boundary of Hellas, and for the trailing IRS to cross most of Hellespontus. At this point, the IRS experimenter requested a 5 deg clock slew to the north in order to cross Hellas at slightly warmer latitudes. Pictures No. 21 through 27 were taken along the third platform swath.

Approximately 8 sec after picture No. 27 was shuttered, the CC&S instructed the platform to slew north to its fourth position. In this position, the remaining TV pictures No. 28 through 33 were taken, with much of picture No. 33 covering the dark side across the terminator. Motion along this swath continued until 8 sec after "picture No. 37" had been shuttered, at which time the CC&S issued instructions for a final clock angle slew of the platform of +21 deg. Performance of this final clock slew delayed the occurrence of excessively oblique viewing angles and extended dark-side coverage for the non-TV instruments.

Closest approach occurred at $05^h00^m49^s.5$ GMT on August 5, at a Martian latitude of -53.3 deg and 78.3 deg east longitude. Shortly thereafter, at about $05^h04^m20^s$, the spacecraft crossed the evening terminator, and then occulted the earth at $05^h14^m09^s$ GMT when loss of radio signal occurred. Occultation occurred on the dark side of Mars at -58.3 deg latitude and 30.3 deg east longitude. The spacecraft was at an areocentric position of -28.6 deg latitude, 124.4 deg east longitude. Occultation ended and the signal reappeared at $05^h43^m51^s$ at 38.1 deg latitude, 211.7 deg east longitude. The spacecraft was now at an areocentric position of -3.8 deg latitude, 137.1 deg east longitude. Reacquisition was completed at $05^h43^m36^s$ GMT. Figure 3-22 shows the areocentric Mariner VII trajectory and the relation between the spacecraft and science events. The events, some of which are labeled on Figures 3-22 are listed below:

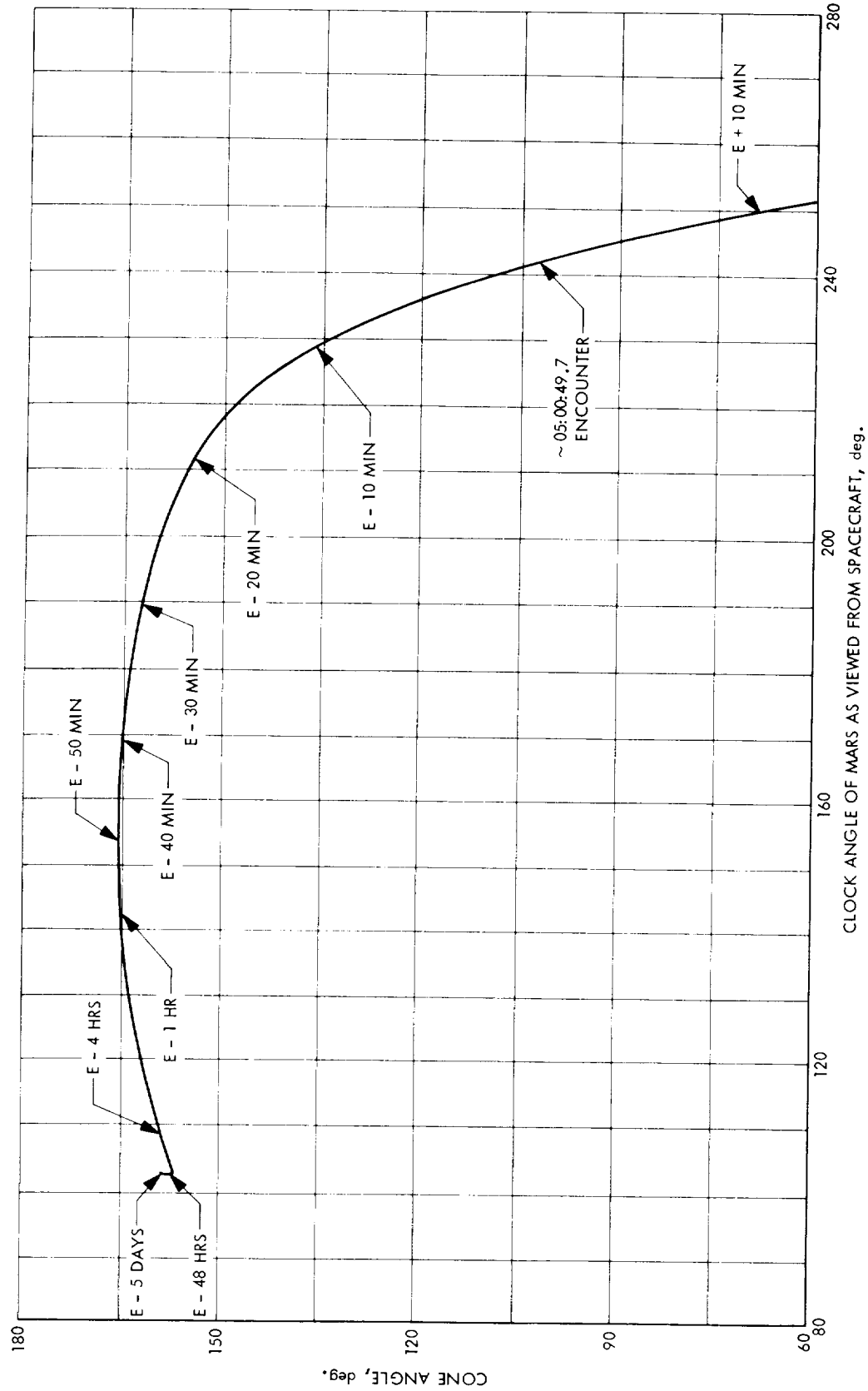

Figure 3-21. Cone Angle vs Clock Angle of Mars at Mariner VII Encounter

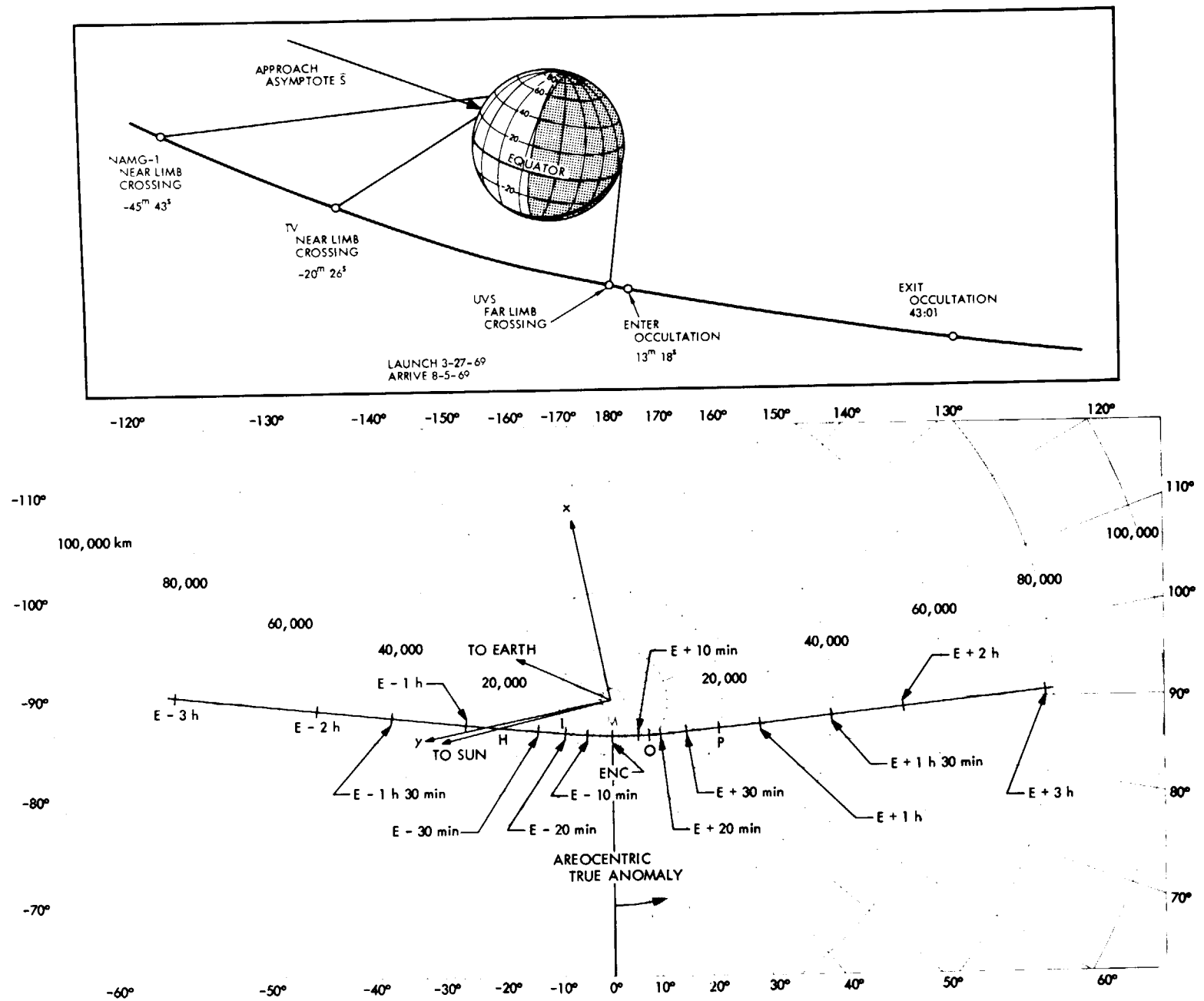

Figure 3-22. Ecliptic View of Near-Mars Mariner VII Trajectory

A Mariner VII "Happening" July 30, 22^h11^m to July 30, 11^h35^m

B Science instrument and scan encounter power turned on August 1, $22^h18^m29^s$

C Spacecraft 2,000,000 km from Mars August 1, $22^h32^m53^s$

D Scan control switched to far-encounter references August 2, $00^h16^m01^s$

E Far-Encounter TV-B Picture No. 1 shuttered August 2, $09^h32^m42^s$

F Far-Encounter TV-B Picture No. 93 shuttered August 4, $23^h59^m30^s$

G Spacecraft crosses Sun-Mars line August 5 $04^h13^m00^s$

H IRS cooldown squibs fired by Pyro - IRS motor started August 5, $04^h15^m07^s$

I Near-encounter TV-A Picture No. 1 shuttered $04^h40^m24^s$

J Initiation of 1st Platform Slew, approximately +33 deg in clock, 9.0 deg in cone performed after shuttering of 9th TV picture $04^h46^m10^s$

K Initiation of 2nd Platform Slew, approximately -17 deg in clock, to 100.0 deg cone, performed after shuttering of 20th TV picture $04^h53^m54^s$

L Initiation of 3rd Platform Slew, approximately -5 deg in clock, performed after shuttering of 27th TV picture $04^h18^m50^s$

M Closest approach to Mars $05^h00^m50^s$

N Initiation of 4th Platform Slew, approximately +6 deg in clock performed after shuttering of 38 TV picture $05^h05^m53^s$

O Spacecraft occults earth $05^h14^m08^s$

P Spacecraft exits earth occultation $05^h43^m51^s$

C. MARINER VI, VII POST-ENCOUNTER

After successfully completing close encounters with Mars, the two Mariner spacecraft have gained energy so that they are in solar orbits with perihelion distances significantly greater than Earth aphelion distance. Though not primarily designed as Mars swingby missions, the trajectories were fairly efficient in this respect. If Mars had been a massless planet, and an impulsive maneuver had been done to change the pre-encounter orbits into the resulting post-encounter orbits, the velocity requirements would have been 1.584 km/sec for Mariner VI and 1.446 km/sec for Mariner VII.

Table 3-8 summarizes the post-encounter trajectory parameters. Notice that both orbits have periods of approximately one and three-quarter years, and that solar conjunctions occur nine and one-half days apart at the end of April and beginning of May, 1970. During the time near solar conjunction, it was possible to perform an extremely sensitive test of general relativity theory by measuring the effect of the Sun's mass on the radio signals being transmitted from the spacecraft.

Figures 3-14, 3-10, 3-13 and 3-11 show probe-Sun distance, probe-Earth distance, Sun-Earth-probe angle, and Earth-probe-Sun angle (Earth cone angle) versus time for Mariner VI and VII. Near the time of conjunction, maximum probe-Earth distance is attained, so that maximum free space attenuation of signal strength occurs. The low-gain antenna, which always points toward the Sun in cruise configuration, also points toward the Earth at this time. Since the high-gain antenna axis makes an angle of 41.6 deg with the low-gain antenna axis, it would be necessary to reorient the spacecraft in order to increase received signal power by transmitting with the high-gain antenna.

Table 3-8. Post-Encounter Heliocentric Trajectory Parameters*

	Mariner VI	Mariner VII
Semi-major axis (km x 10^6)	216.57	210.43
Semi-minor axis (km x 10^6)	211.68	205.93
Period (days)	636.24	609.35
Longitude of ascending node (deg)**	342.64	347.13
Argument of periapsis (deg)**	203.54	173.08
Eccentricity	0.2113	0.2056
Inclination (deg)**	1.78	1.82
Time of aphelion (GMT)	02/03/70 13^h20^m	01/19/70 09^h10^m
Aphelion distance (km x 10^6)	262.35	253.70
Time of solar conjunction (GMT)	04/30/70 01^h20^m	05/09/70 13^h50^m
Distance from Sun at conjunction (km x 10^6)	251.13	236.32
Distance from Earth at conjunction (km x 10^6)	401.96	387.07
Sun-Earth-probe angle at conjunction (deg)	0.95	1.79
Earth-Sun-probe angle at conjunction (deg)	178.48	177.06
Earth-probe-Sun angle at conjunction (deg)	0.57	1.16
Time of perihelion (GMT)	12/18/70 16^h10^m	11/20/70 01^h20^m
Perihelion distance (km x 10^6)	170.80	167.16

*Based on osculating conic at conjunction.
**With respect to ecliptic plane and vernal equinox.

Figure 3-23. Mariner VII Near Encounter TV Coverage

SECTION IV
MANEUVER ANALYSIS

R. T. Mitchell

A. PURPOSE OF MANEUVERS

Midcourse correction maneuvers were required on the Mariners VI and VII trajectories in order to achieve the accuracy on the encounter parameters necessary to satisfy the objectives of the scientific experiments to be performed. These maneuvers were accomplished by means of small changes in spacecraft velocity vector, thus causing their trajectories to be slightly perturbed from the nominal trajectories, but with the desired end conditions. The Mariner VI and VII spacecraft were capable of performing two such corrective maneuvers. This capability was required in order to ensure an acceptable pre-launch probability of achieving a satisfactory encounter. The likelihood of achieving such an encounter at injection was essentially zero for two reasons. First, because of normally occurring in-tolerance injection errors, the resulting dispersions at encounter were much larger than the acceptable encounter region. Second, in order to satisify the planetary quarantine constraint, it was necessary to target the spacecraft approximately 20, 000 km from the nominal desired final aiming point at injection. Similarly, although it was not anticipated that the first maneuver aiming point would have to be biased to satisfy the planetary quarantine constraint, in-tolerance execution errors associated with this maneuver were sufficiently large to lead to a significant probability of requiring a second maneuver. Although the Atlas-Centaur is the most accurate launch vehicle used to date, and could have satisfied the requirements of some previous interplanetary missions with no maneuvers, the stringent accuracy requirements placed on the Mariner Mars 1969 mission required the capability of executing two maneuvers for each spacecraft.

A considerable amount of effort went into pre-mission maneuver strategy studies in order to maximize the probability of executing successful maneuvers, and to prepare operations personnel for various contingency plans. An important part of the maneuver strategy was the injection targeting procedure. The process of injection targeting included selecting the spacecraft separation direction, the Centaur deflection direction, and aiming points for pre- and post-separation and post-deflection. Some of the considerations that went into selecting these values were:

1) Spacecraft separation direction.

   a) Send spacecraft toward planet, launch vehicle away from planet.

   b) Point low gain antenna in lower hemisphere (containing earth) for rapid acquisition of signal.

   c) Have orientation such as to acquire sun before entering earth's shadow, when injection was in sunlight.

   d) Avoid pointing sensitive instruments to sun.

2) Launch vehicle deflection direction.

   a) Minimize probability of launch vehicle impacting planet.

   b) Insure that deflection direction was such that launch vehicle would not collide with separated spacecraft.

   c) Insure that deflection exhaust gases did not impinge on spacecraft.

   d) Insure that launch vehicle did not come within the field of view of the spacecraft Canopus sensor.

3) Aiming point Selection (at injection).

   a) Minimize velocity increment required to remove injection bias.

   b) Bias arrival time consistent with a) above.

   c) Insure that a nominal maneuver violated no constraints on the maneuver sequence.

d) Attempt to aim such that the midcourse maneuver would be in such a direction as to cause maximum maneuver execution errors to map parallel to the limb of the planet.

During operations, the final midcourse aiming points were selected by the principal investigators as a function of orbit determination and expected maneuver execution errors so as to maximize the value of the scientific experiments and minimize the likelihood of needing a second maneuver. Avoiding a second maneuver was desirable for reliability reasons.

B. MANEUVER CONSTRAINTS

A number of constraints existed which had to be taken into consideration when calculating midcourse maneuvers. These constraints appeared as limitations on the turns that could be made, the time the maneuver was to be performed, and the possible aiming points that could be selected.

The major considerations affecting the design of the Mariner VI and VII maneuvers were:

1) Due to the CC&S design, turns could be equal to or greater than 0.18 deg, and not larger than approximately 360 deg. The minimum motor burn time was 0.05 sec, the maximum was 102.35 sec. These constraints did not significantly affect the maneuver design.

2) The maneuver had to be performed such that the Earth range and cone angle would allow telecommunications throughout the maneuver. This constraint turned out to be a very important consideration for these missions, and was a factor in deciding to perform the first midcourse maneuver on Mariner VI quite soon after launch.

3) A firm constraint in designing any maneuver was that enough tracking data have been obtained and processed to give an orbit estimate that will not improve appreciably by taking more data.

4) The star acquired by the Canopus tracker had to be known prior to the maneuver computations.

5) The total velocity correction capability for either spacecraft was about 56 m/sec.

6) In order to avoid damage to the UVS, IRS and TVB, it was necessary that the pitch turn lie within the range of -79.5 deg to +180 deg. The 180 deg constraint was necessary to prevent damage to the instruments during reacquisition.

7) It was a desirable constraint for reliability reasons that the sun not pass through the Canopus sensor field of view, which would activate the Canopus sensor sun shutter.

8) It was desirable, if convenient, to limit the pitch turn to lie in the range ±67 deg. This would prevent the power system from using the battery during the maneuver.

9) Due to the geometrical configuration of the spacecraft, an inaccessible cone existed about the plus and minus cruise orientation of pitch axis within which the thrust axis could not be pointed. The half angle of this cone was 1.085 deg for Mariner VI and 1.2625 deg for Mariner VII.

C. MANEUVER IMPLEMENTATION

After the desired post maneuver aiming point was selected by the principal investigators, and orbit determination personnel had determined a best estimate of the trajectory, the required velocity correction was computed by utilizing a linear search scheme with the integrating trajectory program (SPACE). The required pitch and roll turns to align the motor thrust axis along the negative velocity direction were computed, and the number of CC&S pulses required to implement these turns was determined as a function of the spacecraft temperature. The duration of the burn could only be controlled to the nearest 0.05 sec. In order to eliminate the effects of this resolution error as much as possible, a modified velocity correction vector was determined with a burn duration an integral multiple of 0.05 sec, the same spatial miss as before, and a slightly altered time of arrival. This was done since the arrival time was generally a less critical parameter than the spatial miss. Also, a bias was included in selecting the maneuver aiming point to account for the small velocity increment to be caused by unlatching the scan platform at a later time on the trajectory.

After the three maneuver parameters, pitch turn, roll turn, and burn duration, had been computed, the appropriate commands were stored in the CC&S, and the maneuver was executed by ground command.

D. INFLIGHT RESULTS

The accuracy requirements for both Mariners VI and VII were satisfied with only one maneuver for each spacecraft. The maneuver for Mariner VI was computed on February 28, 1969 based on the best estimate of the orbit at that time. It was determined that no constraints were violated, and the motor ignition occurred at $00^h54^m44^s$ GMT on March 1, 1969. The maneuver for Mariner VII proved to be more involved. The standard maneuver with Canopus as the roll position reference would have required a pitch turn of 69.5 deg, causing a battery share condition (tilting the solar panels by this amount).

Maneuver computations were made using the stars Vega and Sirius for the roll reference. A similar problem existed using Vega, but a more advantageous maneuver resulted using Sirius. Consequently, on April 7, 1969, the command was sent to acquire Sirius, the final maneuver calculations were made, and motor ignition occurred at $20^h22^m09^s$ GMT on April 8, 1969.

Table 4-1 indicates the actual maneuver parameters calculated, the commanded maneuvers, which differed from those calculated due to quantization of the commands, and estimates of the actual maneuvers performed. Also given are statistics on the maneuvers. The encounter parameters resulting from injection and the maneuver for each spacecraft are shown in Table 4-2. Table 4-3 shows the sensitivity of the maneuver parameters to the time of maneuver execution. Figures 4-1 and 4-2 show B plane diagrams (see Ref. 27 for B plane definition) of the Mars capture radius with actual and desired injection and maneuver aiming points. The cone and clock angles of the earth and sun during the midcourse turns for each spacecraft are given in Figures 4-3 and 4-4.

Figure 4-5 shows the 1 m/sec capability ellipses at the time of the maneuver for each spacecraft along with actual and desired injection aim points and desired post maneuver aim points. The actual post maneuver values quoted are exclusive of the effects of the scan platform unlatch. Although the nominal arrival times for Mariner VI and VII were $05^h18^m00^s$ and $05^h05^m00^s$ respectively,

Table 4-1. Mariner VI and VII Maneuver Parameters and Statistics

	Mariner VI			Mariner VII		
	PT (deg)	RT (deg)	ΔV (m/sec)	PT (deg)	RT (deg)	ΔV (m/sec)
Computed	-23.33	78.68	3.0679	-35.64	-12.83	4.2920
Commanded:						
Values	-23.44	78.72	3.0679	-35.58	-12.84	4.2920
Times (sec)	130.0	454.0	5.350	193.0	71.0	7.600
Best estimate of actual value	-24.11	77.97	3.1456	-36.25	-12.65	4.2879
Estimated error	-0.67	-0.76	0.0777	-0.67	0.19	-0.0041
A priori standard deviation	0.400	0.378	0.038	0.384	0.352	0.054
Error in standard deviations	1.68	2.01	2.04	1.74	0.54	0.076
Standard deviations in estimate of actual value	0.23	0.03	0.008	0.077	0.185	0.015

the desired times shown above for the midcourse maneuver are those which were determined to lead to zero resolution error as discussed in the text.

MCR is the midcourse correction requirement to null the injection error at the time of the maneuver; that is, the velocity required to alter the trajectory to pass through the desired injection aim point rather than that actually achieved.

E. MANEUVER PROGRAM

This section will be devoted to a description of the computer program used in flight operations to do maneuver calculations, including trajectory integration, determination of velocity correction requirements, maneuver parameter calculations, and analyses of constraints and statistics. The program, called MOPM (Maneuver Operations – Mariner), ran on the IBM 7094

Table 4-2. Desired and Actual Encounter Parameters and Statistics

	Mariner VI		Mariner VII	
	Desired	Actual	Desired	Actual
Injection				
$\overline{B} \cdot \overline{R}$ (km)	-17900	-13077	18109	29324
$\overline{B} \cdot \overline{T}$ (km)	5920	3684	-1324	-6840
TCA	7-31-69 05:46:39	7-31-69 04:41:26	8-05-69 05:10:18	8-05-69 04:49:13
MCR (m/s)	2.075		1.936	
Midcourse				
$\overline{B} \cdot \overline{R}$ (km)	-643	-410	3439	3537
$\overline{B} \cdot \overline{T}$ (km)	7400	7786	6520	6669
TCA	7-31-69 05:17:26	7-31-69 05:18:44	8-05-69 05:01:02	8-05-69 05:00:11
Miss in number of standard deviations	0.29		0.25	

computer under the trajectory monitor JPTRAJ. It consisted of nine subprograms, each of which could be run serially or individually, to perform various tasks of the overall maneuver determination and analysis problem. Brief descriptions of the functions of each of these subprograms follows. (See Figure 4-6).

INTRO-INTRO is the basic control link of MOPM. It interfaces with the orbit determination program to obtain the best estimate of the achieved trajectory initial conditions, calls other subprograms to determine the resulting trajectory, and prints all input, in addition to preliminary trajectory data. Control of MOPM returns to INTRO after the execution of any requested series of subprograms.

Table 4-3. Sensitivity of Maneuver Parameters to Maneuver Time

Mariner VI*				
Date	Maneuver Time (GMT)	ΔV (m/sec)	PT (deg)	RT (deg)
2/28	00:50:00	3.122	-23.65	78.66
3/01	00:50:00	3.073	-23.49	78.38
3/02	00:50:00	3.032	-23.31	78.11
3/07	00:50:00	2.874	-22.12	76.88
Mariner VII*				
4/02	20:30:00	4.332	-40.32	-13.75
4/05	20:30:00	4.300	-38.46	-13.32
4/08	20:30:00	4.282	-36.64	-13.02
4/12	20:30:00	4.273	-34.24	-12.79
*Mariner VI turns are based on a Canopus roll reference, Mariner VII turns on a Sirius roll reference.				

SPACE-SPACE is the single precision trajectory program which is used for all trajectory integration in MOPM, and is called by a number of the other subprograms for this purpose.

SEARCH-SEARCH is a program which iteratively determines the required values of a set of independent variables in order to achieve a specified set of dependent variables. In this application, it uses SPACE to determine the required velocity components for a fixed set of position components to achieve specified values of $\overline{B} \cdot \overline{R}$, $\overline{B} \cdot \overline{T}$ and time of flight. The maneuver is assumed to be impulsive, or of zero time duration.*

*After the maneuver has been calculated (modified to satisfy any constraints as required) SPACE is run with an integrated burn. If this results in a significant change, a bias is introduced to eliminate this change and the entire process is repeated.

ANAPAR-ANAPAR supplies analytic partials of the encounter parameters with respect to the velocity components for use in SEARCH

DECPR – the DECPR subprogram computes the maneuver parameters (pitch and roll turns) required to implement the velocity correction vector determined in SEARCH. It then evaluates this maneuver for various constraints, such as antenna pointing during the turns for communications, a requirement to point the motor in the inaccessible cone, or a velocity magnitude exceeding the spacecraft capability. Logic exists to modify the maneuver in a minimal way, if possible, to satisfy the constraints, and determines the consequences of these modifications. The modification to eliminate the timer resolution error discussed previously is also done in this link.

PRPLS-PRPLS simulates the midcourse propulsion system, and uses such data as maneuver velocity magnitude, spacecraft temperatures and pressures, and engine operating characteristics to determine the required burn duration. The subprogram is used iteratively with DECPR in determining the modified velocity which nulls the resolution error.

COMGN-COMGN originally was used to convert the final maneuver parameters into a binary code to be transmitted to the spacecraft. This function was performed elsewhere for the '69 mission, but the link was retained because of other calculations performed within it. Among these were post maneuver encounter statistics, the probability of impacting the planet for a given maneuver, the change in geocentric range rate during the maneuver, and various angles during the turns, including the cone and clock angles of various inertial directions, the angles between spacecraft fixed vectors and inertial directions, and the celestial latitude and longitude of spacecraft fixed vectors. COMGN also writes a save tape for telecommunications analysis.

CAPEL-CAPEL is a capability ellipse generator and is used only for maneuver analysis for non-standard events, such as very large injection errors.

PLOTZ-PLOTZ is a plotting routine which may be called to plot capability ellipses, execution and OD error ellipses, residual miss data from DECPR, and cone and clock angles of the Earth and Sun during the turns.

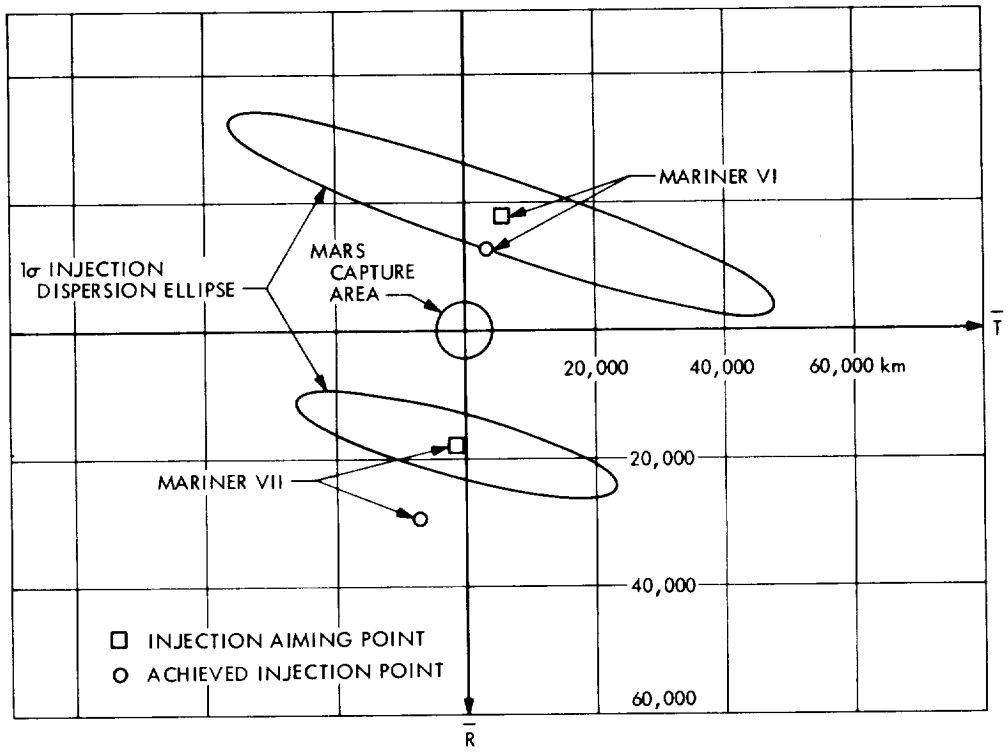

Figure 4-1. Injection Dispersions and Aiming Points

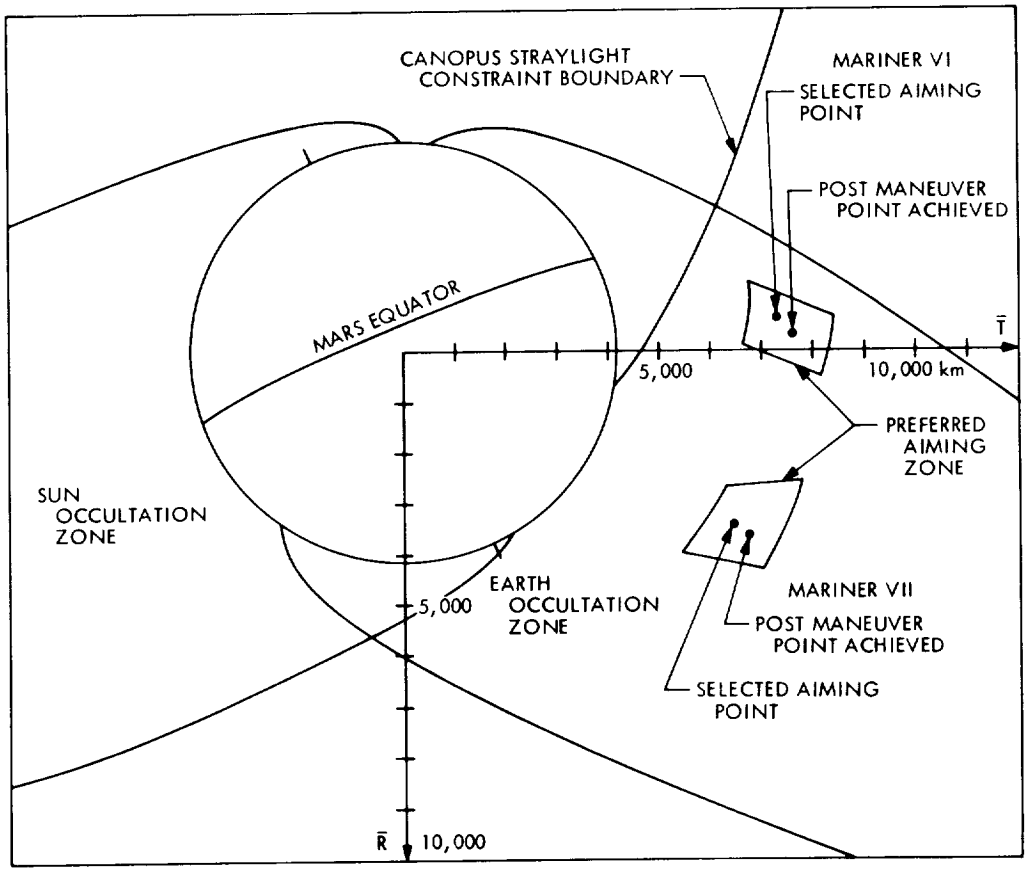

Figure 4-2. Midcourse Aiming Points and Encounter Geometry for Mariners VI and VII

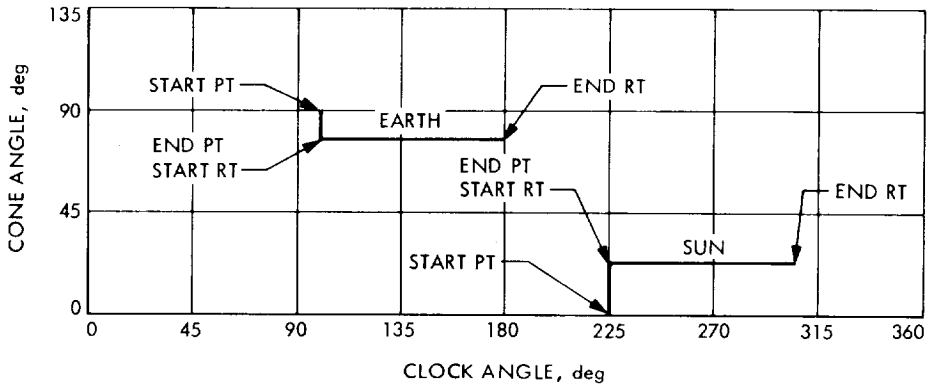

Figure 4-3. Cone and Clock Angles of Sun and Earth During Midcourse Turns, Mariner VI

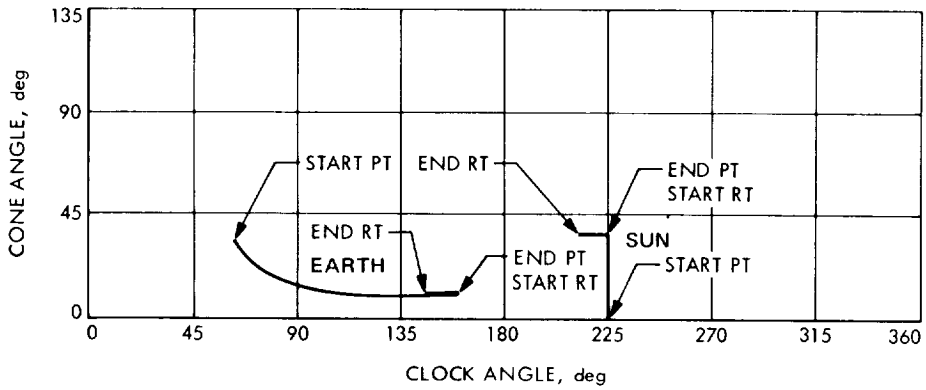

Figure 4-4. Cone and Clock Angles of Sun and Earth During Midcourse Turns, Mariner VII

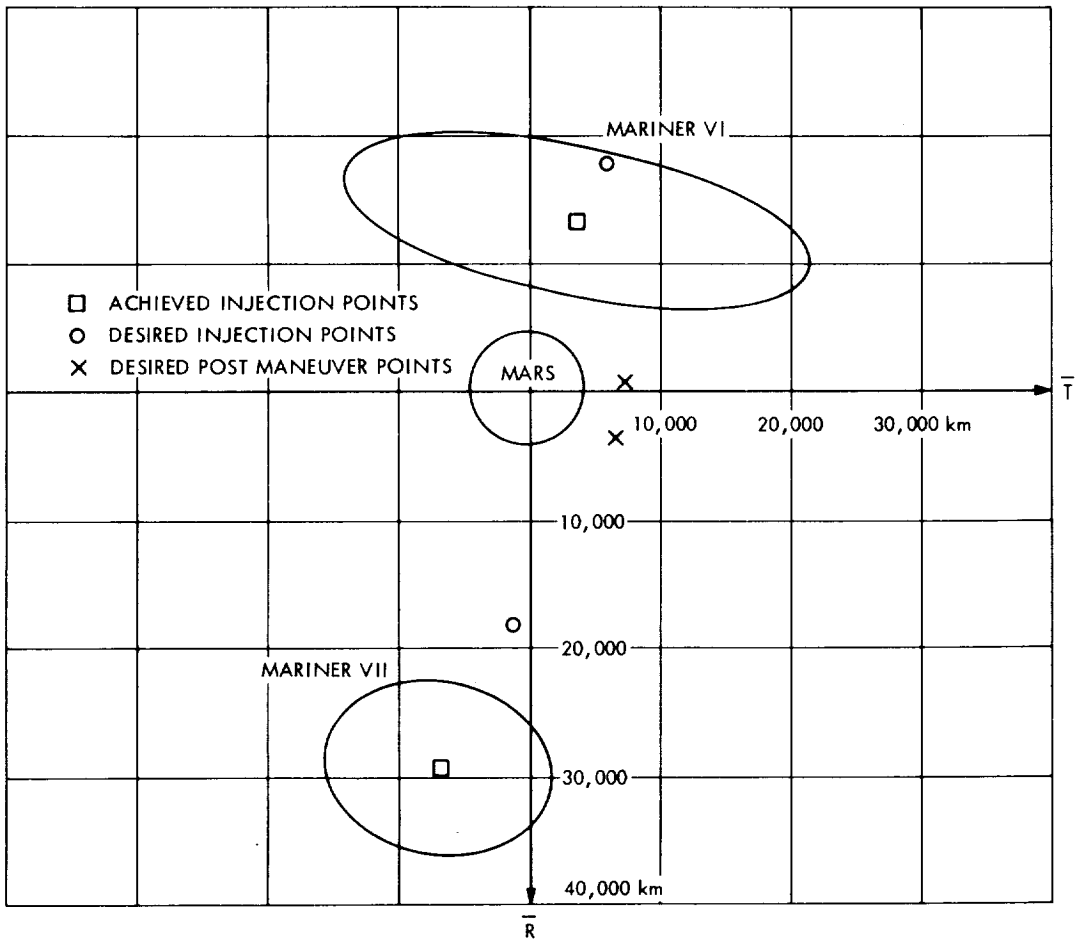

Figure 4-5. One m/sec Capability Ellipses and Aiming Points

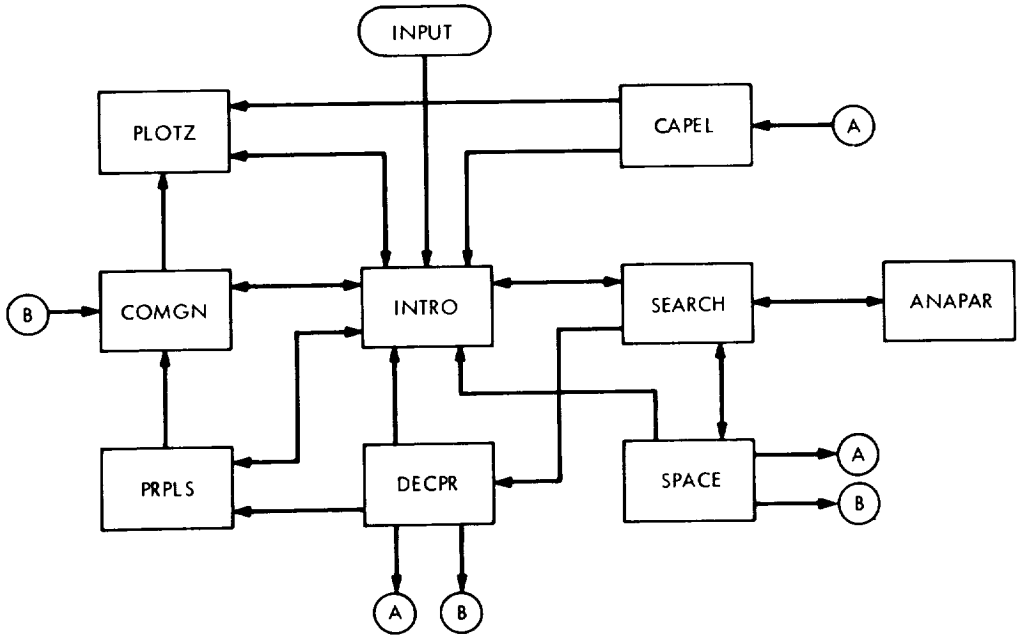

Figure 4-6. MOPM Flow Diagram

SECTION V
OPTICAL OBSERVABLES

J. E. Ball, W. G. Breckenridge, T. C. Duxbury, R. E. Koch

A. INTRODUCTION

This section describes the results of the optical-approach navigation experiment on the 1969 Mariner Mission to Mars. Telemetered data from the Mariner spacecraft (Mariner VI and Mariner VII) were used with earth-based doppler data to estimate the trajectories of both spacecraft in near-real time operations. The telemetered data used included television (TV) pictures of Mars and measurements of the TV pointing direction and spacecraft attitude during the last few days before encounter. Processing of these data yielded the spacecraft-centered and celestially-referenced direction to Mars; the direction was used as the observable in a trajectory-estimation process. The experiment represented the first effort to use spacecraft-based data from an interplanetary spacecraft for the purpose of navigation. The experiment has laid the ground work for future interplanetary missions requiring spacecraft-based navigation data by demonstrating the feasibility of using this data type, within mission time constraints, to successfully produce trajectory estimates.

B. SPACECRAFT MEASUREMENT SYSTEM

Instruments aboard the Mariner spacecraft which were used to obtain navigation data included the narrow-angle TV camera, the far-encounter planet sensor (FEPS), the two-degree-of-freedom scan platform, and the attitude-control sensors. The TV camera and FEPS were mounted on the scan platform (Fig. 5-1) such that their optical axes were parallel. During Mars approach, the FEPS provided error signals for controlling the two gimbal axes of the scan

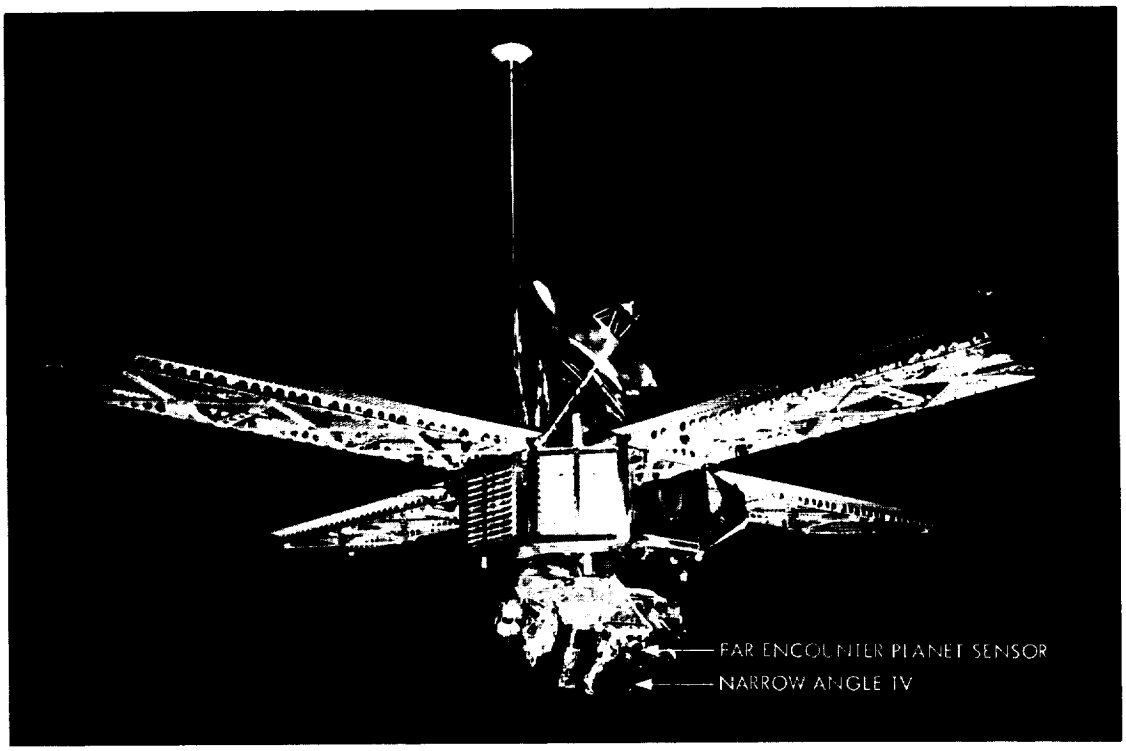

Figure 5-1. Mariner Mars 1969 Spacecraft

platform to keep the TV camera pointed at Mars. The attitude-control sensors (Fig. 5-2) consisted of a two-axis sun sensor and a star sensor. These sensors produced error signals which acted through electronics and gas jets to control the spacecraft attitude with respect to the sun and the star, Canopus. The FEPS and attitude-control sensor error signals, the position of the scan platform gimbals, and TV picture of Mars were telemetered to earth during the approach to Mars.

C. SPACECRAFT-BASED OBSERVABLE EQUATIONS

The spacecraft-centered direction to Mars, $\hat{p}$ (Fig. 5-3) in a celestial reference coordinate system is measured by combining measurements (Fig. 5-4) from the spacecraft instruments. The line-of-sight to Mars, $\hat{V}$, is defined in the TV or planet sensor measurement system. The transformation from the nominal measurement system to the celestial reference system, L, is computed from the scan platform gimbal angle and attitude-control sensor measurements. The transformation from nominal to actual measurement coordinates (I + E),

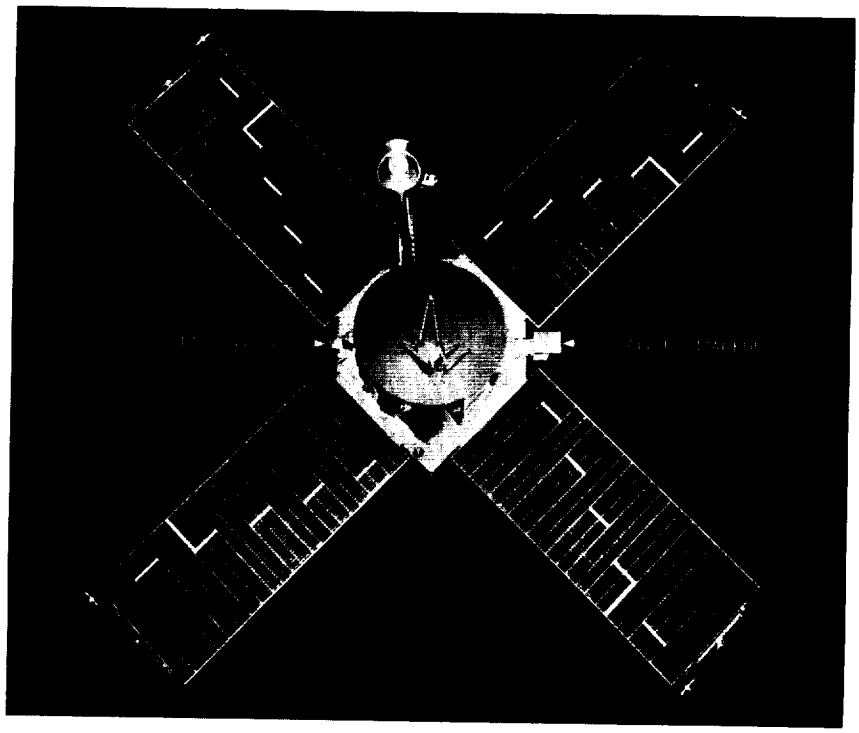

Figure 5-2. Celestial Sensors

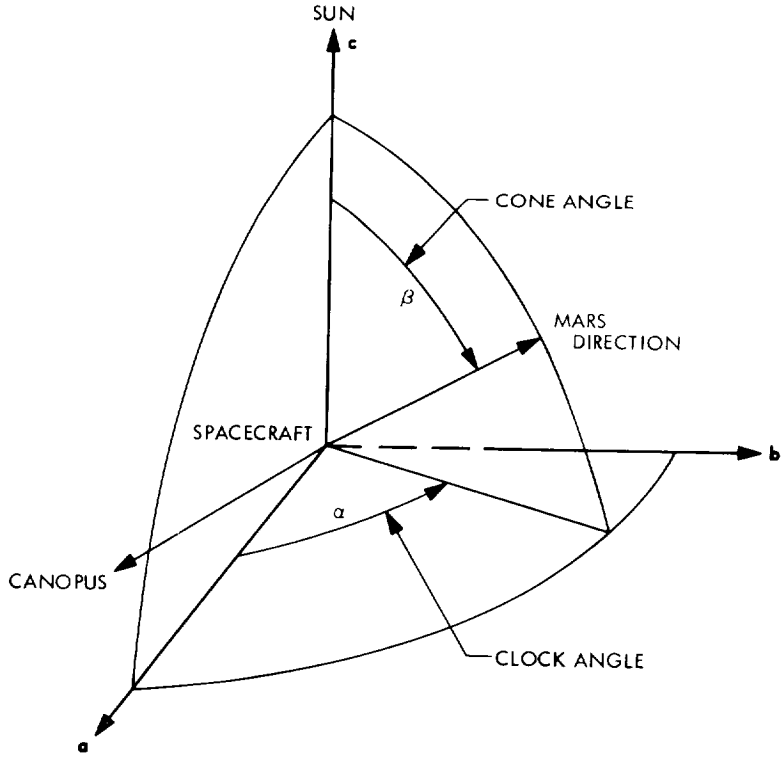

Figure 5-3. Mars Celestial Direction

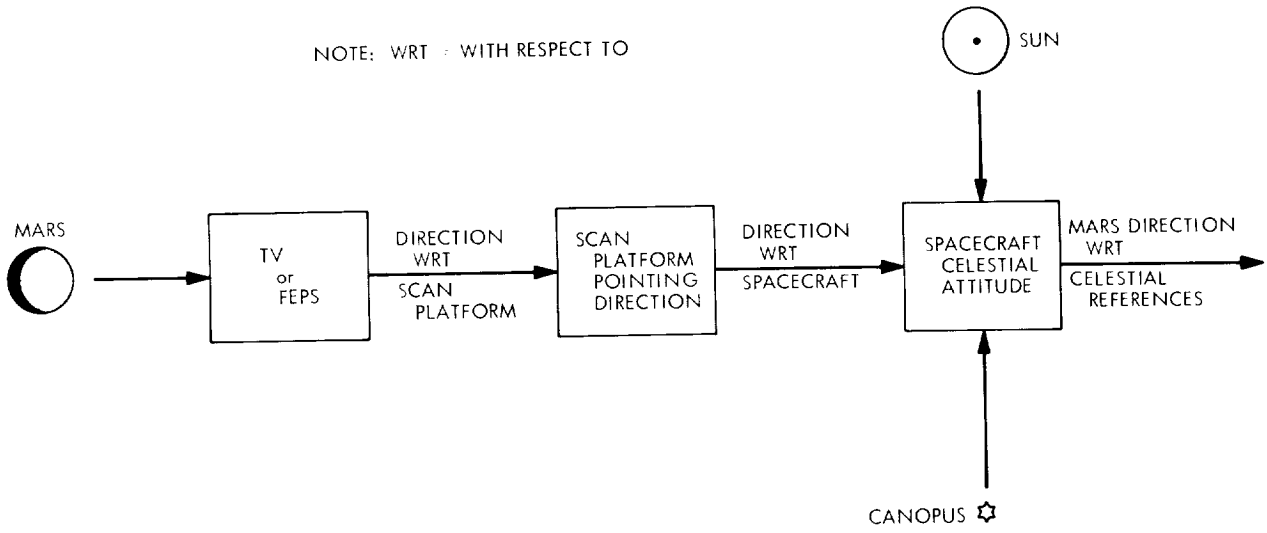

Figure 5-4. Determination of Mars Direction

contains all the measurement error sources (except noise) mapped into $\bar{\epsilon}$, three equivalent coordinate rotations. Assuming that these are small angles, the transformation is represented as

$$(I + E) \approx \begin{bmatrix} 1 & \epsilon_3 & -\epsilon_2 \\ -\epsilon_3 & 1 & \epsilon_1 \\ \epsilon_2 & -\epsilon_1 & 1 \end{bmatrix} \tag{1}$$

where

$$\bar{\epsilon} = \begin{bmatrix} \epsilon_1 \\ \epsilon_2 \\ \epsilon_3 \end{bmatrix} = \begin{bmatrix} e_1 + k_1\Phi + d_1 \\ e_2 + k_2\Phi + d_2 \\ e_3 \end{bmatrix} \tag{2}$$

The terms e_1, e_2, and e_3 represent the three equivalent constant biases; k_1 and k_2 are two proportional center-finding errors; d_1 and d_2 are the two drifts; and Φ is angular diameter. Subscripts m and n are used to denote measured and nominal vectors.

The actual spacecraft-planet vector is perturbed from the nominal by $d\hat{p}$. This is mapped to the actual sensor measurement coordinate system and perturbed by noise $\bar{\eta}_v$ to obtain the equation for $\hat{V}_m$

$$\hat{V}_m = (I + E)L^{-1}(\hat{p}_n + d\hat{p}) + \bar{\eta}_v \tag{3}$$

This sensor measurement is mapped to the celestial coordinate system by L and differenced with the nominal to get the measured deviation from nominal

$$d\hat{p}_m = L\hat{V}_m - \hat{p}_n = L(I + E)L^{-1}(\hat{p}_n + d\hat{p}) - \hat{p}_n + L\eta_v \tag{4}$$

Using $\hat{p}_n = L\hat{V}_n$ and keeping only first order error terms,

$$d\hat{p}_m = d\hat{p} + LE\hat{V}_n + L\bar{\eta}_v \tag{5}$$

Two of the observables used in the demonstration were the Mars clock angle α and cone angle β defined in the celestial reference coordinate system with axes $\hat{a}$, $\hat{b}$, and $\hat{c}$.

$$\hat{c} = (\bar{R} - \bar{r})/|\bar{R} - \bar{r}| = \left[c_1 c_2 c_3\right]^T$$

$$\hat{b} = (\hat{c} \times \hat{C})/|\hat{c} \times \hat{C}| = \left[b_1 b_2 b_3\right]^T \tag{6}$$

$$\hat{a} = \hat{b} \times \hat{c} = \left[a_1 a_2 a_3\right]^T$$

where $\bar{r}$ is the Mars-spacecraft vector, $\bar{R}$ is the Mars-sun vector, and $\hat{C}$ is the spacecraft-Canopus direction. The transformation M, from a Mars-centered inertial reference system to the abc system, is expressed as

$$M = \begin{bmatrix} a_1 & a_2 & a_3 \\ b_1 & b_2 & b_3 \\ c_1 & c_2 & c_3 \end{bmatrix} \tag{7}$$

The actual spacecraft-Mars direction, expressed as a function of $\bar{r}$, is given by

$$\hat{p} = -M \frac{\bar{r}}{|\bar{r}|} = -M\hat{r} = \begin{bmatrix} p_a \\ p_b \\ p_c \end{bmatrix} \tag{8}$$

where p_a, p_b, p_c are the abc direction cosines of $\hat{p}$. Mars clock and cone angles are expressed as

$$\begin{aligned} \alpha &= \tan^{-1}(p_b/p_a) \\ \beta &= \cos^{-1}(p_c) \end{aligned} \tag{9}$$

The partial derivative of measured clock and cone angles with respect to the measured Mars direction is obtained from Eq. (9).

$$\begin{bmatrix} d\alpha \\ d\beta \end{bmatrix}_m = \begin{bmatrix} -\frac{\sin\alpha}{\sin\beta} & \frac{\cos\alpha}{\sin\beta} & 0 \\ \cos\alpha\cos\beta & \sin\alpha\cos\beta & -\sin\beta \end{bmatrix} d\hat{p}_m = A d\hat{p}_m \tag{10}$$

The partial derivative of the measured Mars direction with respect to the spacecraft state mass of Mars, and measurement errors is obtained from Eqs. (5) and (8), giving

$$d\hat{p}_m = -M\, d\hat{r} + PL\, d\bar{\epsilon} + L\bar{\eta}_v \tag{11}$$

where

$$P = \begin{bmatrix} 0 & -p_c & p_b \\ p_c & 0 & -p_a \\ -p_b & p_a & 0 \end{bmatrix} \tag{12}$$

The deviations of the observables from variations of the parameters to be estimated and random noise are obtained by combining Eqs. (10) and (11) to give

$$\begin{bmatrix} d\alpha \\ d\beta \end{bmatrix}_m = -AM\, d\hat{r} + APL\, d\bar{\epsilon} + \bar{n} \tag{13}$$

where $\bar{n}$ is the measurement noise, $\bar{\eta}_v$, mapped to α and β as

$$\bar{n} = AL\bar{\eta}_v$$

Parameters estimated in the investigation were the spacecraft state and mass of Mars defining $d\hat{r}$ and the measurement errors, e_1, e_2, e_3, k_1, k_2, d_1, and d_2.

From Eqs. (2) and (13) and the partial derivative matrix, Q, of $\hat{r}$ with respect to the six state parameters and mass of Mars, the deviations of the observables, α and β, with respect to the six orbital parameters and seven measurement errors used in the linear estimation process are

$$\begin{bmatrix} d\alpha \\ d\beta \end{bmatrix}_m = \left\{ -AMQ \;\middle|\; APL \begin{bmatrix} 1 & 0 & 0 & \Phi & 0 & 1 & 0 \\ 0 & 1 & 0 & 0 & \Phi & 0 & 1 \\ 0 & 0 & 1 & 0 & 0 & 0 & 0 \end{bmatrix} \right\} \begin{bmatrix} d\bar{q} \\ d\bar{e} \end{bmatrix} \qquad (14)$$

where

$$d\bar{e} = \left[e_1 e_2 e_3 \; k_1 k_2 \; d_1 d_2 \right]^T$$

D. MISSION OPERATIONS

The near-Mars phase of the MM'69 mission was divided into two phases: far encounter (FE), and near encounter (NE). The FE phase began a few days before Mars encounter and continued until a few hours before Mars encounter. Directly following FE was NE which continued until one hour past encounter (E + 1h). During FE, the scan platform pointing was controlled by the FEPS and a TV picture was recorded about every 40 min. Recorded pictures were played back to earth while the spacecraft was being tracked by the Deep Space Network station at Goldstone, California. FEPS, scan platform, and attitude-control measurements were telemetered to earth in real time as part of the spacecraft engineering data. The optical-approach navigation experiment used data from FE.

The FE TV picture sequences of the first spacecraft, Mariner VI, and the second spacecraft, Mariner VII, are illustrated in Fig. 5-5. The MM'69 mission was committed to make the Mariner VI TV and engineering data available to the optical-approach navigation experiment before E - 20h. For Mariner VII, the mission was committed to make the first sequence of data available before E - 40h and the second sequence of data available before E - 20h. The last sequence of FE data from either spacecraft would not be used in real time so that the navigation experiment would not interface with the mission at the height of its pre-encounter operations. Trajectory estimates for the spacecraft, based on available earth-based and spacecraft-based data, were to be made available to the mission before E - 12h.

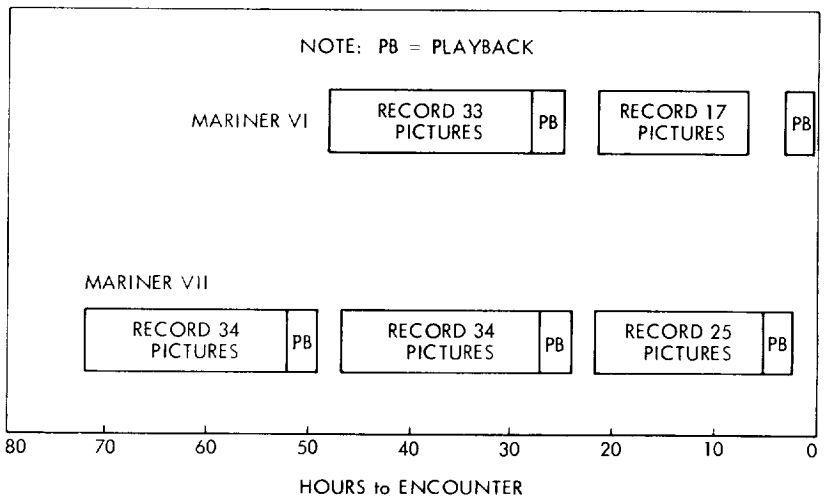

Figure 5-5. Far-Encounter Picture Sequence

A block diagram showing the software programs and information flow of the software system for the real time demonstration is shown in Figure 5-6.

All programs to the right of the dashed line were part of the real time approach on-board demonstration while the programs and other data to the left of the dashed line were part of the mission real time system. There were two programs computing corrections to the spacecraft orbit, one was the Radio Optical Orbit Determination Program (ROODP) and the other was the Optical Observable Processor Program (OOPP). The difference between the two programs are described in a later section. The solutions for the spacecraft's orbit from the two programs were monitored by the FPAC Director and available for his use only.

The operating policy of the demonstration was that it would have minimum interference with the routine operations of the mission. The nominal trajectory used for processing the optical data was obtained from Earth-based data taken before the beginning of FE. The mission computers were used to process the data only during the regular idle period of the mission operations.

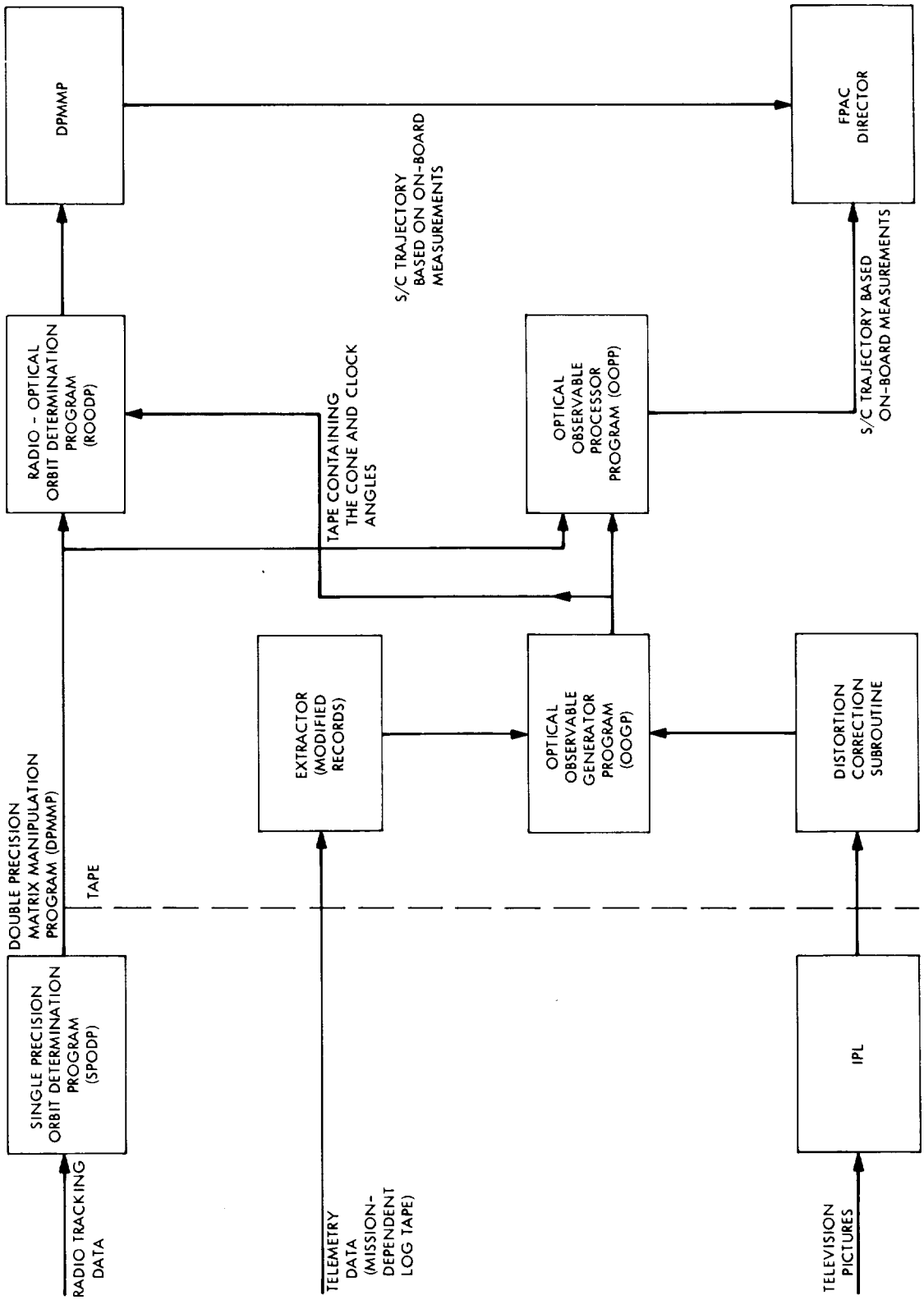

Figure 5-6. Software Programs

E. REAL-TIME OPERATIONS

Telemetered engineering data from Mariner VI were obtained at E - 46h, E - 36h, and E - 20h. The TV pictures were available at E - 25h. These data were processed at the scheduled times of E - 44h, E - 34h, and E - 20h. Trajectory estimates were available within a short period after these times.

The time needed for processing the raw data to produce a trajectory estimate was approximately two hours. A majority of this time (~1. 5h) was used to determine the location of the center of Mars in the TV pictures. Locations determined by two observers were averaged. Approximately 30 min were needed at the computer site to obtain a trajectory estimate from the formatted input data. Each of the three computer programs comprising the software system used about three minutes of central processor time (IBM-7094). The remainder of the 30 min was used for input/output and output evaluation.

Telemetered engineering data from Mariner VII were obtained at E - 70h, E - 46h, and E - 20h. The TV pictures were available at E - 48h, E - 25h, and E - 20h. These data were processed at the scheduled times of E - 68h, E - 44h, and E - 20h. Because a trajectory anomaly affected the earth-based tracking data and because of the success of the navigation experiment on Mariner VI, the FE sequence of events was changed to allow the experiment to obtain an additional 10 pictures during the period E - 24h to E - 22h to help estimate the trajectory of Mariner VII.

All of the real-time objectives of the experiment were met. Spacecraft-based measurements were obtained from the Mariner spacecraft and processed by navigation software developed for the experiment. The data gathering and processing were performed in near real time, and trajectory estimates were made available to mission operations for use in encounter operations.

F. MARINER VI RESULTS

Mariner VI encountered Mars at 05:19 GMT on July 31, 1969. The spacecraft operations associated with taking on-board measurements for navigation started two days earlier (E - 2d) when the scan platform was pointed toward Mars. In each of these two days was a TV picture sequence. The spacecraft data and TV pictures (Figs. 5-7 and 5-8 are typical of FE) from this far-encounter period were used to obtain estimates of the Areocentric trajectory.

Figure 5-7. Mariner VI Picture

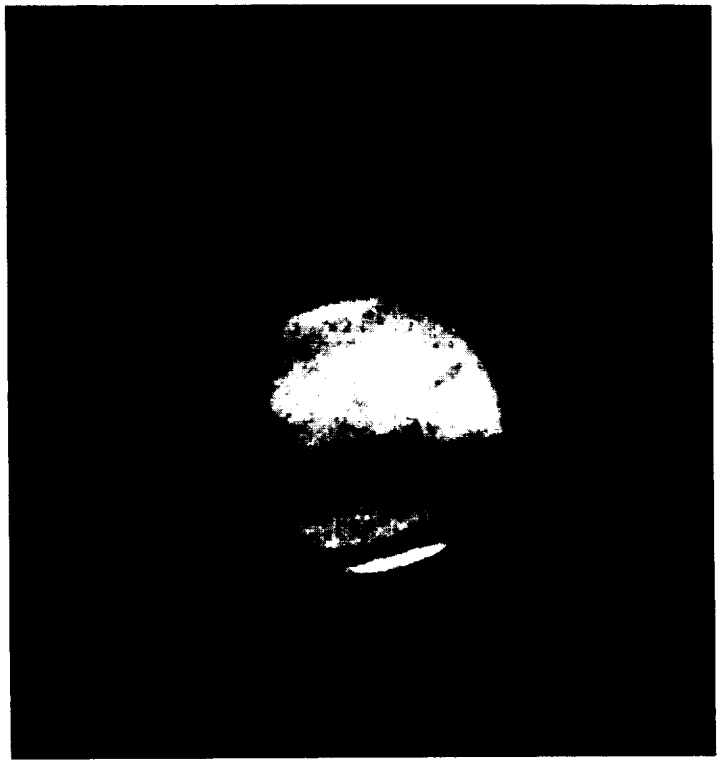

Figure 5-8. Mariner VII Picture

Initial estimates and *a priori* statistics were based on radio tracking data. Short data arcs were used to produce these starting conditions so that the initial estimate differed from the best estimate available at that time and the *a priori* statistics were fairly "loose." This was done so that the optical data would be able to change the estimate.

The parameters of the trajectory to be used in presenting the results are the coordinates in the B plane (Fig. 5-9) of the approach asymptote intersection, $\bar{B} \cdot \bar{R}$ and $\bar{B} \cdot \bar{T}$. The uncertainty of this aim point will be given as the 1σ(40%) error ellipse in the B plane, the semi-major axis $\times$ the semi-minor axis oriented at the angle θ (clockwise) from $\bar{T}$ to the major axis. For Mariner VI the nominal (*a priori* for approach navigation) aim point was (-15 km, 7489 km) with an error ellipse of 361 km $\times$ 79 km at -75 deg. The current best estimate, as determined from the latest radio tracking data, is (-336 km, 7596 km) and will be referred to as the true aim point.

To demonstrate the feasibility of using these spacecraft-based data for mission operations, the data were processed as they became available and trajectory estimates were made in near-real time. Twenty four of the 34 far-encounter TV pictures were used. Of the pictures not used, two were only partial pictures of Mars; the times associated with three of the pictures were not accurately known, and five pictures were not available to the experiment during the near-real time operations. The 24 pictures were taken during the time period from E - 46h to E - 31h. Engineering data were obtained for the time period from E - 49h to E - 20h. The pre-encounter trajectory estimate using the TV data is shown in Fig. 5-10. The deviation of this trajectory estimate from the true trajectory (~50 km) is well within the uncertainty of the estimate (~300 km - 1σ). The deviation of the pre-encounter trajectory estimate using FEPS data from the true trajectory was over 700 km. This deviation is attributed to the difference of the flight performance of the FEPS from the expected performance as determined from pre-flight calibration.

After encounter, a complete set of data was collected, filling gaps of, and extending, the data obtained in near-real time. A total of 46 TV pictures and 40h of planet tracking was then available. These data were used to estimate the trajectory using the *a priori* trajectory parameter covariance matrix with both the *a priori* and current best (true) trajectories.

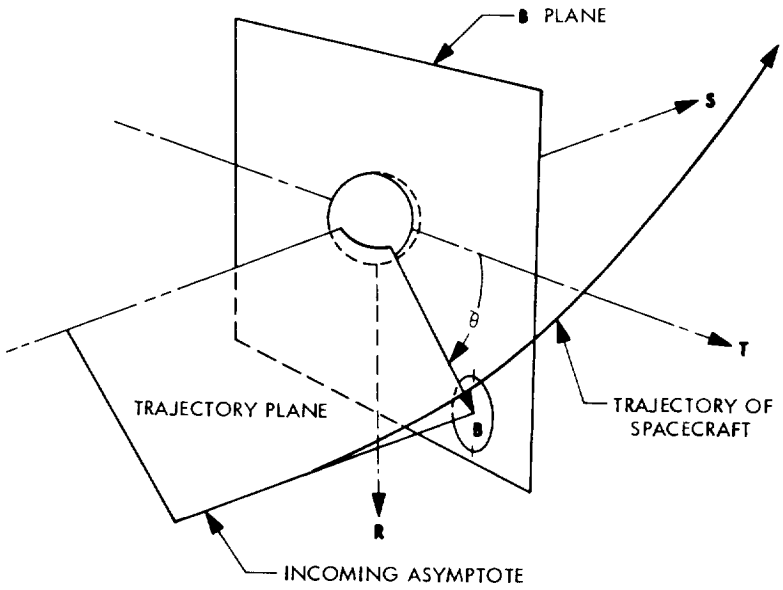

Figure 5-9. B-Plane Sketch

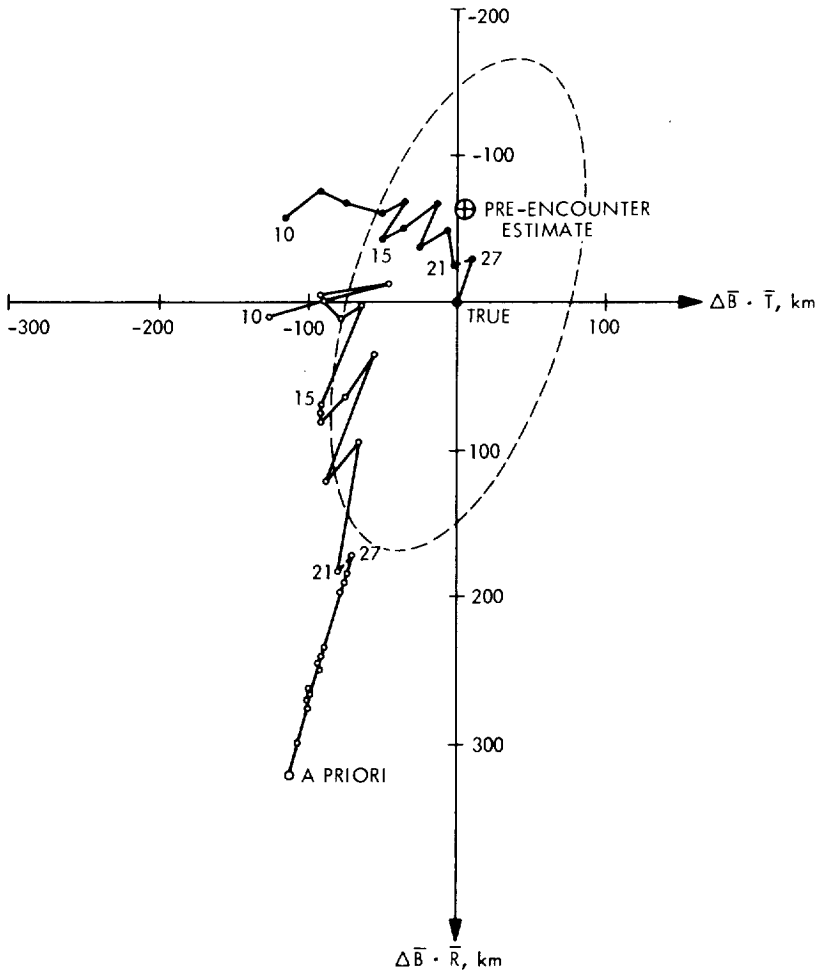

Figure 5-10. Mariner VI Aim-Point Estimates and Error Ellipse Using TV Data

The results of using the TV data are shown in Fig. 5-10 as the trace of the estimated aim point with respect to the true aim point. Time marks along the trace indicate the number of hours to encounter. The error ellipse, centered on the true aim point, shows the expected uncertainty of the estimated aim point at 10h from encounter, the time of the last TV picture used. This ellipse is 173 km × 74 km at -74 deg. After E - 24h, there is a shift in the negative $\overline{T}$ direction, apparently caused by a systematic or unmodeled error source. The most likely source for this error is a change in the ability to locate the planet center in the TV picture as the image gets larger and begins to fill the field of view. Even with this shift, the estimate has just over a 1σ error in the $\overline{T}$ direction and much less than 1σ in the $\overline{R}$ direction.

The estimate using FEPS data showed a large systematic error from the beginning. The FEPS error signals at the times of TV pictures and the TV coordinates of the planet center were used to re-calibrate the FEPS with respect to the TV frame. The OOGP was re-run using the new calibration and the output used for trajectory estimation. The results are shown in Fig. 5-11 as the traces of the estimated aim point. These traces now follow very closely the TV estimates up to E - 24h from where the estimates still degrade badly. Again a systematic error in modeling the FEPS response to a larger, brighter Mars is suspected. This also appears as a significant signature in the residuals, measurement deviations not corrected by the estimated parameters. Figure 5-12 shows the clock angle residuals for the day before encounter. Also evident are deviations of the estimate spaced 24h apart, indicating shifts in the tracked center of brightness as Martian surface features move across the planet image. The error ellipse shown in Fig. 5-11 is 183 km × 74 km at -74 deg.

For Mariner VI the estimate of the trajectory using TV data was within the expected range of uncertainty, while the estimate based on FEPS data was good to E - 24h but not after this time. Work is continuing on the evaluation of the sensor performance and on improvements in the data-processing techniques and software.

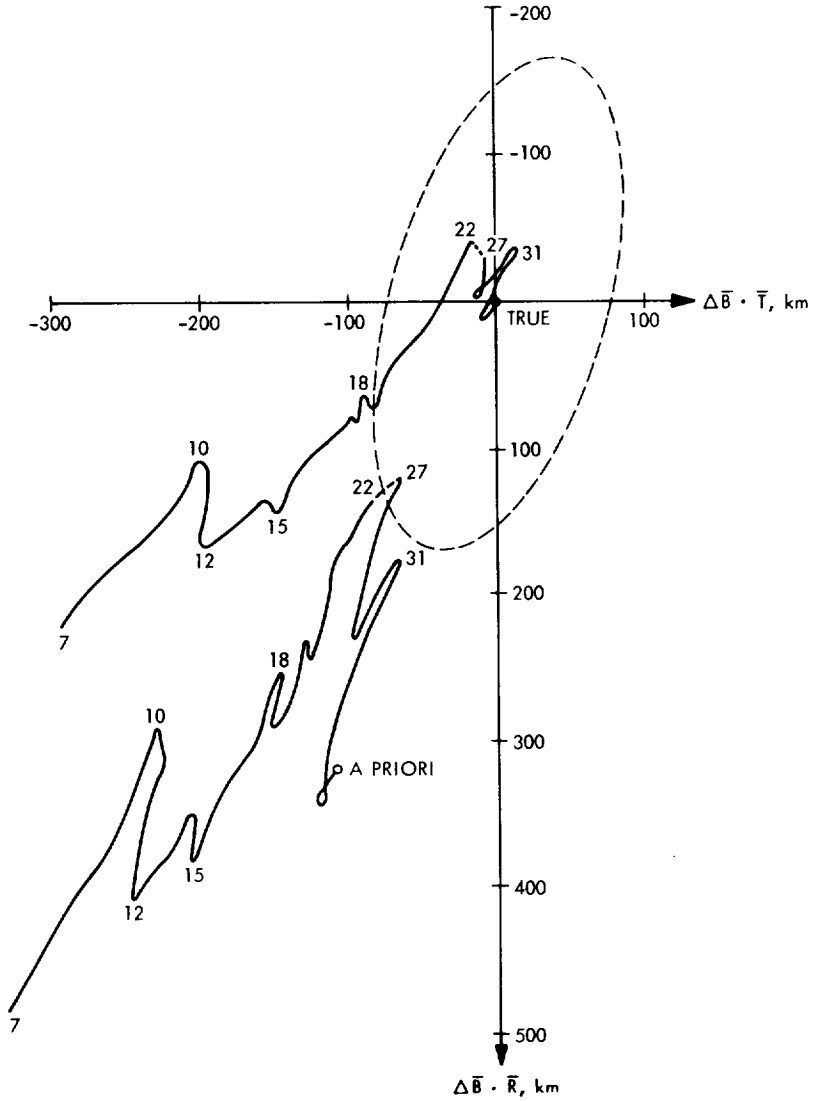

Figure 5-11. Mariner VI Aim-Point Estimates and Error Ellipse Using FEPS Data

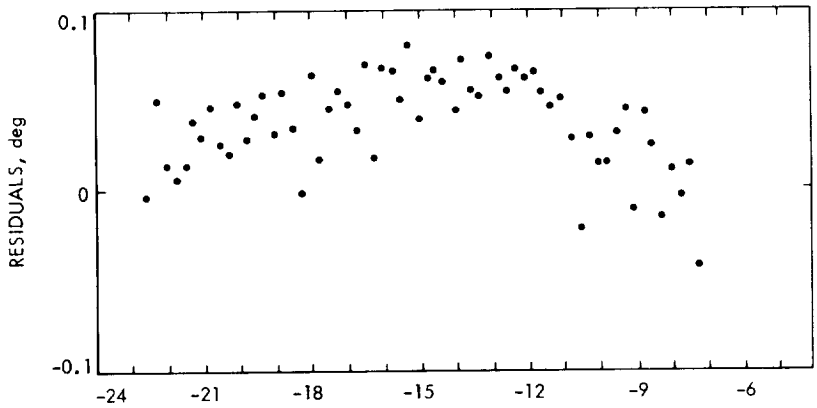

Figure 5-12. Mariner VI Residuals of FEPS Derived Clock Angle Between E - 24 and E - 6 Hours

G. MARINER VII RESULTS

Mariner VII encountered Mars at 05:01 GMT on August 5, 1969 after three days of planet tracking and TV picture taking. However, a few days earlier Mariner VII had experienced a "happening" from which it recovered but without some telemetry channels. Among those channels lost were the fine sun-sensor signals, gyro position signals, FEPS error signals, cone gimbal coarse and fine readouts, and clock gimbal coarse readout. The approach navigation measurements left were the coarse sun sensors and star tracker, the clock gimbal fine readout, and the TV pictures, from which it was possible to reconstruct only the clock angle measurement of planet direction using TV data, and the scan platform clock position, assumed to point to Mars if the planet tracking error averaged zero.

Since the "happening" affected the trajectory of the spacecraft, the radio tracking data for the *a priori* trajectory was doppler data from E - 5d to E - 3d, and the only parameters solved were six trajectory coordinates, the mass of Mars, and three small forces acting on the spacecraft. This gave an *a priori* aim point of (3799 km, 6759 km) with an error ellipse of 360 km × 182 km at -74 deg. The current best estimate (true aim point) is (3615 km, 6720 km).

Modifications were made to the software to account for lost data, and the spacecraft trajectory estimates were made in near-real time as planned. Fifty-three far-encounter TV pictures were used: 26 from the first sequence, 17 from the second sequence, and 10 from the additional sequence. The pictures were taken during the time period from E - 67h to E - 22h. Engineering data were used from the time period E - 68h to E - 20h.

The pre-encounter trajectory estimate using TV data is shown in Fig. 5-13 and the estimate using scan-platform pointing direction is shown in Fig. 5-14. The estimate using TV data was more accurate than the estimate using scan-platform data. Both trajectory estimates were within their expected accuracy from the true trajectory.

After encounter, the complete data set collected had a total of 65 TV pictures and 50h of planet tracking. Using only the clock-angle measurement, trajectory estimates were made using the *a priori* trajectory covariance matrix and both the *a priori* and true trajectories.

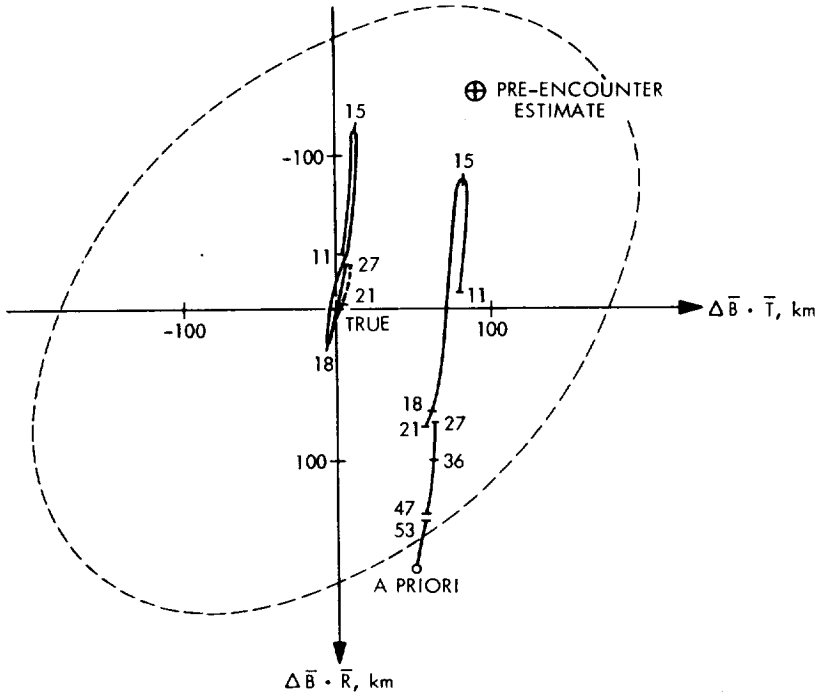

Figure 5-13. Mariner VII Aim-Point Estimates and Error Ellipse Using TV Data

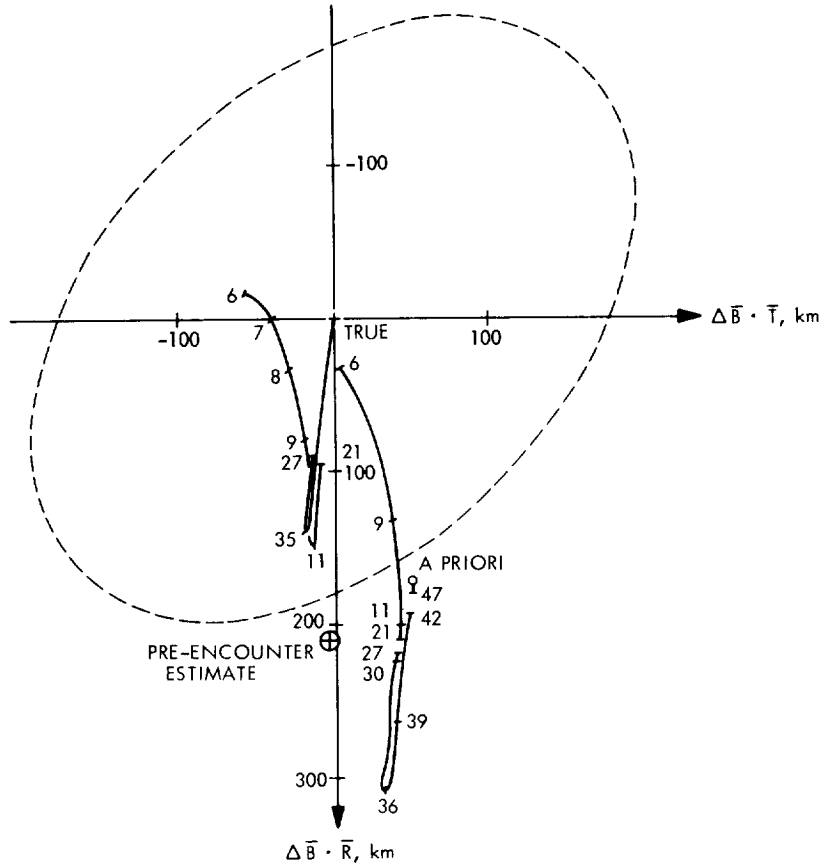

Figure 5-14. Mariner VII Aim-Point Estimates and Error Ellipse Using Platform Clock Angle

The time marked traces of the estimates using TV data are shown in Fig. 5-13, referenced to the true aim point. The error ellipse showing the expected 1σ deviation of the estimate from the true aim point, at the last picture time, is 223 km × 151 km at -40 deg. The television data estimates show no outstanding anomalies and lie well within the error ellipse.

The estimates using the clock angle of the scan-platform pointing direction are shown in Fig. 5-14 with the error ellipse at E - 6h of 230 km × 155 km at -45 deg. These estimates are again well within the error but do show some anomalies. Like Mariner VI, there are deviations spaced 24h apart (E - 11h and E - 35h) that are probably related to shifts in the tracked center of brightness as surface features move across the planet image. There is also a systematic shift of the estimate between E - 11h and E - 6h probably due to shifts in FEPS calibration with the larger brighter planet. Figure 5-15 shows the signature in the platform clock-angle residuals for the day before encounter.

In general, the Mariner VII trajectory estimates using on-board optical data were good despite the loss of some telemetry. This loss of data will, however, preclude any detailed performance analysis.

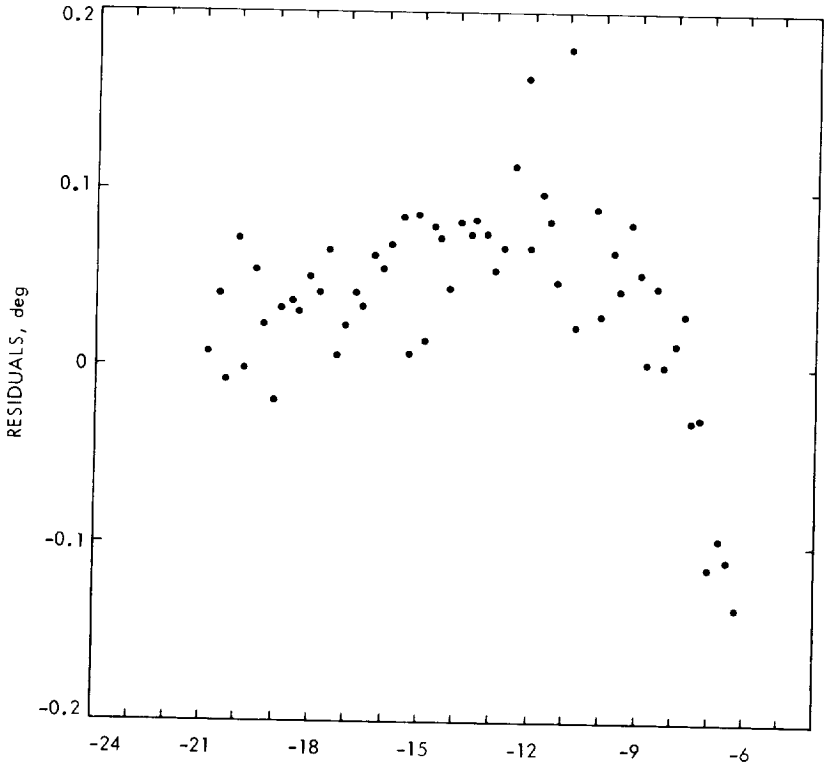

Figure 5-15. Mariner VII Residuals of Scan Platform Clock Angle Between E - 24 and E - 6 Hours

H. RADIO OPTICAL ORBIT DETERMINATION PROGRAM RESULTS

The operation of the programs is described schematically in Fig. 5-16. Radio tracking data and a set of initial injection conditions are first input to the SPODP. The SPODP creates a DPMMP tape which contains the probe ephemeris, variational equations, and information for each radio-tracking observation. This DPMMP tape is next input to ROODP along with optical approach guidance observations, and ROODP constructs a new DPMMP tape which is enriched with optical information in a format suitable for interpretation by the DPMMP. ROODP contains a bias error model which can estimate up to 5 biases in the optical measurements: 3 bias errors in the orientation of the scan platform on board the spacecraft, and 2 biases to estimate the difference between the center of brightness and true geometrical center of Mars.

The DPMMP processes the information on this ROODP-generated DPMMP tape and computes increments to the initial injection conditions. Various data types and data spans may be specified in any combination by the analyst. The DPMMP process is a least squares fit which may be expressed roughly as

$$J^*\Delta Q = R$$

where ΔQ are the increments to the original values of the estimated parameters, J^* is an accumulated matrix of partials; $J^* = \sum_{i=1}^{N} \phi_i \phi_i^T$, N observations, ϕ_i = vector of weighted partials of the data type with respect to the estimated parameters for the i^{th} observation, and R is an accumulated vector of residuals and partials; $R = \sum_{i=1}^{N} \phi_i \Delta F_i$, N observations, ΔF_i = residual for the i^{th} observation, i.e., the difference between the observed value of a data type and the theoretical value based on the present orbit estimate.

Statistics describing the confidence of the new estimate are obtained from the covariance matrix $\Gamma = J^{*-1}$.

Since the DPMMP could not map the new injection conditions into the encounter plane, the SPODP was used to perform this mapping operation. The final result was a new value for $\overline{B} \cdot \overline{R}$, $\overline{B} \cdot \overline{T}$ and the time of closest approach.

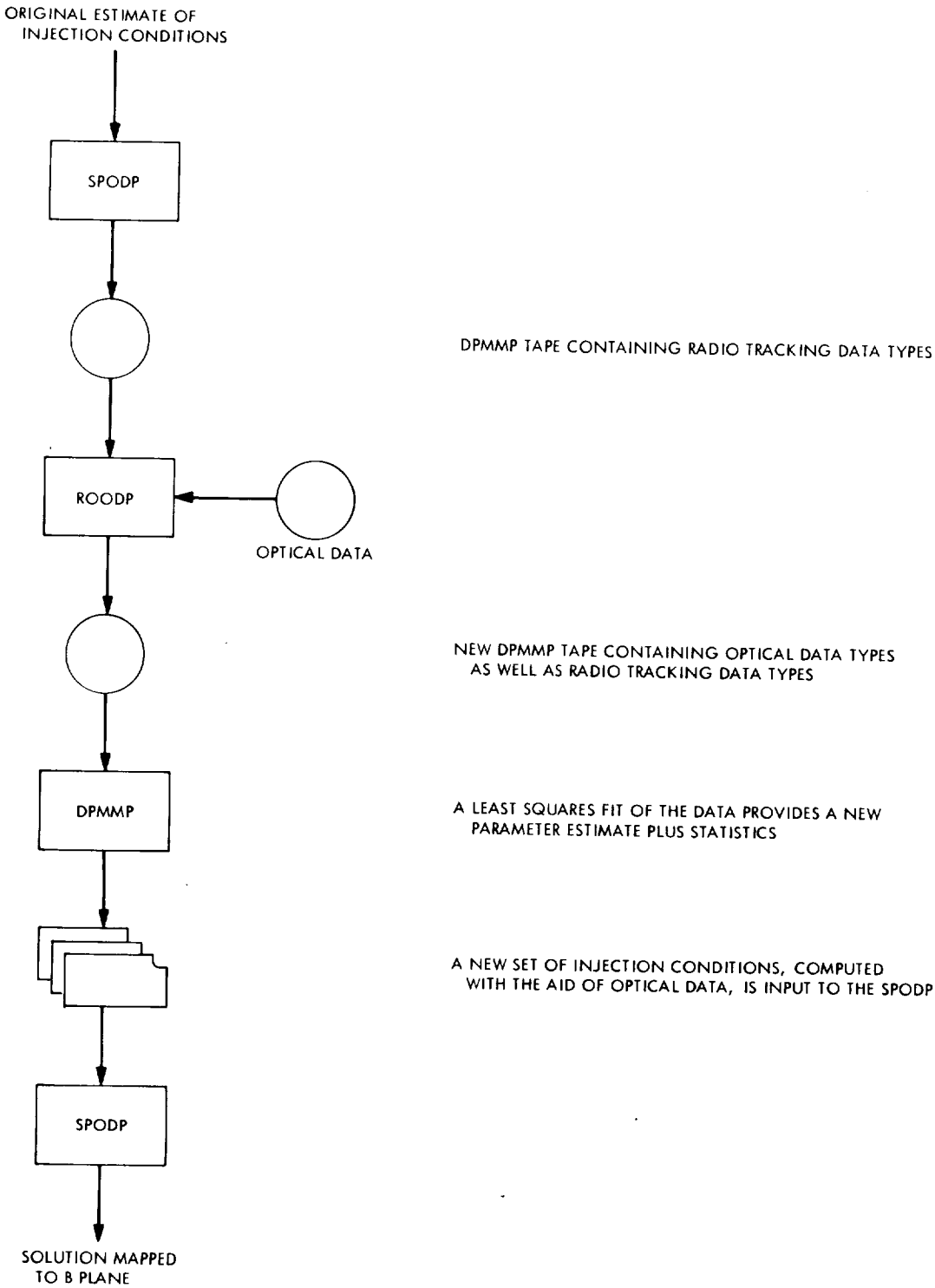

Figure 5-16. ROODP Flow Diagram

The Radio Optical Orbit Determination Program results are tabulated in Table 5-1 through 5-4. Table 5-1 lists the B-plane coordinates of the Mariner VI and VII trajectories input into ROODP. These initial estimates were obtained from the radio data solutions of the spacecraft trajectories taken at ten days and five days respectively before encounter. The final estimate of the spacecraft trajectory after processing the on-board measurements is also listed. The initial estimate from radio data was not the "best" radio solution available, but was selected for demonstrating the power of the on-board data.

The spacecraft trajectory error ellipses in the B-plane are tabulated in Table 5-2 for the corresponding solutions of Table 5-1.

Table 5-3 gives the B-plane coordinates of the "best" available B-plane coordinates for the encounter spacecraft trajectory. Note that the differences in $\overline{B} \cdot \overline{R}$ between Tables 5-1 and 5-3 are only 41 and 38 km respectively.

Table 5-4 is similar to Table 1 except the results are from the Optical Observable Processor Program (OOPP).

One variation between ROODP and OOPP is that ROODP modified equation 2 to the form

$$\bar{\epsilon} = \begin{bmatrix} \epsilon_1 \\ \epsilon_2 \\ \epsilon_3 \end{bmatrix} = \begin{bmatrix} e_1 + K_1\Phi \\ e_2 + K_2\Phi \\ e_3 \end{bmatrix}$$

This modification eliminated the two drifting parameters d_1 and d_2 from the solution. The solutions for the spacecraft trajectory tended to be further away from the correct solution when the optical data furthest from the planet was used. However, when all of the optical data especially the data nearest the planet was processed, the two programs obtained the same solutions for the spacecraft's orbit as can be seen by comparing Table 5-1 with Table 5-4.

Figure 5-17 is a typical plot of the Mariner VI optical observables residuals (observed data minus the computed data) after iterating on the 24 point

Table 5-1. Optical Tracking Data (ROODP)

		$\bar{B} \cdot \bar{R}$, km	$\bar{B} \cdot \bar{T}$, km	TCA, GMT
MA 6	Original Estimate	-14	7485	$7/31\ 05^h19^m05^s.920$
	Optical Result	-368	7473	$7/31\ 05^h18^m56^s.999$
MA 7	Original Estimate	3795	6746	$8/05\ 05^h00^m53^s.001$
	Optical Result	3597	6774*	$8/05\ 05^h00^m50^s.000$

*Loss of cone angle telemetry at E_7 - 127 hrs makes $\vec{B} \cdot \vec{T}$ estimate less accurate than $\vec{B} \cdot \vec{R}$ estimate.

Table 5-2. Statistics of 1σ Error Ellipse (ROODP)

		SMAA, km	SMIA, km	TCA, sec
MA 6	Original Estimate	360	80	6
	Optical	159	73	6
MA 7	Original Estimate	360	182	60
	Optical	217	141	13

Table 5-3. Radio Tracking Data

	$\bar{B} \cdot \bar{R}$, km $\pm 1\sigma$	$\bar{B} \cdot \bar{T}$, km $\pm 1\sigma$	TCA, GMT $\pm 1\sigma$
MA 6	-327 ±3	7603 ±2	$7/31\ 05^h19^m07.^s1$ ±0.5
MA 7	3635 ±5	6711 ±3	$8/05\ 05^h00^m49^s.5$ ±0.5

Table 5-4. Optical Tracking Data (OOPP)

	$\vec{B} \cdot \vec{R}$, km	$\vec{B} \cdot \vec{T}$, km	TCA, GMT
MA 6	-327	7469	$7/31\ 05^h19^m00^s$
MA 7	3599	6788*	$8/05\ 05^h00^m52^s$
*Loss of cone angle telemetry at E_7 - 127 hrs makes $\vec{B} \cdot \vec{T}$ estimate less accurate than $\vec{B} \cdot \vec{R}$ estimate.			

obtained from the television pictures during real time. Figure 5-18 is a typical plot of the doppler residuals from the Mariner VI optical solution.

I. CONCLUSIONS

All of the objectives of the optical-approach navigation experiment were met during the pre-encounter and post-encounter activities. In meeting the objectives, the use of spacecraft-based measurements for navigation, within the time constraints of mission operations, has been shown feasible. Trajectory estimates within their expected accuracy were obtained long before the spacecraft entered the sphere of influence of Mars, demonstrating the accuracy potential of spacecraft-based measurements. Future interplanetary missions should expect significant increase in accuracy performance by using instruments specifically developed for producing navigation data.

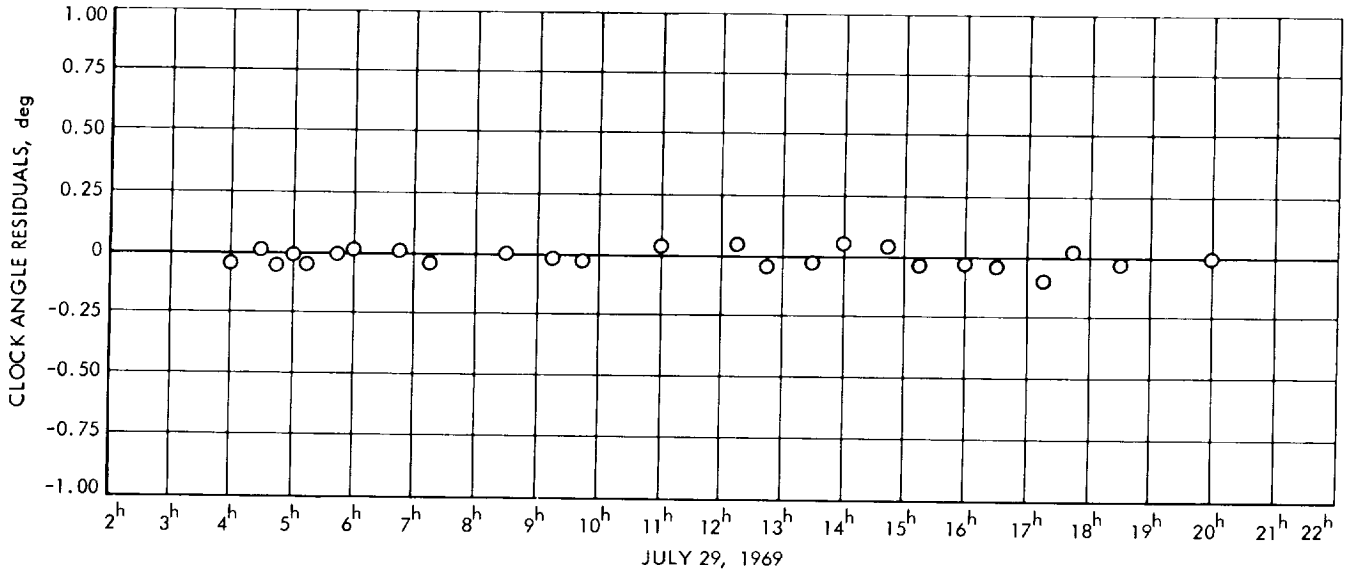

Figure 5-17a. Mariner VI Clock Angle Residuals

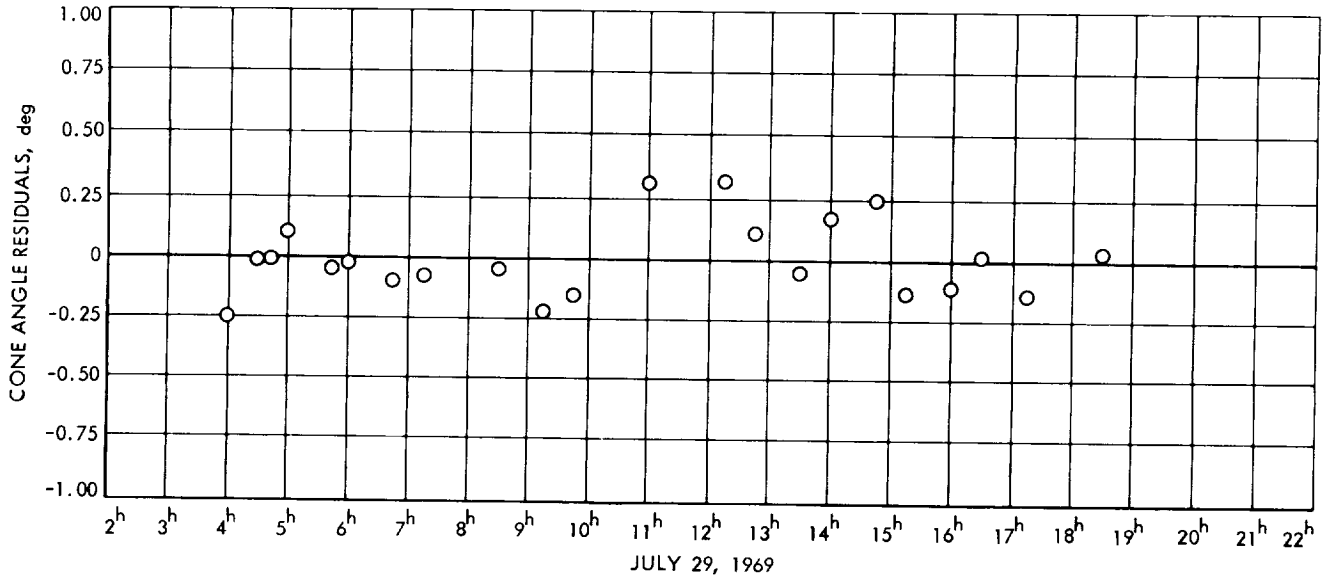

Figure 5-17b. Mariner VI Cone Angle Residuals

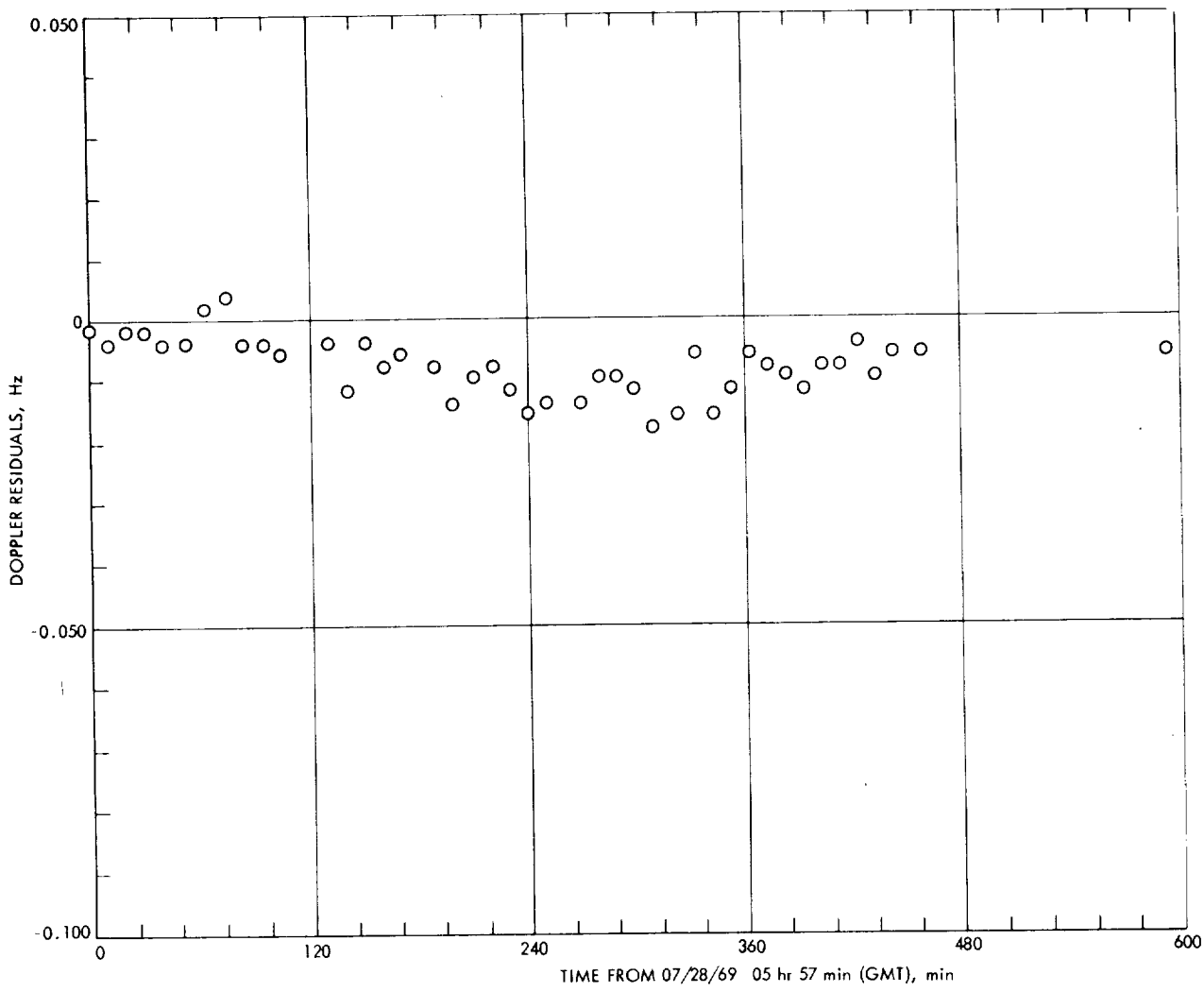

Figure 5-18. Mariner VI Doppler Residuals After Fitting Optical Data

REFERENCES

1. Gordon, H. J., Wong, S. K., and Ondrasik, V. J., "Analysis of Mariner VII Pre-encounter Anomaly," Paper 70-1065, presented at the AAS/AIAA Astrodynamics Conference, Santa Barbara, Calif., Aug. 21, 1970.

2. Hamilton, T. W., Grimes, D. C., and Trask, D. W., "Critical Parameters in Determining the Navigational Accuracy for a Deep Space Probe During the Planetary Encounter Phase," in The Deep Space Network, Space Programs Summary 37-44, Vol. III, pp. 4-11. Jet Propulsion Laboratory, Pasadena, Calif., Mar. 31, 1967.

3. Melbourne, W. G., and O'Handley, D. A., "A Consistent Ephemeris of the Major Planets in the Solar System," in Supporting Research and Advanced Development, Space Programs Summary 37-51, Vol. III, pp. 4-13. Jet Propulsion Laboratory, Pasadena, Calif., June 30, 1968.

4. O'Handley, D. A., Holdridge, D. B., Melbourne, W. G., and Mulholland, J. D., JPL Development Ephemeris Number 69, Technical Report 32-1465. Jet Propulsion Laboratory, Pasadena, Calif., Dec. 15, 1969.

5. Brouwer, D., and Clemence, G. M., Methods of Celestial Mechanics, p. 241, Academic Press, Inc., New York, 1961.

6. Hamilton, T. W., and Melbourne, W. G., "Information Content of a Single Pass of Doppler Data from a Distant Spacecraft," in The Deep Space Network, Space Programs Summary, Vol. III, pp. 18-23. Jet Propulsion Laboratory, Pasadena, Calif., May 31, 1966.

7. Mulhall, et al., Tracking System Analytic Calibration Activities for the Mariner Mars 1969 Mission, Technical Report 32-1499. Jet Propulsion Laboratory, Pasadena, Calif., in press.

8. Mottinger, N. A., "Status of DSS Location Solutions for Deep Space Probe Missions: Third Generation Orbit Determination Program Solutions for Mariner Mars 1969 Mission," in The Deep Space Network, Space Programs Summary 37-60, Vol. II, pp. 77-89. Jet Propulsion Laboratory, Pasadena, Calif., Nov. 30, 1969.

9. Mottinger, N. A., "Status of DSS Location Solutions for Deep Space Probe Missions: Comparison with the SAO Standard Earth 1969 Station Locations," in The Deep Space Network, Space Programs Summary 37-62, Vol. II, pp. 41-45. Jet Propulsion Laboratory, Pasadena, Calif., Mar. 31, 1970.

10. Trask, D. W., and Muller, P. M., "Timing: DSIF Two-Way Doppler Inherent Accuracy Limitations," in The Deep Space Network, Space Programs Summary 37-39, Vol. III, pp. 7-16. Jet Propulsion Laboratory, Pasadena, Calif., May 31, 1966.

11. Explanatory Supplement to the Ephemeris, Her Majesty's Stationery Office, London, 1961.

12. Muller, P. M., "Polar Motion and DSN Station Locations," in The Deep Space Network, Space Programs Summary 37-45, Vol. III, pp. 10-14. Jet Propulsion Laboratory, Pasadena, Calif., May 31, 1967.

13. Guinot, B., and Feissel, M., BIH Annual Report for 1968, Bureau International De L'Heure, Paris, France.

14. Muller, P. M., and Chao, C. C., "New Timing Polynomial Program and Data," in The Deep Space Network, Space Programs Summary 37-57, Vol. II, pp. 42-51. Jet Propulsion Laboratory, Pasadena, Calif., May 31, 1969.

15. Yumi, S., Annual Report of the International Polar Motion Service for 1968, Mizusawa, Japan.

16. Curkendall, D. W., and McReynolds, S. R., "A Simplified Approach for Determining the Information Content of Radio Tracking Data," J. Spacecraft Rockets, Vol. 6, No. 5, pp. 520-525, May 1969.

17. Moyer, T., "Theoretical Basis for the Double Precision Orbit Determination Program (DPODP): III Probe Trajectory," in The Deep Space Network, Space Programs Summary 37-41, Vol. III, p. 24-31. Jet Propulsion Laboratory, Pasadena, Calif., Sep. 30, 1966.

18. Warner, M. R., and Nead, M. W., SPODP – Single Precision Orbit Determination Program, Technical Memorandum 33-204. Jet Propulsion Laboratory, Pasadena, Calif., Feb. 15, 1965.

19. DeSitter, W., and Brouwer, D., "On the System of Astronomical Constants," Boll. Astron. Inst. (Netherlands), Vol. 8, p. 213, 1938.

20. Van Den Bosch, C. A., De Massa's van de Groote Planeten, dissertation, University of Utrecht (Netherlands), p. 126, 1927.

21. Ash, M. E., Shapiro, I. E., and Smith, W. B., "Astronomical Constants and Planetary Ephemerides Deduced from Radar and Optical Observations," Astron. J., April 1967.

22. Null, G. W., Gordon, H. J., and Tito, D. A., The Mariner IV Flight Path and Its Determination from Tracking Data, Technical Report 32-1108. Jet Propulsion Laboratory, Pasadena, Calif., Aug. 1, 1967.

23. Vegos, C. J., and Trask, D. W., "Ranger Combined Analysis, Part II: Determination of the Masses of the Earth and Moon from Radio Tracking Data," in The Deep Space Network, Space Programs Summary 37-44, Vol. III, pp. 11-28. Jet Propulsion Laboratory, Pasadena, Calif., Mar. 31, 1967.

24. Labrum R. G., Wong, S. K., and Reynolds, G. W., The Surveyor V, VI and VII Flight Paths and Their Determination from Tracking Data, Technical Report 32-1302. Jet Propulsion Laboratory, Pasadena, Calif., Dec. 1, 1968.

25. Pease, G., Bourke, R. D., McReynolds, S., Thuleen, K., Borras, J. A., and Mitchell, R., The Mariner V Flight Path and Its Determination from Tracking Data, Technical Report 32-1363. Jet Propulsion Laboratory, Pasadena, Calif., July 1, 1969.

26. Chao, C. C., "Perturbation in JPL Adopted Timing Data Due to Newly Input Raw Data," in The Deep Space Network, Space Programs Summary 37-59, Vol. II, pp. 110-114. Jet Propulsion Laboratory, Pasadena, Calif., Sep. 30, 1969.

27. Kizner, W., A Method of Describing Miss Distances for Lunar and Interplanetary Trajectories, External Publication 674. Jet Propulsion Laboratory, Pasadena, Calif., Aug. 1, 1959.